

STRENGTH AND STIFFNESS OF COMPOSITE
BEAMS IN UNBRACED FRAMES

by

C

EZZAT H.A. FAHMY, B.Sc., M.Eng.

A Thesis

Submitted to the School of Graduate Studies
in Partial Fulfilment of the Requirement

for the Degree

Doctor of Philosophy

McMaster University

October, 1978

STRENGTH AND STIFFNESS OF COMPOSITE

BEAMS IN UNBRACED FRAMES

To My Dear Wife NADIA

Whose

Patience, Understanding and Assistance

are Deeply Appreciated

DOCTOR OF PHILOSOPHY (1978)
(Civil Engineering)

McMASTER UNIVERSITY
Hamilton, Ontario

TITLE: Strength and Stiffness of Composite Beams In Unbraced
Frames

AUTHOR: Ezzat Hassan Ahmed Fahmy, B.Sc. (Cairo Univ.)
M.Eng. (McMaster Univ.)

SUPERVISOR: Professor H. Robinson

NUMBER OF PAGES: xxiv, 371

ABSTRACT

Composite steel-concrete beams often form part of multi-story frames. However, very little information is available on which to base the design of composite beam-to-column connections. As a result, these connections are currently designed on the basis of the connecting steel elements. Most of the information available is limited to continuous composite beams subjected to gravity loads which may be used as a part of braced multi-story frames. Limited information is available on the behaviour of composite beams in unbraced multi-story frames subjected to combined gravity and lateral loads.

The object of this thesis is to study the behaviour of composite beams with ribbed metal deck in an unbraced multi-story frame. Of particular importance in this investigation is the effective slab width which is to be used in evaluating the strength of the composite beam at the connection and the effective slab width which is to be used in evaluating the stiffness of the composite beams in the positive and negative moment regions of an unbraced frame subjected to combined gravity and lateral loads. A combined analytical and experimental investigation was conducted.

A method of analysis has been developed using a combination of the finite difference and finite elements methods to model the composite steel-concrete beams in the various moment regions. The analytical model was used to study the parameters affecting the effective slab widths, for strength and stiffness, and consequently the behaviour of composite beams in an unbraced frame. Curves showing the variation of

the effective slab width for strength and the effective slab width for stiffness with the side ratio (L/b) and the column width to slab width ratio (c/b) in the case of complete interaction and a method for evaluating the effective slab width for stiffness for any degree of interaction are presented.

The analytical model was used to study the effective slab widths for composite simple beams subjected to a central point load, and the results were compared with the different code formulae. The results showed that the AIJ formula agrees very well with the analytical results of the effective slab width for strength while the CSA S16.1 formulae provides a good estimate for the effective slab width for stiffness especially for (L/b) greater than 4.

In the experimental program, 10 composite beam-to-column connections were tested under positive moment conditions to simulate that portion of the composite beam in an unbraced frame between the point of contraflexure and the column face and subjected to positive moment. The test results showed that the strength, stiffness and ductility depend on the (L/b) and (c/b) ratios, steel beam size, slab thickness and the existence of lateral support. The test results showed also that the composite beam-to-column connections possess sufficient rotation capacity to enable plastic design to be applied to unbraced frames with composite beams.

The test beams were analysed using the analytical model and very good agreement was obtained between the experimental and analytical results.

ACKNOWLEDGEMENTS

I wish to express my sincere thanks and appreciation to Professor H. Robinson for his guidance during the course of this study.

I am also indebted to the members of my supervisory committee, Dr. R.M. Korol, Dr. W.K. Tso and Dr. D.S. Weaver for their valuable suggestions.

I would like to take this opportunity to thank McMaster University, The National Research Council of Canada and the Canadian Steel Industries Construction Council for financial support.

I also wish to thank the technicians of the Applied Dynamics Laboratory for their assistance in the experimental work. My thanks are also due to Betty Petro and Pat Dillon from the Word Processing Centre who made this thesis presentable.

Last but not the least, I must mention my deepest appreciation to my parents without whose help and encouragement this work would have been difficult to complete.

TABLE OF CONTENTS

	PAGE
ABSTRACT	iv
ACKNOWLEDGEMENTS	vi
NOTATION	xxi
CHAPTER 1: INTRODUCTION	
1.1 Foreward	1
1.2 Purpose and Scope	5
1.3 Outline of the Thesis	6
CHAPTER 2: LITERATURE REVIEW	
2.1 Introduction	8
2.2 Effective Slab Width	9
2.3 Behaviour of Composite Beams	19
2.3.1 Behaviour of Simple Composite Beams	19
2.3.2 Behaviour of Continuous Composite Beams	22
2.4 Composite Beam-to-Column Connection	26
2.5 Summary	35
CHAPTER 3: ANALYTICAL METHOD AND DESCRIPTION OF THE COMPUTER PROGRAM	
3.1 Introduction	36
3.2 Analytical Model	37
3.3 Idealization of Actual Material Properties	41
3.3.1 Steel Beam	43
3.3.2 Concrete Slab	43

TABLE OF CONTENTS (continued)

	Page
3.3.3 Steel Reinforcement	45
3.3.4 Shear Connectors.	45
3.4 Finite Difference Formulation	47
3.4.1 General Definition	48
3.4.2 Basic Assumptions	48
3.4.3 Basic Equations	50
3.4.4 The Computational Procedure	54
3.5 Finite Elements Formulation	55
3.5.1 General	55
3.5.2 Assumptions	58
3.5.3 Stiffness Matrix for a Plate Element	58
3.5.3.1 System of Axes and Nodal Coordinates	59
3.5.3.2 Displacement Formulation	60
3.5.4 Assemblage of Elements	71
3.5.5 Evaluation of the Stresses and Strains	71
3.5.6 Post-Elastic Analysis	72
3.5.6.1 Concrete Element in Compression and Reinforcing Steel	74
3.5.6.2 Concrete Element in Tension	74
3.6 Effective Slab Widths	76
3.7 Method of Computation	82
3.8 Computer Program Description	83
3.9 Summary	85
 CHAPTER 4: ANALYTICAL INVESTIGATION OF THE EFFECTIVE SLAB WIDTHS	
4.1 General	86
4.2 Check of the Reliability of the Program	86
4.2.1 Check of the Finite Element Section	87
4.2.2 Check of the Over-all Program	89
4.2.2.1 Prediction of the Effective Slab Width for Strength	89
4.2.2.2 Behaviour of the Composite Beam-to-Column Connections	90

TABLE OF CONTENTS (continued)

	Page
4.3 Analytical Investigation	95
4.4 Effective Slab Width for Strength (b_e)	96
4.4.1 Variation of the Effective Slab Width for Strength Along the Span	97
4.4.2 Variation of the Effective Slab Width (b_e) with the Load	102
4.4.3 Effect of the Concrete Strength (f'_c) on the Effective Slab Width for Strength in the Positive Moment Region	107
4.4.4 Effect of the Total Slab Thickness, Steel Beam Size and Number of Connectors on the Effective Slab Width for Strength	109
4.4.5 Effect of the Slab Length to Width Ratio (L/b) and Column Face Width to Slab Width Ratio c/b on the Effective Width	113
4.5 Average Effective Slab Width for Stiffness (b_{av})	114
4.6 Effective Slab Width for Stiffness at any Section of the Composite Beam (b_{es})	124
4.7 A Method for Elastic Analysis of Composite Beams	130
4.8 Discussion on the Effective Slab Width Formula for Simple Composite Beams in the Different Codes	133
4.9 Summary	138
 CHAPTER 5: DESCRIPTION OF THE TEST PROGRAM	
5.1 Introduction	142
5.2 Description of the Test Beams and Test Set-up	143
5.3 Design of Test Specimens	147
5.4 Construction	154
5.5 Instrumentation	155
5.6 Test Procedure and Loading	157
5.7 Actual Material Properties	161

TABLE OF CONTENTS (continued)

	Page
5.8 Summary	165
 CHAPTER 6: EXPERIMENTAL RESULTS	
6.1 General	166
6.2 Presentation of the Test Results	166
6.3 Test Results	170
6.3.1 Beam A	170
6.3.1.a End A ₂	170
6.3.1.b End A ₁	177
6.3.2 Beam B	182
6.3.2.a End B ₁	183
6.3.2.b End B ₂	189
6.3.3 Beam C	195
6.3.3.a End C ₁	195
6.3.3.b End C ₂	202
6.3.4 Beam D	208
6.3.4.a End D ₂	208
6.3.4.b End D ₁	214
6.3.5 Beam E	220
6.3.5.a End E ₁	221
6.3.5.b End E ₂	230
6.4 Evaluation of the Test Results	236
6.4.1 Effect of the Column Face Width to the Slab Width Ratio	238
6.4.2 Effect of the Slab Length to Width Ratio	240
6.4.3 Effect of the Total Slab Thickness	242
6.4.4 Effect of the Steel Beam Size	247
6.4.5 Effect of the Lateral Support	249
6.4.6 Effect of the Existence of the Longitudinal Crack Before Testing	253
 CHAPTER 7: COMPARISON OF THE EXPERIMENTAL AND TEST RESULTS	
7.1 General	256
7.2 Ultimate Moment Capacity	257
7.3 End Moment Versus End Deflection Curves	259

TABLE OF CONTENTS (continued)

	Page
7.4 Bottom Fibre Steel Strain	272
7.5 Moment-Curvature Curves	283
7.6 Strain Distribution Across the Slab Width	295
7.7 Prediction of the Strain Distribution across the Composite Beam Depth	314
7.8 Rotation Capacity	315
CHAPTER 8: SUMMARY AND CONCLUSIONS	
8.1 Summary	321
8.2 Conclusions	324
APPENDIX A: Numerical Method for the Finite Difference Computation	327
APPENDIX B: Computer Program Listing	332
REFERENCES	366

LIST OF FIGURES

FIGURE		PAGE
1.1	Bending Moment in an Unbraced Multi-Story Frame	3
1.2	Bending Moment Regions in the Beams of Multi-Story Unbraced Frames under Combined Loading	3
3.1	Unbraced Frame and One-Story Assemblage	38
3.2	A Typical Composite Steel-Concrete Beam	40
3.3	Analytical Model	42
3.4	Idealized Stress-Strain Curve for the Steel Beam	44
3.5	Stress-Strain Curve for concrete	44
3.6	Idealized Stress-Strain Curve for the Slab Reinforcement	46
3.7	Idealized Load-Slip Curve for the Connectors	46
3.8.a	Composite Beam Showing Connectors and Panels	49
3.8.b	Positive Direction of the Interaction Forces	49
3.9	General Cross Section	51
3.10	Forces, Moments and Strains for Incomplete Interaction	51
3.11	Slip in the (i)th Panel	51
3.12	Layered System	57
3.13	Plate Subdivision and System of Axes	61
3.14	Construction of a Typical Layered System	69
3.15	Iteration Method	73
3.16	Effective Slab Width for Strength	77
3.17	Flow Chart of the Computation Method	84
4.1	Comparison between the Calculated b_e/L and the Results given in Reference (18)	91

LIST OF FIGURES (continued)

FIGURE		PAGE
4.2	Comparison between the Computed Load-Deflection Curve and the Experimental Results Reported in Reference (48) for Beam B ₁	93
4.3	Comparison between the Computed Load-Deflection Curve and the Experimental Results Reported in Reference (48) for Beam F ₁	94
4.4	Analytical Model and Finite Elements Discretization	98
4.5	Variation of the Effective Slab Width for Strength (b_e) along the Span in the Positive Moment Region	100
4.6	Variation of the Effective Slab Width for Strength (b_e) along the Span in the Negative Moment Region	101
4.7	Variation of the Minimum Effective Slab Width for Strength with the Applied Load in the Positive Moment Region for $L/b = 2$	103
4.8	Variation of the Minimum Effective Slab Width for Strength with the Applied Load in the Positive Moment Region for $L/b = 4$	104
4.9	Variation of the Top Fibre Concrete Stress Distribution across the Slab Width at the Column Face with the Applied Load	106
4.10	Variation of the Minimum Effective Slab Width for Strength with the Applied Load in the Negative Moment Region for $L/b = 2$	108
4.11	Effect of f'_c on the Minimum Effective Slab Width for Strength	110
4.12	Variation of the Minimum Effective Slab Width for Strength with (L/b) and (c/b) Ratios in the Positive Moment Region	115
4.13	Variation of the Minimum Effective Slab Width for Strength with (L/b) and (c/b) Ratios in the Negative Moment Region	116
4.14	Variation of the Average Effective Slab Width for Stiffness with (L/b) and (c/b) Ratios in the Positive Moment Region	121

LIST OF FIGURES (continued)

FIGURE		PAGE
4.15	Variation of the Average Effective Slab Width for Stiffness with (L/b) and (c/b) Ratios in the Negative Moment Region	122
4.16	Comparison between the Analytical Effective Slab Width for Strength and the Different Code Formulae	134
4.17	Comparison between the Analytical Effective Slab Width for Stiffness and the Different Code Formulae	137
4.18	One-story Assemblage Showing the Inertia of the Composite Beam in the Different Moment Regions	140
5.1	Typical Test Beam	145
5.2	Schematic View of the Test Set-Up	146
5.3	General View of the Test Set-Up for Beam E	148
5.4	Details of Shear Connectors for Beams A, B, C and E	150
5.5	Details of Shear Connectors for Beam D	151
5.6	Details of the End Plate	153
5.7	Locations of the Dial Gauges	156
5.8	Locations of the Strain Gauges	158
5.9	Strain Gauges and Demec Points on the Concrete Slab	159
5.10	Loading System	160
6.1	Explanation of End Rotation Calculation	168
6.2	Live Load End Moment - End Deflection Results for Ends A ₁ and A ₂	172
6.3	Live Load Moment versus Bottom Fibre Steel Strain for End A ₂	173
6.4	Live Load Moment - Curvature Results for End A ₂	174
6.5	Live Load Moment - End Rotation Results for End A ₂	175

LIST OF FIGURES (continued)

FIGURE		PAGE
6.6	Top Fibre Strain Distribution Across the Slab Width for End A ₂	176.
6.7	Live Load Moment versus Bottom Fibre Steel Strain for End A ₁	178
6.8	Live Load Moment - Curvature Results for End A ₁	179
6.9	Live Load Moment - End Rotation Results for End A ₁	180
6.10	Top Fibre Strain Distribution across the Slab Width for End A ₁	181
6.11	Live Load End Moment - End Deflection Results for Ends B ₁ and B ₂	184
6.12	Live Load Moment, versus Bottom Fibre Steel Strain for End B ₁	185
6.13	Live Load Moment - Curvature Results for End B ₁	186
6.14	Live Load Moment - End Rotation Results for End B ₁	187
6.15	Top Fibre Strain Distribution across the Slab Width for End B ₁	188
6.16	Live Load Moment versus Bottom Fibre Steel Strain for End B ₂	191
6.17	Live Load Moment - Curvature Results for End B ₂	192
6.18	Live Load Moment - End Rotation Results for End B ₂	193
6.19	Top Fibre Strain Distribution across the Slab Width for End B ₂	194
6.20	Live Load End Moment - End Deflection Results for End C ₁	196
6.21	Live Load Moment versus Bottom Fibre Steel Strain for End C ₁	197
6.22	Live Load Moment - Curvature Results for End C ₁	198
6.23	Live Load Moment - End Rotation Results for End C ₁	199

LIST OF FIGURES (continued)

FIGURE		PAGE
6.24	Top Fibre Strain Distribution across the Slab Width for End C ₁	200
6.25	Live Load End Moment - End Deflection Results for End C ₂	203
6.26	Live Load Moment versus Bottom Fibre Steel Strain for End C ₂	204
6.27	Live Load Moment - Curvature Results for End C ₂	205
6.28	Live Load Moment - End Rotation Results for End C ₂	206
6.29	Top Fibre Strain Distribution across the Slab Width for End C ₂	207
6.30	Live Load End Moment - End Deflection Results for End D ₂	209
6.31	Live Load Moment versus Bottom Fibre Steel Strain for End D ₂	210
6.32	Live Load Moment - Curvature Results for End D ₂	211
6.33	Live Load Moment - End Rotation Results for End D ₂	212
6.34	Top Fibre Strain Distribution Across the Slab Width for End D ₂	213
6.35	Live Load End Moment - End Deflection Results for End D ₁	215
6.36	Live Load Moment versus Bottom Fibre Steel Strain for End D ₁	216
6.37	Live Load Moment - Curvature Results for End D ₁	217
6.38	Live Load Moment - End Rotation Results for End D ₁	218
6.39	Top Fibre Strain Distribution across the Slab Width for End D ₁	219
6.40	Live Load End Moment - End Deflection Results for End E ₁	222
6.41	Live Load Moment versus Bottom Fibre Steel Strain for End E ₁	223

LIST OF FIGURES (continued)

FIGURE		PAGE
6.42	Live Load Moment - Curvature Results for End E ₁	224
6.43	Live Load Moment - End Rotation Results for End E ₁	225
6.44	Top Fibre Strain Distribution across the Slab Width for End E ₁	226
6.45	Flexural Cracks in the Slab of End E ₁	227
6.46	End E ₁ after Testing	228
6.47	Failure of End E ₁	229
6.48	Live Load End Moment - End Deflection Results for End E ₂	231
6.49	Live Load Moment versus Bottom Fibre Steel Strain for End E ₂	232
6.50	Live Load Moment - Curvature Results for End E ₂	233
6.51	Live Load Moment - End Rotation for End E ₂	234
6.52	Top Fibre Strain Distribution Across the Slab Width for End E ₂	235
6.53	Comparison between the Top Fibre Concrete Strain for Ends A ₁ and A ₂	241
6.54	Comparison between the Top Fibre Concrete Strain for Ends A ₁ and D ₁	243
6.55	Comparison between the Top Fibre Concrete Strain for End A ₂ and D ₂	244
6.56	Comparison between the Bottom Fibre Steel Strain for Ends A ₁ and D ₁	245
6.57	Comparison between the Bottom Fibre Steel Strain for Ends A ₂ and D ₂	246
6.58	Comparison between the Top Fibre Concrete Strain for Ends A ₁ and E ₂	248
6.59	Comparison between the Top Fibre Concrete Strain Distribution across the Slab Width for Ends E ₁ and E ₂	250

LIST OF FIGURES (continued)

FIGURE		PAGE
6.60	Comparison between the Bottom Fibre Steel Strain for Ends E_1 and E_2	251
6.61	Comparison between the Top Fibre Concrete Strain for Ends E_1 and E_2	252
7.1 - 7.9	Comparison between the Experimental and Analytical Moment - Deflection Curves for the Test Beams	260-268
7.10 - 7.18	Comparison between the Experimental and Analytical Moment - Bottom Fibre Steel Strain Curves for the Test Beams	274-282
7.19 - 7.27	Comparison between the Experimental and Analytical Moment - Curvature Curves for the Test Beams	286-294
7.28 - 7.45	Comparison between the Experimental and Analytical Top Fibre Concrete Strain Distribution across the Slab Width	296-313
7.46	Comparison between the Experimental and Theoretical Strain Distribution across the Depth of the Test Beams	317
7.47	Definition of Rotation Capacity	318

LIST OF TABLES

TABLE		PAGE
4.1	Comparison between the Finite Element Results and those Given in Reference (63)	88
4.2	Effect of the Degree of Interaction on the Effective Slab Width for Strength	111
4.3	The Average Effective Slab Width for Stiffness for the Analysed Beams	118
4.4	The Effective Slab Width for Stiffness at the Column Face for the Analysed Beams	126
5.1	Details of the Test Beams	144
5.2	Properties of the Concrete	163
5.3	Properties of the Steel	164
6.1	Summary of the Test Results	237
6.2	Maximum Strength Ratio, Initial Stiffness Ratio and Ductility Factor of the Test Beams	239
6.3	Effect of Increasing c/b Ratio	254
6.4	Effect of Increasing L/b Ratio	254
6.5	Effect of Increasing Slab Thickness	254
6.6	Effect of Increasing the Steel Beam Size	255
6.7	Effect of the Transverse Support	255
6.8	Effect of the Existence of the Pre-Longitudinal Crack before Testing	255
7.1	Comparison between the Experimental and Analytical Ultimate Moment Capacity	258
7.2	Calculated Deflection for the Transformed Composite Section and the Steel Beam Alone	271

LIST OF TABLES (continued)

TABLE		PAGE
7.3	Bottom Fibre Steel Strain and Curvature for the Transformed Section and the Steel Beam Alone	284
7.4	Calculated and Experimental Concrete and Steel Strains	316
7.5	Rotation Capacity of the Test Beams	319

NOTATION

A_{sc}	Cross sectional area of the connector
A_c	Cross sectional area of the concrete slab
A_s	Cross sectional area of the steel beam
b	Total width of the concrete slab
b_{av}	Average effective slab width for stiffness
b_e	Effective slab width for strength
b_{es}	Effective slab width for stiffness at any section
C_s	Coefficient
d_c	Thickness of the ribbed part of the slab
$d_{(i)}$	Depth of the steel beam in the (i)th panel
E_c	Initial Modulus of elasticity of concrete
E_s	Modulus of elasticity of steel
F	Interaction force
F'	Interaction force for complete interaction
$F_{c(i)}$	Interaction force acting on the concrete slab in the (i)th panel
$F_{s(i)}$	Interaction force acting on the steel beam in the (i)th panel
f'_c	Uniaxial compressive strength of the concrete
f_r	Modulus of rupture of the concrete
f_t	Uniaxial tensile strength of the concrete
f_y	Yield stress of the steel
I_{av}	Average moment of inertia of the composite beam

NOTATIONS (continued)

$(I_{av})_c$	Average moment of inertia of the composite beam for complete interaction
$(I_{av})_i$	Average moment of inertia of the composite beam for incomplete interaction
I_c	Moment of inertia of the concrete slab about its axis
I_{eff}	Moment of inertia of the composite beam at any point along the span
$(I_{eff})_c$	Moment of inertia of the composite beam at any point along the span for complete interaction
$(I_{eff})_i$	Moment of inertia of the composite beam at any point along the span for incomplete interaction
I_s	Moment of inertia of the steel beam about its major axis
J	Joint modulus
K	Modulus of shear connectors
k_i	Modulus of the i th shear connector
L	Length of the composite beam
M	External moment
$M_{(i)}$	External moment applied on the (i) panel
M_c	Bending moment on the concrete slab
$M_{c(i)}$	Bending moment on the concrete slab in the (i) th panel
M_{exp}	Experimental bending moment
M_s	Bending moment on the steel beam
$M_{s(i)}$	Bending moment on the steel beam in the (i) th panel
M_p	Plastic moment of the steel beam
M_u	Ultimate moment of the composite section
N	Number of connectors
P	Applied point load

NOTATIONS (continued)

Q	Connector force
Q_i	Q at the ith connector
Q_u	Ultimate capacity of the connectors in ribbed slab
Q_{us}	Ultimate capacity of the connectors in solid slab
$S_{(i)}$	Lengthh of the (i)th
t_s	Thickness of the solid part of the slab
u	Displacement in x direction
u'	Displacement in x' direction
v	Displacement in y direction
v'	Displacement in Y' direction
X, Y, Z	Global axes
X', Y', Z'	Local axes
y	Distance from the top of the slab to the centre of the uncracked depth
y_b	Distance from the centroid of the composite section to the extreme bottom fibre of the steel beam
z	Distance between the C.G of the steel beam and the centre of the slab
c/b	Column width to total slab width ratio
L/b	Slab length to width ratio
1/c	Interaction coefficient
\overline{EA}	$= \frac{E_s \cdot A_s \cdot E_c \cdot A_c}{E_s \cdot A_s + E_c \cdot A_c}$
$(\overline{EA})_{av}$	The value of EA based on the average effective slab width for stiffness

NOTATIONS (continued)

\overline{EI}	$= E_s I_s + E_c I_c + \overline{EA} \dots (z)^2$
$(\overline{EI})_{av}$	The value of EI based on the average effective slab width for stiffness
γ	Slip
γ_i	Slip at the ith connector
ϵ_{cb}	Bottom fibre concrete strain
ϵ_{ct}	Top fibre concrete strain
ϵ_{cu}	Maximum compressive concrete strain
ϵ_{sb}	Bottom fibre steel strain
ϵ_{st}	Top fibre steel strain
θ	Joint rotation
θ'_x	Rotation about x' axis
θ'_y	Rotation about y' axis
ν_c	Poisson's ratio for concrete
ϕ	Curvature
ϕ_c	Curvature of the concrete slab
$\phi_{D.L}$	Curvature due to D.L
ϕ_s	Curvature of the steel beam

CHAPTER 1
INTRODUCTION

1.1 Foreword

Unbraced multi-story steel frames are used as the structural system for high-rise buildings. As a result of research, the stage has been reached where an unbraced multi-story frame or portion of it can be accurately analyzed to determine its maximum strength and stiffness under gravity or combined gravity and lateral loads. However, the steel frames do not present the complete structural system for a typical high-rise building. The structure usually consists of the multi-story steel frames plus the concrete floor slabs. These two structural elements will interact to share in carrying the applied gravity and lateral loads. The degree of interaction will depend on the type of connection between the slabs and the steel frames.

With today's demands for increasingly economical structures, which at the same time must provide adequate strength and stiffness to resist gravity or combined gravity and lateral loads, attention has been given to the use of the composite action in multi-story frames. Composite steel-concrete beams are now used in the design of such frames. However, such use has been limited to continuous beams subjected to only gravity loads which may be used in the design of braced frames with composite beams. The information available about

frames which are subjected to combined gravity and lateral loads due to the discontinuity of the bending moment at the connection between the beams and the columns is very limited.

When an unbraced frame is subjected to combined gravity and lateral loads the columns apply end moments to the beams at the beam-to-column connections (Figure 1.1). If the lateral loads are large enough to result in positive bending moments adjacent to the leeward side of one or more columns, the distribution of bending moments will determine four regions which must be considered in the investigation of the behaviour of composite beams under combined load conditions. These regions, which are shown in Figure 1.2, are defined as follows.

Region 1 - An interior region in which the cross sections are subjected to positive bending moments, slab in compression, where the compressive force can act over the full effective slab width.

Region 2 - A transition zone consisting of the positive moment region between region 1 and the cross section adjacent to the leeward side of an interior or a windward exterior column. The effective slab width in this region will vary between the full effective width adjacent to region 1 to a minimum value adjacent to the column face.

Region 3 - A negative moment region between region 1 and the cross section adjacent to the windward side of an interior column. The slab reinforcement, if it exists, can be extended past the column.

Region 4 - A negative moment region between region 1 and the cross section adjacent to the windward side of the leeward exterior column. The slab reinforcement in this region cannot be extended past

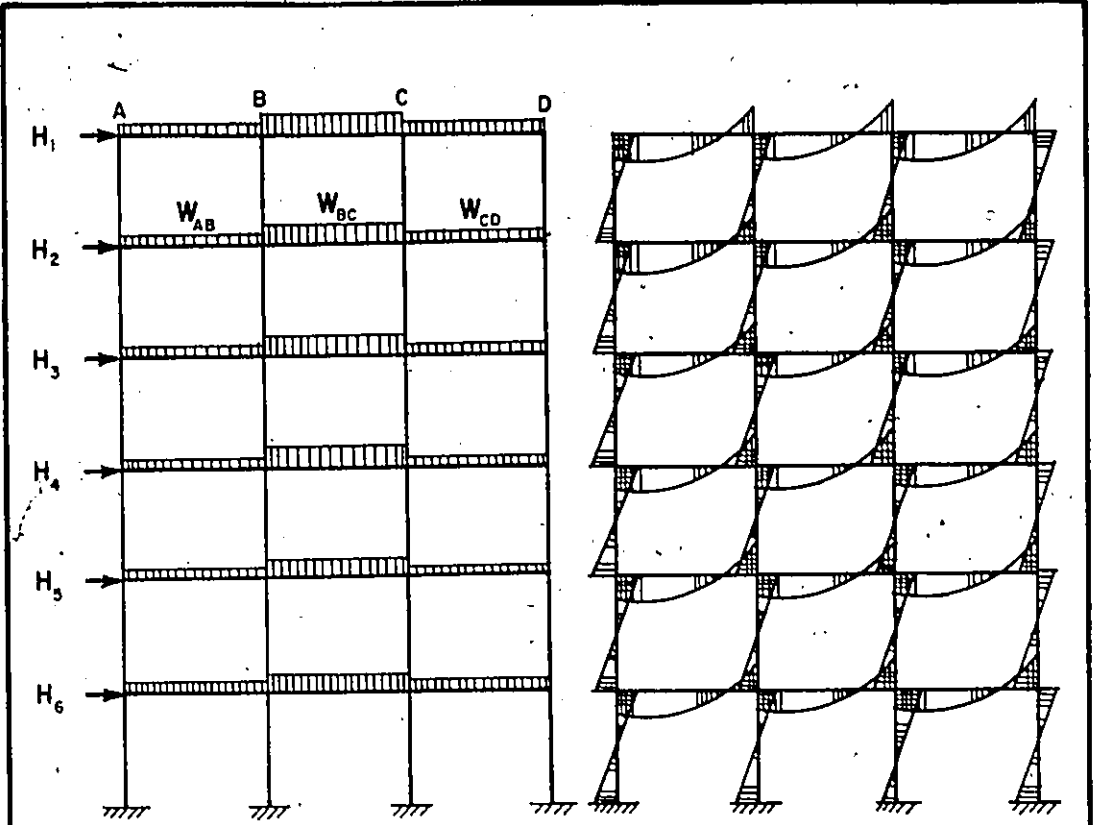


FIGURE 1.1 BENDING MOMENT IN AN UNBRACED MULTI-STORY FRAME

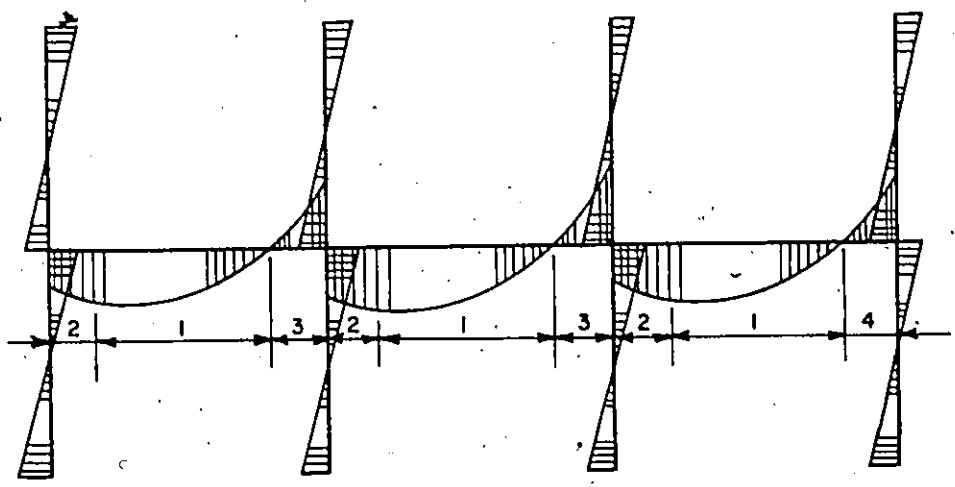


FIGURE 1.2 BENDING MOMENT REGIONS IN THE BEAMS OF MULTI-STORY UNBRACED FRAMES UNDER COMBINED LOADING

the exterior column.

Regions 1 and 3 do not differ appreciably from similar regions of continuous composite beams subjected only to gravity loads. Very little information is available on the behaviour of the composite beams in regions 2 and 4.

Virtually no information is available on which to base the design of composite beam-to-column connections in unbraced frames. In current practice the continuous floor slab at the beam-to-column joint is ignored in the design and the connection is detailed on the basis of the connected steel elements. This practice is always uneconomical and may lead to unsafe column design.

Although tangible benefits in the stiffness and strength of the frame may result by considering the composite action in the design⁽⁴⁰⁾, this system remained non-feasible due to the lack of design information. The required design parameters for the design of this system are⁽⁷²⁾:

- The negative and positive moment strength of the composite beams at the connection with the column.
- The equivalent effective slab width to be used to compute the composite beam moment of inertia in the various moment regions.
- The required capacity of shear studs in the positive and negative moment regions.
- The rotation capacity of the composite beam-to-column connection.

1.2 Purpose and Scope

The primary objective of this investigation is to contribute to the knowledge of the behaviour of composite beams with ribbed metal deck in multi-story frames subjected to combined gravity and lateral loads. In a more restrictive sense the major area of investigation is concerned with the study of:

- a) The effective slab widths for strength and stiffness to be used in the design of the composite beams with ribbed metal deck in the positive and negative moment regions.
- b) The ultimate strength of the composite steel-concrete on ribbed metal deck at the connections in the positive and negative bending moment regions of unbraced frames subjected to combined gravity and lateral loads.
- c) The moment-rotation characteristics of the composite connection to study the possible extension of the existing plastic design method for steel unbraced frames to accommodate the composite structure.

The investigation described in this thesis consists of analytical and experimental components. The main objectives of the analytical investigation was to develop an analytical model to predict the behaviour of the composite beam in a multi-story frame in the positive moment regions. Of particular interest in this analytical study were the effective slab width, the strength and stiffness of the composite beam. The experimental program was designed to provide the required information about the composite beams in the positive moment region and

the experimental results were compared with those predicted by the analytical model to examine the validity of the model.

After examining the validity of the analytical model in the positive moment region it was extended to predict the behaviour of the composite beam in the negative moment regions.

The behaviour of the steel columns in the unbraced frame was beyond this investigation.

The analytical model was also used to study the effective slab width of simply supported composite beams to examine the validity of the current formulae in the different codes.

1.3 Outline of the Thesis

To help the reader to follow the organization of the contents of the thesis, the outline of the thesis is presented in this section.

Chapter 2 contains a literature review of the work pertinent to the study of composite beam-to-column connections. Chapter 3 contains the mathematical formulation of the analytical model and all the assumptions used in the analysis. The development of the computer program used in the analysis is also included in this chapter. The analytical results and a parametric study of the factors affecting the behaviour of the composite beams in the unbraced frames is discussed in Chapter 4. At the end of this chapter a study of the current formulae for the effective slab width in the different codes is presented. Chapter 5 contains the description of the experimental program and the details of the test specimens. The experimental results and the

evaluation of these results are discussed in Chapter 6 and a comparison between the analytical and experimental results for all the test beams is presented in Chapter 7. Finally in Chapter 8 a brief summary of the thesis contents and results and final conclusions are presented.

CHAPTER 2

LITERATURE REVIEW

2.1. Introduction

A considerable amount of research has been devoted to the field of composite concrete-steel structures in recent years. Topics such as limit analysis, ultimate strength, fatigue behaviour, shear connection distribution and effective slab width for simple and continuous beams have been studied in some depth. However, very little attention has been devoted to composite beam-to-column and beam-to-girder connections. Most of the investigations of the strength and behaviour of beam-to-column connections have accompanied studies and experimental investigations of the negative moment regions of continuous composite beams. This chapter will be devoted to the review of the pertinent literature dealing with the particular aspects related to the study of composite beam-to-column connections.

For the sake of convenience, the literature review is organized into three major groupings each dealing with information related to specific aspect of this investigation. These are:

- a: Effective slab width
- b: Behaviour of simple and continuous composite beams
- c: Behaviour of composite beam-to-column connections.

2.2 Effective Slab Width

Most of the studies of the effective slab width related to the study of simple span beams. Very limited studies have been devoted to the effective slab width in the negative moment regions of continuous beams.

Mackey and Wong⁽⁶⁾ presented the results of the effective slab width of simple span composite T-beams which had been determined from laboratory tests carried out on four small scale composite beam and slab floors and from theoretical analysis. Each of the test specimens consisted of a continuous solid 2 inch thick concrete slab over four simply supported steel I-beams. The slab was effectively anchored to the steel beams by means of continuous double spiral shear connectors welded to the top flange of the beams. Each specimen was loaded by four point loads applied at the mid-span of each steel beam. The only variable in these tests was the spacing between the steel beams (b) and hence the beam span to beam spacing (L/b) ratio.

The effective slab width was evaluated experimentally by measuring the longitudinal strains at the top surface of the slab across its width. Since the specimens were loaded only in the elastic range, the concrete stresses were considered to be proportional to the concrete strains. The effective slab width at any section of the composite beam was defined as the area of the top surface concrete stress across the slab width divided by the maximum top surface concrete stress over the steel beam at that particular section.

In the theoretical analysis, Airy stress function was assumed to

represent the stress distribution in the slab. It was also assumed that the stresses due to the applied moment on the slab are constant across its width.

This experimental and theoretical investigation showed that the values of effective width increase with the increase in the beam span to beam spacing ratio. It was also concluded that the experimental effective widths vary along the span of the beam but in an opposite sense to that obtained by analysis.

Although the same definition for the effective width was used in the experimental and theoretical studies, the assumption of constant stress due to the applied moment across the slab width resulted in an effective width that represents the effect of the in-plane stresses only. This explains the discrepancy between the theoretical and experimental results.

Savern^(5,8,9) analyzed simple span T-beams consisting of solid concrete slab and rectangular concrete beam. He assumed full interaction between the slab and the beam and considered only the elastic conditions in his study. The transverse deflection (w) of the T-beam and the plane stress function (f) representing the stresses in the slab were expressed in series form. The boundary conditions at the slab-beam junction were found from the equilibrium conditions between the internal forces acting on the slab and the beam and from the compatibility of deformation between both elements at the junction position. The longitudinal stresses at the upper surface of the slab were expressed as the summation of the stresses due to in-plane and

bending effects.

The same definition for the effective slab width used by Macky and Wong⁽⁶⁾ was used in this study. The effective slab width was calculated for various geometric properties and for three loading conditions, namely; uniformly distributed load over the slab and the beam, uniformly distributed load over the beam only and single point load applied at mid-span of the beam.

This theoretical study of the effective slab width showed that the effective width when the T-beam was subjected to a single point load at mid-span was less than that which occurred when the T-beam was subjected to uniformly distributed load. It was also concluded that the effective slab width varies along the span of the beam and that it increases with the increase in the beam span to beam spacing ratio.

VanDalen⁽¹⁷⁾ tested 17 composite specimens simulating the portion of a continuous composite beam between the points of contraflexure and subjected to negative moment. The slab in these tests was solid concrete and reinforced with top longitudinal and transverse reinforcement. These tests showed that the longitudinal tensile strain at the level of the slab reinforcement was variable across the slab width. VanDalen suggested an equation in the form $\epsilon = \epsilon_0(1-y/9t)$ to represent this variation in the steel reinforcement strain; where in this equation (ϵ) is the longitudinal strain at distance (y) from the steel beam centre line, (ϵ_0) is the longitudinal strain over the steel beam centre line and (t) is the slab thickness. These results together with the stress-strain relationship for the reinforcing steel enables

the effective slab width, in the case of negative moment, to be determined.

Although all the previous work in the effective width field showed that the variation in the longitudinal strains and hence the effective slab width depends on the side ratio (L/b), the equation suggested by VanDalen did not include this parameter in determining the variation in the longitudinal strains across the slab width.

A rational basis for the determination of effective width taking the parameters relevant to the geometry and material properties of the section into account was reported by Adekola⁽¹⁸⁾. He presented the solution for the case of a continuous solid concrete slab spanning identical simply supported steel I-beams. An Airy's stress function and transverse deflection function were assumed in a series form to represent the plane-stress in the slab and the deflection of both the slab and the steel beam. By applying the equilibrium conditions and compatibility of strains between the slab and the steel beam, an expression for the longitudinal stresses in the middle surface of the slab was obtained.

The effective width was defined in this study as the width of slab that would sustain a force equal to the force in the slab, assuming the longitudinal stress is constant across the slab width at the peak stress in the slab at the centre line plane of the web of the steel beam. This expression is given mathematically by

$$b_e = \frac{2 \int_0^{b/2} \sigma_x dy}{[\sigma_x]_{y=0}}$$

where in this expression (b_e) is the effective slab width, (σ_x) is the longitudinal stress at the middle surface of the slab, $[\sigma_x]_{y=0}$ is the peak longitudinal stress over the steel beam and (b) represents the steel beam spacing.

Since in this analysis the determination of the longitudinal stresses at the middle slab surface required the knowledge of the position of the neutral axis of the composite section which in turn required the knowledge of the effective slab width, an iterative method was used by assuming a certain position for the neutral axis and calculating the effective slab width which was used to define the corresponding position of the neutral axis. The assumed and calculated positions of the neutral axis were compared and the effective width when they have nearly the same position was taken as the true effective slab width.

Curves and tables showing the variation of the effective slab width along the beam span for different values of beam span to beam spacing (L/b) ratio were presented for the case of simply supported composite beams loaded with central point loads together with a uniform loading representing the self weight of the beam.

This study showed that the effective slab width varied along the span with the minimum width occurring at the point of maximum moment for the loading case considered. It was also concluded that the variation

in the effective width along the span decreases with the increase in side ratio (L/b) so that for side ratios of five or more, the variation is slight and the effective slab width may be assumed to be constant over the span. It was also found that the ratio of effective to total slab width (b_e/b) increases with the increase in the side ratio and that the variation in the slab thickness to steel beam depth ratio has small effect on the effective slab width, especially for large side ratios.

Since in this analytical study complete interaction between the slab and the beam was assumed and only elastic conditions were considered, the presented results and conclusions are limited to these conditions.

An experimental investigation on the behaviour of simple and continuous composite T-beams subjected to positive and negative moment was conducted by Tachibana⁽³³⁾. Effective slab width in both positive and negative moment regions was one of the main interests in this investigation. In this experimental study four sets of composite T-beam specimens were tested. The main variables in this investigation were the steel reinforcement percentage in the slab, steel reinforcement diameter, pitch of shear connectors and slab width. Simple beams to be subjected to positive moment were loaded with downward two-point load, while simple beams to be subjected to negative moment were inverted and loaded in the same manner. In some tests the beam was tested first under negative moment which caused slab cracks before testing it under positive moment to compare the behaviour of composite beams with cracked slab with those with uncracked slab.

Comparison between the experimental strain distribution in the slabs of the beams tested with virgin concrete and those tested with cracked concrete showed that when the composite beam is subjected to positive moment, the effective width of a cracked slab was the same as that of uncracked one. Also, by comparing the measured strain distribution in the steel reinforcement of the slab when the composite beam was subjected to negative moment with the strain distribution in the slab under positive moment, it was concluded that the effective slab width under negative moment is nearly equal to that under positive moment.

Adekola⁽⁵⁵⁾ studied theoretically the effective slab width for simply supported composite beams with partial interaction. In this study the constitutive equations which relate partial interaction with shear lag were formulated and solved by series solutions for deflection and in-plane stress in the slab to satisfy all the known boundary conditions.

He concluded from this study that the traditionally defined effective slab width on the basis of the longitudinal stress distribution across the slab width⁽¹⁸⁾ is dependent on the degree of interaction and that this effective slab width slightly decreases with increase of the degree of interaction. Such a phenomenon would be inconsistent with the physical expectation. To avoid this inconsistency, he introduced a definition for the effective slab width based on the deflection of the beam. According to this definition, the effective slab width is considered as the width of the slab to be

considered in composite action with the steel beam so that the calculated deflection using the transformed section is equal to the deflection of the actual composite beam. This new definition showed that the effective slab width increases with increase of the degree of interaction.

Effective slab width for composite beams at ultimate load was studied by Heins and Fan⁽⁷¹⁾. In this study, a continuous solid concrete slab spanning several simply supported steel I-beams was considered and full interaction between the concrete slab and the steel beam was assumed. A stress function and deformation function were assumed to describe the stresses and deformation of the slab of the composite beam. Applying the equilibrium and compatibility conditions between the steel beam and the concrete slab resulted in a set of equations which were solved numerically by using the finite difference technique.

The same definition for the effective width used by Adekola⁽¹⁸⁾ was used in this analysis. The analytical results of this study showed that the effective slab width at ultimate load was greater than the elastic effective width for all the studied cases when the girder was an interior one. However, when the edge girder was studied the effective width at ultimate load was less than that in the elastic range. No discussion on this discrepancy between the behaviour of the interior and edge girders was included in this work. The results showed also that the effective slab width to the total width ratio increases with the increase in the side ratio (L/b). The results of this analytical model

were compared with the experimental results of the same model tested by Hagood, Guthrie and Hoadley⁽²⁰⁾. This comparison showed a good correlation between the experimental and analytical results.

Most of the codes and specifications contain rules for calculating maximum slab widths for both interior and edge beams in bridges and buildings. The derivation of these rules have not been explained in any supporting documents.

The current CSA standards⁽⁶²⁾ requirement for the effective slab width for simple composite beams limits the effective width to the least of the following:

$$b_e \leq 16 t_s + b'$$

$$b_e \leq b$$

$$b_e \leq 0.25 L$$

where in these equations (b_e) is the effective slab width, (t_s) is the effective slab thickness, (b') is flange width of the steel beam, (b) is the spacing between the beams and (L) is the span of the simple beam. These limitations are similar to those used in the design of concrete T-beams.

For composite sections subjected to negative bending moment, the steel reinforcement parallel to the beam and within the design effective width of the slab may be included in computing the properties of the composite section provided that:

- a) Reinforcement is adequately anchored by embedment in concrete which is in compression
- b) Shear connectors are provided in the negative moment region to

resist shear equal to the product of the area of the effective longitudinal reinforcement and its yield stress.

In the British Standard Code of Practice^(12,14), the effective slab width for simply supported beams in buildings is limited to 0.25 the span of the beam while the effective slab width for simply supported composite beams for bridges is given by the following equations which are dependent on the beam spacing to beam span ratio (b/L)

$$b_e = \left[\frac{1}{\sqrt{1 + 12(b/L)^2}} \right] b \quad \text{for } L/b < 10$$

$$b_e = b \quad \text{for } L/b > 10$$

The Architectural Institute of Japan Standards⁽⁶⁵⁾ defines the effective slab width for T-shaped beams with rectangular beam cross section as a function of the beam span to beam spacing ratio. According to this standard the effective slab width on each side of simply supported beams is defined as follows

$$b_e = (0.5 - 0.3 a/L) a \quad \text{for } L/a > 1$$

$$b_e = 0.2 L \quad \text{for } L/a \leq 1$$

where in these equations (a) is the distance between the side faces of the beams and (L) is the span of the simply supported beam. The AIJ standard states that the effective width of slab for the design of composite beams of concrete slab and steel I-beam may be computed using the same formula for the T-beams of concrete slab and rectangular concrete beam.

2.3 Behaviour of Composite Beams

Many investigations have been conducted in the field of composite beams to determine the type, amount and distribution of shear connection required to achieve full composite action and to study the behaviour of composite beams. Most of this work has been conducted on conventional simply supported composite beams while less amount of work has been conducted to study the composite system under negative moment and to study the behaviour of continuous composite beams.

2.3.1 Behaviour of Simple Composite Beams

Newmark, Siess and Viest⁽¹⁾ developed a differential equation for incomplete interaction for a beam consisting of two interacting elements in the elastic range. They also reported test results of six simply supported composite steel and concrete T-beams and the results of push-out tests on steel channel shear connectors. The test results were compared with those predicted by the proposed incomplete interaction theory and showed a good agreement.

Robinson⁽⁷⁾ investigated the introduction of ribbed metal decking into the composite system. He concluded that the system was effective and recommended the use of only the solid part of the slab as resisting compressive stresses in the design.

Slutter and Driscoll⁽¹³⁾ concluded, after testing thirteen simple composite beams with different types and arrangement of shear connectors, that the equation developed by Newmark et al⁽¹⁾ is sufficiently good for predicting strains and deflections within the

elastic range but cannot be used to determine the number of connectors required on a beam. They also concluded that the spacing between the connectors did not affect the ultimate capacity provided that there was an adequate number of connectors.

They proposed a method of determining the ultimate bending capacity of the composite beams and obtained good correlation with the experimental results. They also concluded that if sufficient number of connectors were provided, the theoretical ultimate moment could be attained even with presence of appreciable slip.

To investigate the influence of the ribs geometry on the load-deflection relationship for composite beams with ribbed metal deck, Robinson⁽¹⁵⁾ performed tests on 15 simple composite beams with ribbed metal deck and 39 push-out tests. He concluded that the rib height to width ratio was an important parameter. With rib height to width ratio equal to one, rib cracking closely followed the local yielding of the beams while with the ratio greater than one, cracking of the ribs occurred in the elastic range. If the ratio is less than one, a load in excess of first yield load can be achieved.

Yam and Chapman⁽²²⁾ presented a numerical method for the analysis of simply supported composite beams which takes account of inelasticity of the steel, concrete and shear connectors. It was assumed in this analysis that the shear connection between the slab and the steel beam acts as a continuous medium along the length of the beam. The analysis was used to explore the effects of cross sectional properties, span, connector distribution, connector strength and stiffness, type of

loading and strain hardening on the beam-slab interaction and on the ultimate load behaviour of composite beams. Analytical results were compared with experimental results and showed to be in good agreement which implies that the assumptions made in the analysis are justified.

Robinson⁽²⁶⁾ presented an elastic analysis for composite beams incorporating cellular metal deck based on the incomplete interaction theory proposed by Newmark et al⁽¹⁾ for beams with solid concrete slab. He also described the computation of the ultimate moment capacity for composite beams with formed metal deck using the stress block method. An experimental test program was also conducted and the analytical method was verified by comparing the analytical and test results.

Thiruvengadam⁽²⁷⁾ presented a numerical method for the analysis of simply supported composite beams which can be used for both the elastic and inelastic analysis using the finite difference technique. In this analysis the shear connection between the slab and the beam was assumed to be provided by shear connectors placed at discrete points along the span of the beam. The load-slip relationship for the connectors was assumed to consist of a series of straight lines as an approximation to a smooth load-slip curve.

Fisher⁽³⁰⁾ analyzed the results of earlier tests and published tentative design recommendations for composite beams with formed metal deck 3 inches or less in depth. He suggested a design relationship for a connector installed in a deck rib that modifies the design value of a connector in a solid slab to reflect the influence of the rib geometry.

Robinson and Wallace⁽⁵⁴⁾ tested 9 simple span composite beams

with ribbed metal deck with various types and arrangement of shear connectors. The theoretical ultimate capacity was compared with the experimental capacity and showed good agreement.

Ma⁽⁵³⁾ modified the technique developed by Thiruvengadam⁽²⁷⁾ to overcome the numerical difficulties which arises in Thiruvengadam's method. A smooth hyperbolic curve was assumed to represent the load-slip characteristic of the connectors. The developed method can be used for the analysis of symmetrically loaded simple span composite beams both in the elastic and inelastic regions. He verified the use of the method by comparing the analytical results with the experimental results reported by Robinson and Wallace⁽⁵⁴⁾.

2.3.2 Behaviour of Continuous Composite Beams

Closely related to the study of composite beam-to-column connections is the study of continuous composite beams. Most of the investigations of the negative moment regions have been conducted on continuous composite beams in which the interior support was more or less central to the negative moment region. This situation commonly arises in bridges and building frames subjected to gravity loads.

Barnard and Johnson⁽¹⁰⁾ reported tests on four three-span continuous composite T-beams with stud shear connectors spaced uniformly between sections of maximum hogging and sagging moments. Top longitudinal slab reinforcement was provided over the internal supports in each specimen.

The test results showed that when flexible shear connectors are

used, some slip occurs before maximum load is reached. This slip increases deflections but does not appear to have any effect on the behaviour of critical sections of the beam. Therefore the ultimate strength theory for composite beams may be used to predict the magnitude of maximum moment of resistance for cross sections in which the concrete slab is in compression. Furthermore, the fully plastic moment of the steel alone based on the minimum yield stress of the beam and reinforcement steel is a safe estimate of the moment of resistance for cross sections in which the concrete slab is in tension.

It was concluded from this investigation that if secondary failures such as buckling of the steel beam and longitudinal splitting of the slab are avoided, it would be possible to design the continuous composite beam using the conventional plastic design method.

VanDalen⁽¹⁷⁾ concluded experimentally, after testing 17 composite specimens simulating the portion of a continuous composite beam between the points of contraflexure and subjected to negative moment, that when adequate shear connection and transverse reinforcement are provided the resistance to bending in a hogging moment region with longitudinal slab reinforcement continues to increase with the increase in the curvature until buckling occurs in the steel beam even though the slab may be cracked in tension throughout its depth. He also concluded that calculating the moment of resistance in a hogging moment region of a continuous composite beam on the basis of the yield stress of the steel beam and slab reinforcement is conservative for composite beams with compact beams.

The behaviour of stud shear connectors in hogging moment regions was explored by Johnson, Greenwood and VanDalen⁽²⁴⁾. They presented results of push-out tests on 5/16 in. diameter studs set in reinforced concrete slabs in tension. Based on this experimental study they recommended that:

- a) Welded stud shear connectors can be used to transmit shear from longitudinal reinforcement to the steel beam in a hogging moment region of composite beams. Where the neutral axis at the hogging moment section is in the steel beam, as is usual, the total shear to be transmitted may be taken as the product of the area of the effective longitudinal reinforcement and its yield stress.
- b) The design load per stud (Q_u) in the hogging moment region should be taken as 64% of the ultimate capacity as found in a standard push-out test.
- c) Ideally, studs should project into the slab to the level of the upper surface of the longitudinal reinforcement.

A review of the research on composite beams from the year 1960 to the year 1970 was reported by Johnson⁽³¹⁾. He concluded at the end of this review that sufficient research has been completed to enable an ultimate strength design method for continuous composite floor structures for buildings to be codified for composite construction in mild steel and normal-density concrete.

Gracia and Daniels⁽³⁵⁾ suggested a theoretical procedure for

analyzing continuous composite steel-concrete beams in which shear connectors were omitted in a certain region over the internal supports which is designated as the free slab region. The theory showed good correlation with the results of an experimental study consisting of tests on two full size continuous composite beams and six full size simple span composite beams which were subjected to negative bending moment.

The elastic-plastic behaviour of two-span continuous composite T-beams was studied by Yam and Chapman⁽⁴⁷⁾. They presented a numerical solution for the system assuming that the shear connection between the slab and the beam acts as a continuous medium along the beam length. The predictor-corrector method of integration was used to solve the two simultaneous non-linear ordinary differential equations of the first order representing the governing equations of equilibrium and compatibility. The analytical results were compared with the experimental results report earlier by Teraszkiewicz⁽¹⁶⁾. It was concluded that for the symmetrical two-span continuous beams considered, with symmetrical point loads at mid-span or uniformly distributed loads, the simple plastic method can be used to calculate the collapse loads since the second hinge will form before the first one deteriorates. In this analysis both the steel beam and the longitudinal slab reinforcement were considered to resist the negative moment.

Hamada and Longworth⁽⁷⁰⁾ investigated analytically and experimentally the ultimate load and failure modes of continuous composite beams. An iterative finite difference method was employed in

the analysis. They presented a behavioural studies for a number of composite beams in which the steel section, concrete slab thickness and amount of longitudinal slab reinforcement were varied.

Based on this study they concluded that failure modes are significantly affected by the amount of longitudinal slab reinforcement in the negative moment region. They also concluded that a maximum compression flange width to thickness ratio should be limited to prevent local buckling and that this limit depends on the amount of longitudinal slab reinforcement. They suggested that this ratio not exceed $54/\sqrt{\sigma_y}$ when the effective area of longitudinal slab reinforcement is less than the web area of the steel beam. If the area of longitudinal slab reinforcement exceeds the web area but is less than twice the web area, this ratio should not exceed $49/\sqrt{\sigma_y}$.

2.4 Composite Beam-to-Column Connection

Compared to the research effort on composite beams, the attention given to composite beam-to-column connections has been nearly nonexistent. Although composite beams are frequently a part of a framed structure, the designer usually ignores the effect of composite action on the frame design.

Some work has been done by Barnard⁽²³⁾, Johnson and Hope-Gill⁽⁴³⁾ and Naka and Wakabayashi⁽³⁹⁾ to study the effect of composite action on the behaviour of braced frames. However, very limited research has been conducted to investigate the effect of composite action on the behaviour of unbraced frames.

Daniels, Kroll and Fisher⁽²⁹⁾ reported the first experimental study of the behaviour of composite beam-to-column connections in unbraced frames. Two test set-ups were used. They were designed to simulate the portion of an actual unbraced frame in the vicinity of the windward and leeward columns as well as in the vicinity of an interior column.

Based on the results of this study it was concluded that the ultimate strength of the cross section of a composite beam adjacent to the column face and subjected to positive bending moment can be conservatively based on the strength of the steel beam plus a portion of the concrete slab which has a width equal to that in contact with the column. Concrete maximum stress of $0.85 f'_c$ is to be used together with the yield stress of the steel beam when estimating the ultimate strength of the cross section using the stress block method. It was also concluded that the ultimate strength of the cross section of a composite beam adjacent to the column and subjected to negative bending moment is in excess of the strength of the steel beam alone and may be conservatively based on:

- a) The strength of the steel beam alone if the column is an exterior leeward column.
- b) The strength of the steel beam plus the continuous longitudinal slab reinforcement in the full slab width if the column is an interior one.

Test results showed that sufficient rotation capacity of the composite beam exists in the vicinity of the joint to enable the plastic

design theory to be used.

It was recommended, at the end of this investigation, that additional theoretical and experimental studies be performed to explore the possible range of the ultimate strength in the vicinity of the column when the composite beam is subjected to positive or negative moment and to study the effect of an initial gap between the column face and the concrete slab on the behaviour of the composite beam-to-column connections.

DuPlessis and Daniels⁽⁴¹⁾ studied experimentally and theoretically the behaviour of composite steel-concrete T-beams which are subjected to concentrated positive end moment, a condition that occurs at the beam-column connection in an unbraced frame subjected to combined lateral and gravity loads. They tested four composite beams fully welded to an end plate which was bolted to a column test fixture to form a cantilever beam. The experimental model was subjected to upward end point load to simulate the portion of the beam in the unbraced frame which is subjected to positive moment. In this study the effect of slab width and slab thickness on the ultimate strength and stiffness of the composite beam was of particular importance. The span to width ratio (L/b) was kept constant in all the tests.

A theoretical investigation using the principles of the theory of plasticity was performed to obtain upper and lower bounds to the ultimate strength of the test beams. For the upper bound, a failure mechanism was assumed for which the limit load was obtained from equating the rate of external work to the total rate of internal

dissipation of energy. The mechanism was chosen to closely simulate the observed failure mechanism. For the lower bound, a stress field which is internally in equilibrium and satisfies a yield criterion was assumed. It was assumed that plane strain conditions exist in the concrete slab at the end plate. The bearing capacity of the concrete immediately in front of the column was estimated according to the slip-line theory and the equivalent truss method. Based on the slip-line theory and considering Tresca yield criterion, the bearing capacity at the end plate was estimated to be $2.57 f'_c$ while the bearing capacity based on the equivalent truss method was $1.5 f'_c$. Both values were used to estimate a lower bound solution using the rectangular stress block method with a concrete slab width equal to the column face width. The following conclusions were drawn from this study.

- a) The ultimate strength of the test beams are independent of slab width and it depends mainly on the column face width, slab thickness, concrete strength and yield strength of the steel beam.
- b) A lower bound for the maximum end moment achieved in the beams can be obtained by using a rectangular stress block of width equal to the column face width and a concrete stress of $2.57 f'_c$.
- c) The initial stiffness of the test beams can be approximated on the basis of a prismatic beam consisting of the steel beam and the full slab width.

Daniels⁽³⁹⁾ studied analytically the effect of composite beams on frame behaviour. In this study a second order elastic-plastic analysis

technique, which was developed at Lehigh University to study the behaviour of multi-story steel frames, was used. Since at the time of this study specific information concerning the composite beams in the frame structures was not available, some approximations were made. A typical 10 equal story apartment building frame was analysed. The frame was first analysed assuming no composite action to exist then it was analysed with larger steel beams having a flexural stiffness equal to that of the transformed composite section while keeping the flexural strength equal to the plastic moment capacity of the original steel beam alone. Finally the frame was analysed assuming the flexural stiffness of the beams to be 80% of the transformed beam stiffness to allow for the cracked concrete slab and the strength was increased by 50% to account for the capacity of typical slab reinforcement at the negative plastic hinge. The relation between the frame drift and the applied wind load was plotted in each case.

A comparison between the obtained three load-drift relationships indicated that consideration of continuous composite beam action resulted in a substantial reduction in the frame drift at all load levels and increased the frame strength.

Based on the results of previous research⁽⁴¹⁾, DuPlessis and Daniels⁽⁴⁸⁾ investigated the effect of other test variables on the behaviour of composite beam-to-column connections subjected to positive moment. In this study the effect of initial shrinkage gap, shear connector spacing near the column face, concrete strength, steel beam depth, concrete slab type and the existence of lateral beams framing

into the column was investigated. Of particular importance was the effect of these variables on the maximum strength, initial stiffness and ductility of the connections.

The study consisted of experimental and theoretical components. Sixteen composite beam-to-column connections were tested. The test set-up and loading were similar to those discussed by the same authors in reference (41). A theoretical study was carried out to find upper and lower bounds for the strength of the connection. The upper bound solution was identical to that presented in reference (41). However, when discussing the lower bound solution the concrete slab was considered in a state of plane stress and not in a state of plane strain as they suggested before. Since the slab is under a state of biaxial compression, a value of $1.3 f'_c$ was considered suitable value for the strength of the concrete near the column face. Thus, the lower bound solution was obtained by using the stress block method in which the stresses in the slab were considered as a rectangular stress block of width equal to the column face width and a concrete stress of $1.3 f'_c$.

This investigation resulted in the following conclusions:

- a) The maximum strength of composite beam-to-column connections using solid slab construction may exceed the maximum strength of the bare steel connection by 64 to 87%. In the case of formed metal deck slab construction, the strength of the composite connection may exceed that of the bare steel connection by 54 to 61%.
- b) A shrinkage gap between the column face and the concrete slab

causes a significant decrease in the initial stiffness of the connection but has no effect on the maximum strength.

- c) A good lower bound for the maximum strength of a composite beam-to-column connection can be obtained by using a concrete stress of $1.3 f'_c$ over a width equal to the column face width.

It was also concluded that increasing the steel beam size or the slab thickness increases the maximum strength of the connection and that the existence of lateral beams framing into the column increases the maximum strength and initial stiffness of the connection. The test results showed that composite beam-to-column connections possess adequate rotation capacity to enable plastic design to be applied to unbraced frames with composite steel-concrete floor system.

The use of concrete strength of $1.3 f'_c$ as suggested in this work is questionable since it applies only to the state of biaxial compression when the ratio of minor to major stresses is about $0.4^{(25)}$, a case which is not likely to occur in the whole region of the column face. Although a concrete strength of $1.3 f'_c$ and concrete slab width equal to the column face provided a good lower bound in this study, the use of the same conditions will provide a poor estimate of the strength of the test beams reported by the same authors in a previous investigation⁽⁴¹⁾.

The finite element technique was applied by Ansourian⁽⁶⁴⁾ to study the full composite action between concrete slabs and steel beams and to the study of beam-to-column connections in the elastic range. The composite floor system analysed in this investigation consisted of a

continuous solid concrete slab rigidly connected to the top flange of series of parallel steel joists of I-sections which themselves spanned between rigid columns. The slab was assumed to be homogenous throughout and no account was made in the analysis for the cracking of the concrete or for the slab reinforcement.

Refined thin plate elements were used to represent the membrane and flexural action in the slab and line elements of a space frame were used to represent the steel joist. In the assembly of the composite system, the slab represented by the thin plate elements at the mid-surface was attached to the beam by vertical links which make the displacements along the beam axis dependent on the displacement of the slab nodes located vertically above.

The principal variables in this investigation were the flexural stiffness ratio of the joist and the slab and the loading type. Two types of loadings on the floor system were considered, a uniform load over the whole slab and a uniform line load along the axis of each beam. The total load on the floor was the same in both cases.

This study showed that the flexural stiffness ratio of the beam and the slab is an important parameter in determining the axial load and bending moment distribution in the steel beam and the slab. It showed also that there was a little difference in the distribution of membrane stresses when the applied load was either uniform over the whole slab or concentrated along the joist axes.

The effective slab width was estimated, using the same definition used by Adekola⁽¹⁸⁾, from the calculated membrane stress distribution

as it varied along the span, with the minimum effective width occurring at the column face. Only one side ratio (L/b) equal to 1.6 was considered in this analysis.

Ansourian and Roderick⁽⁶⁹⁾ presented an experimental investigation of the composite beam-to-column connections. In this investigation 10 specimens representing beam-to-column connections in which the composite beams were subjected to negative moment were tested. Each specimen consisted of a cantilever composite steel and solid concrete slab fixed to a concrete encased steel column and subjected to downward end point load. Particular attention was given in this investigation to the slab reinforcement to determine the conditions under which it contributes to the composite action of the system.

Strain measurements at a section located 8 inches from the column face showed that the strain in the compression flange at 95% of the collapse load was 6 times the yield strain indicating substantial rotation capacity. The strains in the top layer of the longitudinal slab reinforcement was markedly nonuniform across the width of the slab; at 2 1/2% of the collapse load the strain in the inner bars was 4 times that of the outer bar and this ratio decreased to 1.7 at 90% of the collapse load indicating more uniform strain distribution. The measured strains across the slab width before cracking were compared with those calculated using the finite element analysis⁽⁶⁴⁾ and showed very good agreement as the error was only 4% in the peak strain.

It was concluded from this study that effective composite action in the beam of a connection to an exterior column exists if the

longitudinal slab reinforcement is well anchored at the end of the slab. This may be achieved either by welding a rod to the steel bars outside the slab or by arranging the bars to have sufficient development length at the end of the slab.

2.5 Summary

In this chapter, the literature review was organized into three major groups each dealing with information related to a specific aspect of the current investigation. These were:

- a) Effective slab width.
- b) Behaviour of simple and continuous composite beams.
- c) Behaviour of composite beam-to-column connections.

Other literature which is relevant to the use of finite elements in the reinforced concrete plate analysis was not reviewed in this chapter but is referenced at the pertinent section.

CHAPTER 3
ANALYTICAL METHOD

3.1 Introduction

As mentioned in Chapter 1, the distribution of bending moments along the beams of an unbraced frame determines four regions that have to be considered in the case of an unbraced frame with composite beams. These four regions may be grouped into two major groups according to the sign of the applied bending moment. Group A where the beams are subjected to positive bending moments, slab in compression, and the concrete slabs are considered in resisting the compressive force due to interaction between the steel beams and the concrete slabs. This group contains regions 1 and 2 in Figure 1.2. Group B contains regions 3 and 4 in which the beams are subjected to negative bending moments, slab in tension, and the slabs are considered in resisting the tensile force due to the interaction. Since the concrete has a limited tensile strength after which cracking occurs, cracking of the concrete slabs is more likely to occur in group B even under small applied load due to the tensile force resulting from the interaction between the steel beams and the concrete slabs.

This chapter contains the description of the analytical method and the computer program developed by the author to analyse the behaviour of composite beams in an unbraced frame, subjected to positive and negative bending moments. Of particular interest in this analytical

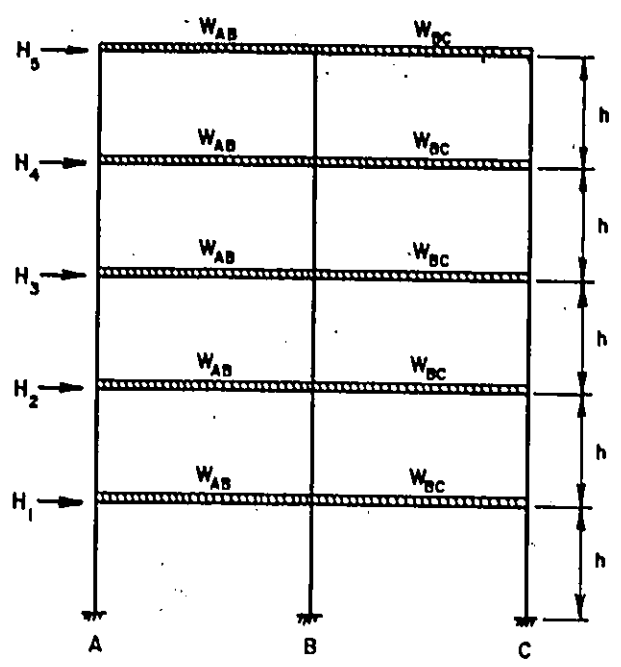
study were the effective slab width at the different moment regions and the strength and stiffness of the composite beams. The analytical models developed in this chapter are based on rational modeling of concrete, steel and their interactive behaviour and takes into account the flexibility of the connectors connecting the steel beams and the concrete slabs, cracking of concrete, slab reinforcement and the inelastic behaviour of the materials.

The analytical results and their evaluation and the comparison between the analytical and experimental results are discussed in the following chapters.

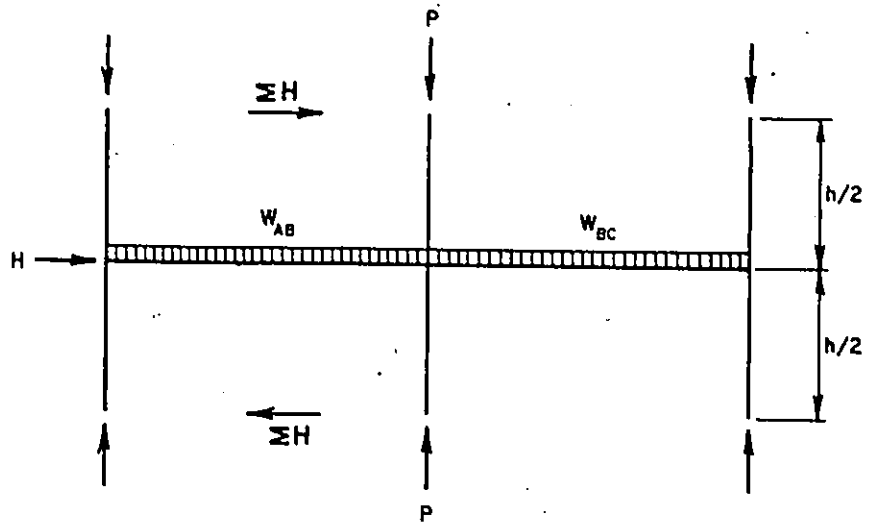
3.2 Analytical Model

Figure 3.1 shows an unbraced frame subjected to combined gravity and lateral loads and a one storey assemblage consisting of the composite beams and steel columns. The assemblage is subjected to column forces P and shear EH resulting from the lateral loads. Because of the story shears resulting from the gravity and lateral loads the columns will apply positive and negative end moments to the composite beams. Thus, the resulting bending moment in the one story assemblage is as that shown in Figure 1.2. As mentioned in Chapter 1, the behaviour of the steel columns is beyond this investigation, thus; only the continuous composite beams of the one story assemblage is considered in the analytical model.

Analytical modeling of simple and continuous composite beams has been discussed in the literature by many authors, Chapter 2, using



a) UNBRACED FRAME SUBJECTED TO COMBINED LOADS



b) ONE-STORY ASSEMBLAGE

FIGURE 3.1 UNBRACED FRAME AND ONE-STORY ASSEMBLAGE

different techniques which are all based on the beam theory and ignoring the variation of the strain and stress distributions across the slab width. Since in the present analysis the stress distribution across the slab width is of main importance in defining the effective slab width, a more rational analytical model is required. The analytical model of a composite beam represents a three dimensional problem with the steel beam lying in a vertical plane and the slab represented by its middle surface lying in a horizontal one (Figure 3.2) and interaction is provided between the two planes by means of mechanical shear connectors. Such a problem can be modeled using any three dimensional technique such as the three dimensional finite element. However, when such a technique is used computer core storage problems arise due to the limited storage capacity of the CDC 6400 computer available at McMaster University computing centre and the computing time and cost per run will be unfeasible. To make the analysis more feasible and suitable for the CDC 6400 computer storage, the three dimensional model was discarded in favour of the model adopted in this thesis which is based on a two step solution. In the first step, the finite difference method was used to find the interaction forces and deformations of the composite beam assuming the stresses are constant across an assumed effective slab width. In the second step, the interaction forces and the deformations were applied to the slab to find the actual stress distributions across the slab width and depth from which the equivalent effective slab width was calculated. The finite element method was used in the second step. The two steps were then repeated until the assumed and calculated

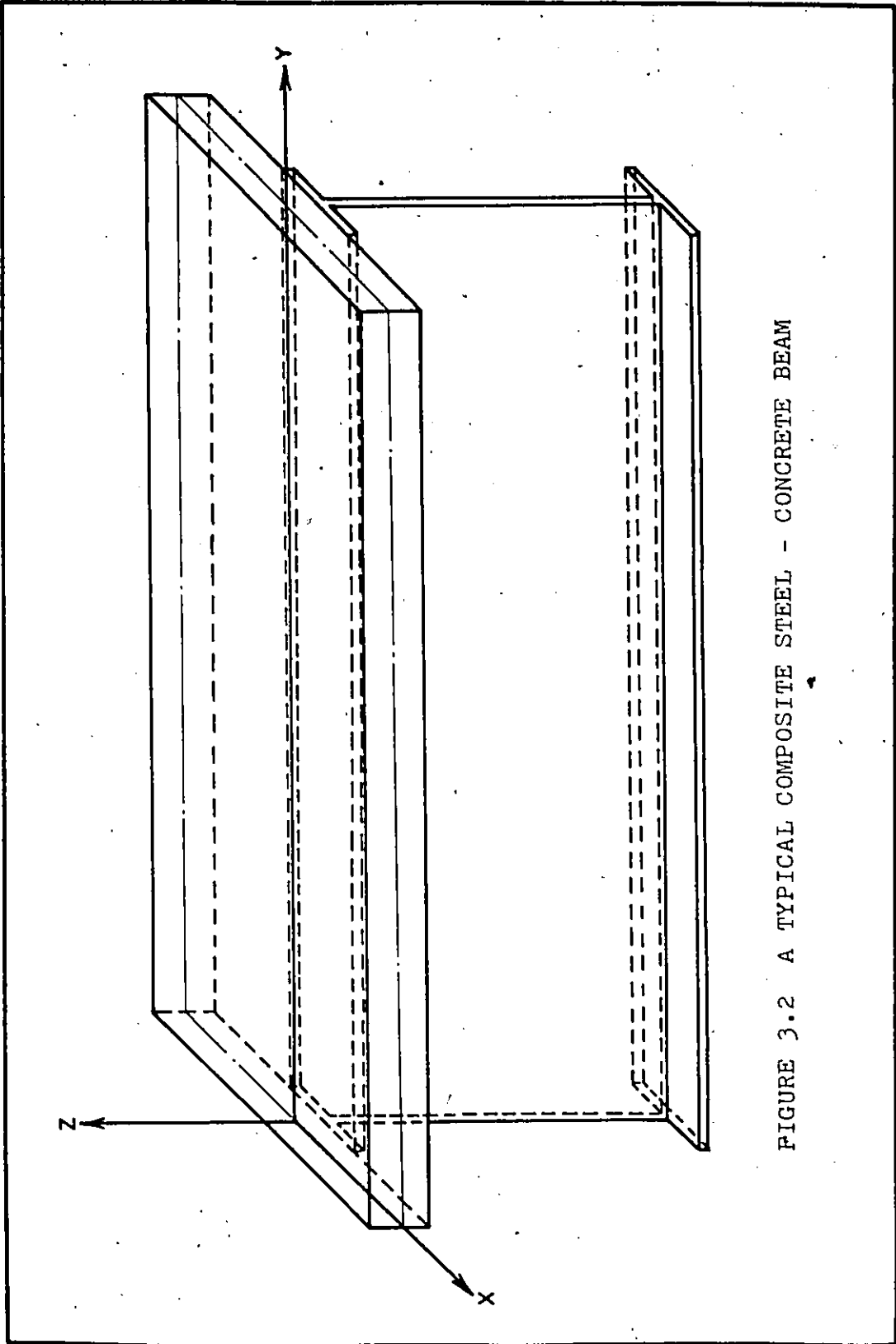


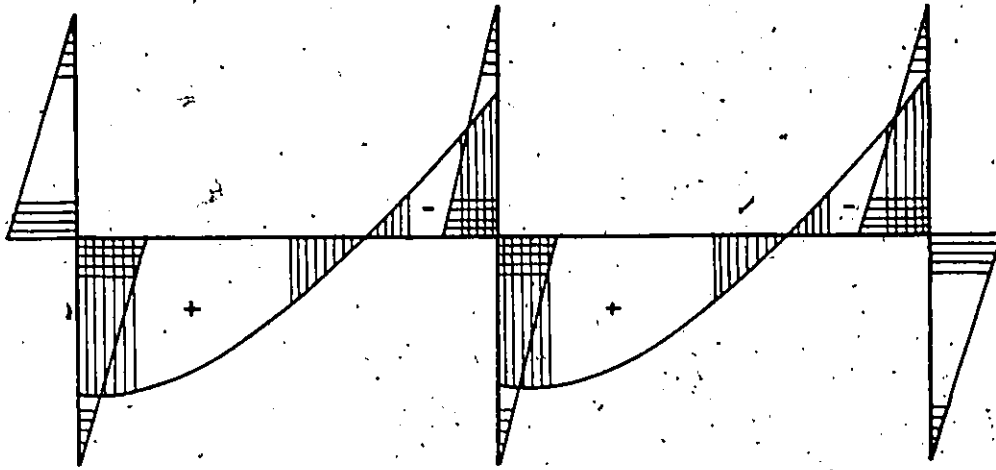
FIGURE 3.2 A TYPICAL COMPOSITE STEEL - CONCRETE BEAM

effective widths are close to each other within a certain prescribed accuracy. In order to allow for the variation in the properties of the concrete slab across its depth due to cracking and due to the existence of the slab reinforcing steel, a two dimensional layered finite element technique was used in the second step. The mathematical formulation and the details of the computation of each step are explained in the subsequent sections.

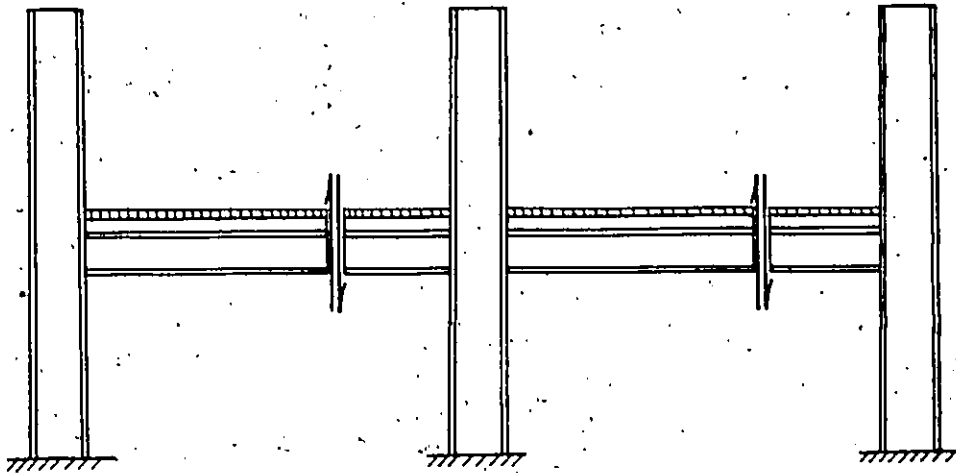
Although the adopted model can accommodate the continuous composite beam as one unit containing positive and negative bending moment regions, it was found unsuitable, due to limited computer core storage, to deal with both negative and positive moment regions in the same computer run. Therefore, in the present analysis it was assumed that the composite beam can be separated in each span at the point of contraflexure and that only shearing forces exist at this position. Thus, each of the positive and negative moment regions can be treated separately. Since the behaviour of the column was beyond the current investigation, each region was modeled as a cantilever beam fixed to the column and subjected to a uniformly distributed load (W) to simulate the gravity load and a point load (P) acting at the free end to simulate the shearing force at the point of contraflexure (Figure 3.3). In the analysis the point load (P) is increased up to the failure of the beam while keeping the load (W) constant.

3.3 Idealization of Actual Material Properties

The following idealization was used in the analysis presented in



a) BENDING MOMENT IN THE ONE-STORY ASSEMBLAGE



b) ASSUMED ANALYTICAL MODEL

FIGURE 3.3 ANALYTICAL MODEL

his thesis to represent the actual material properties of the composite steel-concrete beams.

3.3.1 Steel Beam

The method of analysis described in this thesis can accommodate either a linear or a smooth stress-strain relationship for the steel beam. However, in the present analysis an elastic-plastic-strain hardening curve, Figure 3.4, is used to idealize the actual stress-strain relationship for the hot-rolled steel. The stress-strain relationship for the steel beam is assumed to be similar under tensile or compressive stresses.

3.3.2 Concrete Slab

While the properties of the steel are generally well defined, those for concrete are more difficult to define because concrete is a heterogeneous material composed of mortar and aggregate. Nevertheless, for purposes of analysis, concrete is generally considered as a homogeneous material in a macroscopic sense. Because of the complexity of analyzing the composite beam model, in this study the nonlinear material properties of the concrete will be made very simple but yet capable of capturing the dominant behaviour of the material.

The actual uniaxial stress-strain relationship for concrete in compression, Figure 3.5a, is idealized in the present analysis by the elastic perfect plastic stress-strain curve shown in Figure 3.5b.

Concrete in tension is assumed to behave elastically up to its

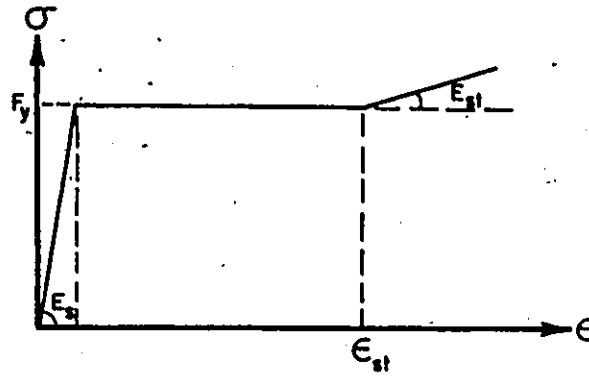
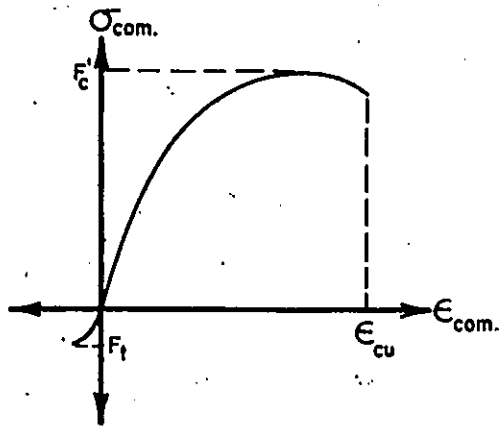
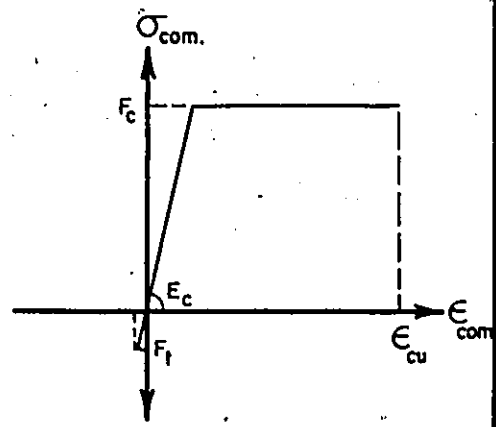


FIGURE 3.4 IDEALIZED STRESS-STRAIN CURVE FOR THE STEEL BEAM



a) ACTUAL UNIAXIAL CURVE



b) IDEALIZED CURVE

FIGURE 3.5 STRESS-STRAIN CURVE FOR CONCRETE

tensile strength. After reaching the tensile strength, concrete is considered to be cracked and its strength drops to zero (Figure 3.5b).

The concrete is assumed to be an isotropic material. Hence, the modulus of elasticity for the idealized curve is considered to be equal in all directions. Poisson's ratio for the concrete is assumed to be independent of the applied load level and is equal in all directions.

3.3.3 Steel Reinforcement

The stress-strain relationship for the slab reinforcing steel is idealized as an elastic-strain hardening with equal yield stress (f_y) and elastic modulus (E_s) in tension and compression. It is further assumed that the reinforcing steel bars carry uniaxial stresses only. Thus, the reinforcing bars are considered to have a modulus of elasticity equal to (E_s) in its longitudinal direction and equal to zero in all other direction with Poisson's ratio equal to zero in all directions. The idealized stress-strain relationship for the reinforcing steel is shown in Figure 3.6.

3.3.4 Shear Connectors

In the analysis presented in this thesis, a hyperbola of the form

$$Q = \frac{C}{\gamma + A} + B$$

was preferred to represent the load-slip characteristic for the connectors. A, B and C are three constants to be determined from the values given by three points which are to be passed by the curve. One

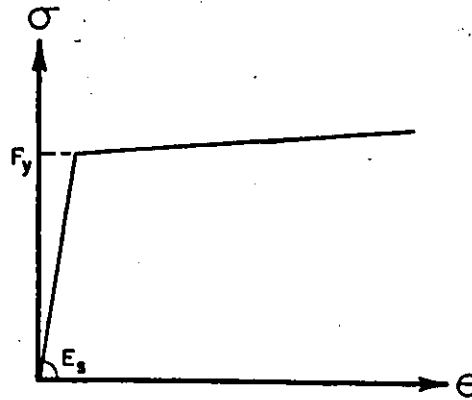


FIGURE 3.6 IDEALIZED STRESS-STRAIN CURVE
FOR THE SLAB REINFORCEMENT

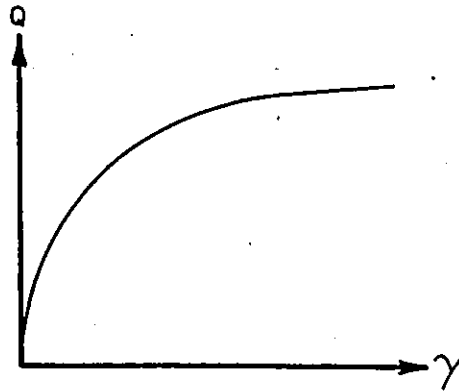


FIGURE 3.7 IDEALIZED LOAD-SLIP CURVE FOR
THE CONNECTORS

of these points is the origin (0,0) and the other two points are properly chosen to define the curve. The hyperbolic curve was found to give the best representation of the load-slip curves obtained from push-out tests by Robinson and Wallace⁽⁵⁴⁾ and shown by Ma⁽⁵³⁾ to predict very closely the performance of composite beams with cellular metal deck. Figure 3.7 shows the idealized load-slip curve for the connectors.

The ultimate shear capacity per connector was considered, in the present analysis, to be 5.4 and 11.3 kips for 1/2 in. and 3/4 in. stud shear connectors respectively. These values are given in the CSA Standards S16.1⁽⁶²⁾ and were shown by Ma⁽⁵³⁾ and Fahmy⁽⁵⁸⁾ to predict very closely the ultimate moment capacity of composite beams and composite open-web steel joists with ribbed metal deck.

The ultimate shear capacity per connector in the case of composite beams with solid slab is evaluated using the formula⁽⁶²⁾

$$Q_{us} = 0.5 A_{sc} \sqrt{f'_c E_c}$$

The load-slip characteristic for the connectors placed in the negative moment region is considered to be similar to that of the connectors in the positive moment region with ultimate shear capacity of 80% of the capacity in the positive moment region as recommended by Johnson et al.⁽²⁴⁾

3.4 Finite Difference Formulation

As mentioned earlier in this chapter, the finite difference

technique was used in the first step of the analysis to find the interaction forces and deformation of the composite beam assuming constant stress distribution across a slab width equal to the predefined effective slab width. In this section the mathematical formulation of the finite difference model and the method of analysis is presented.

3.4.1 General Definition

The composite concrete and formed metal deck on steel beam shown in Figure 3.8a has n panels and n shear connectors. The space between connector i and $i+1$ is referred to as the (i) th panel. If parentheses are not used, the letter i denotes the i th connector.

In the following analysis, the connector forces are defined as positive when they act in the direction shown in Figure 3.8b and negative in the other direction. Bending moments producing tension in the bottom fibre of the steel beam are defined as positive.

3.4.2 Basic Assumptions

The basic assumptions used in deriving the finite difference equation in the present analysis are:

1. Concrete slab and steel beam deflects equally at all points along the span.
2. The distribution of strain is linear over the depth of the slab and the depth of the steel beam respectively.
3. Shear connection between the slab and the steel beam is provided by shear connectors placed at discrete points along the composite

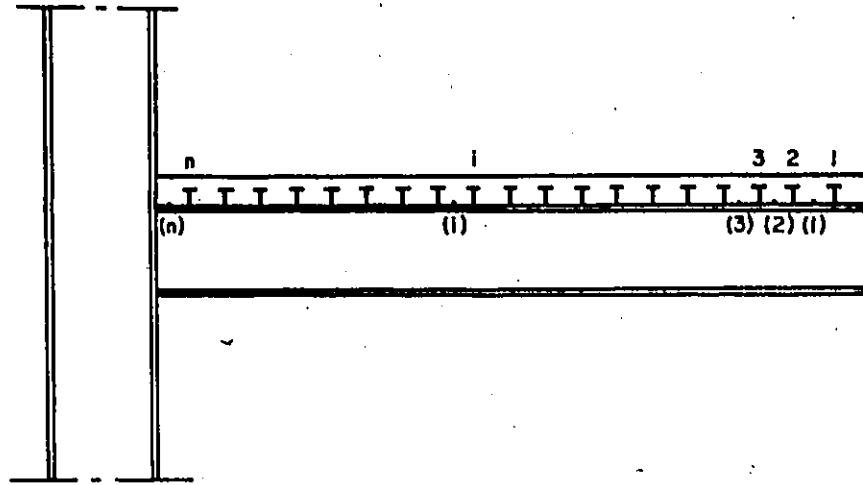


FIGURE 3.8-a COMPOSITE BEAM SHOWING CONNECTORS AND PANELS

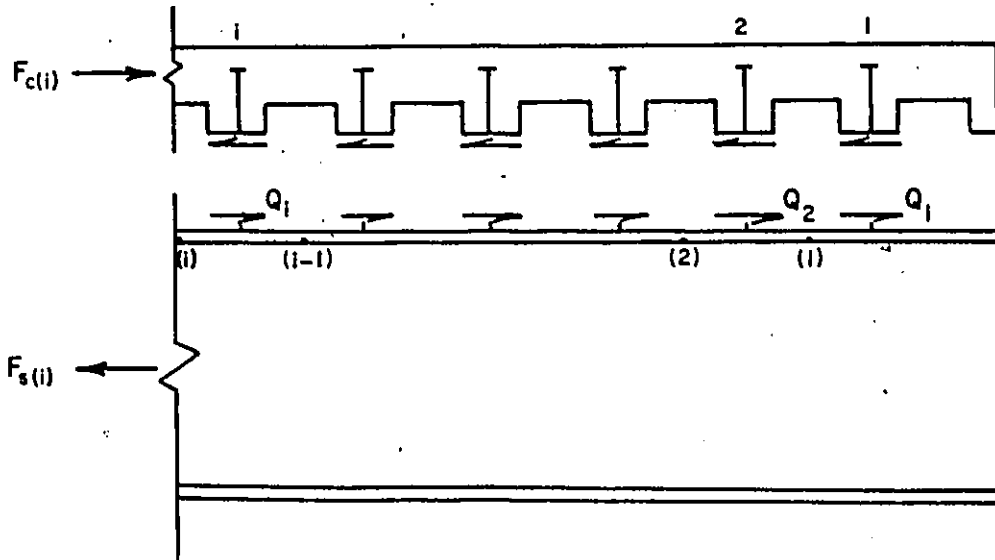


FIGURE 3.8-b POSITIVE DIRECTION OF THE INTERACTION FORCES

beam length.

4. Strain distribution across the slab width, at any section of the composite beam, is constant and equal to the strain distribution over the steel beam centre line.

3.4.3 Basic Equations

The cross section for a general composite beam is shown in Figure 3.9 and the forces, moments and strain distribution are shown in Figure 3.10. The equilibrium equations are

$$F_{s(i)} - F_{c(i)} = 0 \quad (3.1)$$

and

$$F_{s(i)} \{d_{(i)}/2 + d_c + t_s - y\} + M_{s(i)} + M_{c(i)} = M_{(i)} \quad (3.2)$$

The compatibility condition, Figure (3.11), at the interface between the concrete slab and the steel beam is

$$Y_{i+1} - Y_i = \int_{s_{(i)}} (\epsilon_{st(i)} - \epsilon_{cb(i)}) ds \quad (3.3)$$

For linearly elastic connectors,

$$Y_i = \frac{Q_i}{k_i} \quad (3.4)$$

From the equilibrium of the horizontal forces, one obtains

$$F_{c(i)} - F_{c(i-1)} = Q_i \quad (3.5a)$$

and

$$F_{c(i+1)} - F_{c(i)} = Q_{i+1} \quad (3.5b)$$

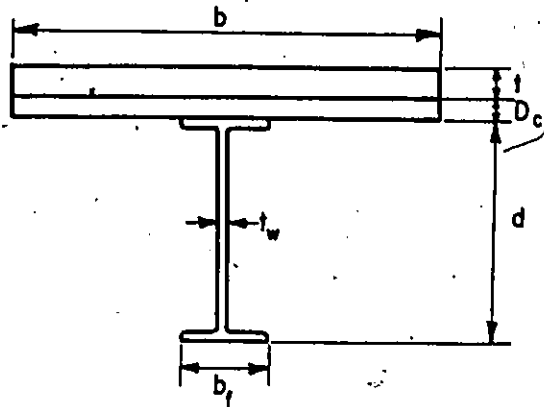


FIGURE 3.9 GENERAL CROSS SECTION

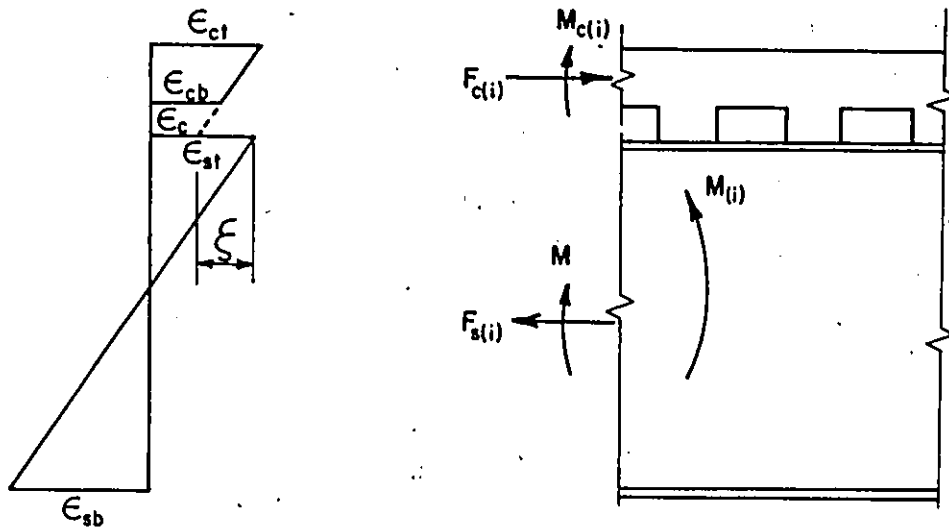


FIGURE 3.10 FORCES, MOMENTS AND STRAINS FOR INCOMPLETE INTERACTION.

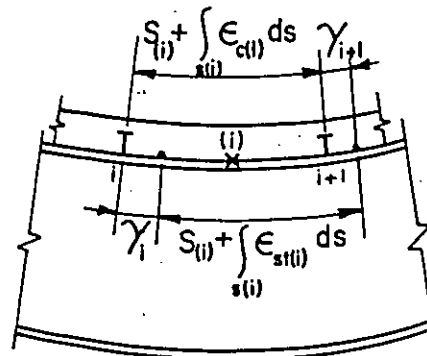


FIGURE 3.11 SLIP IN THE (i)th PANEL

If the steel beam and the concrete slab are both in the elastic range, the strains can be expressed in terms of the forces and moments as follows

$$\epsilon_{st(i)} = \frac{F_{s(i)}}{E_s A_{s(i)}} - \frac{M_{s(i)} \cdot d(i)/2}{E_s I_{s(i)}} \quad (3.6a)$$

and

$$\epsilon_{cb(i)} = -\frac{F_{c(i)}}{E_c A_{c(i)}} + \frac{M_{c(i)} \cdot (d_c + t_s - y)}{E_c I_{c(i)}} \quad (3.6b)$$

The assumption of equal curvature yields

$$\frac{M_{s(i)}}{E_s I_{s(i)}} = \frac{M_{c(i)}}{E_c I_{c(i)}} = \frac{M_{(i)} - z(i) \cdot F_{c(i)}}{\Sigma E I} \quad (3.7)$$

Substitutions of equations (3.4) through (3.7) into equation (3.3) yields

$$\frac{F_{c(i+1)}}{k_{i+1}} - \frac{F_{c(i)}}{k_{i+1}} - \frac{F_{c(i)}}{k_i} + \frac{F_{c(i-1)}}{k_i} = \int_{s(i)} \left[\frac{F_{c(i)}}{E_s A_{s(i)}} - \frac{M_{(i)} - z(i) \cdot F_{c(i)}}{\Sigma E I} \right. \\ \left. - \frac{d(i)}{2} + \frac{F_{c(i)}}{E_c A_{c(i)}} - \frac{M_{(i)} - z(i) \cdot F_{c(i)}}{\Sigma E I} (d_c + t_s - y) \right] ds$$

This equation can be written in the form

$$\frac{F_{c(i-1)}}{k_i} - \left(\frac{1}{k_i} + \frac{1}{k_{i+1}} + \alpha(i) \cdot s(i) \right) F_{c(i)} + \frac{F_{c(i+1)}}{k_{i+1}} = - \int_{s(i)} \beta(i) M_{(i)} ds \quad (3.8)$$

where

$$\alpha_{(i)} = \frac{1}{E_s A_{s(i)}} + \frac{1}{E_c A_{c(i)}} + \frac{z_{(i)}^2}{\Sigma EI}$$

and

$$\beta_{(i)} = \frac{z_{(i)}}{\Sigma EI}$$

Equation (3.8) is a typical finite difference equation for the panel (i) in the case of elastic stress-strain relationships for both the concrete slab and the steel beam with linearly elastic shear connections. This equation is valid for the composite beam in both the positive and negative moment regions. For a composite beam with n panels there will be n such equations resulting in a set of n simultaneous equations. By solving these equations the interaction forces and consequently the stress and strain distributions at the different cross sections will be obtained.

Since the load-slip characteristic for the connector, adopted in the present analysis, is non-linear and the post-elastic analysis is considered, the elastic finite difference equation, equation (3.8), can no longer be used and the original compatibility equation, equation (3.3), has to be solved. It is possible to express the strain difference as a complex non-linear function of F and M. However, since the digital computer is used to perform the computation, it is preferable to use numerical techniques to determine the strain difference corresponding to a given force and moment.

The numerical method used in the analysis does not necessarily need to solve the finite difference equations, hence it can accommodate

any load-slip and stress-strain relationships. In this method a value is first assumed for the end slip, the slip at the first connector, then the slip at the other end, at the column face, is found through the computation. If the slip at the column face is sufficiently close to zero, the solution is obtained otherwise a revised value for the end slip is used and the computation is repeated. The details of the numerical method of computation are given in Appendix A.

3.4.4 The Computational Procedure

- 1) The constants used in the analytical expression for the smooth load-slip curve for the connectors are first determined.
- 2) The bending moment at the centre of each panel due to the applied external loads is computed.
- 3) A trial value for the end slip γ_1 is assumed. By knowing that $F_{(0)} = 0.0$, the force $F_{(1)}$ and the slip at the second connector γ_2 can be computed using the technique described in Appendix A.
- 4) After computing $F_{(1)}$ and γ_2 , by setting $i = 2, 3, \dots, n$, $F_{(2)}$ and γ_3 , $F_{(3)}$ and $\gamma_4 \dots F_{(n)}$ and γ_{n+1} are found successively. γ_{n+1} is the slip at an imaginary connector placed at the column face. The inclusion of such an imaginary connector in the analysis will not affect the results since the slip and hence the shear carried by this connector is equal to zero.
- 5) The computation is performed until the slip at the imaginary connector placed at the column face γ_{n+1} is computed. This slip should be equal to zero since it is assumed that slip is not

permitted at the beam to column connection. If the computed slip is sufficiently close to zero, the solution is obtained; otherwise steps (3) to (5) are repeated using a revised value for the end slip γ_1 . The computation continues until the solution is obtained.

- 6) Through the computation, the forces in the panels and at the connectors, the strains and curvature in each panel are already obtained. The strains are checked for yielding or cracking. If any panel or panels have yielded, steps (3) to (5) are repeated with these panels treated inelastically in computing step (4).
- 7) The deflection of the composite beam along the centre line of the steel beam is computed by numerically integrating the curvature along the span which is already obtained through the computation.

3.5 Finite Element Formulation

The finite element method is used in the second step of the analysis to obtain the strain and stress distributions across the slab width and depth and consequently to define the effective slab widths.

3.5.1 General

The finite element method is essentially a discretization procedure through which a continuum with infinite degrees of freedom can be approximated by an assemblage of discrete elements each with a specified finite number of unknowns.

The finite element method has been described extensively in the

literature. A comprehensive discussion of the theory and application of the method to two-dimensional and three-dimensional systems involving plane stress, plane strain and plate bending is given by Zienkiewicz⁽³⁸⁾. The method has been successfully applied to study the behaviour of reinforced concrete structures by many authors⁽⁴⁴⁾.

Studies of reinforced concrete slabs by the finite element method have been presented by Jofriet and McNeice⁽³⁶⁾ using semi-empirical bilinear moment-curvature relationships.

Scanlon⁽³⁷⁾ developed a layered finite element for reinforced concrete slabs which can account for the effect of cracking. The layered plate bending finite element was used by Wanchoo⁽⁴⁶⁾ to study the elastic and post-elastic behaviour of reinforced concrete slabs subjected to lateral loads.

Lin^(51,67) in his work on combined in-plane and plate bending systems, has extended Scanlon's approach⁽³⁷⁾ to include elasto-plastic behaviour for the steel in tension or compression and for concrete in compression.

In the present analysis, the layered finite element technique is used to study the behaviour of the reinforced concrete slab of the composite beam. In this technique each element is divided into imaginary layers as shown in Figure 3.12. Each layer may have different material properties from other layers according to the strain or stress level in this layer. Thus by using the layered finite element, the variation in the material properties across the slab depth due to the existence of the reinforcing steel, yielding and cracking of concrete

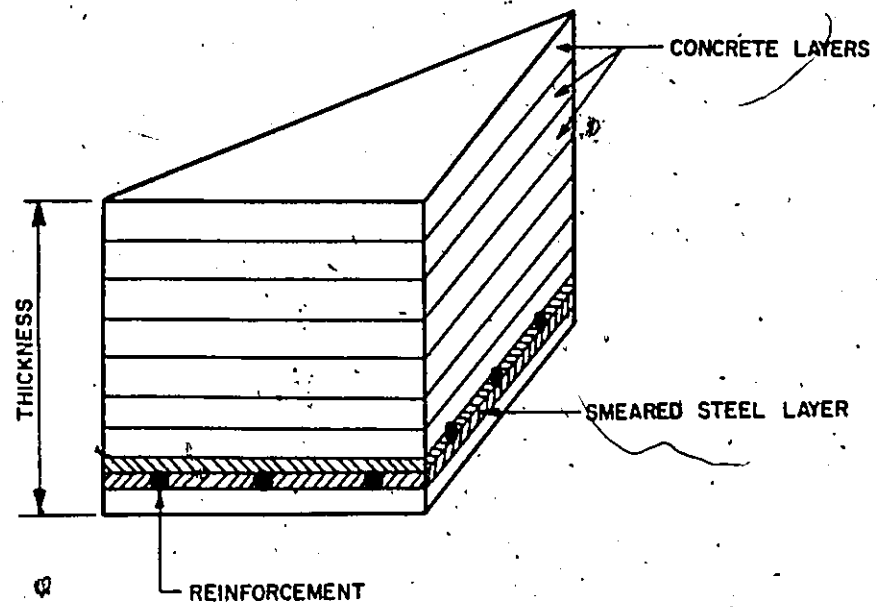


FIGURE 3.12 LAYERED SYSTEM

can be considered in the analysis.

3.5.2 Assumptions

The equation formulated in this section have been derived subject to the following assumptions:

1. Static loading only is assumed.
2. Lateral deflection is small compared to the thickness of the plate, hence the small deflection theory applies.
3. Transverse normal stresses are negligible.
4. Membrane and bending effect are considered.
5. Individual layers are sufficiently bonded at the interface to transfer shear forces.
6. For sufficiently thin layers, stress variation through the layer is neglected; i.e., each layer is represented by the state of stress at its centre.
7. The straight fibres of the plate which are perpendicular to the reference surface before deformation remain so after deformation and do not change their length.

3.5.3 Stiffness Matrix for a Plate Element

The derivation of the element stiffness matrix, using the displacement finite element method, starts with the subdivision of the original continuum into an assemblage of discrete elements and the assumption of an expression for displacement. In the present analysis, triangular elements with 15 degrees of freedom, 5 at each node, is used.

The element derives from incorporating a linear curvature triangular bending element with a constant strain triangular membrane element.

The linear curvature triangular bending element possesses 9 degrees of freedom which are the transverse deflection w and the rotations θ_x and θ_y about the x and y axes at each of the three nodes. The constant strain triangular membrane element possesses 6 degrees of freedom which are the displacements u and v in the x and y direction at each node.

Various conforming and non-conforming functions can be used to represent the displacement within each element. For the bending element, a conforming function satisfies both the displacement and slope continuity along the common edges between the adjacent elements. If a complete slope continuity is required on the interface between the various elements, mathematical and computational difficulties often arise. It is however relatively simple to obtain a displacement function which ensures the displacement continuity but violates the slope continuity. Such a function is called a non-conforming function. An alternate way is to ensure the displacement continuity and satisfy the transverse slope continuity along one of the sides of the element, resulting in a displacement function which is partially conforming.

In the present analysis a partially conforming function is used to express the transverse deflection (w) and a conforming function to represent the in-plane displacements (u) and (v).

3.5.3.1 System of Axes and Nodal Coordinates

The middle surface of the plate, the solid part of the ribbed

slab, is subdivided into triangular elements as shown in Figure 3.13. The nodes of each element are defined by their coordinates. Two sets of right handed axes are used to describe each element. The first set is the global axes x , y and z . Considering the plate to lie in the x - y plane, the coordinates of the nodes in the global axes are denoted by $(x_i, y_i, 0)$, $(x_j, y_j, 0)$ and $(x_k, y_k, 0)$. The second set of axes are the local axes denoted by x' , y' and z' . By considering the element to lie in the x' - y' plane and choosing the origin to be node i and y' axis along the side ij , the local coordinates of the nodes i , j and k are $(0, 0, 0)$, $(0, y'_j, 0)$ and $(x'_k, y'_k, 0)$ respectively. Figure 3.13 shows the global and local axes.

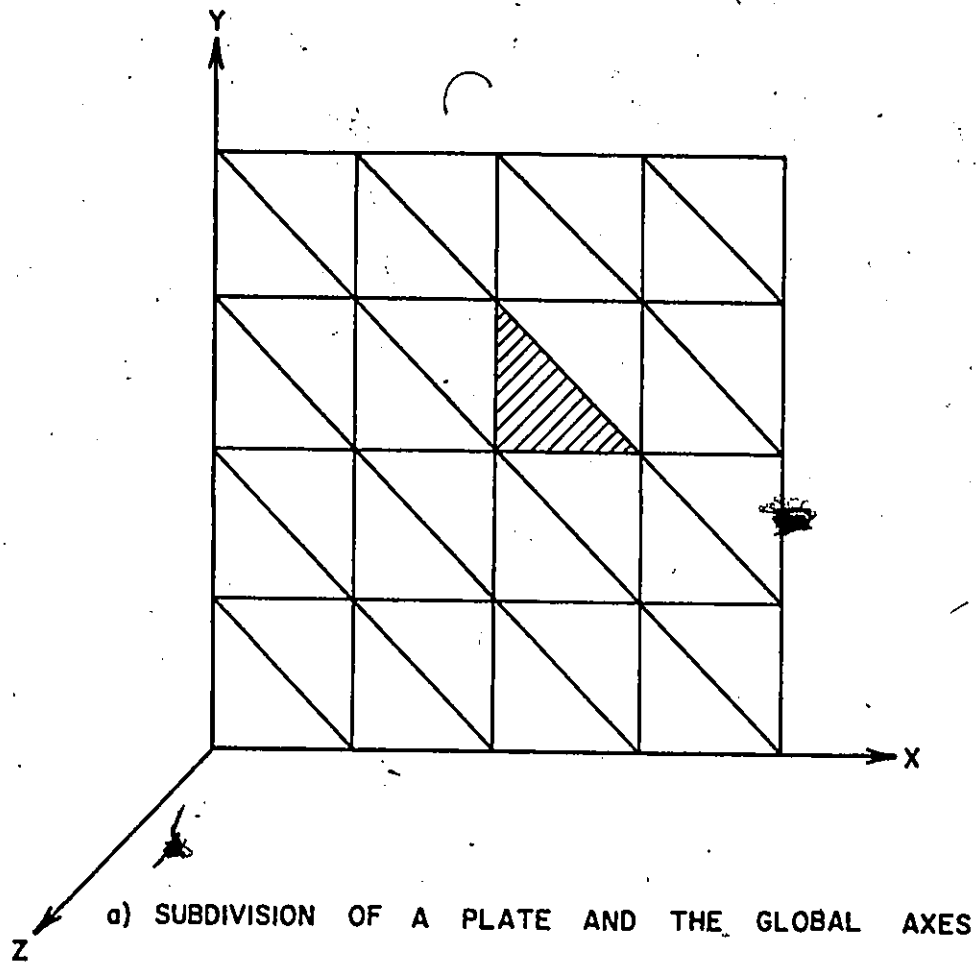
3.5.3.2 Displacement Formulation

Five displacement components are considered as nodal parameters. These nodal parameters are the in-plane displacement u' in the x' direction, in-plane displacement v' in the y' direction, the displacement w' in the z' direction, the rotation θ'_x about the x' axis and the rotation θ'_y about the y' axis.

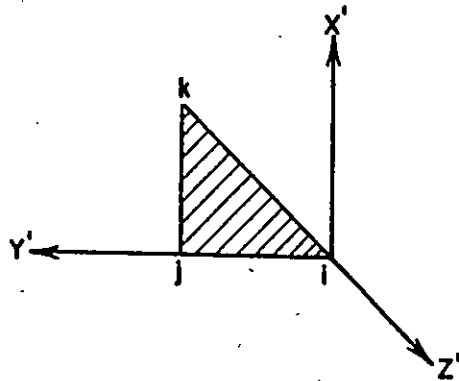
For the constant strain triangular membrane element, the following displacement functions are considered

$$\begin{aligned} u' &= \alpha_1 + \alpha_2 x' + \alpha_3 y' \\ v' &= \alpha_4 + \alpha_5 x' + \alpha_6 y' \end{aligned}$$

A partially conforming displacement function suggested by Rawtani and Dokainish⁽³²⁾ is used to express the displacement w' for the bending element. This function is in the form



a) SUBDIVISION OF A PLATE AND THE GLOBAL AXES



b) LOCAL AXES FOR AN ELEMENT

FIGURE 3.13 PLATE SUBDIVISION AND SYSTEM OF AXES

$$\omega' = \alpha_7 + \alpha_8 x' + \alpha_9 y' + \alpha_{10} x'^2 + \alpha_{11} x' y' + \alpha_{12} y'^2 + \alpha_{13} x'^3 + \alpha_{14} x'^2 y' + \alpha_{15} y'^3$$

where α_i , $i = 1, 15$ are arbitrary constants.

The displacement at any node can be written in matrix form as

$$\{\delta'_i\} = [a] \{\alpha\} \quad (3.9)$$

where

$$\{\delta'_i\} = \begin{Bmatrix} u' \\ v' \\ \omega' \\ \theta'_x \\ \theta'_y \end{Bmatrix} = \begin{Bmatrix} u' \\ v' \\ \omega' \\ \frac{\partial \omega'}{\partial x'} \\ \frac{\partial \omega'}{\partial y'} \end{Bmatrix}$$

$$[a] = \begin{bmatrix} 1 & x' & y' & 0 & 0 & 0 & 0 & 0 & 0 & 0 & 0 & 0 & 0 & 0 & 0 \\ 0 & 0 & 0 & 1 & x' & y' & 0 & 0 & 0 & 0 & 0 & 0 & 0 & 0 & 0 \\ 0 & 0 & 0 & 0 & 0 & 0 & 1 & x' & y' & x'^2 & x' y' & y'^2 & x'^3 & x'^2 y' & y'^3 \\ 0 & 0 & 0 & 0 & 0 & 0 & 0 & 0 & 1 & 0 & x' & 2y' & 0 & x'^2 & 3y'^2 \\ 0 & 0 & 0 & 0 & 0 & 0 & 0 & -1 & 0 & -2x' & -y' & 0 & -3x'^2 & -2x' y' & 0 \end{bmatrix}$$

and

$$\{\alpha\} = \{\alpha_1, \alpha_2, \alpha_3, \alpha_4, \alpha_5, \alpha_6, \alpha_7, \alpha_8, \alpha_9, \alpha_{10}, \alpha_{11}, \alpha_{12}, \alpha_{13}, \alpha_{14}, \alpha_{15}\}^T$$

The element displacement vector $\{\delta'_e\}$ referred to the local axes is given

by the listing of the nodal displacements, thus

$$\{\delta'_e\} = \{u'_i, u'_j, u'_k, v'_i, v'_j, v'_k, \omega'_i, \theta'_{xi}, \theta'_{yi}, \omega'_j, \theta'_{xj}, \theta'_{yj}, \omega'_k, \theta'_{xk}, \theta'_{yk}\}^T \quad (3.10)$$

From equations (3.9) and (3.10), the element displacement vector referred to the local axes becomes

$$\{\delta'_e\} = [A] \{\alpha\} \quad (3.11)$$

where

$$[A] = \begin{bmatrix} 1 & 0 & 0 & 0 & 0 & 0 & 0 & 0 & 0 & 0 & 0 & 0 & 0 & 0 \\ 1 & 0 & y'_j & 0 & 0 & 0 & 0 & 0 & 0 & 0 & 0 & 0 & 0 & 0 \\ 1 & x'_k & y'_k & 0 & 0 & 0 & 0 & 0 & 0 & 0 & 0 & 0 & 0 & 0 \\ 0 & 0 & 0 & 1 & 0 & 0 & 0 & 0 & 0 & 0 & 0 & 0 & 0 & 0 \\ 0 & 0 & 0 & 1 & 0 & y'_j & 0 & 0 & 0 & 0 & 0 & 0 & 0 & 0 \\ 0 & 0 & 0 & 1 & x'_k & y'_k & 0 & 0 & 0 & 0 & 0 & 0 & 0 & 0 \\ 0 & 0 & 0 & 0 & 0 & 0 & 1 & 0 & 0 & 0 & 0 & 0 & 0 & 0 \\ 0 & 0 & 0 & 0 & 0 & 0 & 0 & 0 & 1 & 0 & 0 & 0 & 0 & 0 \\ 0 & 0 & 0 & 0 & 0 & 0 & 0 & 0 & -1 & 0 & 0 & 0 & 0 & 0 \\ 0 & 0 & 0 & 0 & 0 & 0 & 1 & 0 & y'_j & 0 & 0 & y_j'^2 & 0 & 0 & y_j'^3 \\ 0 & 0 & 0 & 0 & 0 & 0 & 0 & 0 & 1 & 0 & 0 & 2y'_j & 0 & 0 & 3y_j'^2 \\ 0 & 0 & 0 & 0 & 0 & 0 & 0 & 0 & -1 & 0 & 0 & -y'_j & 0 & 0 & 0 \\ 0 & 0 & 0 & 0 & 0 & 0 & 1 & x'_k & y'_k & x_k'^2 & x'_k y'_k & y_k'^2 & x_k'^3 & x_k'^2 y'_k & y_k'^3 \\ 0 & 0 & 0 & 0 & 0 & 0 & 0 & 0 & 1 & 0 & x'_k & 2y'_k & 0 & x_k'^2 & 3y_k'^2 \\ 0 & 0 & 0 & 0 & 0 & 0 & 0 & -1 & 0 & -2x'_k & -y'_k & 0 & -3x_k'^2 & -2x'_k y'_k & 0 \end{bmatrix}$$

hence

$$\{\alpha\} = [A^{-1}] \{\delta'_e\} \quad (3.12)$$

At any point on the middle surface, the strains $\{\epsilon'_o\}$ and curvature $\{\psi'\}$ are given by

$$\{\bar{\epsilon}\} = \begin{Bmatrix} \epsilon_0 \\ \psi \end{Bmatrix} = \begin{Bmatrix} \epsilon_x \\ \epsilon_y \\ \gamma_{xy} \\ \psi_x \\ \psi_y \\ \psi_{xy} \end{Bmatrix} = \begin{Bmatrix} \frac{\partial u'}{\partial x'} \\ \frac{\partial v'}{\partial y'} \\ \frac{\partial u'}{\partial y'} + \frac{\partial v'}{\partial x'} \\ \frac{\partial^2 \omega'}{\partial x'^2} \\ \frac{\partial^2 \omega'}{\partial y'^2} \\ \frac{2\partial^2 \omega'}{\partial x' \partial y'} \end{Bmatrix} \quad (3.13)$$

by substituting the expressions of u' , v' and ω' , equation (3.13) can be written in the form

$$\{\bar{\epsilon}\} = [\beta] \{\alpha\} \quad (3.14)$$

where

$$[\beta] = \begin{bmatrix} 0 & 1 & 0 & 0 & 0 & 0 & 0 & 0 & 0 & 0 & 0 & 0 & 0 & 0 \\ 0 & 0 & 0 & 0 & 0 & 1 & 0 & 0 & 0 & 0 & 0 & 0 & 0 & 0 \\ 0 & 0 & 1 & 0 & 1 & 0 & 0 & 0 & 0 & 0 & 0 & 0 & 0 & 0 \\ 0 & 0 & 0 & 0 & 0 & 0 & 0 & 0 & 0 & 2 & 0 & 0 & 6x' & 2y' & 0 \\ 0 & 0 & 0 & 0 & 0 & 0 & 0 & 0 & 0 & 0 & 0 & 2 & 0 & 0 & 6y' \\ 0 & 0 & 0 & 0 & 0 & 0 & 0 & 0 & 0 & 0 & 2 & 0 & 0 & 4x' & 0 \end{bmatrix}$$

From the assumption of linear strain distribution across the depth of the plate, the strain $\{\epsilon'\}$ at any depth z from the middle surface can be expressed in terms of the strain at the middle surface $\{\epsilon_0\}$ and the

curvature $\{\psi'\}$ at that point. Thus, $\{\epsilon'\}$ can be expressed as follows

$$\{\epsilon'\} = \{\epsilon'_0\} - z \{\psi'\} \quad (3.15)$$

where

$$\{\epsilon'\} = \begin{Bmatrix} \epsilon'_x \\ \epsilon'_y \\ \gamma'_{xy} \end{Bmatrix}$$

and

$$\{\psi'\} = \begin{Bmatrix} \frac{\partial^2 w'}{\partial x'^2} \\ \frac{\partial^2 w'}{\partial y'^2} \\ \frac{2\partial^2 w'}{\partial x' \partial y'} \end{Bmatrix}$$

Equation (3.15) can be written as

$$\{\epsilon'\} = [G] [\beta] \{\alpha\} \quad (3.16)$$

where

$$[G] = \begin{bmatrix} 1 & 0 & 0 & | & -z & 0 & 0 \\ 0 & 1 & 0 & | & 0 & -z & 0 \\ 0 & 0 & 1 & | & 0 & 0 & -z \end{bmatrix}$$

The general stress-strain relation may be expressed by

$$\{\sigma'\} = [C] \{\epsilon'\} \quad (3.17)$$

where $[C]$ represents the constitutive relations of the material. For a concrete layer,

$$[C] = \frac{E_c}{(1-\nu_c^2)} \begin{bmatrix} 1 & \nu_c & 0 \\ \nu_c & 1 & 0 \\ 0 & 0 & \frac{1-\nu_c}{2} \end{bmatrix} \quad (3.18a)$$

A steel layer is assumed to consist of reinforcing steel placed in two perpendicular directions, longitudinal and transverse reinforcement, and it is further assumed that the reinforcing steel resists stresses in its longitudinal direction only. Thus, the matrix [C] for a steel layer is given by

$$[C] = E_s \begin{bmatrix} 1 & 0 & 0 \\ 0 & 1 & 0 \\ 0 & 0 & 0 \end{bmatrix} \quad (3.18b)$$

substitution of equation (3.16) into equation (3.17) yields

$$\{\sigma'\} = [C] [G] [\beta] \{\alpha\} \quad (3.19)$$

Substituting for $\{\alpha\}$ from equation (3.12)

$$\{\sigma'\} = [C] [G] [\beta] [A^{-1}] \{\delta_e'\} \quad (3.20)$$

The internal energy E_i is given by

$$\begin{aligned} E_i &= \int_{\text{vol}} \frac{1}{2} \{\epsilon'\}^T \{\sigma'\} dv \\ &= \int_{\text{vol}} \frac{1}{2} \{\delta_e'\}^T [A^{-1}]^T [\beta]^T [G]^T [C] [G] [\beta] [A^{-1}] \{\delta_e'\} dv \end{aligned}$$

and the external energy is given by

$$E_e = \{\delta_e'\}^T \{P_e'\}$$

Equating the external and internal energy gives

$$\{\delta'_e\}^T \{P'_e\} = \int_{\text{vol}} \frac{1}{2} \{\delta'_e\}^T [A^{-1}]^T [\beta]^T [G]^T [C] [G] [\beta] [A^{-1}] \{\delta'_e\} dv$$

Taking variation, the above equation yields

$$\{P'_e\} = \int_{\text{vol}} [A^{-1}]^T [\beta]^T [G]^T [C] [G] [\beta] [A^{-1}] \{\delta'_e\} dv \quad (3.21)$$

Since $[A^{-1}]$ is independent of x' , y' and z' and $[\beta]$ is independent of z' , equation (3.21) is written in the form

$$\{P'_e\} = [A^{-1}]^T \int_{\text{area}} [\beta]^T \int_z [G]^T [C] [G] dz [\beta] dA [A^{-1}] \{\delta'_e\} \quad (3.22)$$

Comparing equation (3.22) with the following equation

$$\{P'_e\} = [K'_e] \{\delta'_e\} \quad (3.23)$$

where $[K'_e]$ is the element stiffness matrix in the local axes. Thus the element stiffness matrix is given by

$$[K'_e] = [A^{-1}]^T \int_{\text{area}} [\beta]^T \int_z [G]^T [C] [G] dz [\beta] dA [A^{-1}] \quad (3.24)$$

Assuming the material properties are constant within each layer, equation (3.24) can be written as follows

$$[K'_e] = [A^{-1}]^T \int_{\text{area}} [\beta]^T \sum_{i=1}^n \int_{z_i}^{z_{i+1}} [G]^T [C] [G] dz [\beta] dA [A^{-1}]$$

$$= [A^{-1}]^T \int_{\text{area}} [\beta]^T \sum_{i=1}^n \int_{z_i}^{z_{i+1}} [F] dz [\beta] dA [A^{-1}] \quad (3.25)$$

where n is the number of layers

z_i and z_{i+1} are the distance from the middle surface to the two faces of the i th layer (Figure 3.14).

$$[F] = [G]^T [C] [G] = \begin{bmatrix} [C] & | & -z[C] \\ \hline -z[C] & | & z^2[C] \end{bmatrix}$$

The inner integration in equation (3.25) can be carried out as follows

$$[D] = \sum_{i=1}^n \int_{z_i}^{z_{i+1}} [F] dz = \sum_{i=1}^n \int_{z_i}^{z_{i+1}} \begin{bmatrix} [C] & | & -z[C] \\ \hline -z[C] & | & z^2[C] \end{bmatrix} dz$$

$$= \sum_{i=1}^n \begin{bmatrix} (z_{i+1} - z_i) [C] & | & -\frac{1}{2} (z_{i+1}^2 - z_i^2) [C] \\ \hline -\frac{1}{2} (z_{i+1}^2 - z_i^2) [C] & | & \frac{1}{3} (z_{i+1}^3 - z_i^3) [C] \end{bmatrix}$$

$$= \begin{bmatrix} \sum_{i=1}^n t_i [C] & | & \sum_{i=1}^n -t_i z_i [C] \\ \hline \sum_{i=1}^n -t_i z_i [C] & | & \sum_{i=1}^n (z_{i+1}^3 - z_i^3) [C] \end{bmatrix}$$

Thus

$$[K_e'] = [A^{-1}]^T \int_{\text{area}} [\beta]^T [D] [\beta] dA [A^{-1}]$$

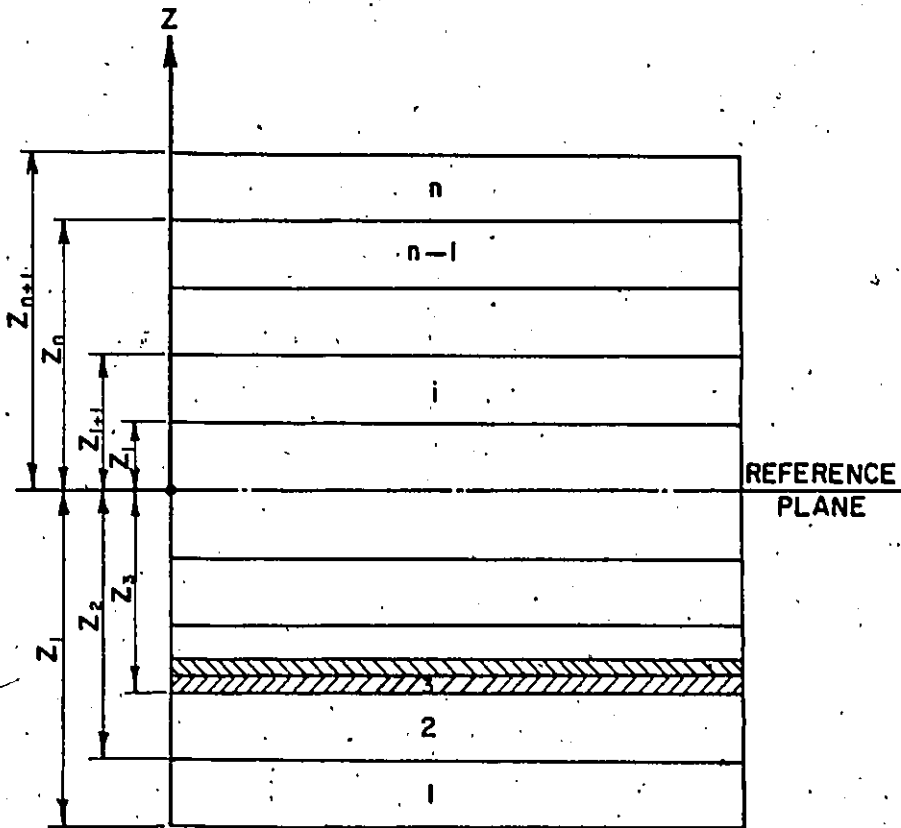


FIGURE 3.14 CONSTRUCTION OF A TYPICAL LAYERED SYSTEM

$$[K'_e] = [A^{-1}]^T [S] [A^{-1}] \quad (3.26)$$

where

$$[S] = \int_{\text{area}} [B]^T [D] [B] dA$$

To assemble the element stiffness matrices into a single total stiffness matrix, all the matrices should be referred to the set of global axes. Thus, each element stiffness matrix must be transformed from the local to the global set of axes.

The element nodal displacements in the local axes, $\{\delta'_e\}$, are related to the element nodal displacements in the global axes, $\{\delta_e\}$, by the relation

$$\{\delta'_e\} = [T] \{\delta_e\} \quad (3.27)$$

where $[T]$ is the transformation square matrix of order equal to the number of element degrees of freedom.

Similarly the element nodal forces in the local axes, $\{P'_e\}$, are related to the element nodal forces in the global axes, $\{P_e\}$, by the relation

$$\{P'_e\} = [T] \{P_e\} \quad (3.28)$$

Substitution of equations (3.27) and (3.28) into equation (3.23) yields

$$[T] \{P_e\} = [K'_e] [T] \{\delta_e\} \quad (3.29)$$

Since the two sets of axes are orthogonal, the transformation matrix $[T]$ is also orthogonal. Hence,

$$[T]^{-1} = [T]^T$$

Thus equation (3.29) can be written in the form

$$\{P_e\} = [T]^T [K'_e] [T] \{\delta_e\}$$

From which the element stiffness matrix in the global axes $[K_e]$ is expressed as

$$[K_e] = [T]^T [K'_e] [T] \quad (3.30)$$

3.5.4 Assemblage of Elements

Having calculated the stiffness matrices $[K_e]$ for the individual elements, the next step is to combine all these matrices, according to the sequence of node numbering employed on the structure, to obtain the total stiffness matrix $[K]$ for the slab. The code numbering method is used to generate the total stiffness matrix.

3.5.5 Evaluation of the Stresses and Strains

The nodal displacements $\{\delta\}$ in the global axes are found by solving the equation

$$\{P\} = [K] \{\delta\} \quad (3.31)$$

Having calculated the nodal displacements, the stresses and strains at any point in an element are found using the following equations

$$\{\sigma\} = [T_1] [C] [G] [\delta] [A^{-1}] [T] \{\delta_e\} \quad (3.32)$$

and

$$\{\epsilon\} = [C]^{-1} \{\sigma\} \quad (3.33)$$

where $[T_1]$ is the stresses transformation matrix.

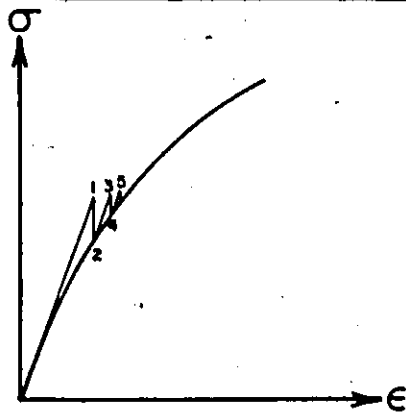
3.5.6 Post-Elastic Analysis

Structures exhibit nonlinear behaviour if either of the following conditions are violated

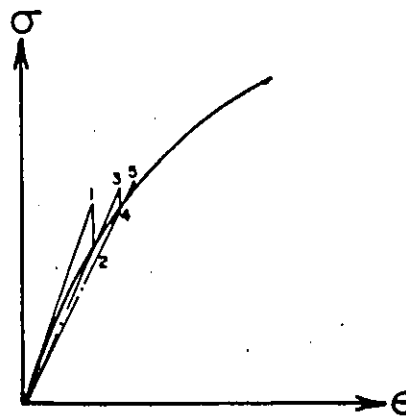
- (1) Linear stress-strain relationship
- (2) Linear strain-displacement relationship.

The nonlinear behaviour caused by the violation of the first condition is called material nonlinearity while the violation of the second condition is called geometrical nonlinearity. In the analysis described in this thesis it is assumed that displacements are small which implies that geometrical nonlinearity can be neglected. Thus only material nonlinearity is considered in the present analysis.

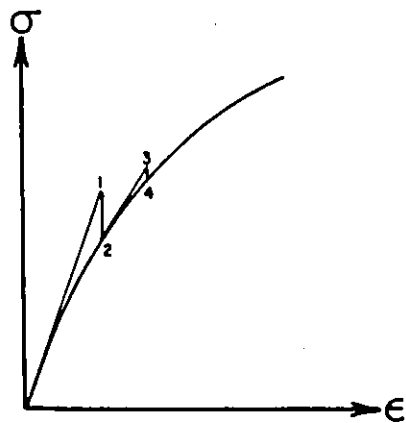
The finite element formulation given in sections 3.5.3, 3.5.4 and 3.5.5 is valid for both linear and nonlinear material properties. Numerous iteration methods for solving systems of nonlinear equations can be used to solve equation (3.31). Three commonly used methods are initial stiffness method, secant stiffness method and tangent stiffness method (Figure 3.15). Two approaches can be used, with respect to the applied loads, to solve equation (3.31); the total load approach and the incremental approach. The selection of the iteration method depends on the adopted approach and idealized stress-strain relation. In the present investigation the total load is applied on the structure, total load approach, and the secant stiffness method of iteration is used. The adopted method of iteration provided a fairly readily convergence for the solution.



a) INITIAL STIFFNESS



b) SECANT STIFFNESS



c) TANGENT STIFFNESS

FIGURE 3.15 ITERATION METHOD

3.5.6.a Concrete Elements in Compression and Reinforcing Steel

The principal stresses at the centre of gravity of each element are calculated for every layer. If one of the principal stresses exceeds the specified f'_c , the elastic limit of the adopted stress-strain relationship for concrete, for a concrete layer or f_y for a steel layer; the material constitutive relations for this layer of the element should be changed and the secant modulus of elasticity is to be used instead of the initial modulus. Thus the element stiffness and consequently the total stiffness matrix are revised according to the new constitutive relation.

The maximum strain failure criterion is adopted in the present analysis. Accordingly, when the maximum principal strain in a layer of an element exceeds the limiting strain, failure of the layer occurs and consequently its stiffness is considered to be zero in the analysis. The limiting concrete strain ϵ_{cu} proposed by Hognestad, et al. ⁽³⁾ as

$$\epsilon_{cu} = 0.004 - \frac{f'_c}{6.5 \times 10^6} \quad (3.34)$$

is used to define the failure of concrete according to its uniaxial compressive strength f'_c . The limiting strain of 0.003 as defined in the CSA Standard A23.3 - 1973 was discarded in favour of the previous equation since it takes account of the variation in the concrete strength.

3.5.6.b Concrete Element in Tension

For concrete in tension, a crack is introduced when the principal

tensile stress exceeds a predetermined tensile strength. The tensile strength was taken as the modulus of rupture. The modulus of rupture (f_r) is given in the CSA standard A23.3 - 1973 as a function of the maximum compressive stress (f'_c) as follows

$$f_r = 7.5 \sqrt{f'_c}$$

Exact modeling of cracking in concrete is difficult because of the different problems associated with the crack formation. — Various approaches for modeling the cracked concrete have been discussed in the literature. The simplest approach is to delete the element from the global matrix when it is cracked. A more sophisticated model is to reduce the stiffness of the element in the direction normal to the crack while keeping the stiffness in its direction unchanged. The most difficult simulation of cracking can be achieved by introducing new nodes in the cracked element and subdividing the element into new elements.

Since the purpose of the present analysis is to study the macro-behaviour of the composite construction rather than the micro-behaviour, the use of sophisticated crack modeling is not necessarily required. Therefore, in the present analysis, when the principal tensile stress at a layer of an element exceeds the modulus of rupture of the concrete, this layer of the element is deleted from the structure by assigning it a modulus of elasticity equal to zero. This approach slightly underestimates the stiffness of the slab and the capacity of the composite beam. The percentage of error, when using this simple method, decreases with the decrease in the element size and decrease of the layer

thickness.

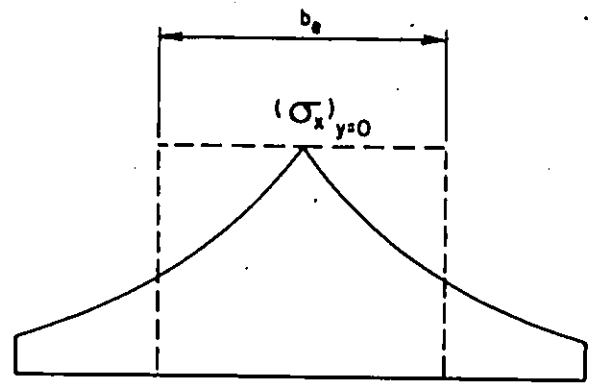
3.6 Effective Slab Widths

As mentioned in section 3.2 the method of analysis is an iteration method which consists of two steps. It was necessary to define two effective slab widths to be used in the first step of the analysis in order to ensure the compatibility of deformations between the steel beam, as obtained from the first step, and the concrete slab, as obtained from the second step, and to ensure the internal force and moment equilibrium. These two effective slab widths are

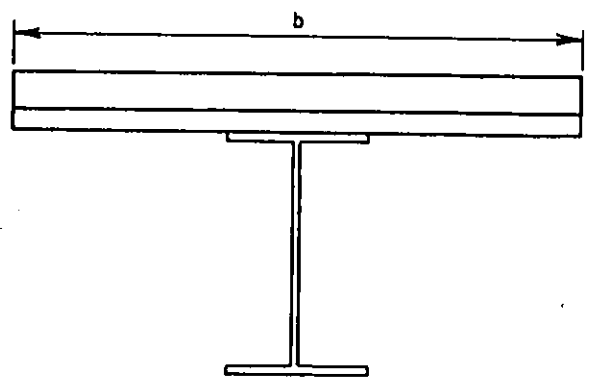
a) Effective Slab Width for In-plane Forces:

This effective slab width is referred to in the literature as the shear effective width since it is the effective slab width that resists the interaction forces provided by the shear connectors.

In the positive moment region the effective slab width for in-plane forces (b_e) will be referred to as the effective slab width for strength in the present analysis. It is defined as that width of slab which would sustain a force equal to the force in the actual slab at that section assuming the longitudinal stresses across the effective slab width are constant and equal to the stresses over the steel beam centre line, Figure 3.16. In a mathematical form, the effective slab width for strength (b_e) is given by



STRESS DISTRIBUTION ACROSS THE SLAB WIDTH



CROSS SECTION

FIGURE 3.16 EFFECTIVE SLAB WIDTH FOR STRENGTH

$$b_e = \frac{t \int_{-b/2}^{b/2} \int_0^t \sigma_x dy dz}{\int_0^t (\sigma_x)_{y=0} dz} \quad (3.35a)$$

where b is the total slab width (spacing between the steel beams)

t is the slab thickness (thickness of the solid part of the ribbed slab)

σ_x is the longitudinal stress in the slab

The above definition of the effective slab width applies in the negative moment region before cracking of the concrete slab. For a section with fully cracked concrete through the whole depth, the effective slab width will be based on the stresses in the slab reinforcement as follows

$$b_e = \frac{\int_{-b/2}^{b/2} \sigma_s dy}{(\sigma_s)_{y=0}} \quad (3.35b)$$

where σ_s is the longitudinal stress in the steel reinforcement

$(\sigma_s)_{y=0}$ is the longitudinal stress in the steel reinforcement over the steel beam centre line.

The definition of the effective slab width for strength (b_e) as given in equations (3.35a) and (3.35b) is valid for both elastic and plastic conditions.

b) Effective Slab Width for Bending Moment:

As mentioned before, the deformation of the composite beam as

computed from the finite difference solution together with the interaction forces were applied on the finite element model to determine the stress and strain distribution in the actual concrete slab. A definition for the effective slab width for bending moment (b_{em}) was required in order to ensure that the moment carried by the slab of the composite beam (M_c) is equal to the moment carried by the actual slab. This definition of the effective slab width for bending moment can be presented as

$$b_{em} = \frac{2 \int_0^{t/2} \int_0^{b/2} \sigma_x z \, dy \, dz}{M_c'} \quad (3.36)$$

where M_c' is the moment per unit width in the slab as obtained from the finite difference solution of the composite beam.

The definition of the effective slab width for bending moment as given in equation (3.36) is valid for the elastic and plastic conditions.

The above two definitions for effective slab width, b_e and b_{em} , were necessary to perform the computer analysis described in sections 3.4 and 3.5. However, the analysis showed that for practical cases the effective slab width for bending moment was not important since the moment carried by the slab is only a small fraction of the moment carried by the composite beam.

In addition to the above two definitions of the effective slab width, two additional definitions are identified in order to facilitate

the simple calculation using the method of the transformed section. These two additional definitions of the effective slab width are:

1. Effective Slab Width for Stiffness

The effective slab width for stiffness at any section is defined as the slab width to be used with the steel beam so that the calculated curvature of the transformed section is equal to the actual curvature of the composite beam at that particular section.

Since the curvature of the composite beam (ϕ) is obtained from the analytical model, the effective slab width at any section can be calculated from the knowledge of the curvature (ϕ) and the applied moment (M) at that section

$$I_{\text{eff}} = \frac{M}{E_s \phi} \quad (3.37)$$

Using the method of transformed section

$$I_{\text{eff}} = I_s + \frac{1}{n} \cdot I_c + \frac{1}{n} \cdot A_c (y_c)^2 + A_s (y_s)^2 \quad (3.38)$$

where A_c area of the concrete slab cross section

A_s area of the steel beam cross section

I_s moment of inertia of the steel beam about the major axis

I_c moment of inertia of the concrete slab about its centre line

I_{eff} effective moment of inertia

n the modular ratio = E_c/E_s

y_s the distance from the centre of the steel beam to the centre of the composite section

y_c the distance from the centre of the slab to the centre of the composite section.

From the knowledge of I_{eff} , the effective slab width for stiffness (b_{es}) at any section is calculated using equation (3.38).

2. Average Effective Slab Width for Stiffness

It was found from the analysis that the effective slab width for stiffness is variable along the beam. Therefore, in order to simplify the every day calculation using the transformed section, an average effective width for stiffness is defined as the uniform effective width to be used with the steel beam so that the calculated deflection using the transformed section is equal to the actual deflection of the composite beam. Thus, for the analytical model described in section 3.2

$$I_{av} = \frac{M L^2}{3 E_s \Delta_c} \quad (3.39)$$

where I_{av} is the average moment of inertia

L the length of the cantilever beam in the model

Δ_c the deflection of the composite beam

From a knowledge of (I_{av}), the average effective slab width for stiffness (b_{av}) can be calculated using equation (3.38).

The two definitions for the effective slab width for stiffness are valid only for the elastic condition. No attempt is made to extend these definitions to the plastic stage since they are not required for the ultimate stress design.

3.7 Method of Computation

The complete method of analysis can be summarized in the following steps:

1. Assuming values for the effective widths b_e and b_{em} , usually starts with the total width b , the composite beam is solved using the finite difference solutions described in steps 1 to 7 in section 3.4.4.
2. The resulting interaction forces (Q) and the deflection at the connectors position is applied to the appropriate nodes of the finite element model of the slab.
3. Using the finite element model, the stresses, strains across the slab width and depth are calculated at the different sections.
4. Stresses in the slab are checked against cracking, crushing and yielding. If any of these conditions occur, steps 3 and 4 are to be repeated using the appropriate material properties. This procedure continues until the cracking, yielding or crushing is stabilized.
5. Effective slab widths b_e and b_{em} are calculated from the resulting stresses in the slab using equations (3.35) and (3.36). The calculated effective widths are compared with the assumed values. If the assumed and calculated values are close to each other within the prescribed accuracy, the solution is obtained otherwise steps (1) to (5) are repeated using the calculated b_e and b_{em} as the assumed value.
6. Effective slab width for stiffness (b_{es}) and the average

effective slab width (b_{av}) is calculated from the resulting curvature (ϕ) and deflection (Δ_c) using equations (3.37), (3.38) and (3.39).

7. Steps 1 to 6 are repeated for each load increment.

3.8 Program Description

A computer program utilizing the finite difference and finite element techniques has been developed. The program has been written to run on the CDC 6400 computer available at McMaster University Computing Centre. Flow chart for the program is given in Figure 3.17.

The program consists of a main program and 12 subroutines. The program was written to study the composite beam-to-column connection under positive moment. Some modifications to the main program and some of the subroutines were required to study the behaviour of the system under negative moment.

The input of the program consists of the geometrical properties of the composite beam and the material properties. The following represents the output of the program:

1. Slip distribution along the composite beam
2. Stress and strain distributions in the steel beam along the span
3. Deflection of the composite beam along the span
4. Stress and strain distributions in the concrete slab across its width and depth both in the longitudinal and transverse directions
5. Cracked, yielded and crushed zones in the concrete slab

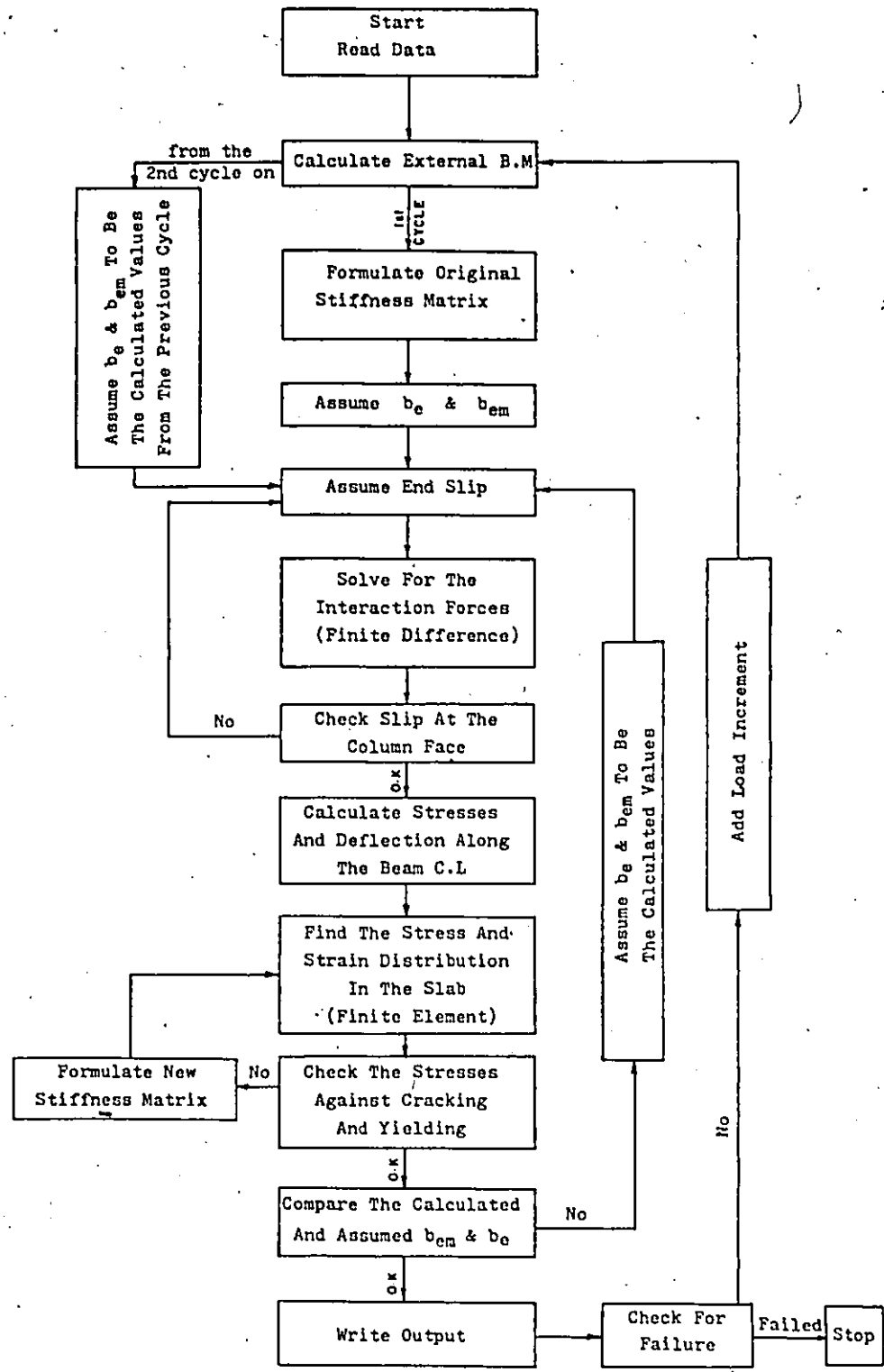


FIGURE 3.17 FLOW CHART OF THE COMPUTATION METHOD

6. Deflection and curvature at the different sections of the composite beam along the span and the concrete slab outside the steel beam.
7. The distribution of the effective slab widths b_e and b_{em} along the span

The complete description and listing of the computer program is given in Appendix B.

3.9 Summary

This chapter contains the mathematical formulation of the analytical model and all the assumptions made in the analysis. The steps of computation and brief description of the computer program are also given in this chapter.

The analytical results are given in the next chapter and a comparison between the analytical and test results for the test beams are given in Chapter 7.

CHAPTER 4

ANALYTICAL INVESTIGATION OF THE EFFECTIVE SLAB WIDTHS

4.1 General

The analytical method described in Chapter 3 was used to determine the effective slab widths, for strength and stiffness, and consequently the strength and stiffness of composite beams with ribbed metal deck in a multi-story frame subjected to lateral loads. The method was applied to both positive and negative analytical models, described in Section 3.2, to study the behaviour of the composite system in the positive and negative bending moment regions. A parametric study of the factors affecting the behaviour of the system is included in this chapter.

Although the main purpose of this investigation was to study the behaviour of composite beams in an unbraced frame, the analytical method was also applied to evaluate the effective slab widths for simple composite beams. A comparison between the analytical results and the current formula for the effective slab width in the different codes is presented at the end of the chapter.

4.2 Check of the Reliability of the Program

Before applying the analytical method to study the behaviour of composite beams in multi-story frames, the reliability and suitability

of the computer program were documented by comparison with the available theoretical and experimental results in the literature. First, the finite element section in the program was checked by solving some classical plate problems and comparing the obtained results with those documented in the literature. Secondly, the whole program was checked by comparing the prediction of the computer program with the available experimental and theoretical results for simple composite beams and composite beam-to-column connections.

4.2.1 Check of the Finite Element Section

The reliability of the finite element formulation was checked by solving a square plate and a rectangular plate with all edges fixed and subjected to a central lateral load perpendicular to the plane of the plate. The square plate was of dimension 8 ft. by 8 ft. while the rectangular plate was 4 ft. by 8 ft. Both plates were 8 in. thick. The modulus of elasticity was assumed to be 3×10^7 psi and Poisson's ratio 0.15. The central deflection and the two slopes, θ_x and θ_y , at the central node were computed for each case.

Szilard⁽⁶³⁾ reported the solution of these classical plate problems using the finite difference method. The central deflection of the plate is given by the equation

$$\Delta_{\max} = C_1 \frac{P a^2}{D} \quad (4.1)$$

where a is the short dimension of the plate

C_1 is a factor depending on the aspect ratio of the plate

D is the flexural rigidity of the plate

P is the applied load

Δ_{\max} is the central deflection.

He tabulated the values of C_1 for different aspect ratios. For the square plate C_1 it is 0.0056 while for the rectangular plate it is 0.0072. The central deflection was calculated for each plate using equation (4.1) and the appropriate value for C_1 . Due to the symmetry of the plate and loading, the two slopes at the central node should be zero.

The results obtained from the finite element program are compared with those computed from equation (4.1) in Table 4.1.

Square Plate			
	Δ_{\max}	θ_x	θ_y
Finite Element Results	0.0335	0.447×10^{-15}	0.881×10^{-16}
From Equation (4.1)	0.033	0	0

Rectangular Plate			
	Δ_{\max}	θ_x	θ_y
Finite Element Results	0.01085	0.107×10^{-15}	0.974×10^{-17}
From Equation (4.1)	0.0106	0	0

Table 4.1: Comparison Between the Finite Element Results and those Given in Reference (63).

The results given in this table show that the computed central deflection is very close to that calculated from equation (4.1) and that the two slopes, θ_x and θ_y , at the central point are approximately equal to zero. This serves as a check of the efficiency and accuracy of the adopted finite element scheme.

4.2.2 Check of the Over-all Program

After checking the finite element section, the reliability of the over-all program was checked. Since the main outputs of the computer program are the distribution of the effective slab width along the composite beam and the behaviour of the composite beam in terms of the deflection and strain distribution along the beam centre line, each of these two outputs was checked by comparison with the available results in the literature.

a) Prediction of the Effective Slab Width for Strength

The developed computer program was used to analyse a simple composite T-beam consisting of a W12x27 steel beam and a 4 in. thick solid concrete slab. The span of the beam was 16 ft. and the width of the slab was 4 ft. The beam was subjected to a central point load (P) and was provided with very stiff connectors to simulate the case of complete interaction between the concrete slab and the steel beam. The distribution of the effective slab width along the span was given as a direct output of the computer program.

The computed values of the effective slab width were compared with the results reported by Adekola⁽¹⁸⁾ in the literature. The results

reported by Adekola⁽¹⁸⁾ are based on a theoretical solution in which an Airy's stress function was assumed to represent the stresses in the middle surface of the slab and a displacement function to represent the deformation of the composite beam. The terms of these functions were chosen so that they satisfy the boundary conditions and the compatibility of deformation between the concrete slab and the steel beam.

Figure 4.1 shows a comparison between the computed effective slab widths along the centre line of the analysed composite beam and the results reported by Adekola⁽¹⁸⁾ for the same aspect ratio (L/b) which was equal to 4 for the analysed beam.

As can be seen from this figure, the computed effective widths agree very well with the reported theoretical results. This serves as a check for the reliability of the output of the computer program concerning the effective slab width.

b) Behaviour of the Composite Beam-to-Column Connections

The final check on the computer program was done by analysing two composite beam-to-column connections tested experimentally by DuPlessis and Daniels⁽⁴⁸⁾. The computed and experimental results were compared for each connection.

The first composite beam-to-column connection, which was labelled (B_1), consisted of a cantilever composite beam fixed to a very stiff column test fixture. The composite beam consisted of a W12x27 steel beam and a 4 in. thick solid concrete slab. The beam was 8 ft. long and the concrete slab width was 4 ft. The material properties of the beam

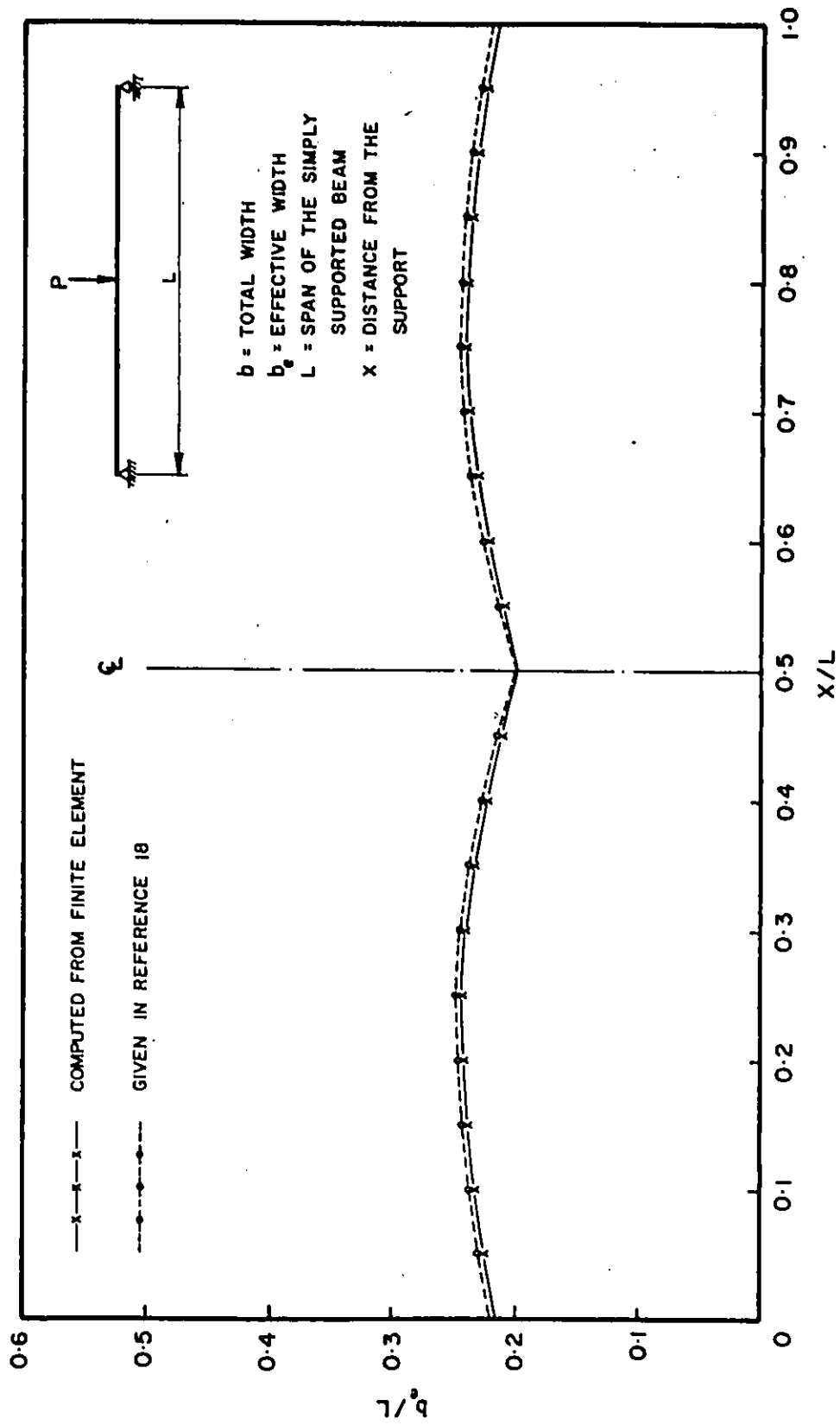


FIGURE 4.1 COMPARISON BETWEEN THE CALCULATED b_e/L AND THE RESULTS GIVEN IN REFERENCE (18)

and the details of the connectors are reported in reference (48). The beam was subjected to a concentrated end load increased from zero up to the failure of the beam.

The second beam-to-column connection, labelled (F_1), was similar to the first one, (B_1), except for the concrete slab which was a ribbed concrete on metal deck. The slab consisted of a 2.5 in. thick solid part and 1.5 in. deep ribs. The material properties and the details of the connectors for this beam are reported in the same reference (48).

The geometric and material properties pertinent to each of the test beams were fed into the computer program and the distribution of the effective slab widths, deflections and curvature along the beam length were given as a direct output of the program.

Figures 4.2 and 4.3 show the computed and experimental end moment versus the chord rotation for tests (B_1) and (F_1) respectively. Since both beams failed by crushing of the concrete slab adjacent to the column face, the computation was terminated when the concrete strain reached the maximum compressive strain computed from equation (3.34). The computed values of M_u/M_p were 1.69 and 1.60 for tests (B_1) and (F_1) respectively. These values correspond to experimental results of 1.67 and 1.57 for the same two beams.

The comparison of the computed and experimental results shows that the computed results agree very well with the reported experimental results. This serves as a check of the reliability and suitability of the computer program concerning the prediction of the behaviour and ultimate capacity of the composite system.

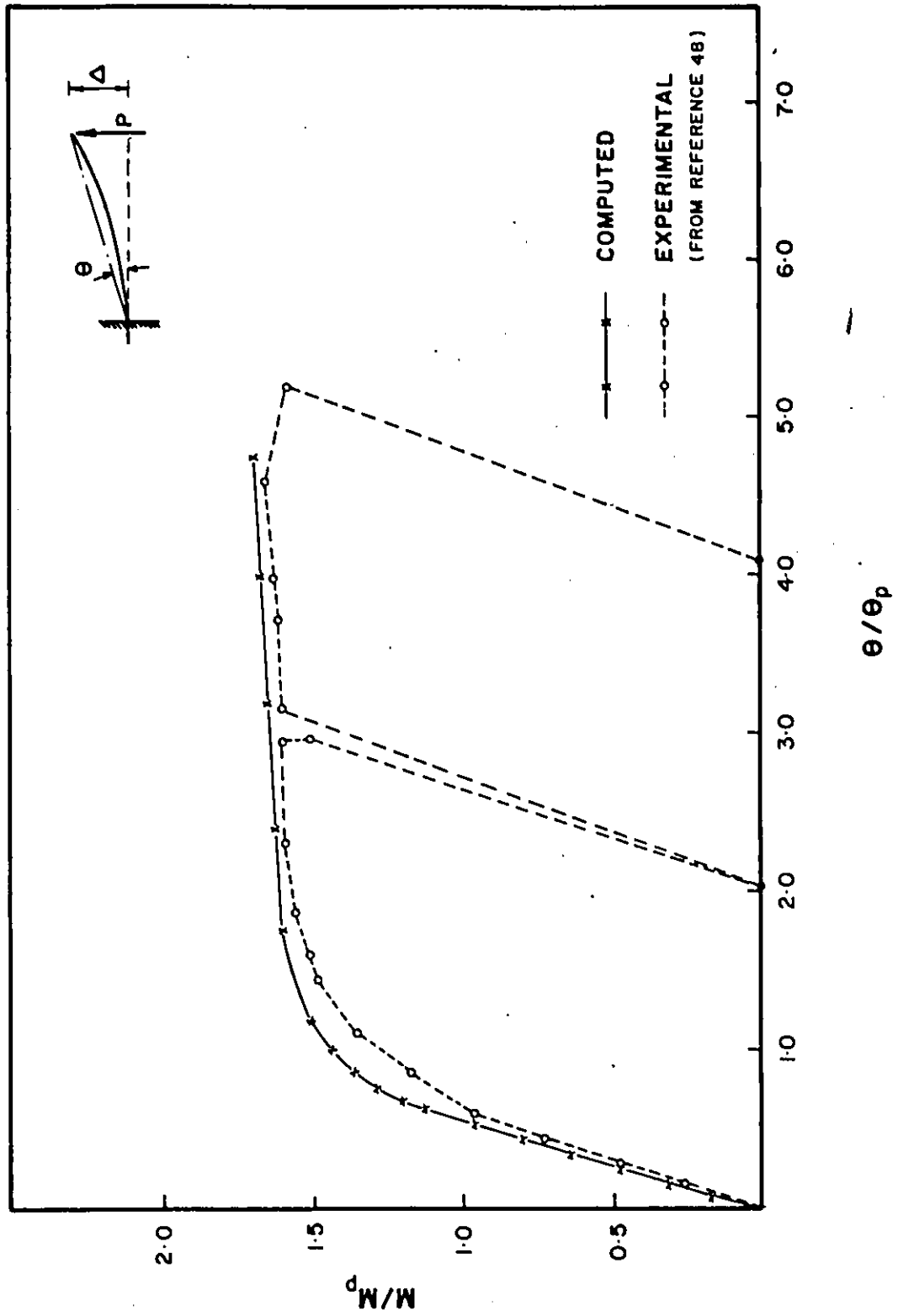


FIGURE 4.2 COMPARISON BETWEEN THE COMPUTED LOAD-DEFLECTION CURVE AND THE EXPERIMENTAL RESULTS REPORTED IN REFERENCE (48) FOR BEAM B1

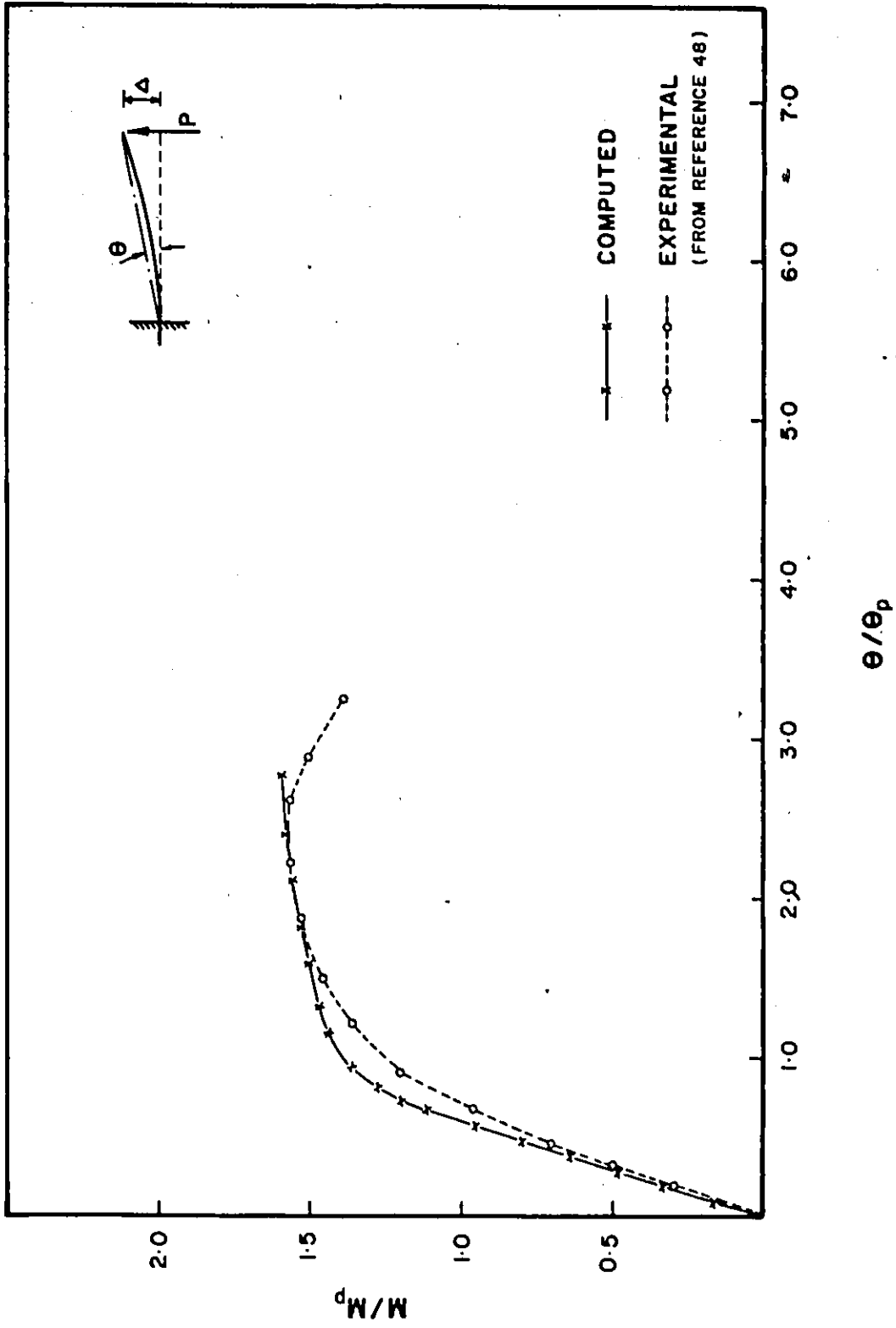


FIGURE 4.3 COMPARISON BETWEEN THE COMPUTED LOAD-DEFLECTION CURVE AND THE EXPERIMENTAL RESULTS REPORTED IN REFERENCE (48) FOR BEAM F1

The good agreement between the analytical results and those reported in the literature, theoretically and experimentally, was considered to provide evidence of the validity and the reliability of the analytical method adopted in this investigation.

4.3 Analytical Investigation

The main purpose of this analytical investigation was to determine an effective slab width to be used in estimating the ultimate moment capacity of the composite beams at the connection with the columns, of an unbraced frame, in both positive and negative moment regions (Figure 3.2). The analytical results were also used to determine the effective slab width to be used in calculating the stiffness of the composite beams in both moment regions. The analytical models in the positive and negative moment regions, Section 3.2, were used in the current analytical investigation.

The effect of the following parameters on the effective slab widths was considered in this analytical study

- a) Slab length to width ratio (L/b).
- b) Column width to slab width ratio (c/b).
- c) Total slab thickness.
- d) Steel beam size.
- e) Degree of connection.

The results of the analytical study are arranged in three major groups based on the three definitions for the effective slab width which are

- a) The effective slab width for strength (b_e).
- b) The average effective slab width for stiffness (b_{av}).
- c) The effective slab width for stiffness at any section (b_{es}).

The results pertinent to each of these three groups are presented and discussed in details in the following sections.

4.4 Effective Slab Width for Strength (b_e)

The effective slab width for strength (b_e) was defined in Chapter 3 as the width of slab which would sustain a force equal to the force in the actual slab assuming the longitudinal stress across the effective slab width is constant and equal to the stress over the steel beam centre line. The effective slab width for strength (b_e) was calculated according to the method of analysis described in Section 3.7 and was given as a direct output of the computer program at several points, mid spacing between connectors, along the span for each load increment applied on the analytical model.

Several composite beams were analysed to determine the effective slab width for strength and to study the effect of each of the parameters mentioned in Section 4.3 in both positive and negative moment regions.

The model in the positive moment region consisted of a cantilever composite beam with ribbed concrete slab on metal deck fixed to a very rigid column. The ribbed slab was reinforced with a 6 in. by 6 in. 10/10 gauge welded wire mesh placed at the middle of the solid part. The beams were subjected to a concentrated point load applied at the

free end. The load was increased from zero up to the failure of each beam. The geometrical and material properties were varied for the different beams to achieve the required parametric study. Figure 4.4 shows the analytical model and the finite element discretization.

A similar model was used in the negative moment region. The slab was reinforced in this case with reinforcing steel bars placed 1/2 in. from the top surface of the slab. The steel reinforcement was assumed to be distributed uniformly across the slab width.

The details of the analysed beams are reported in the pertinent sections of the following discussion.

4.4.1 Variation of the Effective Slab Width for Strength Along the Span

To study the variation of the effective slab width along the span of the composite beam, nine beams were analysed under each of the positive and negative moment conditions. The analysed composite beams consisted of W12x27 steel beams and 4 in. thick ribbed concrete slab on metal deck. The slab width was 4 ft. and was constant for all beams while the span of the beam was changed to obtain different L/b ratios. Three L/b ratios were considered namely 2, 3 and 4. For each L/b ratio, three column widths were considered so that c/b ratio was 0.25, 0.5 and 1.0 for each case. Each beam was provided with eighteen 3/4 in. diameter stud shear connectors.

The data pertinent to each beam were fed into the computer program and the distribution of the effective slab width along the span was computed for every load increment up to the failure of the beam.

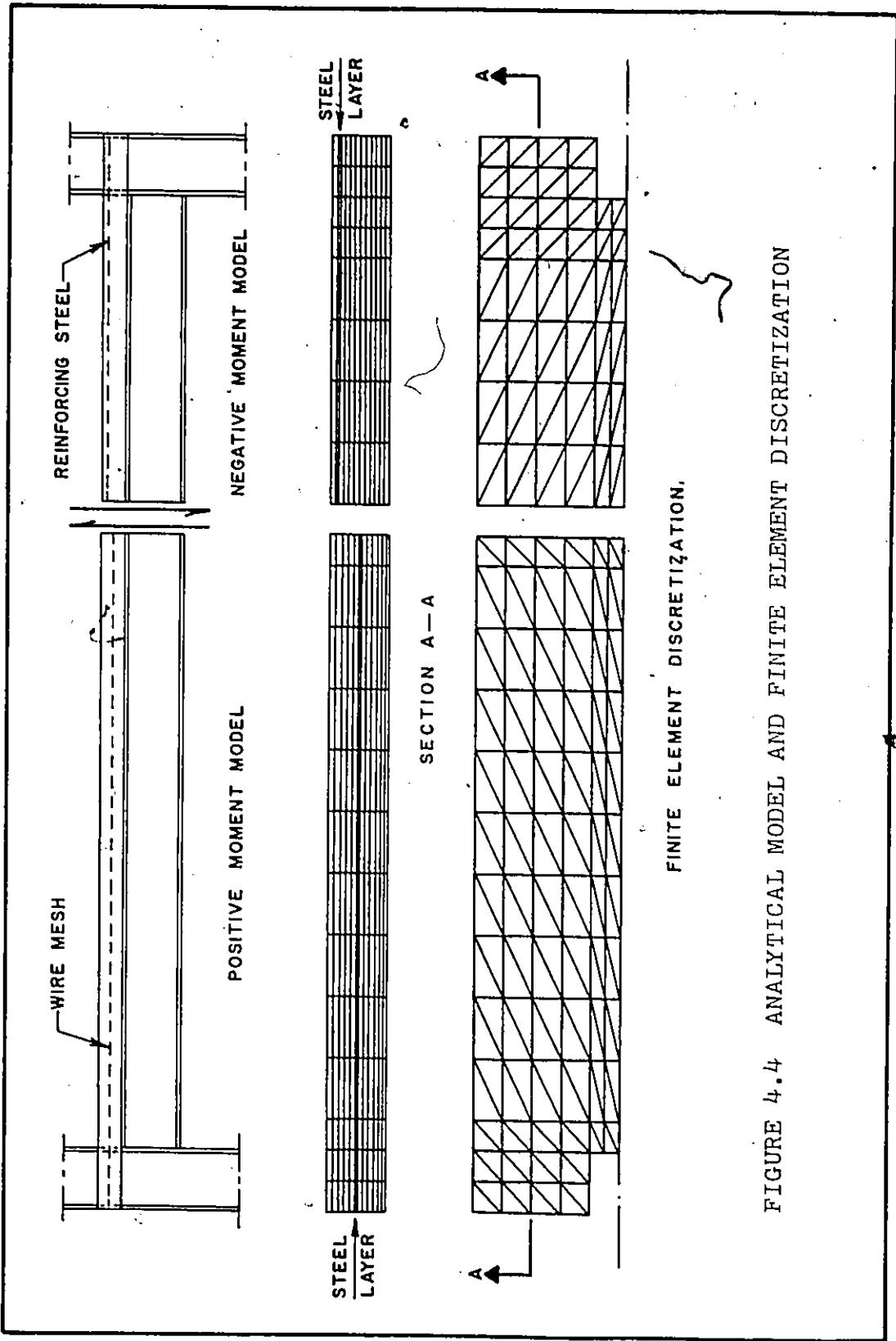


FIGURE 4.4 ANALYTICAL MODEL AND FINITE ELEMENT DISCRETIZATION

Figure 4.5 shows the variation of the effective slab width along the span for the composite beams subjected to positive moment condition and Figure 4.6 shows the distribution under negative moment condition. Each figure shows the distribution of the effective slab width (b_e) for the nine cases considered.

The effective slab width for strength (b_e) was nonuniform along the beam centre line with the minimum effective slab width located at the column face. The degree of uniformity increases with the increase in L/b and c/b ratios as shown in Figures 4.5 and 4.6.

Although the case of c/b equal to one is not a practical case considering the practical size of the column and the spacing between the frames, it was included in the analysis since it simulates the case of a simple composite beam having a span equal to $2L$ and subjected to a central point load equal to $2P$. The distribution of the effective slab width along the beam in this case agrees with the results presented by Adekola⁽¹⁸⁾ as shown in Figure 4.1.

Since the main purpose of the current investigation is to determine the effective slab width that can be used to determine the moment capacity of the beam at the position of the connection, the rest of the parametric study was devoted to the minimum effective slab width, at the column face, and the notation (b_e) was used to represent the effective slab width for strength at this position in the rest of the thesis.

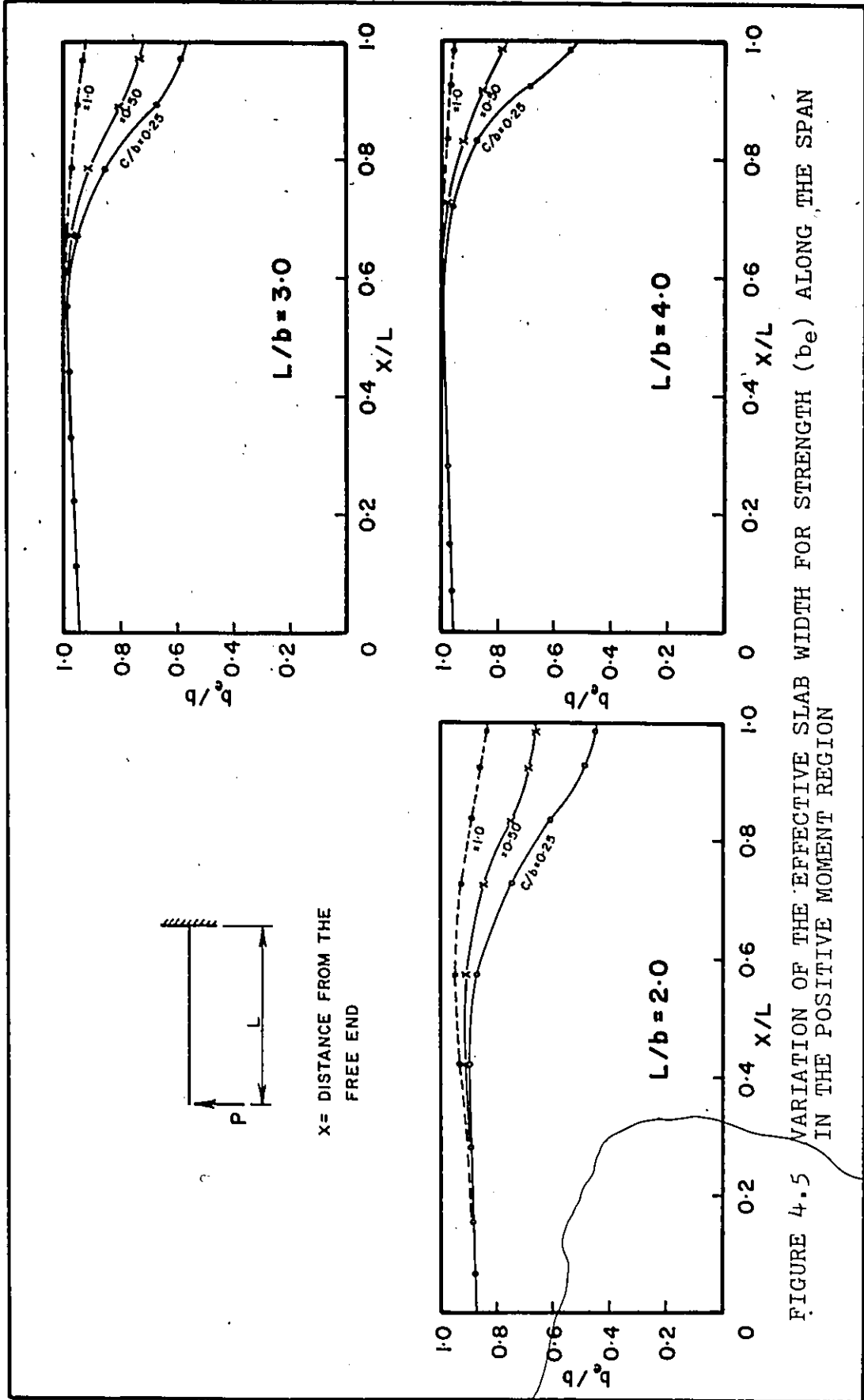


FIGURE 4.5 VARIATION OF THE EFFECTIVE SLAB WIDTH FOR STRENGTH (b_e) ALONG THE SPAN IN THE POSITIVE MOMENT REGION

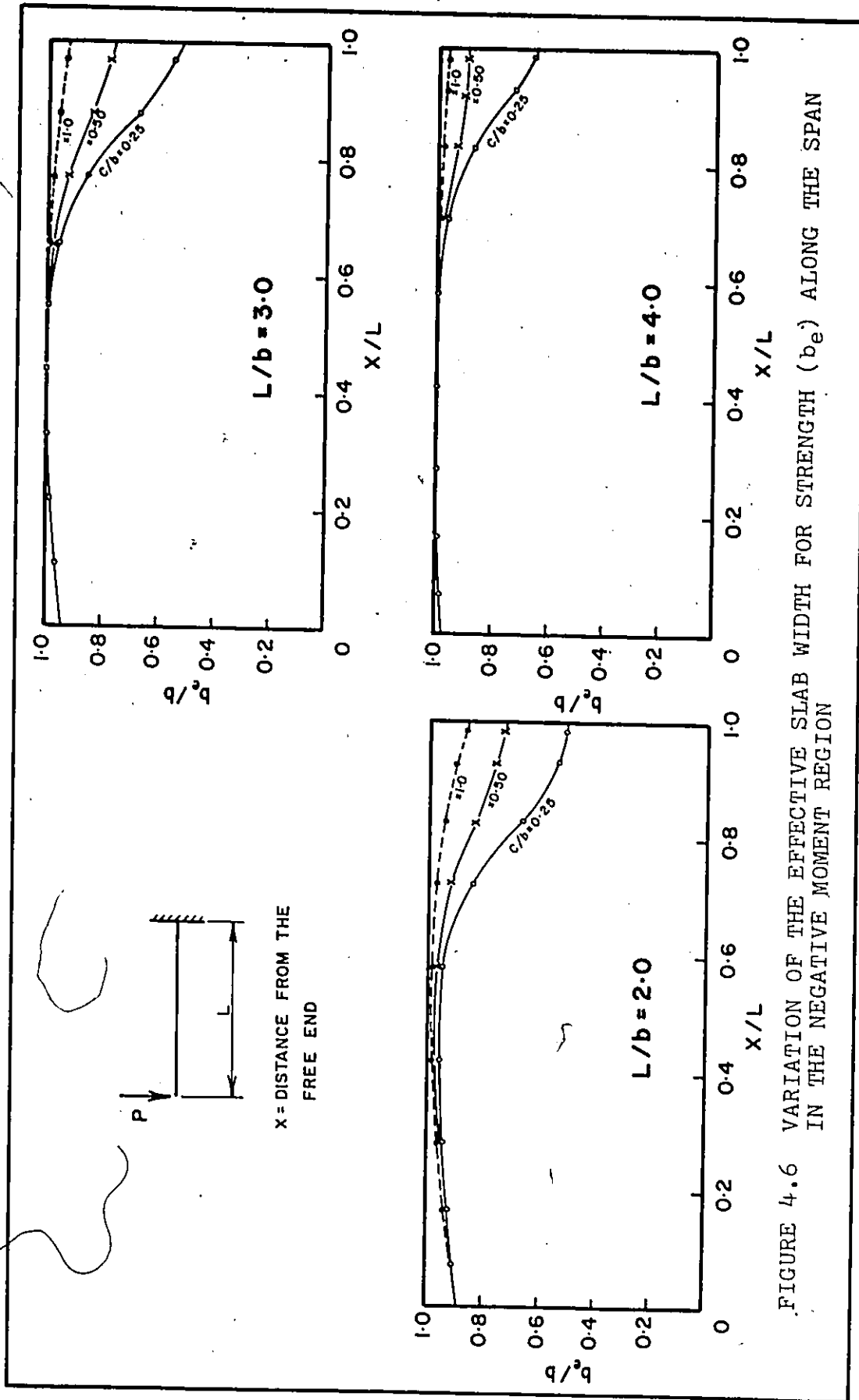


FIGURE 4.6 VARIATION OF THE EFFECTIVE SLAB WIDTH FOR STRENGTH (b_e) ALONG THE SPAN IN THE NEGATIVE MOMENT REGION

4.4.2 Variation of the Effective Slab Width (b_e) with the Applied Load

Since the main concern of the current investigation is to determine an effective slab width to be used to determine the ultimate capacity of the composite beam, it was necessary to study the variation of the effective slab width with increase in the applied load.

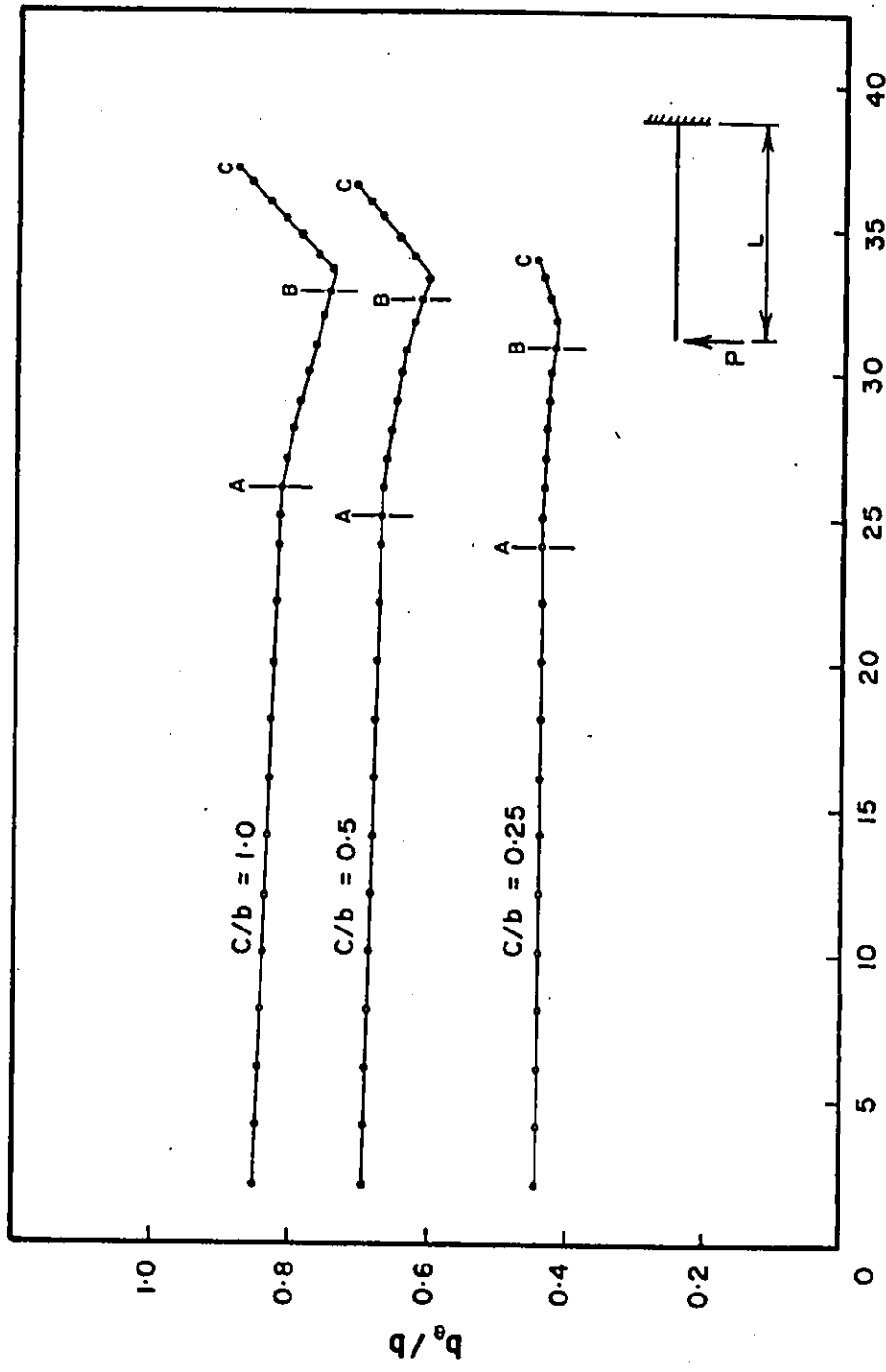
The computer results of the beams described in Section 4.4.1 were used for the purpose of this study. The minimum effective slab width for strength (b_e), at the column face, is plotted in Figures 4.7 and 4.8 against the applied load on the beam for L/b ratio equal to 2 and 4 for the positive moment region. Each figure contains three curves corresponding to a c/b ratio of 0.25, 0.5 and 1. Three points are marked on each curve.

Point A: start of yielding of the steel beam bottom flange.

Point B: reaching a stress of $0.85 f'_c$, the limit of the elastic portion of the idealized stress-strain curve, in the concrete slab.

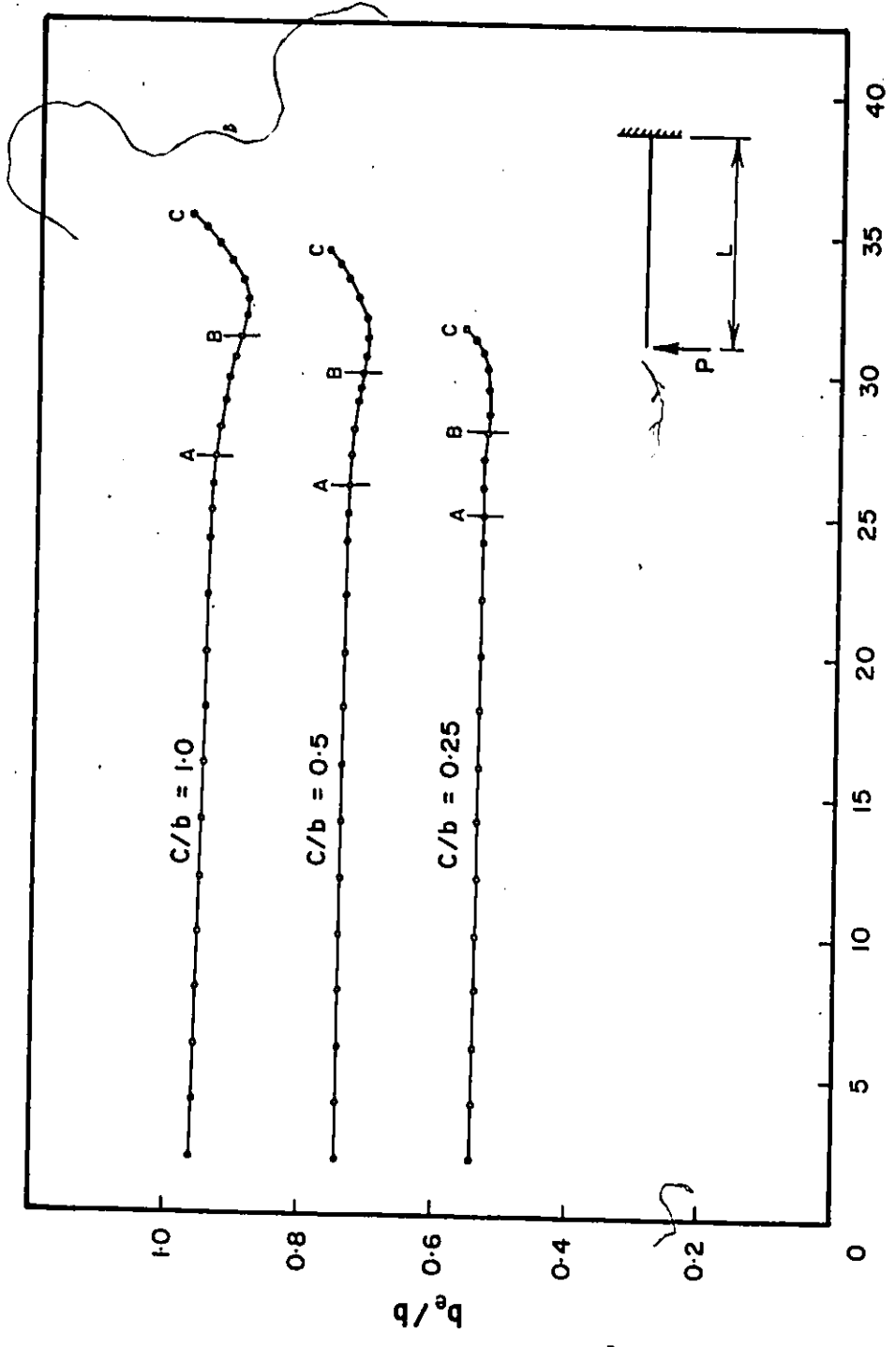
Point C: failure of the beam.

The curves shown in these two figures show that before yielding of the steel beam the minimum effective slab width (b_e) slightly decreased with increasing the applied load. The decrease in the effective slab width is greater for larger c/b ratios. However, even for a c/b ratio of 1.0 the effective slab width when the steel beam started yielding, point A, was less than the initial one by about 4% for L/b equal to 2 and about 2% for L/b equal to 4. After yielding of the steel beam the rate of decrease of the minimum effective slab width was



APPLIED LOAD (kips)

FIGURE 4.7 VARIATION OF THE MINIMUM EFFECTIVE SLAB WIDTH FOR STRENGTH WITH THE APPLIED LOAD IN THE POSITIVE MOMENT REGION FOR $L/b = 2$



APPLIED LOAD (kips)

FIGURE 4.8 VARIATION OF THE MINIMUM EFFECTIVE SLAB WIDTH FOR STRENGTH WITH APPLIED LOAD IN THE POSITIVE MOMENT REGION FOR $L/b = 4$

higher and was much more noticeable for larger c/b ratios. Upon reaching the maximum stress in the concrete, $0.85 f'_c$, the effective slab width started to decrease at a lower rate and then started to increase again. At failure, point C, the effective slab width was larger than the initial one or at least equal to it. This observation applies to all the beams analysed as shown in Figures 4.7 and 4.8.

These results agree with the results obtained by Heins and Fan⁽⁷¹⁾ for the case of simply supported beams. They studied the effective slab width of simple composite beams using the finite difference technique. The study showed that the effective slab width at ultimate is slightly greater than the elastic one and that this difference decreases with the increase in L/b ratio.

The increase in the effective slab width after reaching the plateau of the idealized stress-strain curve for the concrete may be explained by considering the variation of the stress distribution across the slab width. Figure 4.9 shows the top fibre stress distribution across the slab width at various load levels for an L/b ratio of 2 and c/b of 0.25. This figure shows that when the peak stress over the steel beam reached the plateau, this peak stress remained constant while the stresses increased on both sides of the slab causing more uniformity of the stress distribution and consequently a larger effective slab width. Although the increase in the effective slab width as explained above is a result of the idealized stress-strain curve, this increase is more conservative than that which would occur if the actual stress-strain curve was used since the peak stress would decrease in this case upon

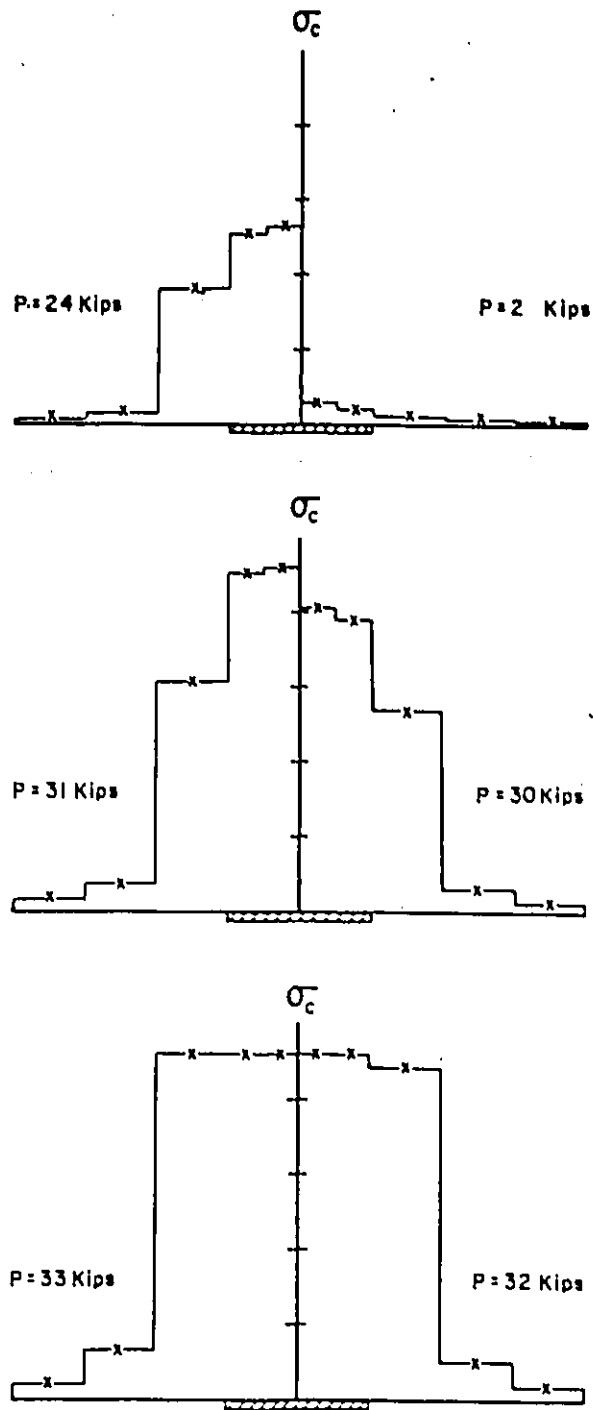


FIGURE 4.9 VARIATION OF THE TOP FIBRE CONCRETE STRESS DISTRIBUTION ACROSS THE SLAB WIDTH AT THE COLUMN FACE WITH THE APPLIED LOAD

reaching f'_c , instead of being constant as for the idealized curve, due to the softening of the concrete and consequently a larger effective slab width would be expected.

The variation of the effective slab width with the applied load in the negative moment region for L/b ratio of 2 is shown in Figure 4.10. Four points are marked on each curve in this figure.

Point A: start of flexural cracking in the slab

Point B: the slab was completely cracked across the whole depth at that section, adjacent to the column face, and only the steel reinforcement is considered

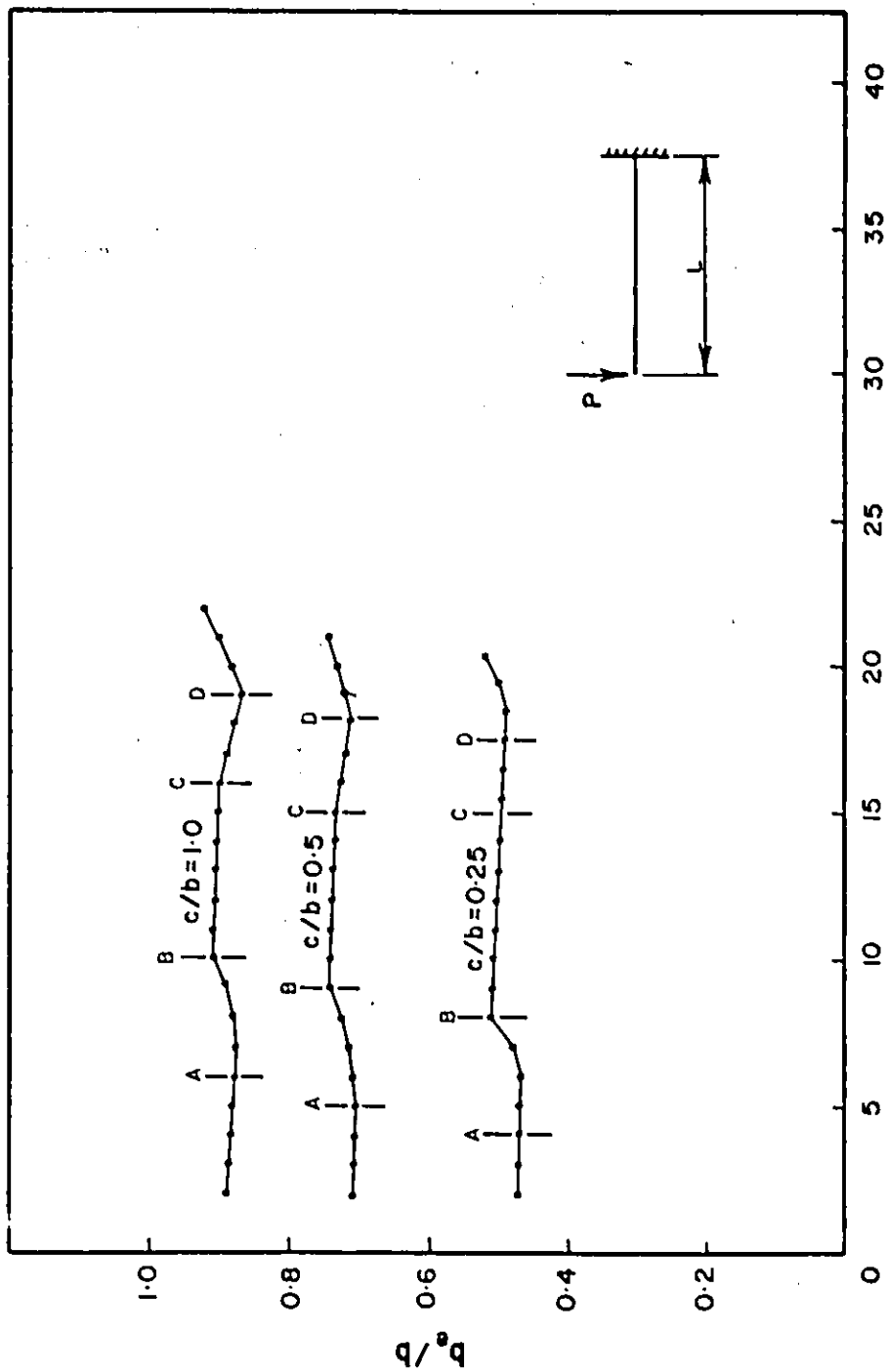
Point C: yielding of the steel beam

Point D: the peak stress in the steel reinforcement reached the elastic limit of the idealized stress-strain relationship.

As the figure shows, a slight increase occurred in the effective slab width after the concrete was completely cracked through the whole depth, point B on the curve, and the effective slab width was calculated from equation (3.35b). A slight decrease in the effective slab width in the elastic region and an increase after the peak stress reached (F_y) of the reinforcing steel occurred in this case similar to that for the positive moment region as described before.

4.4.3 Effect of the Concrete Strength (f'_c) on the Effective Slab Width for Strength in the Positive Moment Region

Since the failure of the analysed composite beams occurred due to



APPLIED LOAD (kips)

FIGURE 4.10 VARIATION OF THE MINIMUM EFFECTIVE SLAB WIDTH FOR STRENGTH WITH THE APPLIED LOAD IN THE NEGATIVE MOMENT REGION FOR $L/b = 2$

crushing of the concrete slab adjacent to the column face, it was important to study the effect of the variation of the concrete strength (f'_c), and consequently the maximum compressive strain (ϵ_{cu}), on the effective slab width for strength.

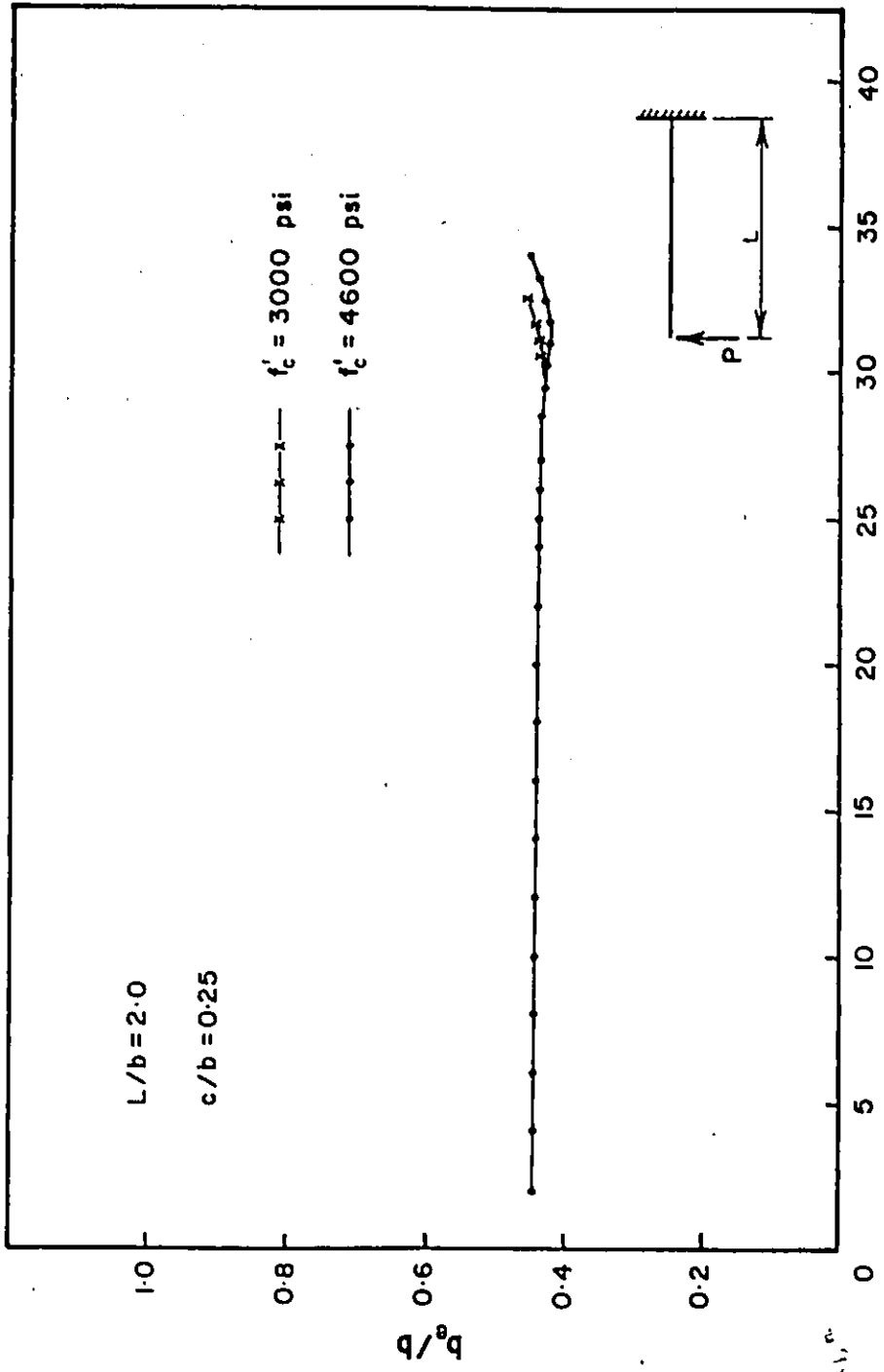
Figure 4.11 shows the variation of the minimum effective slab width for strength, at the column face, with the applied load for two different values of (f'_c), 3000 and 4600 psi, for L/b ratio of 2 and c/b ratio of 0.25.

As can be seen from the figure, the effective slab width was equal for both cases up to the point of reaching the plateau of the idealized stress strain curve, $0.85 f'_c$, of the concrete with the lower strength. The effective slab width started to increase after the peak concrete stress reached the value of $0.85 f'_c$ corresponding to each case. At failure the effective slab width was slightly in excess of the initial one for both cases.

4.4.4 Effect of the Total Slab Thickness, Steel Beam Size and Number of Connectors on the Effective Slab Width for Strength

To study the effect of each of these parameters on the effective slab width for strength, several beams were analysed by the computer. The analysed beams had the same beam length and slab width and consequently the same L/b ratio. The c/b ratio was 0.25 for all the analysed beams.

Three beam sizes were considered; W10x49, W12x27 and W16x40. The total slab thickness was changed from 4 in. (2.5 in. solid part and 1.5



APPLIED LOAD (kips)

FIGURE 4.11 EFFECT OF f'_c ON THE MINIMUM EFFECTIVE SLAB WIDTH FOR STRENGTH

in. ribs) to 5 in. (3.5 in. solid part and 1.5 in. ribs). The number of connectors was changed from nine pairs to nine single 3/4 in. diameter shear connectors.

Table 4.2 shows the dimensions of each beam and the calculated ratio of b_e/b for each case. The ratios of b_e/b given in this table are calculated at the column face, the minimum effective width, for an applied load of 2 kips.

Steel Beam Size	Beam Length (in)	Slab Width (in)	Slab Thickness		Number of connectors	1/c	b_e/b
			Solid part (in)	Total (in)			
W12x27	96	48	2.5	4	18	15.64	.446
W12x27	96	48	2.5	4	9	7.82	.449
W12x27	96	48	3.5	5	18	14.94	.446
W16x40	96	48	2.5	4	18	10.34	.447
W10x49	96	48	2.5	4	18	9.73	.448

Table 4.2: Effect of the Degree of Interaction on the Effective Slab Width for Strength

In order to make the study more feasible, the degree of interaction was considered as the major parameter to be investigated since it includes the three parameters (slab thickness, steel beam size and number of connectors) under consideration. The degree of interaction is represented in terms of the interaction coefficient $1/c$ which is defined as follows⁽¹⁾

$$\frac{1}{c} = \frac{4 \cdot K \cdot L^2 \cdot \overline{EI}}{S \cdot \pi^2 \cdot \overline{EA} \cdot \Sigma EI} \quad (4.2)$$

where

$$\frac{1}{\overline{EA}} = \frac{1}{E_c A_c} + \frac{1}{E_s A_s}$$

$$\Sigma EI = E_c I_c + E_s I_s$$

$$\overline{EI} = \Sigma EI + \overline{EA} \cdot z^2$$

A_s, A_c cross-sectional area of the beam and the slab respectively

E_s, E_c moduli of elasticity of the beam and slab respectively

I_s, I_c moments of inertia of the beam and slab respectively

K modulus of shear connectors

L Span length of the composite cantilever beam

s average spacing between shear connectors

z distance between the centroidal axes of the slab and the beam.

The values of the factor $1/c$ corresponding to each of the analysed beams are given in Table 4.2. It can be concluded from the results given in this table that the effective slab width for strength slightly decreases with the increase of the degree of interaction. A similar conclusion was reported by Adekola⁽⁵⁵⁾ for the case of simple composite beams with partial interaction. However, the decrease in the effective slab width with the increase of the degree of interaction is very small, as shown in Table 4.2, and may be neglected for all practical purposes and consequently the effective slab width for strength could be considered as independent of the slab thickness, steel beam size and number of connectors.

4.4.5 Effect of the Slab Length to Width Ratio (L/b) and Column Face Width to Slab Width Ratio c/b on the Effective Width

In this section the effect of L/b and c/b ratios on the effective width ratio b_e/b is investigated. Since the results presented in section 4.4.2 showed that the effective slab width varies slightly with the applied load and that the effective slab width at failure is slightly larger than that in the elastic range, the initial elastic effective slab width for strength is considered in the analysis to represent the effective slab width in both the elastic and plastic ranges. For the negative moment region, the effective slab width when the concrete is fully cracked across its depth, point B in Figure 4.10, is considered to represent the effective slab width in this case.

Several beams were analysed by the computer to cover a wide range of L/b and c/b ratios. All the analysed beams consisted of a W12x27 steel beam and a 4 in. thick ribbed concrete slab. The beams had the same slab width (4 ft.) and the same number of connectors (nine pairs of 3/4 inch diameter stud shear connectors). The span of the beam was changed so that the L/b ratio ranged from 1 to 6 and the column face width was changed so that the c/b ratio ranged from 0.1 to 1. For the negative moment region top reinforcement was placed in the concrete slab at 1/2 in. from the top surface. The percentage of the reinforcement was about 0.8% and was distributed uniformly across the slab width. The steel bars in front of the column face were assumed to be welded to the column so that they could transmit a tensile force to the column. It should be mentioned here that the reinforcing bars outside the column

face were assumed to be extended beyond the column to simulate region 3, Figure 1.2, and that region 4, Figure 1.2, where the steel reinforcement can not be extended beyond the column was not considered in the present analysis. The current practice is to consider only the steel beam in resisting the negative moment in region 4. However, an experimental investigation by Ansourian and Roderick⁽⁶⁹⁾ showed that if the steel bars are arranged so that a sufficient development length exists beyond the column face, effective composite action may be said to exist in region 4. In this case the results presented in this section may be also applicable in region 4.

Figures 4.12 and 4.13 show the variation of the effective width ratio (b_e/b) at the column face for the positive and negative moment regions respectively. These two figures show that for the same c/b ratio, the minimum effective slab width for strength increases with increasing L/b ratio. A similar conclusion was reported by Adekola⁽¹⁸⁾ for the case of simple composite beams, c/b equal 1, with complete interaction. For the same L/b ratio, the effective slab width ratio (b_e/b) increases with the increase in c/b ratio.

4.5 Average Effective Slab Width for Stiffness (b_{av})

The average effective slab width for stiffness is defined, Chapter 3, as the uniform slab width to be considered in composite action with the steel beam so that the calculated deflection using the transformed section will be equal to the deflection of the actual beam with the variable effective slab width along its span. For the positive

b = TOTAL WIDTH

b_e = EFFECTIVE WIDTH

c = COLUMN WIDTH

L = SPAN

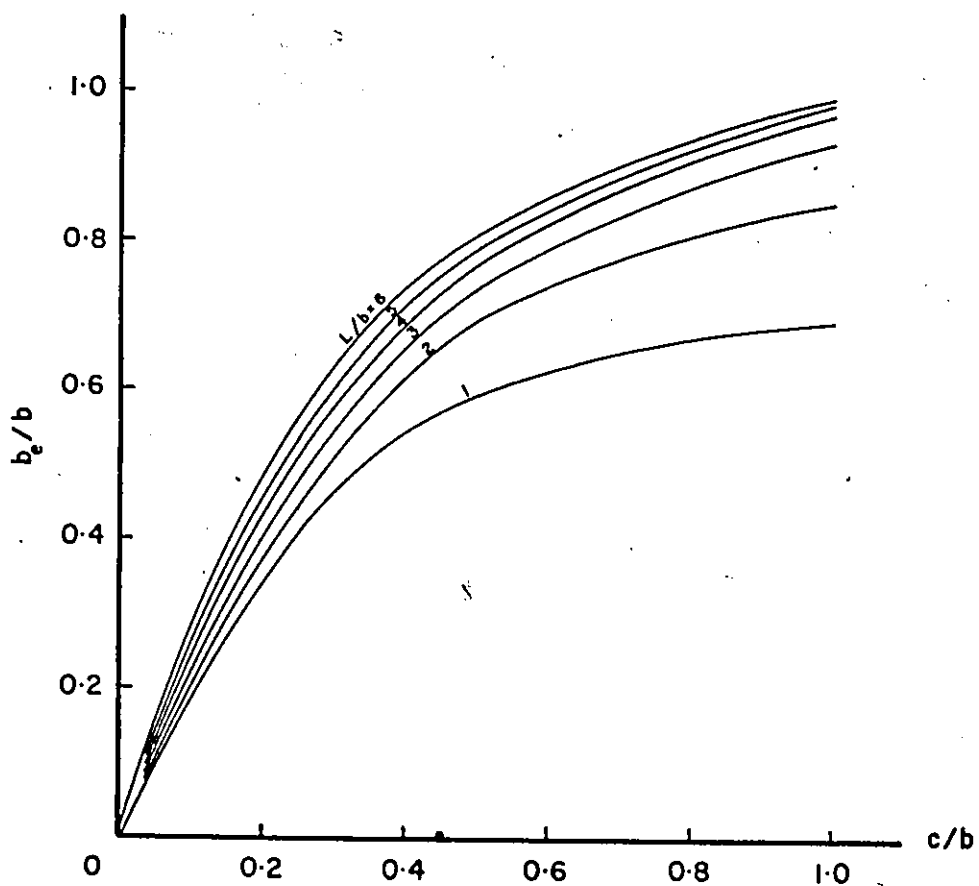
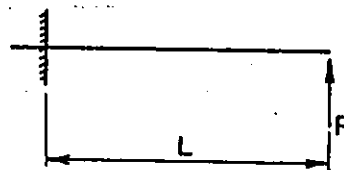


FIGURE 4.12 VARIATION OF THE MINIMUM EFFECTIVE SLAB WIDTH FOR STRENGTH WITH (L/b) AND (c/b) RATIOS IN THE POSITIVE MOMENT REGION

b = TOTAL WIDTH
 b_e = EFFECTIVE WIDTH
 c = COLUMN WIDTH
 L = SPAN

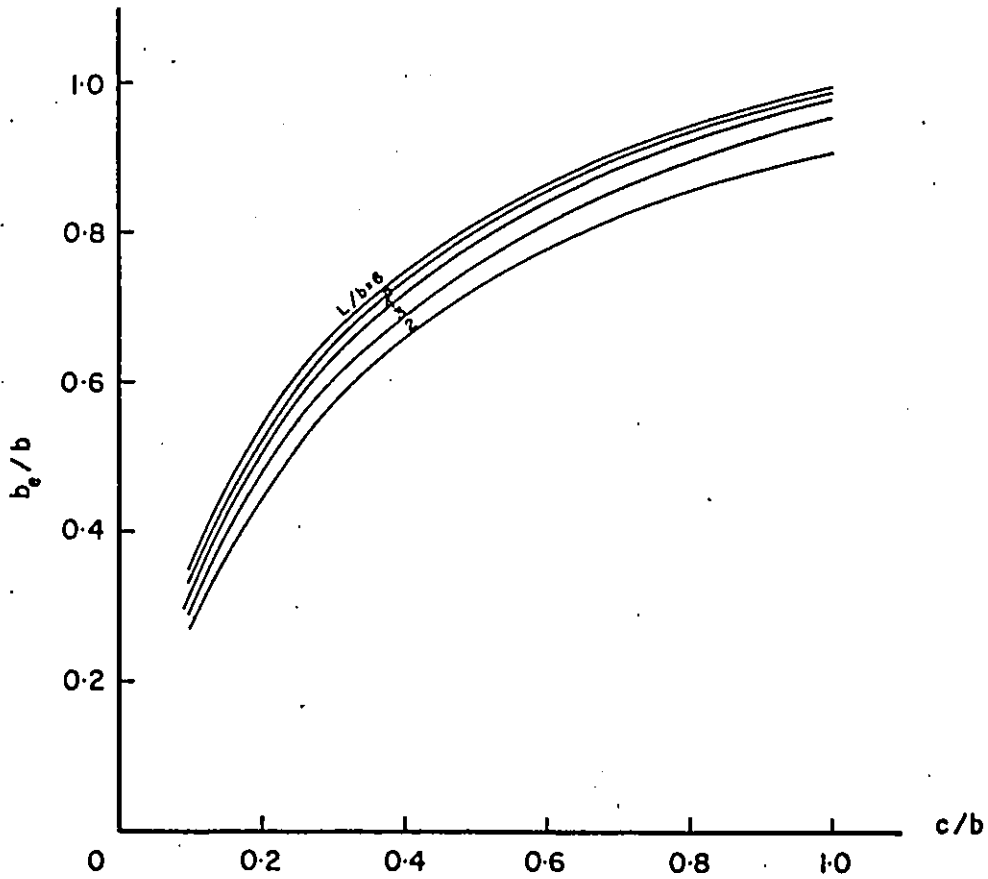
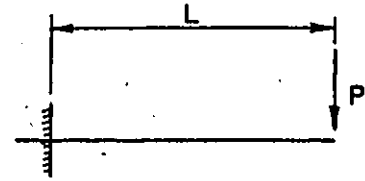


FIGURE 4.13 VARIATION OF THE MINIMUM EFFECTIVE SLAB WIDTH FOR STRENGTH WITH (L/b) AND (c/b) RATIOS IN THE NEGATIVE MOMENT REGION

moment region the transformed section consists of the steel beam and a concrete slab having the average effective slab width (b_{av}). For the negative moment region the transformed section consists of the steel beam and the slab reinforcement, if it exists, within the average effective slab width.

The average effective slab width for stiffness was evaluated for some of the analysed beams described in section 4.4 in the elastic range using the cantilever beam deflection formula, equation (3.39), and the relation between the moment of inertia of the transformed section and the effective slab width given in equation (3.38). The computed deflection, from the computer analysis, was substituted in equation (3.39) and the average moment of inertia (I_{av}) was calculated and was substituted into equation (3.38) to obtain the average effective slab width for stiffness for each beam. The results are given in Table 4.3. The results given in this table show that for the same L/b and c/b ratios, the average effective slab width for stiffness varies with the variation in the steel beam size, total slab thickness and number of connectors or in other words, it varies with the variation in the degree of interaction.

For the case of complete interaction when no slip occurs at the interface between the concrete slab and the steel beam, the flexural stiffness at any section ($E_s I_{eff}$) in the positive moment region is given by

$$E_s I_{eff} = E_s I_s + E_c I_c + \frac{E_s A_s E_c (t.b_e)}{E_s A_s + E_c . t.b_e} z^2$$

Steel Beam Size	Slab thickness (in)	% of slab Reinforcement	o/b	L/b	Number of connectors	Computer Results			Computed Results from Eqn. 4.6			
						I_{av}	b_{av}/b	F^*	F/F	I_{av}	b_{av}/b	F^*
W12x27	4	-	0.25	2	36	470	.51	10.60	.850	466	0.50	10.85
W12x27	4	-	0.50	2	36	492	.59	11.21	.842	491	0.58	11.34
W12x27	4	-	1.00	2	36	505	.63	11.52	.840	504	0.63	11.54
W16x40	4	-	0.25	2	36	985	.50	7.12	.814	980	0.49	7.36
W10x49	4	-	0.25	2	36	535	.50	10.10	.810	530	0.49	10.49
W12x27	4	-	0.25	2	18	444	.43	9.94	.780	438	0.42	10.10
W12x27	5	-	0.25	2	18	494	.34	10.33	.781	492	.34	10.55
W12x27	4	-	0.25	3	18	481	.54	16.10	.820	475	0.52	16.10
W12x27	4	-	0.50	3	18	495	.59	16.70	.816	489	0.58	16.53
W12x27	4	-	1.00	3	18	503	.63	17.00	.814	498	0.61	16.80
W12x27	4	-	0.50	3	36	519	.69	17.60	.870	515	0.68	17.60
W12x27	4	0.8	0.25	3	9	295	.72	23.97	.815	291	0.70	24.40
W12x27	4	0.8	0.50	3	9	309	.84	26.88	.807	304	0.81	26.90
W12x27	4	0.8	1.00	3	9	312	.88	37.80	.803	309	0.86	37.50

Table 4.3: Average Effective Slab Width for Stiffness (b_{av})

* Value of the interaction force at the column face

The second term on the right hand side of this expression is the contribution due to plate bending whilst the third term represents the contribution due to the interaction force. I_c , the moment of inertia of the slab, is based on the effective width for bending moment (b_{em}), Section 3.6, which is different from (b_e). However, for composite beams with ribbed metal deck the term $E_c I_c$ is very small compared to the other terms and can be neglected for all practical cases. Based on this approximation the effective slab width for the stiffness at a section (b_{es}) for the case of complete interaction is approximately equal to the effective slab width for strength (b_e) at the same section. The same approximation applies in the negative moment region. Thus, for complete interaction the transformed section at any point along the composite beam is considered to consist of the steel beam and a concrete slab having width equal to (b_e) in the positive moment region whilst it consists of the steel beam and the slab reinforcement, if it exists, within the effective slab width (b_e) for the negative moment region.

The deflection of the composite beam, which is of variable moment of inertia, can be computed by double integrating the curvature along the span. Thus,

$$\Delta_c = \int \int \frac{M}{L E_s I_{eff}} dx dx \quad (4.3)$$

in which

I_{eff} the moment of inertia of the transformed section

M the applied external moment on the section

Δ_c the deflection of the composite beam with complete

interaction

The average moment of inertia (I_{av}) and consequently the average effective slab width for stiffness (b_{av}) can be found by substituting the value of Δ_c into equation (3.39).

Since the average effective slab width for stiffness (b_{av}) in the case of complete interaction depends on the effective slab width for strength (b_e) and its distribution along the span, which in turn was shown, Section 4.4, to be dependent on the L/b and c/b ratio, the average effective slab width for stiffness (b_{av}) will also be dependent on these two ratios. Figures 4.14 and 4.15 show the variation of (b_{av}) for the case of complete interaction with the variation of L/b and c/b ratios for the positive and negative moment regions respectively.

A composite beam with complete interaction between the concrete slab and the steel beam is a hypothetical one. In actual practice, however, all composite members do suffer some loss of interaction due to the slip which occurs at the interface between the concrete slab and the steel beam. The general equation for deflection of the composite beam with incomplete interaction is⁽¹⁾

$$\Delta_t = \Delta_c + \frac{ML^2}{EI} \cdot \frac{c}{\pi^2} \frac{\overline{EA} \cdot z^2}{\Sigma EI} \cdot \frac{F}{F'} \quad (4.4)$$

where Δ_t is the deflection of the composite beam with incomplete interaction

Δ_c is the deflection of the composite beam with complete interaction

F/F' in the ratio of the interaction force in the case of

b = TOTAL WIDTH

b_{ov} = AVERAGE EFFECTIVE WIDTH

c = COLUMN WIDTH

L = SPAN

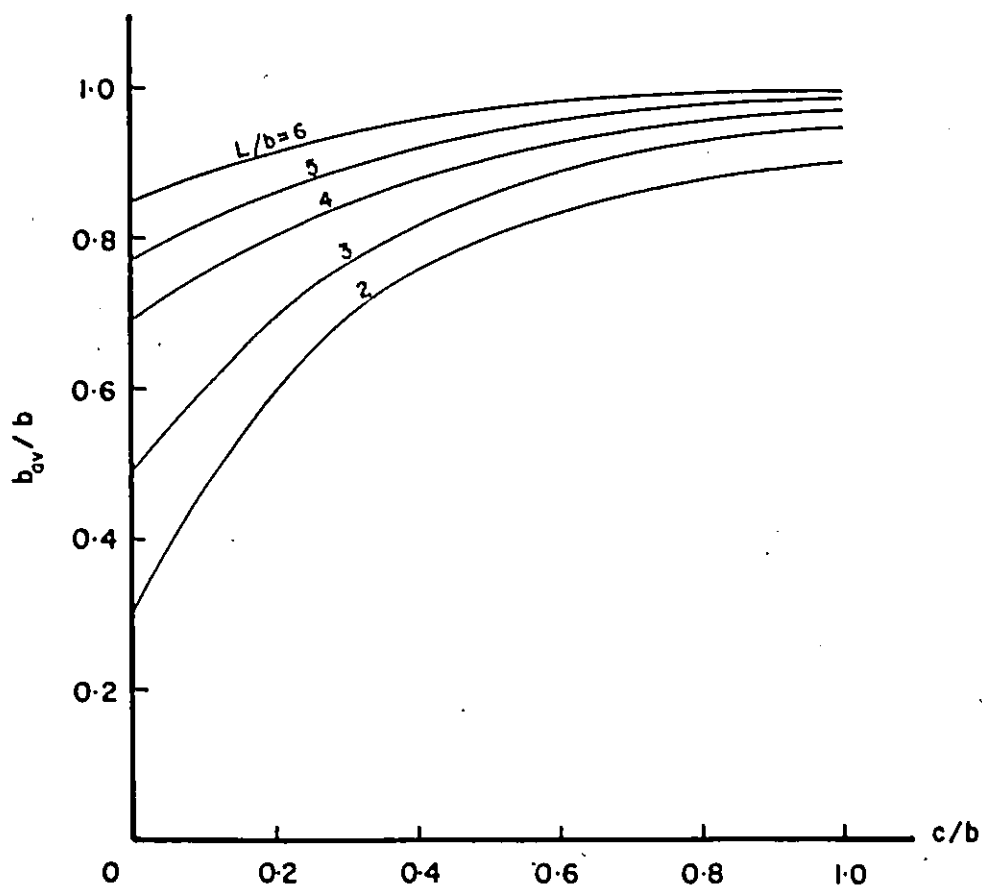
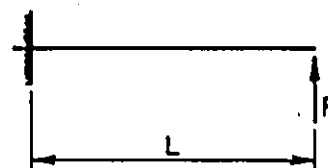


FIGURE 4.14 VARIATION OF THE AVERAGE EFFECTIVE SLAB WIDTH FOR STIFFNESS WITH (L/b) AND (c/b) RATIOS IN THE POSITIVE MOMENT REGION

b = TOTAL WIDTH

b_{ov} = AVERAGE EFFECTIVE WIDTH

c = COLUMN WIDTH

L = SPAN

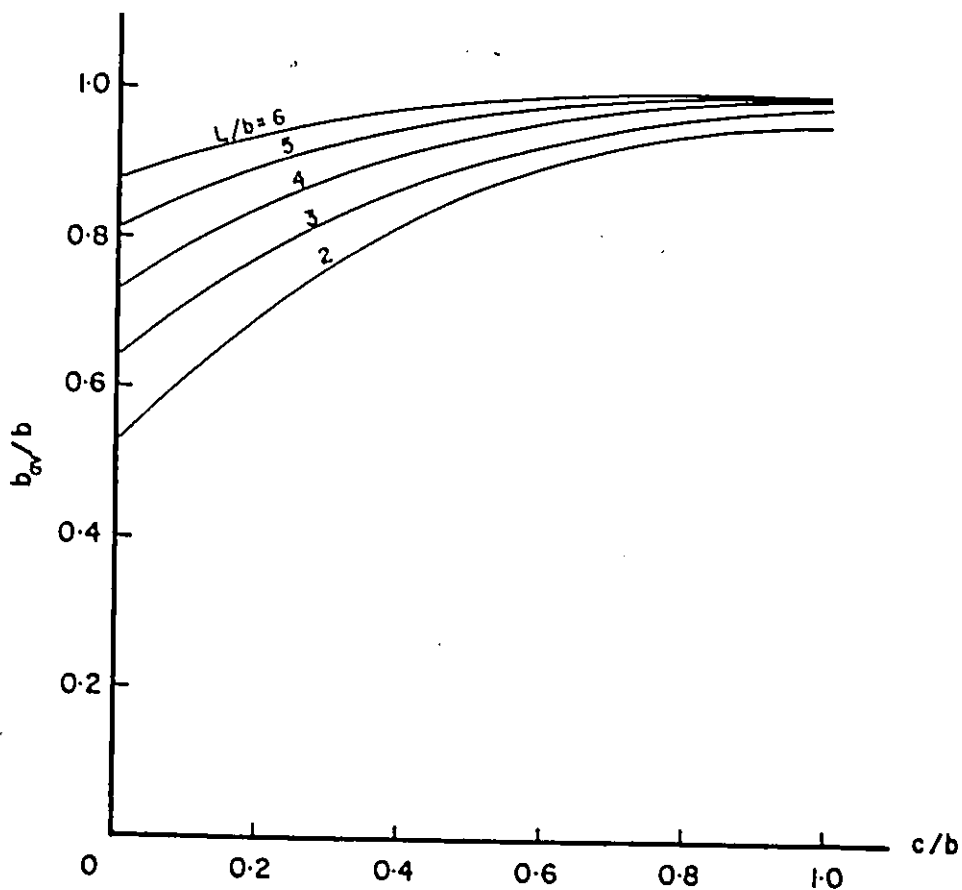
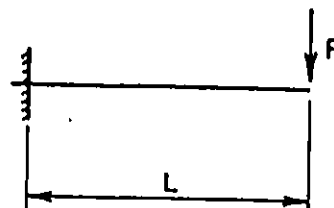


FIGURE 4.15 VARIATION OF THE AVERAGE EFFECTIVE SLAB WIDTH FOR STIFFNESS WITH (L/b) AND (c/b) RATIOS IN THE NEGATIVE MOMENT REGION

incomplete to that in the case of complete interaction at the section of the maximum moment (at the column face in this case).

The rest of the terms in equation (4.4) were defined before with equation (4.2). The value of F/F' for the load case under consideration is given by⁽¹⁾

$$\frac{F}{F'} = 1 - \frac{4\sqrt{c}}{\pi} \cdot \frac{\sinh^2(\pi/2\sqrt{c})}{\sinh(\pi/\sqrt{c})} \quad (4.5)$$

Equation (4.4) and (4.5) were derived for a composite beam with a constant slab width and consequently for a constant value of \overline{EA} , \overline{EI} and \overline{EI} along the beam. The average effective slab width for stiffness (b_{av}) in the case of complete interaction is considered in the following analysis to represent this uniform slab width along the beam.

Equation (4.4) can be written as

$$\Delta_t = \left(1 + 12 \frac{c}{\pi^2} \cdot \frac{\overline{EA} \cdot z^2}{\overline{EI}} \cdot \frac{F}{F'}\right) \Delta_c$$

or

$$\Delta_t = c_d \Delta_c \quad (4.6)$$

in which c_d is a dimensionless coefficient given by

$$c_d = 1 + 12 \frac{c}{\pi^2} \cdot \frac{\overline{EA} \cdot z^2}{\overline{EI}} \cdot \frac{F}{F'}$$

Thus, the average moment of inertia for the case of incomplete interaction (I_{av})_i can be written as

$$(I_{av})_i = \frac{(I_{av})_c}{c_d} \quad (4.7)$$

where $(I_{av})_i$ and $(I_{av})_c$ are the average moments of inertia in the case of incomplete and complete interaction respectively.

Equation (4.7) shows that the average moment of inertia and consequently the average effective slab width for stiffness in the case of incomplete interaction depends on the degree of interaction since the coefficient c_d depends on it. The coefficient c_d decreases and consequently $(I_{av})_i$ increases with the increase in the degree of interaction.

The degree of interaction and the average moment of inertia were calculated for each of the analysed beams using equation (4.7) and the results are shown in Table 4.3. The results given in this table show that the average effective slab width for stiffness (b_{av}) computed from equation (4.7) was very close to that obtained from the computer analysis which takes account of the incomplete interaction.

4.6 Effective Slab Width for Stiffness at any Section of the Composite Beam (b_{es})

The effective slab width for stiffness at any section (b_{es}) is defined, Chapter 3, as the slab width to be used with the steel beam so that the calculated curvature of the transformed section is equal to the actual curvature of the composite beam at that particular section. The definition of (b_{es}) was introduced in the present analysis to facilitate the calculation of the curvature of the composite beam and the strain

and stress distributions across the beam depth in the elastic range.

Since the curvature and stress distribution at the composite section adjacent to the column face are of main importance, the analytical investigation was concentrated on the value of (b_{es}) at that particular section of the composite beam.

The effective moment of inertia of the composite beam (I_{eff}) at the column face was calculated from each of the analysed beams described in section (4.4) using equation (3.37) and the effective slab width for stiffness at that section (b_{es}) was obtained from equation (3.38) by substituting the value of (I_{eff}) for each beam. The obtained results are given in Table 4.4. The results given in this table show that (b_{es}) varies with the variation in L/b and c/b ratios and that for the same L/b and c/b ratio the value of (b_{es}) varies with the variation in the steel beam size, total slab thickness and the number of connectors.

For the case of complete interaction where no slip occurs between the concrete slab and the steel beam, the effective slab width for stiffness (b_{es}) was shown in the previous section, Section 4.5, to be approximately equal to the effective slab width for strength (b_e) at that section. For the practical cases, where slip occurs between the slab and the steel beam, a reduction in the moment of inertia of the composite section and consequently in the value of (b_{es}) occurs.

Since the curvature of the steel beam is equal to the curvature of the composite beam at any section,

Steel Beam Size	Slab thickness (in)	% of slab Reinforcement	a/b	L/b	Number of connectors	Computer Results		Computed Results from Eqn. 4.10		
						l_{eff}	b_{es}/b	F/P	l_{eff}	b_{es}/b
W12x27	4	-	0.25	2	36	414	0.35	0.919	409	0.34
W12x27	4	-	0.50	2	36	432	0.39	0.875	454	0.40
W12x27	4	-	1.00	2	36	448	0.44	0.849	446	0.43
W16x40	4	-	0.25	2	36	871	0.34	0.917	865	0.33
W10x49	4	-	0.25	2	36	469	0.34	0.917	460	0.33
W12x27	4	-	0.25	2	18	382	0.26	0.849	379	0.25
W12x27	5	-	0.25	2	18	417	0.22	0.830	420	0.22
W12x27	4	-	0.25	3	18	420	0.36	0.895	417	0.35
W12x27	4	-	0.50	3	18	437	0.42	0.839	435	0.41
W12x27	4	-	1.00	3	18	447	0.44	0.820	444	0.43
W12x27	4	-	0.50	3	36	463	0.49	0.894	455	0.47
W12x27	4	0.8	0.25	3	9	273	0.53	0.990	272	0.53
W12x27	4	0.8	0.25	3	9	285	0.63	0.871	283	0.62
W12x27	4	0.8	1.00	3	9	292	0.7	0.817	286	0.66

Table 4.4: Effective Slab Width for Stiffness (b_{es}) at the Section of Maximum Moment

$$\frac{(M_s)_c}{E_s I_s} = \frac{M}{E_s (I_{eff})_c} \quad (\text{for complete interaction})$$

and

$$\frac{(M_s)_i}{E_s I_s} = \frac{M}{E_s (I_{eff})_i} \quad (\text{for incomplete interaction})$$

where

$(I_{eff})_c$ and $(I_{eff})_i$ are the moment of inertia of the transformed section for complete and incomplete interaction respectively.

$(M_s)_c$ and $(M_s)_i$ are the moment carried by the steel beam alone in the case of complete and incomplete interaction respectively.

M is the applied external moment on the section.

From these two equations the effective moment of inertia in the case of incomplete interaction can be expressed as

$$(I_{eff})_i = \frac{(M_s)_c}{(M_s)_i} \cdot (I_{eff})_c \quad (4.8)$$

The moment carried by the steel beam (M_s) may be expressed in terms of the external moment (M) , the interaction force (F) and the moment carried by the slab (M_c) as

$$M_s = M - M_c - F.z$$

However, M_c for the case of composite steel and concrete slab is usually very small compared to the other terms, about 1.2% of the total moment

for the case of L/b equal 3 and c/b equal 1, and may be neglected to simplify the calculation. Thus, equation (4.8) can be written as

$$(I_{\text{eff}})_i = \frac{M - F' \cdot z}{M - F \cdot z} \cdot (I_{\text{eff}})_c \quad (4.9)$$

where F' and F are the interaction forces in the case of complete and incomplete interaction respectively.

Since F' at any section is given by

$$F' = \frac{\overline{EA} \cdot z}{EI} \cdot M$$

Thus, equation (4.9) may be written as

$$(I_{\text{eff}})_i = \frac{\{\overline{EI}/(\overline{EA} \cdot z)\} - z}{\{\overline{EI}/(\overline{EA} \cdot z)\} - (F/F') \cdot z} (I_{\text{eff}})_c$$

or

$$(I_{\text{eff}})_i = C_s \cdot (I_{\text{eff}})_c \quad (4.10)$$

in which

$$C_s = \frac{\{\overline{EI}/(\overline{EA} \cdot z)\} - z}{\{\overline{EI}/(\overline{EA} \cdot z)\} - (F/F') \cdot z} \quad (4.11)$$

Equation (4.10) can be used to determine the effective slab width for stiffness at any section for the case of incomplete interaction by substituting the values of \overline{EA} , \overline{EI} , F/F' , z and $(I_{\text{eff}})_c$ at the particular section.

The value of (F/F') at the position of the maximum moment was solved before⁽¹⁾ for a similar load condition for the case of a composite beam with constant slab width as given in equation (4.5).

Since the effective slab width (b_e) and consequently (\overline{EA}) and (\overline{EI}) are variable along the beam length, the solution given in equation (4.5) will be inappropriate for this case. Presenting a solution for (F/F') at the column face for this complicated case was discarded in favour of using the simple equation (4.5) assuming a uniform slab width equal to $(b_{av})_c$, as discussed in section 4.5, together with a correction factor (α) which reflects the effect of the variation in the effective slab width. It was found from the analysis that the computed value of the interaction force (F) at the column face on the basis of the average effective slab width for stiffness $(b_{av})_c$ is very close to the value obtained from the computer analysis, which accounts for the variation in the slab width, as given in Table 4.3. Thus the value of (F) at the column face may be written as

$$F = \left(\frac{F}{F'}\right)_{av} \cdot \frac{(\overline{EA})_{av} \cdot z}{(\overline{EI})_{av}} \cdot M$$

where in this equation (F/F') _{av}, $(\overline{EA})_{av}$ and $(\overline{EI})_{av}$ are calculated on the basis of the average effective slab width for stiffness (b_{av}) . The interaction force at the column face in the case of complete interaction is given by

$$F' = \frac{\overline{EA} \cdot z}{\overline{EI}} \cdot M$$

where \overline{EA} and \overline{EI} are calculated on the basis of the minimum effective slab width (b_e). Thus,

$$\left(\frac{F}{F'}\right)_{\text{at the column face}} = \left(\frac{F}{F'}\right)_{\text{av}} \cdot \frac{\overline{EA}_{\text{av}} \cdot \overline{EI}}{(\overline{EI})_{\text{av}} \cdot (\overline{EA})}$$

or

$$\left(\frac{F}{F'}\right)_{\text{correct}} = \alpha \left(\frac{F}{F'}\right)_{\text{av}}$$

where

$$\alpha = \frac{(\overline{EA})_{\text{av}} \cdot (\overline{EI})}{(\overline{EI})_{\text{av}} \cdot (\overline{EA})}$$

Thus the factor C_s in equation (4.11) can be written as

$$C_s = \frac{\{\overline{EI}/(\overline{EA} \cdot z)\} - z}{\{\overline{EI}/(\overline{EA} \cdot z)\} - \alpha(F/F')_{\text{av}} \cdot z} \quad (4.12)$$

The effective moment of inertia (I_{eff}) and consequently the effective slab width for stiffness (b_{es}) at the column face was calculated for each of the analysed beams using equation (4.10) and the results are given in Table 4.4. As shown in this table the calculated results were very close to those obtained from the computer analysis which accounts for incomplete interaction.

4.7 A Method for Elastic Analysis of Composite Beams

Based on the results presented in this chapter, the following method can be used for elastic analysis of composite beams, simple or as a part of a multi-story frame, to determine the curvature and stress distribution at the section of maximum moment and the deflection of the

beam. The method described in this section does not require computer facilities and is suitable for hand calculation. The method is described in the following steps:

1. Form the geometric properties of the beam the ratios of L/b and c/b are determined. For the case of a simple beam (L) is half the span of the beam while for composite beams in a multi-story frame (L) is the distance from the point of contraflexure to the column face.
2. From a knowledge of L/b and c/b ratios the effective slab width for strength (b_e) and the average effective slab width for complete interaction (b_{av}) can be determined from Figures 4.12, 4.13, 4.14 and 4.15 for the positive and negative moment regions respectively.
3. For the value of (b_{av}) the values $(\overline{EA})_{av}$, $(\overline{EI})_{av}$ and hence the value of $1/c$ and $(F/F')_{av}$ are computed (equations (4.2) and (4.5)).
4. The coefficients c_d and c_s are computed for the computed value of (F/F') and the average moment of inertia (I_{av}) and the effective moment of inertia (I_{eff}) at the section under consideration are determined from equations (4.7) and (4.10). From the calculated (I_{eff}) the value of (b_{es}) and the distance from the centroidal axis to the bottom fibre of the steel beam (y_b) are determined.
5. The curvature (ϕ) of the composite section is given by

$$\phi = \frac{M}{E_s (I_{eff})}$$

The bottom fibre steel strain (ϵ_{sb}) and the top fibre steel strain (ϵ_{st}) are given by

$$\epsilon_{sb} = \frac{M \cdot y_b}{E_s I_{eff}}$$

and

$$\epsilon_{st} = \epsilon_{sb} - \phi d$$

in which d is the depth of the steel beam.

The interaction force (F) can be calculated from the steel strain as

$$F = \frac{(\epsilon_{sb} - \epsilon_{st})}{2} \cdot E_s \cdot A_s$$

hence, the top and bottom fibre concrete strains, ϵ_{ct} and ϵ_{cb} , are determined as follows

$$\epsilon_{ct} = \frac{F}{E_c (b_e \cdot t_s)} + \phi \cdot \frac{t_s}{2}$$

$$\epsilon_{cb} = \frac{F}{E_c (b_e \cdot t_s)} - \phi \cdot \frac{t_s}{2}$$

This method was used to analyse the experimental beams at the working load level and the results of this analysis are presented in Chapter 7.

4.8 Discussion of the Effective Slab Width Formula for Simple Composite Beams in the Different Codes

The analytical effective slab widths for the case of simple composite beams are compared in this section with the formula provided in the different codes.

According to the current Canadian Standard S16.1, the effective slab width for simply supported composite beams is determined by the lesser of the following limitations

$$b_e \leq 16 t_s + b_o$$

$$b_e \leq L/4$$

$$b_e \leq b$$

where

b is the spacing between the composite beams

b_e effective slab width

b_o the width of the steel beam flange

L the span of the beam

t_s thickness of the slab

For the practical case where the spacing between the composite beams (b) is about 5 ft. and the slab thickness is 4 in., 2.5 in. solid part and 1.5 in. ribs, the first limitation will be greater than the third one. Thus either the second or third limitation will define the effective slab width. Based on these two limitations the effective slab width will be equal to $L/4$ up to a value of (L/b) equal to 4 and after that it will be equal to the total width (b). The variation of the effective slab width with (L/b) based on these two limitation is shown in Figure

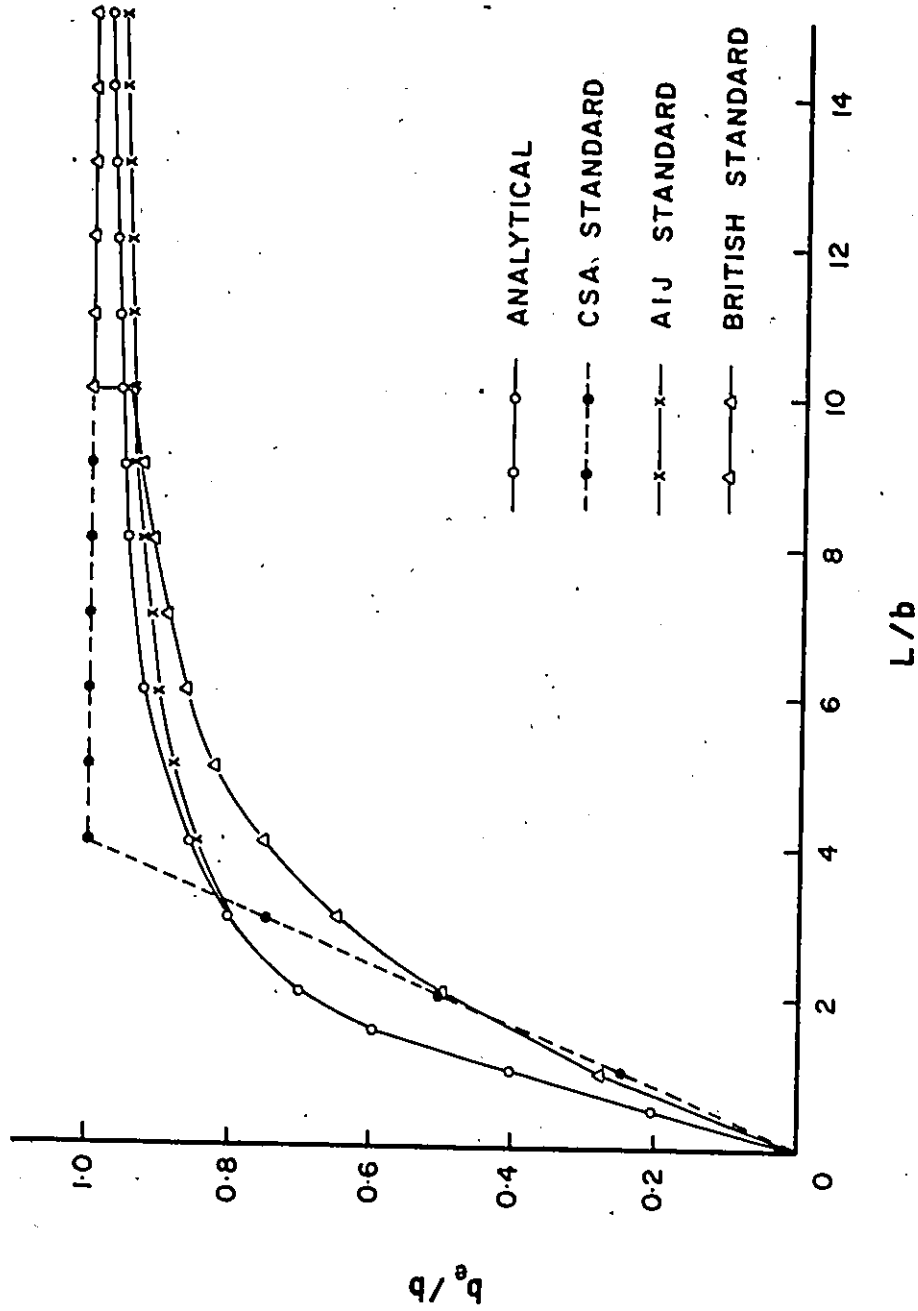


FIGURE 4.16 COMPARISON BETWEEN THE ANALYTICAL EFFECTIVE SLAB WIDTH FOR STRENGTH AND THE DIFFERENT CODE FORMULAE

4.16. Also presented in this figure is the variation of the analytical effective slab width for strength with (L/b) for the case of simple composite beam subjected to central point load. Although no direct relation between the effective slab width (b_e) and the span to width ratio (L/b) is given in the CSA limitation, the effective slab width obtained from these limitations depends on the (L/b) ratio as shown in Figure 4.16. A comparison between the variation of the analytical effective slab width with (L/b) ratio and the CSA limitations, Figure 4.16, shows that the code limitations are conservative for all (L/b) ratios less than 3 and for greater values of (L/b) the CSA limitations are unconservative.

According to the British Standard Code of Practice [CP 117, Part 2 (Beams for Bridges), 1967], the effective slab width is given as a function of the (L/b) ratio in two limitations

1.
$$b_e = \left\{ \frac{1}{\sqrt{1 + 12 (b/L)^2}} \right\} b \quad \text{for } L/b < 10$$
2.
$$b_e = b \quad \text{for } L/b > 10$$

The effective slab width based on these two limitations is shown in Figure 4.16. The figure shows that the curve representing the variation of the effective slab width with (L/b) ratio based on the British Standards is almost of the same shape as that obtained analytically but on the conservative side up to (L/b) equal 10. After that value it is unconservative but close to the analytical values.

Also presented in Figure 4.16 is the variation of the effective slab width with the (L/b) ratio based on the AIJ Specification⁽⁶⁵⁾ which

limits the effective slab width on each side of the composite beam (b_e') as

$$\begin{aligned} b_e' &= (0.5 - 0.3 b/L) b && \text{for } b < L \\ b_e' &= 0.2 b && \text{for } b \geq L \end{aligned}$$

A very good agreement occurs between the analytical effective slab width and that obtained based on the AIJ Specification as shown in Figure 4.16.

The above discussion shows that for the purpose of stress calculation, the AIJ specification⁽⁶⁵⁾ provides a very good estimation for effective slab width for all (L/b) ratios while the CSA standards⁽⁶²⁾ provides unconservative effective slab width for (L/b) ratio greater than 3.

Since the analytical investigation showed that another effective slab width is required for the calculation of the composite beam deformation, defined as the average effective slab width for stiffness (b_{av}), and that this width was different from that one for strength (b_e), a comparison between the average effective slab width for stiffness (b_{av}) and the provisions of the different standards was required. This comparison is presented in Figure 4.17. The Figure shows that all standards are conservative for values for (L/b) less than 4 and that the AIJ limitation is the closest one to the analytical values up to L/b equal to 3. For (L/b) greater than 4, the CSA standard provides a good estimation for the average effective slab width for stiffness. The AIJ and the British standards are more conservative than the CSA standard for (L/b) ratio greater than 4 with respect to the average effective

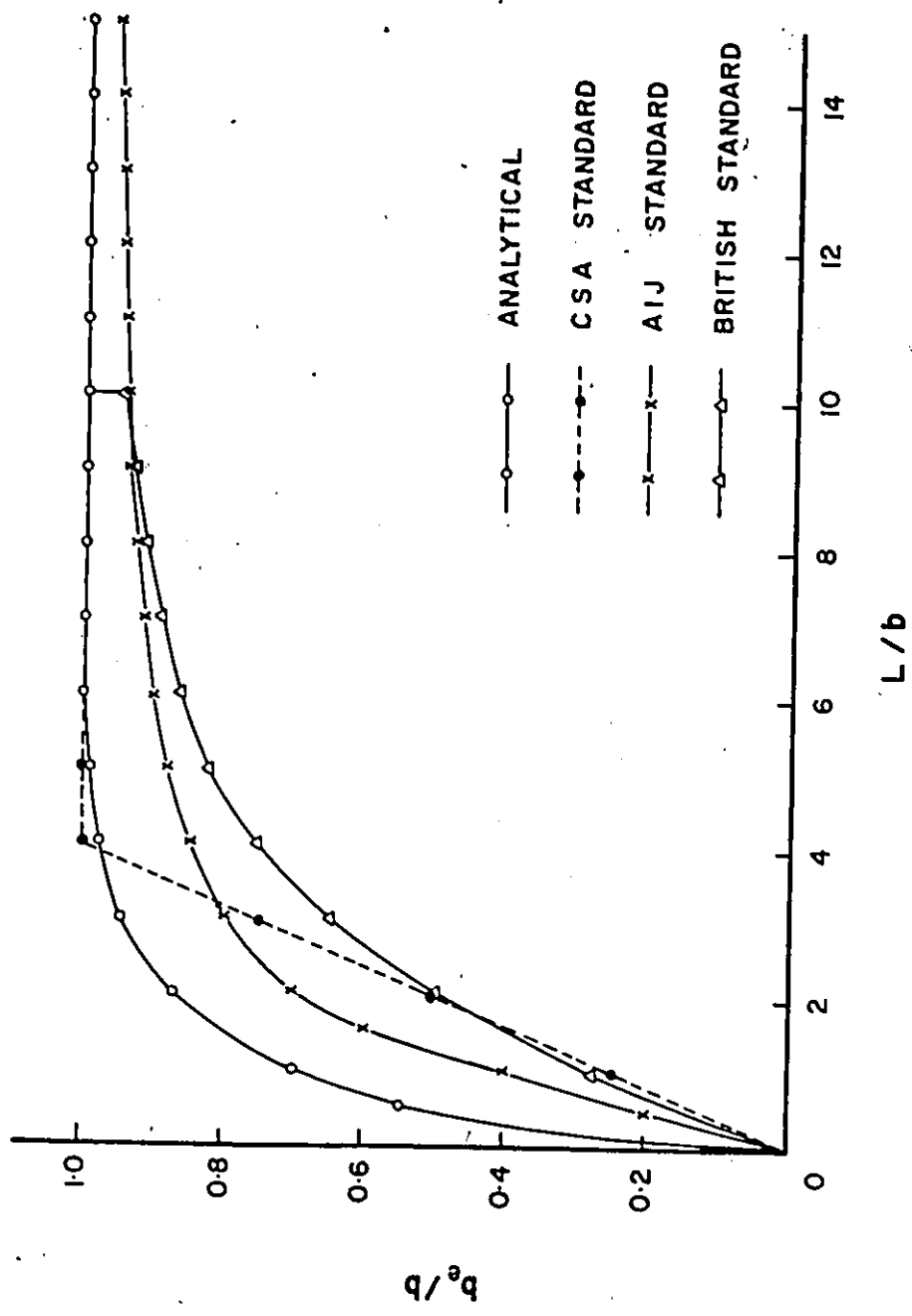


FIGURE 4.17 COMPARISON BETWEEN THE ANALYTICAL EFFECTIVE SLAB WIDTH FOR STIFFNESS AND THE DIFFERENT CODE FORMULAE

slab width for stiffness.

4.9 Summary

This chapter contains the results of the analytical study of the effective slab widths. Three definitions for the effective slab width are introduced in this chapter namely the effective slab width for strength (b_e), the effective slab width for stiffness (b_{es}) and the average effective slab width for stiffness (b_{av}).

The analytical study of the effective slab width for strength (b_e), Section 4.4, showed that this effective slab width varies along the span of the beam with the minimum effective width occurring at the section of the maximum moment. It was also shown that a slight variation occurs in the effective slab width for strength with the variation in the applied load. However, for practical consideration the initial elastic effective slab width is considered to represent the effective slab width at any load level in the positive moment region and the effective slab width when the concrete slab width is completely cracked through the whole depth to represent the effective slab width for strength in the negative moment region. The analysis showed also that the effective slab width for strength depends mainly on the slab length to width ratio (L/b) and the column width to slab width ratio (c/b) and it may be considered as independent of the slab thickness, steel beam size and number of connectors.

Design curves relating the effective slab width ratio b_e/b to the two major parameter (L/b) and (c/b) are presented in this chapter for

the positive and negative moment regions.

The strength of the composite section in the positive moment region is to be based on the steel beam and a concrete slab having the effective slab width for strength (b_e) whilst in the negative moment region the strength is to be based on the steel beam and the slab reinforcement, if it exists, within the effective slab width (b_e).

A definition for the effective slab width for stiffness at the section of the maximum moment (b_{es}) was introduced to facilitate the computation of the curvature and the stress and strain distribution at that section in the elastic range using the transformed section method. The analytical study showed that for the case of complete interaction the effective slab width for stiffness (b_{es}) is approximately equal to that one for strength (b_e). A method was presented to calculate the effective slab width for stiffness (b_{es}) for any degree of interaction.

In order to simplify the calculation of the composite beam stiffness and deformation using the transformed section, the definition of the average effective slab width for stiffness (b_{av}) was introduced. Design curves relate the average effective slab width for stiffness (b_{av}) to (L/b) and (c/b) ratios in the case of complete interaction and a method to find (b_{av}) for any degree of interaction are presented for the positive and negative moment regions.

The average effective slab width (b_{av}) is one of the major parameters required in the design of a multi-story frame with composite beams. It is required to calculate the stiffness of the composite beam in the positive and negative moment regions, Figure 4.18, and

I_{+ve} The moment of inertia of the transformed section based on the steel beam and a concrete slab having a width equal to (b_{av})

I_{-ve} The moment of inertia of the transformed section based on the steel beam and the slab reinforcement, if it exists, within the average effective slab width (b_{av})

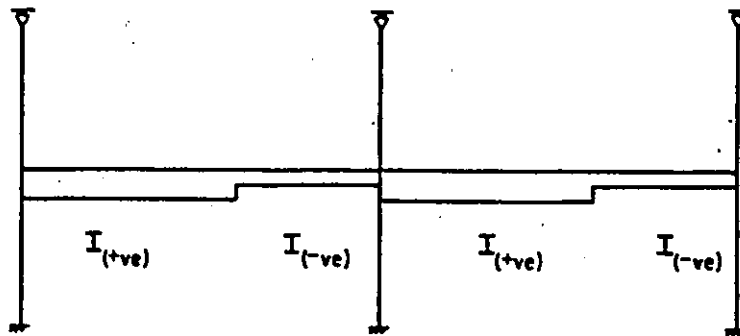


FIGURE 4.18 ONE STORY ASSEMBLY SHOWING THE MOMENT OF INERTIA OF THE COMPOSITE BEAM IN THE DIFFERENT MOMENT REGIONS

consequently the bending moment distribution in the statically indeterminate multi-story frame.

At the end of the chapter a comparison between the analytical results and the provisions for the effective slab width for simple composite beams in the different codes was presented.

CHAPTER 5

DESCRIPTION OF TEST PROGRAM

5.1 Introduction

To examine the theoretical model and to verify the theoretical parametric study, a series of tests was performed. The test program consisted of tests of five composite beams with ribbed metal deck. Each beam was bolted at one end to a column test fixture to form a cantilever beam and was loaded with upward end load to simulate that portion of the composite beam in a multi-story frame which is subjected to positive moment due to the effect of lateral loads. Each beam was tested from both sides, thus; a total of ten tests were performed.

The tests were designed to study the effect of five primary variables on the ultimate strength, stiffness of composite steel-concrete beam-to-column connections and on the effective slab width especially at the connection. These parameters are:

1. Column face width to the slab width ratio.
2. Slab length to slab width ratio
3. Total slab thickness
4. Steel beam size
5. Existence of lateral beams framing into the column and connected to the slab.

This chapter contains information on details of the test specimens, material properties, test set-up, instrumentation and test procedure.. The test results and the evaluation of these results and a comparison between the test and analytical results are presented and discussed in the following chapters.

5.2 Description of the Test Beams and Test Set-Up

Each test specimen consisted of a concrete slab with ribbed metal deck attached to a steel I-beam by 3 in. long $3/4$ in. diameter stud shear connectors. A five foot wide slab was used in all the beams. The 5 foot width was chosen to represent the practical spacing between the composite beams. The beam length was varied to provide the required information for the parametric study.

In order to study the effect of the column face width to the slab width ratio, it was necessary to change the column face width since the slab width was constant in all the tests. Changing the column face width requires the use of more than one column test fixture. A more convenient and economical method was used to change the column face width while using the same column test fixture. This was achieved by welding a thick steel plate to each end of the beams which was bolted to the column test fixture so that the beam and end plate constituted a rigid beam to column connection. The width of the steel plate was varied to simulate the required variation in the column face width.

Two different I-beam sizes, W12x27 and W16x40, were used to study the effect of the steel beam size on the behaviour of the composite

beam-to-column connection. The total slab thickness was 4 in. for four beams and 5 in. for the fifth one.

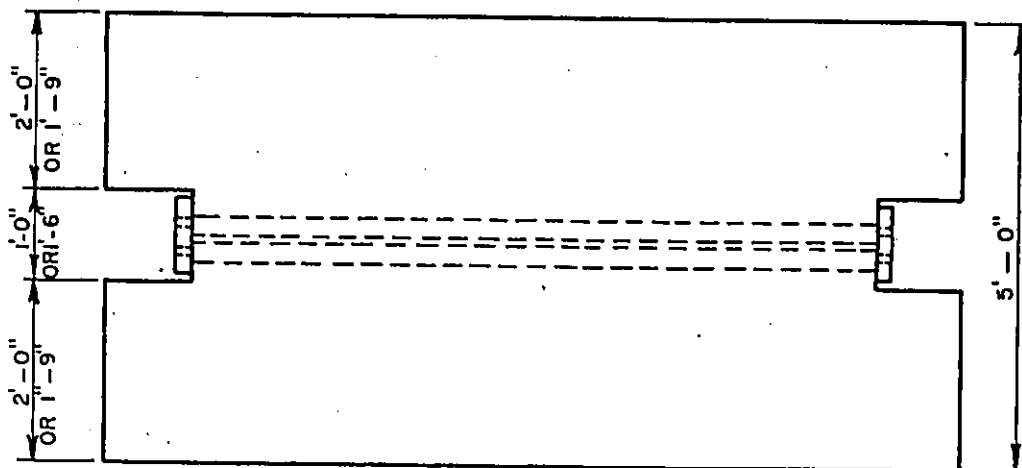
Figure 5.1 shows a typical test beam and the details of all the test beams are given in Table 5.1.

Beam No.	Test No.	Steel Beam Size	Total Slab thick (in)	Existance of transverse support	length >ft.	Steel plate width (in)	No. of connectors
A	A1	W12x27	4	without	8	10	21
	A2			without		15	
B	B1	W12x27	4	without	8	10	21
	B2			without		15	
C	C1	W16x40	4	without	8	10	21
	C2			without		10	
D	D1	W12x27	4	without	12	10	23
	D2			without		15	
E	E1	W12x27	5	with	8	10	15
	E2			without		10	

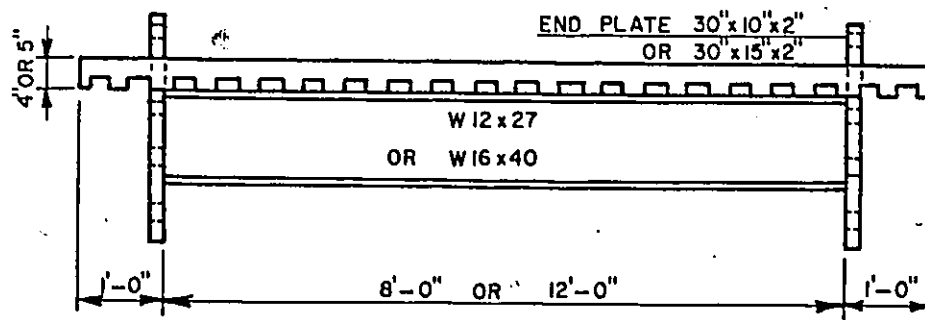
Table 5.1: Details of the Test Beams

Figure 5.2 shows a schematic view of the test set up. Each beam was bolted to the column test fixture with eight 1.0 in. diameter A490 bolts. After one end was tested, the test beam was turned around and the other end plate was bolted to the column test fixture.

Before the last test, a W12x27 steel I-beam was welded to the



PLAN



ELEVATION

FIGURE 5.1 TYPICAL TEST BEAM

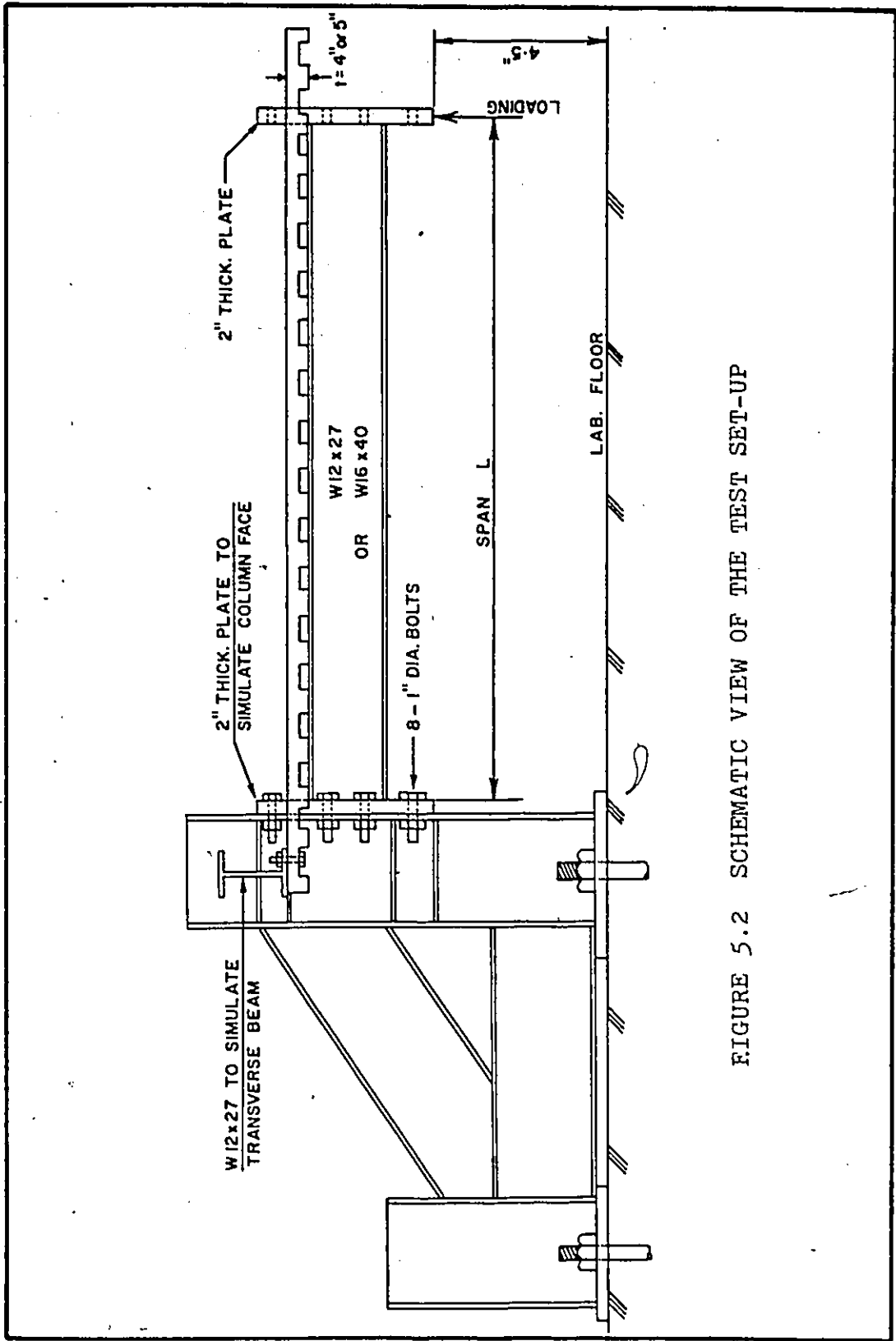


FIGURE 5.2 SCHEMATIC VIEW OF THE TEST SET-UP

column test fixture on each side to simulate the transverse beam framing into the column. Each of these beams was bolted to the concrete slab of the last test beam using three 1/2 in. diameter bolts to simulate the existence of shear connectors connecting the concrete slab to the transverse beams in the actual frame. Figure 5.3 shows the view of the test set-up for the last test beam.

5.3 Design of Test Specimens

It was important in the design of the test beams to ensure that each beam will fail by crushing of the concrete slab at the end plate not by shearing of the connectors or fracture of the steel beam so that the beam can be turned around to test the other end without changing the original properties except in a very small region around the end plate at the free end. This requirement necessitates the knowledge of the maximum compressive force which the steel plate will exert on the slab. This force was calculating using the effective slab width predicted from the analytical model explained in the previous chapters. Minimum compressive concrete strength (f'_c) of 4000.0 psi was assumed in the design since the actual concrete strength was not known at this stage of the experimental program. Thus, the maximum compressive force (C) exerted by the end plate on the slab is given by:

$$C = 0.85 f'_c \cdot b_e \cdot t$$

where f'_c is the design compressive concrete strength

b_e is the effective slab width at the column face

t is the thickness of the solid part of the slab.

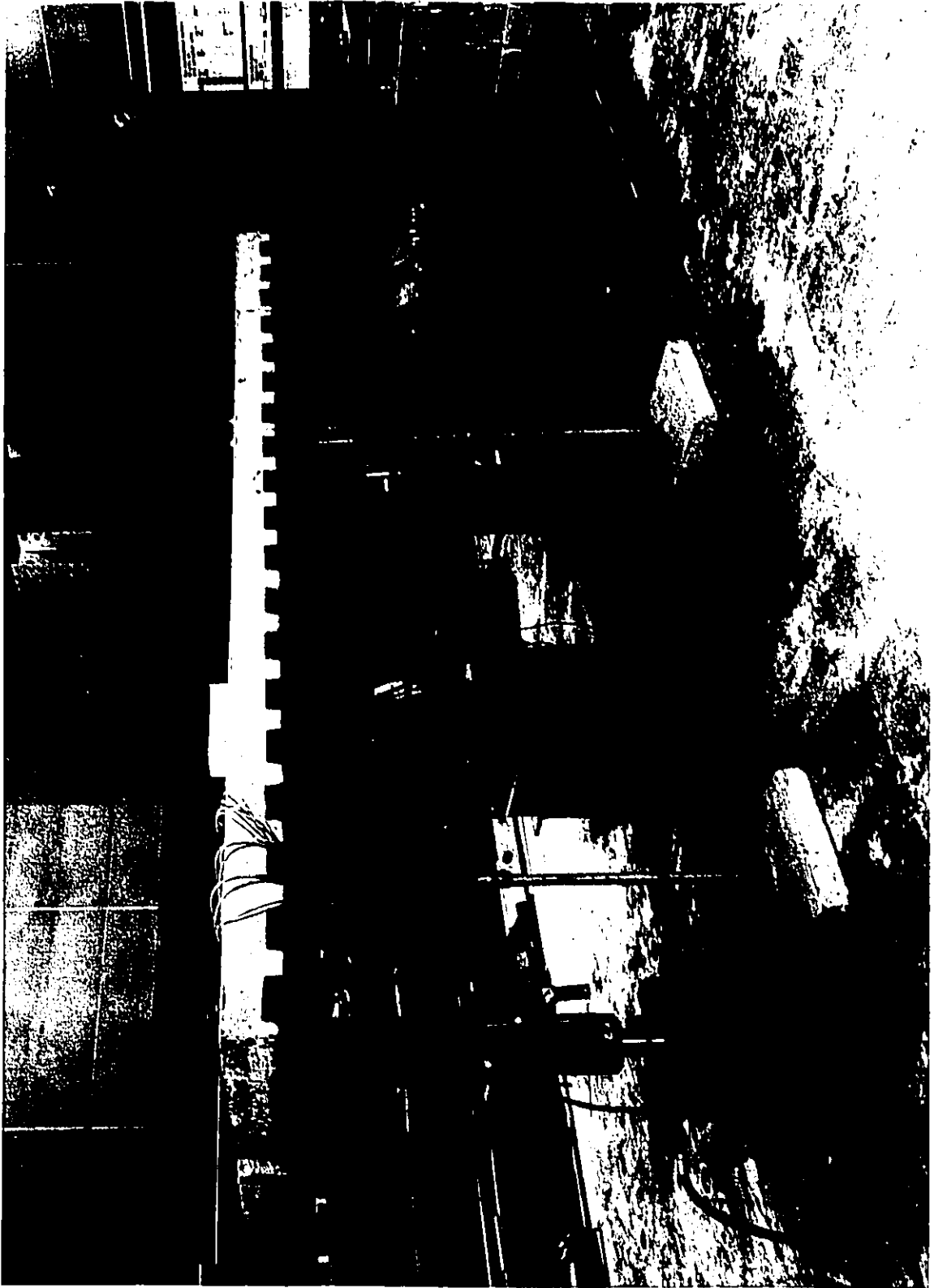


Figure 5.3 Construction site of the tunnel. The tunnel is located in the

A W12x27 steel section was chosen for four of the test beams since it represents one of the practical steel sections commonly used. A nominal yield stress of 50.0 ksi was assumed in the design. The product of the steel beam area and its assumed nominal yield stress, i.e. $A_s F_y$, was greater than the estimated maximum compressive force in the slab (C) which ensured the occurrence of failure in the slab rather than the steel beam. A W16x40 steel section was chosen for the fifth test beam to study the effect of the steel beam size on the behaviour of the composite beam-to-column connection.

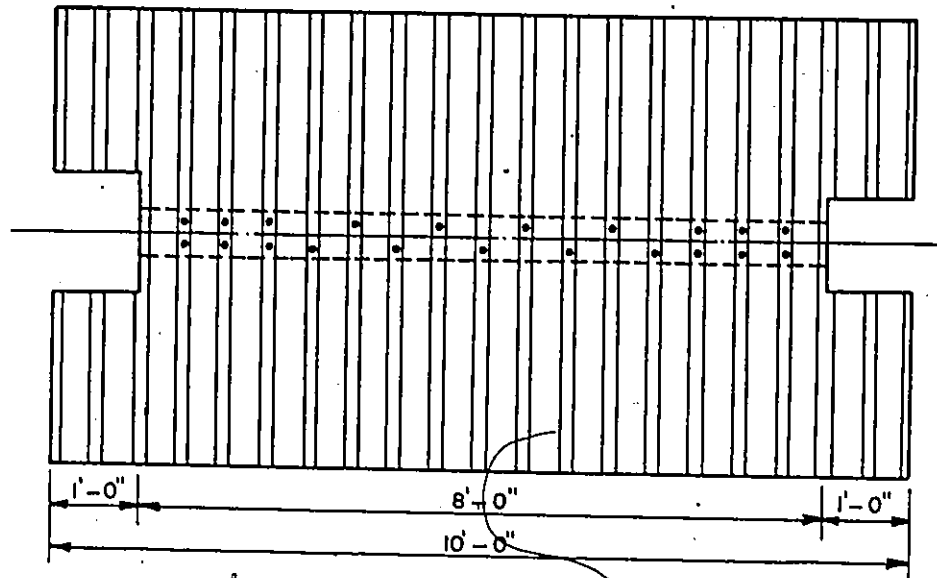
Shear connection between the steel beam and the concrete slab was provided by means of 3/4 in. diameter stud shear connectors. The required number of shear connectors was estimated according to the CSA specifications⁽⁶²⁾ for the case of full shear connection. An ultimate shear capacity (Q_u) of 11.3 kips per each connector, as provided in the CSA standard⁽⁶²⁾, was used in the design of the connectors. Thus the number of the stud shear connectors provided in each beam is given by

$$N = \frac{0.85 f'_c b_e t}{Q_u}$$

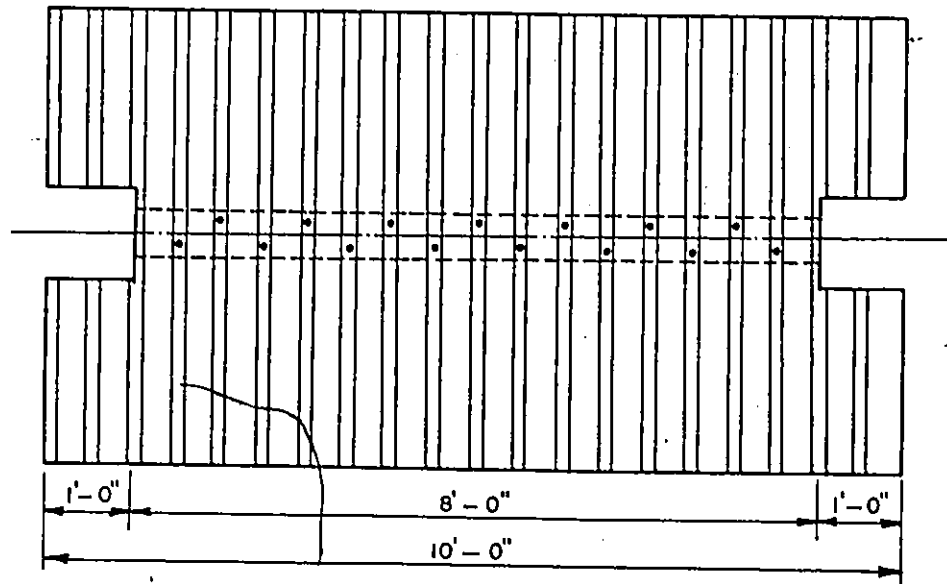
For the beams with two different end plate sizes, the effective slab width (b_e) based on the wider end plate was used to estimate the required number of shear connectors for these beams.

Figures 5.4 and 5.5 show the details of the shear connectors for the different test beams.

The concrete slab was reinforced with a 6 in by 6 in 10/10 gauge welded wire mesh. This amount of reinforcement represents the specified



a) BEAMS A, B and C



b) BEAM E

FIGURE 5.4 DETAILS OF SHEAR CONNECTORS FOR BEAMS A, B, C AND E

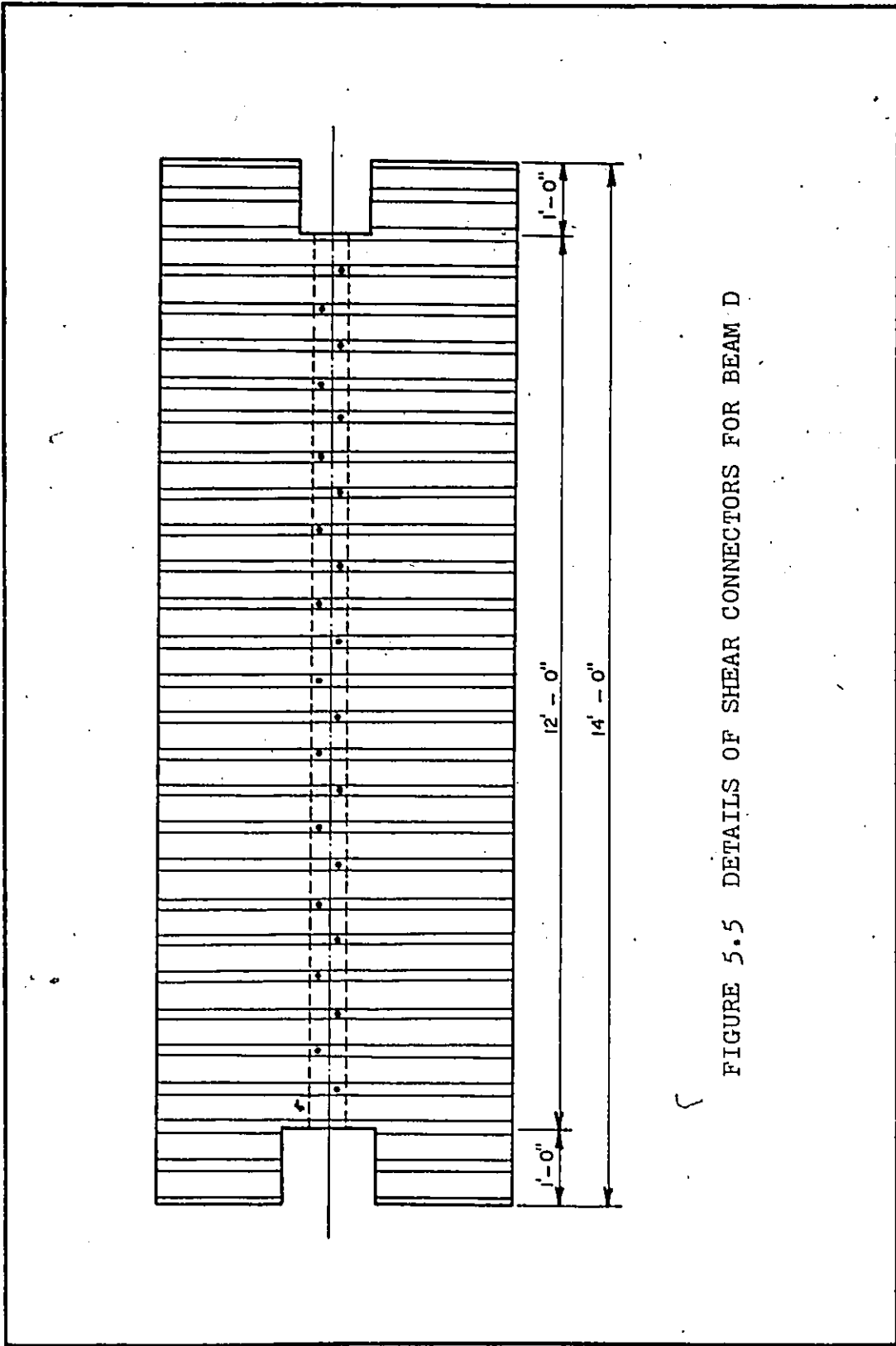



FIGURE 5.5 DETAILS OF SHEAR CONNECTORS FOR BEAM D

minimum reinforcement and is commonly used to reinforce the slab of composite beams with ribbed metal deck.

The 8 ft length of the test beams between the steel end plates was selected on the basis of the results obtained from a previous test program on composite beams with solid concrete slab conducted by Duplessis and Daniels^(41,48). The results of these tests showed that a length of 8 ft would be sufficient to prevent any significant interaction between the ends of the beam. The 12 ft length was selected as a second value to study the effect of the span length to width ratio on the behaviour of the connection.

As mentioned before a steel end plate was welded to each end of the test beams to simulate the column face. Two types of end plates were used; type A was 10" x 30" x 2" while type B was 15" x 30" x 2". The 10 in. and 15 in. plate widths were selected to represent practical column face widths. A 2 in. thickness was chosen to minimize the deformation of the end plate during the loading of beams. The details of the end plates are shown in Figure 5.6.

The column test fixture and the bolts connecting each of the test beams to it were designed so that the stresses produced in these elements remain well below the elastic limit of the material during loading to avoid any permanent deformation so that these elements can be used for the subsequent tests and to minimize the effect of the deformation of these parts on the test results.



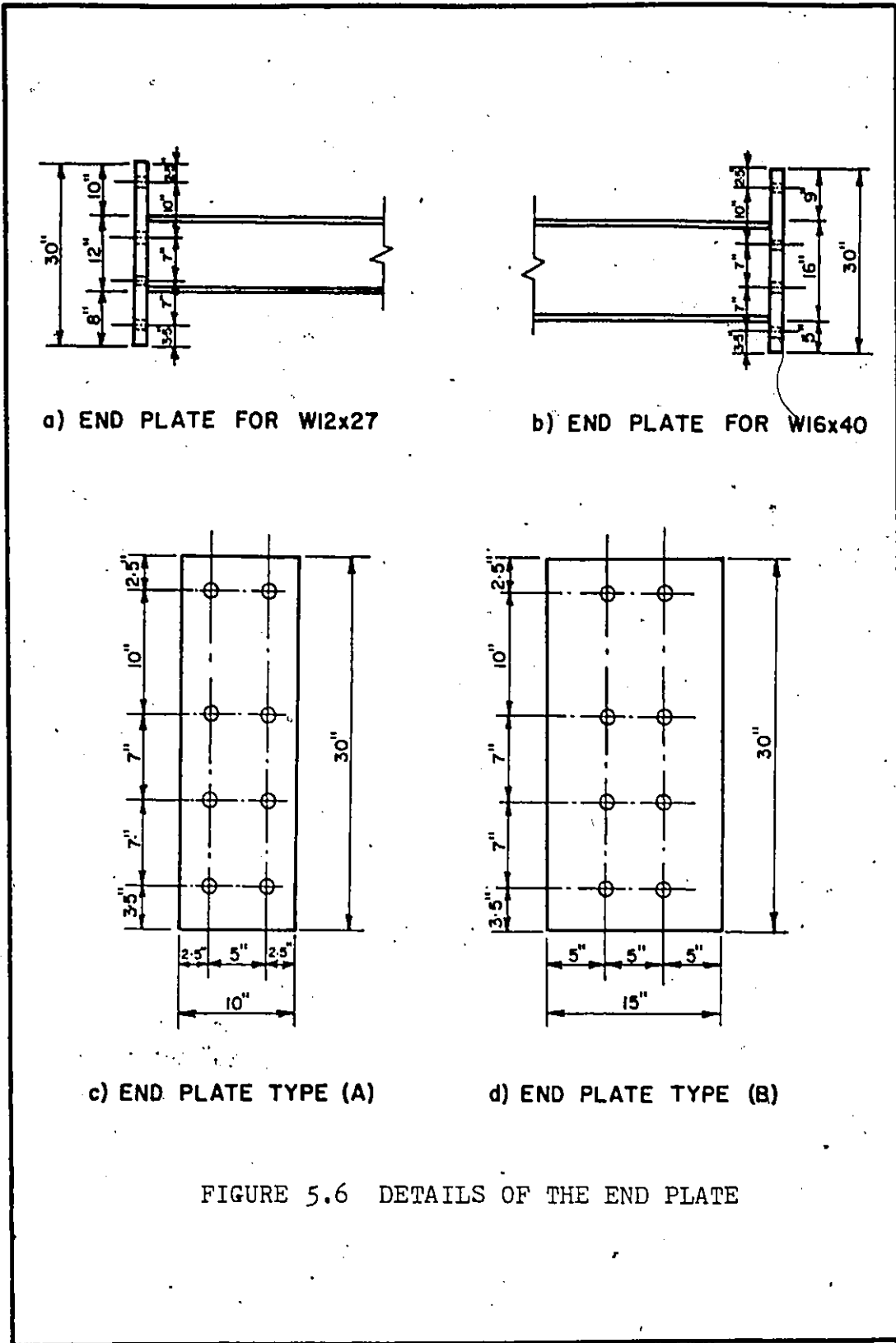


FIGURE 5.6 DETAILS OF THE END PLATE

5.4 Construction

The steel beams were delivered to the laboratory with the appropriate lengths and the end plates were also delivered with the required sizes and with the required holes, which were machine drilled, in each plate. The end plates were welded to each beam in the laboratory using E107 electrodes. The web was fillet welded to the plate while the flanges were bevelled and butt welded to the plate. The column test fixture was also collected and welded in the laboratory.

Welding of the stud shear connectors was performed in the laboratory using the standard stud welding equipment. The stud connectors were welded to the steel beams through the decking as in the standard practice.

The concrete slab was poured in a 1.5 in. cellular metal decking with 6 in. rib spacing. The solid part thickness above the ribs was 2.5 in. for four beams and 3.5 in. for the fifth one. The concrete was poured up to half the solid part thickness when the reinforcing wire mesh was placed; then the concrete was poured again to fill the forms. The concrete was internally vibrated using 1 1/4 in. diameter poker type vibrator. The concrete used for all the beams was ready-mixed and having 3 in. slump. The concrete was poured for all test beams at the same time. The decking was shored at several points along its length during pouring of the concrete.

About five hours after placing, when the concrete had begun to harden, wet burlap was placed over the specimens and kept moist for 7 days.

Three concrete cylinders were poured with each beam and were cured alongside the beams.

5.5 Instrumentation

Each test beam was instrumented to measure the applied load, the deflection at the applied load position and at several points near the fixed end, the relative horizontal movement between the end plate and the column test fixture, the strains in the steel beam at different locations and the longitudinal strain in the top fibre of the concrete slab at several locations across the slab width.

Deflections were measured by means of dial gauges. The precision with which the dial gauges could be read was one-thousandth of an inch. For each test beam, eight dial gauges were positioned at the locations shown in Figure 5.7. The two dial gauges mounted at the free end were installed to measure the vertical deflection at the applied load position. The three gauges placed underneath the beam near the fixed end were installed to measure the vertical deflection at these locations which was used to calculate the end rotation. Two gauges were mounted opposite to the end plate and one opposite to the column face, these gauges were used to measure the horizontal movement and the rotation of the end plate.

Steel strains were measured by 1/4 in. electric resistance foil strain gauges and were read by means of manual strain indicators. The precision with which the strain gauges could be read was 1×10^{-6} in/in. Twelve gauges were mounted on each end of the test beams at the

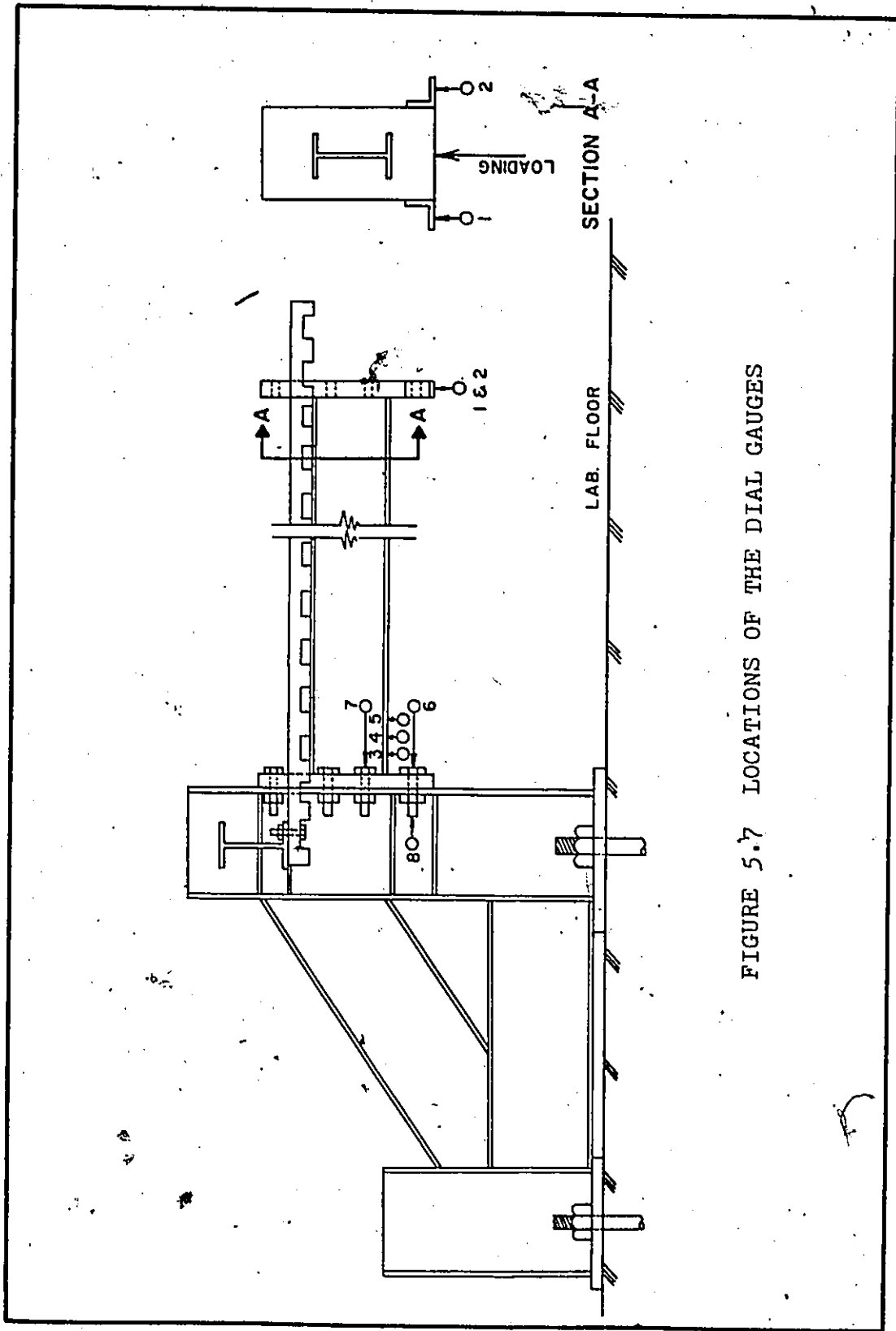


FIGURE 5.7 LOCATIONS OF THE DIAL GAUGES

locations shown in Figure 5.8.

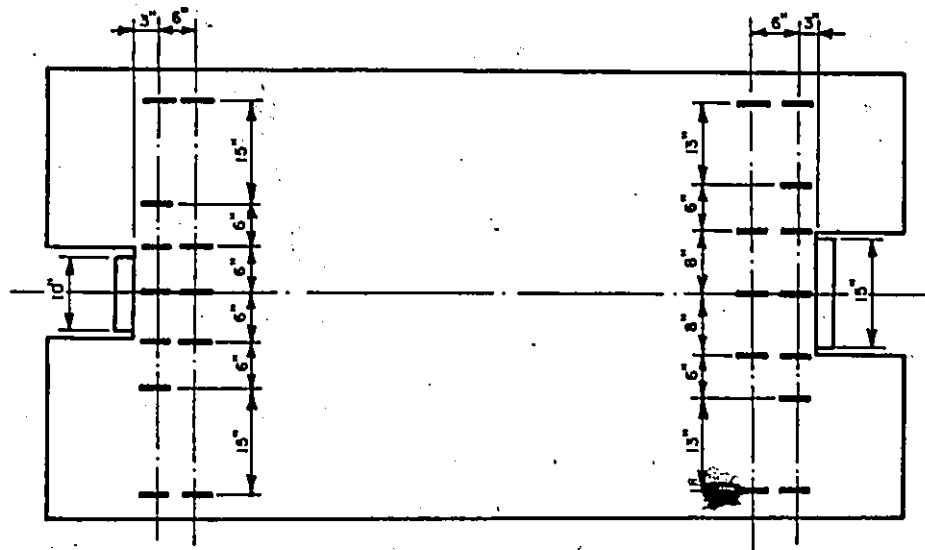
Concrete strains were measured by using 6 in. long paper-backed electric resistance filament strain gauges and were read by means of manual strain indicators with a precision of 1×10^{-6} in/in. Twelve gauges were mounted on the top surface of the slab near each end of the test beams. Concrete gauges were positioned on two lines perpendicular to the beam centre line to measure the longitudinal strain distribution across the slab width at these two positions. The locations of the concrete gauges are shown in Figures 5.8 and 5.9.

Demec points were installed on the top surface of the slab in some specimens to measure the transverse strains in the top surface of the slab along the beam centre line as shown in Figure 5.9.

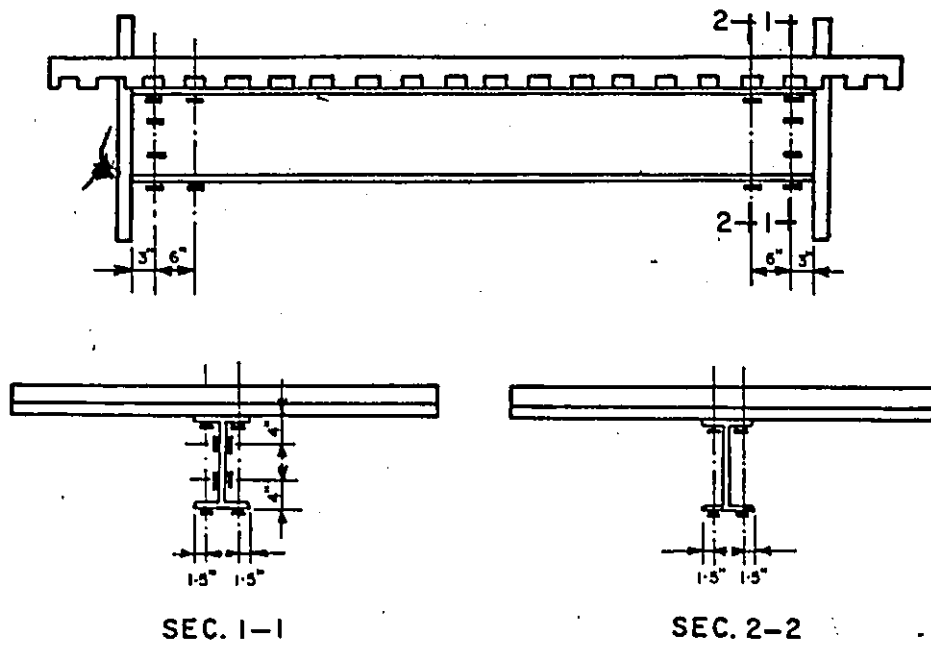
5.6 Test Procedure and Loading

Each of test beams was bolted at one end to the column test fixture by the eight 1 in. diameter bolts. The bolts were fastened using the turn-of-nut method.

An upward load was applied at the other end, the free end, of the beam by means of a hydraulic jack resting directly on the laboratory floor. A calibrated load cell was used to accurately control the applied load. The load cell was placed over the piston of the jack and was attached to a universal ball bearing, placed between the load cell and the free end of the test beam, to allow for the rotation of the end of the test beam (Figure 5.10). The load cell was calibrated immediately before each test.



a) STRAIN GAUGES ON THE CONCRETE SLAB



b) STRAIN GAUGES ON THE STEEL BEAM

FIGURE 5.8 LOCATIONS OF THE STRAIN GAUGES

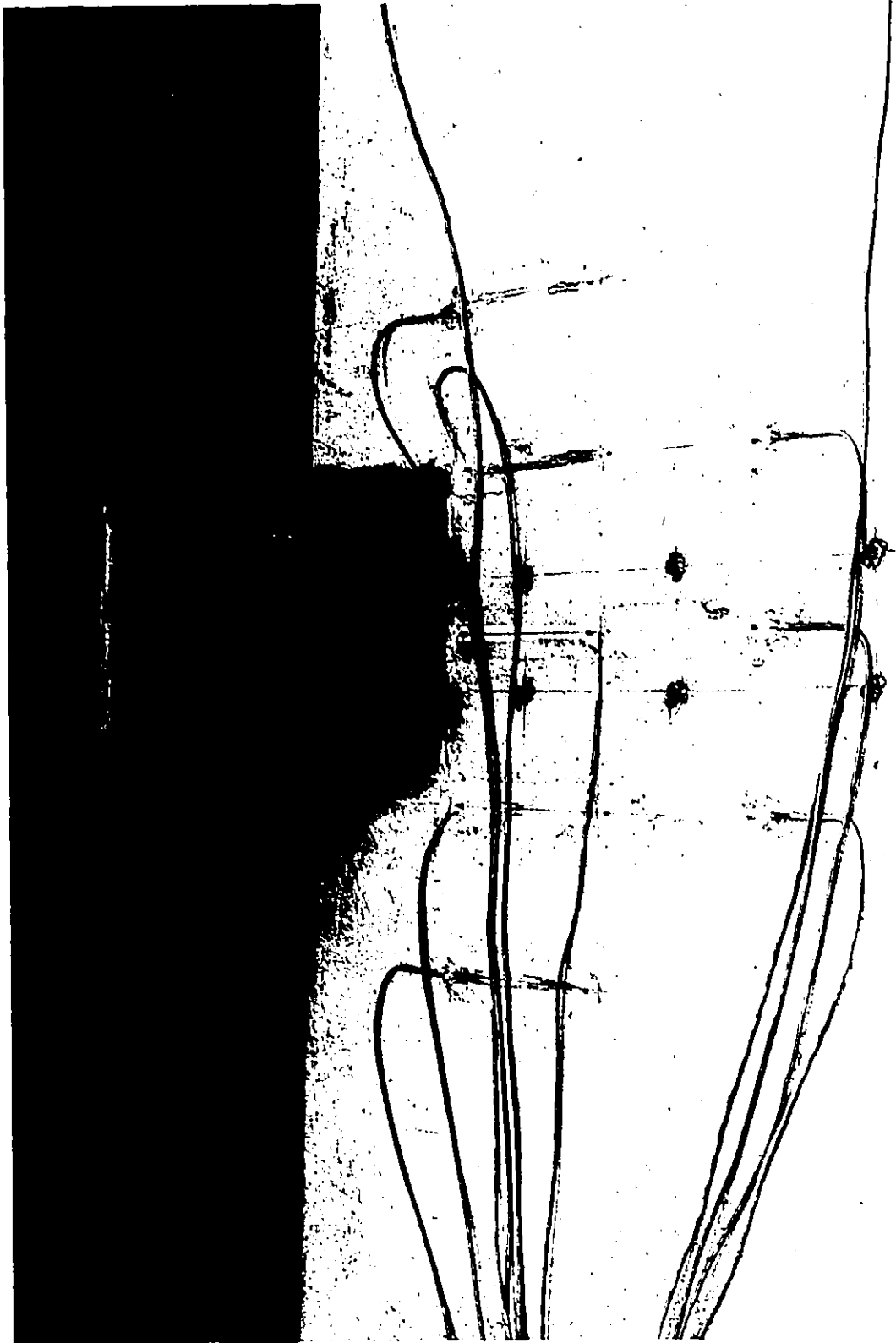


FIGURE 5.9 REINFORCING BAR PATTERN ON THE CONCRETE SLAB

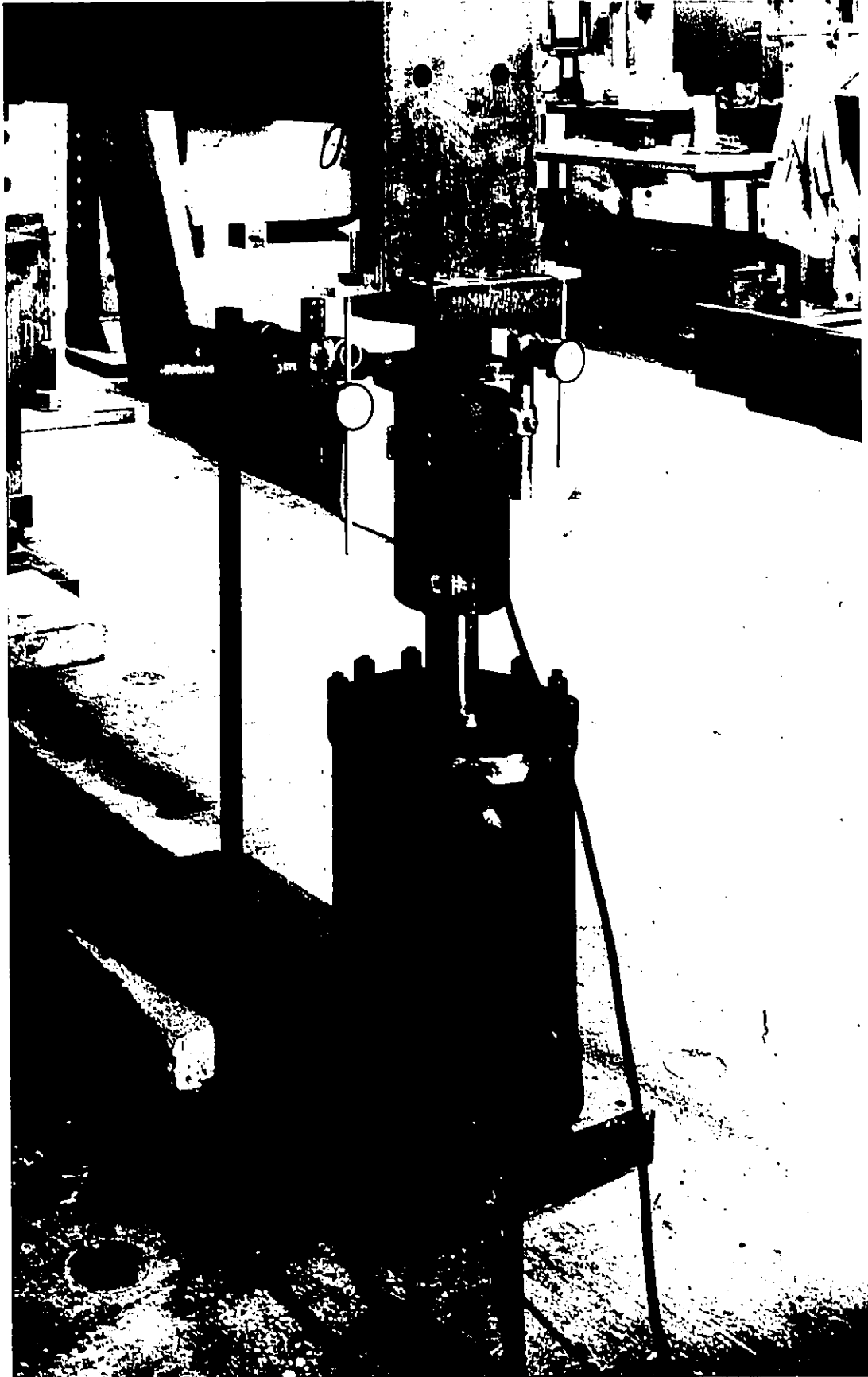


FIGURE 5.10 LOADING SYSTEM

The zero load position for a test beam was taken as the position at which there would, theoretically, be no moment at the fixed end. This corresponded to applying a small load at the free end equal to half the calculated weight of the test beam.

Initial readings were taken, then the load was applied in increments of 2.0 kips up to the yielding of the steel beam when the increment was decreased to 1.0 kip up to the failure of the specimen.

Dial gauge and strain gauge readings were recorded after the application of each load increment. In the non-linear region, the readings were recorded after the stabilization of the load. The beam was inspected after each load increment to detect the occurrence of any cracking or crushing in the concrete slab.

After completing the test on one end, the beam was turned around and the other end was bolted to the column test fixture and the test procedure was repeated.

5.7 Actual Material Properties

The actual material properties of the concrete and the steel were determined from testing of the control specimens.

As mentioned before, three standard 6 in. diameter concrete cylinders were poured and cured alongside with each beam. The cylinders were capped with a molten sulphur compound and were tested in a 300 kip capacity hydraulic Tinius Olson testing machine. The cylinders were tested after testing one end of the test beam and before testing the second end. The average strength of the three test cylinders was

considered as the strength of the concrete slab at both ends.

The tensile strength of the concrete and its modulus of elasticity were calculated using the appropriate CSA equations. The tensile strength of concrete in flexure, known as modulus of rupture was obtained using the formula

$$f_r = 7.5 \sqrt{f'_c}$$

while the split-cylinder tensile strength was obtained using the formula

$$f_t = 6.7 \sqrt{f'_c}$$

The modulus of elasticity for the concrete was obtained from the CSA equation

$$E_c = 33 (W)^{1.5} \sqrt{f'_c}$$

where $W = 145$ pcf for normal weight concrete.

The actual material properties of the concrete is shown in Table 5.2.

Table 5.3 shows the mechanical properties of the steel beams. These properties were obtained by performing tensile tests on steel specimens cut from the web and the flange of each beam after testing both ends. The location from which these tensile specimens were taken was chosen close to the centre of the beam to avoid the parts at which plastic deformations occurred during the tests. The tensile tests specimens were tested in a 120 kip Tinius Olson Universal machine at a speed of 0.025 inch per minute until fracture occurred. The stress-strain relationship was recorded automatically on a graph paper by the machine.

Beam No.	f'_c (psi)		f_t^* (psi)	f_r^{**} (psi)	E_c^{***} (psi)
	Test result	Average			
A	4187 4481 4668	4445	446	500	3.8×10^6
B	4410 4560 4350	4440	446	499	3.8×10^6
C	4304 4297 4640	4413	445	498	3.8×10^6
D	4208 4597 4244	4350	442	494	3.7×10^6
E	4889 4836 4792	4839	466	521	3.9×10^6

Table 5.2: Properties of the Concrete

$$* \quad f_t = 6.7 \sqrt{f'_c}$$

$$** \quad f_r = 7.5 \sqrt{f'_c}$$

$$*** \quad E_c = 33 (W)^{1.5} \sqrt{f'_c}$$

Beam Number	PART	Yield stress ksi		Ultimate Stress ksi		Elastic Modulus psi x 10 ⁶	
		Test	Average	Test	Average	Test	Average
A	Flange	50.30	50.10	76.32	76.42	3.10	3.00
		49.90		76.52		2.90	
	Web	54.12	54.35	77.39	77.80	2.85	2.92
		54.58		78.21		2.99	
B	Flange	50.00	50.02	76.50	76.30	2.97	2.93
		50.04		76.10		2.90	
	Web	55.21	54.90	77.95	77.67	2.93	2.99
		54.58		77.39		3.05	
C	Flange	55.5	55.10	88.9	88.5	3.00	2.98
		54.7		88.1		2.97	
	Web	62.50	62.00	85.43	85.20	3.03	3.04
		61.50		84.96		3.06	
D	Flange	57.30	57.45	81.4	81.15	2.95	3.00
		57.60		80.9		3.05	
	Web	62.4	61.58	82.76	82.25	3.20	3.05
		60.77		81.75		2.90	
E	Flange	51.90	51.70	77.70	77.50	2.99	2.97
		51.50		77.30		2.95	
	Web	55.06	55.27	78.50	78.21	2.83	2.97
		55.49		77.93		3.10	

Table 5.3: Properties of the Steel

5.8 Summary

In this chapter the description of the test set-up, design of the test specimens, test procedure and the material properties for the concrete and the steel used in the fabrication of the test specimens were discussed. Care was taken in the fabrication and testing of the specimens in order to reduce the influence of test variability. This was especially important because of the limited number of test specimens planned for this investigation. The test results and comparison between the experimental and analytical results are discussed in the following chapters.

CHAPTER 6
EXPERIMENTAL RESULTS

6.1 General

The description of the test specimens and the test procedure were discussed in the previous chapter. The test results and observations and the evaluation of these results are presented in this chapter. A comparison between the analytical and test results for each of the test specimens are presented in the next chapter.

6.2 Presentation of the Test Results

To represent the test results, a group of five graphs are plotted for each end of every beam tested. These graphs represent the following characteristics.

a) End-Moment versus End-Deflection

By end-moment is meant the moment reaction at the fixed end of the test beam. The end deflection is the deflection of the free end of the beam where the load is applied. The end deflection was measured at two points, one at each side of the load cell as shown in Figure 5.10, and the plotted deflection is the average of these two readings.

b) Applied Moment Versus Bottom Fibre Steel Strain

The bottom fibre steel strain at a section labelled 1-1 and located 3 inches from the column face, the location of the first line of the mounted strain gauges, is plotted against the applied moment at that

section. The plotted strain is the average of the two strain gauges mounted on the lower flange of the steel beam at that section.

c) Moment-Curvature Curve

The curvature at Section 1-1 is plotted against the applied moment on that section. Section 1-1 was chosen since it is adjacent to the column face where a plastic hinge is likely to form in a multi-story frame.

The curvature was calculated from the measured top and bottom steel strains assuming linear strain distribution across the beam depth. Thus,

$$\phi = \frac{\epsilon_b - \epsilon_t}{h} \quad (6.1)$$

where in this equation

h is the distance between the gauges mounted on the top and bottom flanges

ϵ_b and ϵ_t are the measured top and bottom steel strains with sign

ϕ is the curvature

d) End Moment versus End Rotation

End rotation represents the slope of the beam at the position of the connection. It is known that the difference in rotation between two points on a beam is given by the equation

$$\theta_2 - \theta_1 = \int_1^2 \phi \, dx \quad (6.2)$$

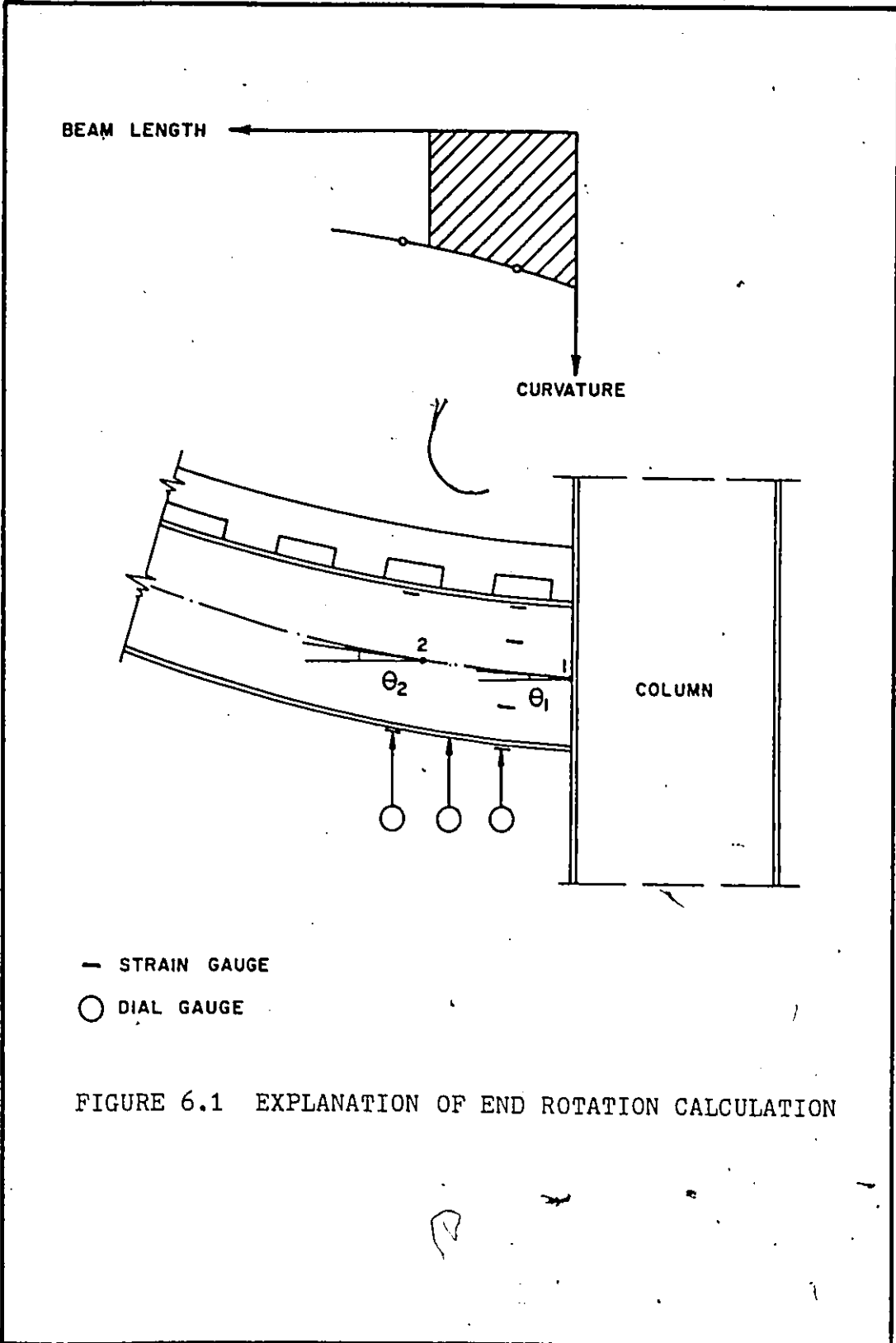


FIGURE 6.1 EXPLANATION OF END ROTATION CALCULATION

where

θ_1 and θ_2 are the rotation at points 1 and 2 respectively

ϕ is the curvature.

The curvature at any section along the composite beam may be expressed in terms of the strains at the top and bottom fibres of the steel beam as given in equation (6.1). Thus, equation (6.2) can be written as

$$\theta_2 - \theta_1 = \int_1^2 \frac{\epsilon_b - \epsilon_t}{h} dx \quad (6.3)$$

or

$$\theta_1 = \theta_2 + \int_1^2 \frac{\epsilon_b - \epsilon_t}{h} dx \quad (6.4)$$

Equation (6.4) was used to determine the end rotation (θ_1). The rotation at point 2 (θ_2) was determined from the dial gauge readings. The integral of the strain was approximated numerically employing the strain gauge readings between point 2 and the connection between the beam and the column. A diagram showing this procedure is given in Figure 6.1.

The end rotation was calculated at each test load and the end moment versus end rotation was plotted for each test.

The joint modulus (J) is a very important joint property and can be calculated from the Moment-Rotation diagram. The joint modulus is defined in the elastic range as the end moment required to produce a unit end rotation. Thus,

$$J = \frac{M}{\theta} \quad (6.5)$$

The joint modulus was calculated for each of the tests from the corresponding M- θ curve using Equation (6.5).

e) Strain Distribution Across The Slab Width

The measured concrete strains across the slab width were plotted at various stages of loading. The strain distribution was plotted for the two sections labelled 1-1 and 2-2 and located at 3 and 6 inches from the column face, (Figure 5.8).

6.3 Test Results

In this section the test results and observations pertinent to each of the test beams are presented and discussed.

6.3.1 Beam A

Beam A was 8 ft. long and was provided with a 10 in. wide plate at one end (A_1) and a 15 in. wide plate at the other end (A_2). (A_2) was tested first up to failure and then the beam was turned around and the end (A_1) was tested.

6.3.1-a End A_2

The end A_2 was bolted to the column and the beam was loaded in a load increment of 2 kips up to a load of 26.0 kips then the increment was changed to 1 kip until failure. The load readings were recorded at the time of reading the gauges and immediately prior to the next application of the load. The load remained steady after each load

increment up to a load of 20.0 kips when it started to drop by small amounts of 0.1 to 0.2 kips after each loading step.

The end deflection increased elastically up to load 24.0 kips then it started deviating. When the specimen failed it had already deflected 2.87 in. Figure 6.2 shows the end moment versus the end deflection curve for end A_1 .

The steel strain readings at sections 1-1 and 2-2 indicated that the yield started at section 1-1 before section 2-2. Steel strain at section 1-1 increased linearly with the increase in the applied load up to a load of 26.0 when the bottom flange yielded and the relation deviated from the straight line. At failure the bottom fibre steel strains at Section 1-1 reached 18000 micro in/in which indicate that the steel beam underwent large plastic strain before failure. Figure 6.3 shows the variation of the bottom fibre steel strain at Section 1-1 with the applied moment on the section.

Figure 6.4 shows the Moment-Curvature curve for section 1-1. The curvature increased linearly with the applied moment and started to deviate from the straight line relation at load 26.0 kips and reached a value of $1380 \times 10^{-6} \text{ in}^{-1}$ at failure.

Figure 6.5 shows the Moment-Rotation curve. It indicates that the end rotation started to deviate from the linear relation at load of 26.0 kips and reached 0.0075 rad. at failure. The calculated elastic joint modulus (J) for this end was $124.8 \times 10^4 \text{ kip. in/rad.}$

The measured top fibre concrete strain distributions across the slab width at sections 1-1 and 2-2 are shown in Figure 6.6. The peak

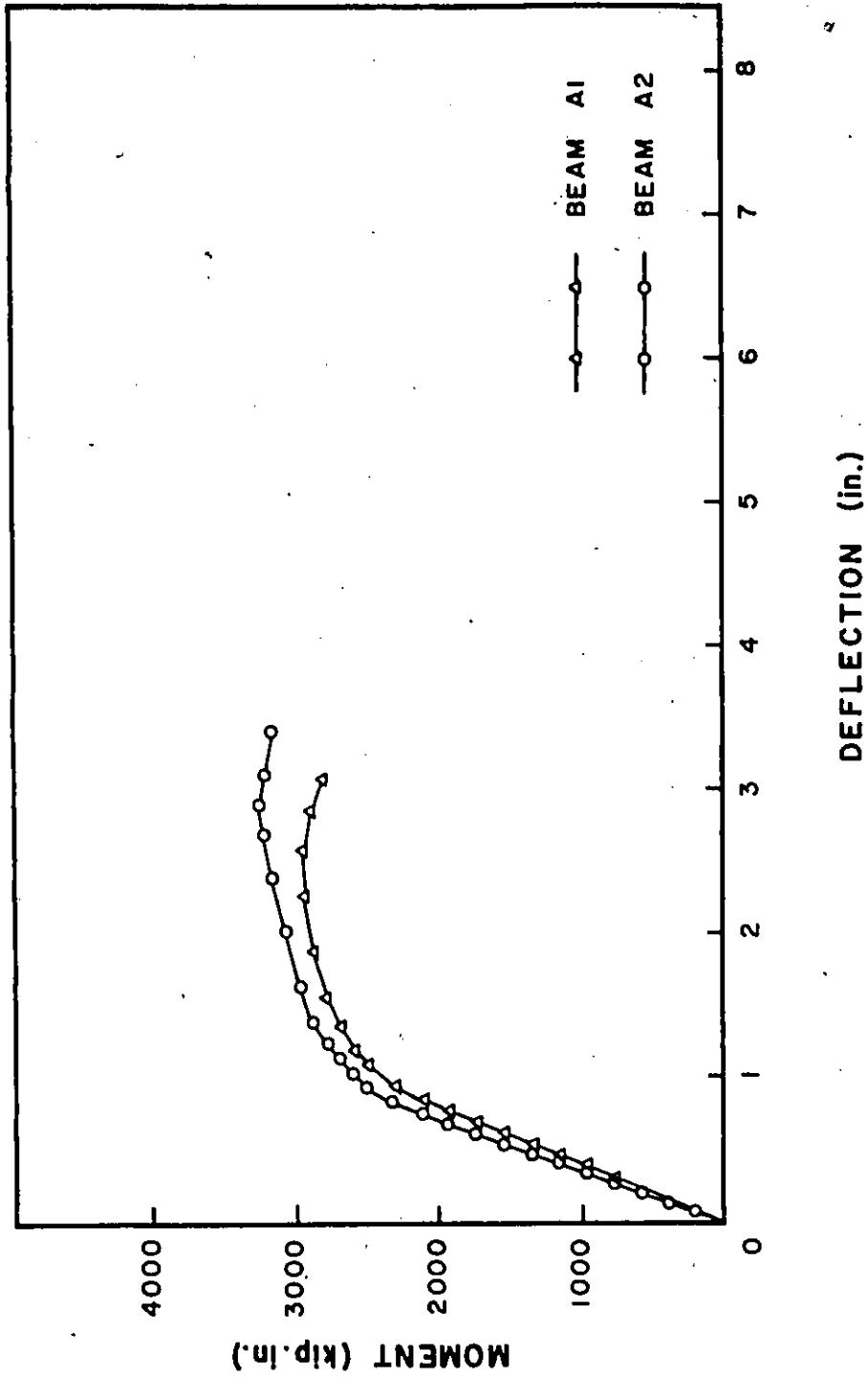
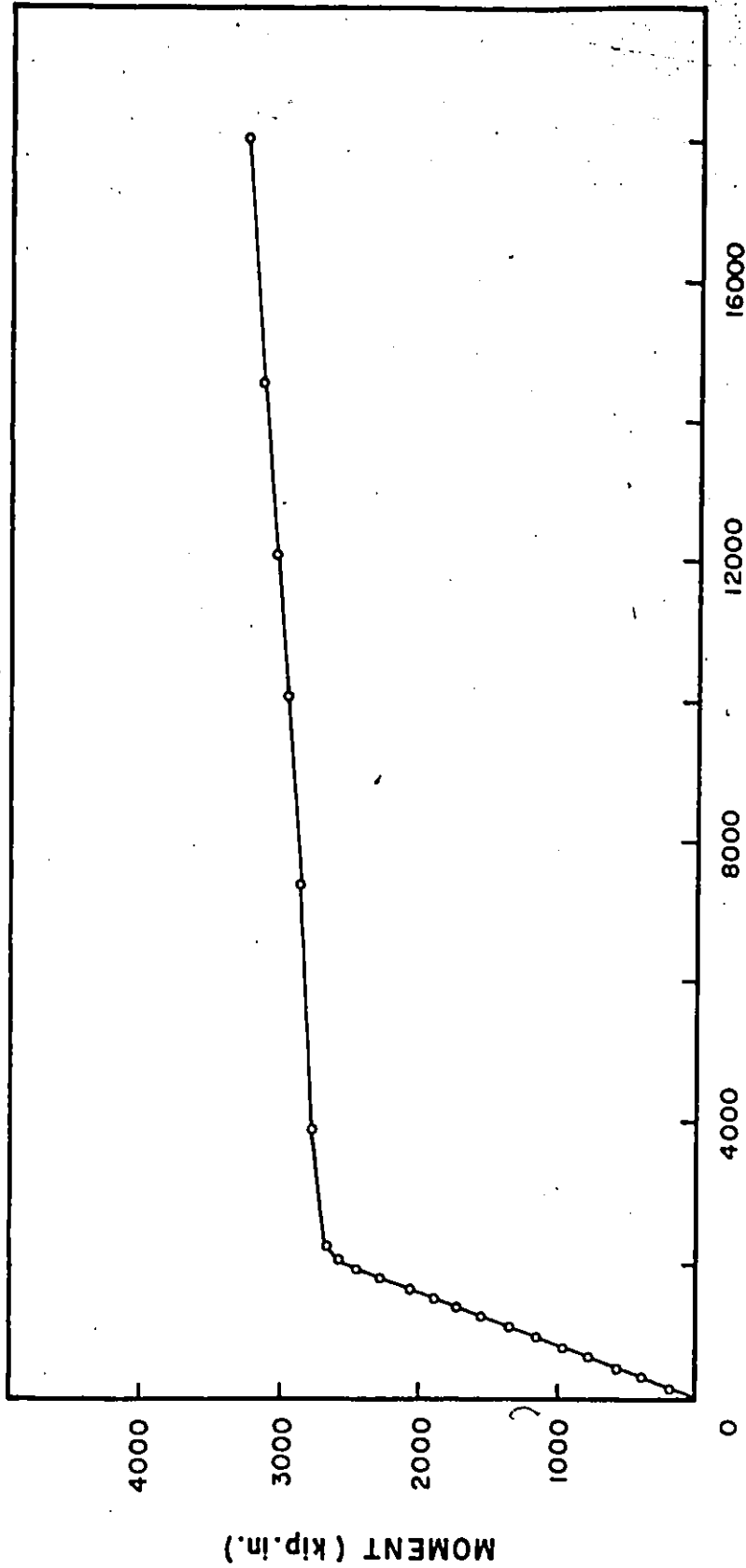


FIGURE 6.2 LIVE LOAD END MOMENT - END DEFLECTION RESULTS FOR ENDS A1 AND A2



STRAIN (micro in./in.)

FIGURE 6.3 LIVE LOAD MOMENT VERSUS BOTTOM FIBRE STEEL STRAIN FOR END A2

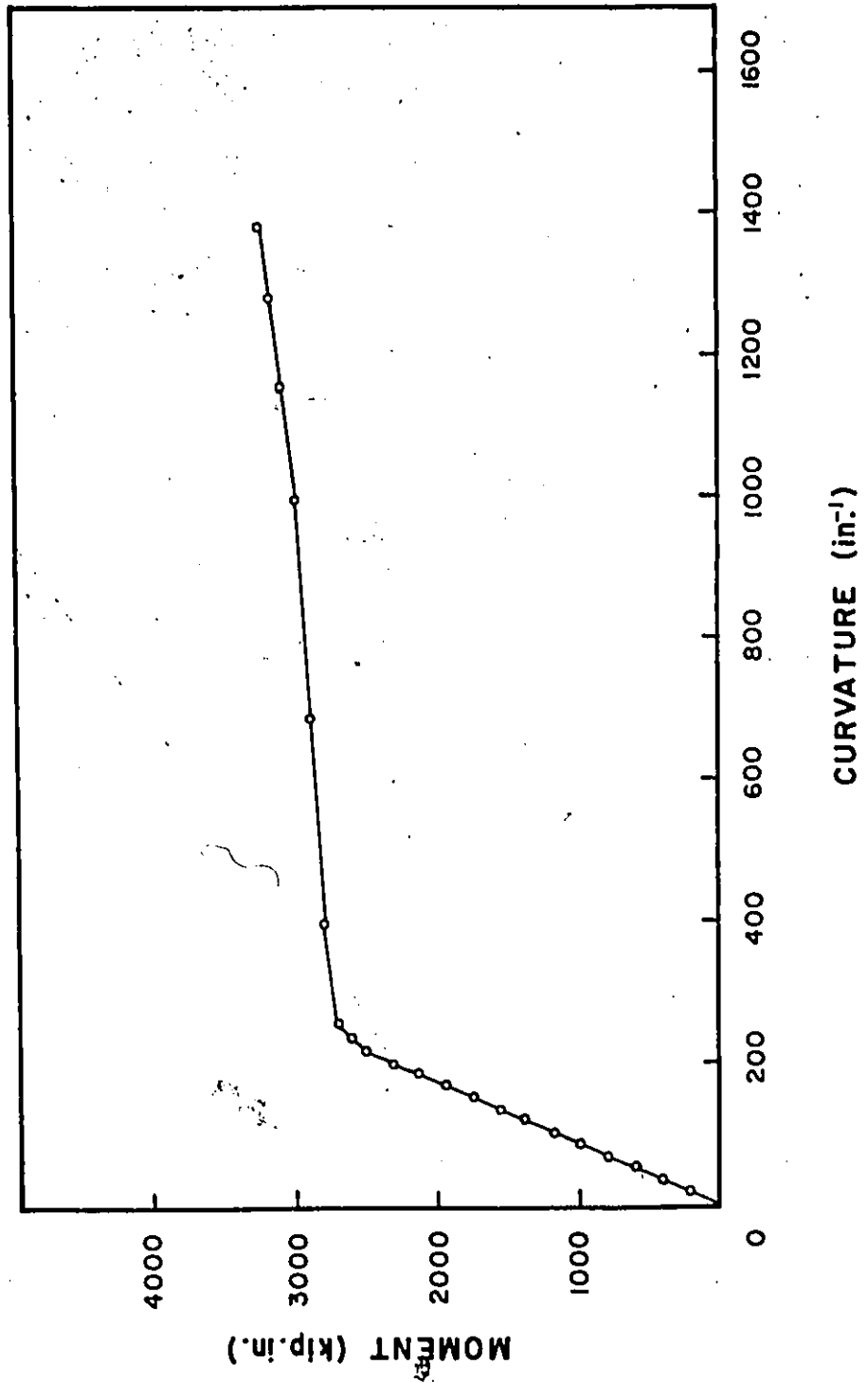


FIGURE 6.4 LIVE LOAD MOMENT - CURVATURE RESULTS FOR END A2

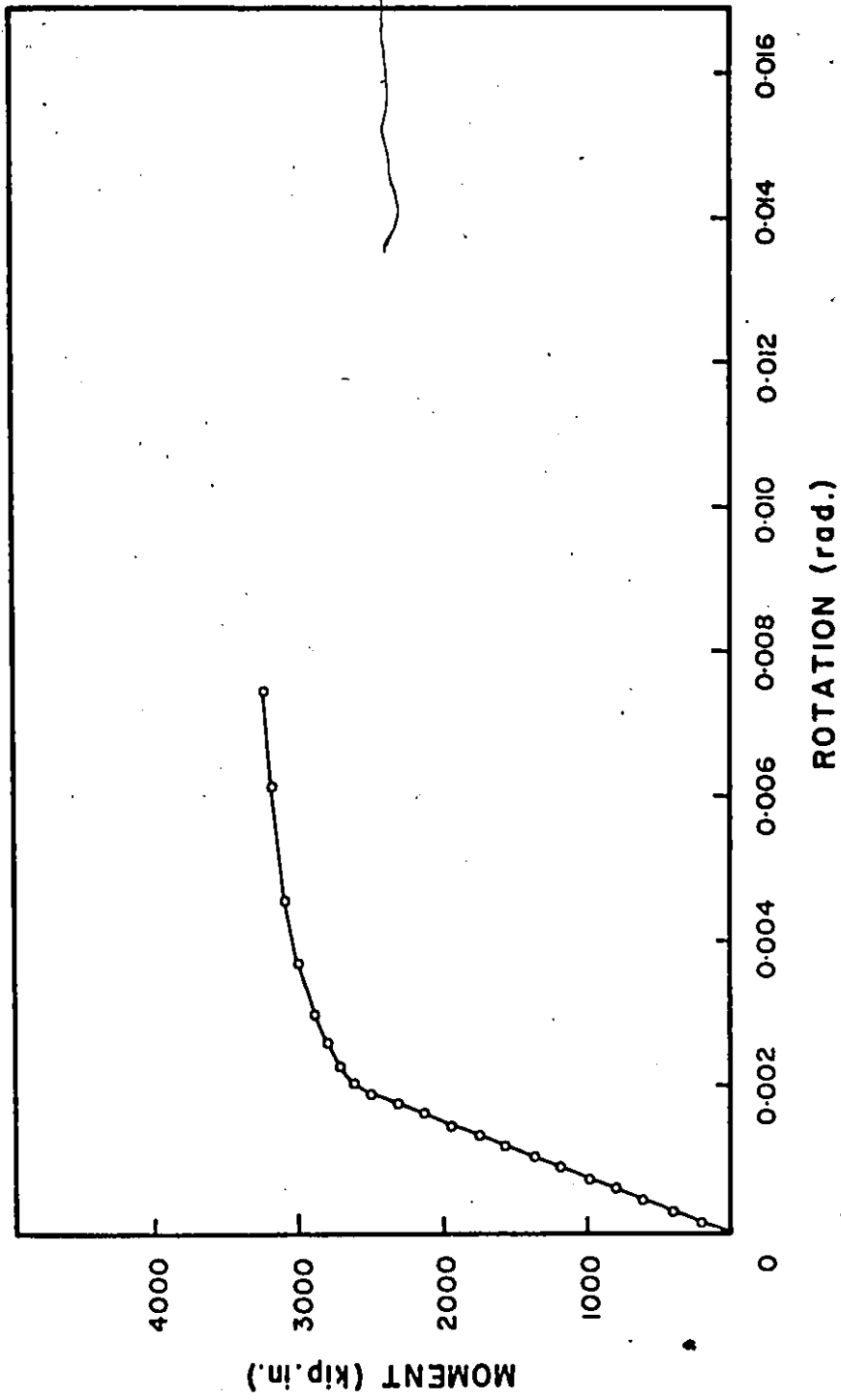
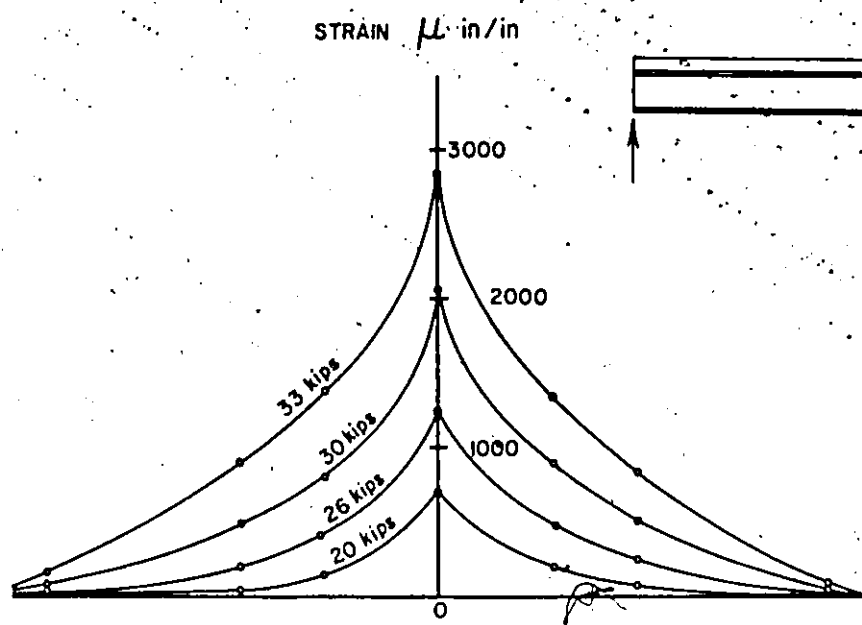
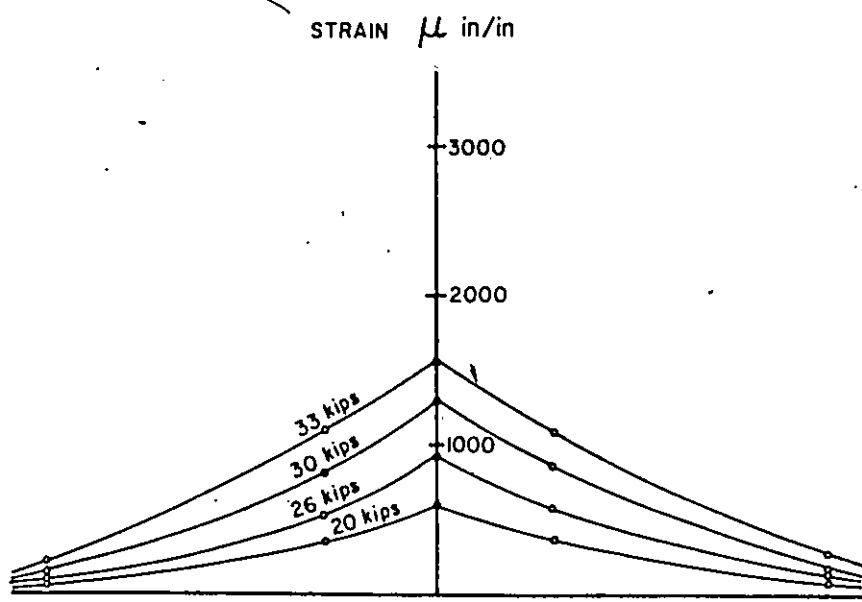


FIGURE 6.5 LIVE LOAD MOMENT - END ROTATION RESULTS FOR END A2



a) AT SECTION 1-1



b) AT SECTION 2-2

FIGURE 6.6 TOP FIBRE STRAIN DISTRIBUTION ACROSS THE SLAB WIDTH FOR END A2

value at both sections occurred over the centre line of the steel beam. The strain distribution across the width was non-uniform at both sections and was more uniform at Section 2-2 than at Section 1-1.

At a load of 29.0 kip a longitudinal crack was visual on the top surface of the concrete slab over the steel beam. The crack started very close to the fixed end and propagated towards the free end with increasing the load to reach the free end at failure.

The specimen failed due to crushing of the concrete slab adjacent to the column face at a load of 33.88 kips. No signs of connector failure or pulling of the concrete slab from the metal deck were observed.

6.3.1-b End A₁

After completing the test on end A₂, the beam was turned around and end A₁ was tested. A longitudinal crack, resulting from testing A₂, was already existing before starting this test.

The beam was loaded in the same manner as for end A₂. The load increment was reduced from 2 kips to 1 kip at load 26.0 kips. The load was steady between consecutive applications and started to drop a small amount of 0.2 kips at load 20.0 kips.

Figure 6.2 shows the end moment versus the end deflection for A₁. The load deflection relationship remained linear up to a load of 22.0 kips and then started to deviate. The end deflection reached 2.6 in. at failure.

Figure 6.7 shows the variation of the bottom fibre steel strain at section 1-1 with the applied moment. The steel strain followed a straight line relationship with the applied moment and started rounding

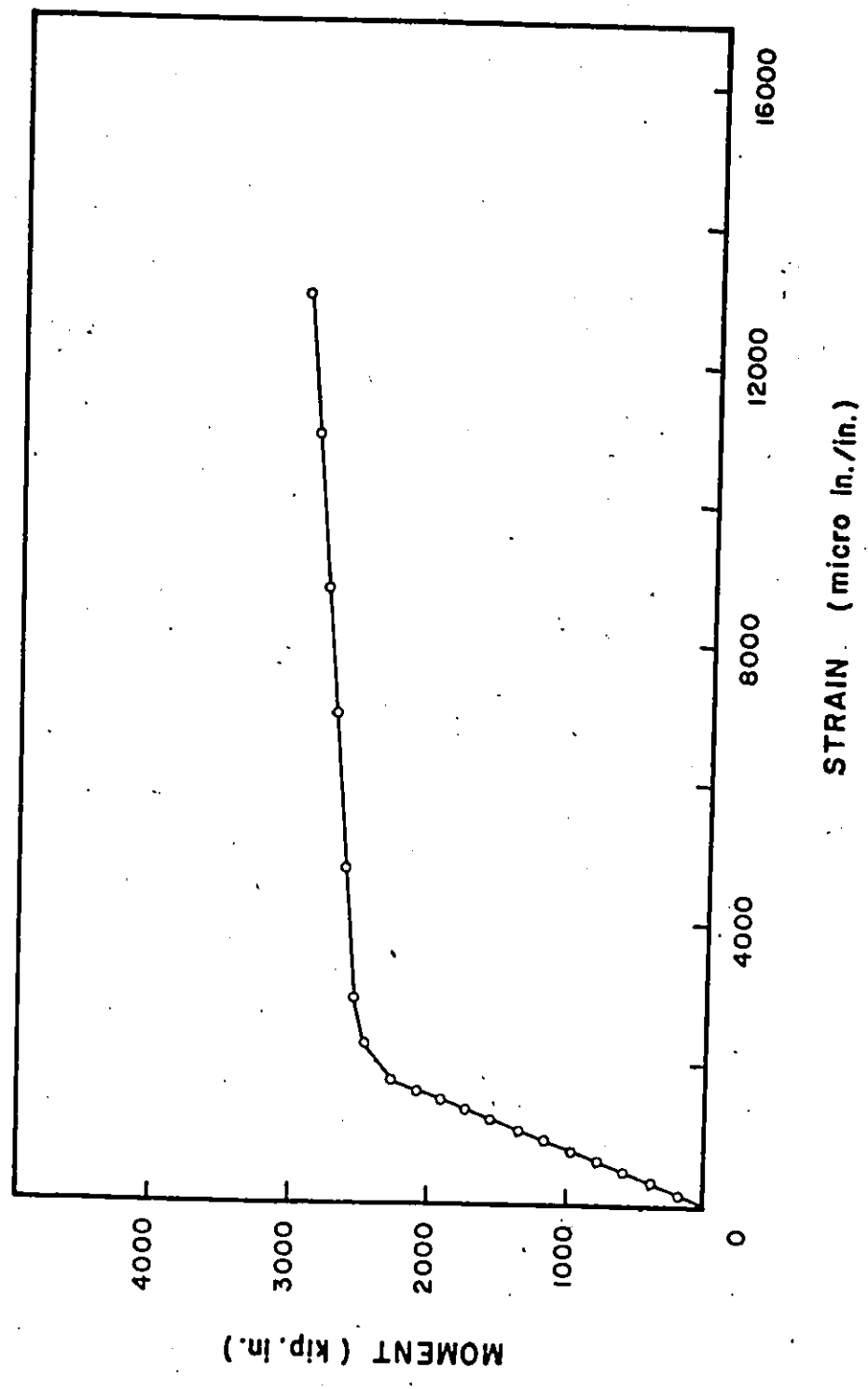


FIGURE 6.7 LIVE LOAD MOMENT VERSUS BOTTOM FIBRE STEEL STRAIN FOR END A1

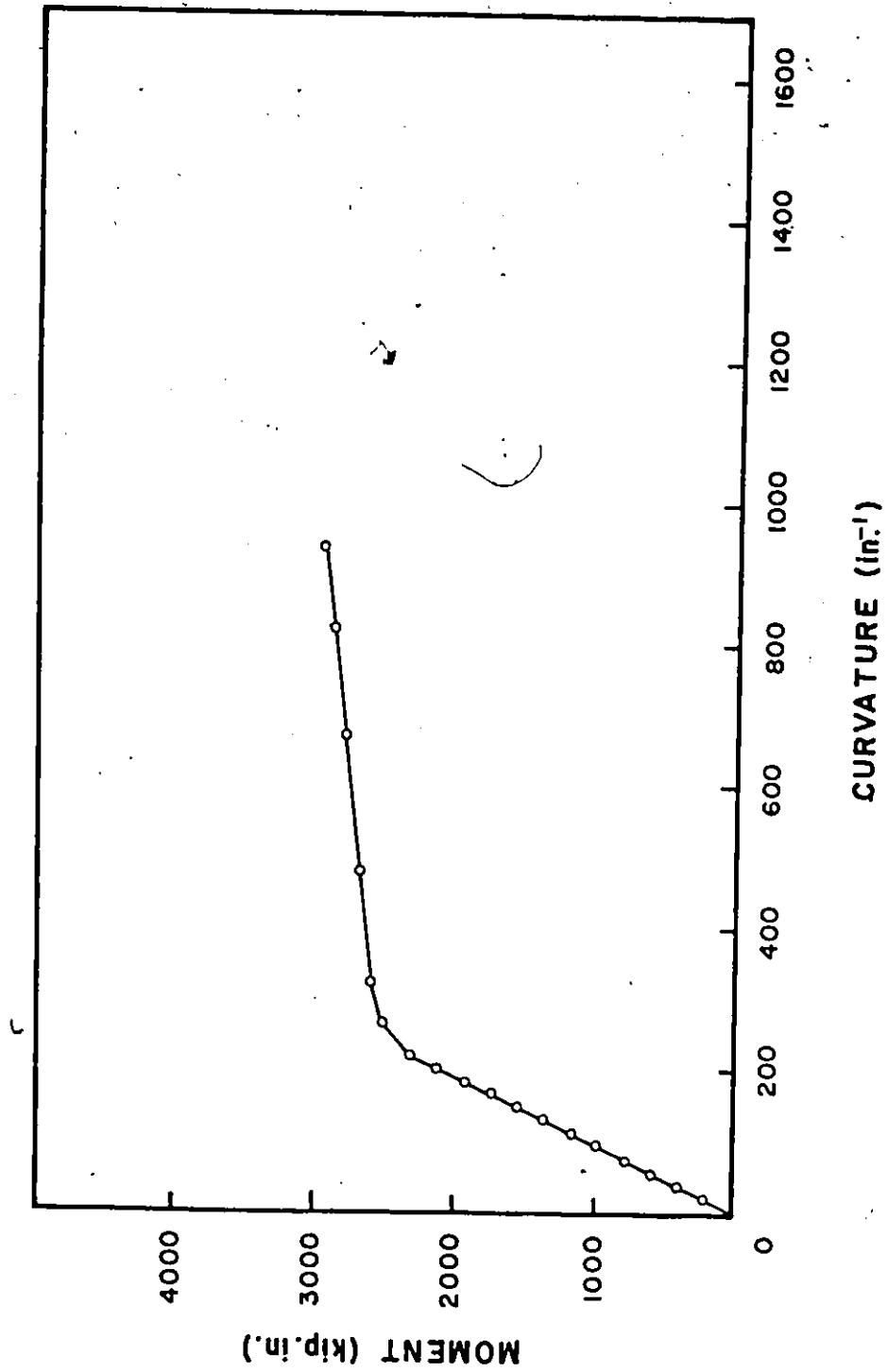


FIGURE 6.8 LIVE LOAD MOMENT - CURVATURE RESULTS FOR END A1

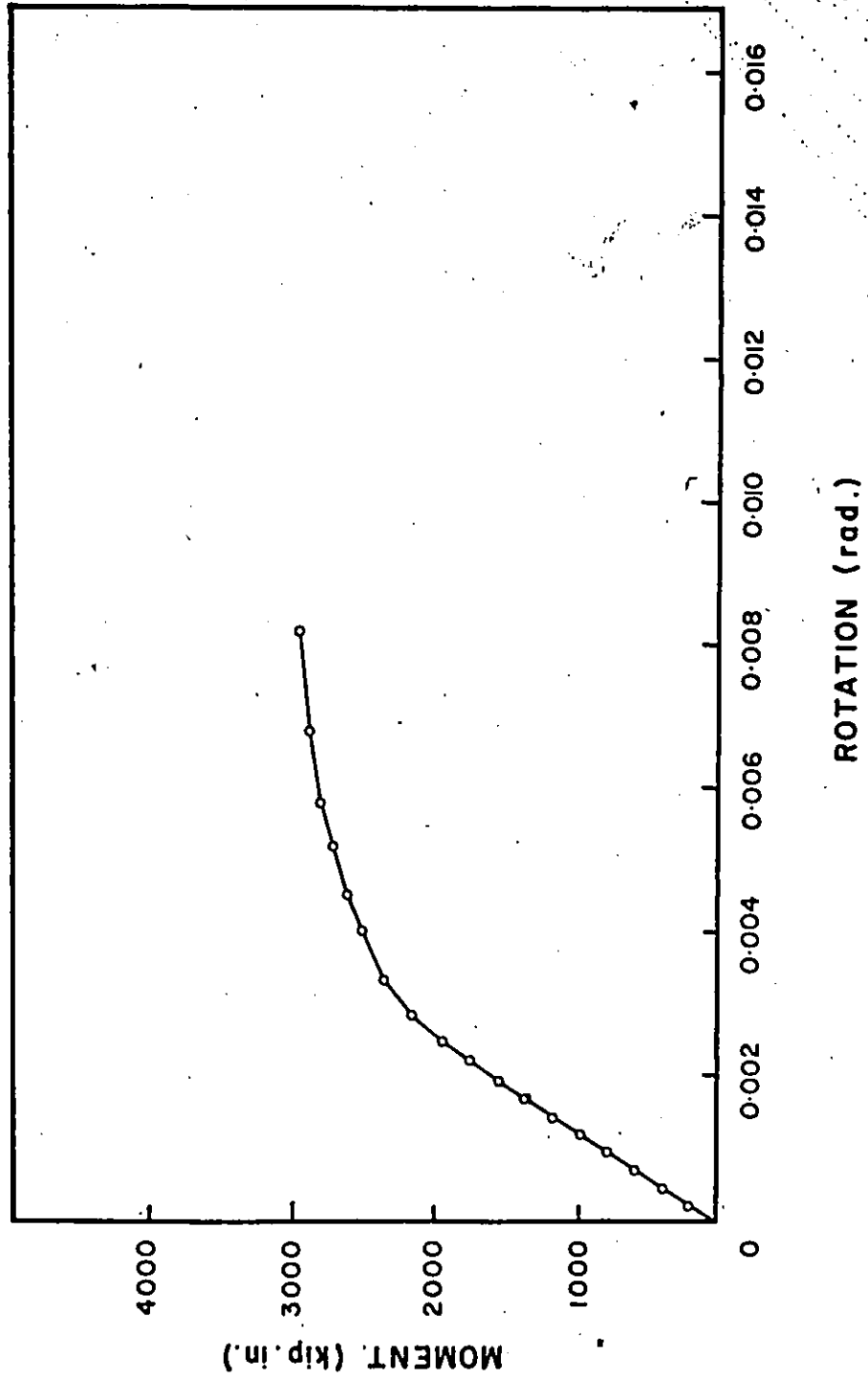
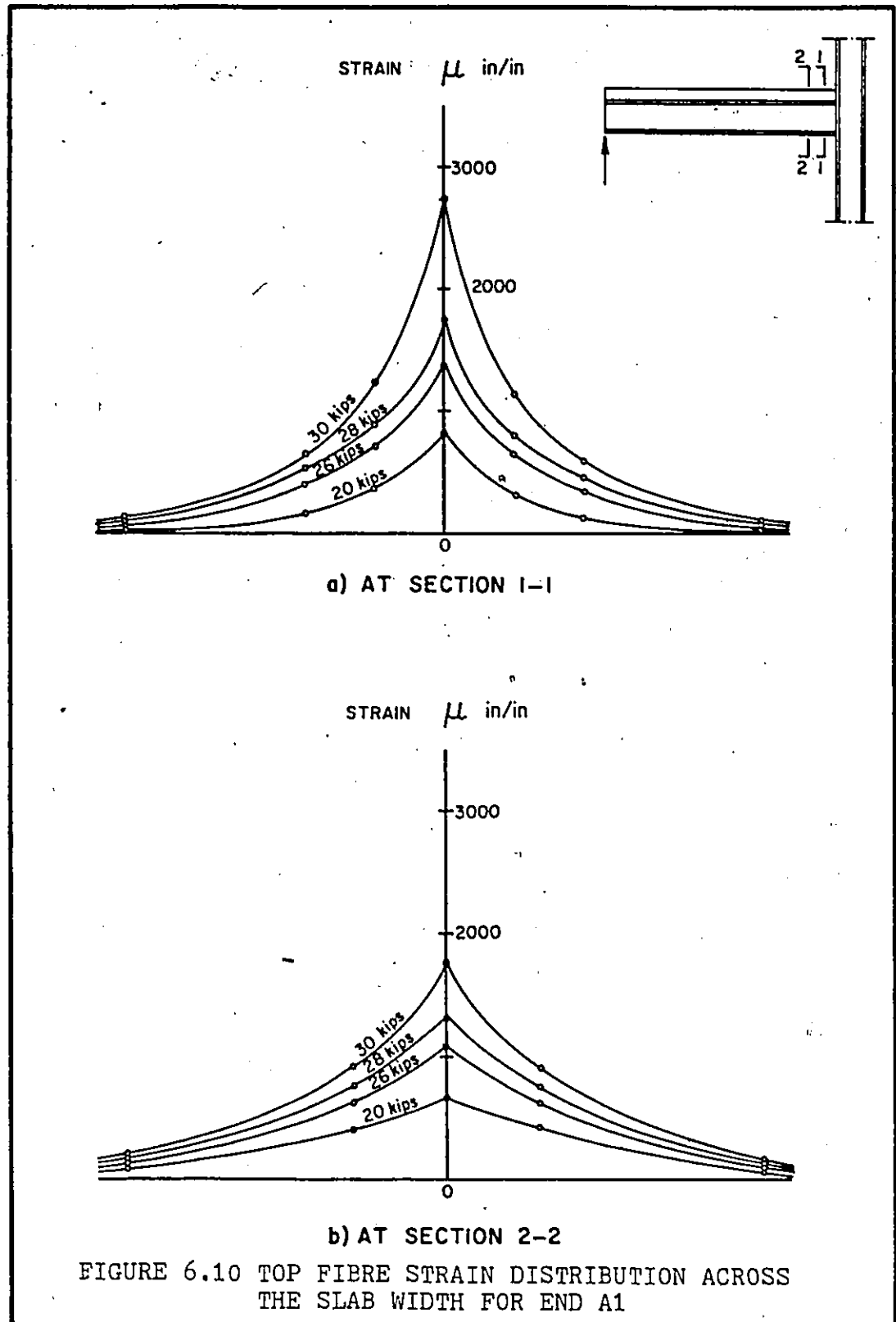


FIGURE 6.9 ' LIVE LOAD MOMENT - END ROTATION RESULTS FOR END A1



at a test load of 24.0 kips. At failure the bottom fibre steel strain at Section 1-1 was 13000 micro in/in.

The curvature of section 1-1 is plotted against the applied moment on the section in Figure 6.8. The curvature followed a straight line relationship with the applied moment up to load 24.0 kips, after which the curvature increased more rapidly to reach a value of $940 \times 10^{-6} \text{ in}^{-1}$ at the maximum load.

The Moment-rotation curve for end A_1 is shown in Figure 6.9. The figure shows that the rotation increased linearly with the applied moment up to test load of 22.0 kips. The end rotation reach 0.0082 rad at failure. The joint modulus calculated from the moment-rotation curve was $82.6 \times 10^4 \text{ kin. in/rad}$.

The variation of the top concrete strains across the slab width at sections 1-1 and 2-2 are shown in Figure 6.10. As observed in testing A_2 , the peak strain at both sections occurred over the steel beam centre line and the strain distribution was more uniform at section 2-2 than at section 1-1.

No signs of connectors punching through the metal deck and no other signs of damage were observed up to failure. Failure of the specimen occurred at load 30.7 kips due to crushing of the concrete slab in front of the column face.

6.3.2 Beam B

Beam B was identical to Beam A. The end with the small plate (B_1) was tested first this time and then the beam was turned around and

the end (B_2) was tested. The effect of the existence of the longitudinal crack was determined for the comparison of end (A_1) with end (B_1) and end (A_2) with (B_2). The result of this comparison is mentioned later in this chapter.

6.3.2-a End B_1

The small end plate B_1 was bolted to the column and the beam was loaded in the same manner as for beam A. Loading started with a load increment of 2 kips up to load 26.0 kips and was reduced after that to 1 kip until failure. The load remained steady up to a test load of 16.0 kips when it started to drop a small amount of 0.1 kip. The amount of the drop in the load increased with increasing the load and reached about 0.8 kip before failure.

The measured free end deflection increased linearly with the increase in the applied end moment. At load 22.0 kips the linear relationship ceased and the deflection increased more rapidly with the increase in the load to reach a value of 2.92 in. at failure. Figure 6.11 shows the measured end deflection versus the applied end moment.

The bottom fibre steel strain at section 1-1 increased linearly with the increase in the applied moment and started to deviate from the linear relationship at load 22.0 kips. At this instant the strain was about 1700 micro in/in. The bottom fibre steel strain reached 14300 micro in/in at failure. The measured strains at section 1-1 and 2-2 indicated that yielding occurred at section 1-1 before section 2-2. Figure 6.12 shows the measured bottom fibre steel strains at section 1-1 versus the applied moment at that section.

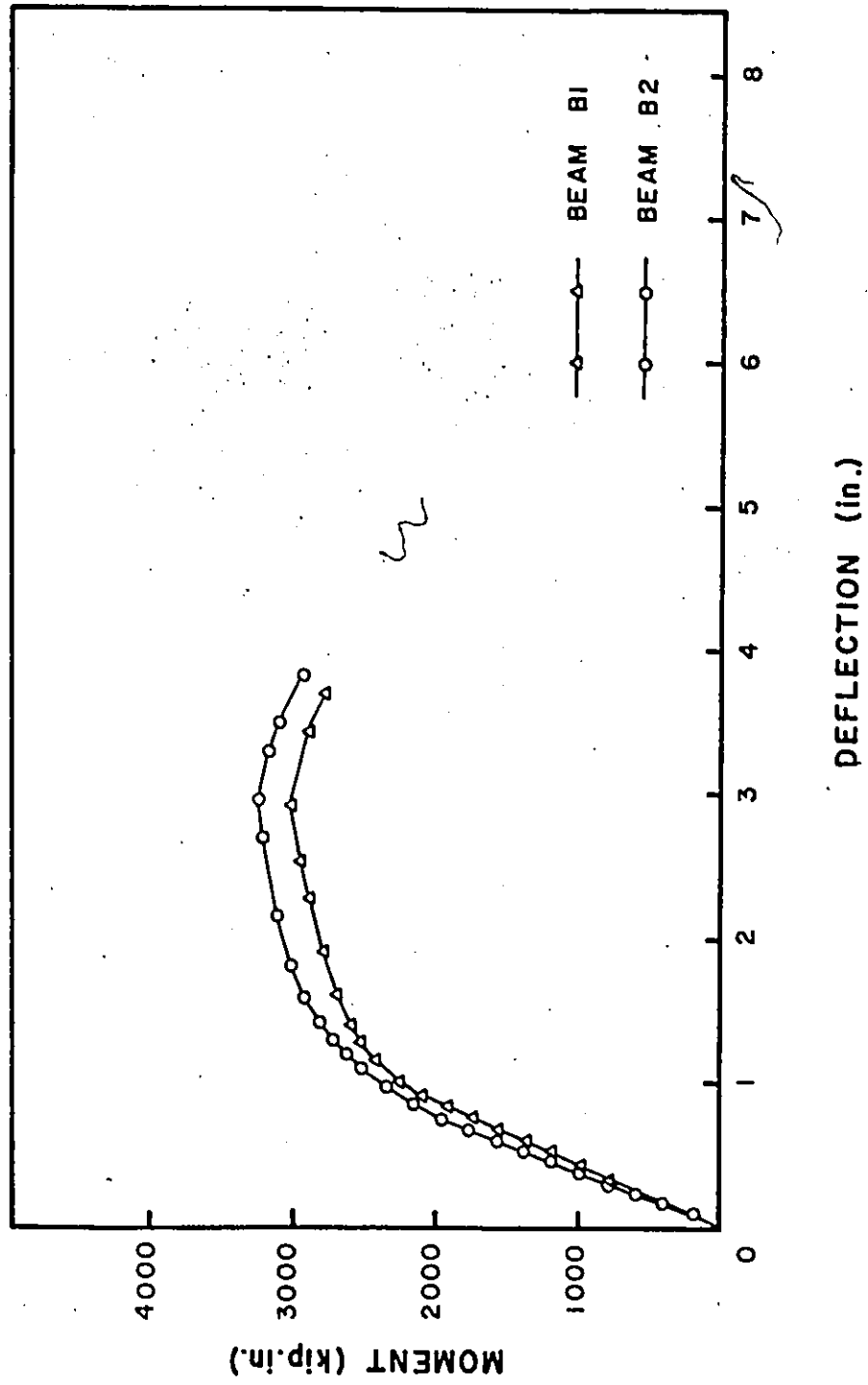


FIGURE 6.11 LIVE LOAD END MOMENT - END DEFLECTION RESULTS FOR ENDS B1 AND B2

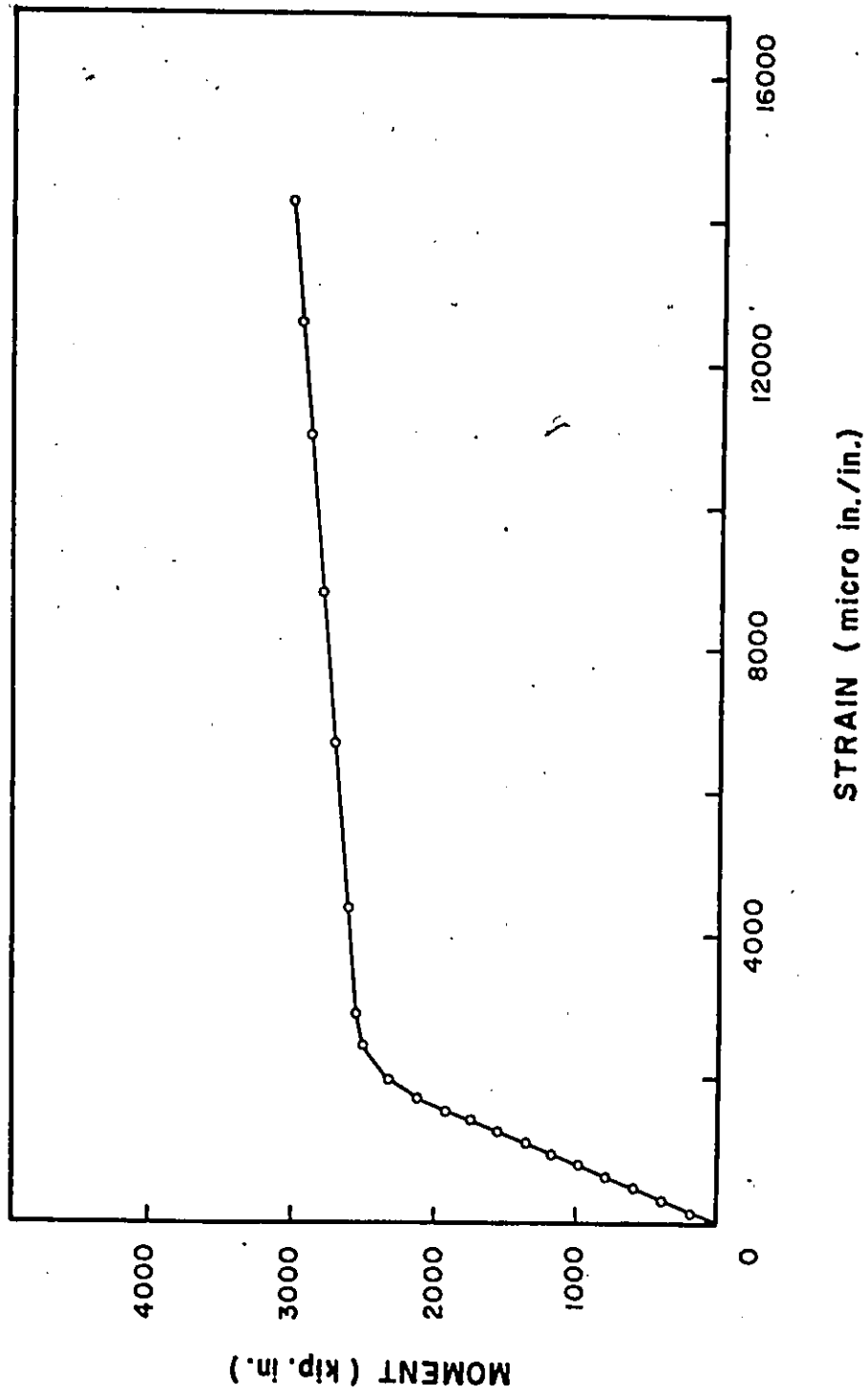


FIGURE 6.12 LIVE LOAD MOMENT VERSUS BOTTOM FIBRE STEEL STRAIN FOR END B1

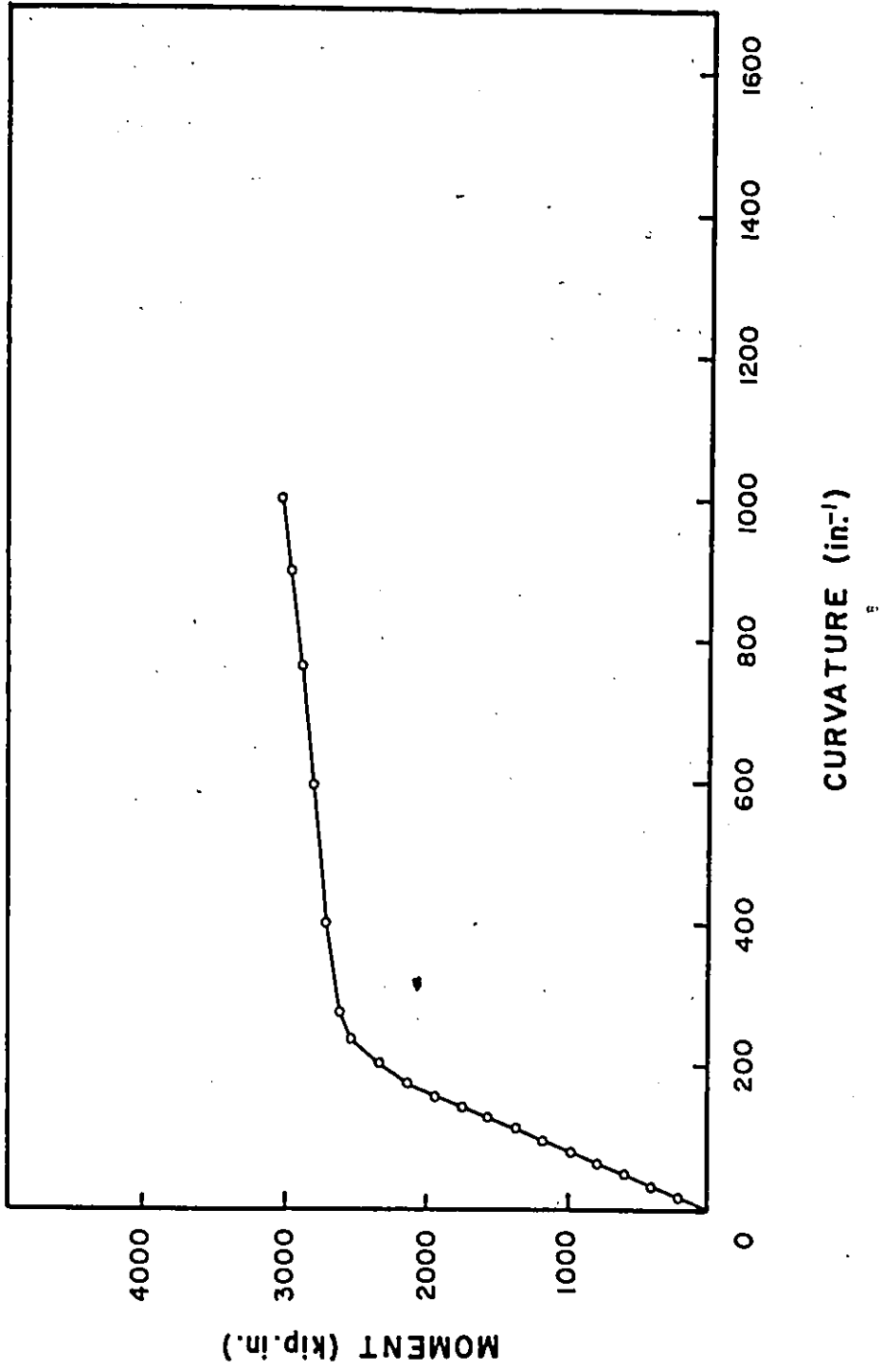


FIGURE 6.13 LIVE LOAD MOMENT - CURVATURE RESULTS FOR END B1

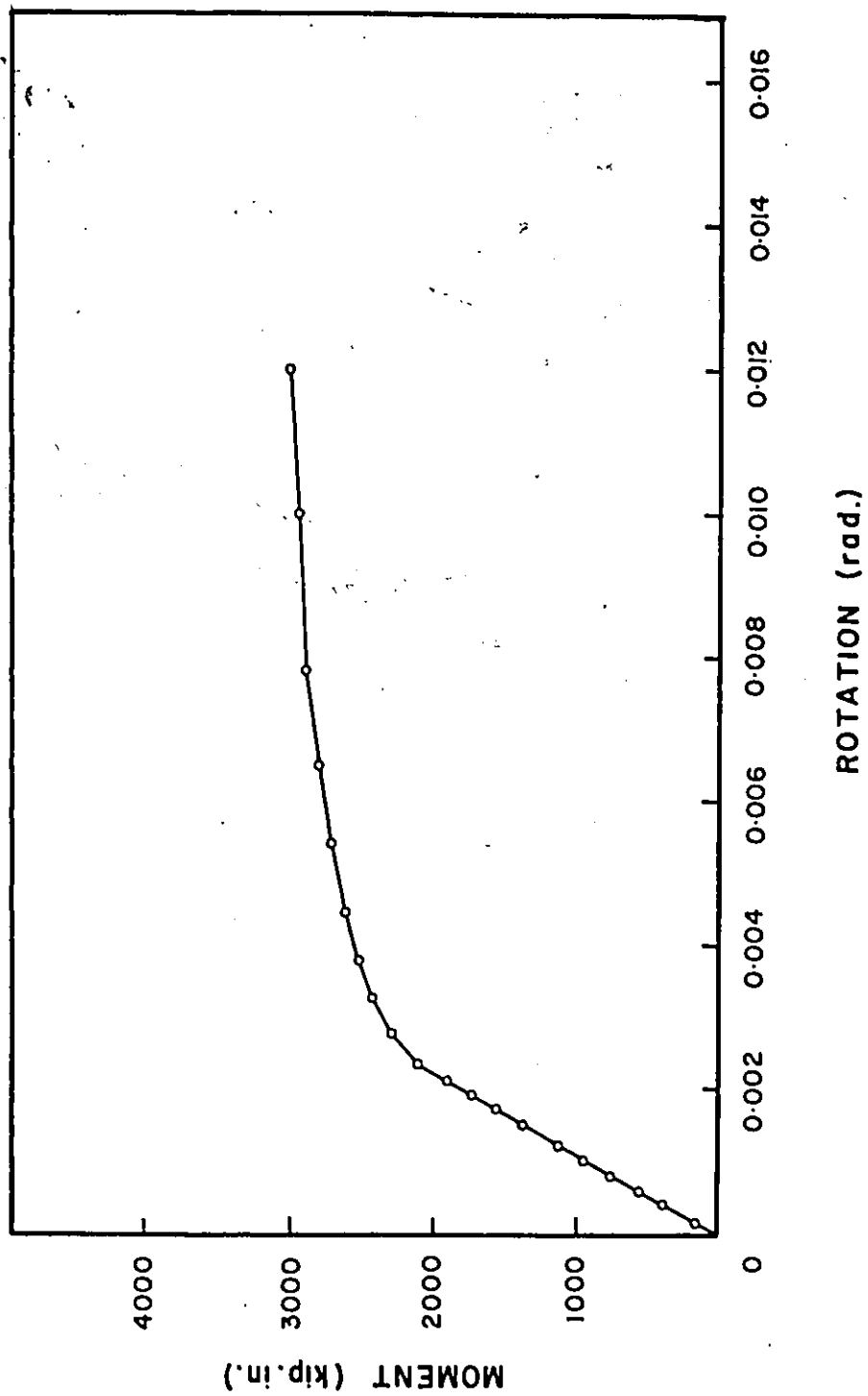


FIGURE 6.14 LIVE LOAD MOMENT - END ROTATION RESULTS FOR END B1

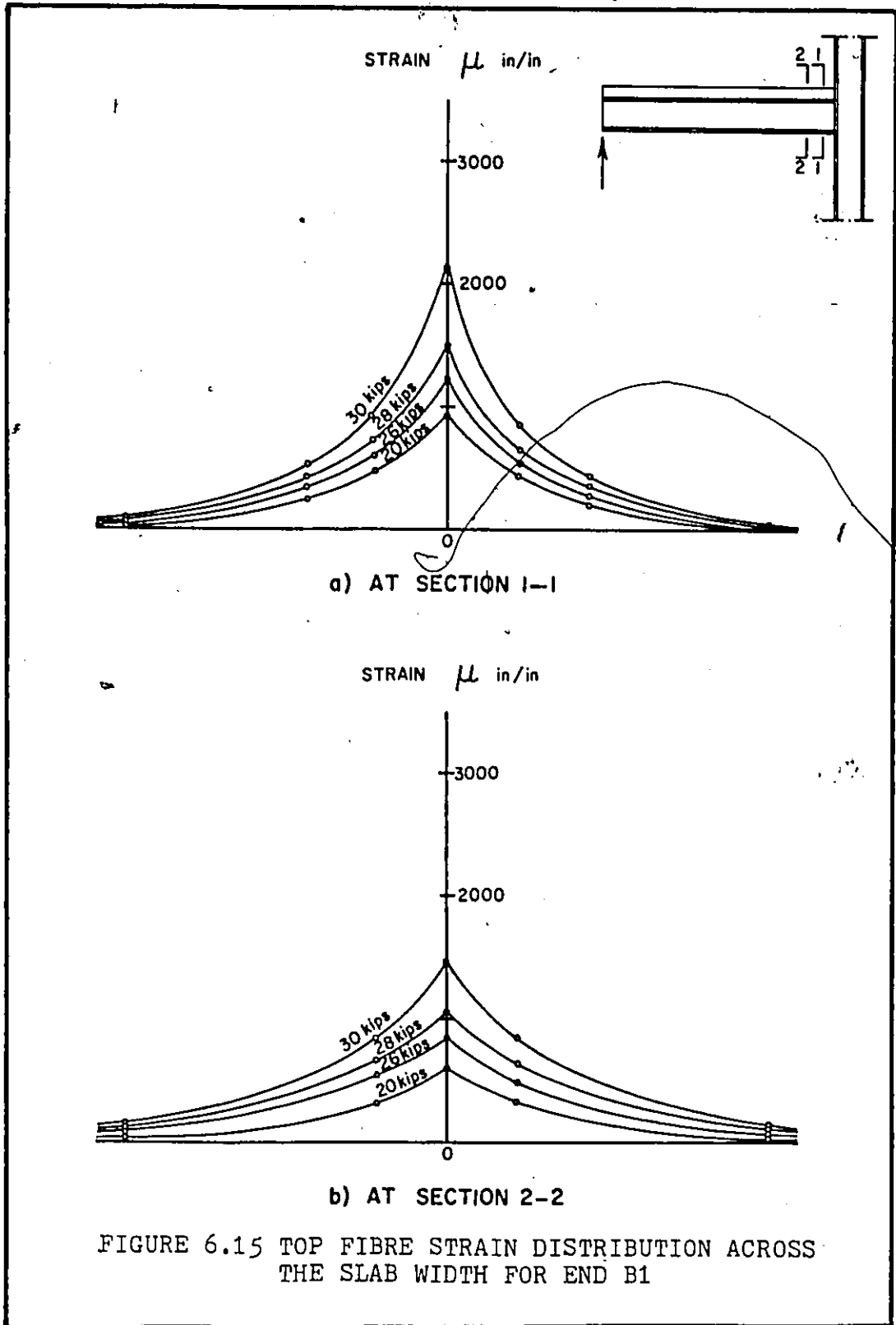


FIGURE 6.15 TOP FIBRE STRAIN DISTRIBUTION ACROSS THE SLAB WIDTH FOR END B1

Figure 6.13 shows the moment-curvature curve at section 1-1. The moment-curvature relationship was also linear up to a load of 22.0 kips when it started rounding. The curvature at this instant was about $175 \times 10^{-6} \text{ in}^{-1}$. The curvature increased more rapidly after that and when the specimen failed the curvature was $1000 \times 10^{-6} \text{ in}^{-1}$.

The moment-rotation curve for end B_1 is shown in Figure 6.14 which shows that the end rotation followed the linear relationship with the applied end moment up to a load of 22.0 kips when it started rounding and the end rotation was 0.012 rad when the specimen failed. The joint modulus for this end was found to be $93.6 \times 10^4 \text{ kip. in/rad}$.

Figure 6.15 shows the top fibre concrete strain distributions at sections 1-1 and 2-2. The strain distribution followed the same pattern as for end A_1 . As observed before the strain distributions were non-uniform across the slab width with the peak strain occurring over the centre line of the steel beam and the distribution at Section 2-2 was more uniform than at Section 1-1 at all load levels.

At a test load of 28.0 kips a longitudinal crack was observed on the top of the slab over the steel beam centre line close to the fixed end. The crack propagated with increasing the load and almost reached the free end at failure.

At a test load of 31.7 kips the specimen failed due to crushing of the concrete slab adjacent to the column face. No other signs of damage or connector failure were observed in the beam.

6.3.2-b End B_2

The end B_2 was tested after completing the test on B_1 . The

concrete slab was already longitudinally cracked over the steel beam along the whole length of the beam before starting the test.

The end plate B_2 was bolted to the column and the specimen was loaded, as before with a load increment of 2 kips up to the load of 26.0 kips and then reduced to 1 kip up to failure. The load started to drop a small amount of 0.1 kip at load 18.0 and was fairly steady before this load.

The end moment-end deflection relationship followed the same pattern as for end B_1 . The linear relationship ceased at a load of 24.0 kips after which the rate of increase in the deflection increased with the applied load and the deflection reached 2.97 in. at failure. The end moment versus the end deflection for end B_2 is shown in Figure 6.11.

Figure 6.16 shows the variation in the bottom fibre steel strains at section 1-1 with the applied moment on the section. As observed before the increase in the strain was linear with the load. The linear relationship ceased at the load of 24.0-kips. At this instant the bottom fibre steel strain was about 1750 micro in/in and it reached a value of 16400 micro in/in at failure.

The moment-curvature curve at section 1-1 is shown in Figure 6.17. The figure shows that curvature followed a linear relationship with the applied moment up to the load of 24.0 kips and increased more rapidly after that. At load 24.0 kips the curvature was $170 \times 10^{-6} \text{ in}^{-1}$ and it reached the value of $1500 \times 10^{-6} \text{ in}^{-1}$ when the specimen failed.

The end rotation followed a linear relationship with the applied end moment up to the same load of 24.0 kips. At failure the

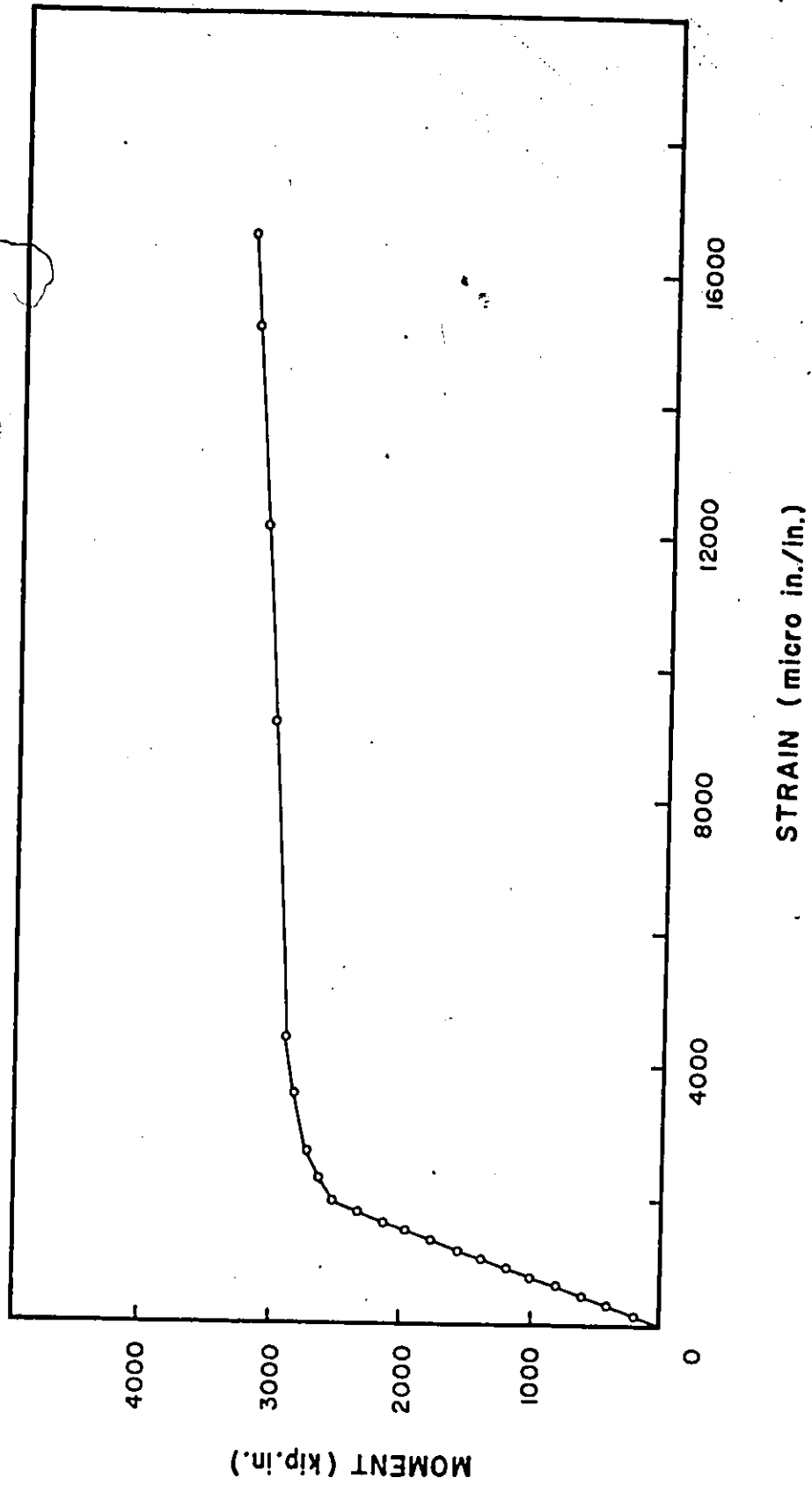


FIGURE 6.16 LIVE LOAD MOMENT VERSUS BOTTOM FIBRE STEEL STRAIN FOR END B2

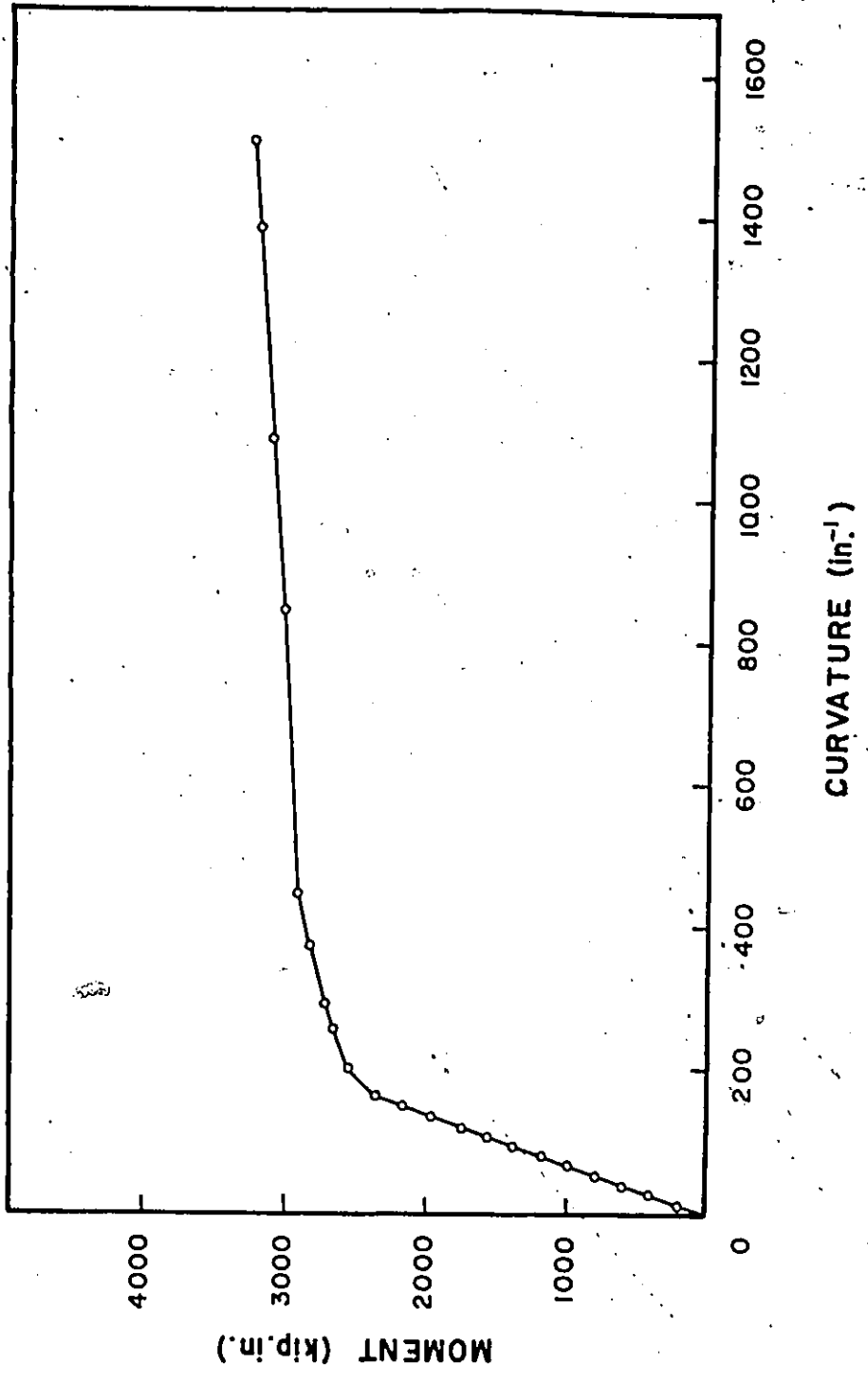


FIGURE 6.17 LIVE LOAD MOMENT - CURVATURE RESULTS FOR END B2

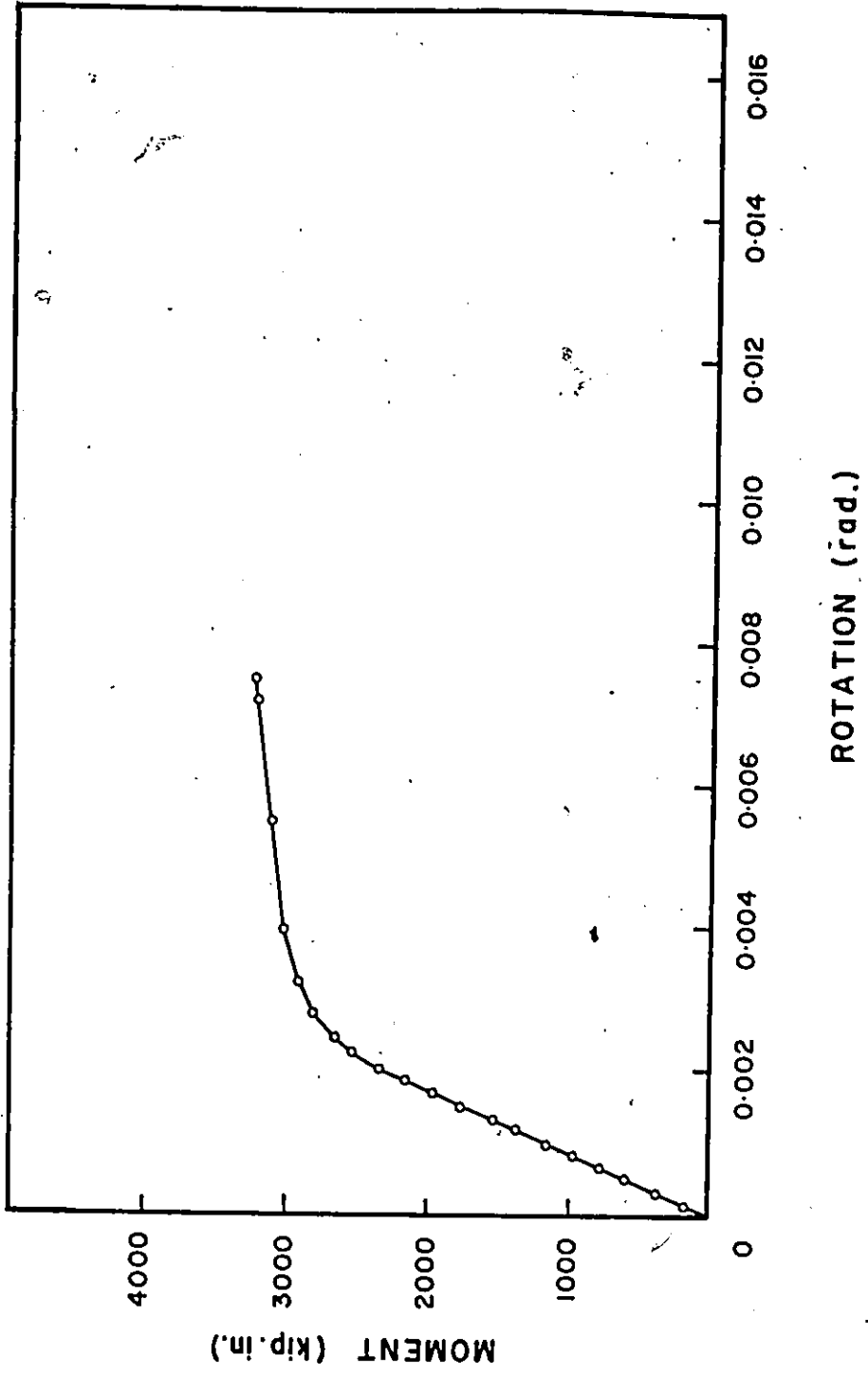
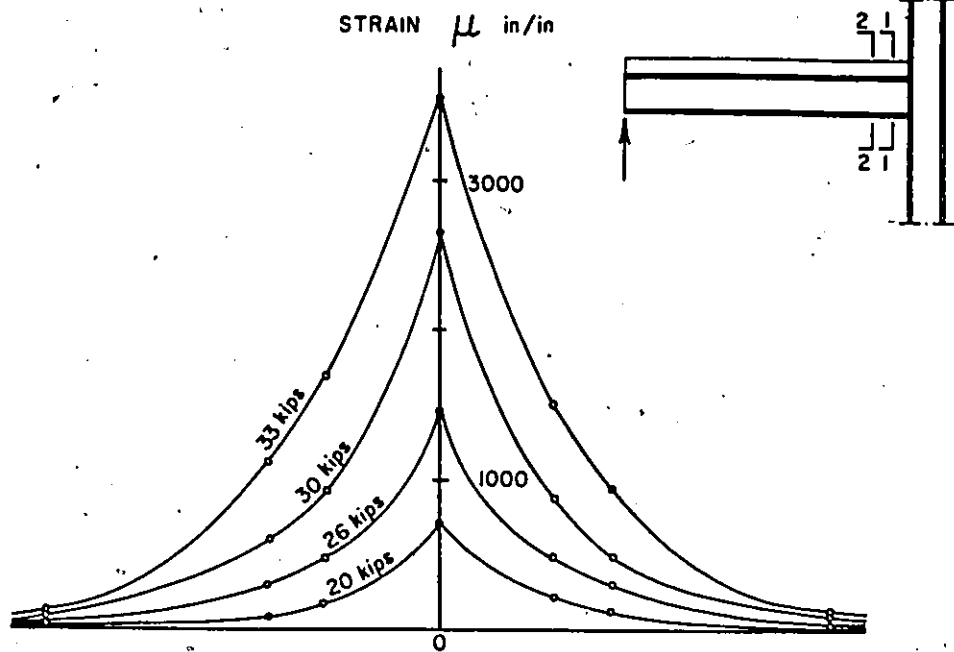
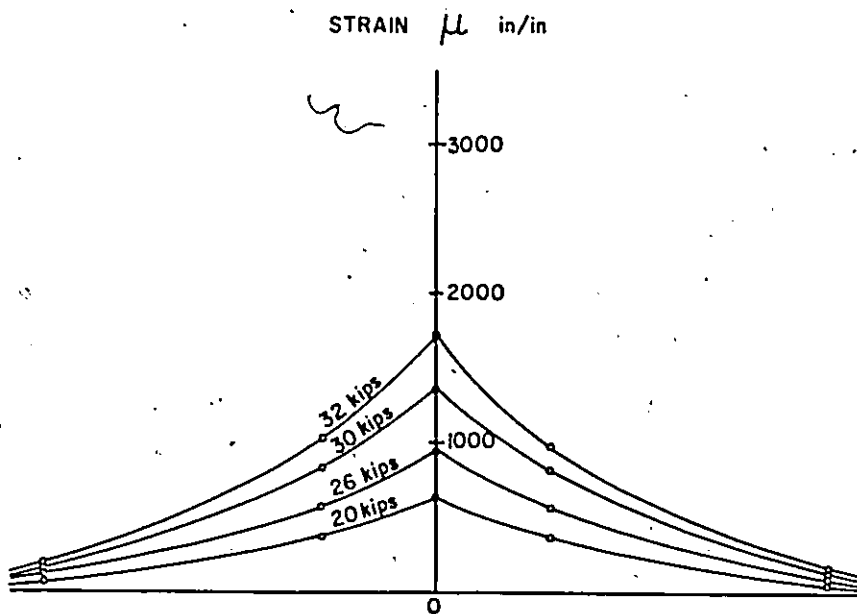


FIGURE 6.18 LIVE LOAD MOMENT - END ROTATION RESULTS FOR END B2



a) AT SECTION 1-1



b) AT SECTION 2-2

FIGURE 6.19 TOP FIBRE STRAIN DISTRIBUTION ACROSS THE SLAB WIDTH FOR END B2

calculated end rotation was .0075 rad. The joint modulus (J) calculated from the moment-rotation curve was found to be 110.4×10^4 kip. in/rad. Figure 6.18 shows the moment-rotation curve for end B₂.

Figure 6.19 shows the distributions of the top fibre concrete strain across the slab width at various load levels. The same observation concerning the characteristics of the strain distribution in the slab were observed for this end.

No signs of connector failure or pulling of the concrete slab from the metal deck were observed. The specimen failed at a load of 33.3 kips due to the crushing of the concrete slab in front of the column face.

6.3.3. Beam C

The steel beam for beam C was a W 16x40. The beam was 8 ft. long and was provided with a 10 in. wide end plate on each end of the beam.

6.3.3-a End C₁

The end plate C₁ was bolted to the column and the specimen was loaded by increments of 4 kips up to a load of 40.0 kips when it was reduced to 2 kips. At a load of 50.0 kips the increment was reduced again to 1 kip and was kept at this value up to failure. The load was steady up to a load of 28.0 kips when it started to drop by an amount of 0.1 kip and the drop reached 0.6 kip at a test load of 58.0 kips (just before failure).

The free end deflection increased linearly with the applied load up to load 36.0 kips when it started to slightly deviate from the linear

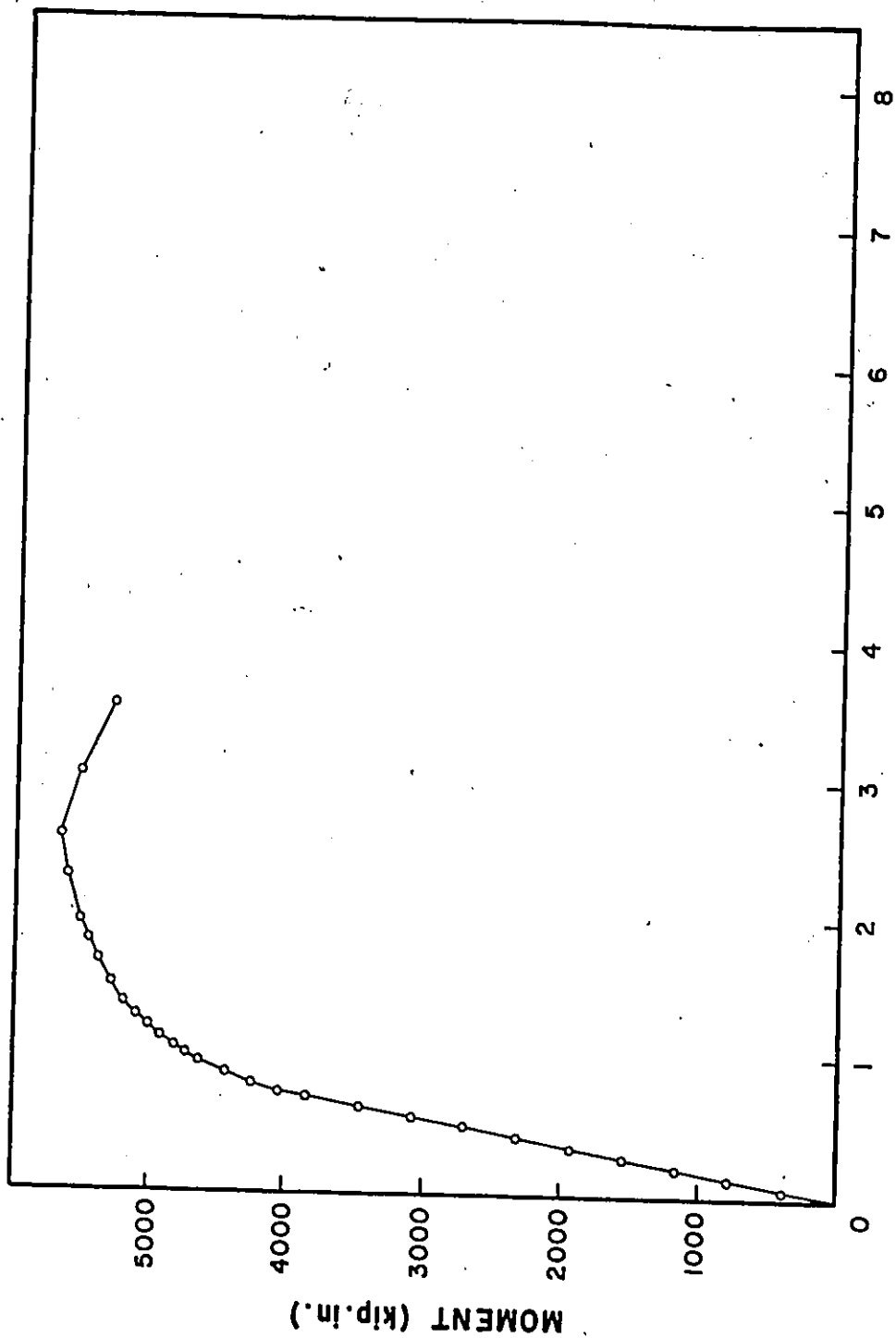


FIGURE 6.20 LIVE LOAD END MOMENT - END DEFLECTION RESULTS FOR END C1

DEFLECTION (in.)

MOMENT (kip.in.)

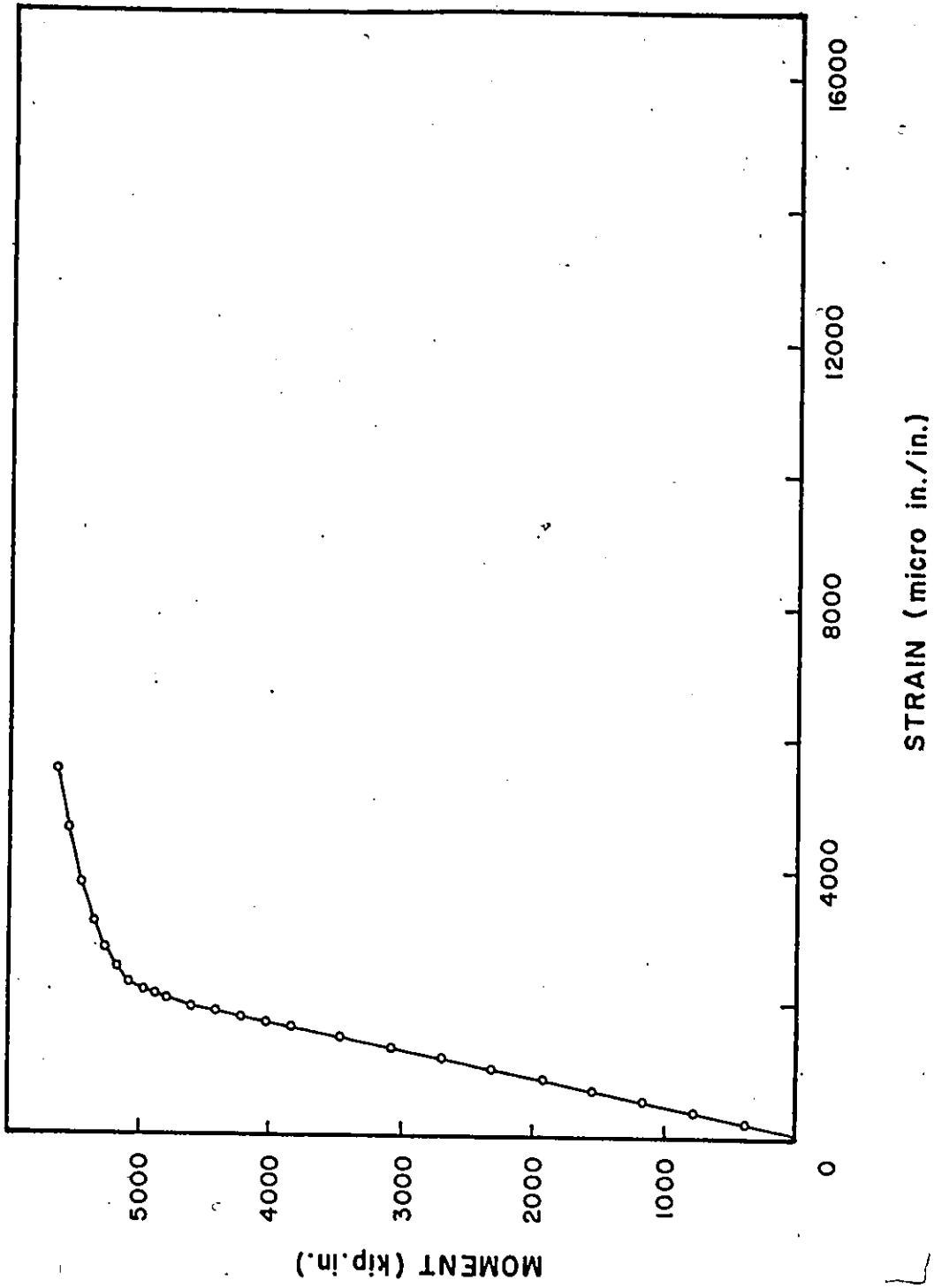


FIGURE 6.21 LIVE LOAD MOMENT VERSUS BOTTOM FIBRE STEEL STRAIN FOR END C1

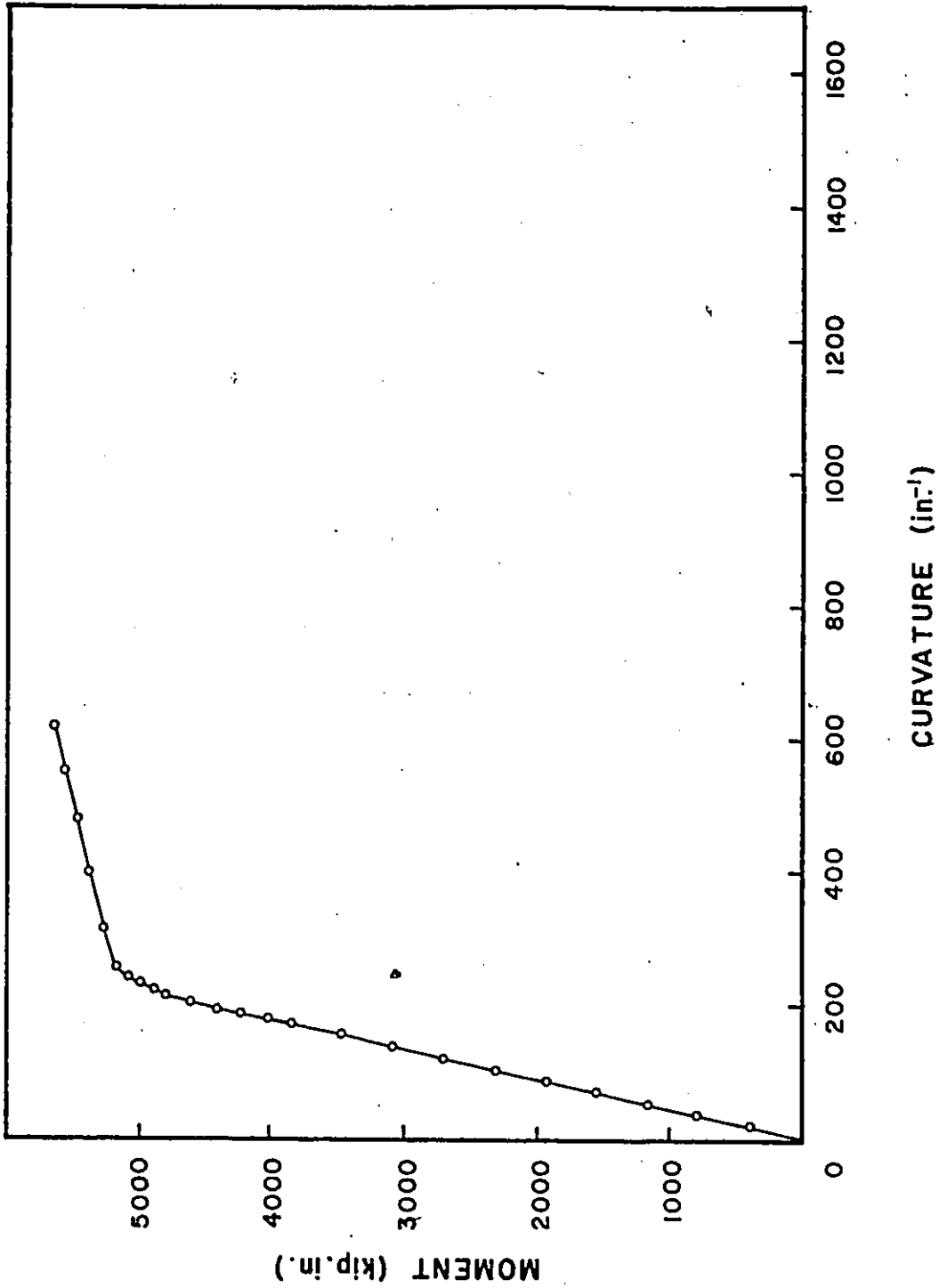


FIGURE 6.22 LIVE LOAD MOMENT - CURVATURE RESULTS FOR END C1

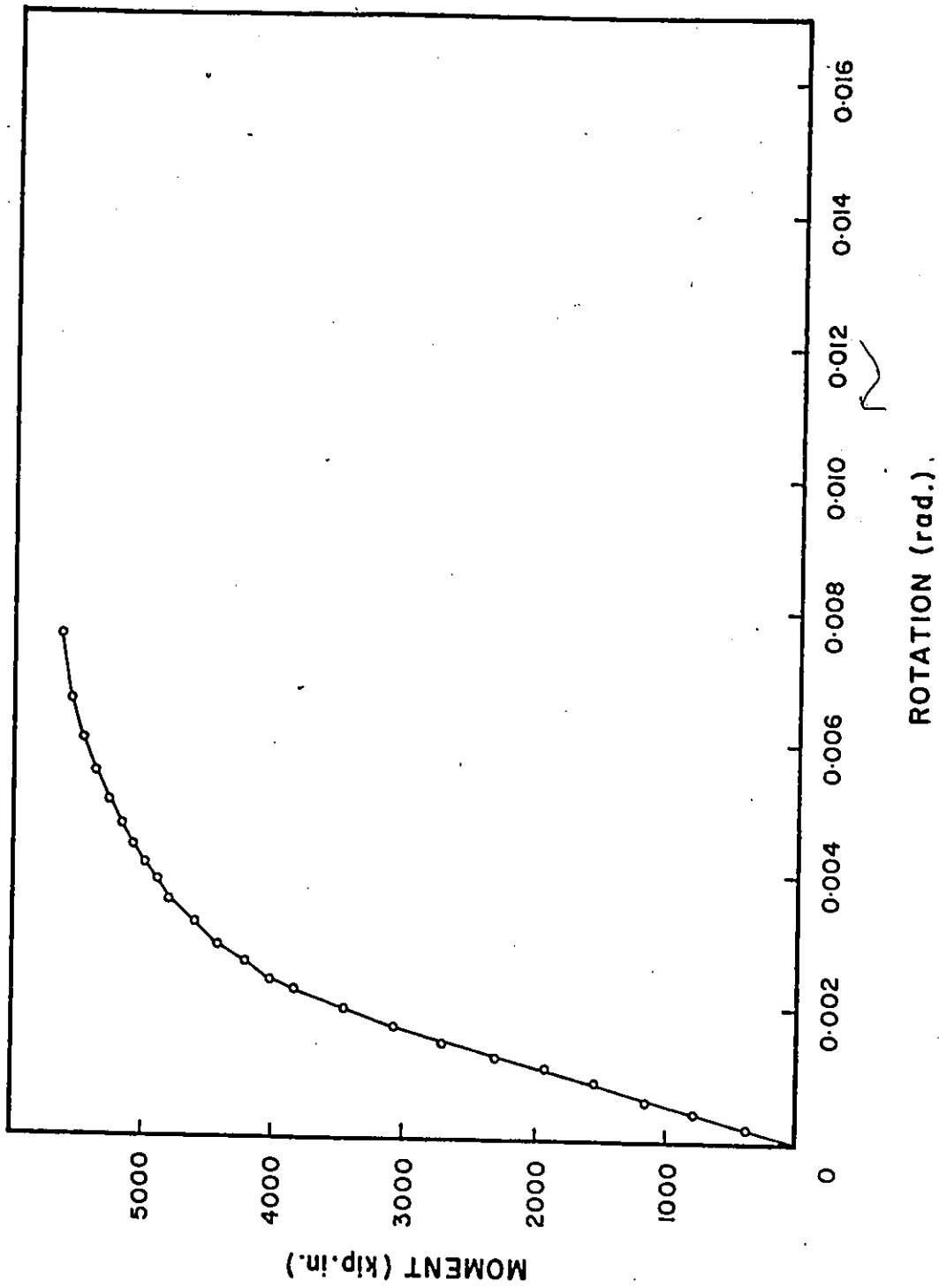
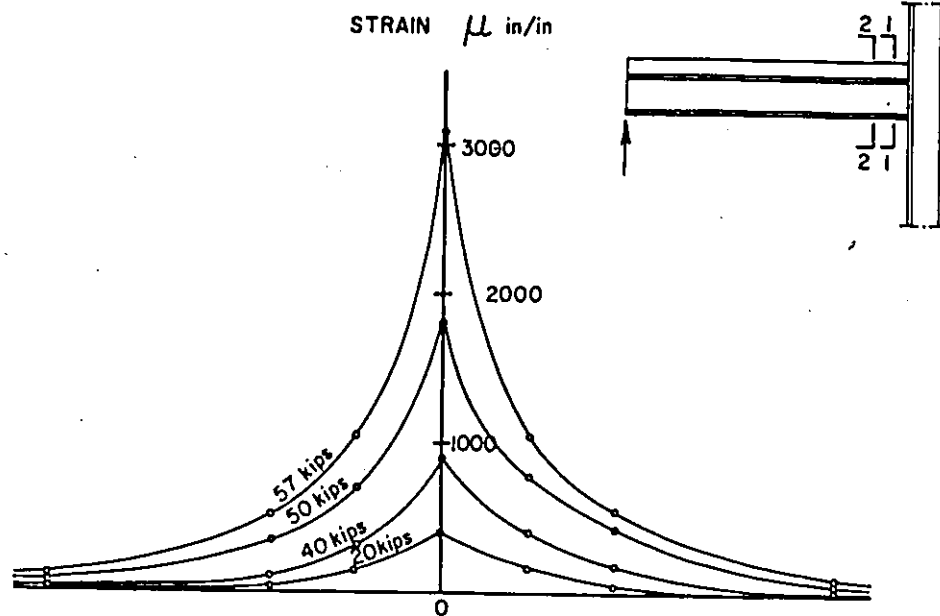
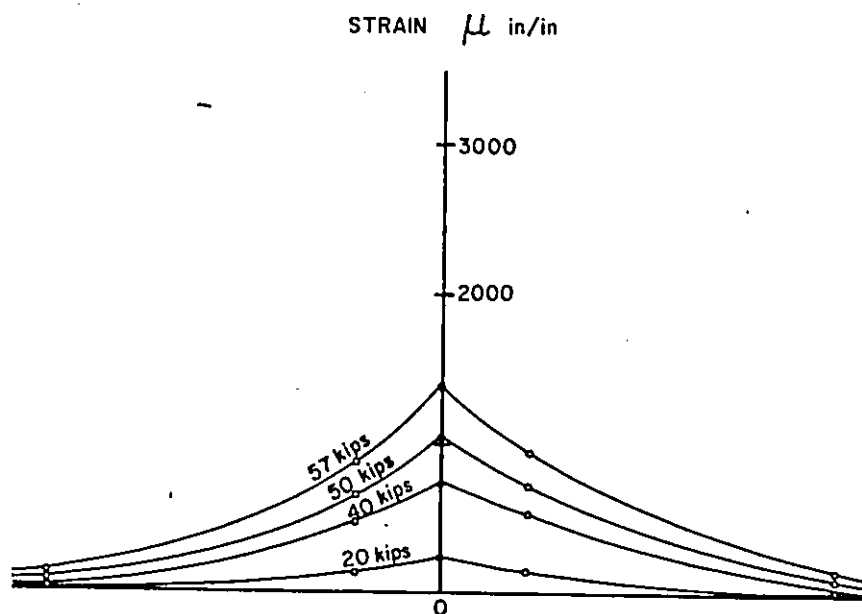


FIGURE 6.23 LIVE LOAD MOMENT - END ROTATION RESULTS FOR END C1



a) AT SECTION 1-1



b) AT SECTION 2-2

FIGURE 6.24 TOP FIBRE STRAIN DISTRIBUTION ACROSS THE SLAB WIDTH FOR END C1

relationship. The deflection at this instant was 0.55 in. At a load of 56.0 kips the rate of increasing the deflection became faster and the deflection reached a value of 2.55 in. at failure. Figure 6.20 shows the free end deflection versus the applied end moment for end C_1 .

The bottom fibre steel strain at section 1-1 followed the linear relationship with the applied moment on the section up to a load of 48.0 kips when the strain was 1950 micro in/in. At failure the bottom fibre steel strain at section 1-1 reached 5500 micro in/in. The variation of the bottom fibre steel strain at section 1-1 with the applied moment on the section is shown in Figure 6.21.

Figure 6.22 shows the moment-curvature curve at the same section. The figure shows that the moment-curvature curve started to round at the load of 48.0 kips. At this instant the curvature was $200 \times 10^{-6} \text{ in}^{-1}$. At a load of 54.0 kips the curvature started to increase more rapidly with the increase in the applied load to reach $620 \times 10^{-6} \text{ in}^{-1}$ when the specimen failed.

The end moment-end rotation relationship was similar to those of the previous beams. The linear relationship ceased at load 42.0 kips. The end rotation reached 0.0076 rad. at failure as shown in Figure 6.23. The calculated joint modulus (J) was $187.2 \times 10^4 \text{ kip. in/rad}$.

Figure 6.24 shows the top fibre strain distributions at sections 1-1 and 2-2 for various load levels.

A longitudinal crack was observed, on the top surface of the slab over the centre line of the steel beam, at a test load of 48.0 kips. The crack started close to the fixed end and almost reached the other

end at failure.

The specimen failed at a test load of 58.9 kips due to crushing of the concrete slab in front of the column face. No other signs of damage were observed.

6.3.3-b End C₂

The end C₂ was tested after completing the test on end C₁. The concrete slab was longitudinally cracked before starting the test.

The load was applied in this case in an increment of 4 kips up to load 40.0 kips when it was reduced to 2 kips up to load 46.0 kips. Then it was reduced to 1 kip and was kept at this value up to the failure of the specimen.

The moment-deflection relationship was similar to that for end C₁ with the end of the linear relation occurring at load 32.0 kips. The deflection reached a value of 2.23 in at failure. Figure 6.25 shows the end moment versus the free end deflection for end C₂.

The bottom fibre steel strain at section 1-1 increased linearly with the applied moment up to a load of 52.0 kips when it started rounding as shown in Figure 6.26. The bottom fibre steel strain reached a value of 2800 micro in/in at failure which indicate that the steel beam did not experience large plastic strains compared to end C₁.

Figure 6.27 shows the moment-curvature at section 1-1. It shows that the linear relationship ceased at load 42.0 kips and that the curvature was $440 \times 10^{-6} \text{ in}^{-1}$ at failure which is relatively small value compared to the curvature of end C₁ at failure.

The moment-rotation curve for this end is shown in Figure 6.28.

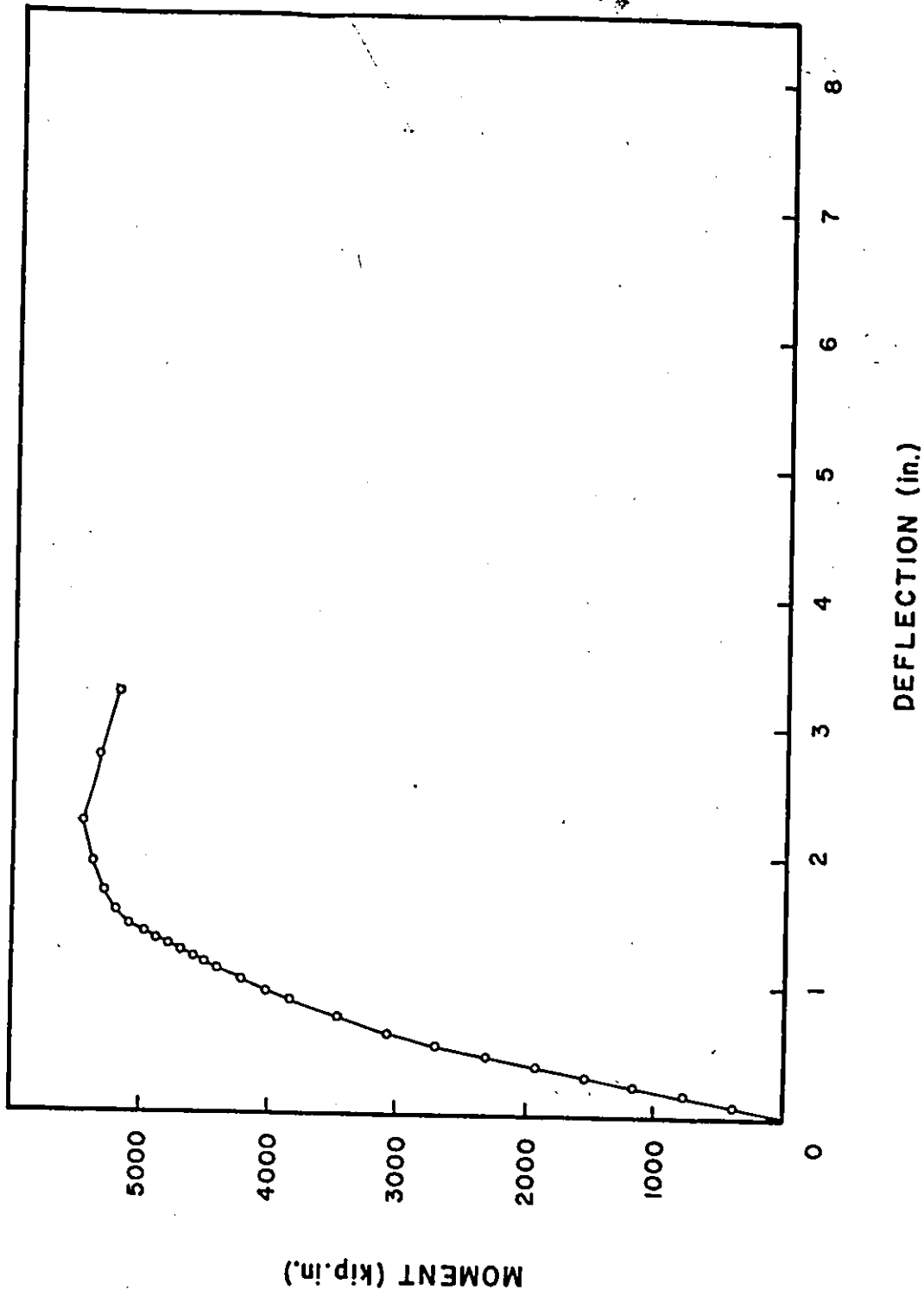


FIGURE 6.25 LIVE LOAD END MOMENT - END DEFLECTION RESULTS FOR END C2

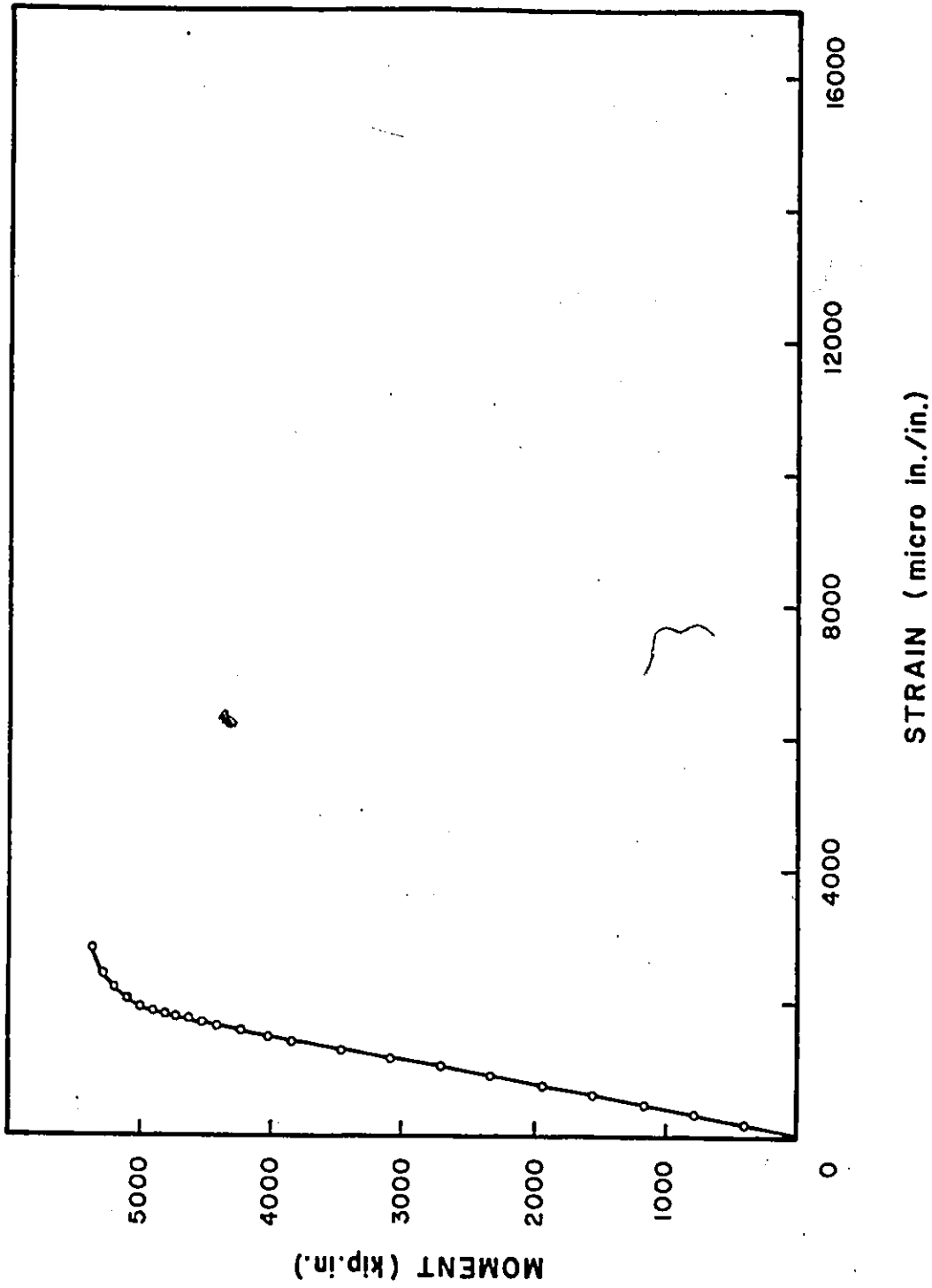
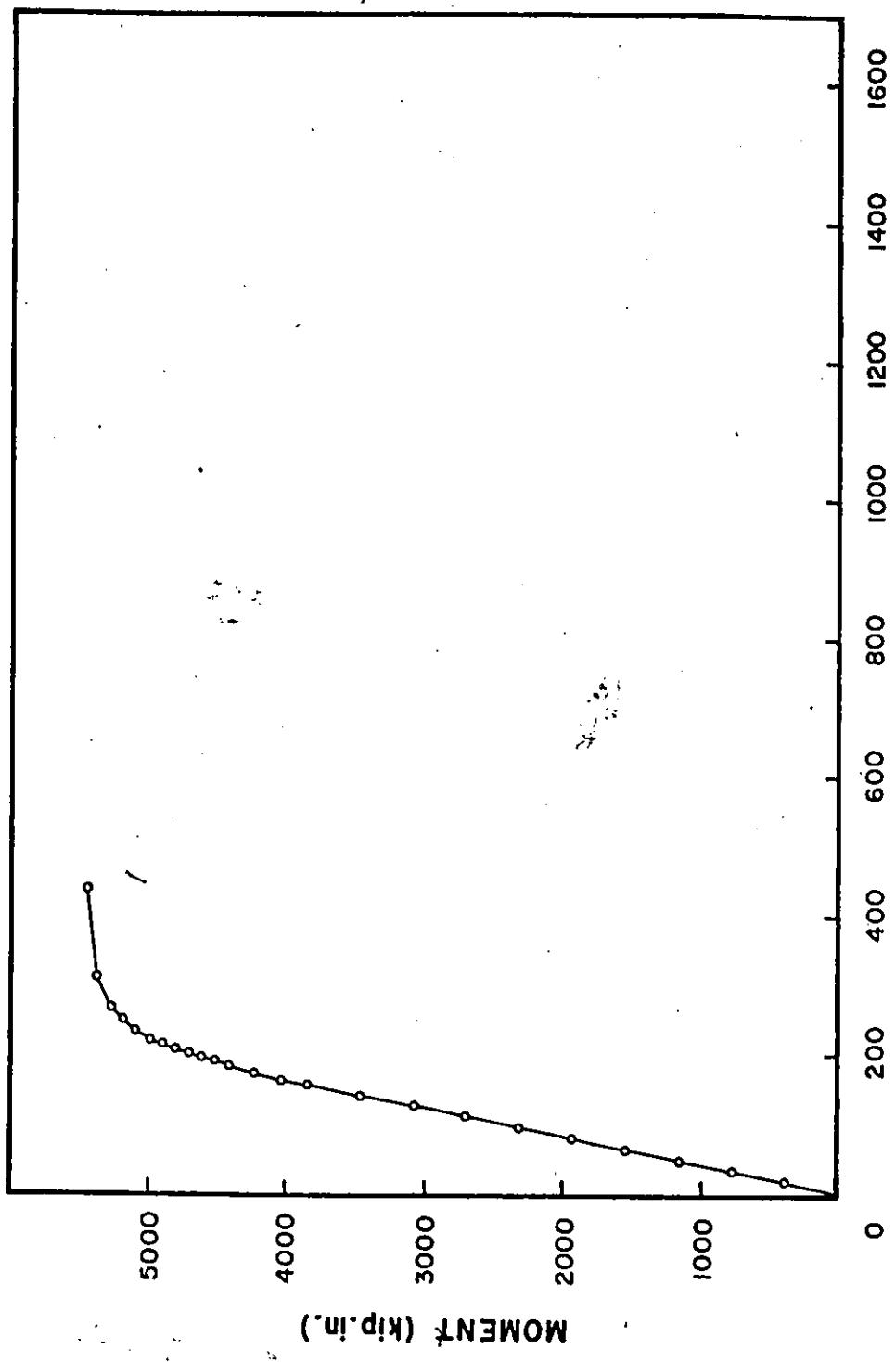
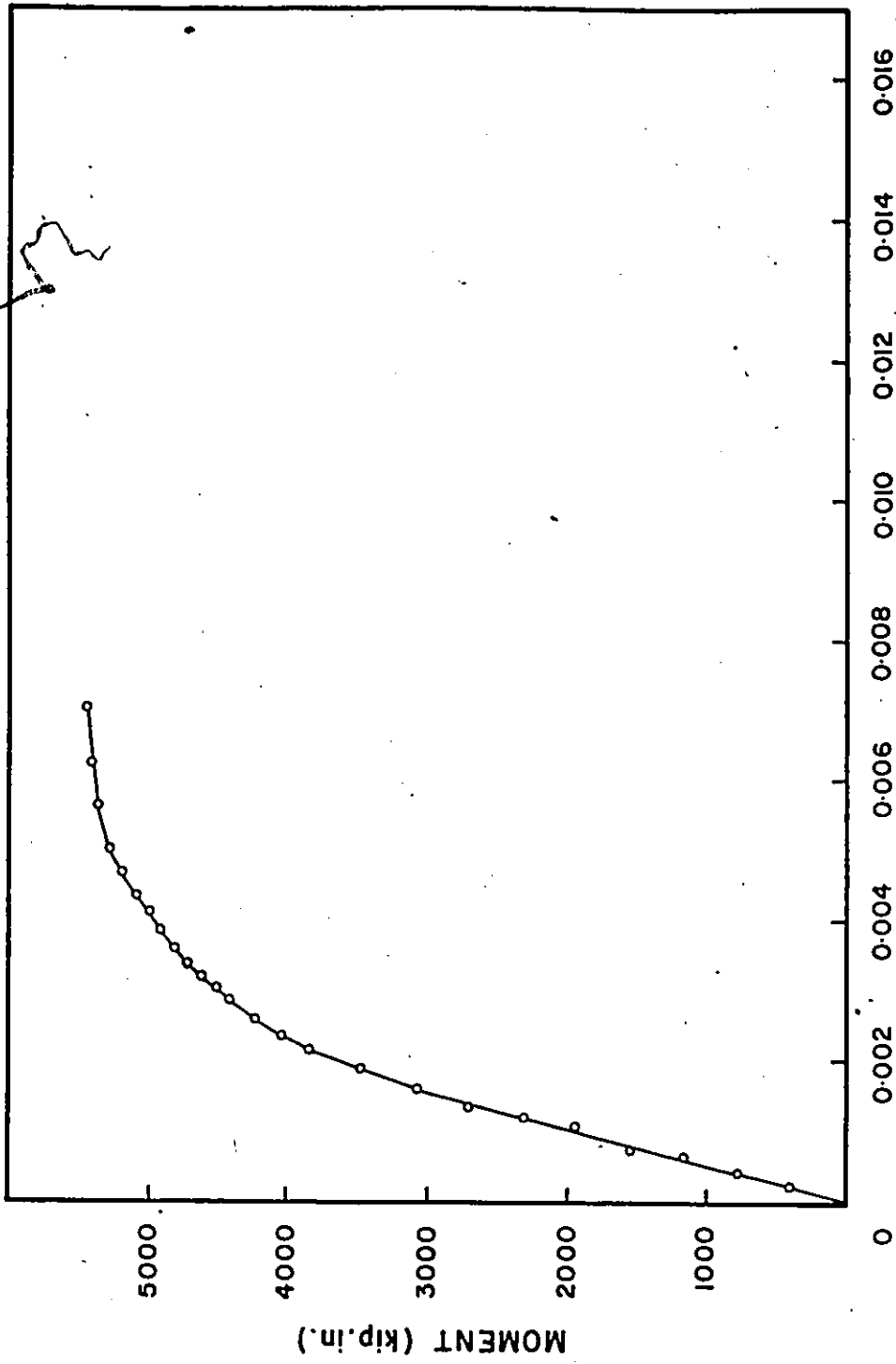


FIGURE 6.26 LIVE LOAD MOMENT VERSUS BOTTOM FIBRE STEEL STRAIN FOR END C2



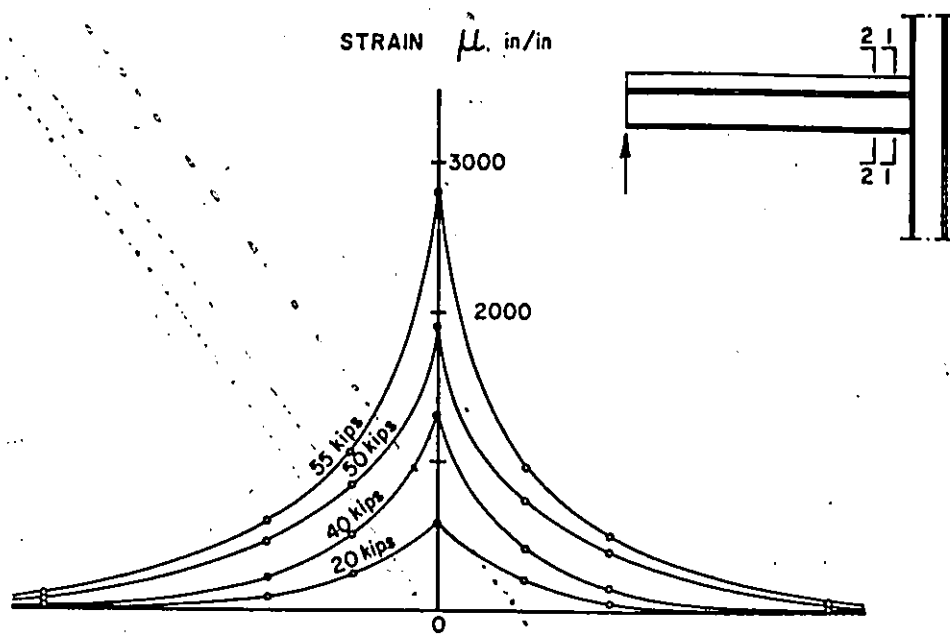
CURVATURE (in.⁻¹)

FIGURE 6.27 LIVE LOAD MOMENT - CURVATURE RESULTS FOR END C2

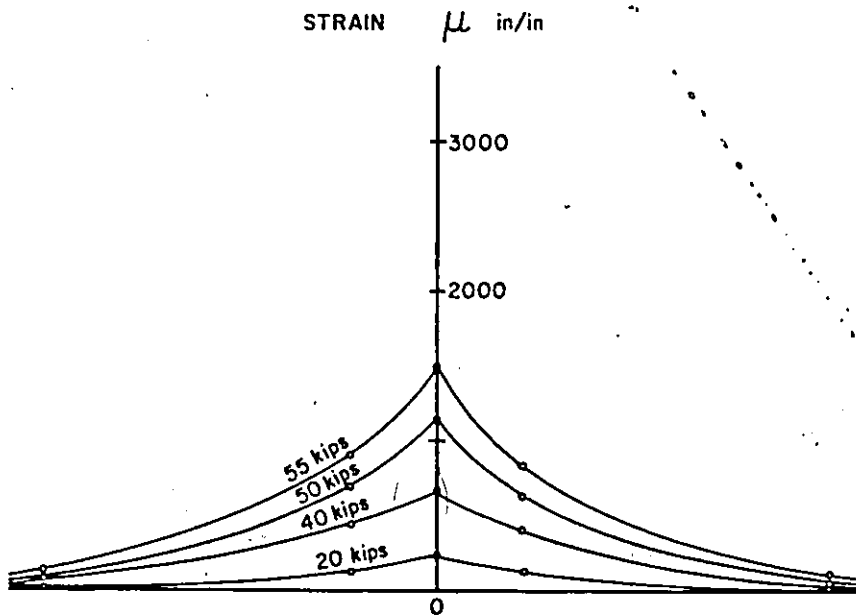


ROTATION (rad.)

FIGURE 6.28 LIVE LOAD MOMENT - END ROTATION RESULTS FOR END C2



a) AT SECTION 1-1



b) AT SECTION 2-2

FIGURE 6.29 TOP FIBRE STRAIN DISTRIBUTION ACROSS THE SLAB WIDTH FOR END C2

The end rotation reached 0.007 rad. at failure and the calculated joint modulus was 180×10^4 kip. in/rad.

Figure 6.29 shows the top fibre concrete strain distributions at sections 1-1 and 2-2 for various load levels.

At a test load of 56.8 kips the specimen failed due to crushing of the concrete slab adjacent to the column. No other signs of failure or damage were observed.

6.3.4 Beam D

Beam D was 12 ft in length. The steel beam for this composite beam was a W12x27 and the beam was provided with a 10 in. wide plate at one end (D_1) and a 15 in. wide plate at the other end (D_2). End (D_2) was tested first.

6.3.4-a End D_2

The beam was bolted to the column and was loaded in the same manner as the previous beams. The load increment was 2 kips and reduced to 1 kip at a test load of 16.0 kips. The load was steady up to the load of 16.0 kips when it started to drop by 0.1 kip, the amount of the load drop increased with the loading to reach about 0.5 kip at test load of 24.0 kips.

The linear relationship between the applied moment and the free end deflection ceased at load 17.0 kips. The deflection was 1.6 in at this instant. At a load of 20.0 kips the deflection started to increase more rapidly to reach 4.3 in. at failure as shown in Figure 6.30.

The bottom fibre steel strain at section 1-1 ceased from

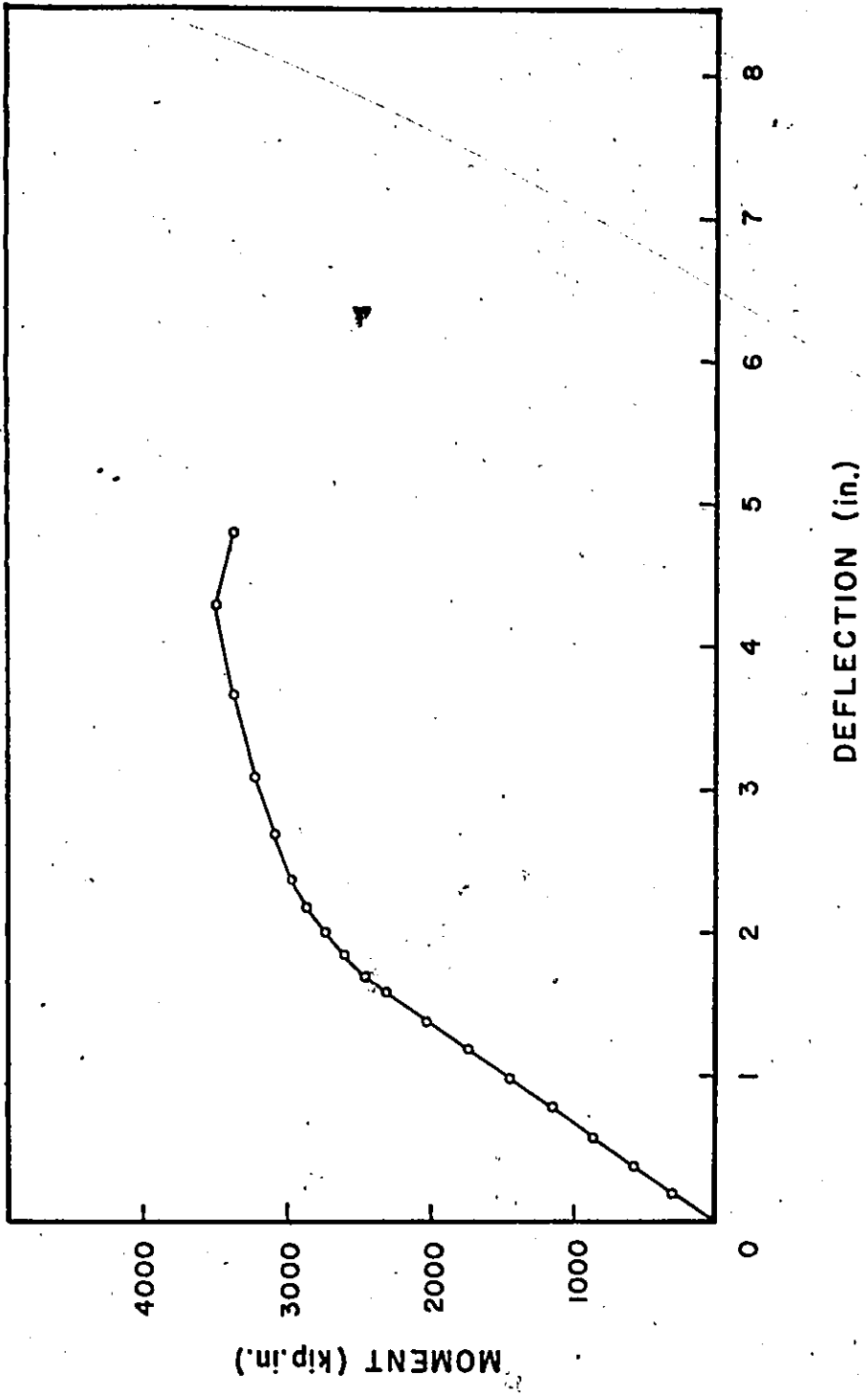


FIGURE 6.30 LIVE LOAD END MOMENT - END DEFLECTION RESULTS FOR END D2

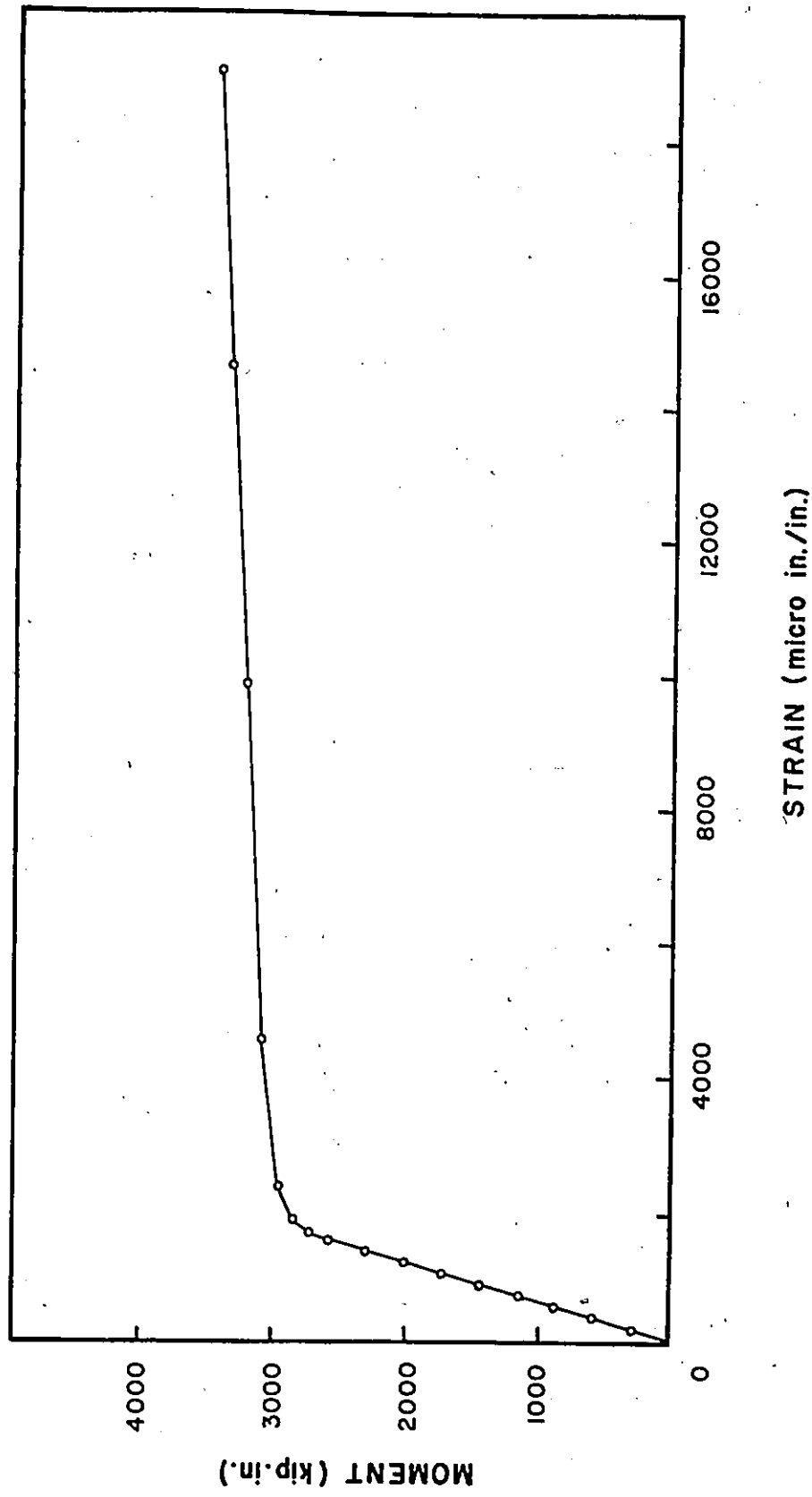


FIGURE 6.31 LIVE LOAD MOMENT VERSUS BOTTOM FIBRE STEEL STRAIN FOR END D2

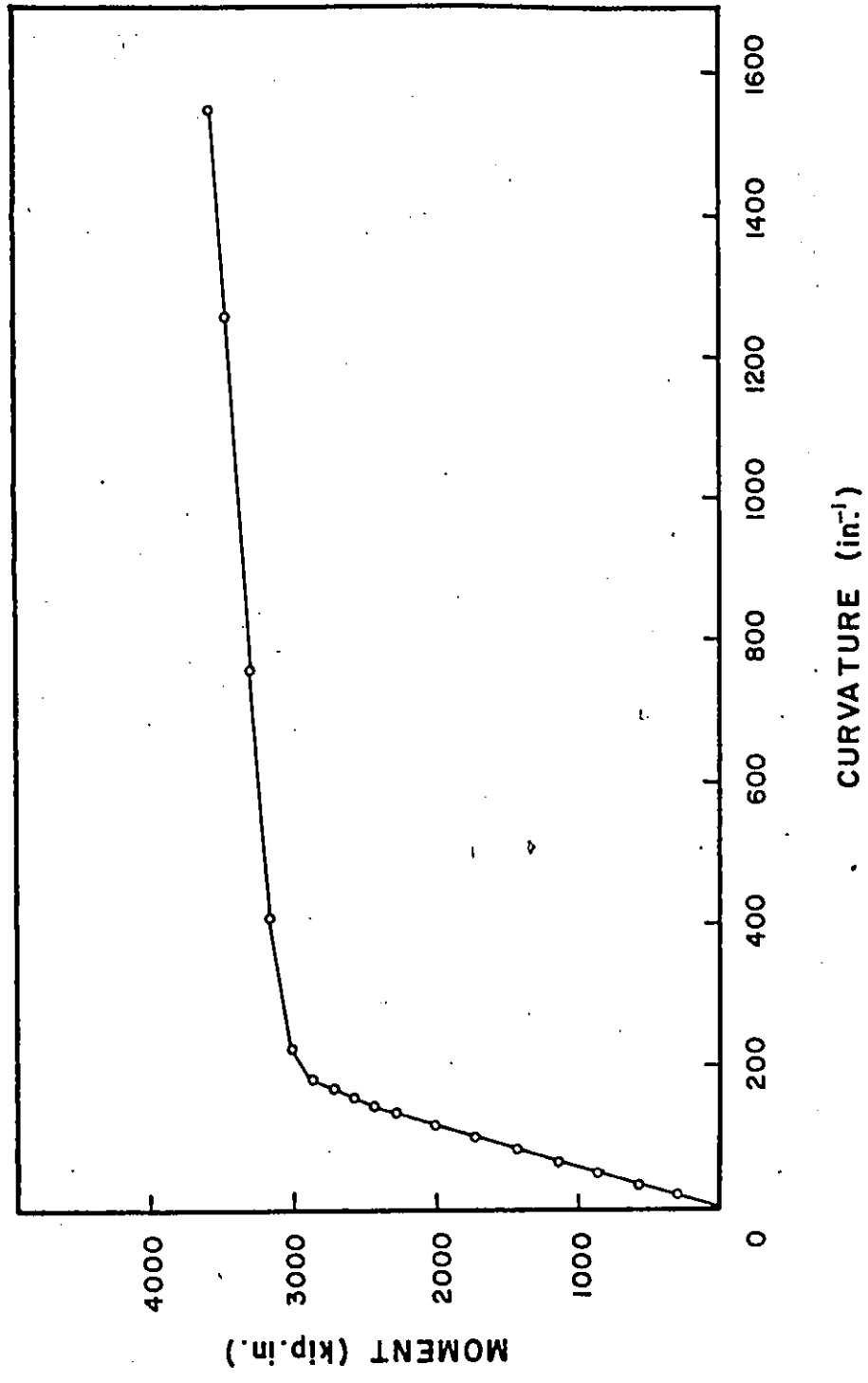


FIGURE 6.32 LIVE LOAD MOMENT - CURVATURE RESULTS FOR END D2

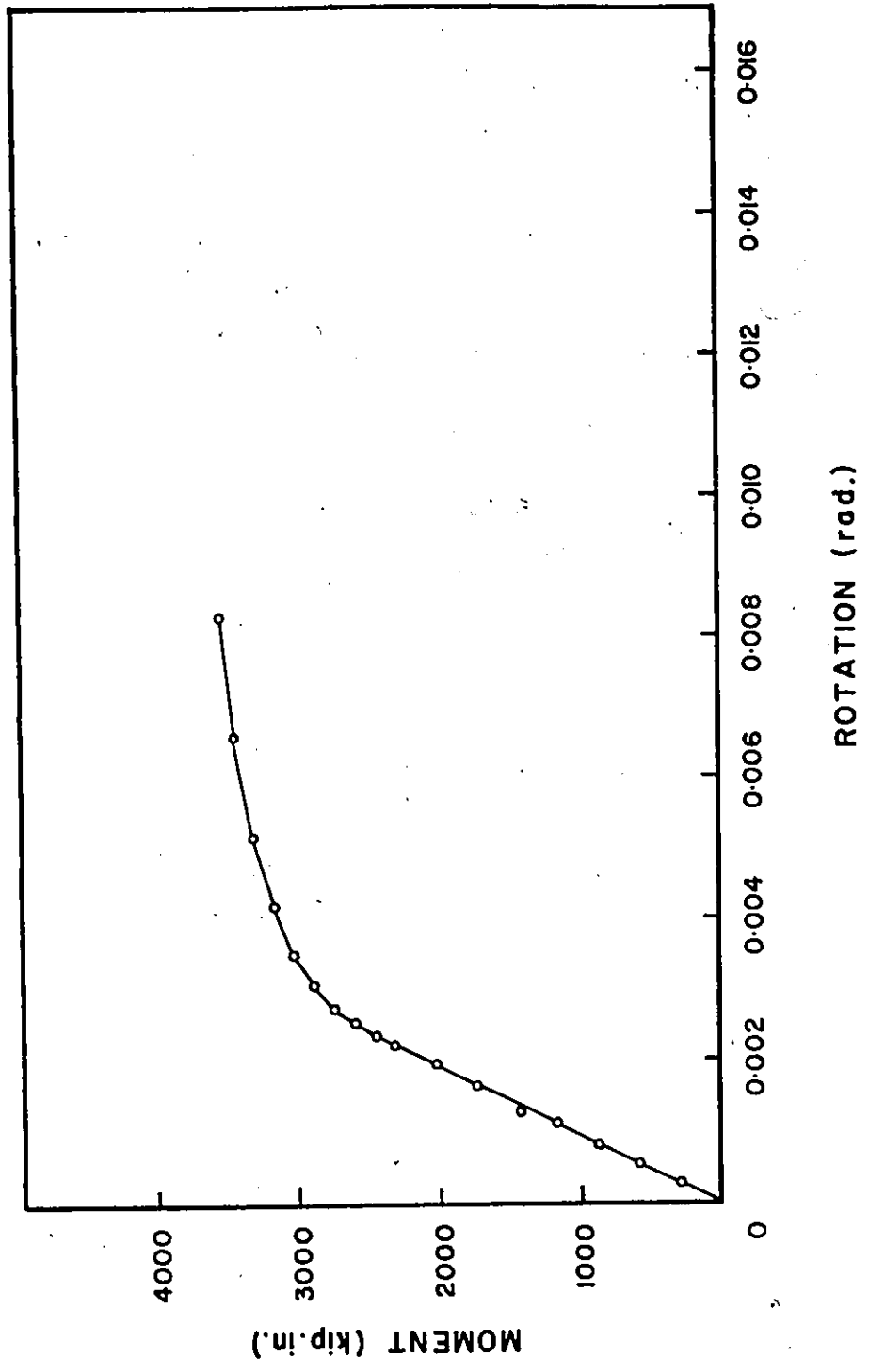
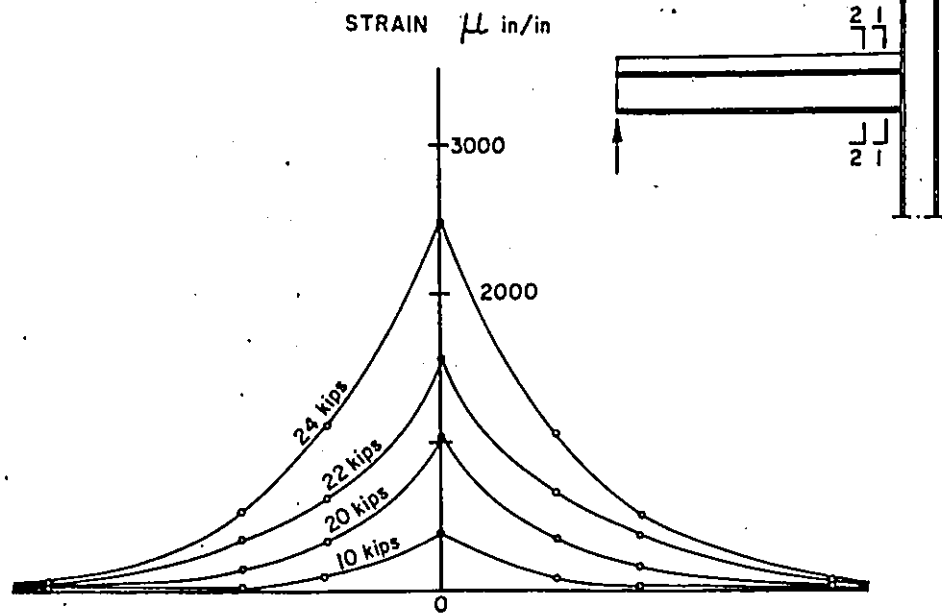
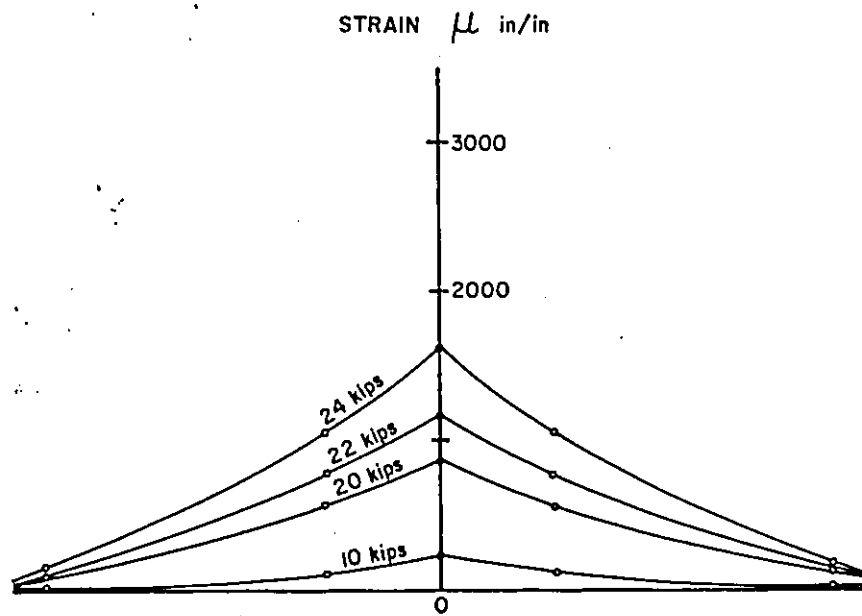


FIGURE 6.33 LIVE LOAD MOMENT - END ROTATION RESULTS FOR END D2



a) AT SECTION 1-1



b) AT SECTION 2-2

FIGURE 6.34 TOP FIBRE STRAIN DISTRIBUTION ACROSS THE SLAB WIDTH FOR END D2

increasing linearly with the applied moment at load of 18.0 kips when it started rounding. The bottom fibre steel strain reached 19000 micro in/in at failure. Steel strain measurements at section 1-1 and 2-2 indicated that yielding occurred at section 1-1 before section 2-2. Figure 6.31 shows the variation of the bottom fibre strain at Section 1-1 with the applied moment.

The moment-curvature curve at section 1-1 is shown in figure 6.32. The linear relationship between the curvature and the applied moment ceased at load 18.0 kips. At a load of 20.0 kips the curvature started to increase more rapidly to reach a value of $1550 \times 10^{-6} \text{ in}^{-1}$ at failure.

Figure 6.33 shows the moment-rotation curve for end D_2 . the end rotation reached 0.0083 rad. at failure. The joint modulus (J) was $103.2 \times 10^4 \text{ kip in/rad}$.

The distributions of the top fibre concrete strain at sections 1-1 and 2-2 are shown in Figure 6.34.

At a load of 20.0 kips a longitudinal crack was observed on the top of the slab near the fixed end and propagated towards the other end with increase in the applied load. The longitudinal crack almost reached the free end at failure.

Failure of the beam occurred due to crushing of the concrete slab at load 24.88 kips. No other signs of connector failure or pulling of the concrete slab from the metal deck was observed.

6.3.4-b End D_1

The concrete slab was already longitudinally cracked before

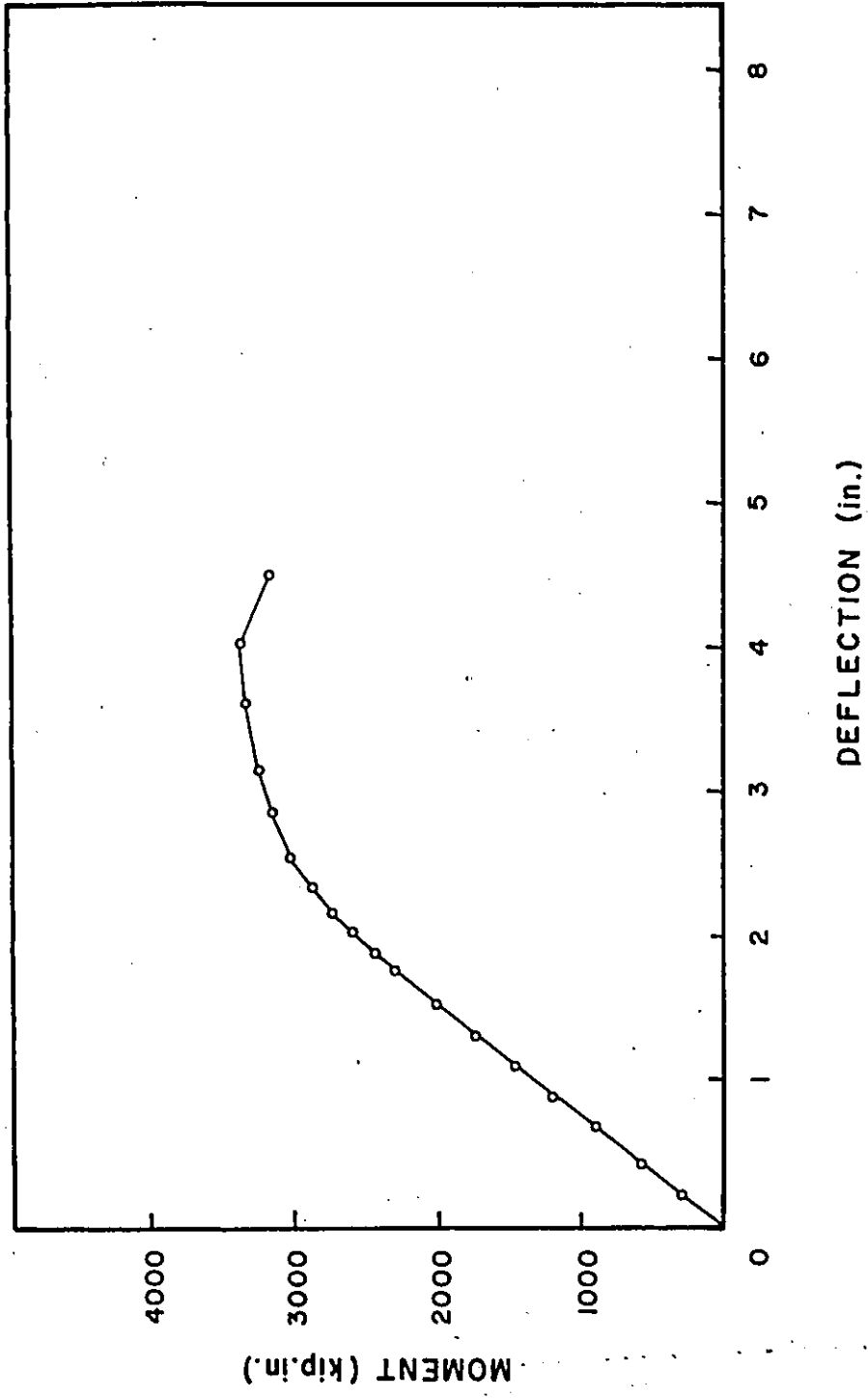


FIGURE 6.35 LIVE LOAD END MOMENT - END DEFLECTION RESULTS FOR END D1

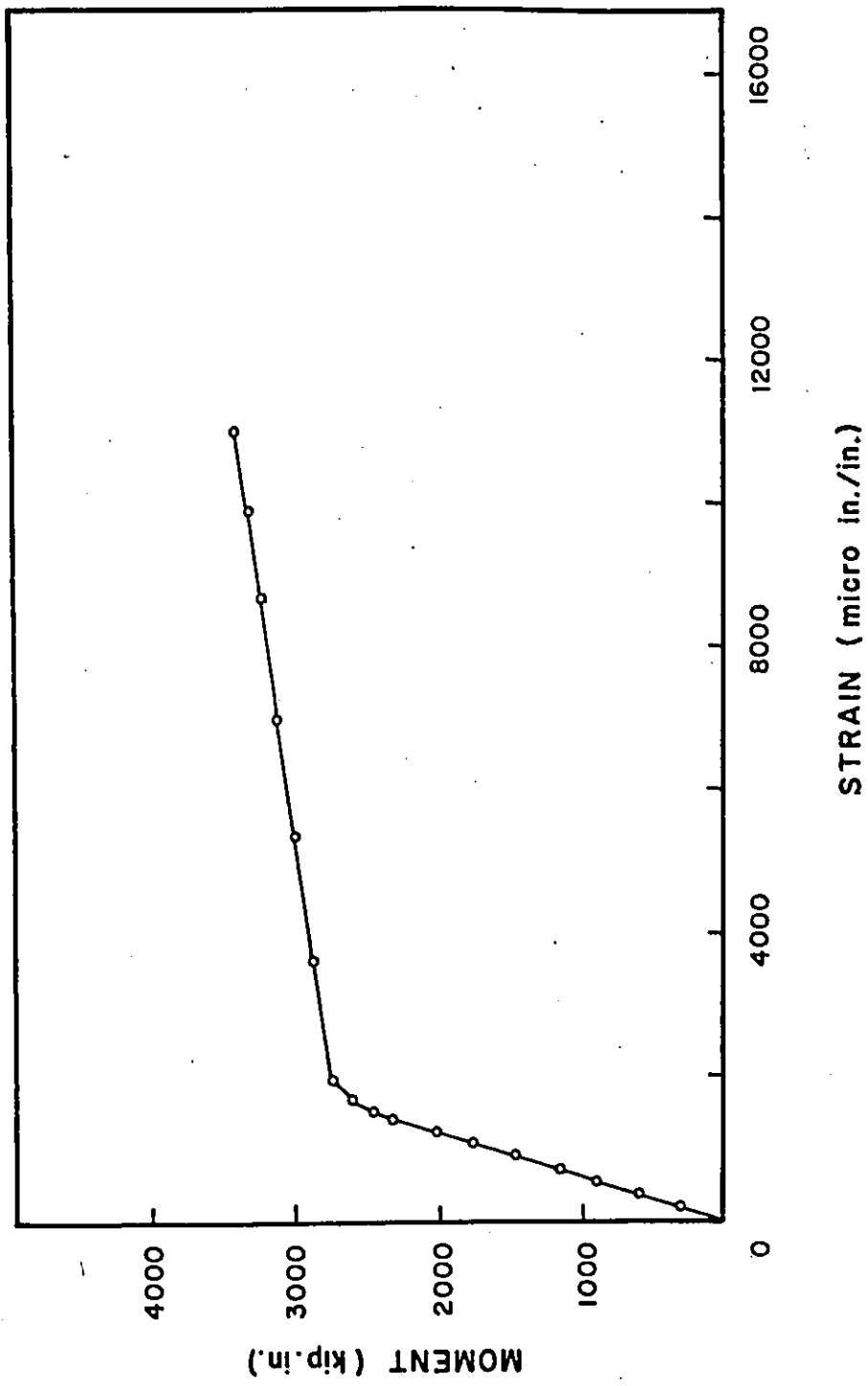


FIGURE 6.36 LIVE LOAD MOMENT VERSUS BOTTOM FIBRE STEEL STRAIN FOR
END D1

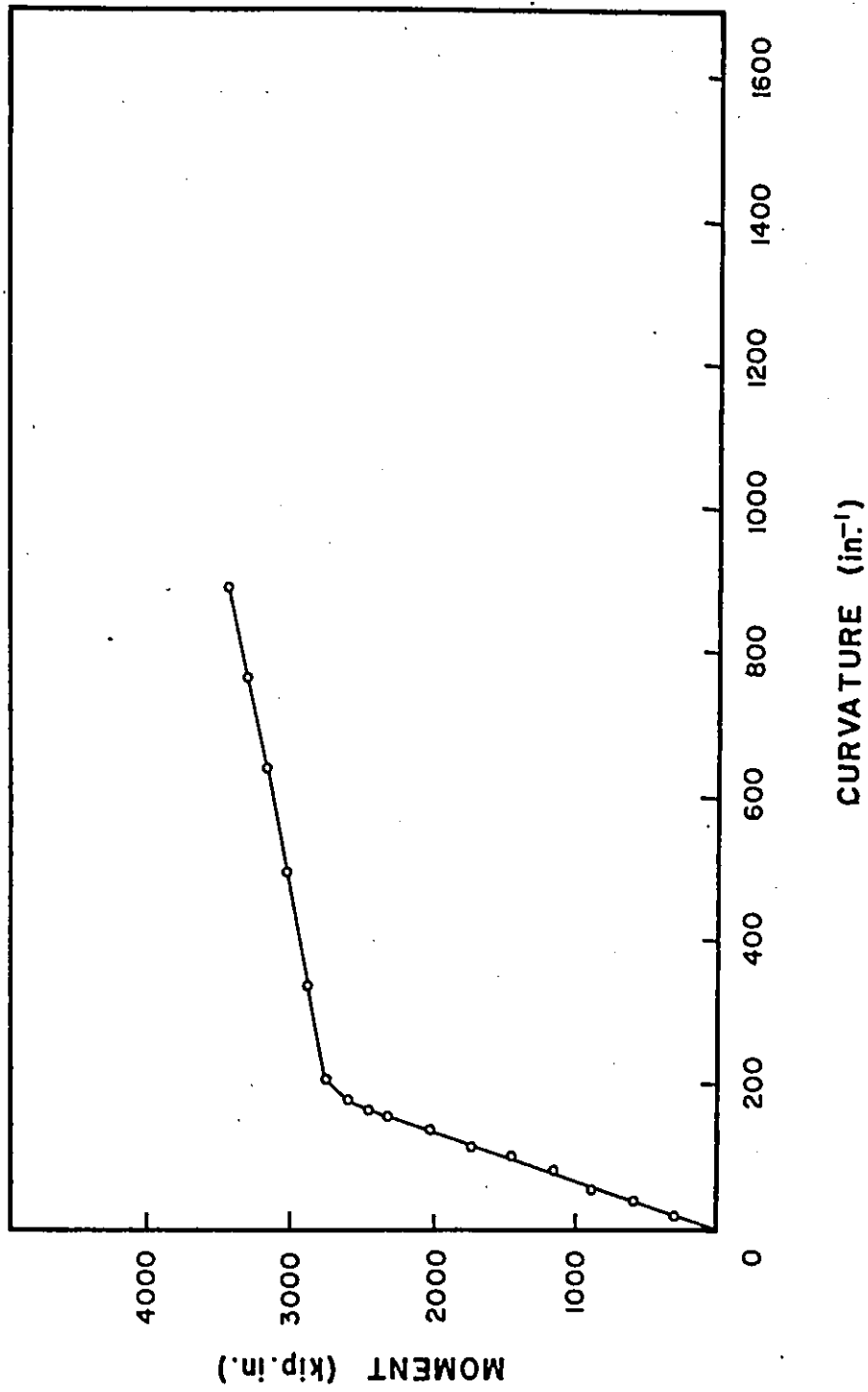


FIGURE 6.37 LIVE LOAD MOMENT - CURVATURE RESULTS FOR END D1

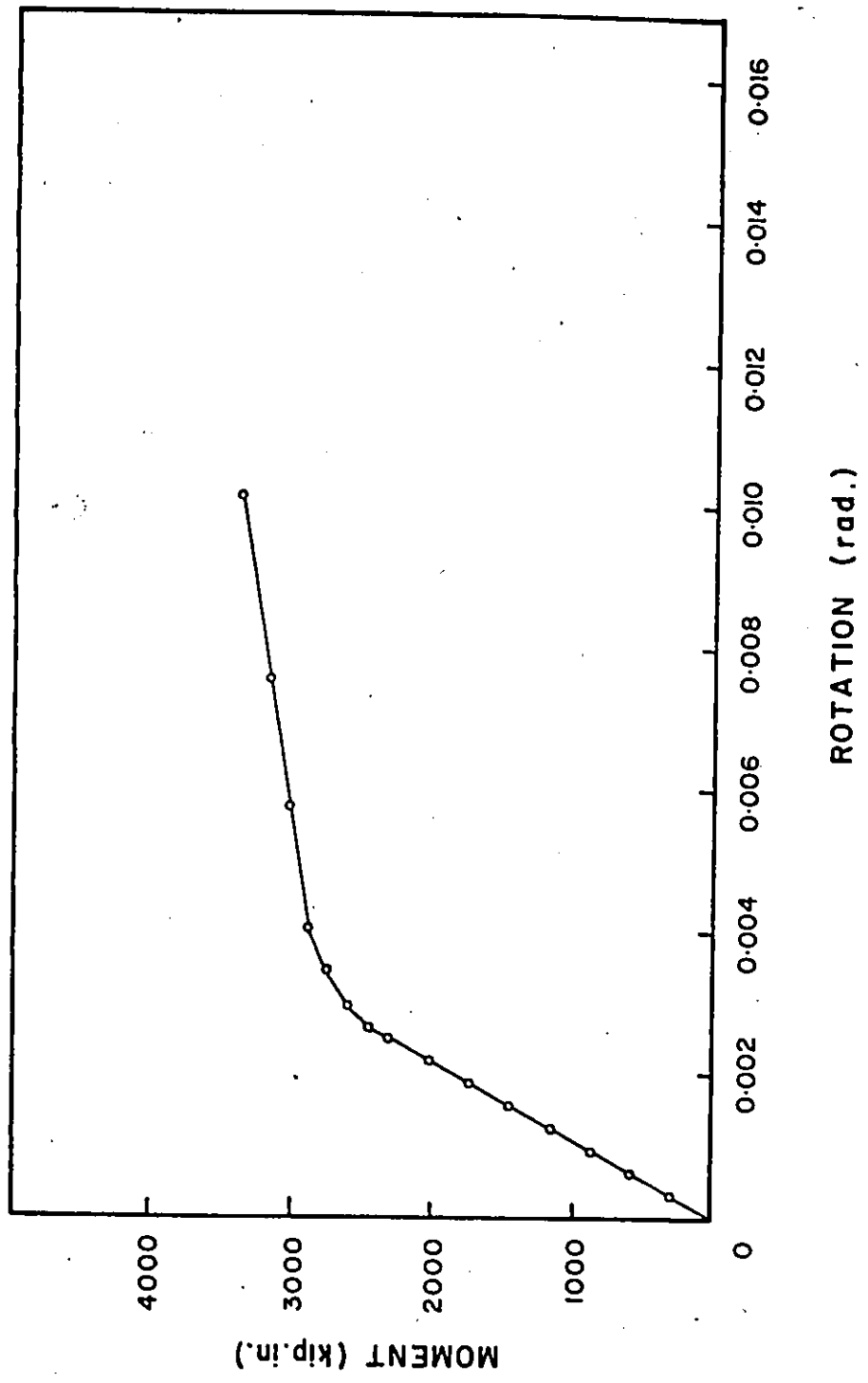
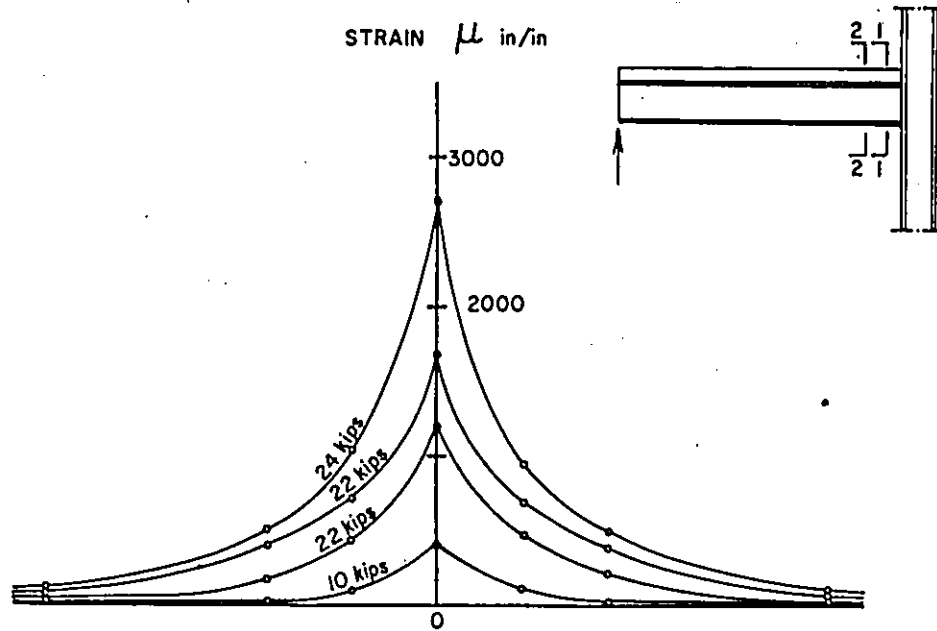
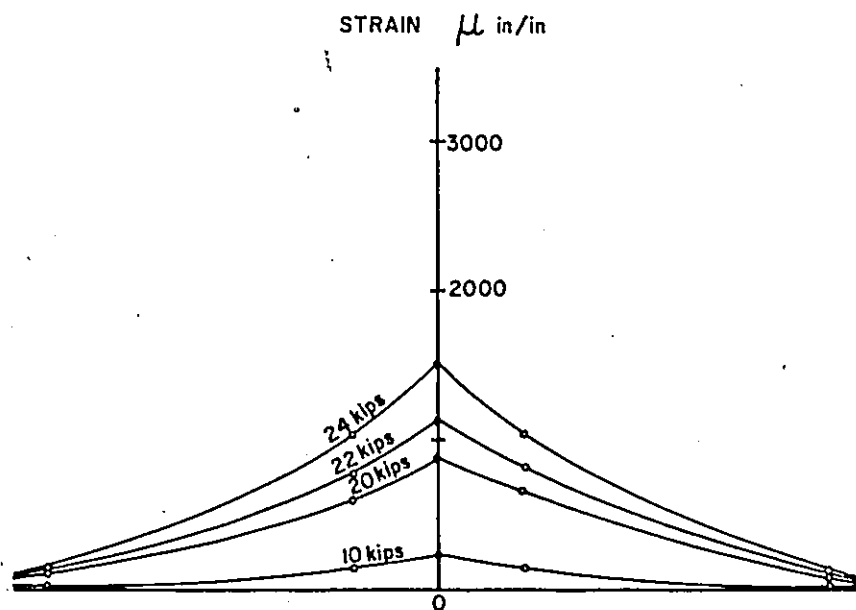


FIGURE 6.38 LIVE LOAD MOMENT - END ROTATION RESULTS FOR END D1



a) AT SECTION 1-1



b) AT SECTION 2-2

FIGURE 6.39 TOP FIBRE STRAIN DISTRIBUTION ACROSS THE SLAB WIDTH FOR END D1

starting the test on D_1 . The beam was bolted to the column and load in the same manner and by the same load increment as for end D_2 .

Figure 6.35 shows the end moment versus the end deflection for end D_1 . The linear relationship ceased at load 16.0 kips and the deflection was 4.05 in. at failure.

The bottom fibre steel strain at Section 1-1 is plotted against the applied moment on the section in Figure 6.36. The figure shows that the moment-strain relationship followed the same general shape as for end D_2 with the end of the linear relationship occurring at load 17.0 kips. The bottom fibre steel strain at section 1-1 reached 11000 micro in/in at failure.

Figure 6.37 shows the moment-curvature at Section 1-1. The curvature increased also linearly up to load 17.0 kips. The curvature at Section 1-1 was $900 \times 10^{-6} \text{ in}^{-1}$ at failure.

Figure 6.38 shows the moment-rotation curve for D_1 . The end rotation was about 0.01 at failure and the calculated joint modulus (J) was $90 \times 10^4 \text{ kip. in/rad.}$

Figure 6.39 shows the distributions of the top fibre concrete strain at sections 1-1 and 2-2.

The specimen failed at load 23.5 kips due to crushing of the concrete slab adjacent to the column face.

6.3.5 Beam E

Beam E was designed to study the effect of increasing the thickness of the solid part of the slab and the existence of a

transverse beam connected to the slab. Beam E was 8 ft. long and the concrete slab for this beam was 5 in. thick (3.5 in. solid part and 1.5 in. rib). The beam was provided with a 10 inch wide end plate at each end.

6.3.5.a End E₁

The End plate E₁ was bolted to the column and the slab was bolted by three 1/2 in. diameter bolts to a transverse W12x27 beam welded on each side of the column.

The load was applied on the free end in an increment of 2 kips up to load 26.0 kips and then reduced to 1 kip. The load was steady and started to drop a small amount of 0.1 kip at load 26.0 kips.

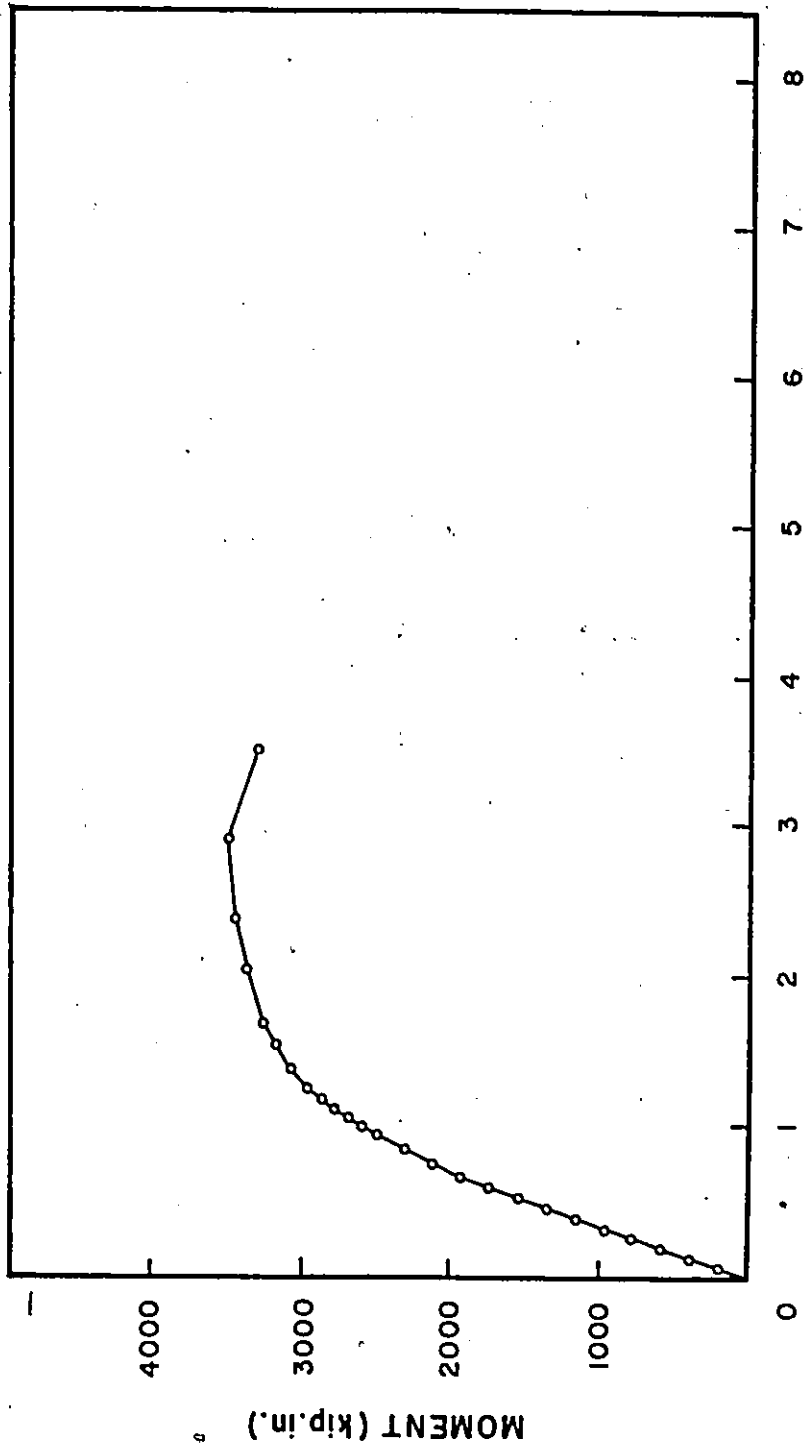
Figure 6.40 shows the variation of the free end deflection with the applied moment. The figure shows that the linear relationship ceased at load 20.0 kips when the deflection was .67 in. The deflection reached a value of 2.9 in. at failure.

The variation of the bottom fibre steel strain at Section 1-1 with the applied moment is shown in Figure 6.41. The strain reached 15000 micro in/in at failure.

Figure 6.42 shows the moment-curvature curve and Figure 6.43 shows the moment-rotation curve. At failure the curvature was $1260 \times 10^{-6} \text{ in}^{-1}$ and the end rotation was 0.0077 rad. The joint modulus (J) was found to be 86.4 kip in/rad.

The top fibre concrete strain distributions at Sections 1-1 and 2-2 are shown in Figure 6.44.

At a load of 8.0 kips a flexural crack started at the bottom of



DEFLECTION (in.)

FIGURE 6.40 LIVE LOAD END MOMENT - END DEFLECTION RESULTS FOR END E1

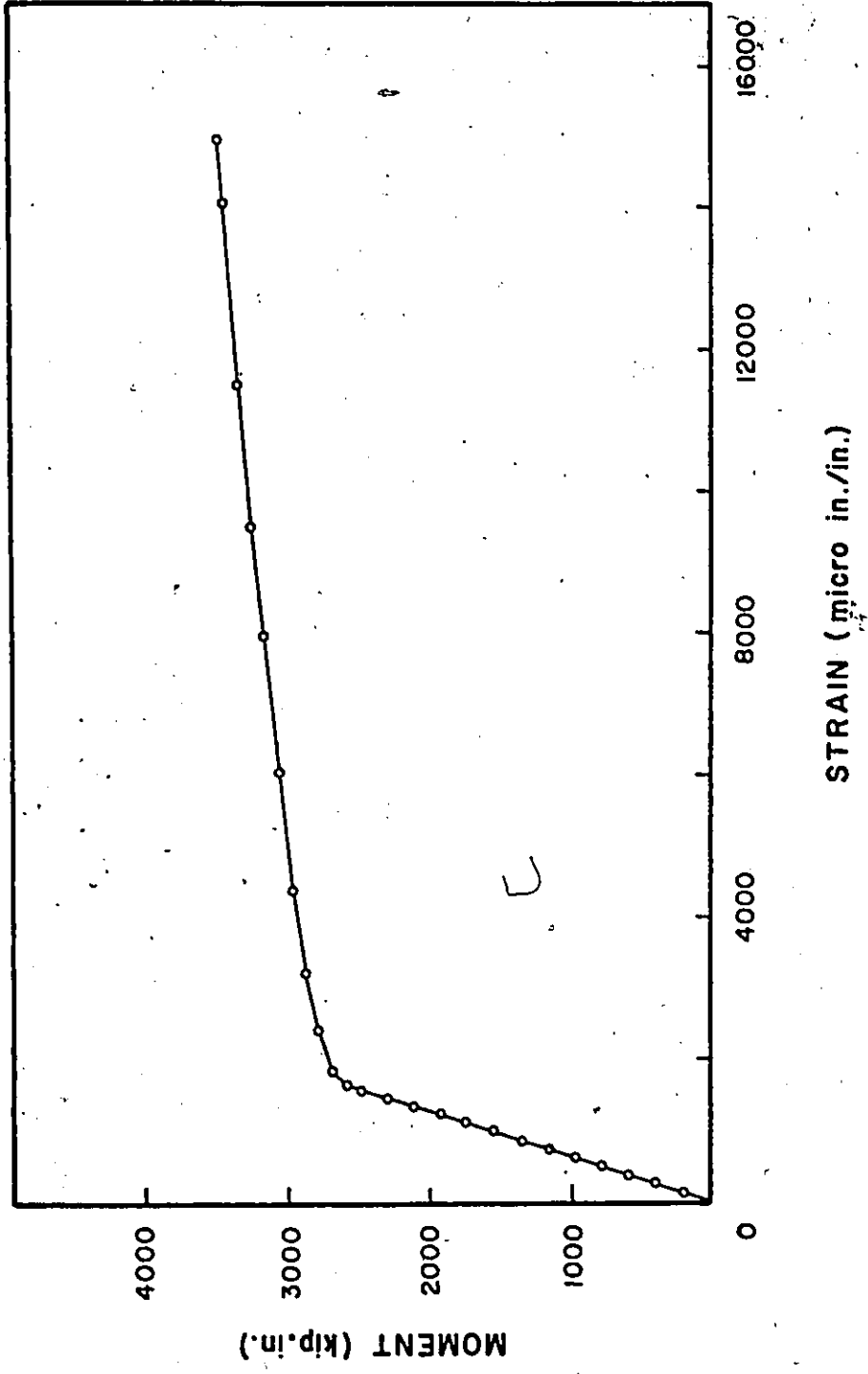


FIGURE 6.41 LIVE LOAD MOMENT VERSUS BOTTOM FIBRE STEEL STRAIN FOR END E1

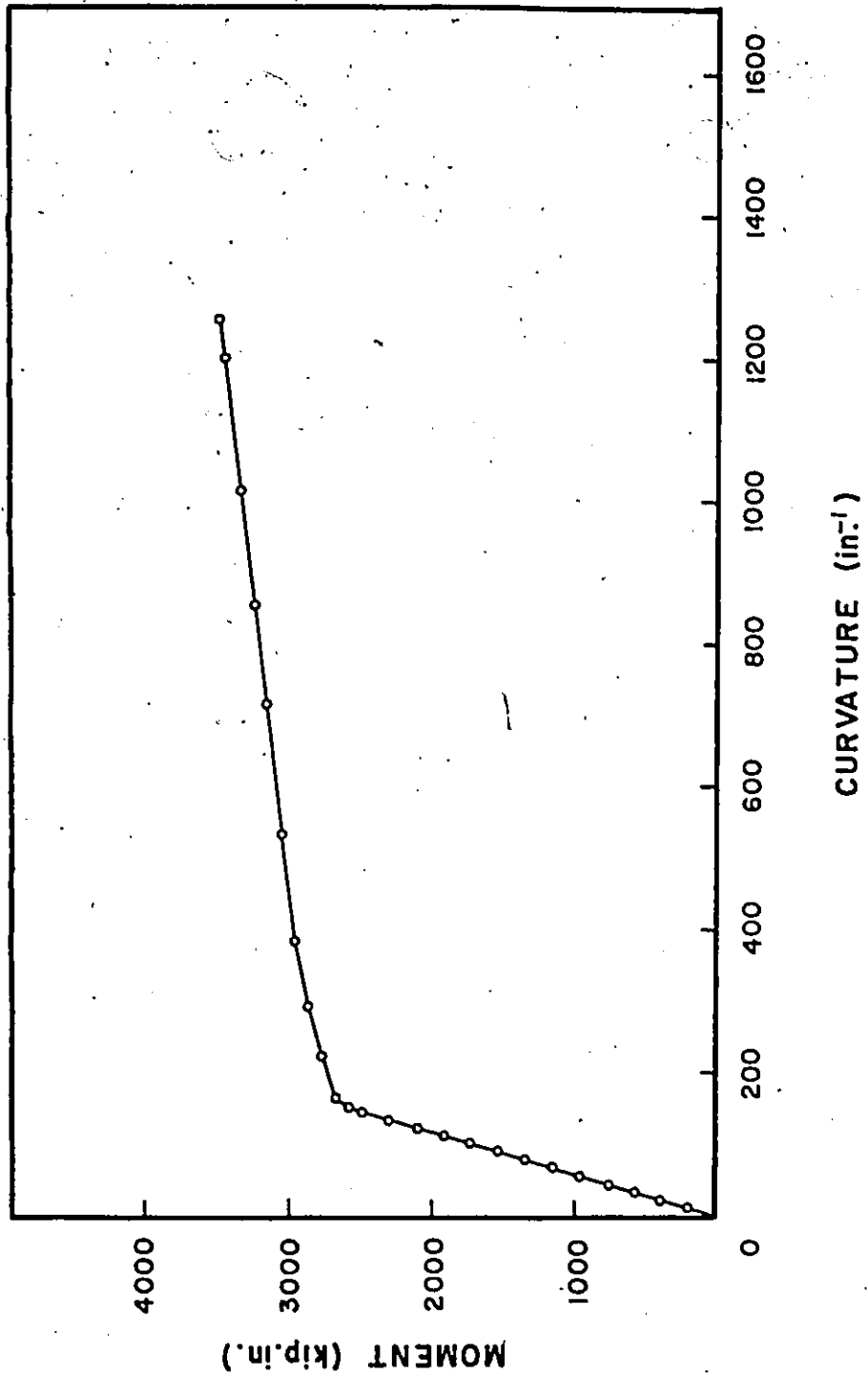


FIGURE 6.42 LIVE LOAD MOMENT - CURVATURE RESULTS FOR END E1

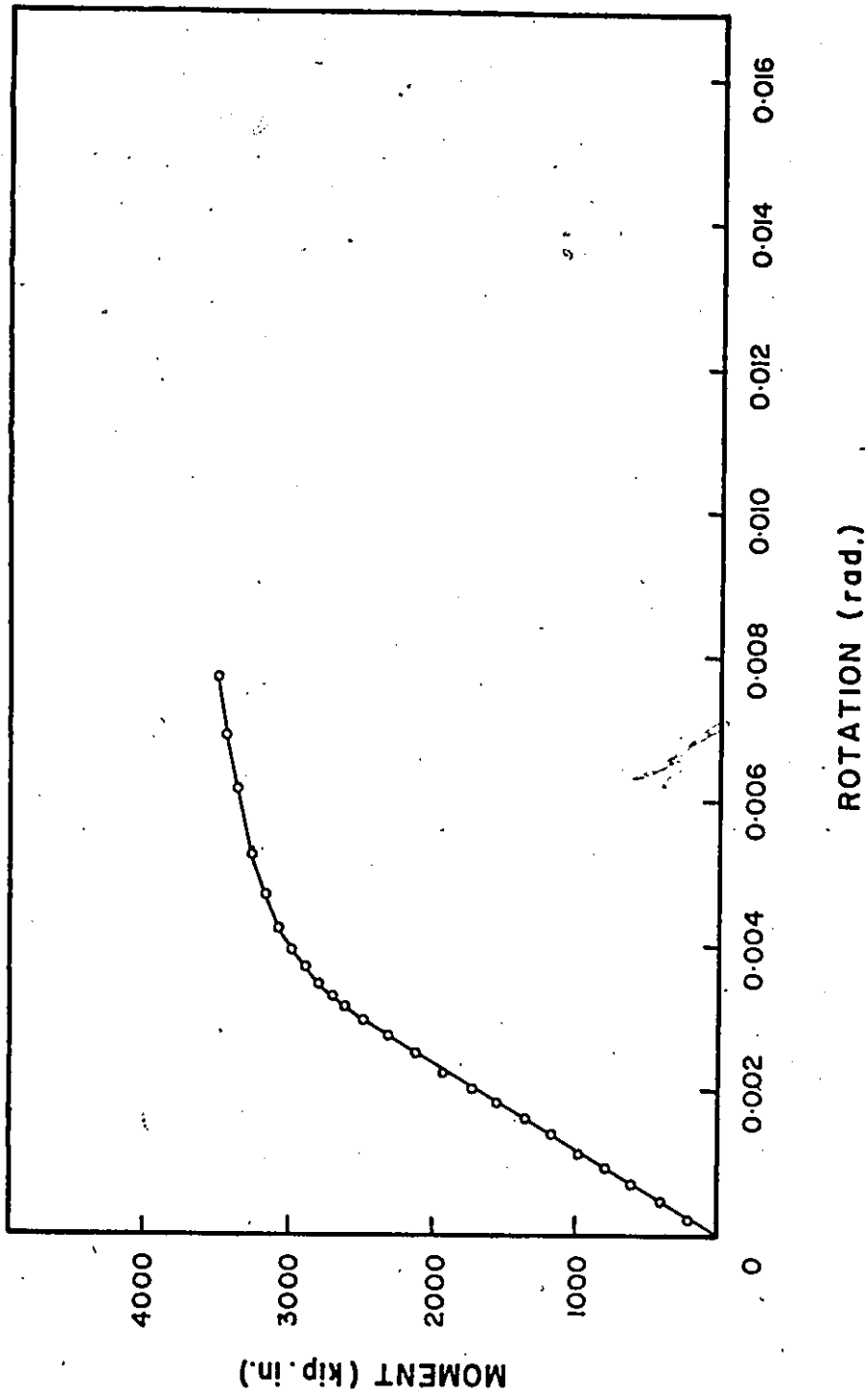
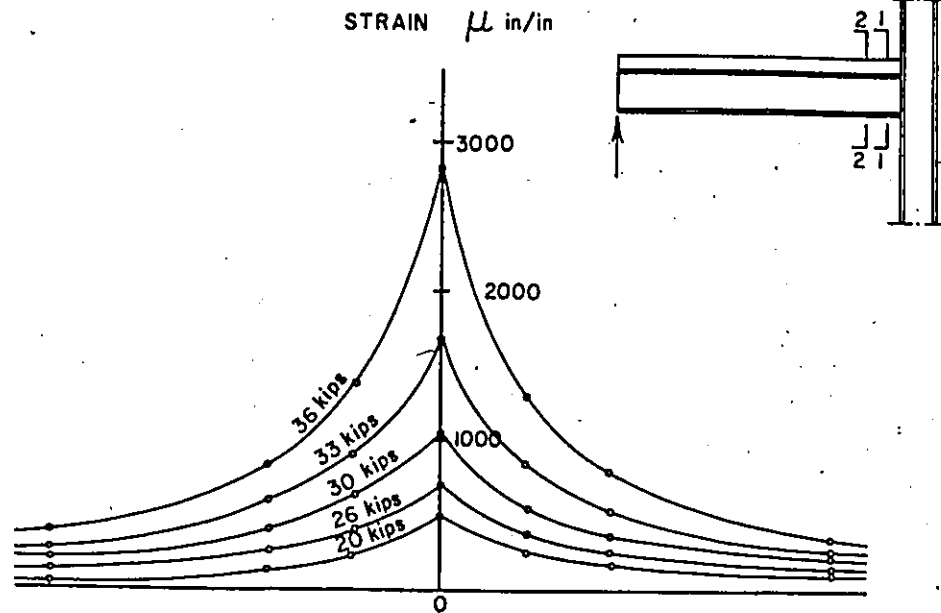
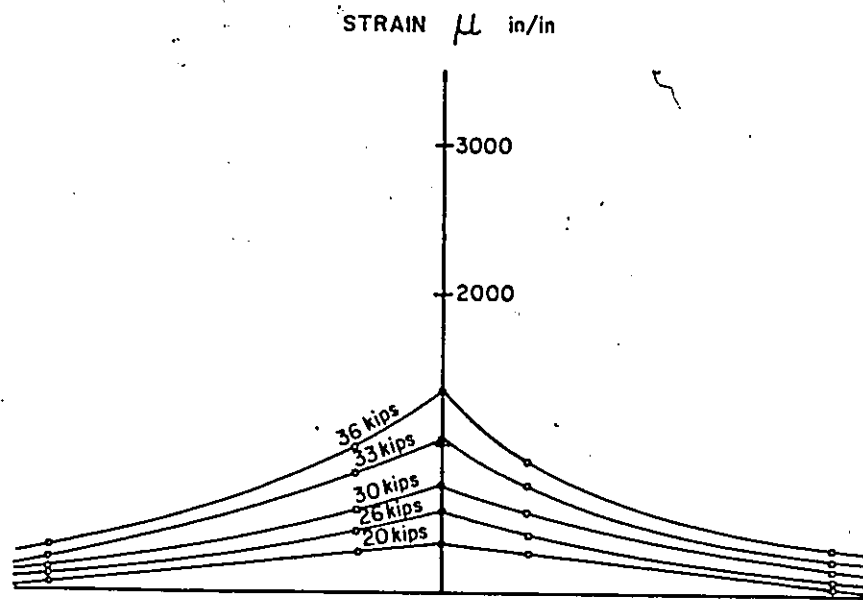


FIGURE 6.43 LIVE LOAD MOMENT - END ROTATION RESULTS FOR END E1



a) AT SECTION 1-1



b) AT SECTION 2-2

FIGURE 6.44 TOP FIBRE STRAIN DISTRIBUTION ACROSS
THE SLAB WIDTH FOR END E1

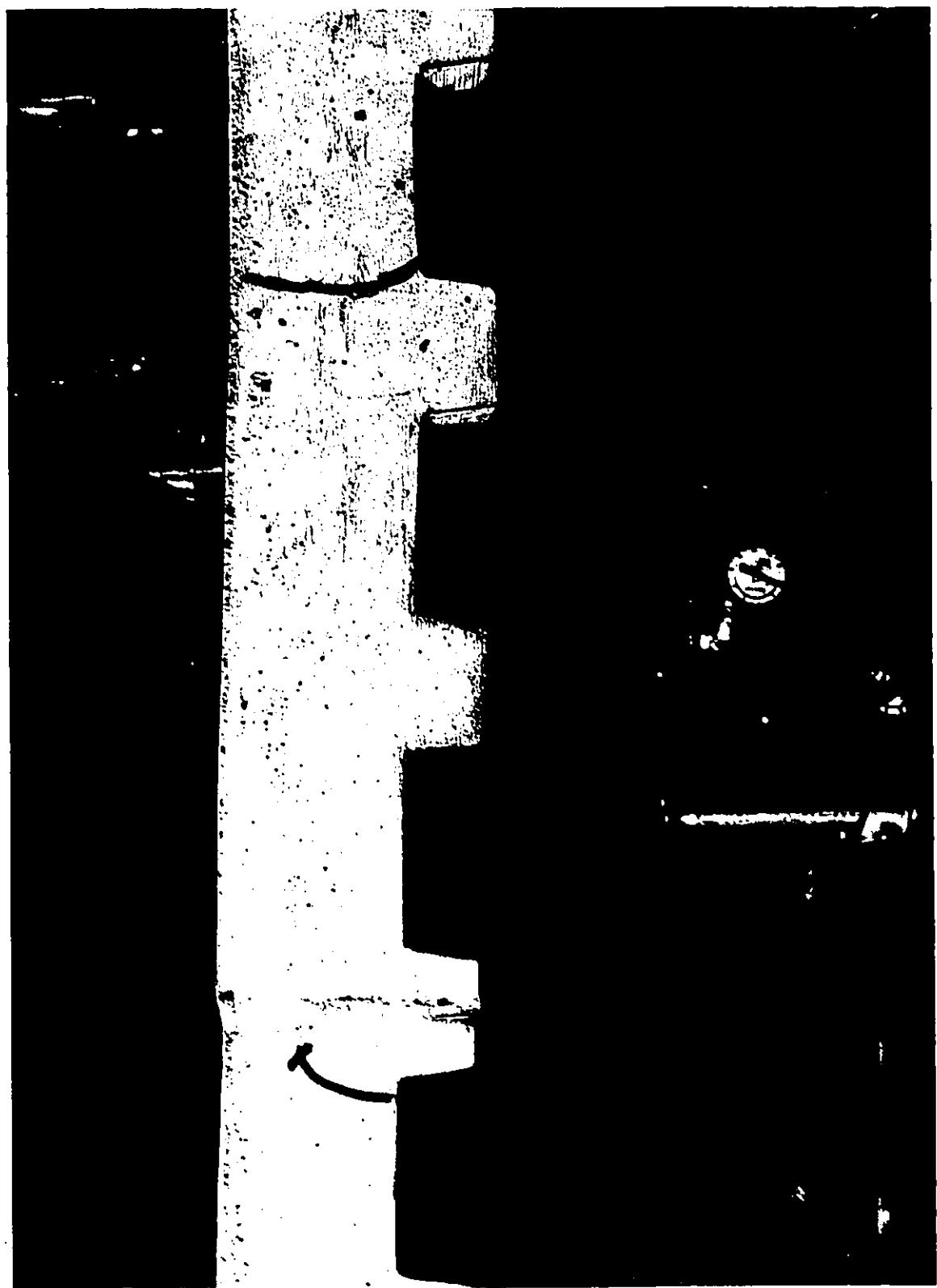


FIGURE 6.45 PIENRAL CMOGHE IN THE SEAL OF END E1



FIGURE 6.46 END OF AFTER TUNING

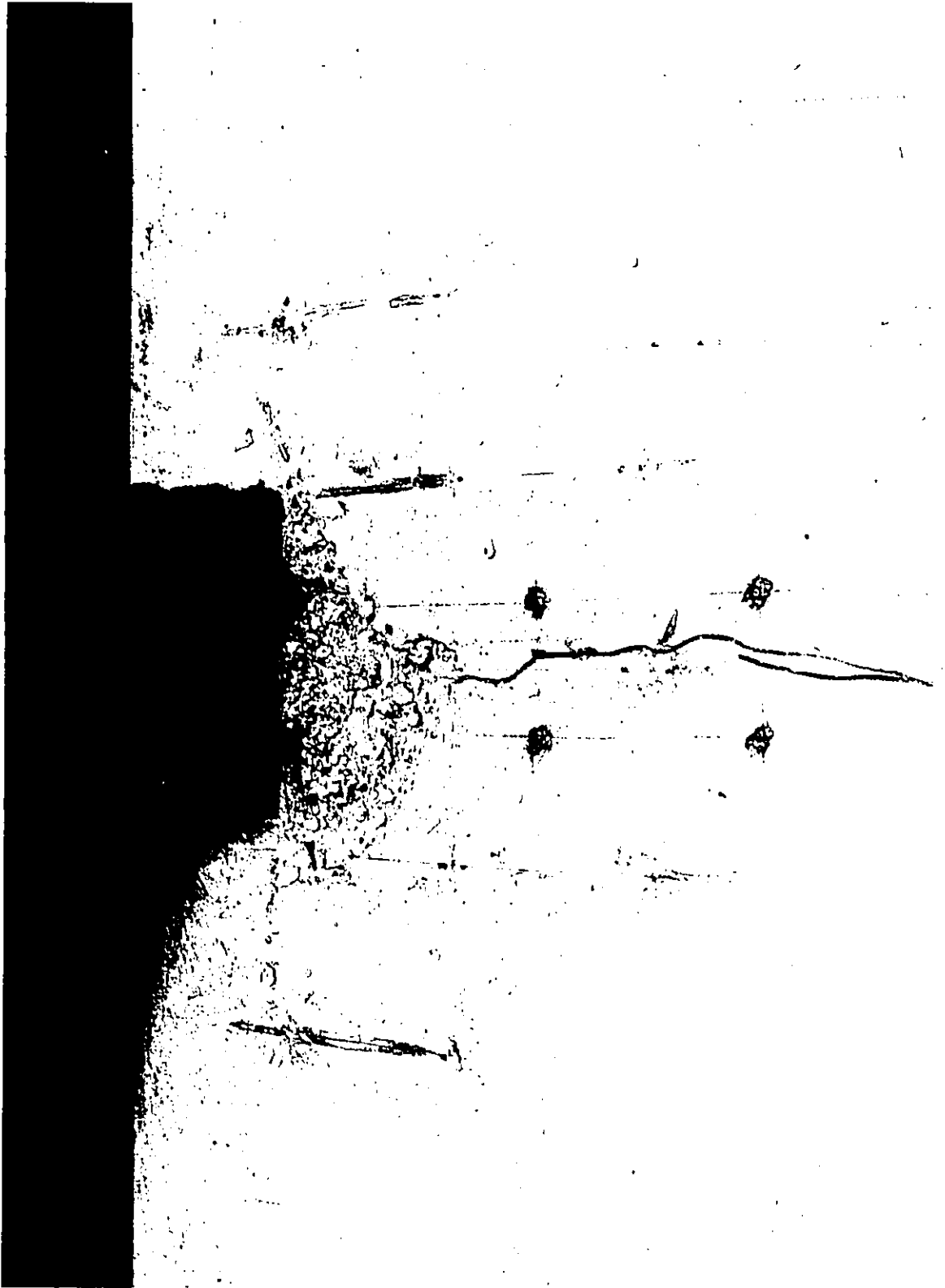


FIGURE 6.47 FAILURE OF THE 15

the solid part of the slab in the first panel adjacent to the transverse beam (in line with the column face). The flexural crack propagated towards the top surface of the slab with increasing the load. A second flexural crack was observed about two panels from the first one at load 22.0 kips as shown in Figure 6.45. At failure the first crack reached the top surface and a transverse crack was visual all over the slab width at this position. The concrete slab pulled off the metal deck adjacent to the transverse support at a test load of 31.0 kips (Figure 6.45).

At a load of 32.0 kips a longitudinal crack was observed on the top of the slab close to the column. At failure the longitudinal crack reached the other end (Figure 6.46).

The beam failed due to crushing of the concrete slab adjacent to the column face at a load of 36.5 kips (Figure 6.47).

6.3.5.b End E_2

End E_2 was similar to end E_1 except it was not bolted to the transverse beam. The existence of the transverse beam had no effect on the results of this test since it was welded to be on the top of the slab, while the slab at this position deflects downward due to the applied load. The concrete slab was already cracked before starting this test.

The load was applied in the same manner and with the same load increment as for end E_1 .

The end moment versus the free end deflection curve is shown in Figure 6.48. The deflection increased linearly up to load 20.0 kips.

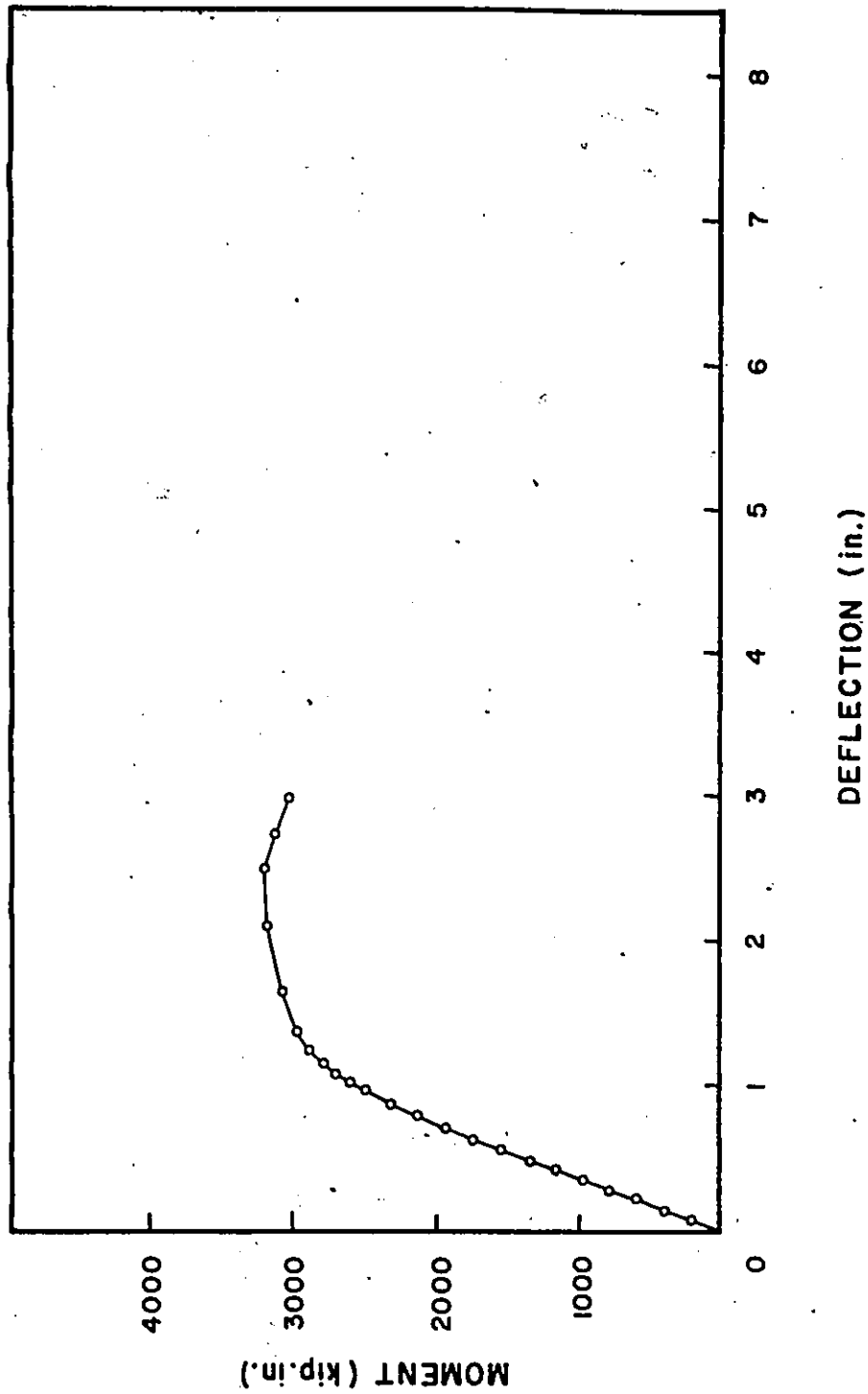


FIGURE 6.48 LIVE LOAD END MOMENT - END DEFLECTION RESULTS FOR END E2.

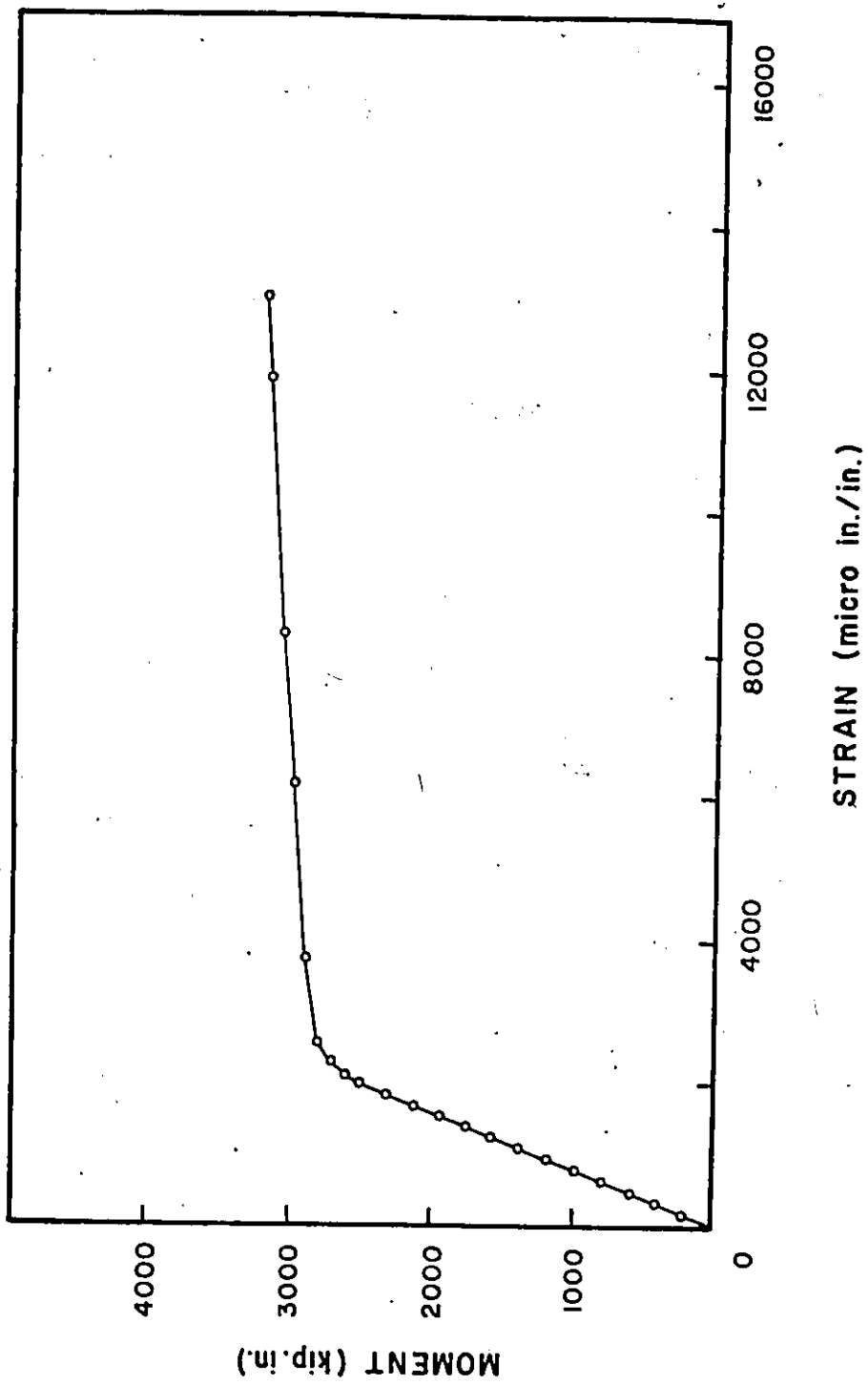


FIGURE 6.49 LIVE LOAD MOMENT VERSUS BOTTOM FIBRE STEEL STRAIN FOR END E2

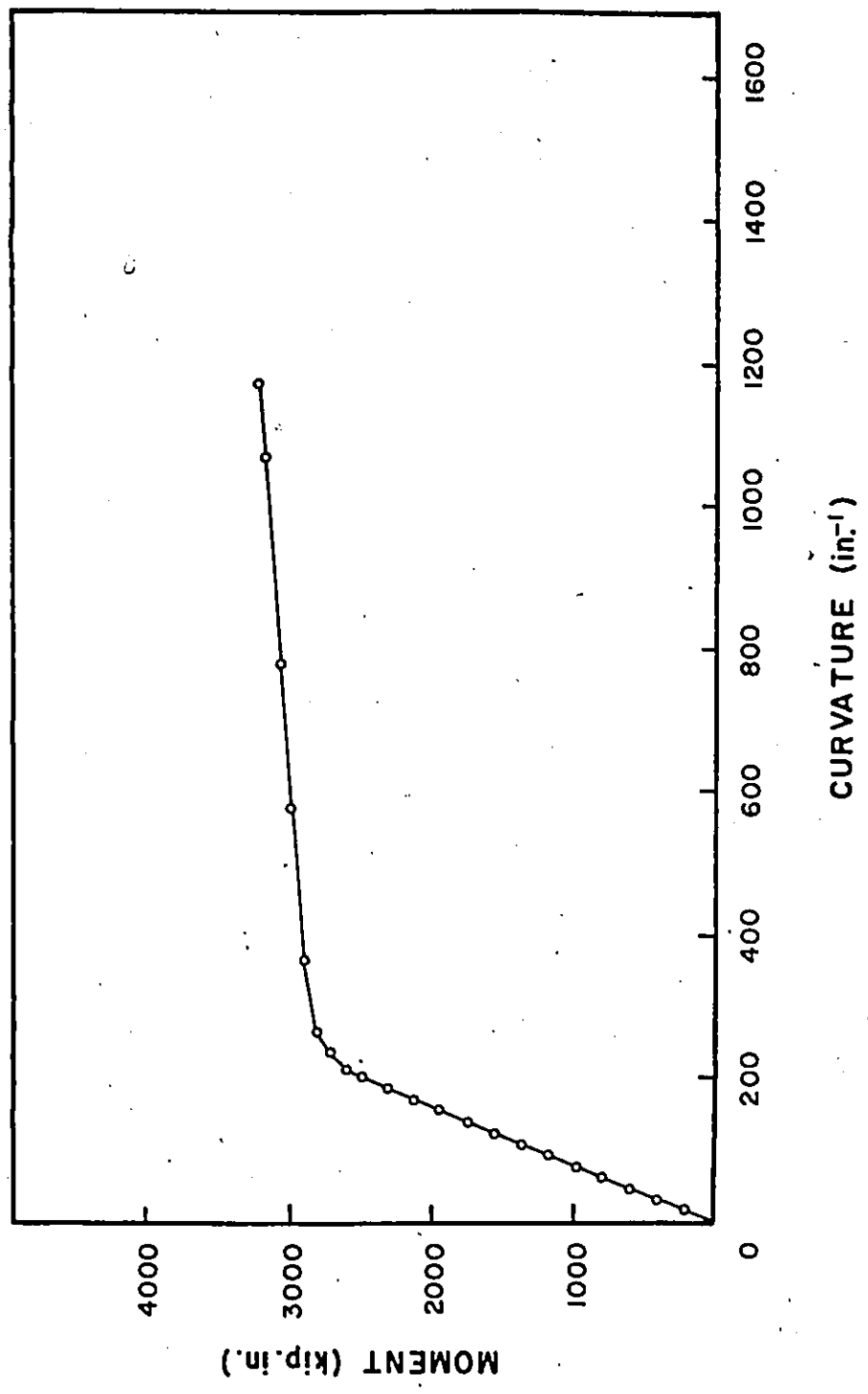


FIGURE 6.50 LIVE LOAD MOMENT - CURVATURE RESULTS FOR END E2



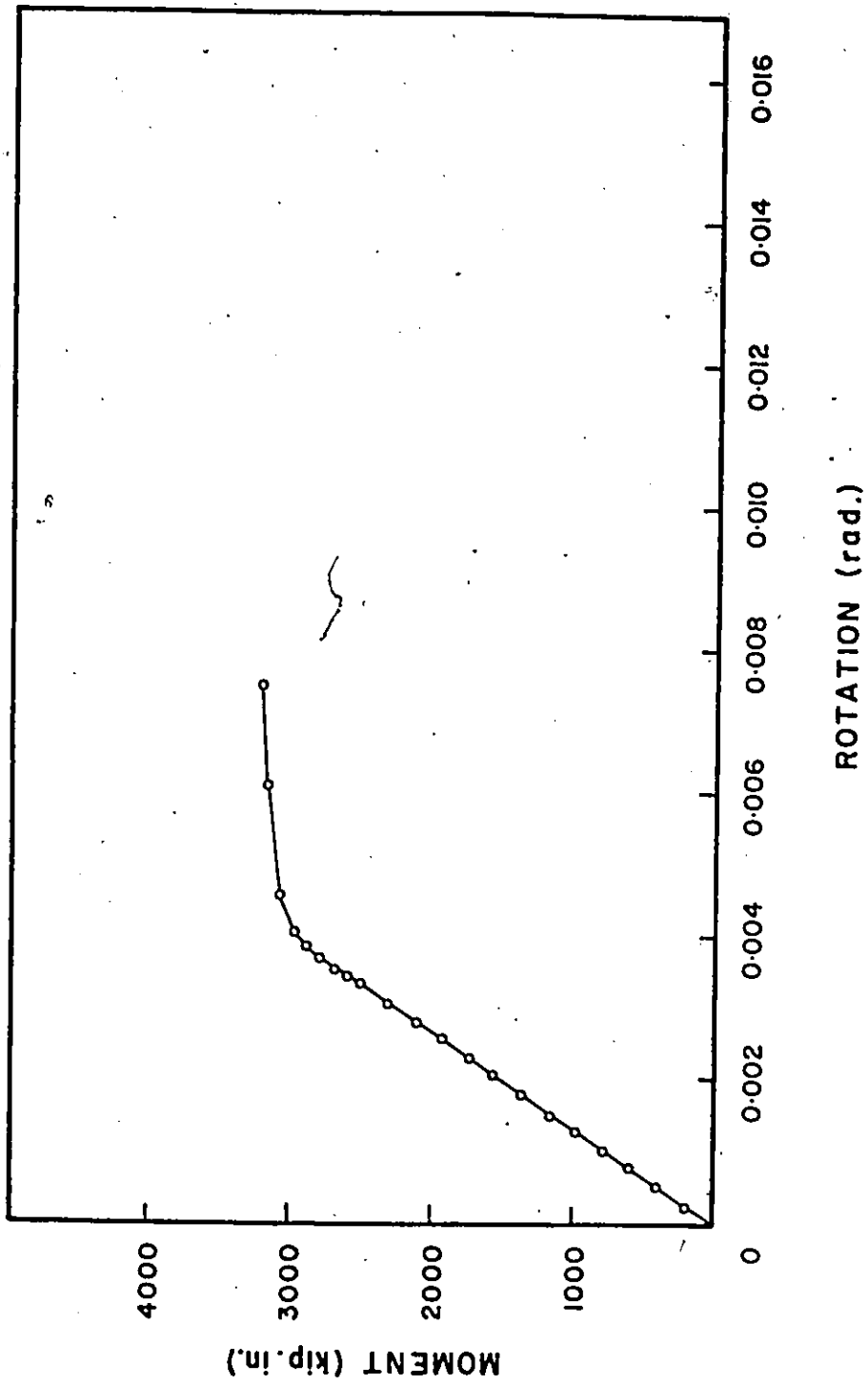
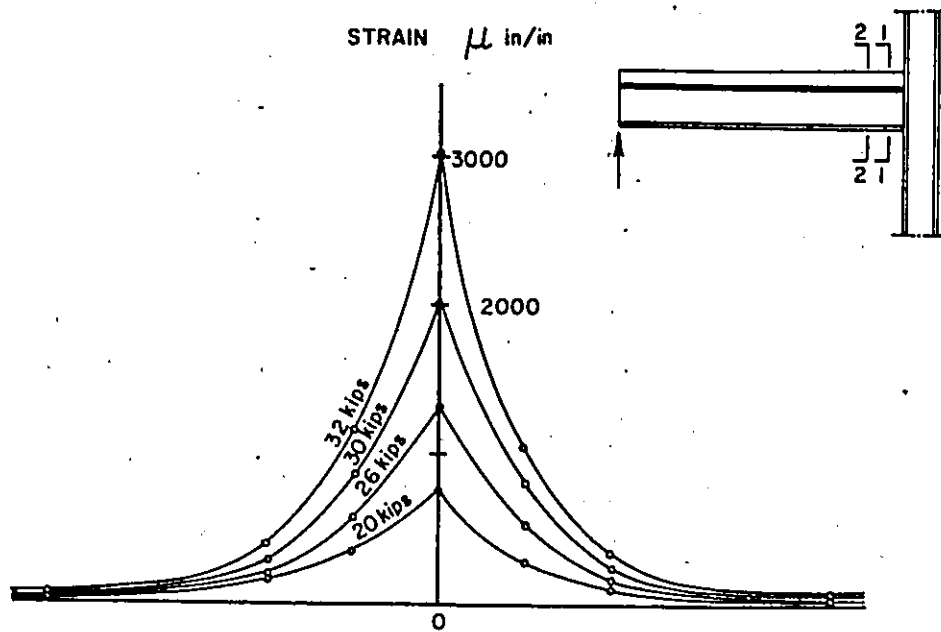
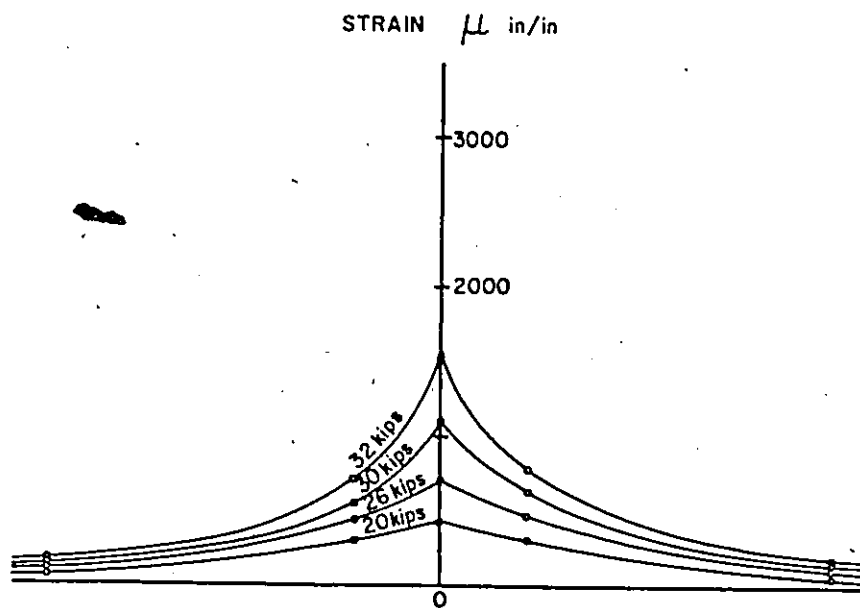


FIGURE 6.51 LIVE LOAD MOMENT - END ROTATION FOR END E2



a) AT SECTION 1-1



b) AT SECTION 2-2

FIGURE 6.52 TOP FIBRE STRAIN DISTRIBUTION ACROSS THE SLAB WIDTH FOR END E2

The deflection at this instant was 0.71 in. and it reached a value of 2.52 in. when the specimen failed.

Figure 6:49 shows the variation of the bottom fibre steel strain at section 1-1 with the applied moment on the section. The steel strain followed a linear relationship with the applied moment up to load 26.0 kips. The bottom fibre steel strain reached 13000 micro in/in at failure.

Figure 6.50 shows the moment-curvature at section 1-1 and Figure 6.51 shows the moment-rotation curve. The curvature reached 1170×10^{-6} in⁻¹ at failure while the end rotation was 0.0075 rad. The calculated joint modulus (J) was 76.8×10^4 kip. in/rad.

No signs of connector failure or pulling of the concrete slab from the metal deck was observed in this test.

The specimen failed at a load of 33.48 kips due to crushing of the concrete slab in front of the column face.

Summary of the test results for all specimens is given in Table 6.1.

6.4 Evaluation of the Test Results

As mentioned in Chapter 5, the experimental program was designed to study the effect of the test parameters on the effective slab width at the connection and on the strength and stiffness of the composite beam. The effect of each of the 5 test variables listed in Chapter 5 is investigated in the light of the following three parameters.

Beam	A ₁	A ₂	B ₁	B ₂	C ₁	C ₂	D ₁	D ₂	E ₁	E ₂
Max. Load kips	30.70	33.88	31.70	33.30	58.90	56.8	23.5	24.88	36.5	33.48
M _{exp} kip in	2947	3252	3043	3197	5654	5453	3384	3583	3504	3214
Max. deflection in	2.60	2.87	2.92	2.97	2.55	2.23	4.05	4.30	2.9	2.52
Max. bottom fibre steel strain micro in/in	13000	18000	14300	16400	5500	2800	11000	19000	15000	13000
Max. curvature in $\times 10^{-4}$	940	1380	1000	1500	620	440	900	1550	1260	1170
Max. end rotation rad	0.0082	0.0075	0.012	0.0075	0.0076	0.007	0.010	0.0083	0.0077	0.0075
Joint Modulus kip in/rad $\times 10^4$	82.6	124.8	93.6	110.4	187.2	180.0	90.0	103.2	86.4	76.8
Longitudinal cracking load kips	--	29.0	28.0	--	48.0	--	--	20.0	32.0	--

Table 6.1: Summary of the Test Results

1. Maximum Strength Ratio: The ratio of the maximum moment attained (M_{exp}) to the plastic moment of the steel beam alone (M_p).
2. Initial Stiffness Ratio: The ratio of the inertia of the transformed section (I_{av}) to the inertia of the steel beam alone (I_s). This ratio may be also expressed as $\Delta_{steel}/\Delta_{comp}$.
3. Ductility Factor: The definition of the section ductility is used to evaluate the ductility factor. The ductility factor is defined as the ratio between the curvature at ultimate (ϕ_u) to the curvature at yield (ϕ_y).

Table 6.2 shows the values of these three parameters, obtained from the test results, for all test beams.

6.4.1 Effect of the Column Face Width to the Slab Width Ratio

The effect of the column face width to the slab width ratio can be determined by comparing the results of ends A_1 with A_2 , B_1 with B_2 and D_1 with D_2 .

The comparison shows that the maximum strength ratio increased for the three cases when the c/b ratio was increased from 0.166 to 0.25. While the increase in the c/b ratio was 50% the increase in the maximum strength ratio ranged from 5.0 to 10.4%.

The initial stiffness ratio increased also with the increase in the c/b ratio. The increase in the initial stiffness ratio ranged from 10 to 24.0%.

The increase in the ductility factor ranged from 50. to 59.7% with the increase in the c/b ratio.

Test Number	Maximum strength Ratio	Initial stiffness Ratio	Ductility Factor
A ₁	1.54	1.25	4.27
A ₂	1.70	1.55	6.42
B ₁	1.59	1.29	5.00
B ₂	1.67	1.42	7.5
C ₁	1.39	1.14	2.90
C ₂	1.34	1.12	3.00
D ₁	1.69	1.52	5.39
D ₂	1.79	1.73	8.61
E ₁	1.78	1.57	7.63
E ₂	1.63	1.42	5.57

Table 6.2: Maximum strength Ratio, Initial Stiffness Ratio and Ductility Factor of the Test Beams

Table 6.3 shows the effect of increasing c/b ratio for the three cases considered. Figure 6.53 shows a comparison between the top fibre concrete strain over the steel beam centre line at Section 1-1 for ends A_1 and A_2 . This comparison shows that for the same load the concrete strain decreased with the increase in c/b ratio.

Since for every case considered in the above comparison the concrete strength and yield stress of the steel beam were almost the same for both ends, the above results lead to the conclusion that the effective slab width must have been increased with the increase in the column face width to the total width ratio.

6.4.2 Effect of the Slab Length to Width Ratio

Comparing tests A_1 with D_1 , B_1 with D_1 , A_2 with D_2 and B_2 with D_2 shows the effect of increasing L/b ratio.

The comparison of the results of these tests shows that the maximum strength ratio, initial stiffness ratio and ductility factor increased with the increase in L/b ratio. The increase in the maximum strength ratio ranged from 5.3 to 9.7% and the increase in the initial stiffness ratio ranged from 11.6 to 21.8%. The results of this comparison are given in Table 6.4.

The increase in the maximum strength ratio, initial stiffness ratio and ductility factor leads to the conclusion that the effective slab width acting with the steel beam must have been increased with the increase in L/b ratio. This conclusion agrees with the analytical results discussed in Chapter 4.

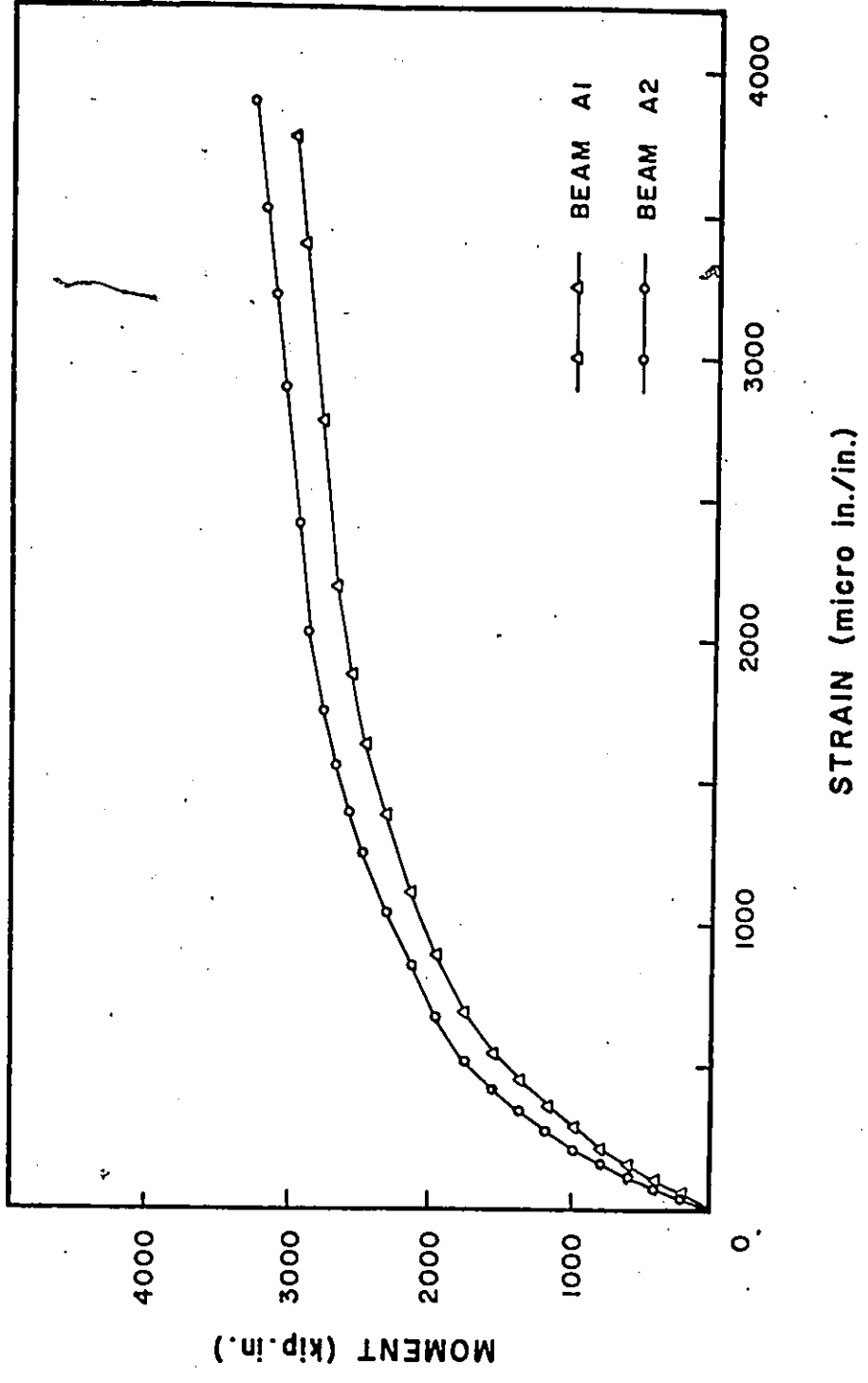


FIGURE 6.53 COMPARISON BETWEEN THE TOP FIBRE CONCRETE STRAIN FOR ENDS A1 AND A2

Figures 6.54 and 6.55 show a comparison between the maximum top fibre concrete strains for ends A_1 and D_1 and end A_2 and D_2 . Figures 6.56 and 6.57 show the comparison between the bottom fibre steel strains for the same ends. These figures show that for the same applied moment on the section, the maximum top fibre concrete strain and bottom fibre steel strain decreases with the increase of L/b ratio. This decrease proves the above conclusion that the effective slab width increases with the increase of the slab length to width ratio.

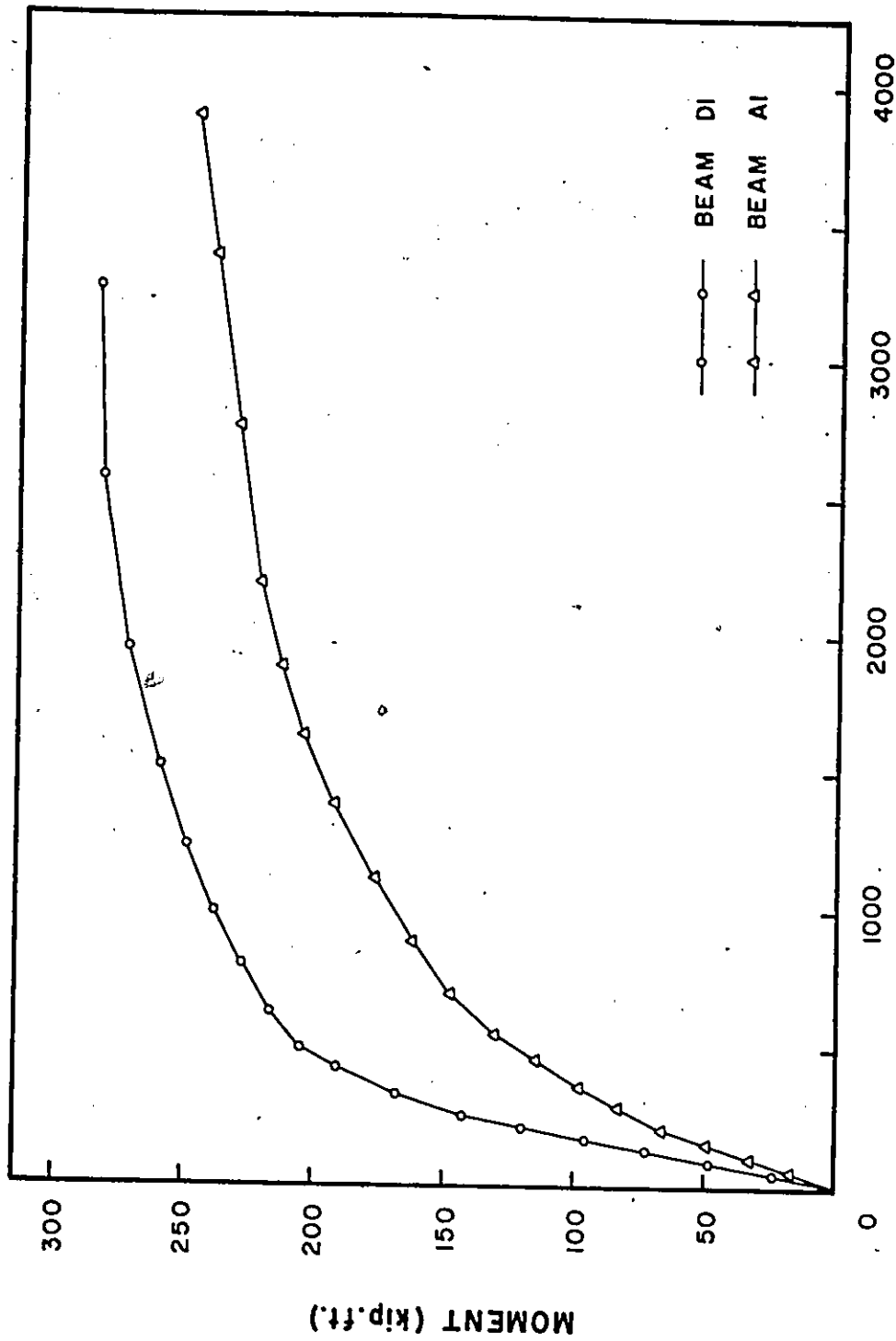
The effect of L/b ratio has been realized by the investigators for the case of simple and continuous beams. However this effect has never been investigated before, to the best of the author's knowledge, when the behaviour of unbraced frames with composite beams was investigated.

6.4.3 Effect of the Total Slab Thickness

The effect of increasing the total slab thickness can be determined by comparing tests A_1 with E_2 and B_1 with E_2 . The effect of increasing the total slab thickness from 4 in to 5 in is given in Table 6.5.

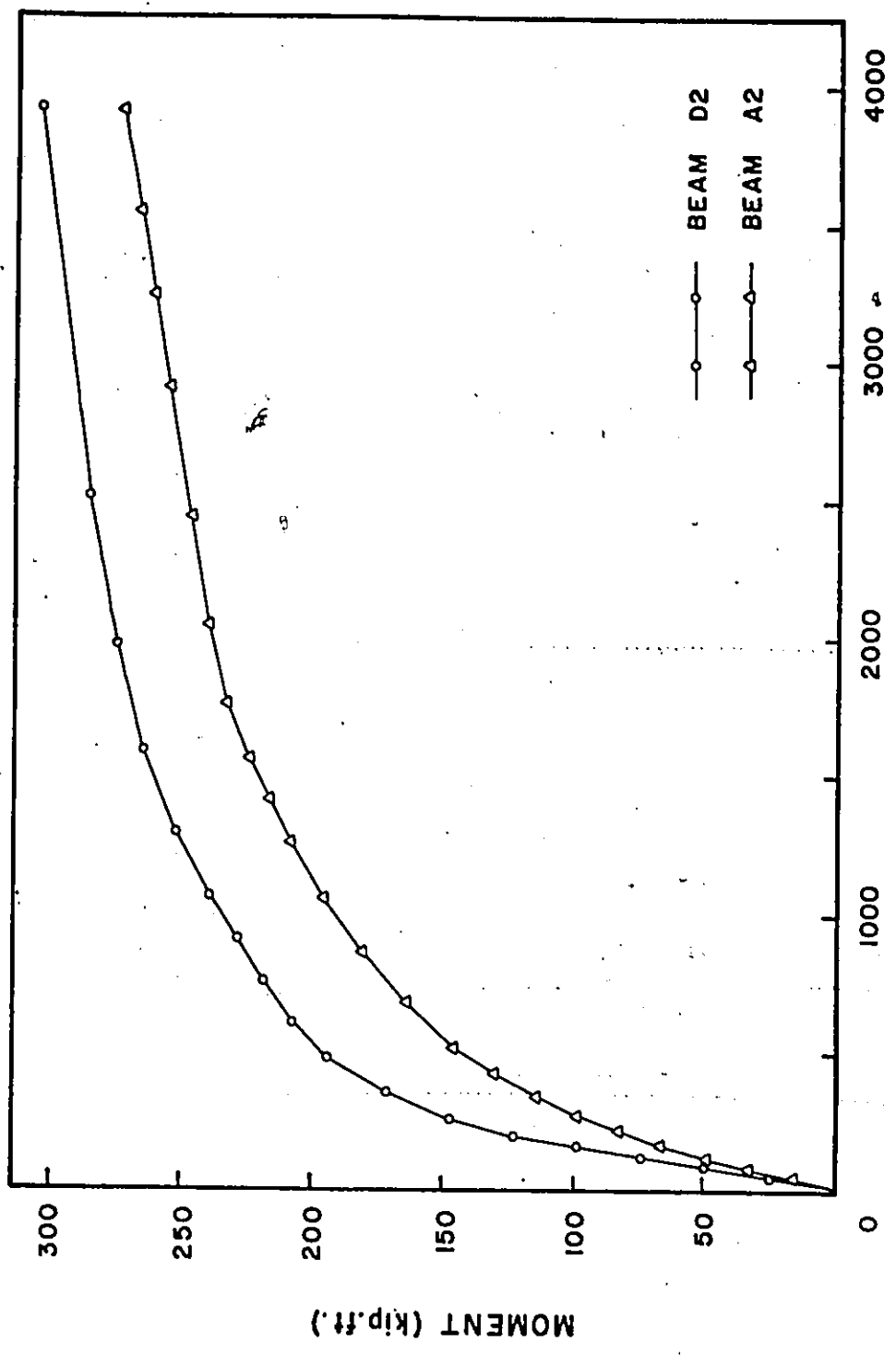
The results in this table show that the maximum strength ratio, initial stiffness ratio and ductility factor increased with increasing the total slab thickness.

The increase in the total slab thickness was shown analytically to have no effect on the effective slab width for strength. A comparison between the top fibre concrete strain distributions across



STRAIN (micro in./in.)

FIGURE 6.54 COMPARISON BETWEEN THE TOP FIBRE CONCRETE STRAIN FOR ENDS A1 AND D1



STRAIN (micro in./in.)

FIGURE 6.55 COMPARISON BETWEEN THE TOP FIBRE CONCRETE STRAIN FOR ENDS A2 AND D2

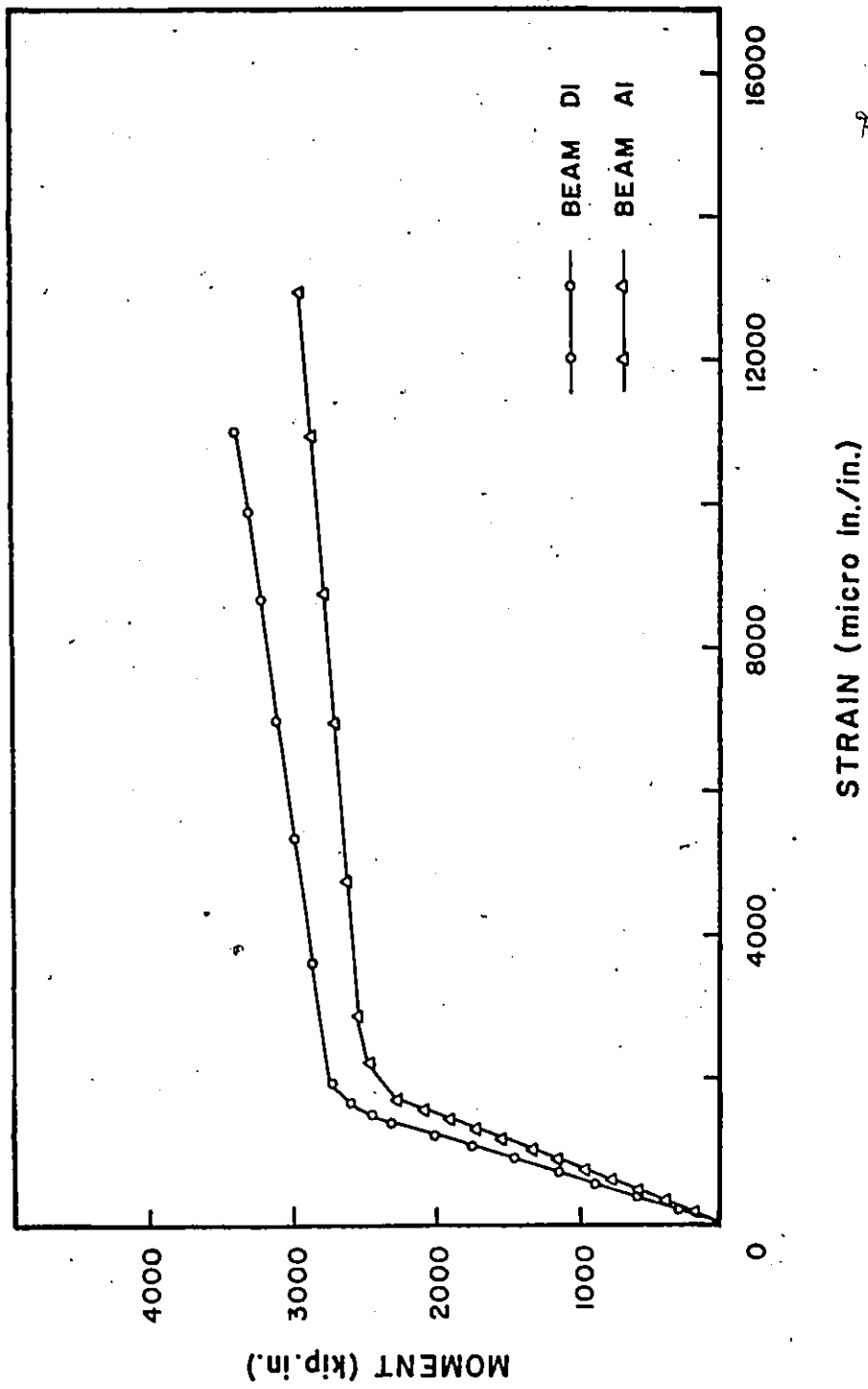


FIGURE 6.56 COMPARISON BETWEEN THE BOTTOM FIBRE STEEL STRAIN FOR ENDS A1 AND D1.

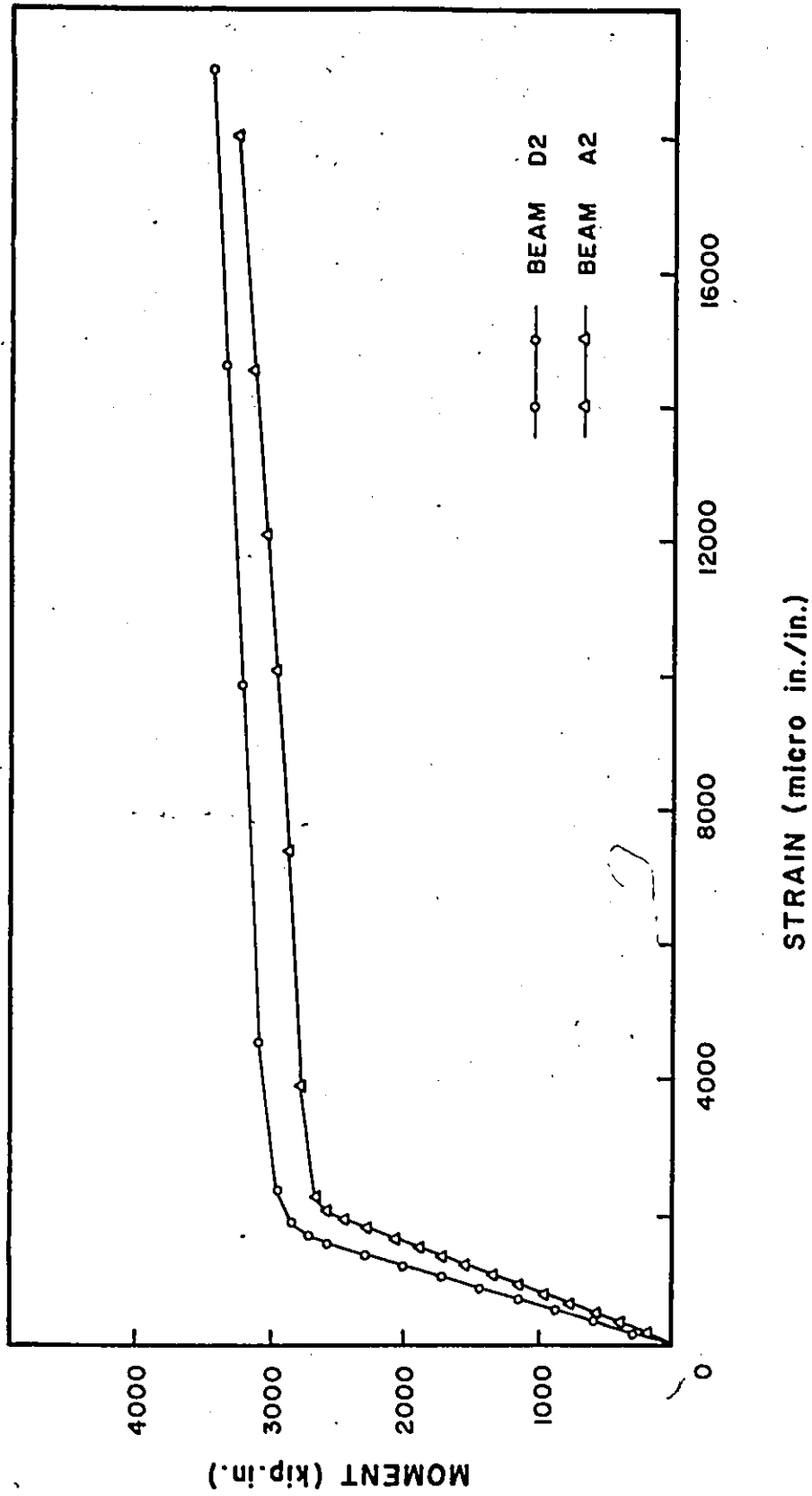


FIGURE 6.57 COMPARISON BETWEEN THE BOTTOM FIBRE STEEL STRAIN FOR ENDS A2 AND D2

the slab width for ends A_1 and E_2 , Figures 6.10 and 6.52, shows that although the strains were higher for the thinner slab, the strain distribution shape is almost the same which leads to the conclusion that the effective slab width for strength is almost the same for both cases.

The increase in the maximum strength ratio, initial stiffness ratio and ductility factor is due to the increase in the slab thickness. The increase of the slab thickness increases the inertia of the section and raises the neutral axis of the section which reduces the concrete strain. Figure 6.58 shows a comparison between the top fibre concrete strains at section 1-1 for ends A_1 and E_2 .

6.4.4 Effect of the Steel Beam Size

A comparison of tests A_1 with C_2 and B_1 with C_1 shows that the only appreciable difference between these tests was the size of the steel beam. Thus the effect of the steel beam size can be determined from the comparison of the results of these tests. The effect of increasing the steel beam size from W12x27 to W16x40 is given in Table 6.6.

Table 6.6 shows that the maximum strength ratio, initial stiffness ratio and ductility factor decreased with the increase in the beam size. The decrease in the maximum strength ratio ranged from 9.7 to 15.7% and the decrease in the initial stiffness ratio ranged from 8.8 to 13.2%. The decrease in the ductility factor was much more larger and ranged from 29.7 to 40%. Increasing the beam size, beam area and inertia, increases the contribution of the steel beam to the maximum

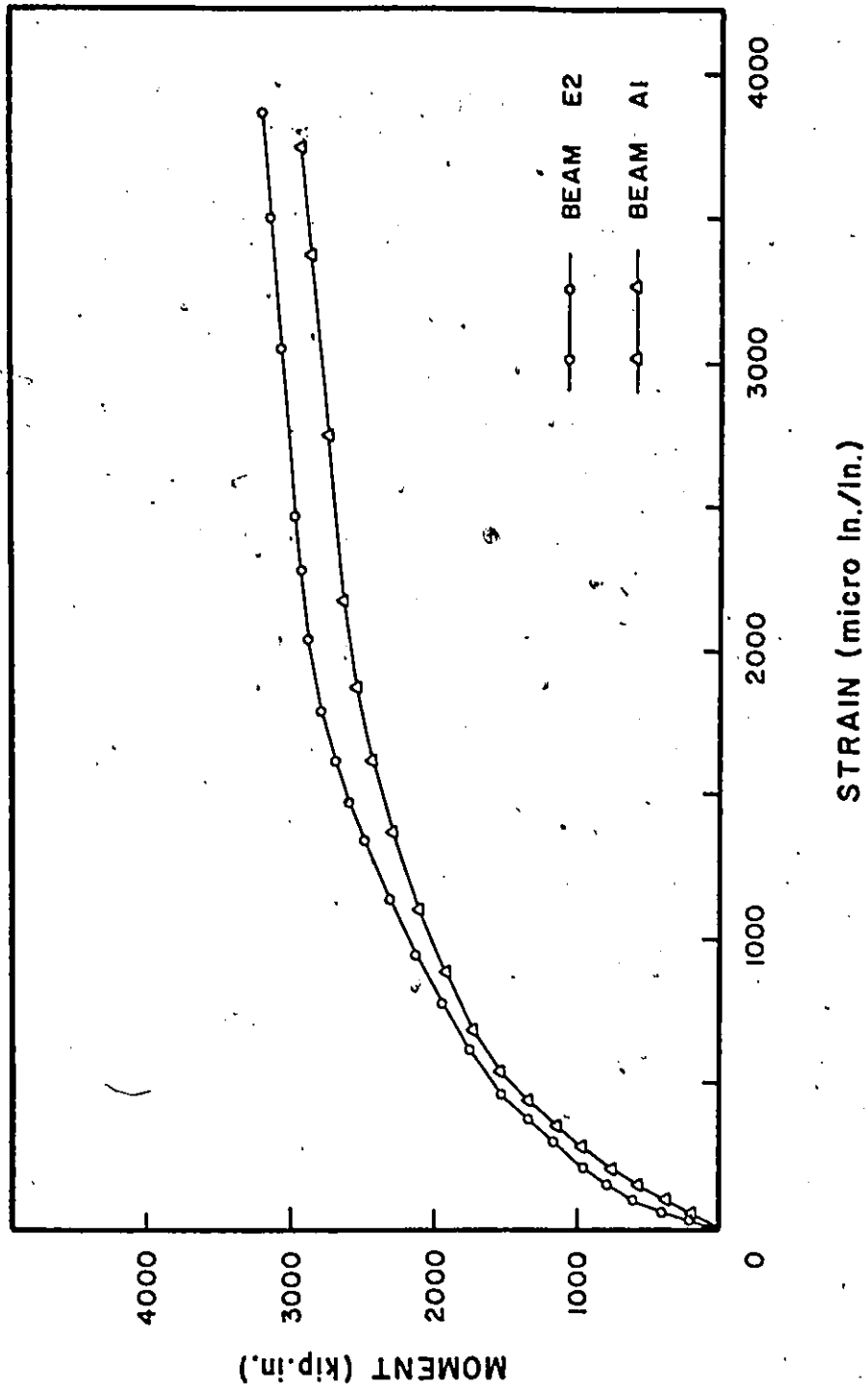


FIGURE 6.58 COMPARISON BETWEEN THE TOP FIBRE CONCRETE STRAIN FOR ENDS A1 AND E2

strength and to the inertia of the composite section and consequently reduces the maximum strength and initial stiffness ratios. Also increasing the beam size lowers the neutral axis of the section and consequently reduces the bottom fibre steel strain and increases the top fibre concrete strain. Thus the connection attains its maximum strength before developing large plastic strains in the beam which reduces the ductility of the section.

6.4.5 Effect of the Lateral Support

The effect of the lateral support can be determined by comparing tests E_1 with E_2 . The only difference between these tests was the existence of the lateral beam which was bolted to the slab of end E_1 .

The effect of the existence of the lateral support is given in Table 6.7. The results in this table show that the maximum strength ratio, initial stiffness ratio and the ductility factors increased with the existence of the lateral support. The maximum strength ratio increased by 9.2%, the initial stiffness ratio by 10.6% and the ductility factor by 36.9%.

To illustrate the effect of the existence of the lateral support, the top fibre concrete strain distribution across the slab width at section 1-1 for end E_1 and E_2 are compared in Figure 6.59. This figure shows that the strain distribution is more uniform for end E_1 than end E_2 which leads to a larger effective slab width. Hence the strength and inertia of the composite section increases and consequently the maximum strength ratio, initial stiffness ratio and ductility factor increase.

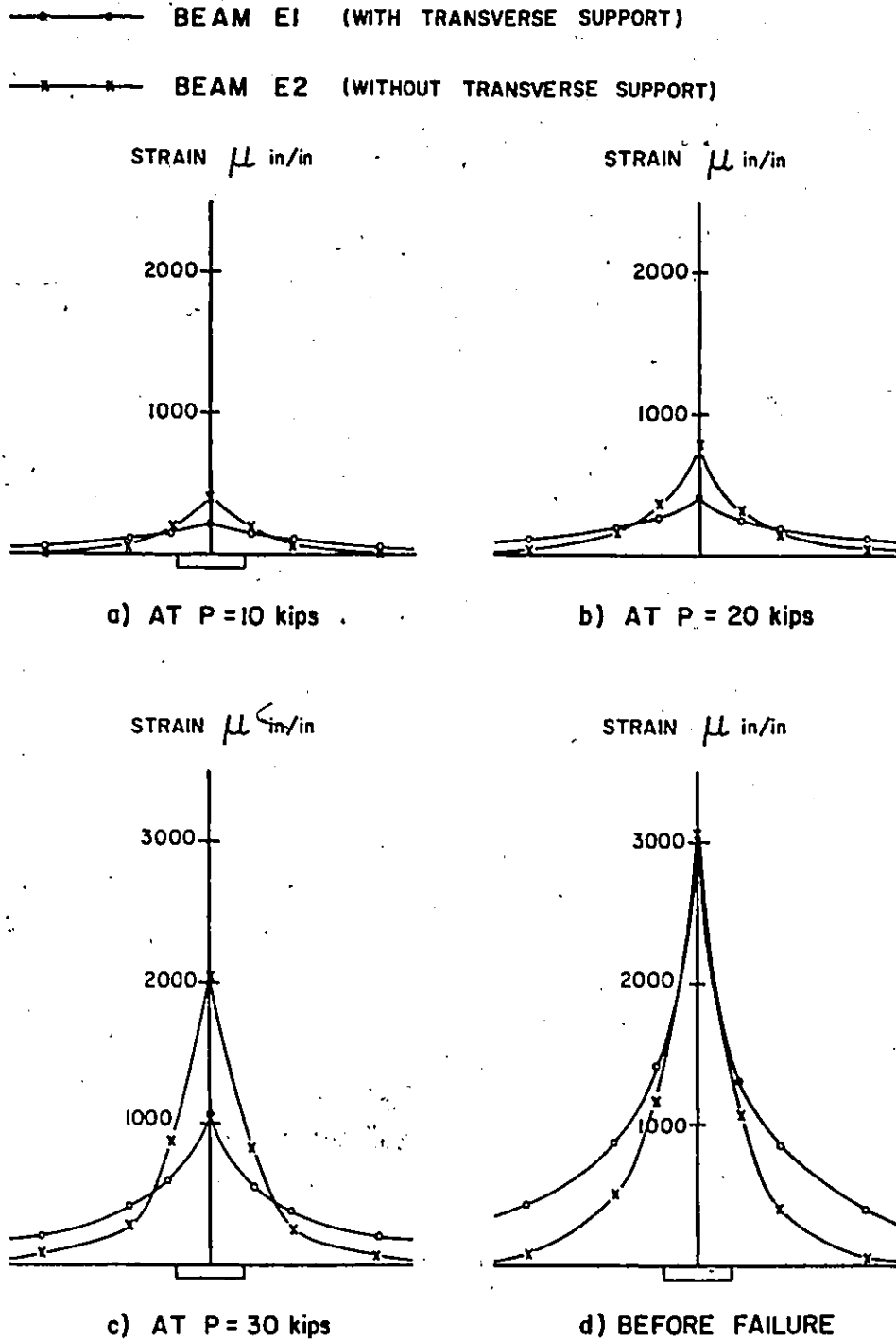


FIGURE 6.59 COMPARISON BETWEEN THE TOP FIBRE CONCRETE STRAIN DISTRIBUTION ACROSS THE SLAB WIDTH FOR ENDS E1 AND E2

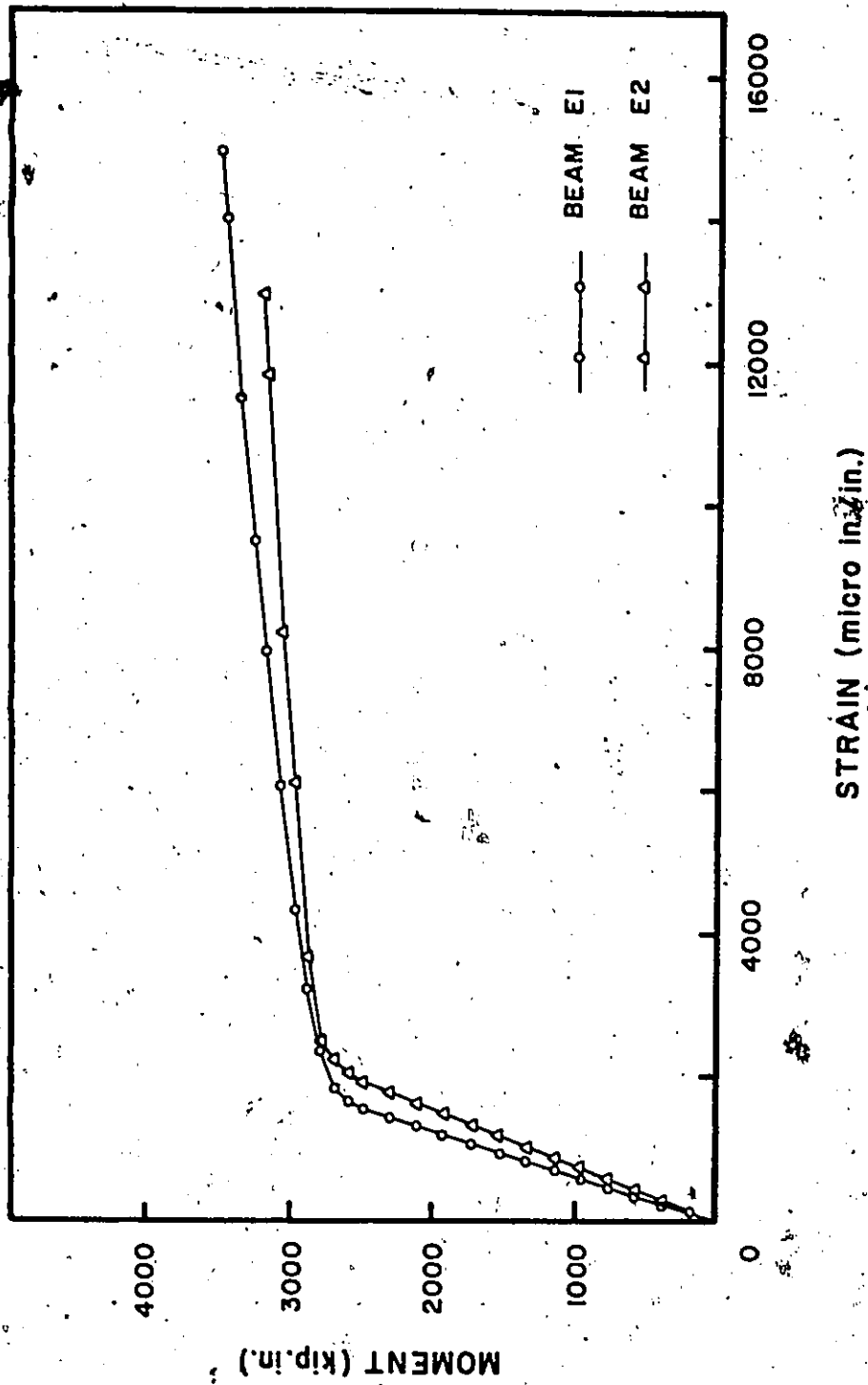


FIGURE 6.60 COMPARISON BETWEEN THE BOTTOM FIBRE STEEL STRAIN FOR ENDS E1 AND E2

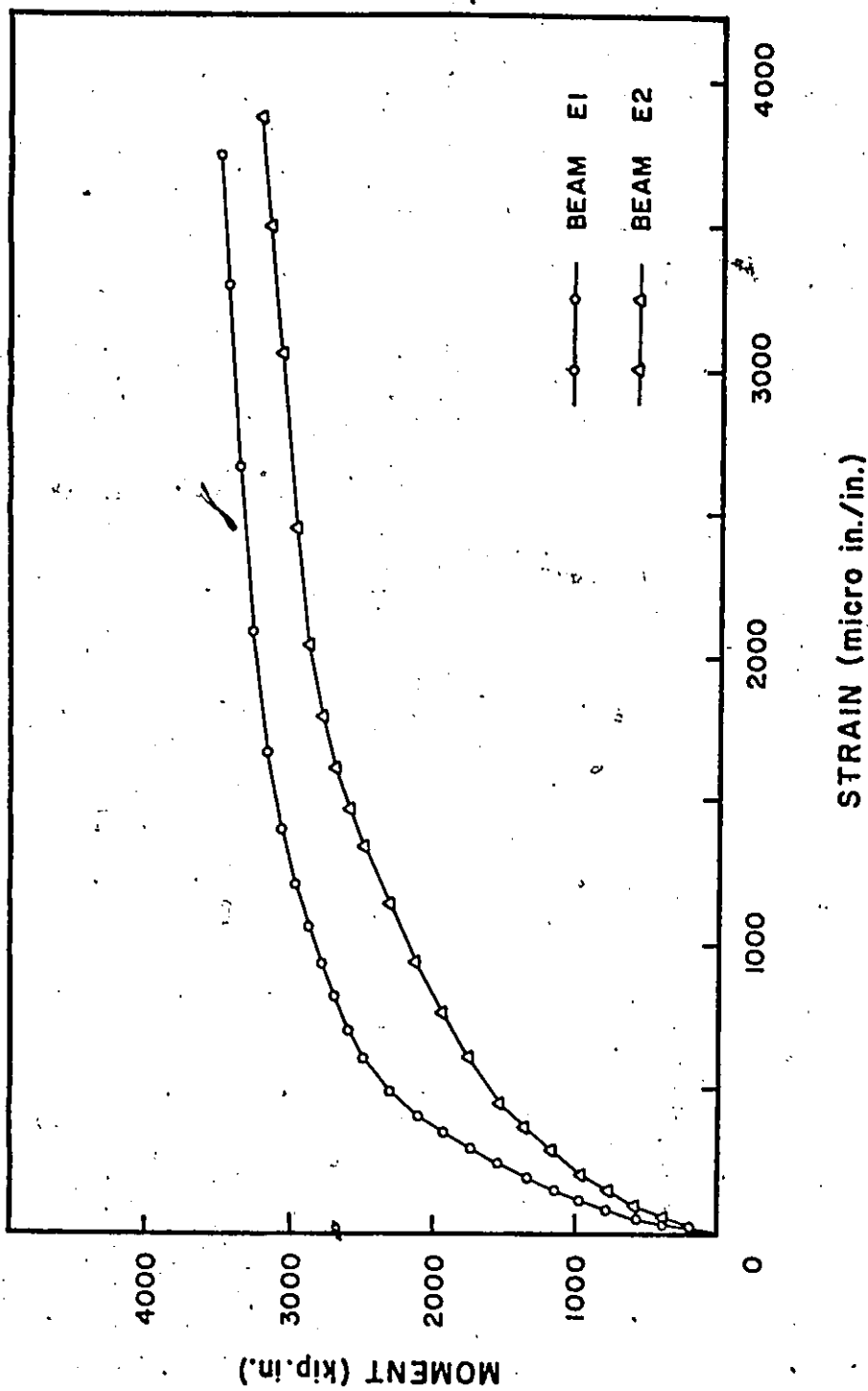


FIGURE 6.61 COMPARISON BETWEEN THE TOP FIBRE CONCRETE STRAIN FOR ENDS E1 AND E2

Figure 6.60 shows a comparison between the bottom fibre steel strain at section 1-1 for ends E_1 and E_2 . Figure 6.61 shows a comparison between the top fibre concrete strain at the Section 1-1 for the same ends.

6.4.6 Effect of Existence of the Longitudinal Crack Before Testing

Although the effect of the longitudinal crack was not one of the factors to be investigated, it was possible to study this effect from the test results. The effect of existence of pre-longitudinal crack can be determined from comparison of tests A_1 with B_1 , A_2 with B_2 and C_1 with C_2 . The results of this comparison is given in Table 6.8.

The results presented in this table show the maximum strength ratio, initial stiffness ratio and ductility factor decreased due to the existence of the crack. The decrease in the maximum strength ratio was small and ranged from 1.8 to 3.5% while the decrease in the ductility factor was large and reached 14.6% when ends A_2 and B_2 were compared. The decrease in the initial stiffness ranged from 1.8 to 8.4%.

c/b = 0.166	c/b = 0.25	Maximum Strength Ratio % increase	Initial Stiffness Ratio % increase	Ductility Factor % increase
A ₁	A ₂	10.4	24.0	50.3
B ₁	B ₂	5.0	10.0	50.0
D ₁	D ₂	5.9	13.8	59.7

Table 6.3: Effect of Increasing c/b ratio

L/b = 1.6	L/b = 2.4	Maximum Strength Ratio % increase	Initial Stiffness Ratio % increase	Ductility Factor % increase
A ₁	D ₁	9.7	21.6	26.2
B ₁	D ₁	6.2	17.8	7.8
A ₂	D ₂	5.3	11.6	34.1
B ₂	D ₂	7.2	21.8	14.8

Table 6.4: Effect of Increasing L/b Ratio

4 in slab	5 in slab	Maximum Strength ratio % increase	Initial Stiffness ratio % increase	Ductility Factor % increase
A ₁	E ₂	5.8	13.6	30.4
B ₁	E ₂	2.5	10.0	11.4

Table 6.5: Effect of Increasing Slab Thickness

W12x27 Steel Beam	W16x40 Steel Beam	Maximum Strength Ratio % Decrease	Initial Stiffness Ratio % Decrease	Ductility Factor % Decrease
A ₁	C ₁	9.7	8.8	32.0
B ₁	C ₁	12.5	11.6	42.0
A ₁	C ₂	12.9	10.4	29.7
B ₁	C ₂	15.7	13.2	40.0

Table 6.6: Effect of Increasing the Steel Beam Size

Without trans- verse support	Without trans- verse support	Maximum Strength Ratio % increase	Initial Stiffness Ratio % increase	Ductility Factor % increase
E ₂	E ₁	9.2	10.6	36.9

Table 6.7: Effect of the Transverse Support

Without pre- crack	with pre- crack	Maximum Strength Ratio % Decrease	Initial Stiffness Ratio % Decrease	Ductility Factor % Decrease
B ₁	A ₁	3.2	3.1	14.6
A ₂	B ₂	1.8	8.4	14.4
C ₁	C ₂	3.5	1.8	3.3

Table 6.8: Effect of the Existence of the Pre-longitudinal Crack Before Testing

CHAPTER 7

COMPARISON OF THE EXPERIMENTAL AND ANALYTICAL RESULTS

7.1 General

To verify the method of inelastic analysis described in Chapter 3 and to compare the prediction of the various methods, the test beams were taken as examples for computation.

In this chapter the results obtained from the analytical model, the transformed section method and the ultimate stress block method are compared with the experimental results. The comparison is organized in six major groups as follows:

1. The ultimate moment capacity of the composite beam at the position of the connection to the column.
2. Moment-deflection behaviour of the composite beam.
3. Variation of the bottom fibre steel strain at the position of the connection with the applied moment on the section.
4. Moment-curvature characteristics of the composite section adjacent to the connection with the column.
5. Top fibre concrete strain distributions across the slab width.
6. Strain distribution across the composite beam depth at the section adjacent to the connection.

The results obtained from various methods are discussed in detail in the subsequent sections.

7.2 Ultimate Moment Capacity

The ultimate moment capacity of each of the experimental beams was calculated using the analytical model and using the ultimate stress block method.

The geometrical and material properties pertinent to each of the test beams were fed as an input into the computer program and the ultimate moment was obtained directly as output. Since all the test beams failed by crushing of the concrete slab, as designed, adjacent to the column face, the computation was terminated when the strain in the concrete slab reached the maximum compressive strain ϵ_{cu} given by equation (3.34) in Chapter 3.

The ultimate moment capacity was evaluated for each beam using the ultimate stress block method. The analytical effective slab width for strength corresponding to L/b and c/b ratio of each beam, Chapter 4, and a maximum concrete strength equal to $0.85 f'_c$ were used in this calculation.

The ultimate stress block method was also used to evaluate the ultimate moment capacity of the test beams assuming effective slab width equal to the column face width and concrete strength equal to $1.3 f'_c$ as recommended by previous investigators⁽⁴⁸⁾.

The results obtained from the inelastic computer analysis and the ultimate stress block method are compared with the experimental results, for each of the test beams, in Table 7.1. End C_2 was excluded from the comparison since it was a repetition of end C_1 .

The ultimate moment capacity obtained from the inelastic analysis

Beam	A ₁	A ₂	B ₁	B ₂	C ₁	D ₁	D ₂	E ₁	E ₂
Analytical Effective slab width for strength in.	19.0	24.9	19.0	24.9	19.0	20.0	26.0	23.7	19.0
M _{exp} kip. in.	2947	3252	3043	3197	5654	3384	3583	3504	3214
M _u (Inelastic) kip. in.	3072	3264	3072	3264	5760	3456	3672	3600	3168
M _u (stress block & effective slab width) kip. in.	2886	3152	2886	3152	5563	3210	3394	3336	3024
M _u (stress block & column face width) kip. in.	2696	2897	2696	2897	5174	2990	3210	3024	3024
$\frac{M_{exp}}{M_u}$ (Inelastic)	0.96	0.99	0.99	0.98	0.98	0.98	0.98	0.97	0.98
$\frac{M_{exp}}{M_u}$ (stress block & ESW)	1.02	1.03	1.05	1.02	1.02	1.05	1.05	1.05	1.02
$\frac{M_{exp}}{M_u}$ (stress block & CFW)	1.1	1.13	1.13	1.13	1.09	1.13	1.12	1.16	1.07

Table 7.1: Comparison of the Experimental and Analytical Ultimate Moment Capacity

is slightly higher than the experimental one. The ratio of the experimental to the computed value ranges from 0.96 to 0.99 as shown in Table 7.1.

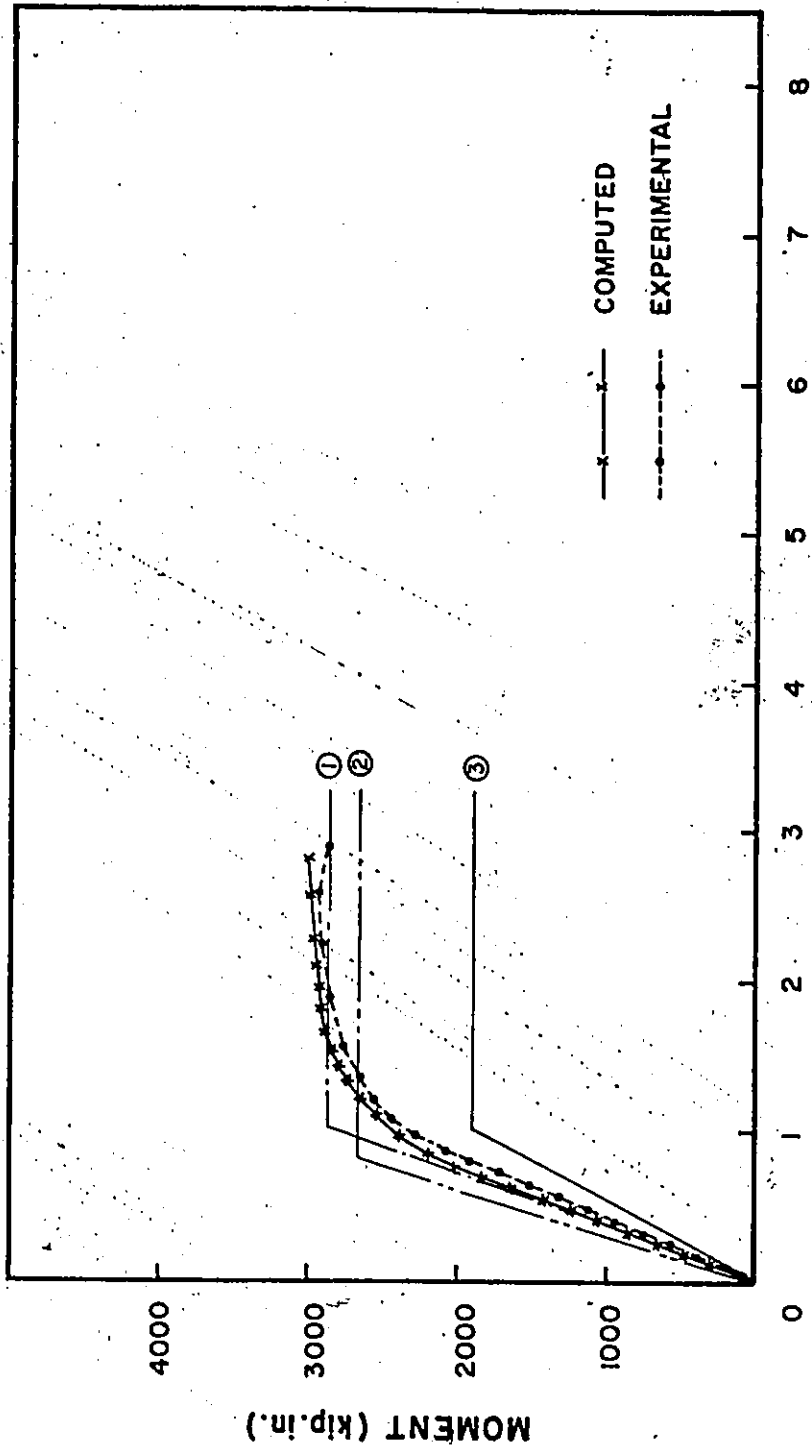
Table 7.1 shows that the ultimate moment capacity obtained from the ultimate stress block method and the analytical effective slab width for strength is slightly less than the experimental value. The ratio between the experimental and computed value ranges from 1.02 to 1.05. However, this ratio ranges between 1.07 and 1.13 when the calculation is performed assuming the effective slab width to be equal to the column face width and considering the concrete strength to be increased to $1.3 f'_c$ due to the biaxial effect.

The above comparison indicates that a very close lower bound for the ultimate strength of the composite beam, at the beam-to-column connection, can be predicted by the ultimate stress block method using the pertinent effective slab width for strength, which has been developed in Chapter 4, and a concrete strength of $0.85 f'_c$.

7.3 End Moment Versus Free End Deflection Curves

Deflections were calculated from the integration of the curvature resulting from the inelastic analysis, described in Chapter 3, which takes into account the effect of the shear lag in the slab and the slip occurring at the interface between the steel beam and the slab. The deflections are given as a direct output from the computer program for every load increment.

Figures 7.1 through 7.9 show the computed and experimental end



DEFLECTION (in.)

FIGURE 7.1 COMPARISON BETWEEN THE EXPERIMENTAL AND ANALYTICAL MOMENT-DEFLECTION CURVES FOR END A1

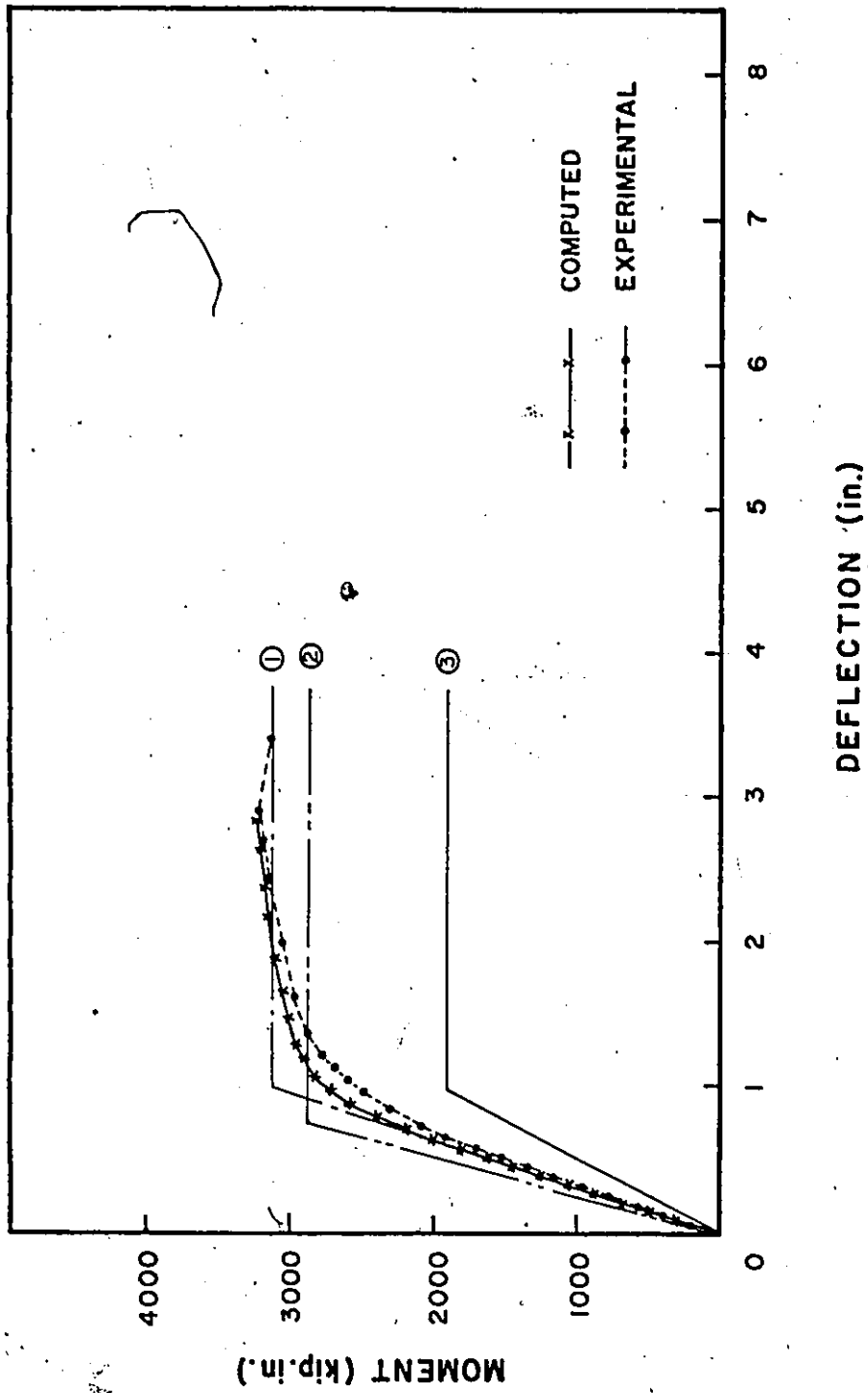


FIGURE 7.2 COMPARISON BETWEEN THE EXPERIMENTAL AND ANALYTICAL MOMENT-DEFLECTION CURVES FOR END A2

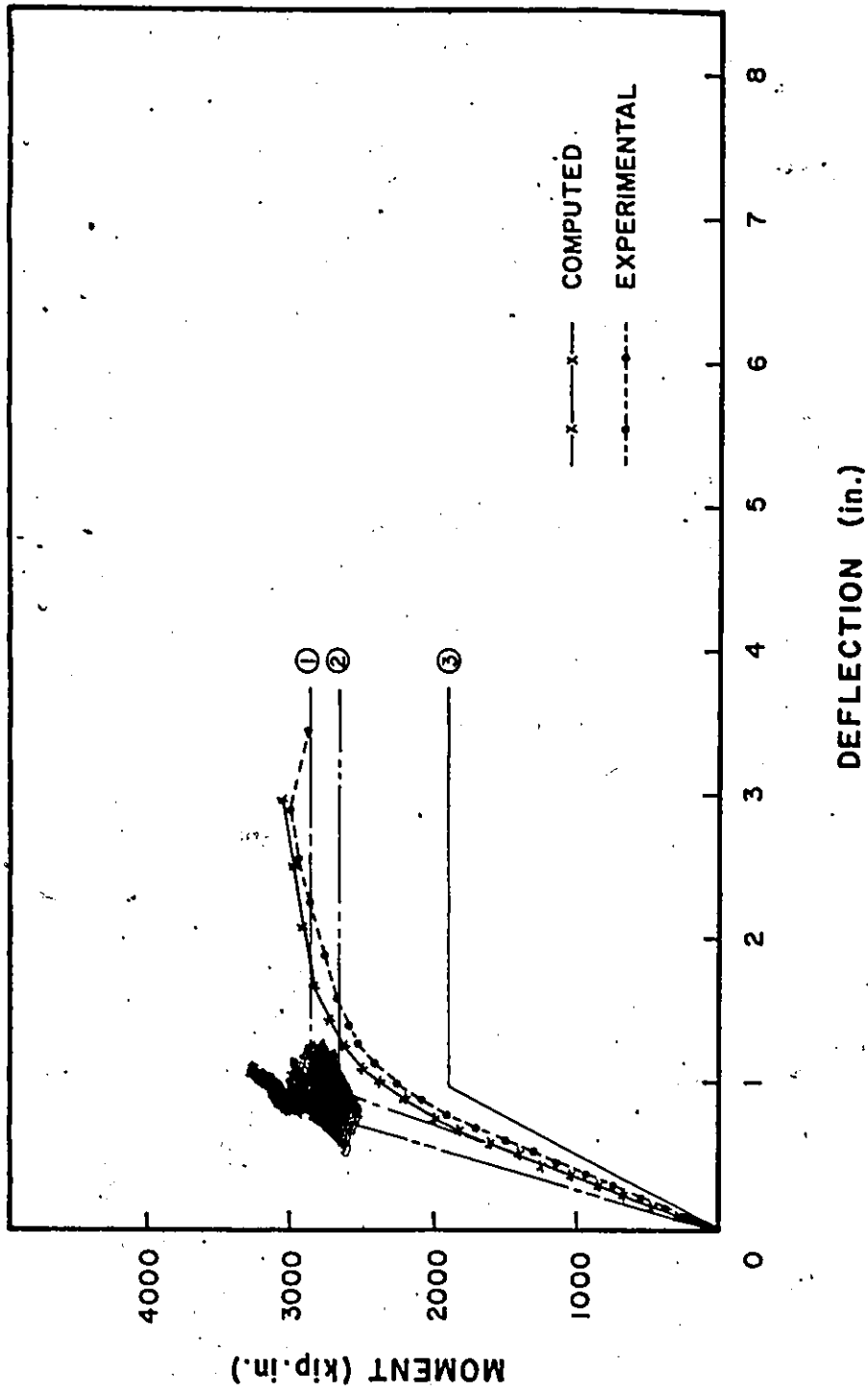
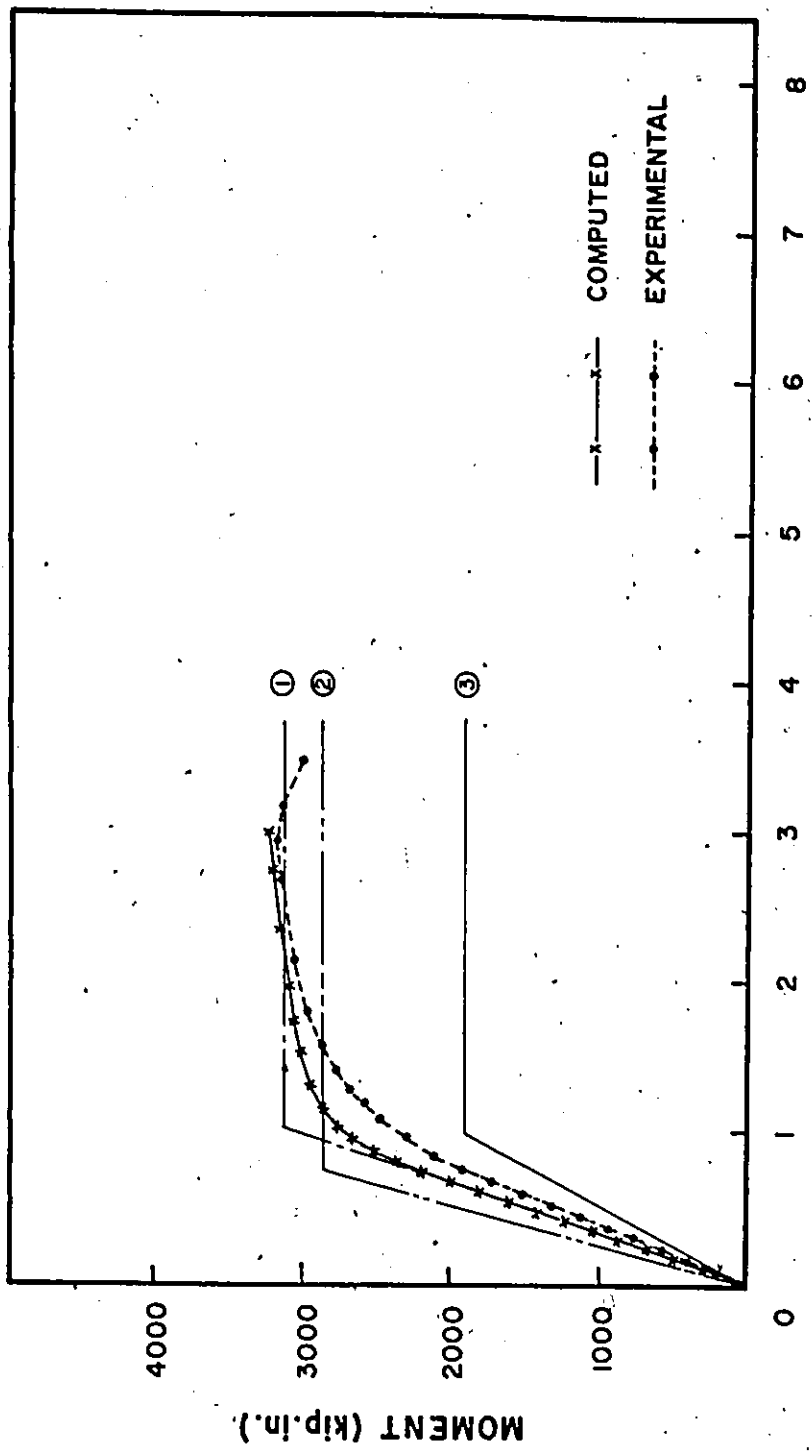


FIGURE 7.3 COMPARISON BETWEEN THE EXPERIMENTAL AND ANALYTICAL MOMENT-DEFLECTION CURVES FOR END B1



DEFLECTION (in.)

FIGURE 7.4 COMPARISON BETWEEN THE EXPERIMENTAL AND ANALYTICAL MOMENT-DEFLECTION CURVES FOR END B2

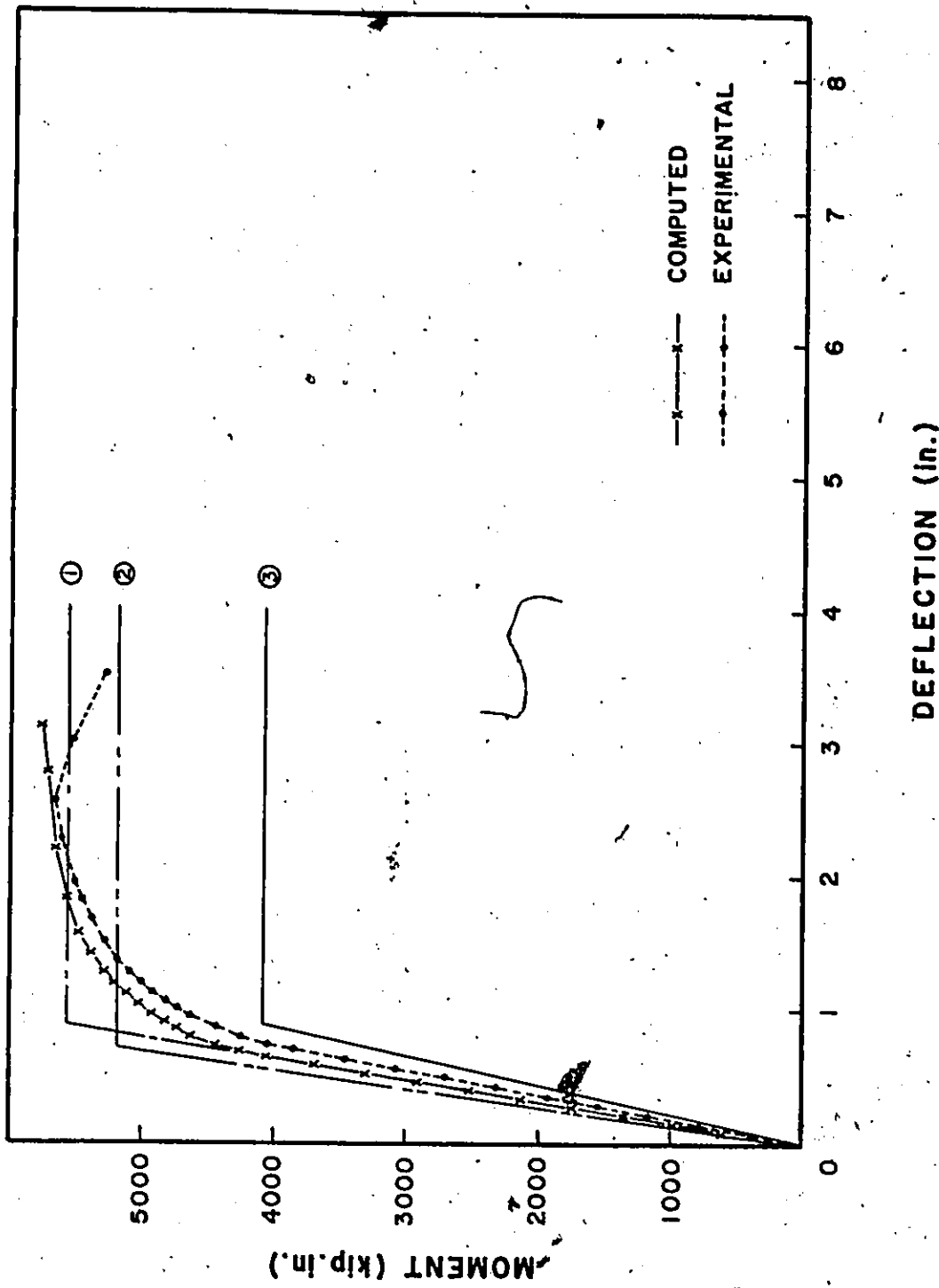


FIGURE 7.5 COMPARISON BETWEEN THE EXPERIMENTAL AND ANALYTICAL MOMENT-DEFLECTION CURVES FOR END C1

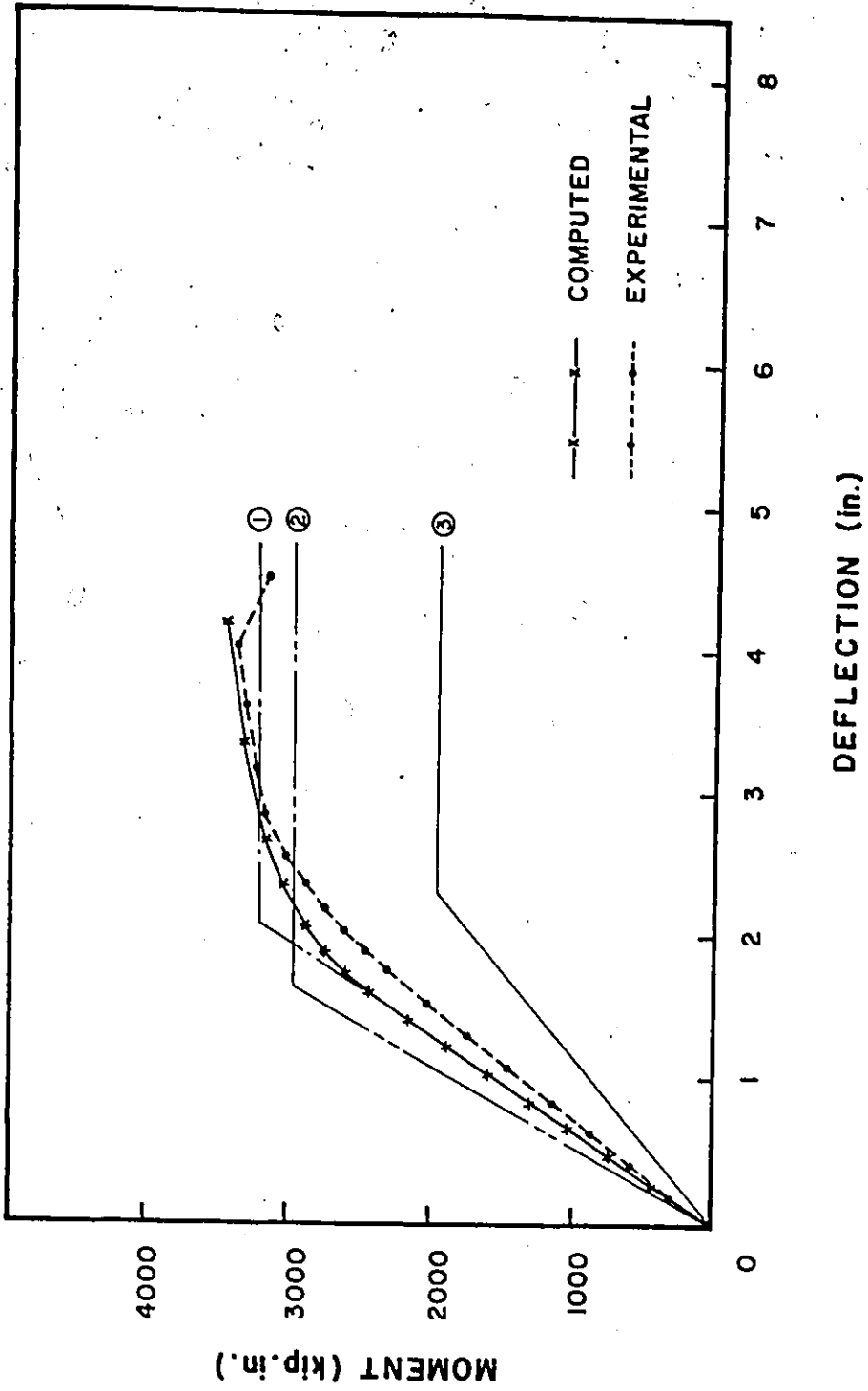


FIGURE 7.6 COMPARISON BETWEEN THE EXPERIMENTAL AND ANALYTICAL MOMENT-DEFLECTION CURVES FOR END D1

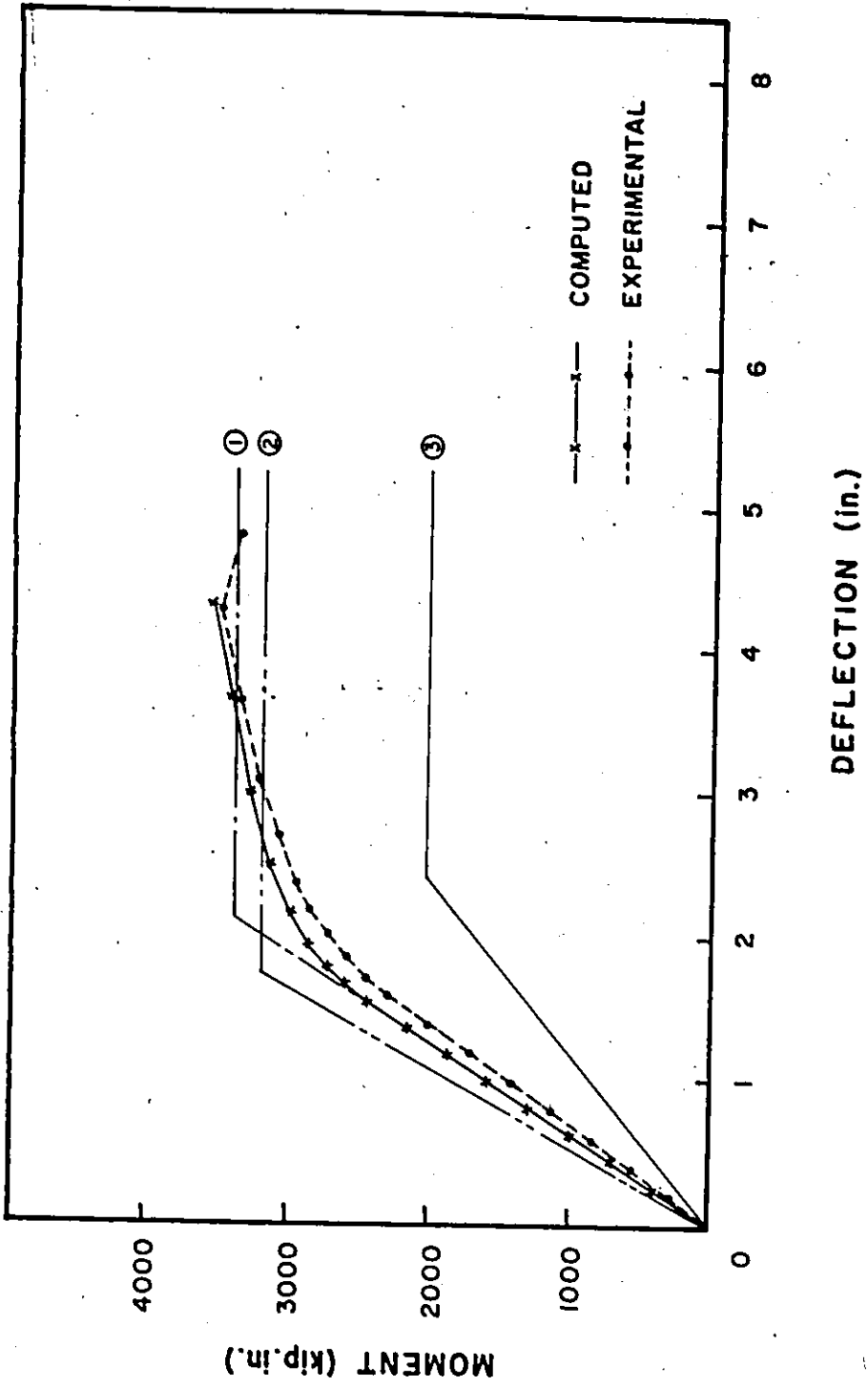


FIGURE 7.7 COMPARISON BETWEEN THE EXPERIMENTAL AND ANALYTICAL MOMENT-DEFLECTION CURVES FOR END D2

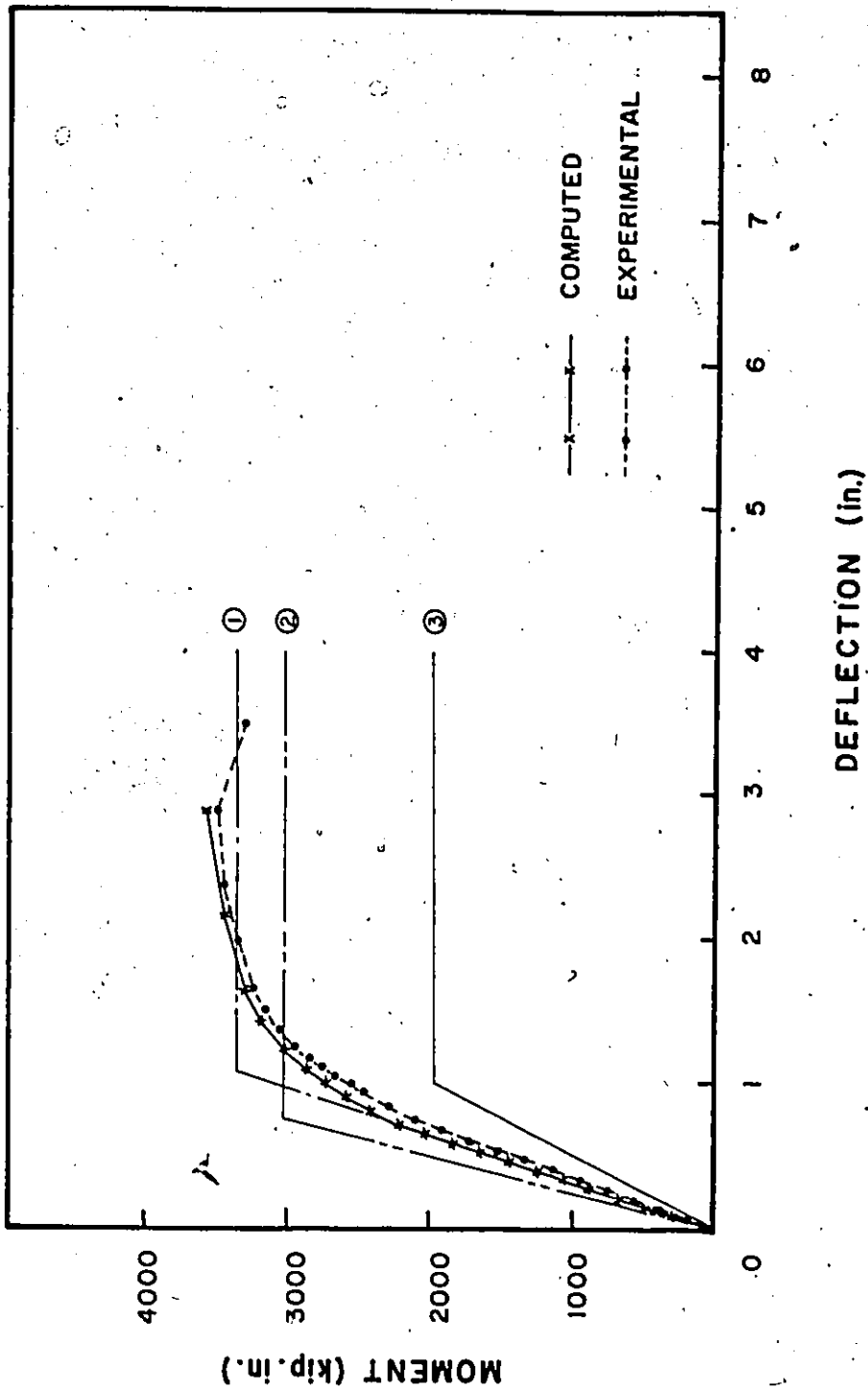


FIGURE 7.8 COMPARISON BETWEEN THE EXPERIMENTAL AND ANALYTICAL MOMENT-DEFLECTION CURVES FOR END E1

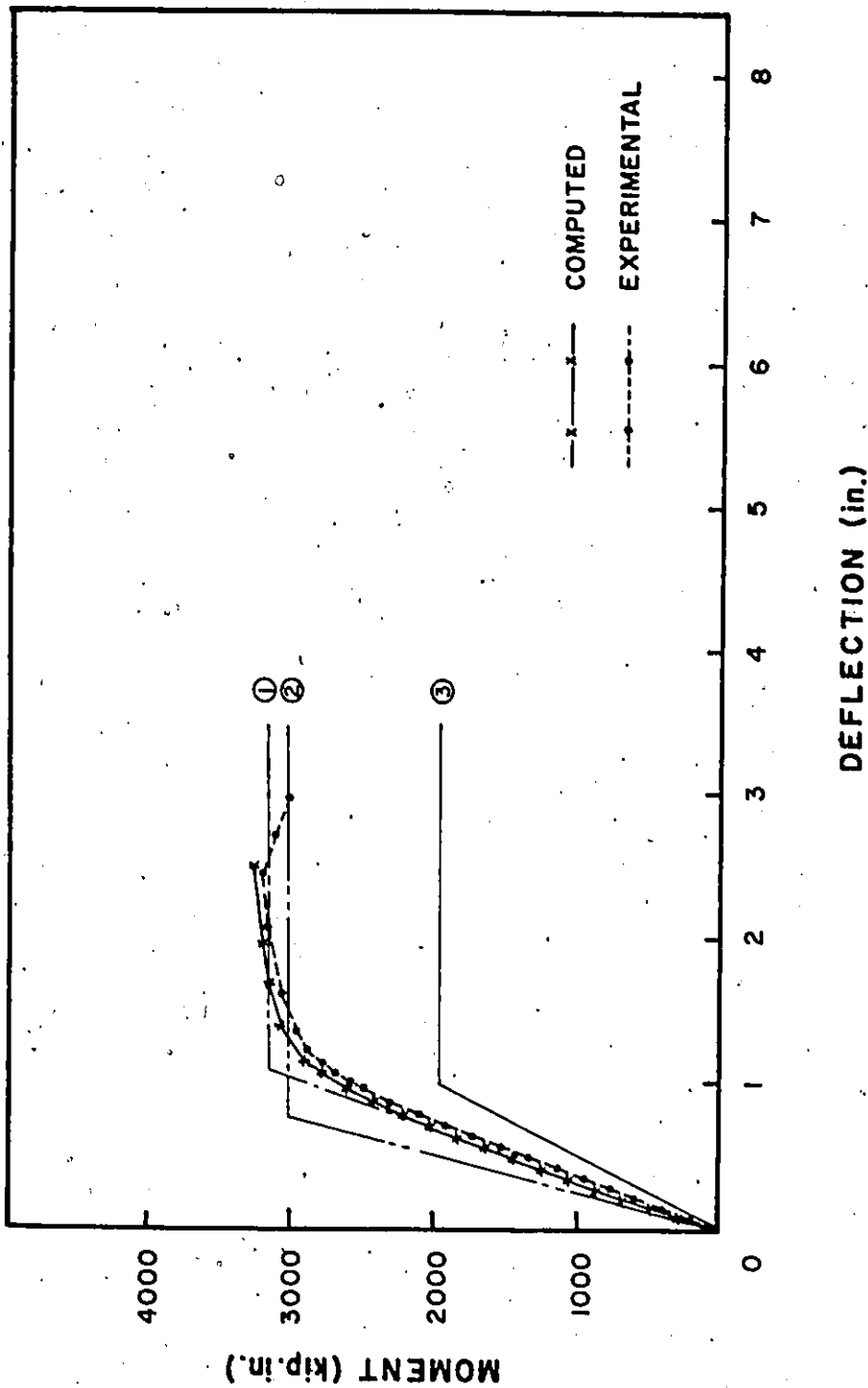


FIGURE 7.9 COMPARISON BETWEEN THE EXPERIMENTAL AND ANALYTICAL MOMENT-DEFLECTION CURVES FOR END E2

moment versus free end deflection curves for the test beams. In addition to the computed and experimental curves each figure contains three theoretical curves described as follows:

1. Moment-deflection curve predicted using the transformed section and the average effective slab width for stiffness.
2. Moment-deflection curve predicted using the transformed section and the total slab width.
3. Moment-deflection curve for the steel beam alone.

Curve (1) was computed using the deflection expression for a cantilever beam subjected to a concentrated load at the free end:

$$\Delta_c = \frac{P L^3}{3 E_s I_{eff}} \quad (7.1)$$

The effective moment of inertia of the composite beam was calculated for the transformed section assuming a concrete slab width equal to the average effective slab width for stiffness (b_{av}) which has been developed in Chapter 4. The Moment-deflection behaviour of the composite beam is idealized to be elastic-perfectly plastic. The composite beam is assumed to behave elastically up to the theoretical ultimate moment calculated using the stress block method and the pertinent effective slab width for strength as described in Section 7.2.

Curve (2) was computed using the same deflection formula. I_{eff} in this case was calculated for the transformed section assuming the total slab width to be effective as recommended by previous investigators⁽⁴¹⁾. The behaviour of the composite beam is considered to

be elastic up to the theoretical ultimate moment calculated using the stress block method and effective slab width equal to the column face width with concrete strength of $1.3 f'_c$.

The deflection of the steel beam alone, Curve 3, was computed by replacing the effective moment of inertia (I_{eff}) by the moment of inertia of the steel beam about its major axis (I_s) in the deflection formula (7.1). The steel beam is considered to behave elastically up to its plastic moment.

The effect of the strain hardening was not considered in computing curves 1, 2 and 3 while it is included in the inelastic computer analysis.

The ultimate moment, plastic moment of the steel beam, moment of inertia and the deflections at the instant of attaining the ultimate moment for each of the curves (1, 2 and 3) are given in Table 7.2. The values of the deflections given in this table for curves (1) and (2) include the effect of the end rotation which was estimated using the following formula:

$$\Delta_{rotation} = \frac{M_u}{J} \cdot L \quad (7.2)$$

where in this equation

$\Delta_{rotation}$ is the deflection at the free end due to the rotation of the fixed end.

M_u is the theoretically calculated ultimate moment for each case.

J is the elastic joint stiffness which was found

Beam	M_u kip. in.	A_1	A_2	B_1	B_2	C_1	D_1	D_2	E_1	E_2
Transformed Section and analytical average effective slab width for stiffness (curve 1)	I_c in ⁴	2886	3152	2886	3152	5563	3210	3394	3336	3168
	Δ in	452	462	452	462	951	500	510	508	498
	Δ/A	1.01	0.97	0.97	1.00	0.91	2.02	2.10	1.07	1.07
Transformed section and total slab width (curve 2)	M_u kip. in.	2696	2897	2696	2897	5174	2990	3210	3024	3024
	I_c in ⁴	606	606	606	606	1166	606	606	720	720
	Δ in	0.78	0.73	0.75	0.72	0.73	1.63	1.71	0.79	0.83
Steel Beam Alone (curve 3)	M_p kip. in.	1910	1910	1912	1912	4060	2010	2010	1965	1965
	I_s in ⁴	204	204	204	204	516	204	204	204	204
	Δ in	0.99	0.99	0.99	0.99	0.84	2.35	2.35	1.02	1.02

Table 7.2: Calculated Deflection for the Transformed Composite Section and the Steel Beam Alone

experimentally for each of the test beams (Chapter 6).

L is the span of the beam

The effect of end rotation was also included in the analytical curve predicted by the inelastic analysis by introducing a rotational spring at the support which had a moment-rotation characteristic similar to the moment-rotation characteristic of each connection.

The analytical moment-deflection curve predicted from the inelastic analysis agreed well with the experimental one for all the test beams. The results presented in Figures 7.1 through 7.9 show that the elastic deflections computed by using the transformed section and the average effective slab width for stiffness were equal to those predicted by the computer analysis and were more realistic than those predicted by considering the total slab width to compositely act with the steel beam.

The above results show that a very good prediction of the deflection in the elastic range can be obtained by using the transformed section method with the analytical average effective slab width for stiffness corresponding to L/b and c/b ratios and the degree of interaction of the beam.

7.4 Bottom Fibre Steel Strain

To verify the analytical method and to compare the prediction of the various methods, the bottom fibre steel strain at section 1-1 of the test beams, which is located 3 in. from the column face, was chosen.

The bottom fibre steel strains were obtained directly as an

output of the inelastic analysis computer program. Figures 7.10 through 7.18 show the experimental and analytical bottom fibre steel strain at section 1-1 versus the applied moment on that section for the test beams. Each figure contains two more theoretical curves labelled (1) and (2) in each figure.

Curve (1) represents the variation of the bottom fibre steel strain with the applied moment obtained by using the transformed section with the analytical effective slab width for stiffness (b_{es}) at that section. The bottom fibre steel strain were calculated from the formula

$$\epsilon_{sb} = \frac{M \cdot y_b}{E_s \cdot I_{eff}} \quad (7.3)$$

where in this equation

M is the applied moment on the section.

I_{eff} is the effective moment of inertia for stiffness of the transformed section based on the analytical effective slab width for stiffness (b_{es}) at that particular section (Chapter 4).

y_b is the distance from the centroid of the transformed section to the lower steel fibre.

ϵ_{sb} is the bottom fibre steel strain.

The composite beam is assumed to behave elastically up to its maximum strength calculated by the stress block method considering slab width equal to the analytical effective slab width for strength (b_e) and a concrete strength of $0.85 f'_c$ as mentioned in Section 7.2.

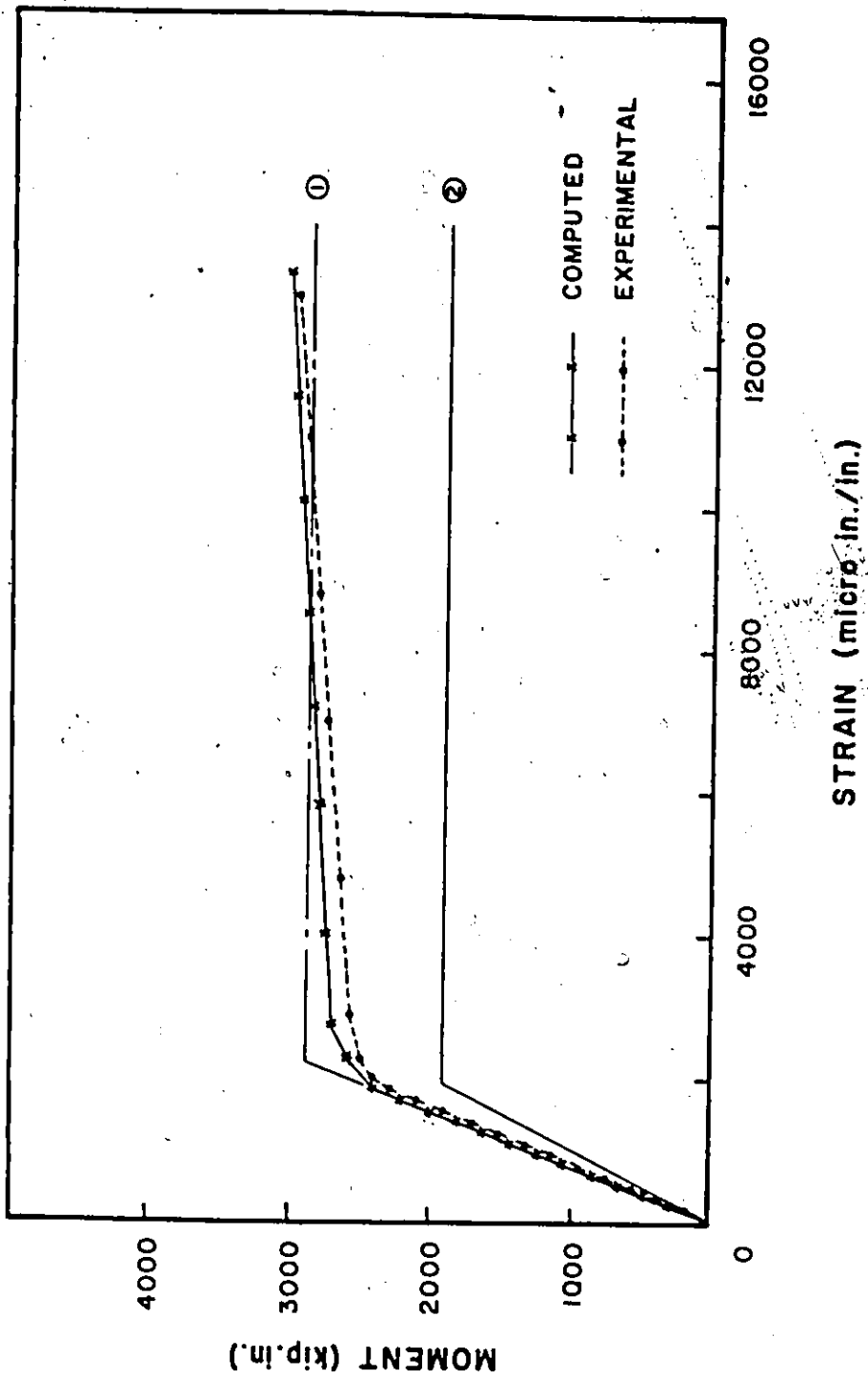


FIGURE 7.10 COMPARISON BETWEEN THE EXPERIMENTAL AND ANALYTICAL MOMENT VERSUS BOTTOM FIBRE STEEL STRAIN CURVES FOR END A1

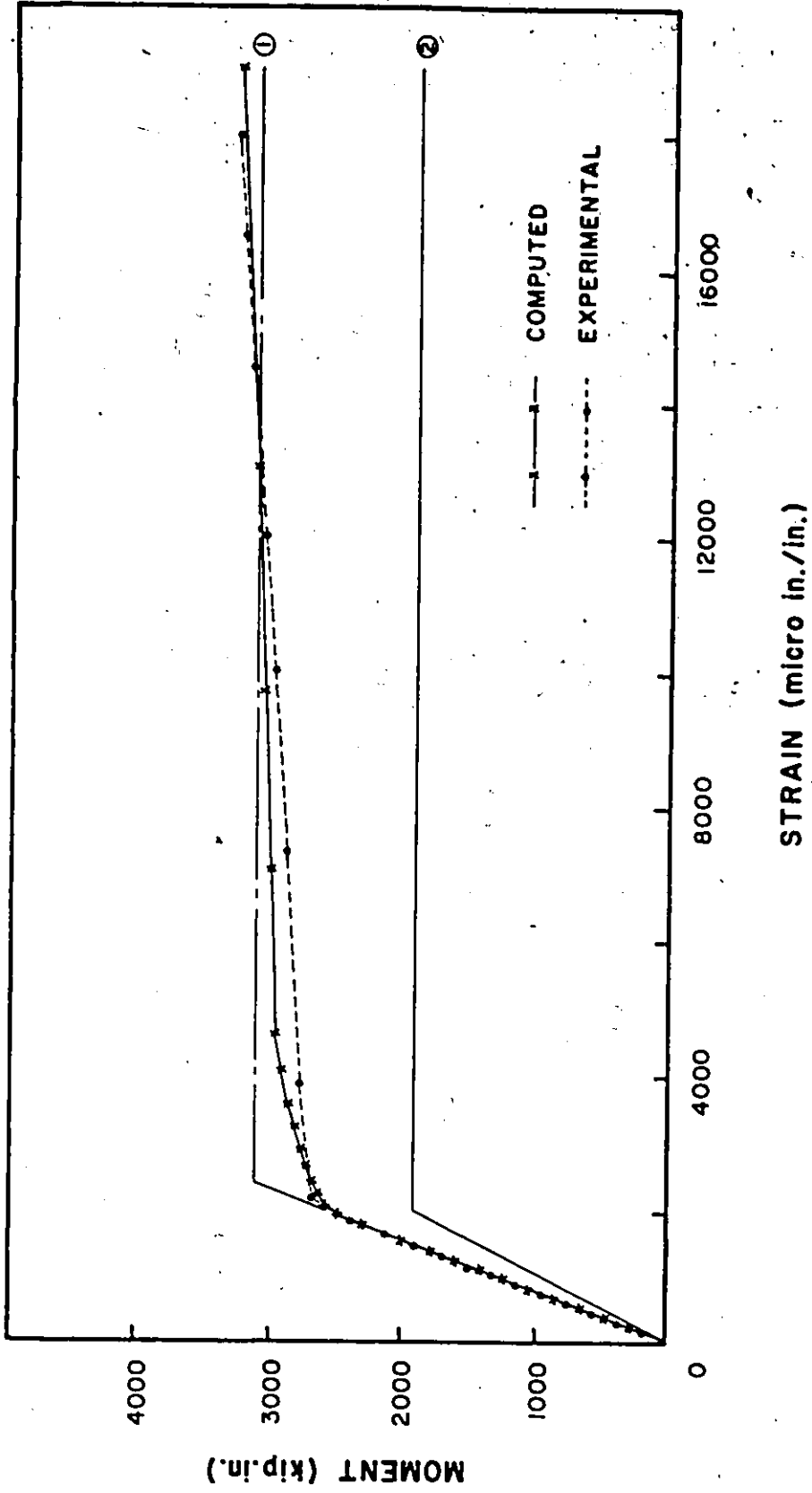


FIGURE 7.11 COMPARISON BETWEEN THE EXPERIMENTAL AND ANALYTICAL MOMENT VERSUS BOTTOM FIBRE STEEL STRAIN CURVES FOR END A2

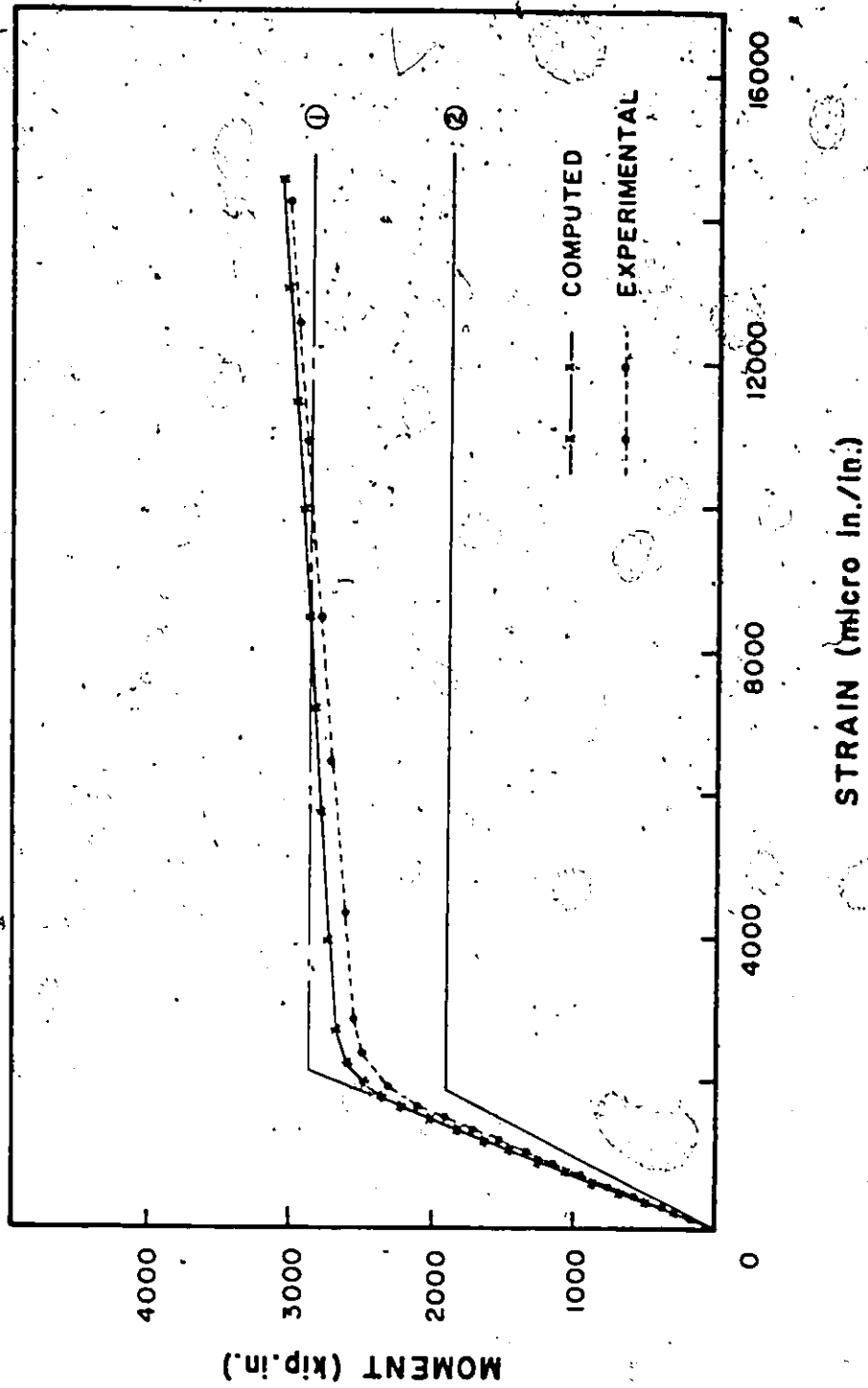


FIGURE 7.12 COMPARISON BETWEEN THE EXPERIMENTAL AND ANALYTICAL MOMENT VERSUS BOTTOM FIBRE STEEL STRAIN CURVES FOR END B1

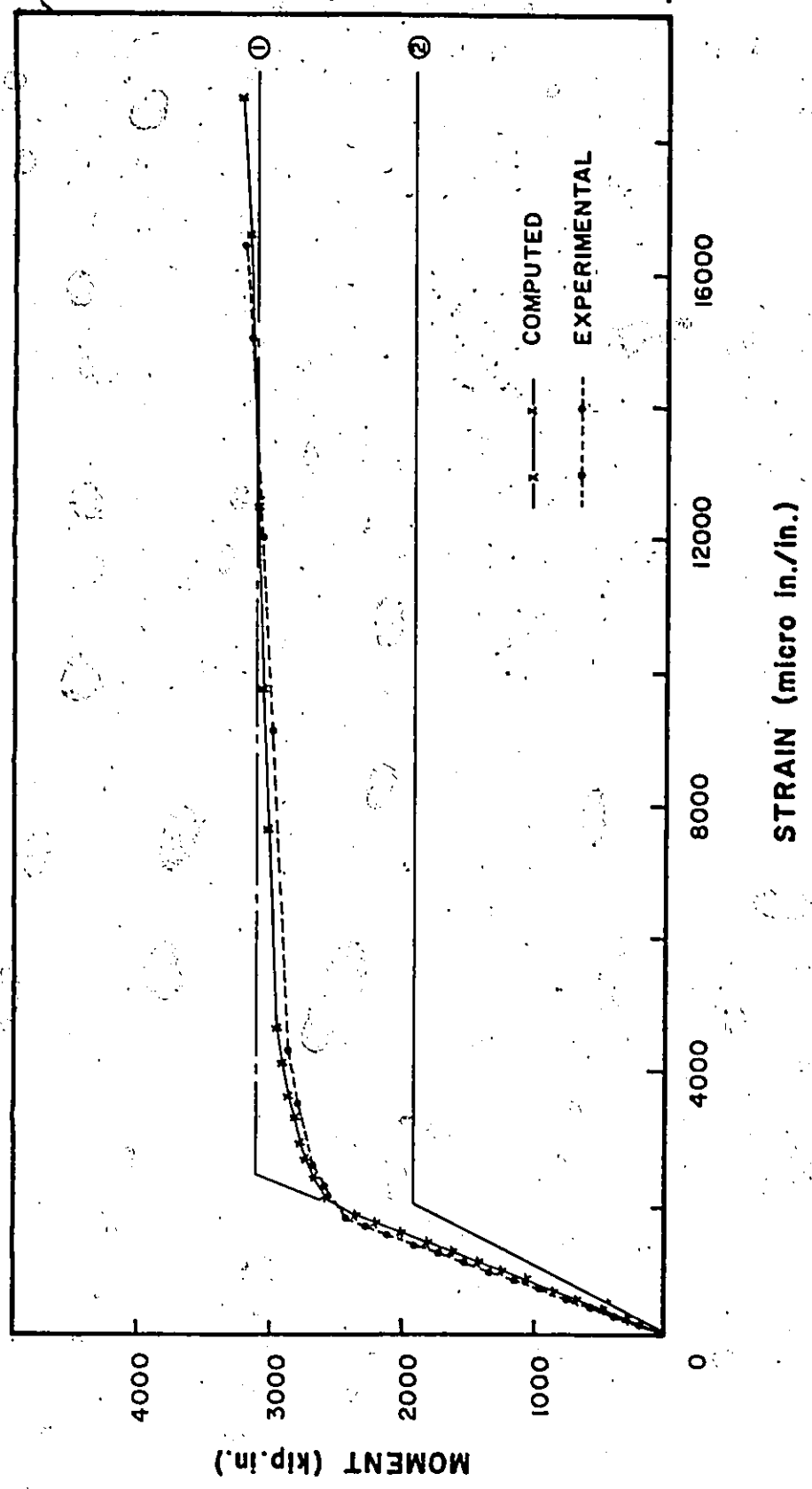


FIGURE 7.13 COMPARISON BETWEEN THE EXPERIMENTAL AND ANALYTICAL MOMENT VERSUS BOTTOM FIBRE STEEL STRAIN CURVES FOR END B2

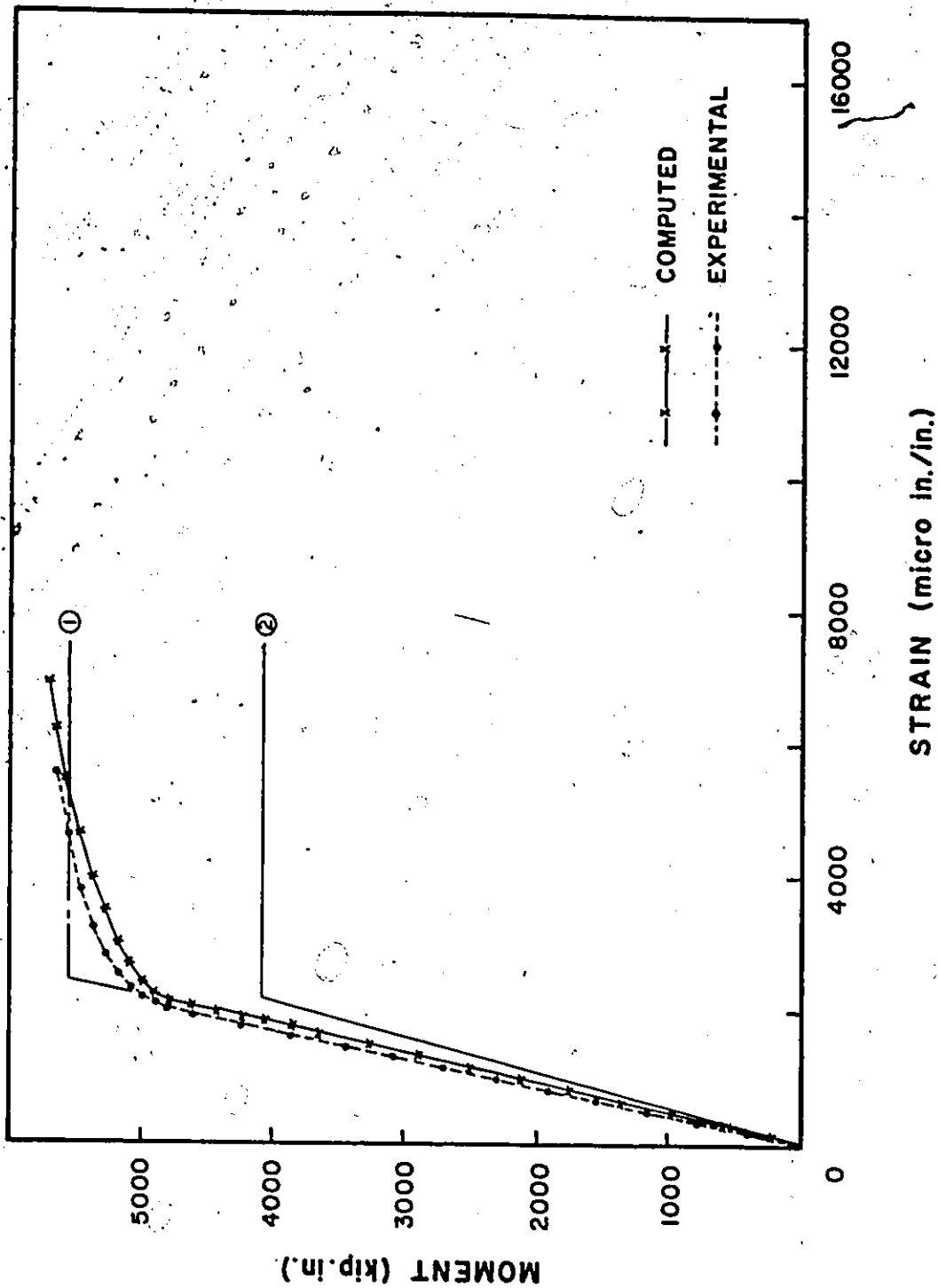


FIGURE 7.14 COMPARISON BETWEEN THE EXPERIMENTAL AND ANALYTICAL MOMENT VERSUS BOTTOM FIBRE STEEL STRAIN CURVES FOR END C1

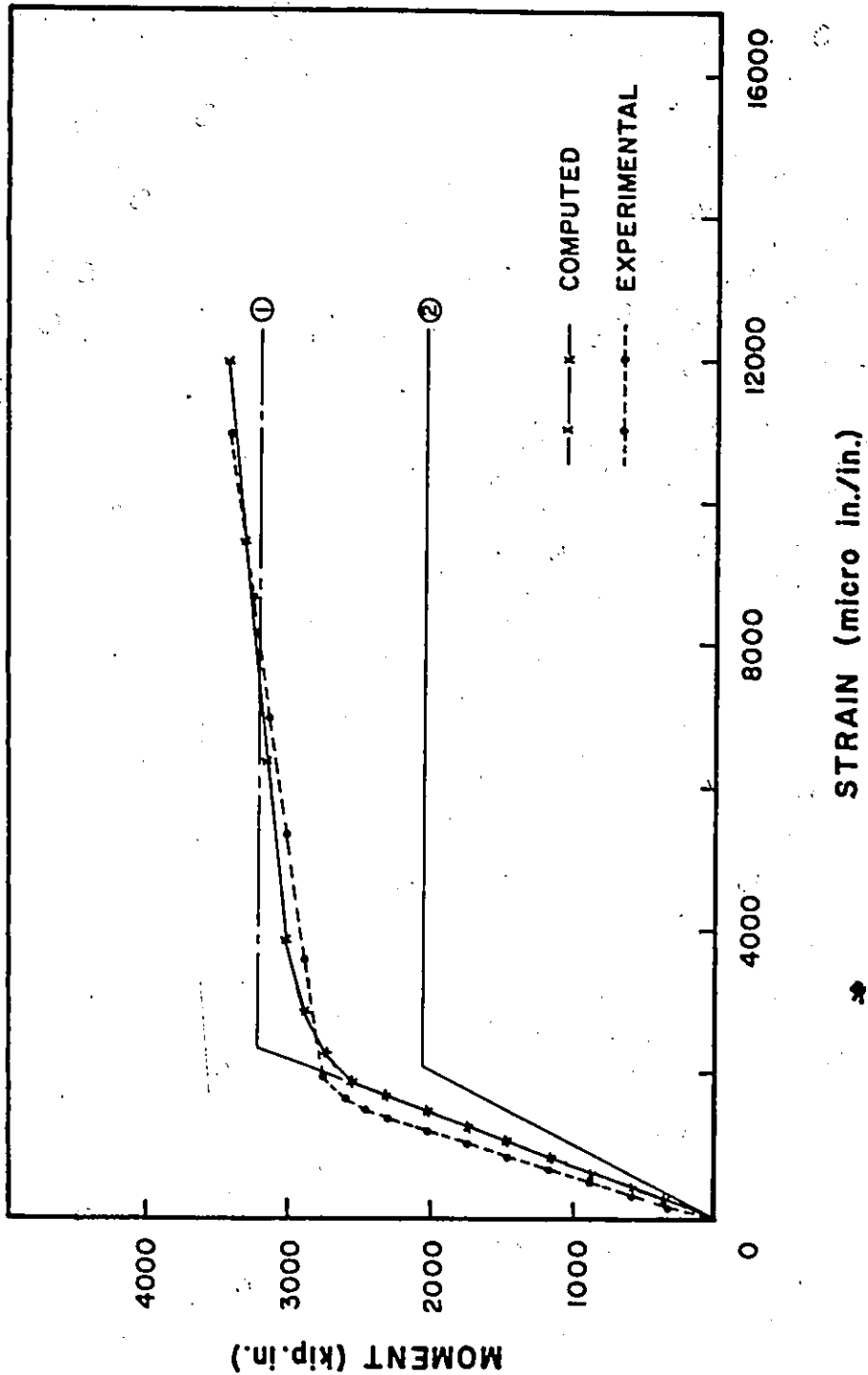


FIGURE 7.15 COMPARISON BETWEEN THE EXPERIMENTAL AND ANALYTICAL MOMENT VERSUS BOTTOM FIBRE STEEL STRAIN CURVES FOR END D1

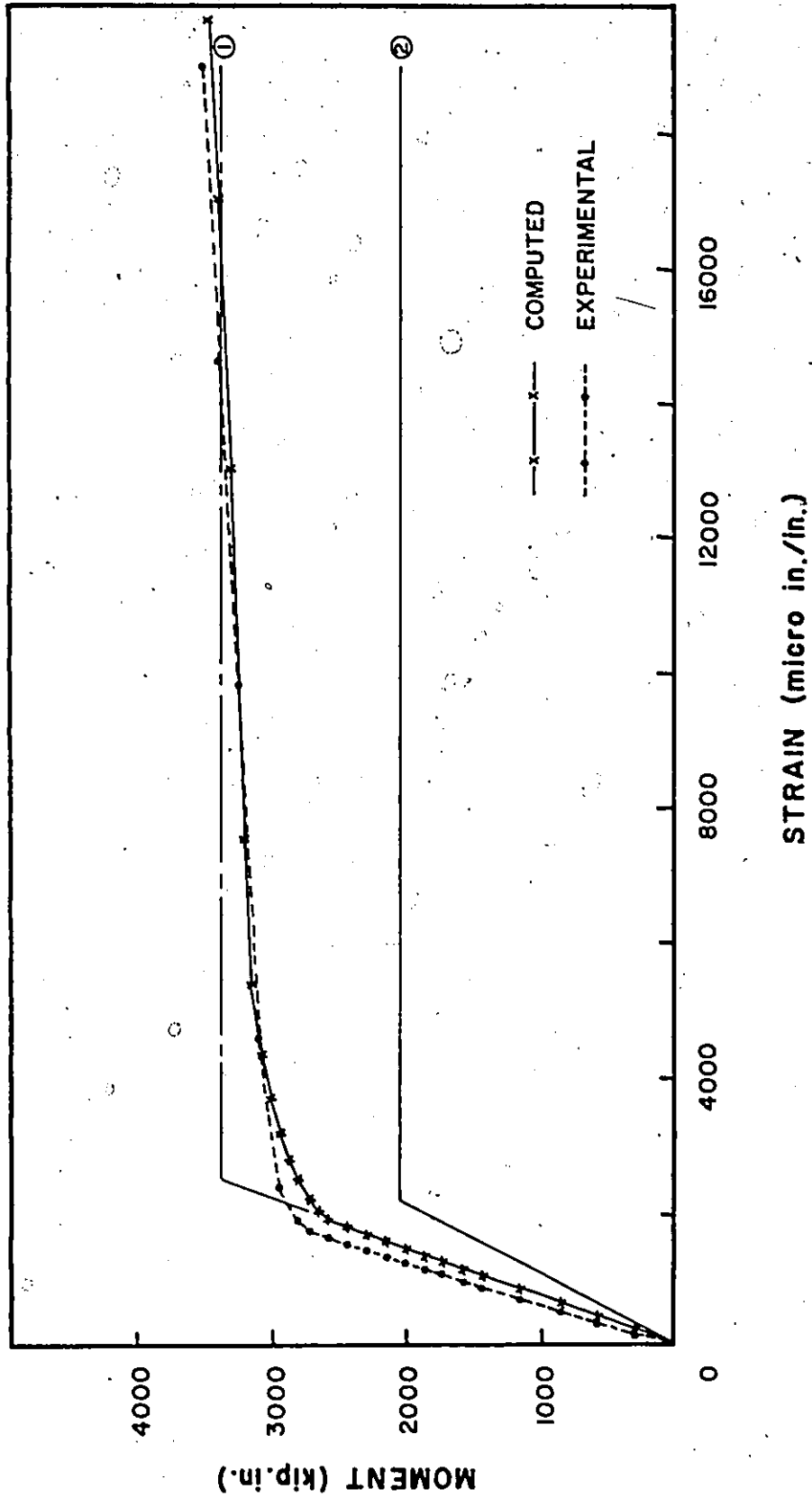


FIGURE 7.16 COMPARISON BETWEEN THE EXPERIMENTAL AND ANALYTICAL MOMENT VERSUS BOTTOM FIBRE STEEL STRAIN CURVES FOR END D2

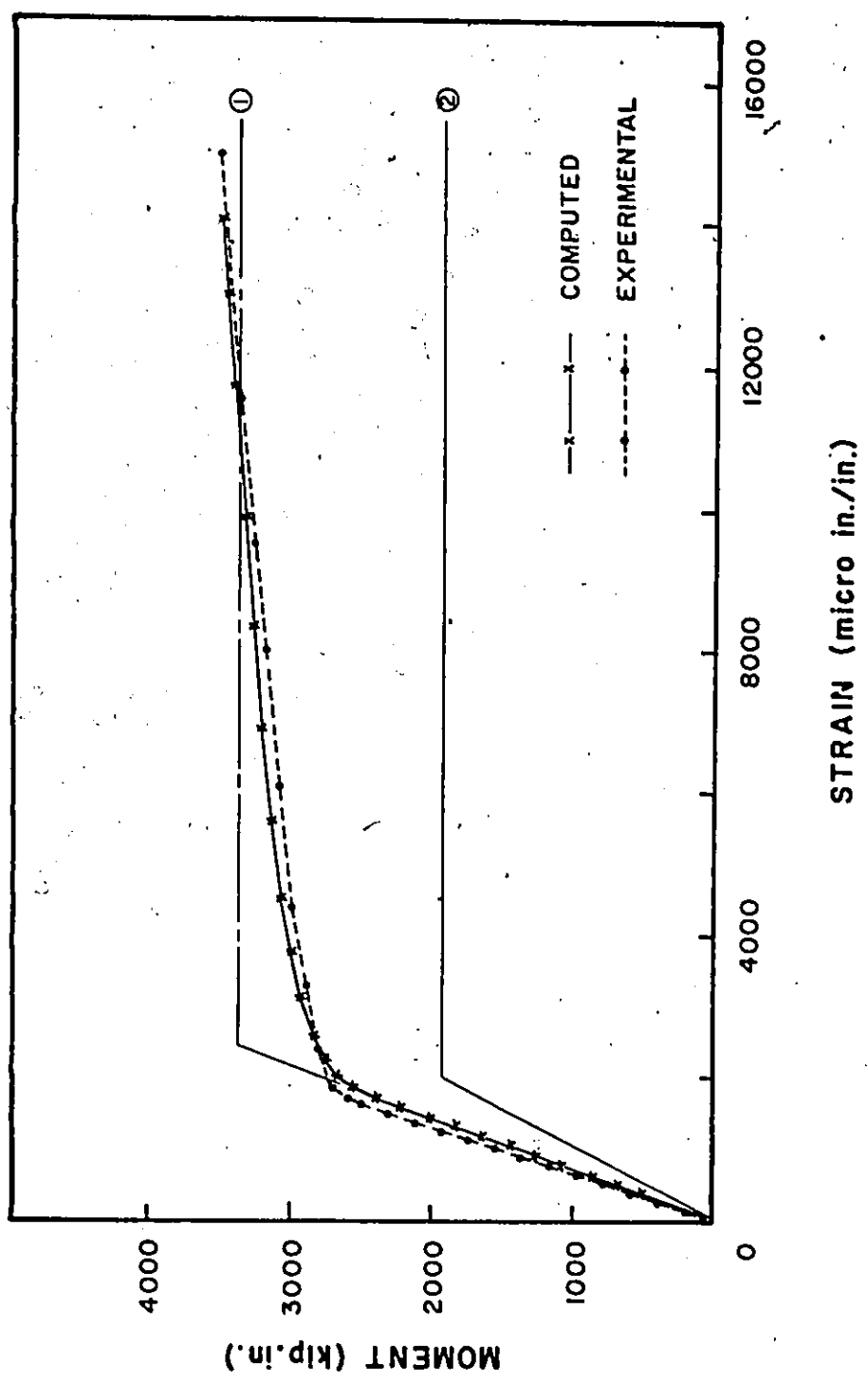


FIGURE 7.17 COMPARISON BETWEEN THE EXPERIMENTAL AND ANALYTICAL MOMENT VERSUS BOTTOM FIBRE STEEL STRAIN CURVES FOR END E1

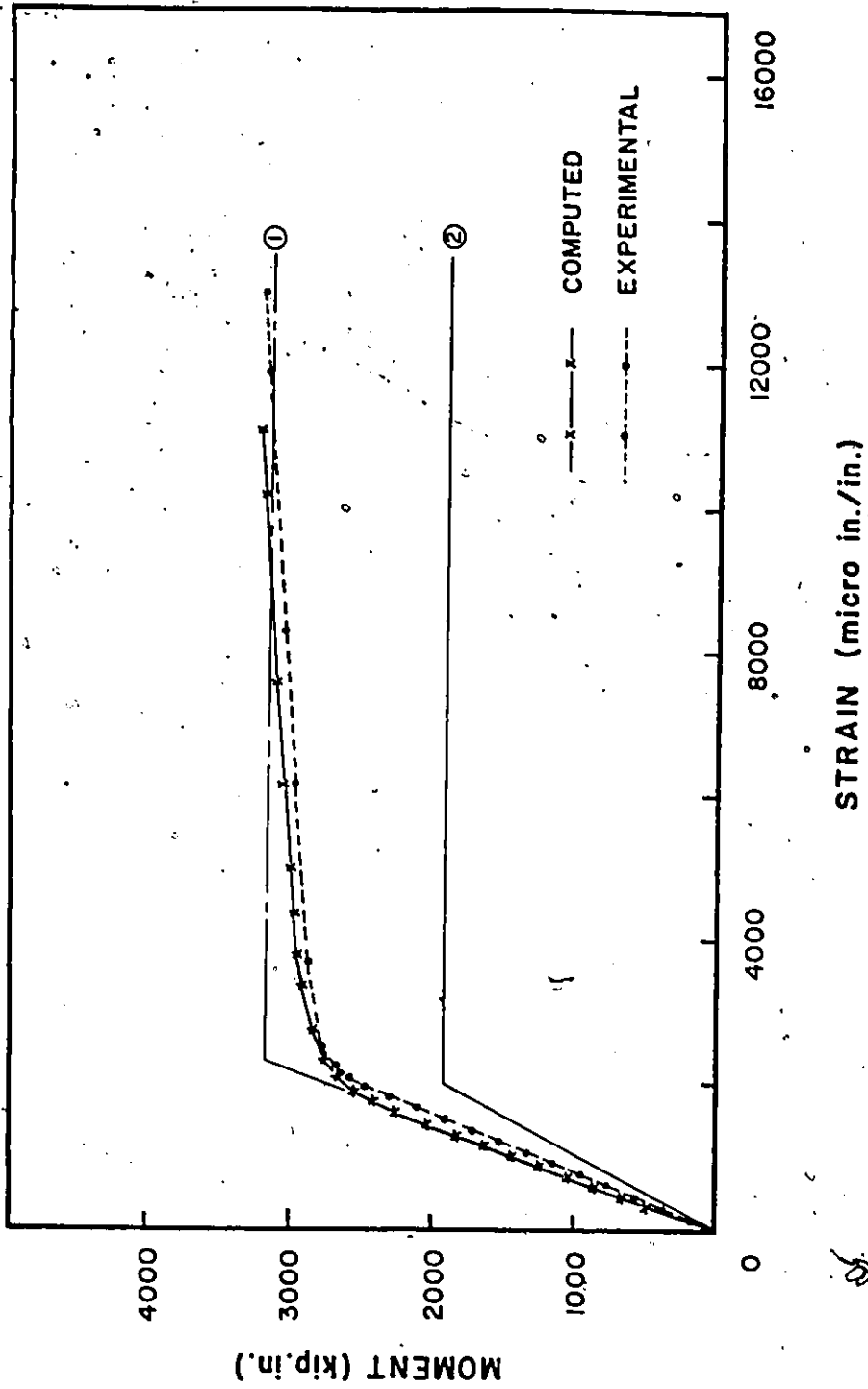


FIGURE 7.18 COMPARISON BETWEEN THE EXPERIMENTAL AND ANALYTICAL MOMENT VERSUS BOTTOM FIBRE STEEL STRAIN CURVES FOR END E2

Curve (2) represents the variation of bottom fibre steel strain with the applied moment for the steel beam alone. The steel strains were calculated using the same strain formula (7.3) and replacing y_b and I_{eff} by $d_b/2$ and I_s respectively. The steel section is assumed to behave elastically up to its calculated plastic moment.

Table 7.3 shows the calculated bottom fibre steel strains for the transformed section and the steel section alone at the instant of attaining the ultimate and plastic moment respectively. The effect of the strain hardening was not considered in calculating the theoretical curves (1) and (2).

The moment-strain curves computed from the inelastic analysis agreed well with the experimental curves for all the beams tested. The strain predicted from the transformed section coincided with the analytical values obtained from the computer results in the elastic region and were very close to the experimental values as shown in Figures 7.10 through 7.18.

In conclusion, if the analytical effective slab width for stiffness (b_{es}) corresponding to L/b and c/b ratios and the degree of interaction of the beam is used, the method of the transformed section provides a very good prediction for the bottom fibre steel strains in the elastic range.

7.5 Moment-Curvature Curves

The prediction of moment-curvature characteristic by the analytical inelastic analysis and the transformed section methods were

Beam No.	A ₁	A ₂	B ₁	B ₂	C ₁	D ₁	D ₂	E ₁	E ₂
Trans- formed section	M _u kip. in.	2886	3152	2886	3152	5563	3210	3394	3168
	I _{eff} in ⁴	398	409	398	409	835	425	447	423
	y _b in	8.8	8.9	8.8	8.9	10.5	9.1	9.3	9.0
	curvature x 10 ⁻⁶	250	265	250	265	230	260	262	258
	ε _{sb} μ in/in	2200	2365	2200	2365	2412	2370	2435	2324
Steel Beam Alone	M _p kip. in.	1910	1910	1912	1912	4060	2085	2085	1965
	I _s in ⁴	204	204	204	204	516	204	204	204
	d/2 in	6	6	6	6	8	6	6	6
	curvature x 10 ⁻⁶	322	322	323	323	271	352	352	332
	ε _s μ in/in	1937	1937	1939	1939	2170	2115	2115	1993

Table 7.3: Bottom Fibre Steel Strain and Curvature for the Transformed Section and the Steel Beam Alone

compared with the experimental one for each beam. The curvature at section 1-1, 3 inch from the column face, was chosen for purpose of the comparison since it is very close to the curvature at the column face where the plastic hinge would occur in an actual multi-story frame.

Figures 7.19 through 7.27 show the moment-curvature curves obtained from the inelastic analysis, transformed section, steel beam alone and experimentally for each test.

Curvature was given as a direct output of the computer program at each load increment.

The transformed section was used to calculate the curvature at a given moment using the elastic relation

$$\phi_c = \frac{M}{E_s I_{eff}} \quad (7.4)$$

where in this equation

I_{eff} is the effective moment of inertia for stiffness of the transformed section based on the analytical effective slab width for stiffness (b_{es}) at that particular section.

M is the applied moment on the section.

ϕ_c is the curvature.

Curve (1) in the figures shows the $M-\phi$ curve obtained from this equation.

Curvature of the steel section alone (ϕ_s) was obtained from the same formula (7.4) by replacing I_{eff} by I_s . Curve (2) in the figures represents the moment-curvature relationship of the steel beam alone.

The curvature obtained from the transformed section for the

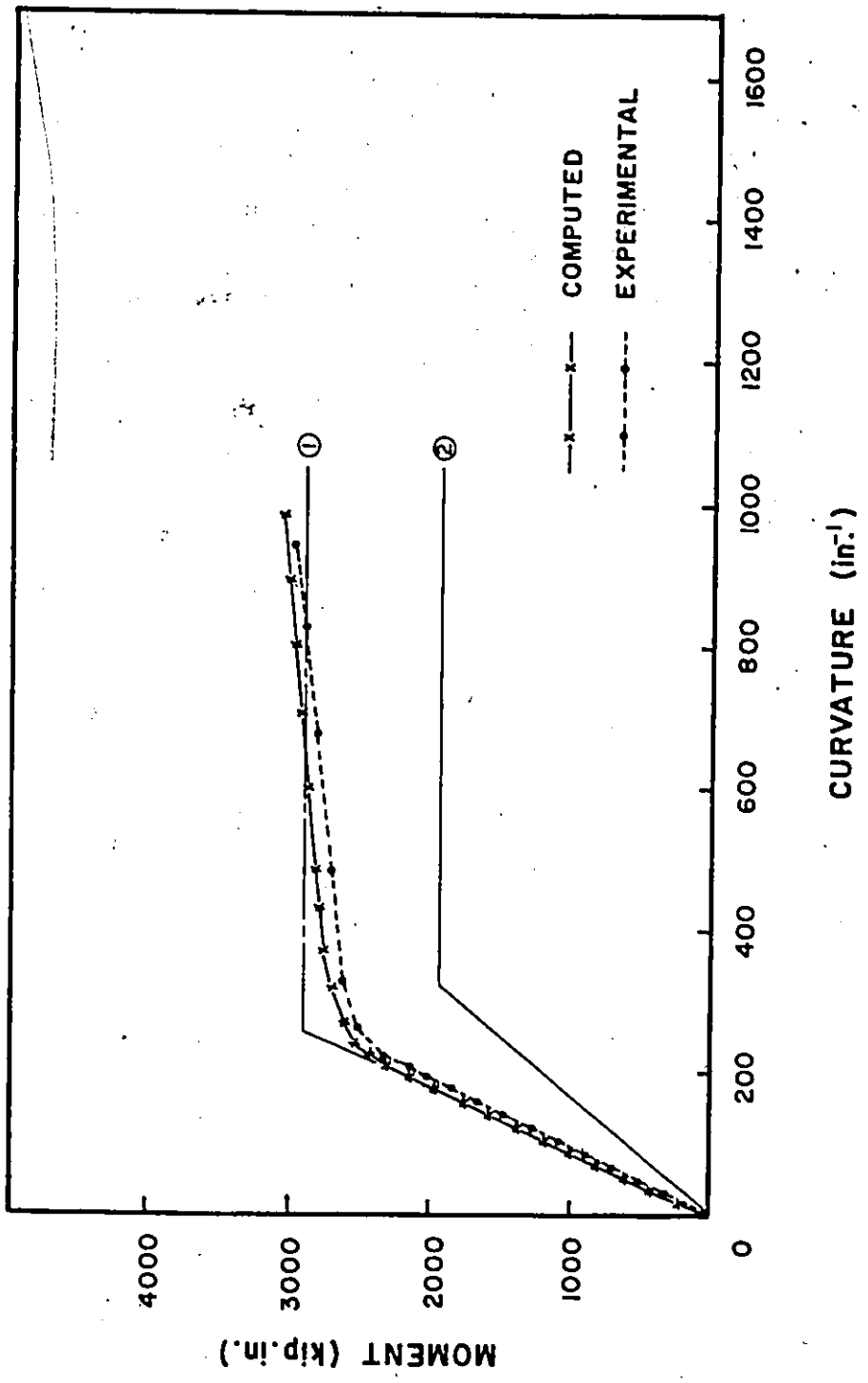


FIGURE 7.19 COMPARISON BETWEEN THE EXPERIMENTAL AND ANALYTICAL MOMENT-CURVATURE CURVES FOR END A1

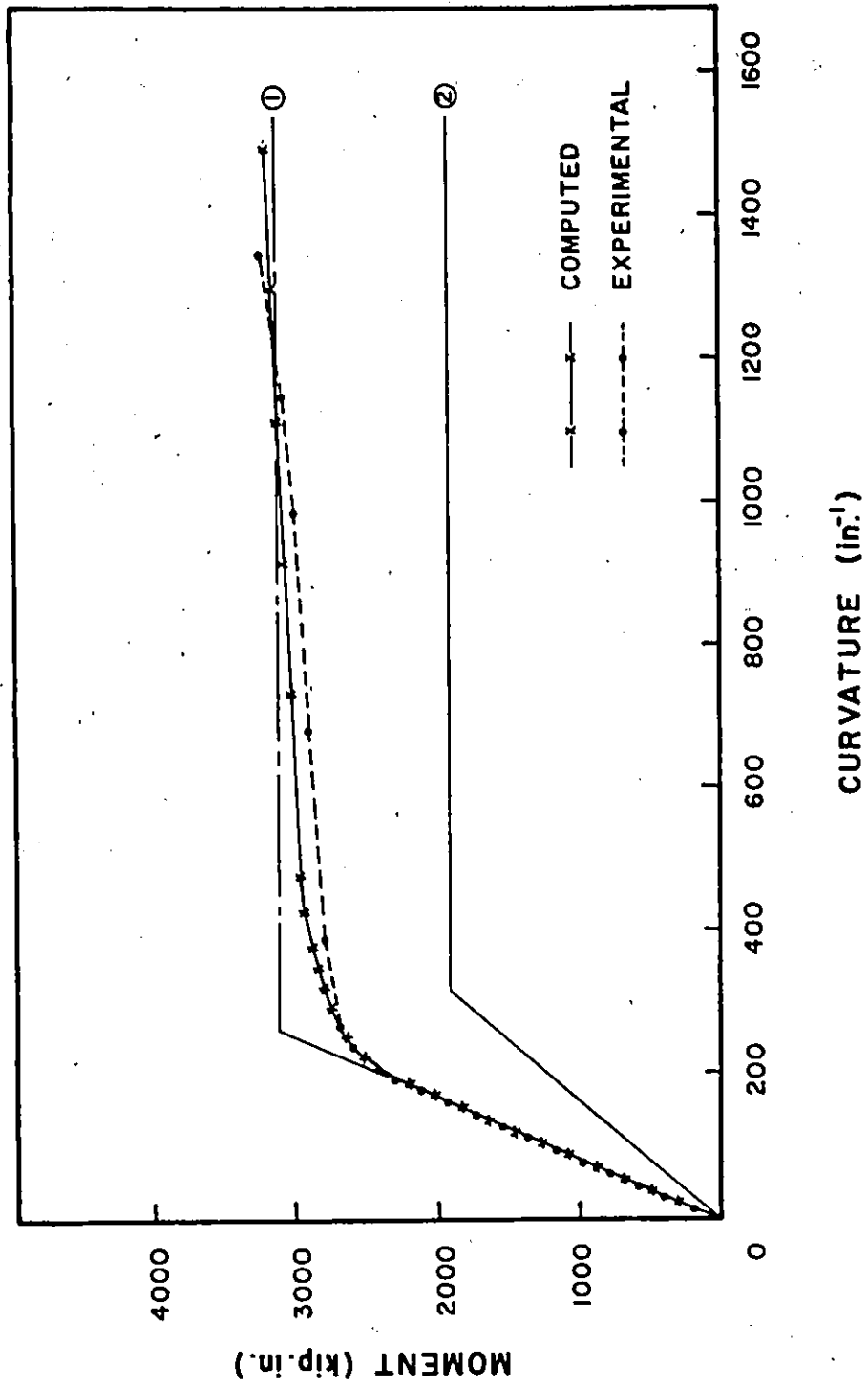


FIGURE 7.20 COMPARISON BETWEEN THE EXPERIMENTAL AND ANALYTICAL MOMENT-CURVATURE CURVES FOR END A2

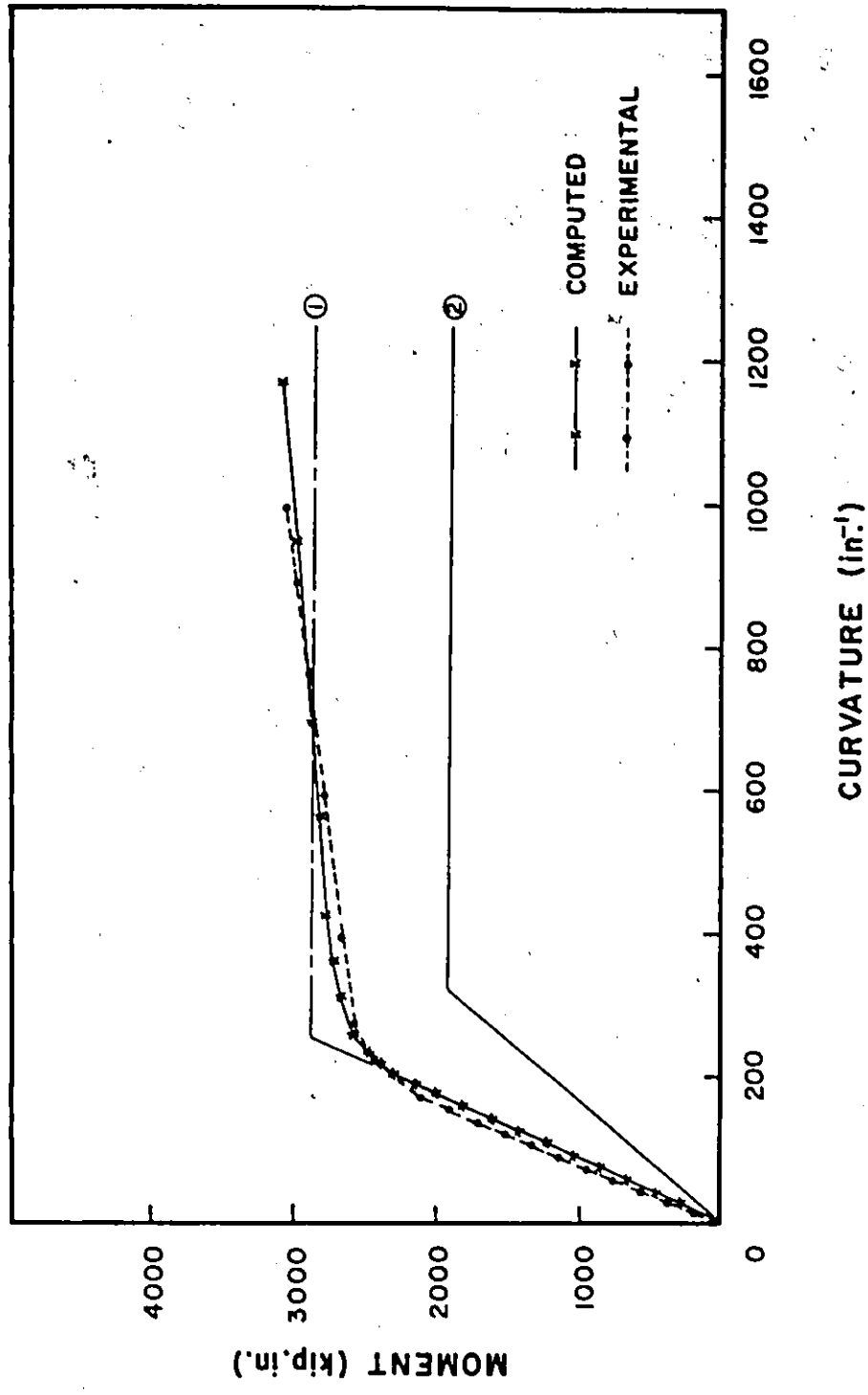


FIGURE 7.21 COMPARISON BETWEEN THE EXPERIMENTAL AND ANALYTICAL MOMENT-CURVATURE CURVES FOR END B1

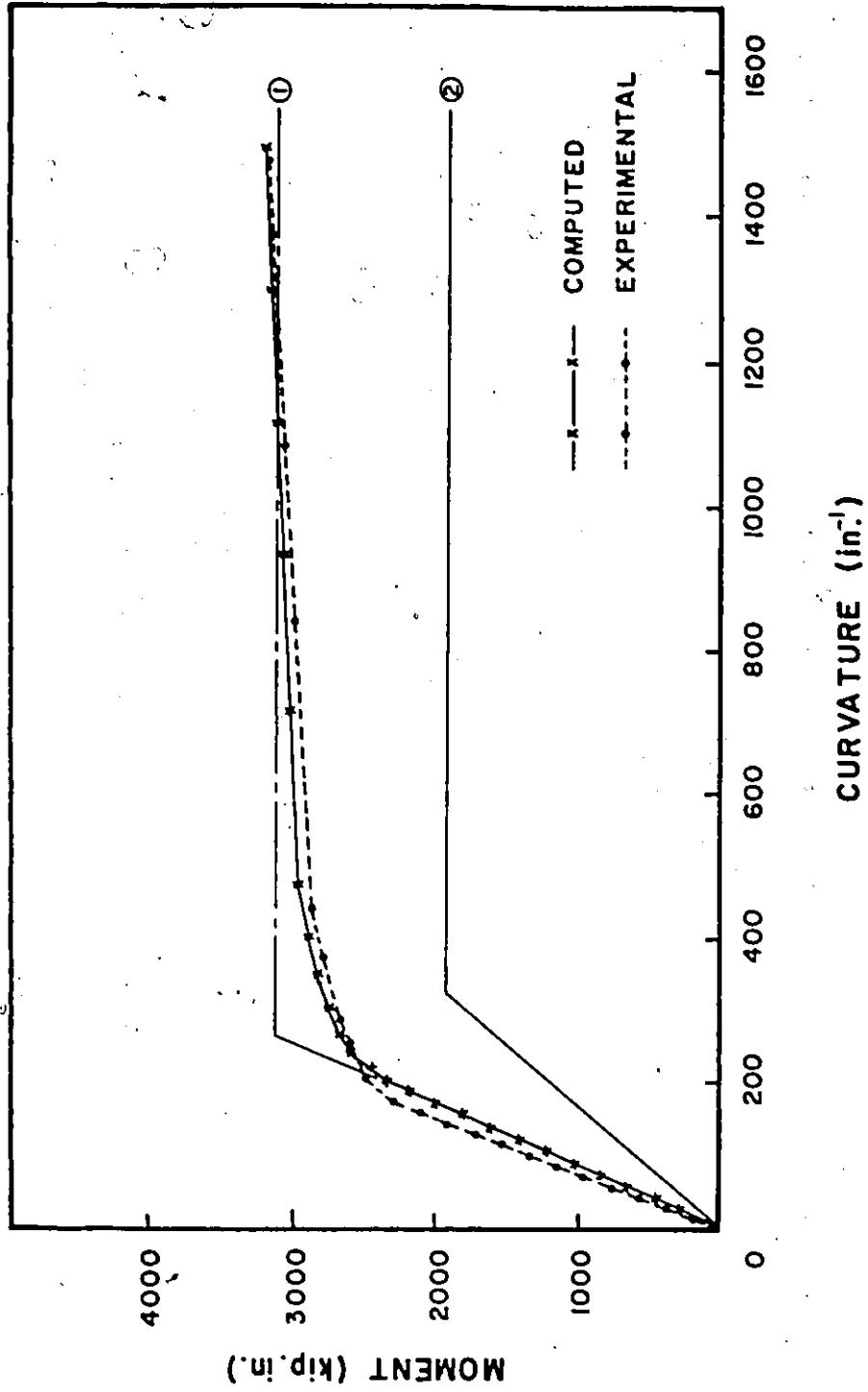


FIGURE 7.22 COMPARISON BETWEEN THE EXPERIMENTAL AND ANALYTICAL MOMENT-CURVATURE CURVES FOR END B2

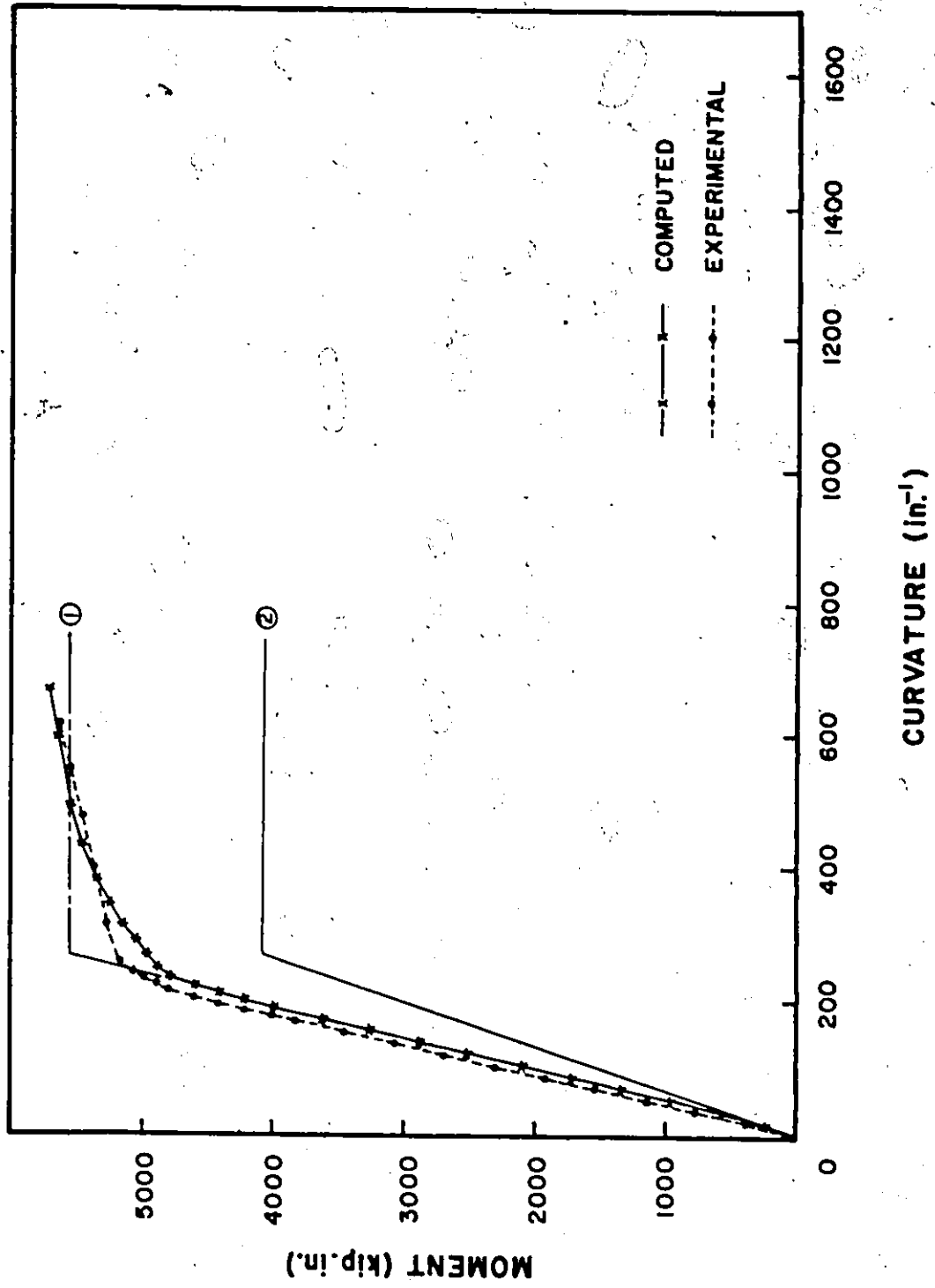


FIGURE 7.23 COMPARISON BETWEEN THE EXPERIMENTAL AND ANALYTICAL MOMENT-CURVATURE CURVES FOR END C1

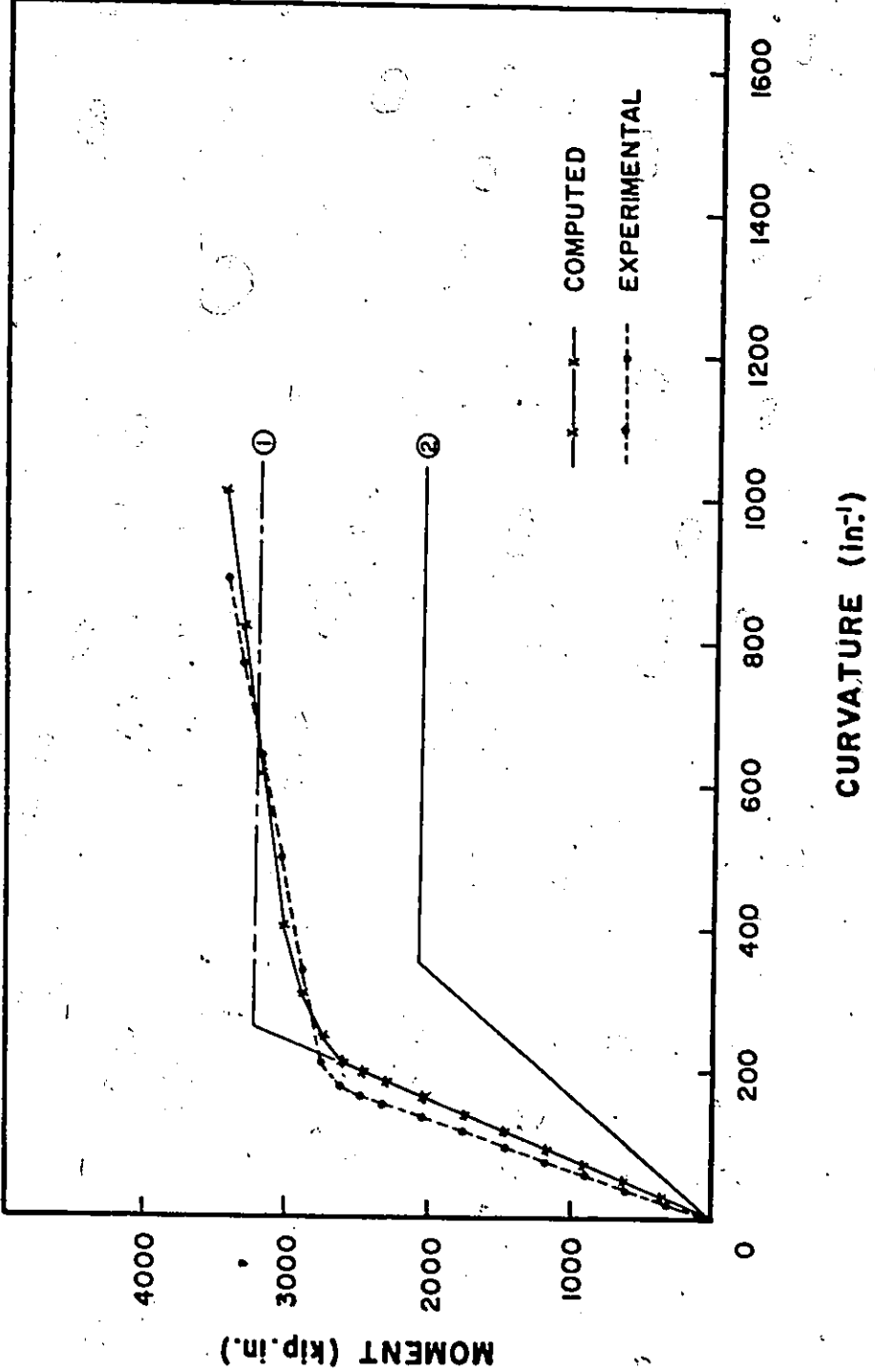


FIGURE 7.24 COMPARISON BETWEEN THE EXPERIMENTAL AND ANALYTICAL MOMENT-CURVATURE CURVES FOR END D1

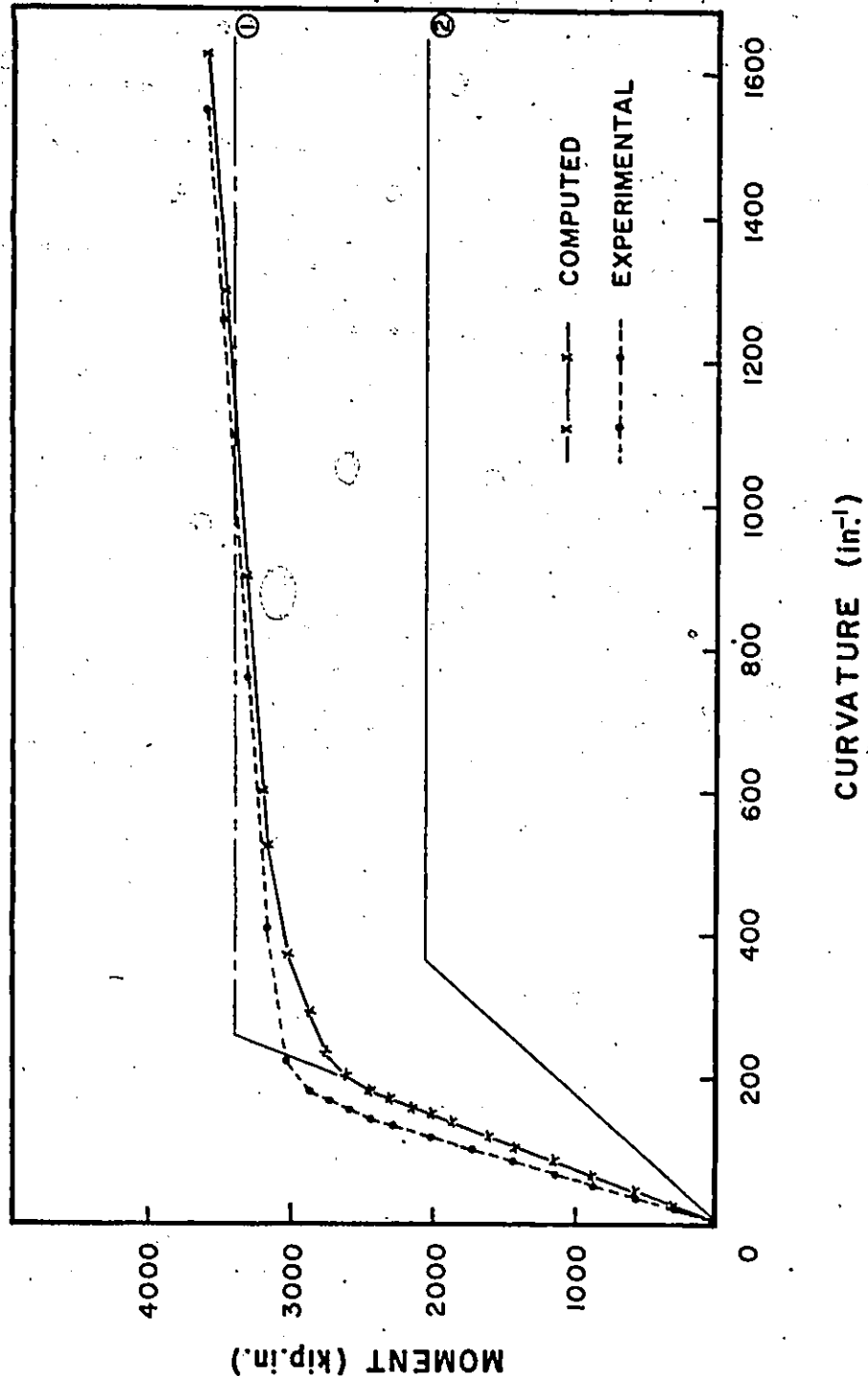


FIGURE 7.25 COMPARISON BETWEEN THE EXPERIMENTAL AND ANALYTICAL MOMENT-CURVATURE CURVES FOR END D2

A

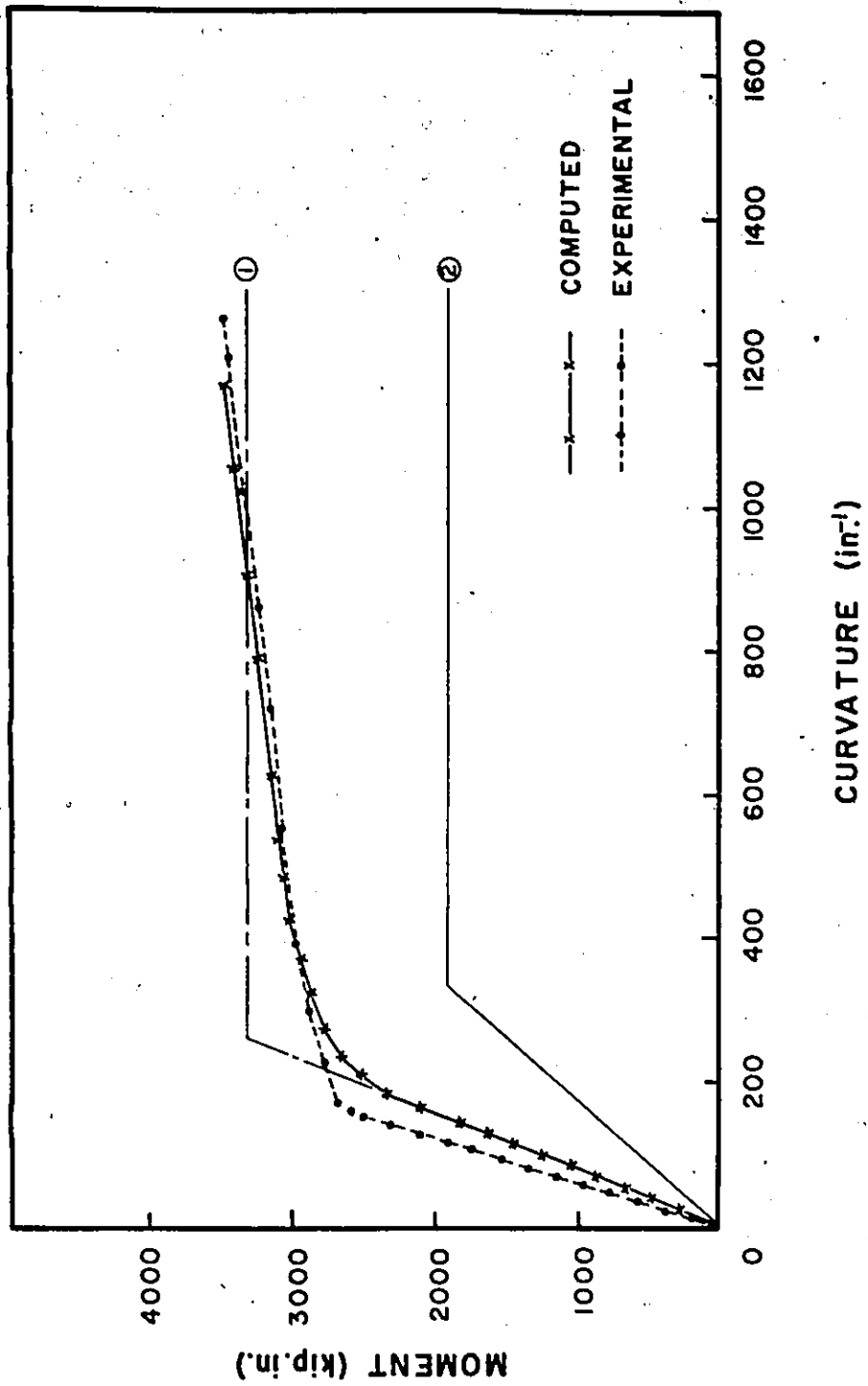


FIGURE 7.26 COMPARISON BETWEEN THE EXPERIMENTAL AND ANALYTICAL MOMENT-CURVATURE CURVES FOR END E1

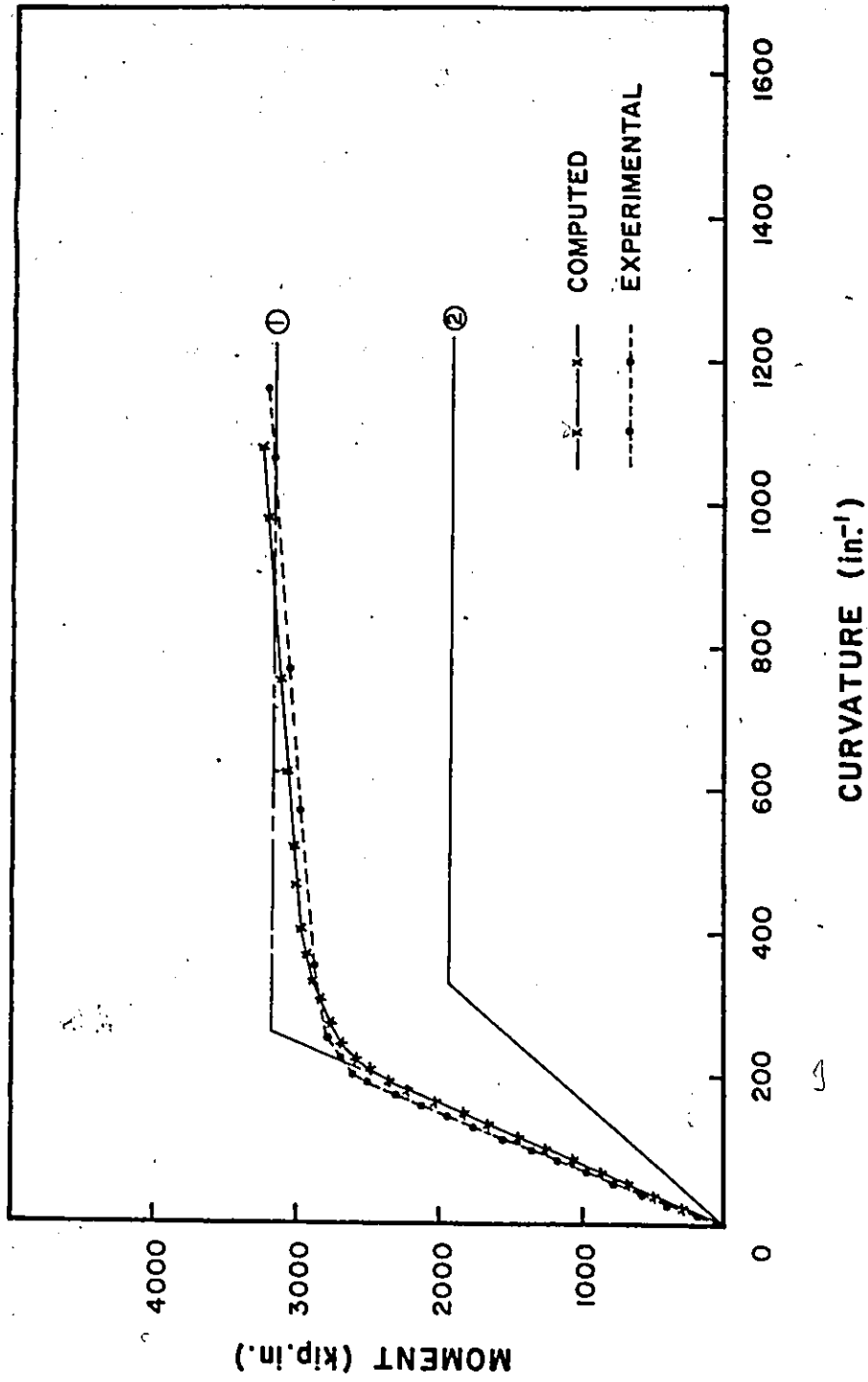


FIGURE 7.27 COMPARISON BETWEEN THE EXPERIMENTAL AND ANALYTICAL MOMENT-CURVATURE CURVES FOR END E2

composite beam and the curvature of the steel beam alone at the ultimate and plastic moment for the composite and steel section respectively are given in Table 7.3.

It can be seen from Figures 7.19 through 7.27 that there is good agreement between the computed and experimental curves for all the test beams. The values of the curvature obtained from the transformed section method were very close to the experimental values in the elastic range. Curvature of the steel beam alone was much greater than the curvature of the composite beam under the same moment.

7.6 Strain Distribution Across the Slab Width

Since one of the main purposes of the current investigation is to provide an evaluation of the effective slab width for strength which can be used to estimate the ultimate moment capacity of the composite beam at the connection and since this effective width, by definition, depends mainly on the distribution of the stress, or strain, across the slab width; it was important to compare the analytically predicted strains across the slab width with those measured experimentally.

The measured and analytical top fibre concrete strains at the two sections located 3 inches and 9 inches from the column face were compared at various loading levels. The results of this comparison are shown in Figures 7.28 through 7.45. These figures show that the shape of the experimental strain distribution across the slab width agrees very well with that predicted analytically. Although the measured and computed magnitudes of strains were not equal, the difference between

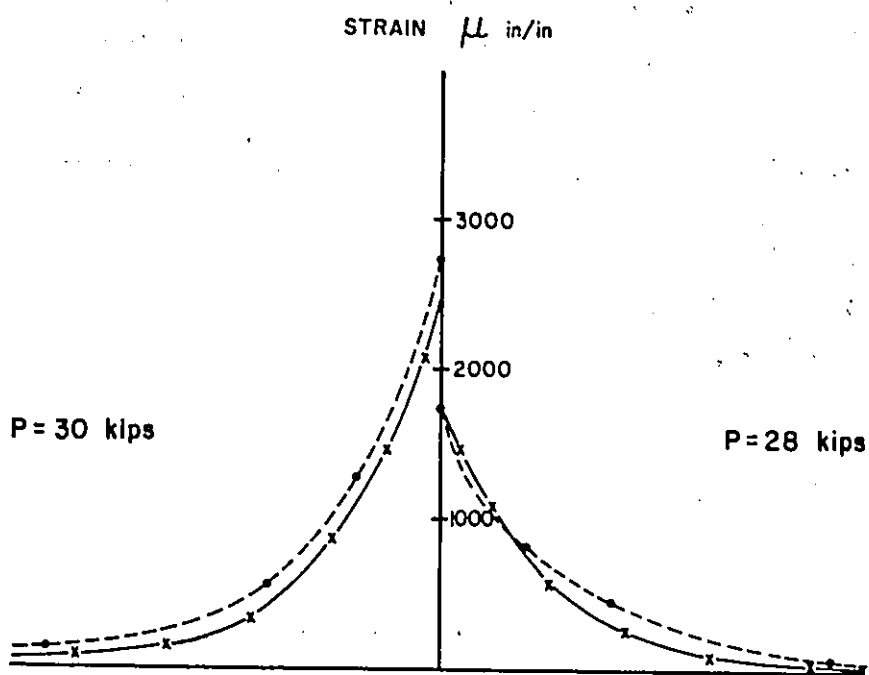
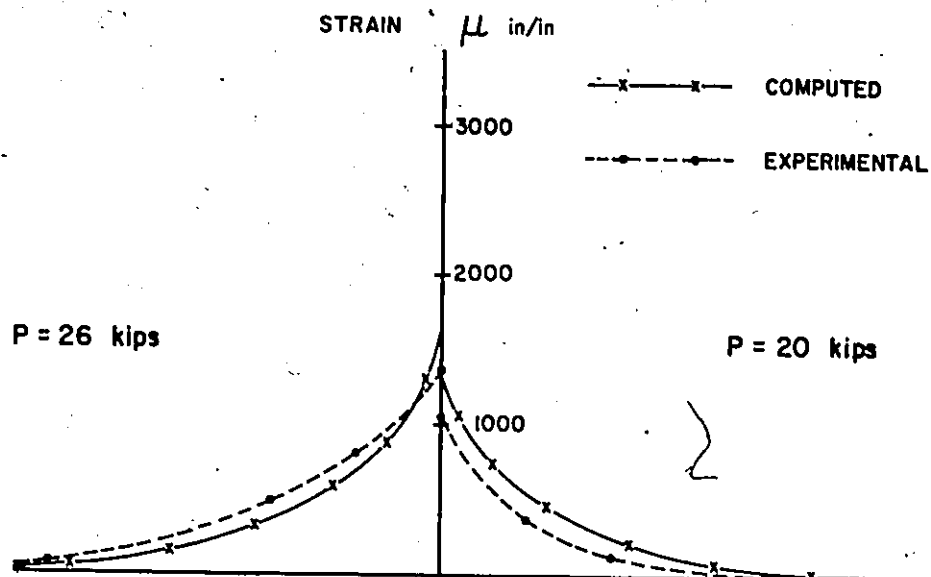


FIGURE 7.28 COMPARISON BETWEEN THE EXPERIMENTAL AND ANALYTICAL TOP FIBRE CONCRETE STRAIN DISTRIBUTION ACROSS THE SLAB WIDTH AT SECTION 1-1 FOR END A1

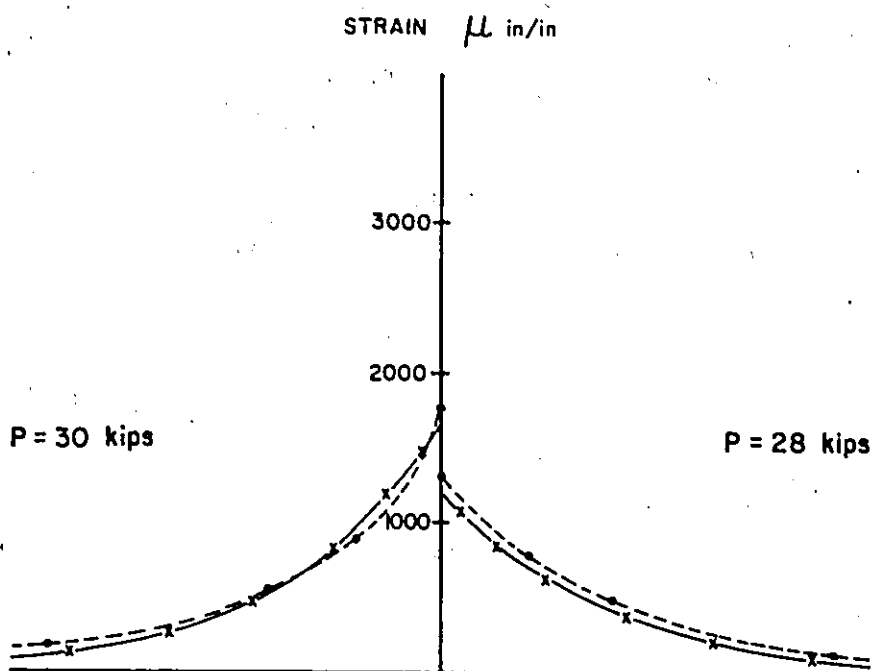
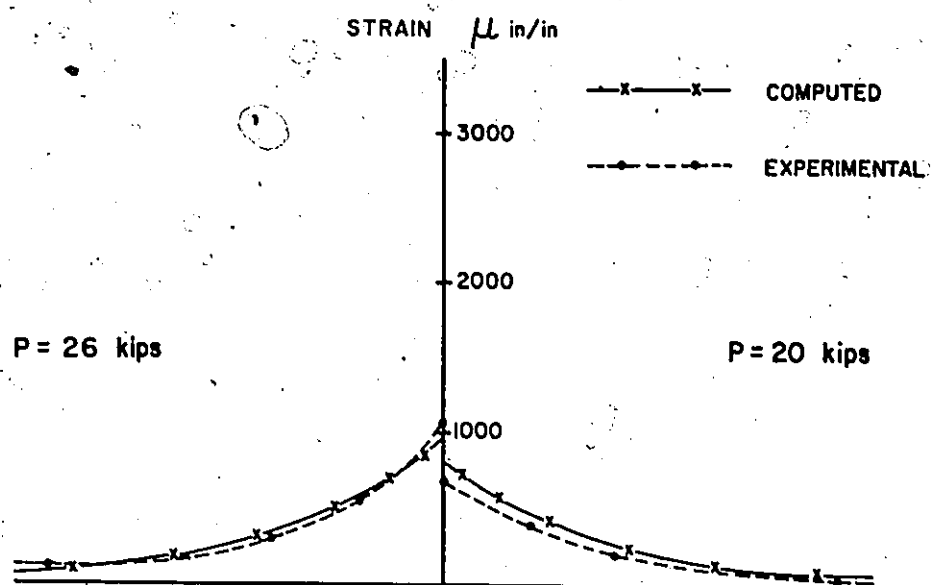


FIGURE 7.29 COMPARISON BETWEEN THE EXPERIMENTAL AND ANALYTICAL TOP FIBRE CONCRETE STRAIN DISTRIBUTION ACROSS THE SLAB WIDTH AT SECTION 2-2 FOR END A1

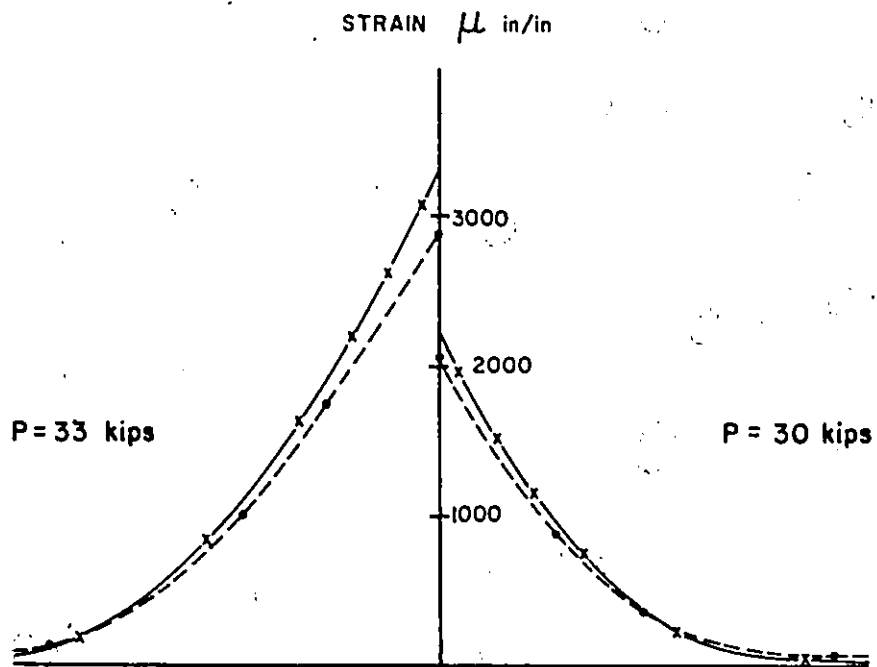
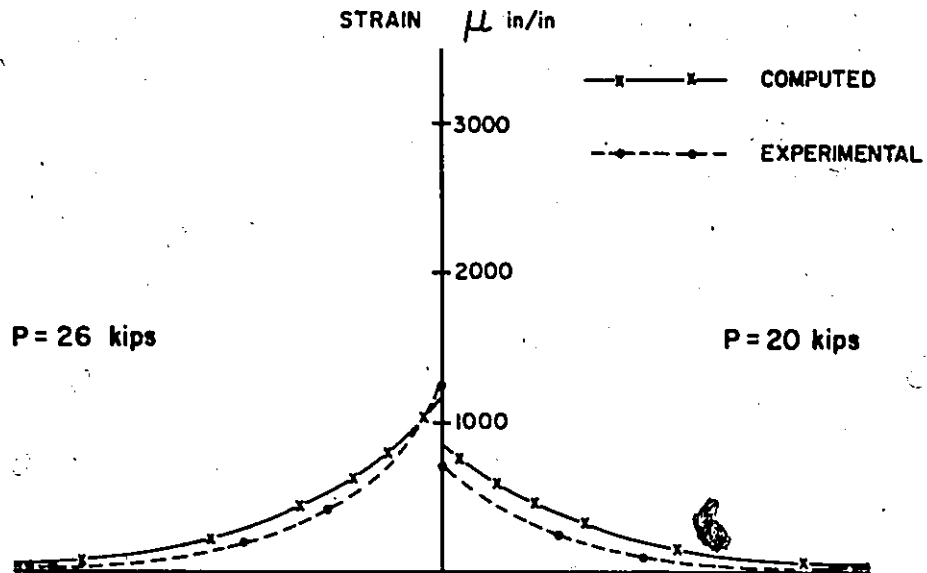


FIGURE 7.30 COMPARISON BETWEEN THE EXPERIMENTAL AND ANALYTICAL TOP FIBRE CONCRETE STRAIN DISTRIBUTION ACROSS THE SLAB WIDTH AT SECTION 1-1 FOR END A2

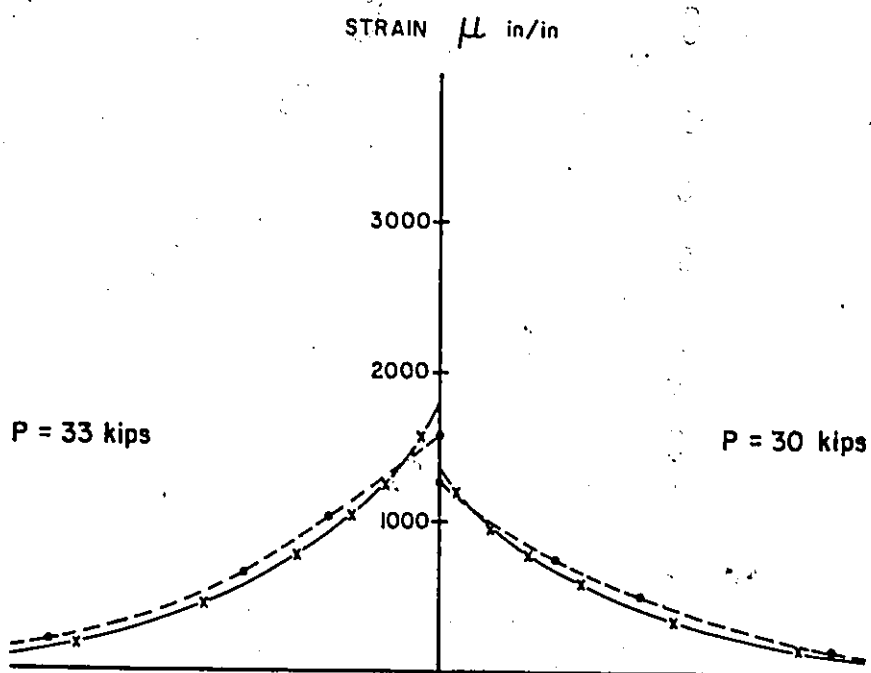
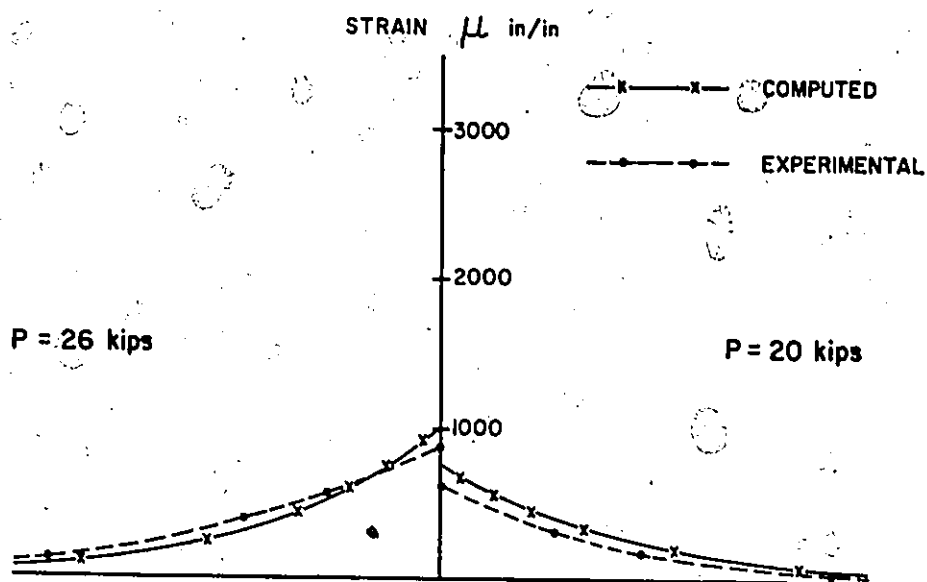


FIGURE 7.31 COMPARISON BETWEEN THE EXPERIMENTAL AND ANALYTICAL TOP FIBRE CONCRETE STRAIN DISTRIBUTION ACROSS THE SLAB WIDTH AT SECTION 2-2 FOR END A2

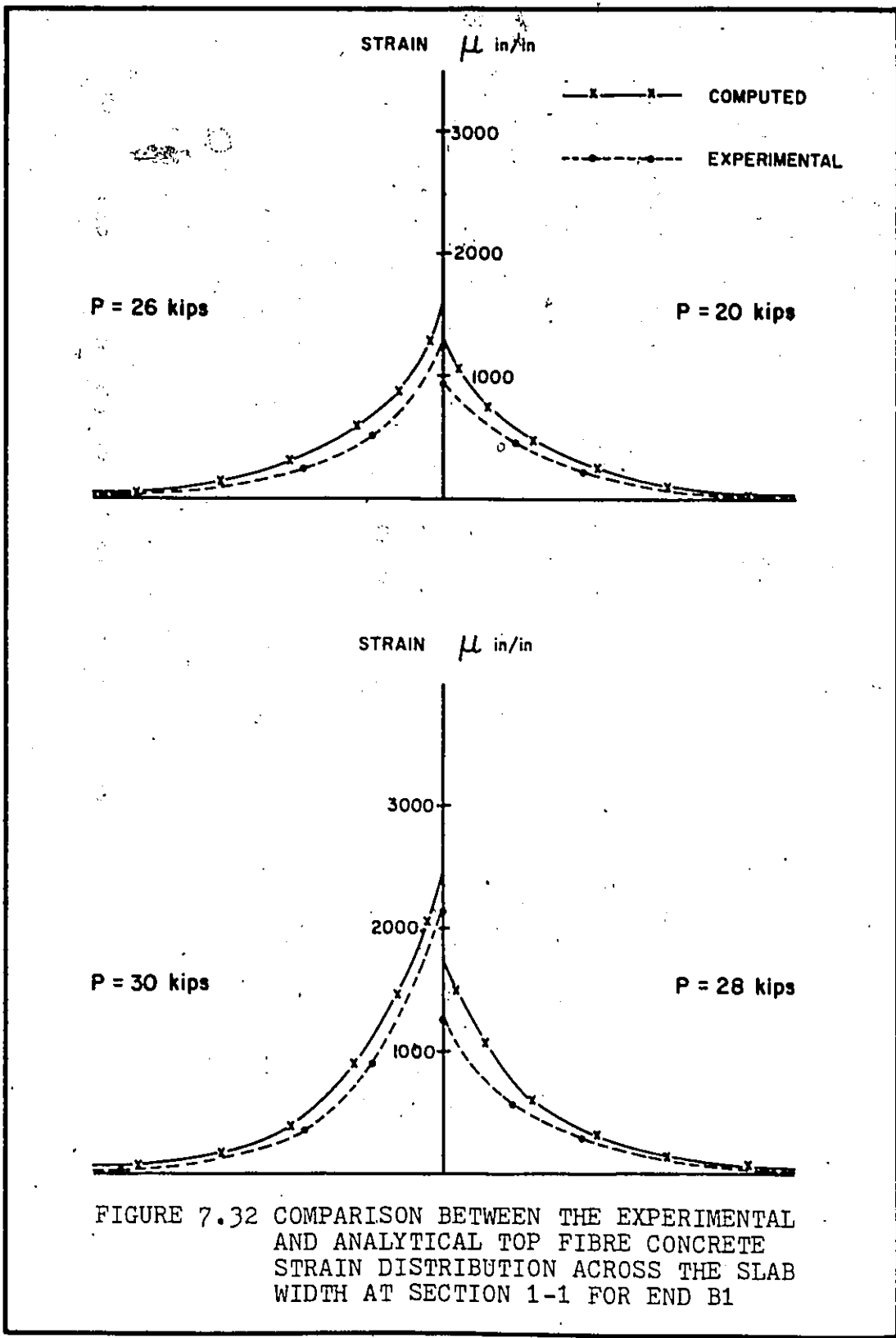


FIGURE 7.32 COMPARISON BETWEEN THE EXPERIMENTAL AND ANALYTICAL TOP FIBRE CONCRETE STRAIN DISTRIBUTION ACROSS THE SLAB WIDTH AT SECTION 1-1 FOR END B1

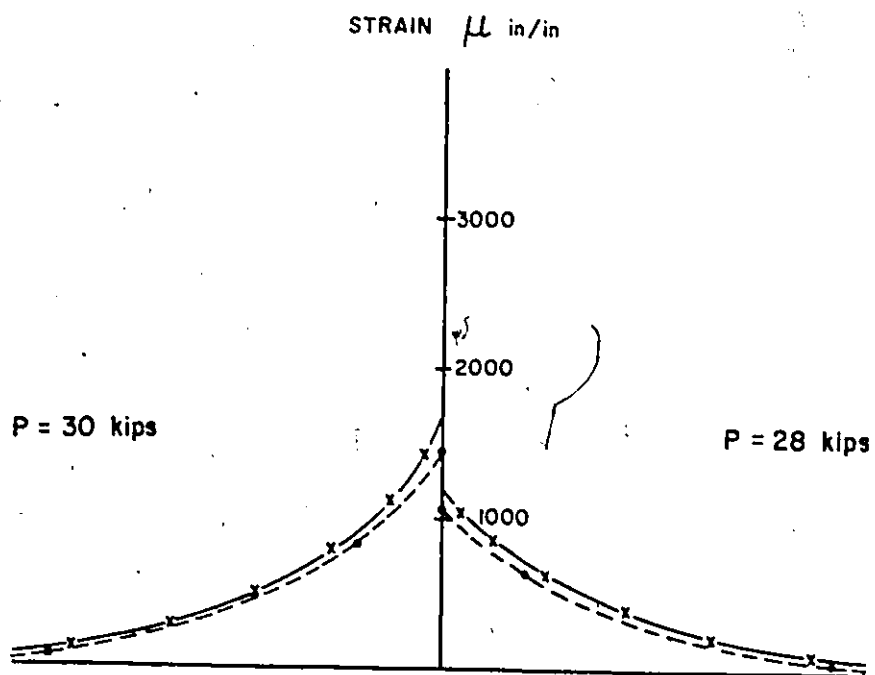
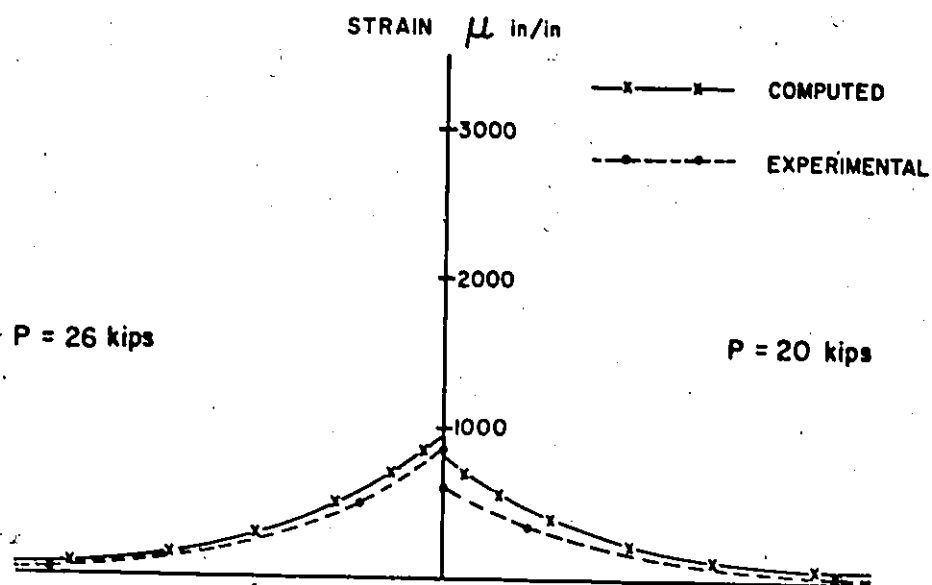
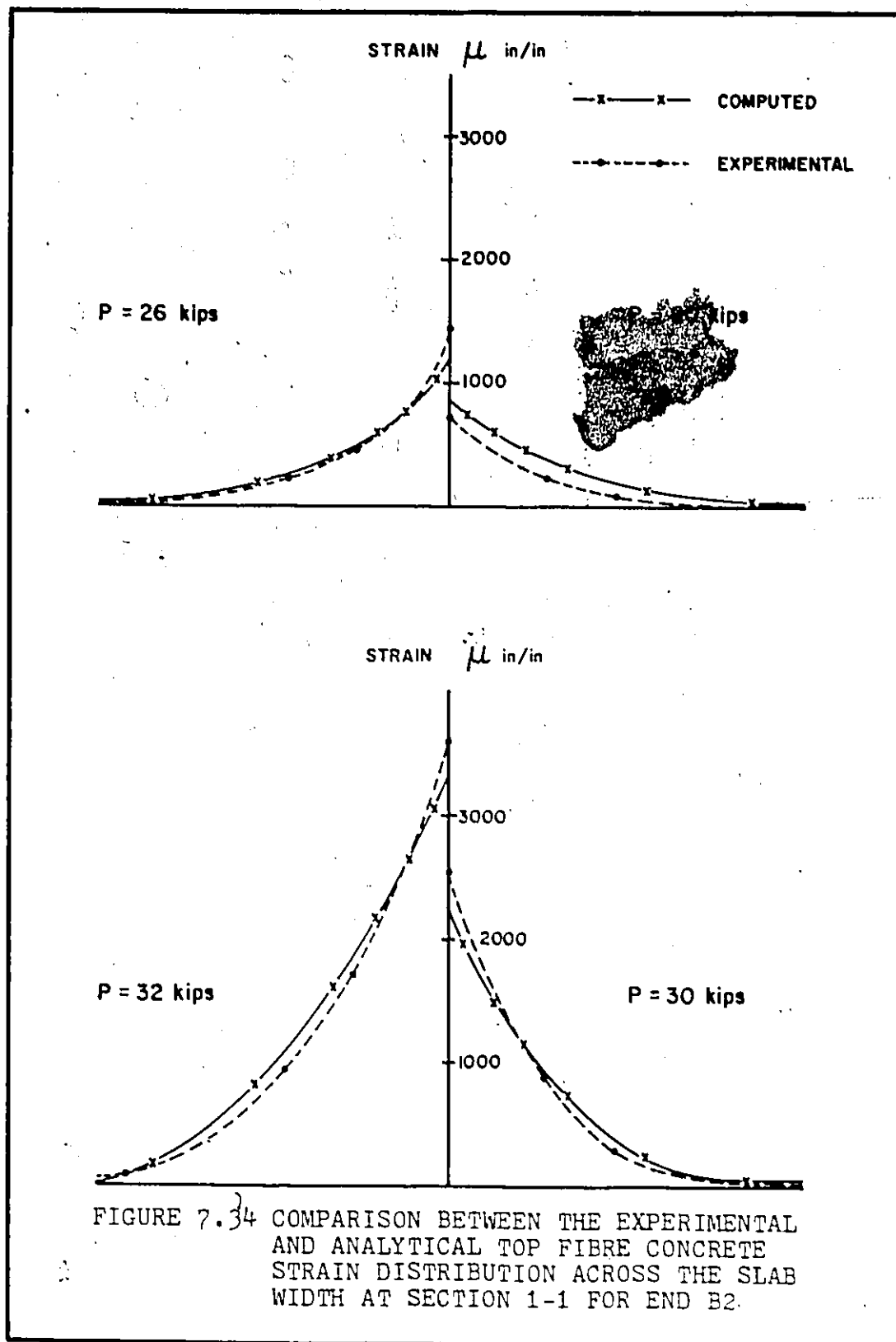


FIGURE 7.33 COMPARISON BETWEEN THE EXPERIMENTAL AND ANALYTICAL TOP FIBRE CONCRETE STRAIN DISTRIBUTION ACROSS THE SLAB WIDTH AT SECTION 2-2 FOR END B1



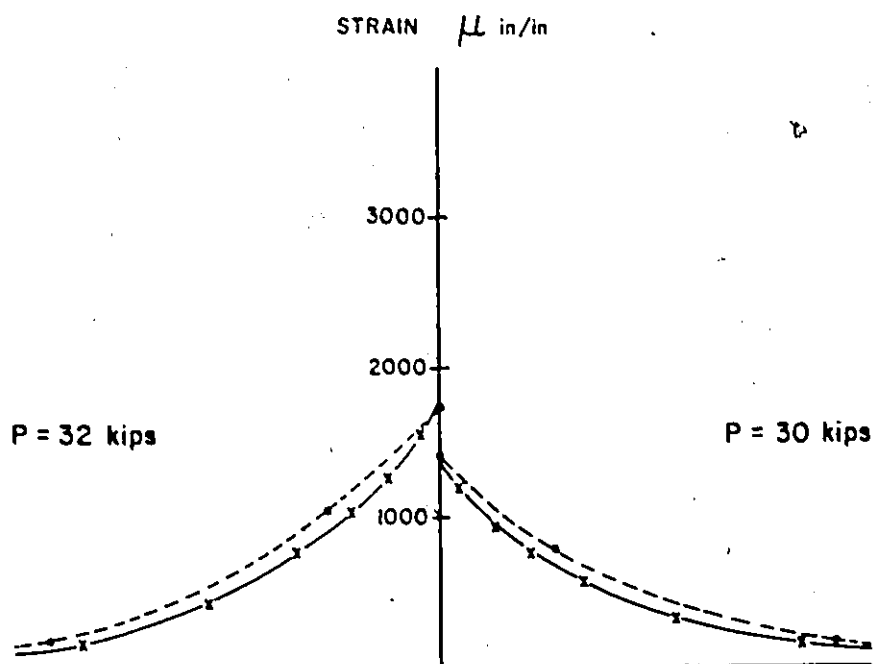
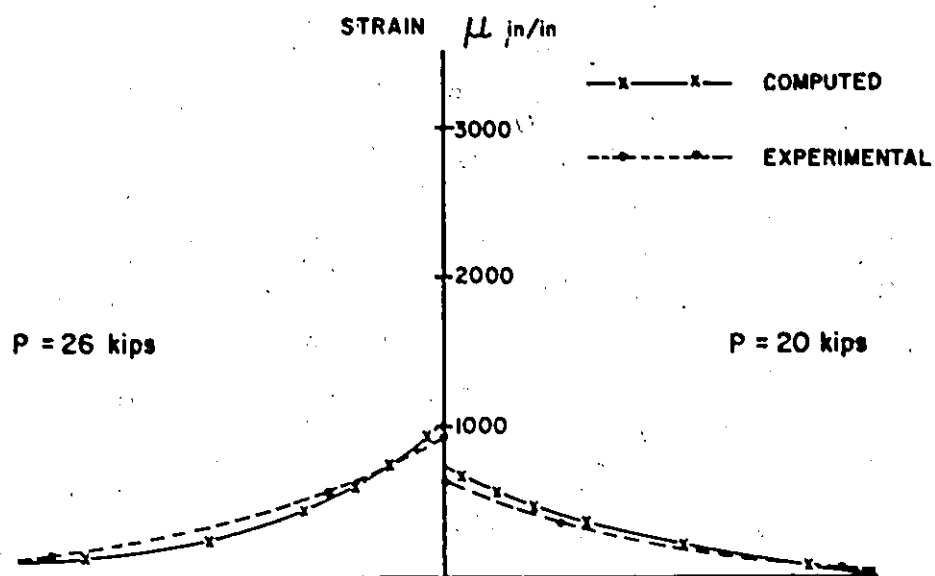


FIGURE 7.35 COMPARISON BETWEEN THE EXPERIMENTAL AND ANALYTICAL TOP FIBRE CONCRETE STRAIN DISTRIBUTION ACROSS THE SLAB WIDTH AT SECTION 2-2 FOR END B2

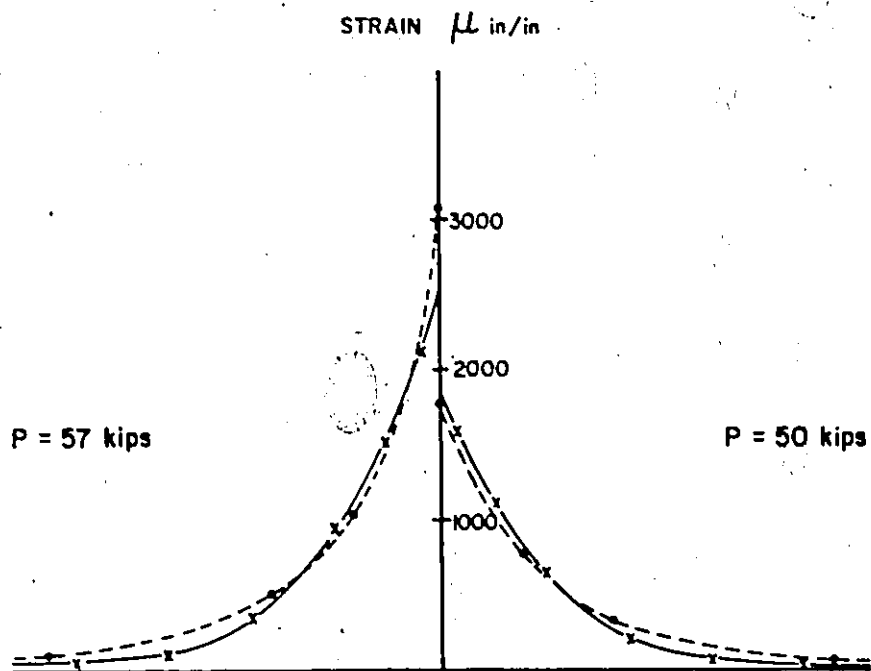
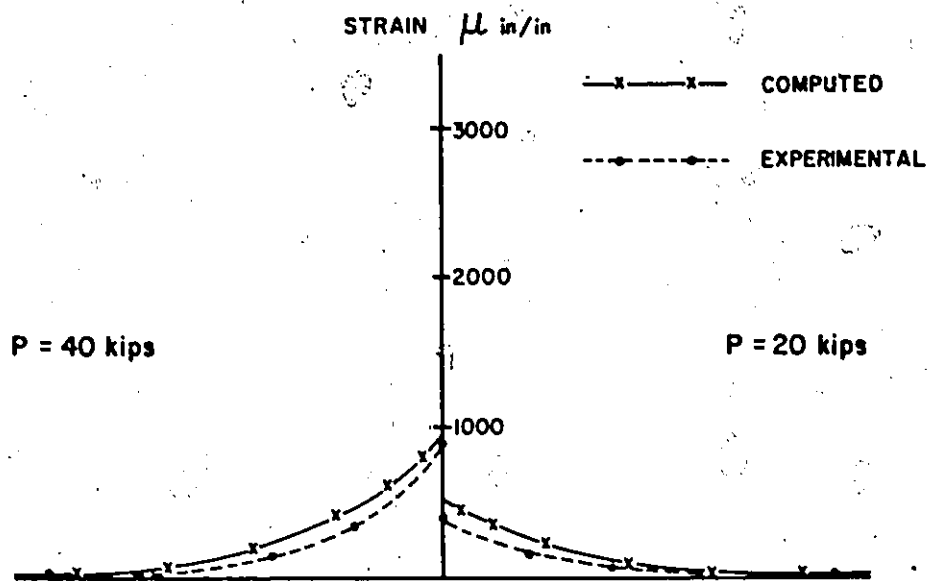


FIGURE 7.36 COMPARISON BETWEEN THE EXPERIMENTAL AND ANALYTICAL TOP FIBRE CONCRETE STRAIN DISTRIBUTION ACROSS THE SLAB WIDTH AT SECTION 1-1 FOR END C1

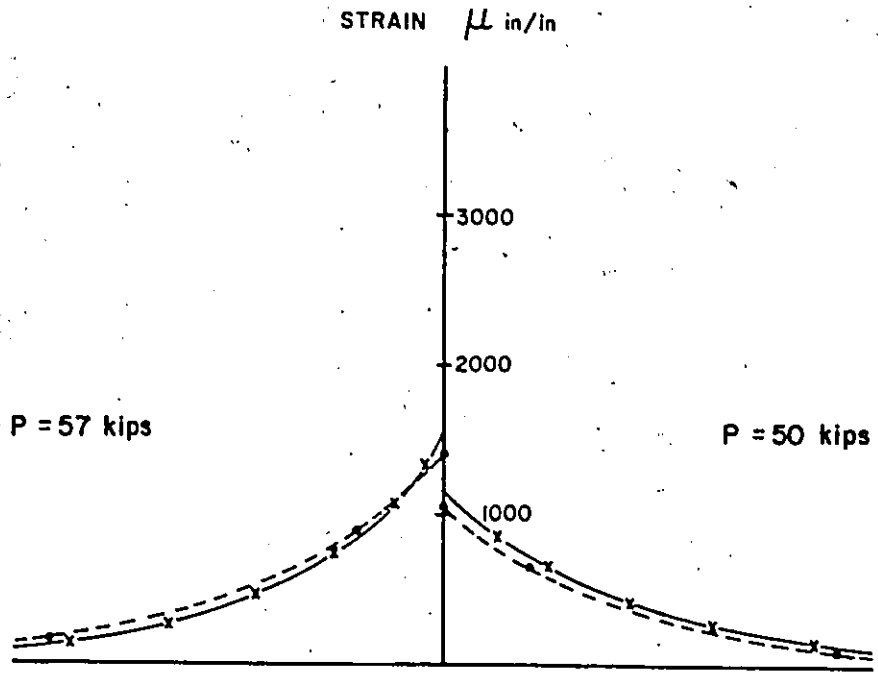
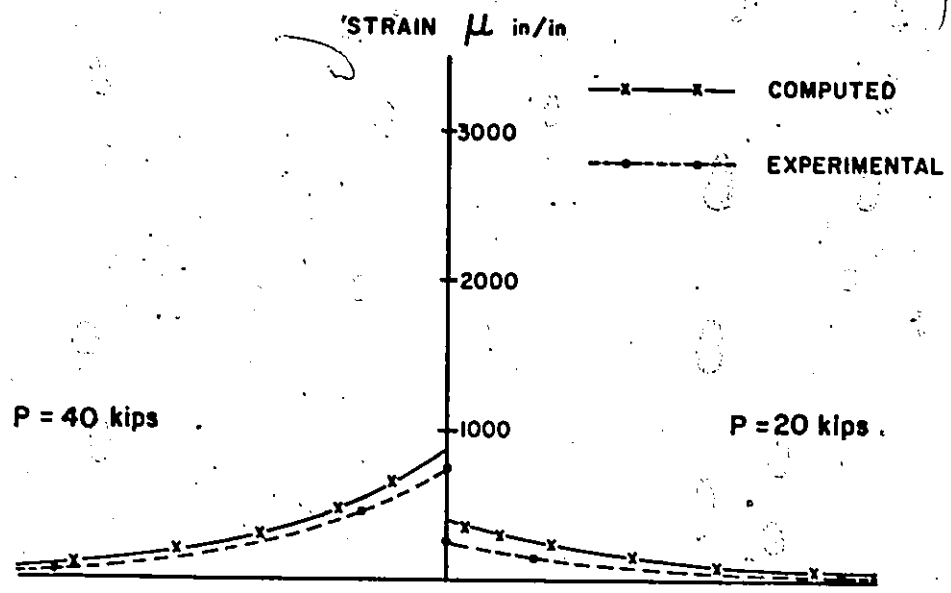
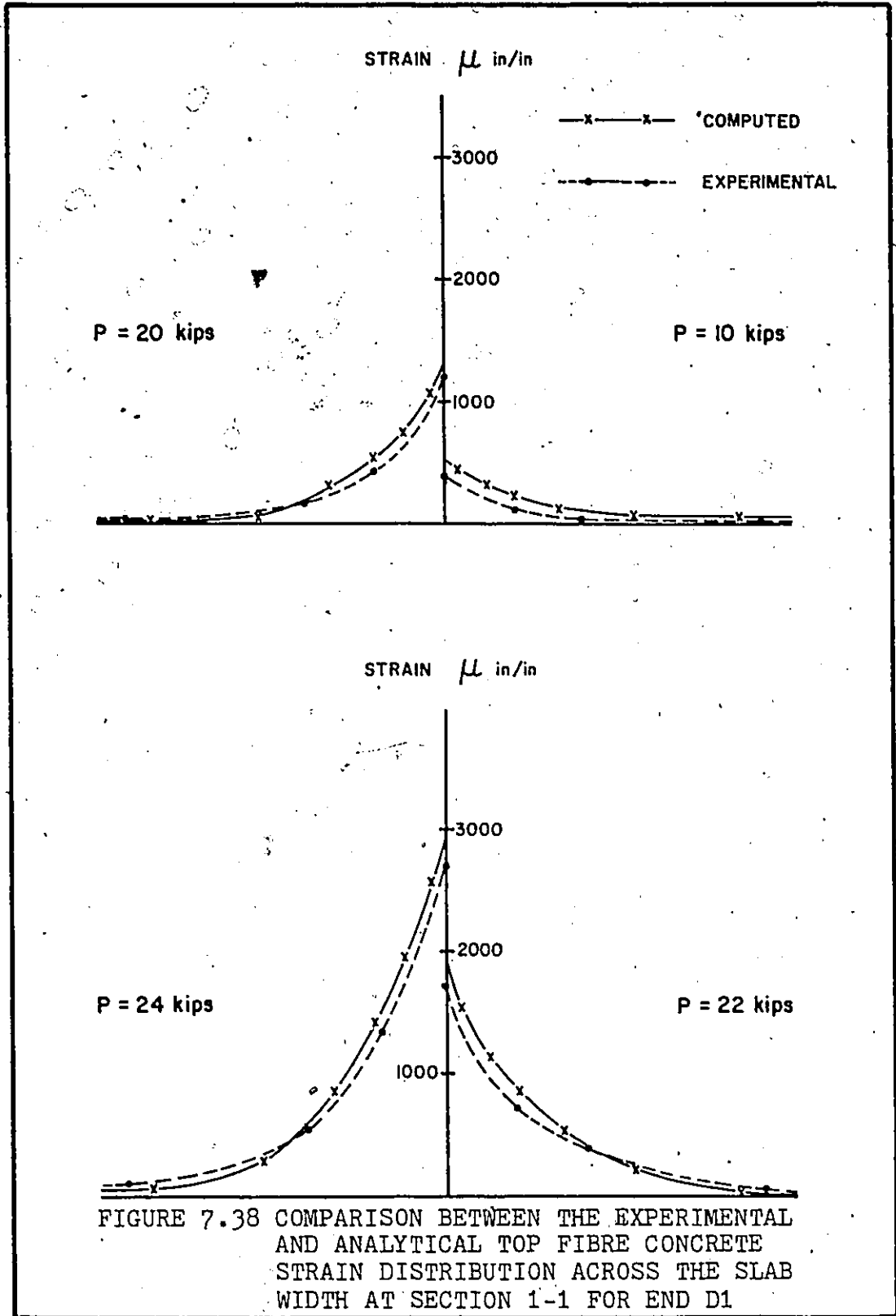
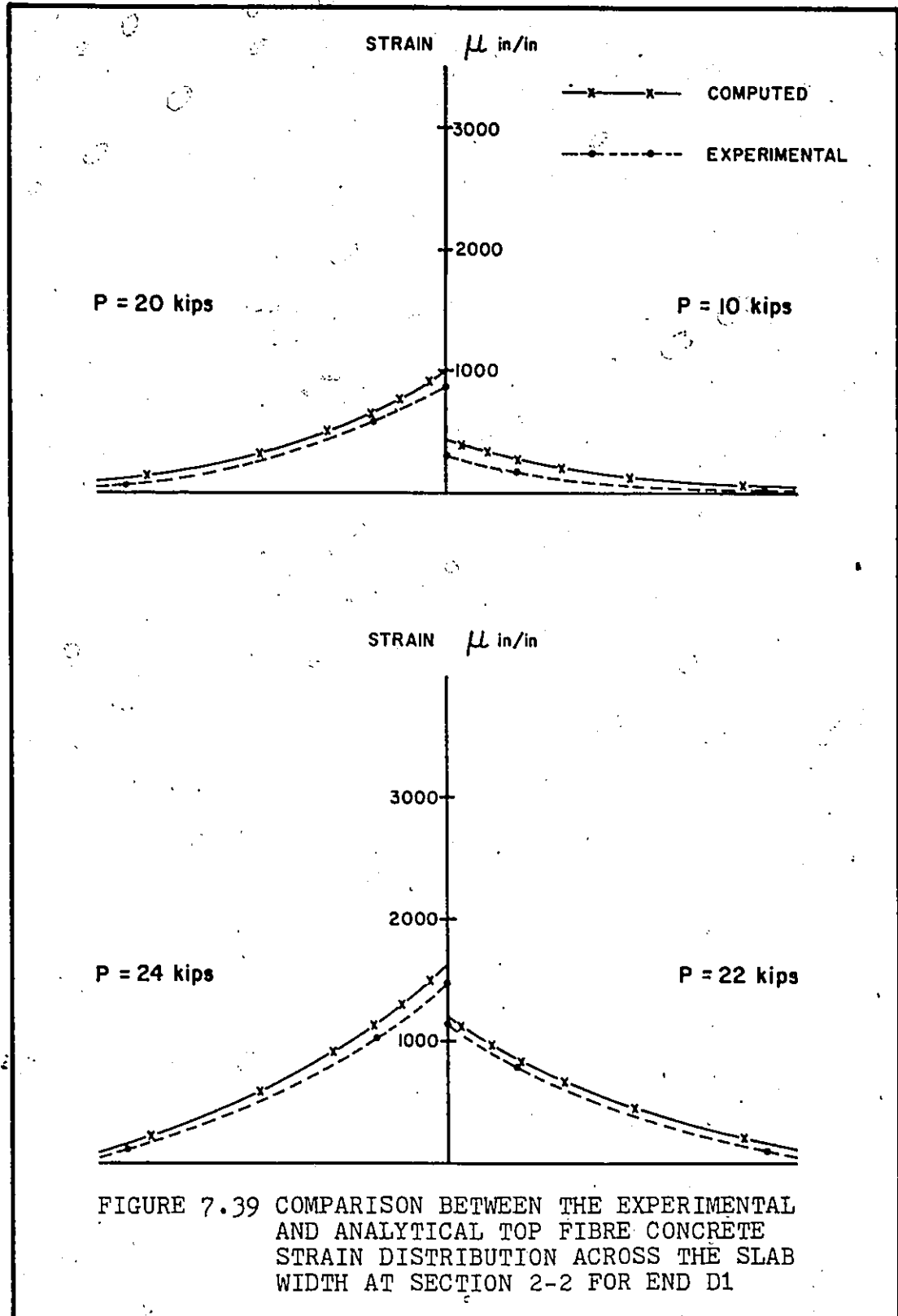
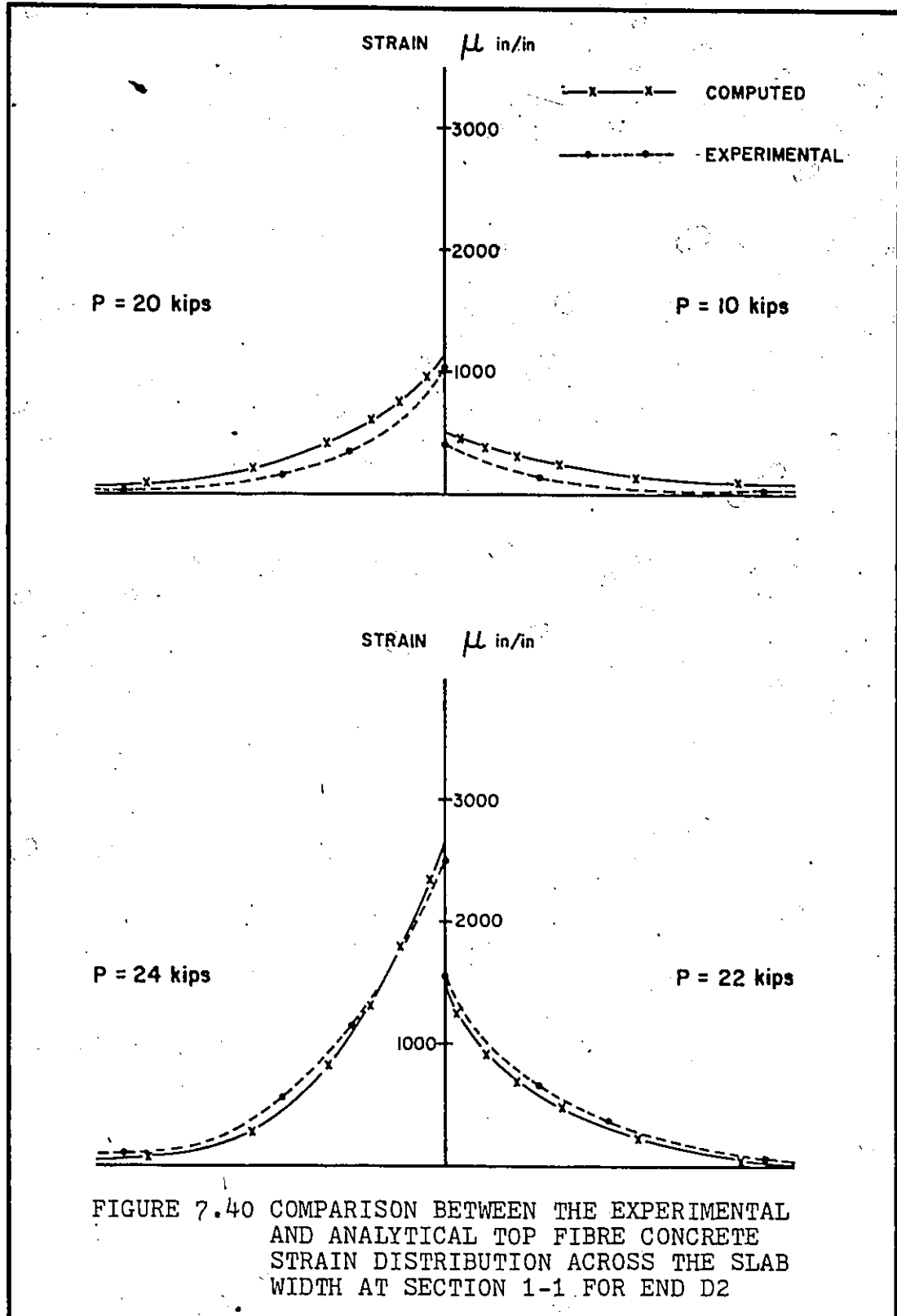
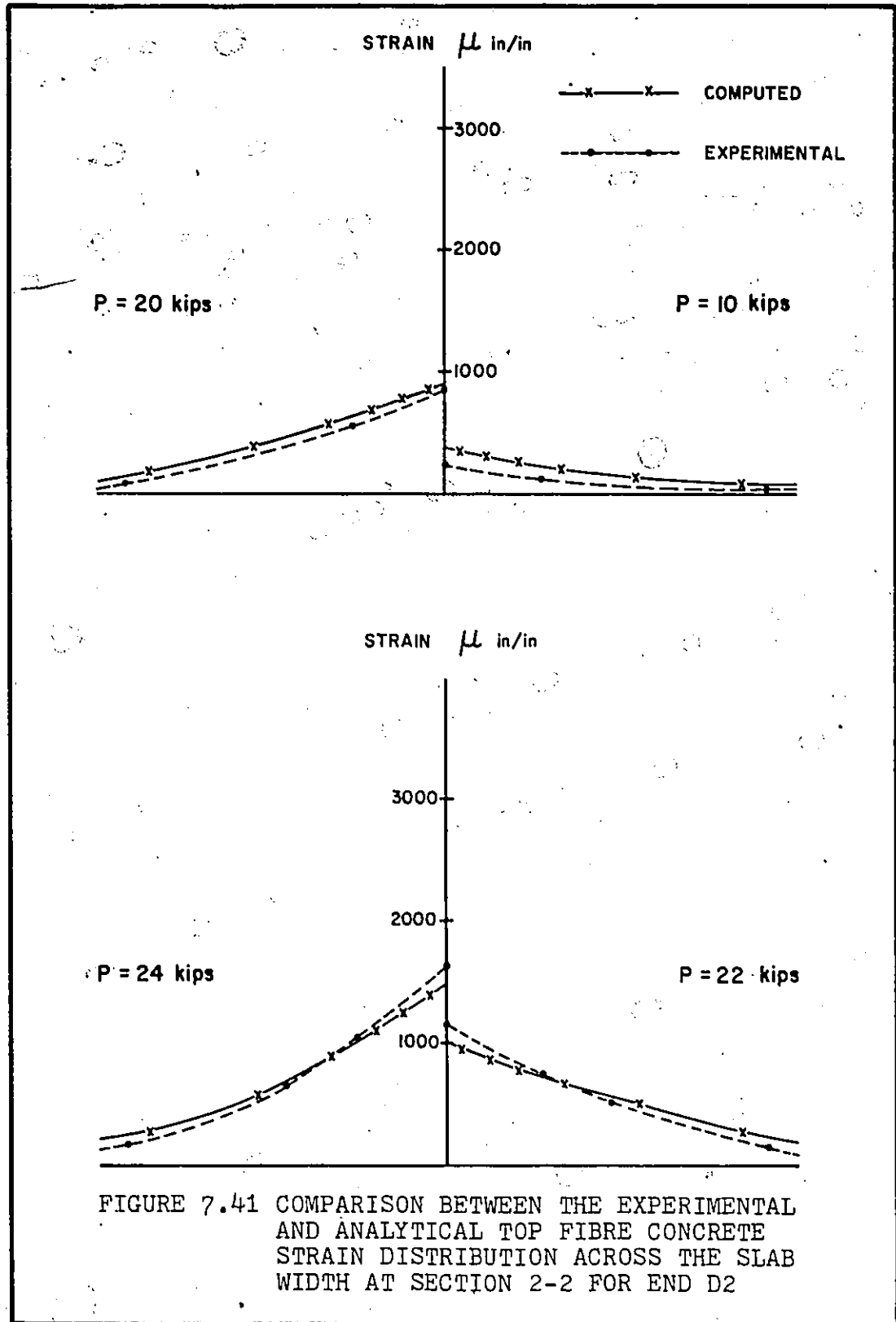


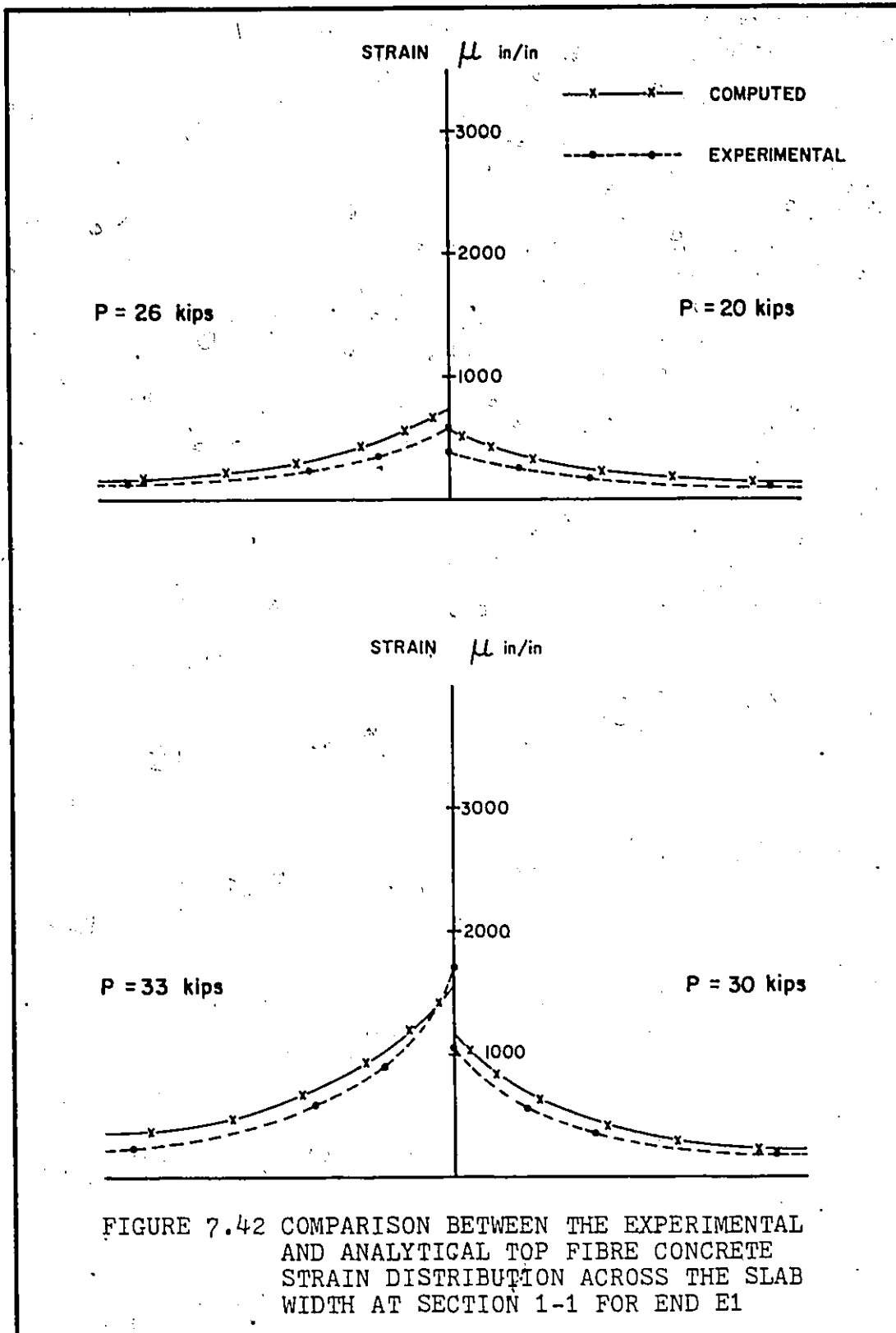
FIGURE 7.37 COMPARISON BETWEEN THE EXPERIMENTAL AND ANALYTICAL TOP FIBRE CONCRETE STRAIN DISTRIBUTION ACROSS THE SLAB WIDTH AT SECTION 2-2 FOR END C1











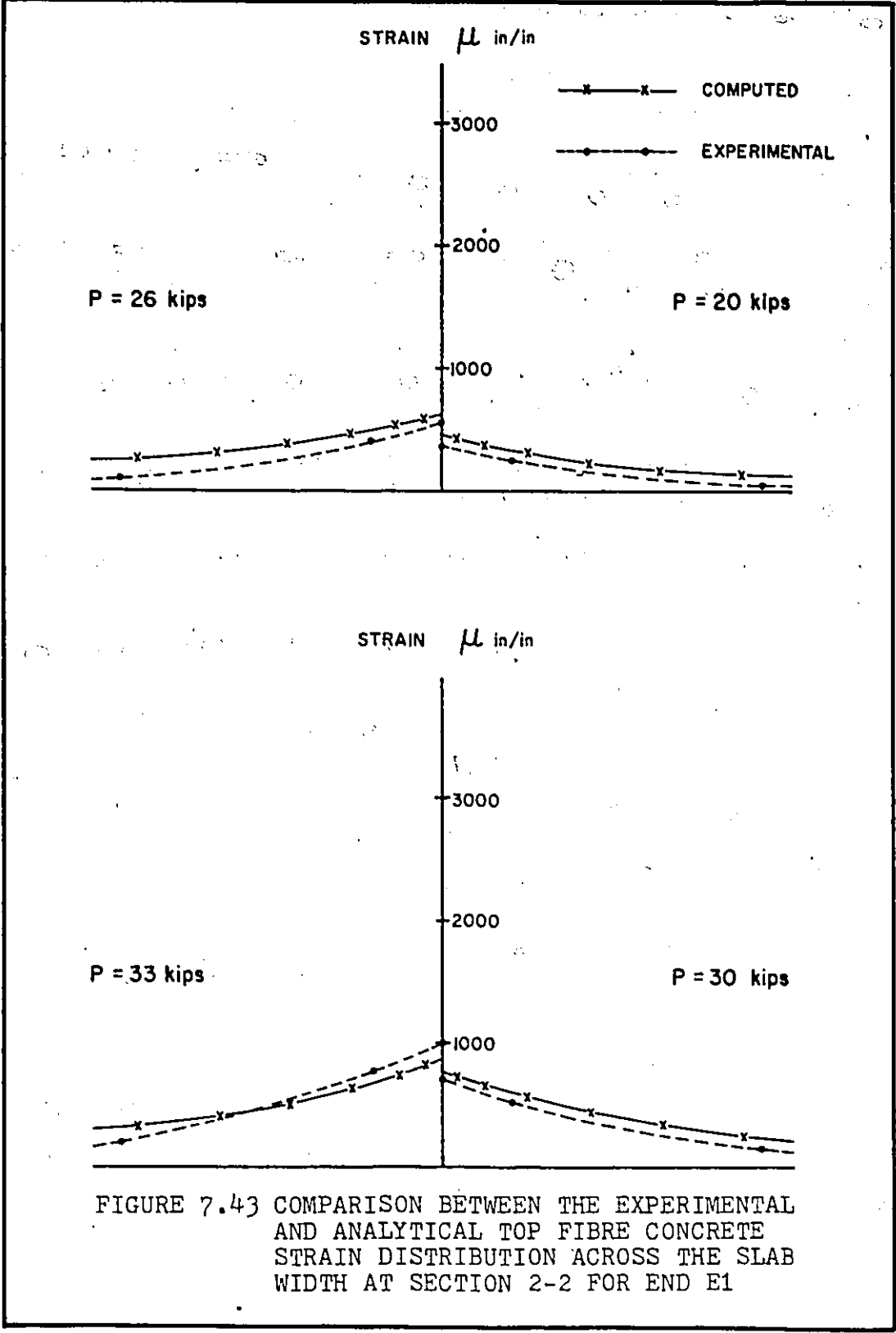


FIGURE 7.43 COMPARISON BETWEEN THE EXPERIMENTAL AND ANALYTICAL TOP FIBRE CONCRETE STRAIN DISTRIBUTION ACROSS THE SLAB WIDTH AT SECTION 2-2 FOR END E1

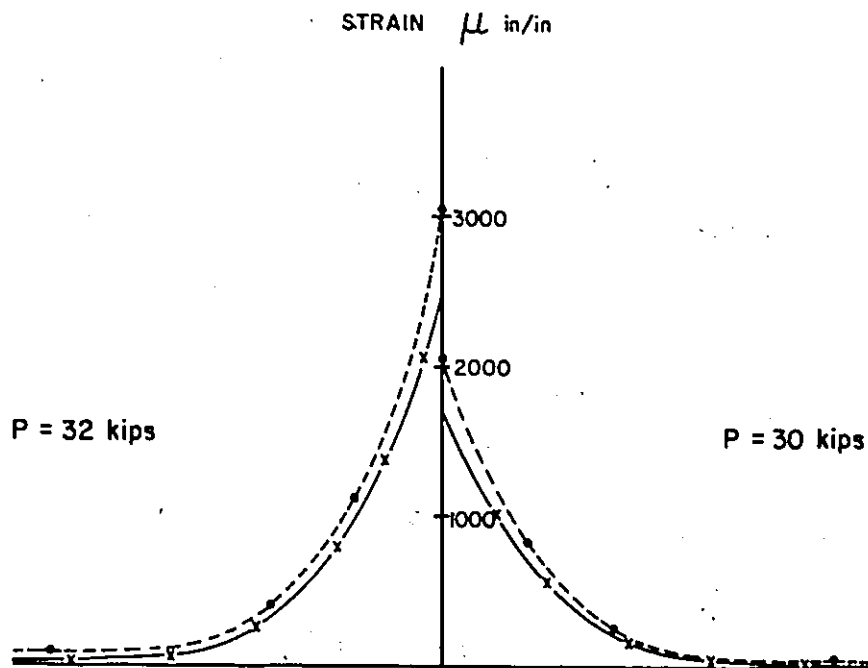
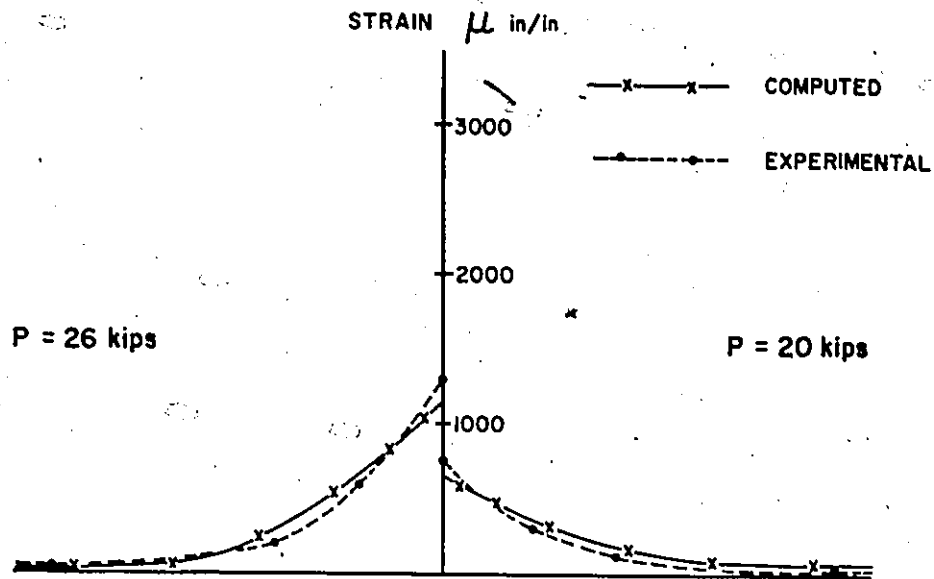
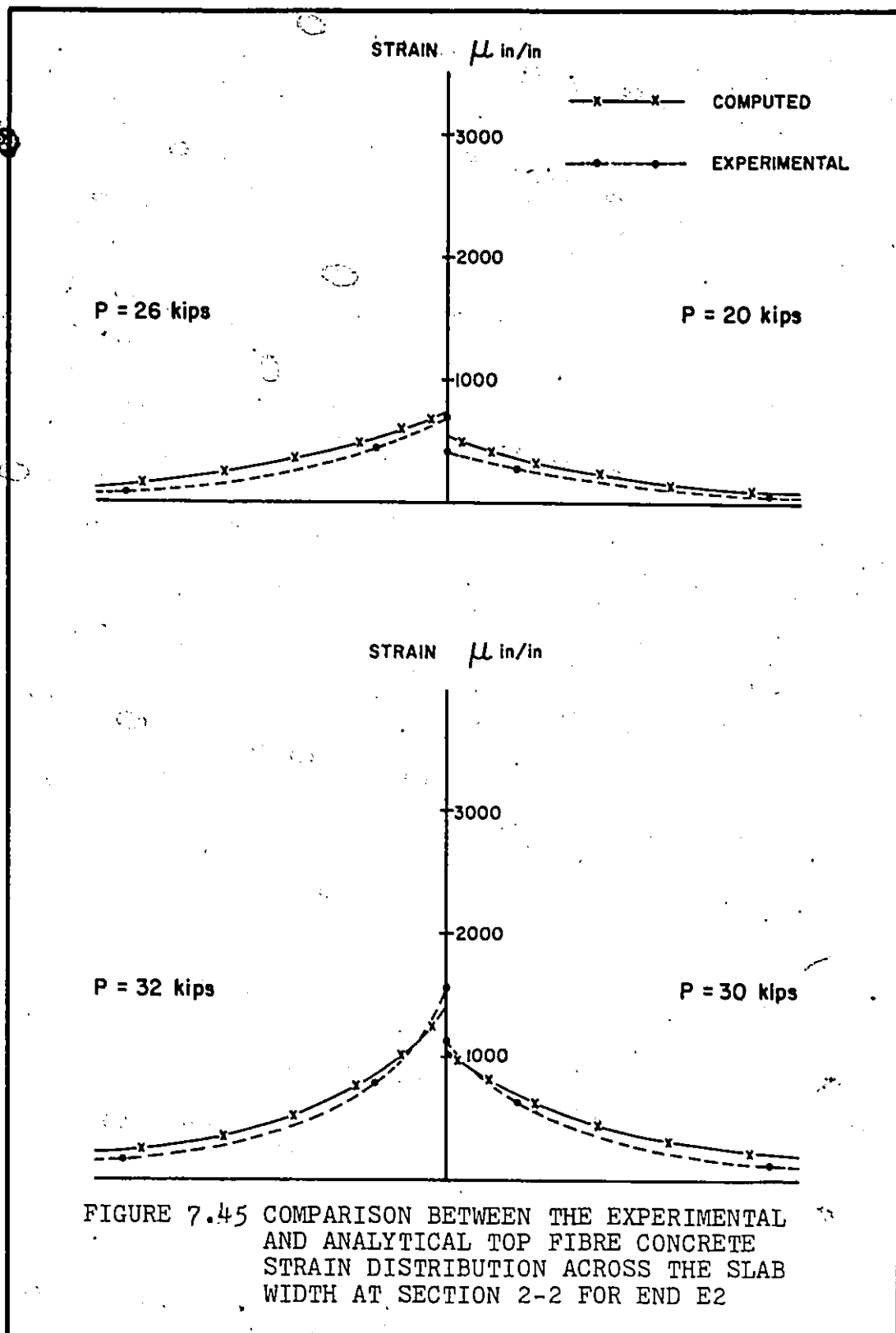


FIGURE 7.44 COMPARISON BETWEEN THE EXPERIMENTAL AND ANALYTICAL TOP FIBRE CONCRETE STRAIN DISTRIBUTION ACROSS THE SLAB WIDTH AT SECTION 1-1 FOR END E2



the two values, which should be expected due to the assumptions made in the analytical model and the accuracy of the experimental measurements, was small as shown in the figures.

Although an experimental value for the effective slab width for strength was not available for comparison with the analytical value, the agreement between the experimental and analytical top fibre strain distribution across the slab width indicates an agreement between the analytical and experimental, if calculated, effective slab widths since the analytical top fibre concrete strains were found from the inelastic method which takes into account the effective slab width. Moreover, the agreement between the experimental and analytical top fibre concrete strain distributions and between the experimental and analytical curvatures leads to an agreement between the experimental and analytical strain distribution across the slab depth and consequently agreement between the two effective widths which are calculated from the integration of these stresses (equation (3.35), Chapter 3).

Both the experimental and analytical strain distributions were more uniform at section 2-2, 9 inches from the column face, than at section 1-1, 3 inches from the column face, which indicates a variation in the effective slab width for strength along the beam length.

Prediction of the Strain Distribution Across the Composite Beam Depth

The method described in Chapter 4 for calculating the strain distribution across the composite beam depth in the elastic range using

the transformed section with the appropriate effective slab widths b_e and b_{es} (Chapter 4) was examined by comparing its strain prediction with the experimental results at section 1-1 (3 inches from the column) for each of the test beams.

For the purpose of comparison, the strain distribution at the experimental working load, defined as the experimental load at which at bottom fibre steel strain of the specimen was $0.66 \epsilon_y$, was chosen. The values of b_e and b_{es} were obtained from the results shown in Chapter 4 for the appropriate L/b and c/b ratios and degree of interaction. The experimental strains at the working load were obtained from the interpolation of the experimental data.

Table 7.4 shows the experimental and calculated results. The results are also shown in Figure 7.46. The results show that the method can predict fairly accurate the strain distribution across the composite beam depth in the elastic range.

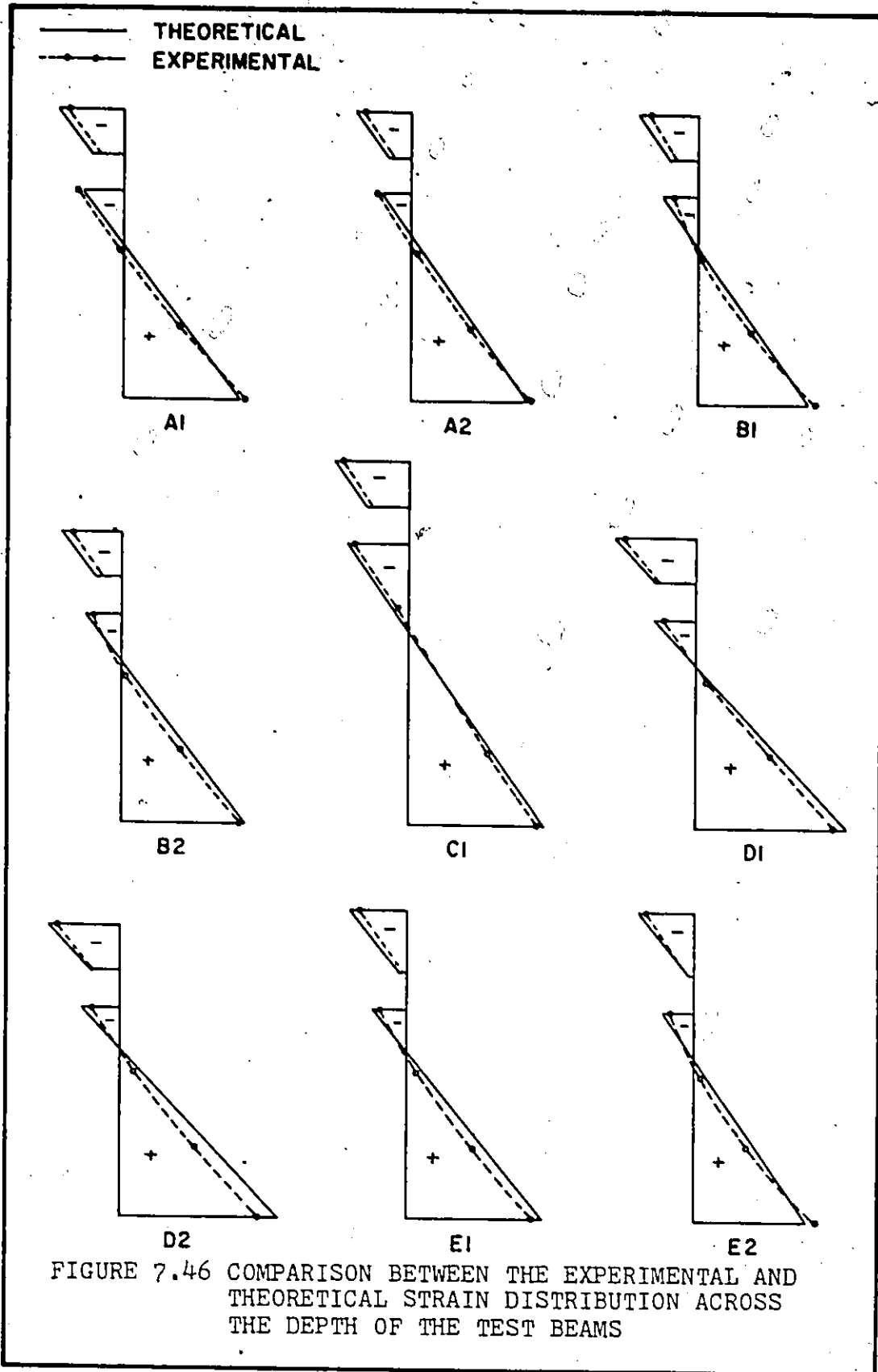
7.8 Rotation Capacity

Rotation capacity is of great importance in plastic design. The rotation is necessary to assure that all the required plastic hinges will form throughout the structure.

In plastic design of steel structures rotation capacity is defined as the angular rotation which a given cross sectional shape can accept at the plastic moment value without prior local failure as indicated in Figure 7.47. The same definition of the rotation capacity was used by Duplessis and Daniels⁽⁴⁸⁾ to evaluate the rotation capacity

Beam No.	A ₁	A ₂	B ₁	B ₂	C ₁	D ₁	D ₂	E ₁	E ₂
Bottom Fibre Steel Strain micro in/in	Exp.	1036	1036	1035	1035	1140	1188	1188	1070
	Theo.	1006	1032	952	1068	1165	1320	1390	1179
Steel strain at the bottom fibre of the top flange micro in/in	Exp.	0402	-302	-200	-241	-503	-320	-250	-206
	Theo.	-316	-298	-301	-320	-550	-360	-330	-280
Top fibre concrete strain micro in/in	Exp.	-450	-400	-420	-425	-600	-650	-575	-450
	Theo.	-550	-477	-520	-490	-664	-730	-630	-478

Table 7.4: Calculated and Experimental Concrete and Steel Strains



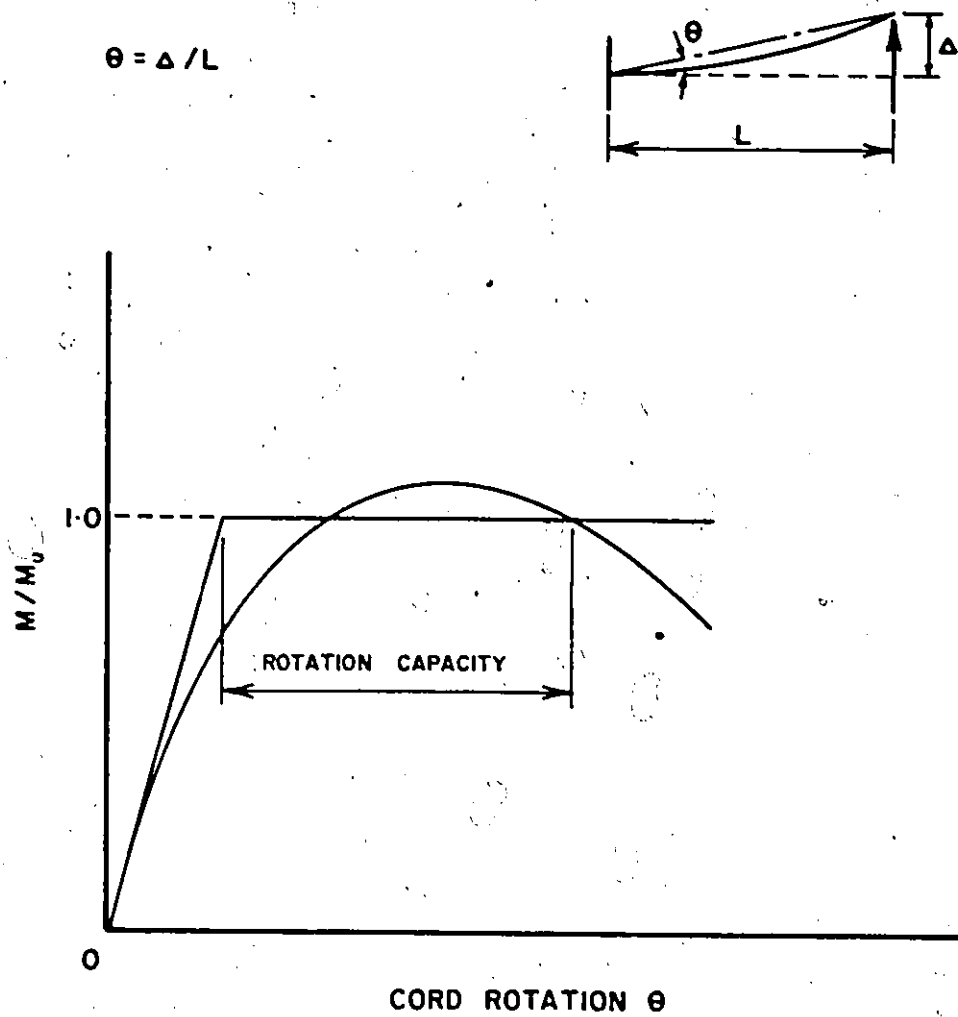


FIGURE 7.47 DEFINITION OF ROTATION CAPACITY

of composite beam-to-column connections.

The rotation capacity, based on the above definition, was calculated for each of the test beams. The calculated ultimate moment on the basis of the analytical effective slab width for strength (b_e) and concrete strength of $0.85 f'_c$, curve (1) in Figures 7.1 through 7.9, was taken as the plastic moment of the composite section. The calculated rotation capacity is given in Table 7.5.

Beam Number	A ₁	A ₂	B ₁	B ₂	C ₁	D ₁	D ₂	E ₁	E ₂
Rotation Capacity	0.020	0.025	0.023	0.023	0.020	0.016	0.020	0.023	0.017

Table 7.5: Rotation Capacity of the Test Beams

There is no definite value for the required rotation capacity of a joint since this value depends on the location of the joint in the structure and the sequence of forming the plastic hinges. However, Duplessis and Daniels⁽⁴⁸⁾ reported that in many unbraced frames the required rotation capacity was of the order of the deflection index at the maximum load. They assumed a typical deflection index of about 0.02 to evaluate the adequacy of the rotation of the composite beam-to-column connections.

Using the same assumption for the required rotation capacity, it can be seen that all the tests except D₁ and E₂ had adequate rotation capacity. The rotation capacity for tests D₁ and E₂ were 0.016 and 0.017 rad. respectively. These values are not far from the assumed

required capacity.

From the results of tests E_1 and E_2 it can be seen that appreciable increase occurred in the rotation capacity, about 35%, due to the existence of the transverse support.

CHAPTER 8

SUMMARY AND CONCLUSIONS

8.1 Summary

Analytical and experimental studies were performed to investigate the strength and stiffness of composite beams with ribbed metal deck in an unbraced multi-story frame subjected to lateral loads. One of the main interests in this investigation was the effective slab width that should be considered in composite action with the steel beam in the various moment region.

An analytical method of analysis was developed, utilizing both the finite difference and finite element methods, to study the behaviour of the composite beams in the positive and negative moment regions. The finite difference technique was used to determine the interaction forces, stresses and deformation of the composite beam along its span, whilst a layered finite element technique was used to determine the distribution of the strains and stresses across the slab width and depth.

A computer program was developed to perform the analysis on the CDC 6400 computer. Although the developed method of analysis can accommodate the continuous composite beam, each of the positive and negative moment regions was treated separately due to core storage limitation of the CDC 6400 computer.

The analytical method was used to study the effective slab

widths in the various bending moment regions. Three definitions for the effective slab width were used in the analysis. These definitions are:

- a) The effective slab width for in-plane forces (b_e). This effective width was called throughout the thesis the effective slab width for strength since it is to be used to determine the ultimate strength of the composite section.
- b) The effective slab width for stiffness at a particular section (b_{es}). This effective slab width is to be used to determine the moment of inertia of that particular section using the transformed section method and consequently the curvature and stress distribution at that position.
- c) The average effective slab width for stiffness (b_{av}) to be used to determine the average stiffness of the composite beam for the purpose of deformation calculations.

The effective slab width for strength (b_e) developed in this thesis is valid in both the elastic and inelastic ranges while the effective slab widths for stiffness (b_{es}) and (b_{av}) were developed in the elastic range only and consequently they are not valid in the inelastic range.

A parametric study was performed to investigate the effect of three major parameters on the effective slab widths. These parameters are:

1. Slab length to slab width ratio (L/b)
2. Column face width to slab width ratio (c/b)
3. Degree of interaction.

The degree of interaction includes the effects of the slab thickness, steel beam size and number and stiffness of the shear connectors.

The analytical results show that the effective slab width for strength (b_e) depends mainly on the (L/b) and (c/b) ratios and can be considered as independent of the degree of interaction. The effective slab widths for stiffness (b_{es}) and (b_{av}) depend on the (L/b) and (c/b) ratios and on the degree of interaction.

A set of curves representing the variation of the effective slab width for strength (b_e) and the average effective slab width (b_{av}) for the case of complete interaction with respect to (L/b) and (c/b) ratios are presented in this thesis. An analytical method to determine the effective slab widths for stiffness (b_{es}) and (b_{av}) for any degree of interaction is also presented.

Although the main purpose of the analysis was to study the behaviour of composite beams in an unbraced multi-story frame, the analytical model was used to investigate the effective slab widths for simply supported composite beams subjected to central point load. The analytical results were compared to the provision for the effective slab width in the CSA Standard, AIJ Standard and the British Standard. The results showed that the AIJ equation for the effective slab width agrees very well with the analytical results of the effective slab width for strength (b_e) and that the CSA standard is unconservative for L/b ratios greater than 3. However the CSA standard provides a very good estimation for average effective slab width for stiffness for L/b equal or greater than 4 and below this value all the standards are

conservative.

A series of tests were performed to investigate the behaviour of the composite beam-to-column connection in the positive moment region. A total of 10 tests were performed to study the effect of (L/b) and (c/b) ratio, slab thickness, steel beam size and the existence of lateral support on the behaviour of the composite beam. The test results showed that the maximum strength ratio, initial stiffness and ductility factor increased with increasing (L/b) ratio, (c/b) ratio and slab thickness and decreased with increasing the steel beam size. The results showed also that the existence of a transverse beam increases the strength, stiffness and ductility of the composite beam.

Each of the test beams was analysed using the developed computer program and the experimental and analytical results were compared. This comparison showed that a very good agreement exists between the experimental and analytical results.

8.2 Conclusions

Based on the analytical and experimental investigation reported in this study, the following conclusions may be drawn.

1. The effective slab width for strength (b_e) for composite beams depends mainly on the slab length to width ratio (L/b) and the column width to slab width ratio (c/b) . The effective slab width ratio (b_e/b) increases with the increase of these two ratios.
2. The effective slab widths for stiffness (b_{es}) and (b_{av}) depend on (L/b) and (c/b) ratios and on the degree of interaction.

3. The AIJ standard provides a very good estimation of the effective slab width for strength for simple composite beams subjected to central point load while the CSA Standard provides a very good estimate for the average effective slab width for stiffness specially for L/b greater than 4.
4. A very good estimate of the maximum strength of a composite beam at the position of the composite beam-to-column connection can be obtained by using the stress block method together with the analytical effective slab width for strength (b_e) corresponding to the (L/b) and (c/b) ratios. In the positive moment region, a concrete block having a width (b_e) and stress of $0.85 f'_c$ is to be considered with the steel beam in the ultimate stress block calculation. In the negative moment region only the slab reinforcement, if it exists, within the effective width (b_e) is to be considered in the stress block calculation.
5. A very good estimate of the average stiffness of the composite beam can be obtained using the transformed section method together with the analytical average effective slab width for stiffness (b_{av}) corresponding to the (L/b) and (c/b) ratios and the degree of interaction. In the positive moment region the transformed section consists of the steel beam and a concrete slab having a width equal to (b_{av}). In the negative moment region the transformed section consists of the steel beam and the slab reinforcement, if it exists, within the average effective width (b_{av}).

6. The maximum strength of composite beams with ribbed metal deck at the position of the composite beam-to-column connections exceeds the maximum strength of the steel beam alone by 34 to 79% depending on the (L/b) and (c/b) ratios, slab thickness, steel beam size and the existence of lateral support framing to the column and connected to the slab of the composite beam.
7. The existence of the lateral support increases the maximum strength, the initial stiffness, ductility and rotation capacity of the composite beam-to-column connections.
8. Composite beam-to-column connections, especially with the presence of lateral support, possess adequate ductility and rotation capacity to enable plastic design to be applied to unbraced frames with composite steel-ribbed concrete floor system.

APPENDIX A

NUMERICAL METHOD FOR THE FINITE DIFFERENCE COMPUTATION

The numerical method used in the finite difference analysis, section 3.4, is described in detail in this Appendix.

a) Computation of the Extreme Fibre Strain in the Slab for Given Force (F) and Curvature (ϕ)

If the curvature of the slab (ϕ_c) and the interaction force (F) acting on the concrete slab are known, a unique strain distribution can be established. Although the force (F) is a function of the extreme fibre strain (ϵ_{ct}) and the curvature (ϕ_c), it is now only a function for the extreme fibre strain (ϵ_{ct}) since the curvature (ϕ_c) has a fixed given value. That is,

$$F = F(\epsilon_{ct})$$

Using Taylor's expansion to express the force (F) and retaining the linear terms only yields

$$F = F(\bar{\epsilon}_{ct}) + \frac{\partial F(\epsilon_{ct})}{\partial \epsilon_{ct}} \delta \epsilon_{ct} \quad (A.1)$$

where F the given force for which ϵ_{ct} is required
 $F(\bar{\epsilon}_{ct})$ the force corresponding to an assumed ($\bar{\epsilon}_{ct}$)
 $\partial F(\epsilon_{ct})/\partial \epsilon_{ct}$ the rate of change of the force with respect to the strain

$\delta \epsilon_{ct}$ strain increment to give the required force (F)

In order to find $\delta \epsilon_{ct}$, the term $\partial F(\epsilon_{ct})/\partial \epsilon_{ct}$ in equation (A.1) must be evaluated first. For this purpose a small strain increment $\Delta \epsilon_{ct}$ is to be added to the strain $\bar{\epsilon}_{ct}$ and the force $F(\bar{\epsilon}_{ct} + \Delta \epsilon_{ct})$ corresponding to strain $(\bar{\epsilon}_{ct} + \Delta \epsilon_{ct})$ and curvature (ϕ_c) is to be computed. Then

$$\frac{\partial F(\epsilon_{ct})}{\partial \epsilon_{ct}} = \lim_{\Delta \epsilon_{ct} \rightarrow 0} \frac{F(\bar{\epsilon}_{ct} + \Delta \epsilon_{ct}) - F(\bar{\epsilon}_{ct})}{\Delta \epsilon_{ct}} \quad (A.2)$$

Hence, from equation (A.1)

$$\delta \epsilon_{ct} = \frac{F - F(\bar{\epsilon}_{ct})}{\frac{\partial F(\epsilon_{ct})}{\partial \epsilon_{ct}}} \quad (A.3)$$

and the required strain ϵ_{ct} is given by

$$\epsilon_{ct} = \bar{\epsilon}_{ct} + \delta \epsilon_{ct} \quad (A.4)$$

If the assumed strain $(\bar{\epsilon}_{ct})$ is not in the neighbourhood of the required strain, equation (A.4) will provide a poor approximation for the required strain and will not provide the desired accuracy. Therefore the procedure should be repeated by taking the computed ϵ_{ct} as $\bar{\epsilon}_{ct}$ and correspondingly the computed (F) as $F(\bar{\epsilon}_{ct})$. This process converges rapidly especially when $\bar{\epsilon}_{ct}$ is chosen properly.

b) Computation of the Strain Distribution in the Composite Beam for a Given Force (F) and External Moment (M)

Although there are four unknowns ϵ_{sb} , ϕ_s , ϵ_{ct} and ϕ_c in this case, only two of them are independent. If ϕ_s is known, ϕ_c can be determined from the relation

$$\phi_c = \phi_s - \phi_{D.L} \quad (\text{for unshored beam})$$

or

$$\phi_c = \phi_s \quad (\text{for shored beam})$$

and if ϕ_s and ϵ_{sb} are known, the force (F) can be found and consequently (ϵ_{ct}) as described in the previous section. Therefore ϵ_{sb} and ϕ_s are the only two independent variables in determining the strain distribution across the composite-beam depth. Thus,

$$F = F(\epsilon_{sb}, \phi_s)$$

and

$$M = M(\epsilon_{sb}, \phi_s)$$

Using Taylor's expansion to express the force (F) and the moment (M) and retaining the linear terms only yields

$$F(\epsilon_{sb}, \phi_s) = F(\bar{\epsilon}_{sb}, \bar{\phi}_s) + \frac{\partial F}{\partial \epsilon_{sb}} \delta \epsilon_{sb} + \frac{\partial F}{\partial \phi_s} \delta \phi_s \quad (\text{A.5})$$

and

$$M(\epsilon_{sb}, \phi_s) = M(\bar{\epsilon}_{sb}, \bar{\phi}_s) + \frac{\partial M}{\partial \epsilon_{sb}} \delta \epsilon_{sb} + \frac{\partial M}{\partial \phi_s} \delta \phi_s \quad (\text{A.6})$$

These two simultaneous equations are to be solved to find $\delta \epsilon_{sb}$ and $\delta \phi_s$. The computation procedure is summarized in the following

steps.

- 1) For starting values $\bar{\epsilon}_{sb}$ and $\bar{\phi}_s$, $F(\bar{\epsilon}_{sb}, \bar{\phi}_s)$ and $M(\bar{\epsilon}_{sb}, \bar{\phi}_s)$ are computed.
- 2) Adding a small strain increment $\Delta \epsilon_{sb}$ to the strain $\bar{\epsilon}_{sb}$ while keeping $\bar{\phi}_s$ constant, the force $F(\bar{\epsilon}_{sb} + \Delta \epsilon_{sb}, \bar{\phi}_s)$ and the moment $M(\bar{\epsilon}_{sb} + \Delta \epsilon_{sb}, \bar{\phi}_s)$ are computed.
- 3) Adding a small curvature increment $\Delta \phi_s$ to the curvature $\bar{\phi}_s$ while keeping $\bar{\epsilon}_{sb}$ constant, the force $F(\bar{\epsilon}_{sb}, \bar{\phi}_s + \Delta \phi_s)$ and the moment $M(\bar{\epsilon}_{sb}, \bar{\phi}_s + \Delta \phi_s)$ are computed.
- 4) The force and moment gradients are computed from

$$\frac{\partial F}{\partial \epsilon_{sb}} = \lim_{\Delta \epsilon_{sb} \rightarrow 0} \frac{F(\bar{\epsilon}_{sb} + \Delta \epsilon_{sb}, \bar{\phi}_s) - F(\bar{\epsilon}_{sb}, \bar{\phi}_s)}{\Delta \epsilon_{sb}}$$

$$\frac{\partial F}{\partial \phi_s} = \lim_{\Delta \phi_s \rightarrow 0} \frac{F(\bar{\epsilon}_{sb}, \bar{\phi}_s + \Delta \phi_s) - F(\bar{\epsilon}_{sb}, \bar{\phi}_s)}{\Delta \phi_s}$$

$$\frac{\partial M}{\partial \epsilon_{sb}} = \lim_{\Delta \epsilon_{sb} \rightarrow 0} \frac{M(\bar{\epsilon}_{sb} + \Delta \epsilon_{sb}, \bar{\phi}_s) - M(\bar{\epsilon}_{sb}, \bar{\phi}_s)}{\Delta \epsilon_{sb}}$$

$$\frac{\partial M}{\partial \phi_s} = \lim_{\Delta \phi_s \rightarrow 0} \frac{M(\bar{\epsilon}_{sb}, \bar{\phi}_s + \Delta \phi_s) - M(\bar{\epsilon}_{sb}, \bar{\phi}_s)}{\Delta \phi_s}$$

- 5) Solving the two simultaneous equations (A.5) and (A.6) to obtain

$\delta \epsilon_{sb}$ and $\delta \phi_s$, then

$$\epsilon_{sb} = \bar{\epsilon}_{sb} + \delta \epsilon_{sb}$$

and
$$\phi_s = \bar{\phi}_s + \delta \phi_s$$

If the desired accuracy is not achieved in the first trial, the same steps are to be repeated using the calculated values of ϵ_{sb} and ϕ_s as $\bar{\epsilon}_{sb}$ and $\bar{\phi}_s$. This process converges rapidly and after a few cycles the desired accuracy can be reached.

c) Computation of the Panel Force $F_{(i)}$ and Connector Slip γ_{i+1} From the Known Panel Force $F_{(i-1)}$ and Connector Slip γ_i

If the slip at the connector i is known, the computation of the slip at the connector $i+1$ can be accomplished by the following method:

- 1) The force Q_i at the connector i is found from the analytical expression of the load-slip curve for the connector.
- 2) The panel force $F_{(i)}$ in the panel (i) can be computed from

$$F_{(i)} = F_{(i-1)} + Q_i$$
- 3) The strains (ϵ_{bt}) and (ϵ_{cb}) due to the force $F_{(i)}$ and the external moment $M_{(i)}$ are computed as described in the previous sections.
- 4) The slip γ_{i+1} is computed from the compatibility equation

$$\gamma_{i+1} = \gamma_i + \int_{s_{(i)}} (\epsilon_{bt} - \epsilon_{cb}) ds$$

APPENDIX B
COMPUTER PROGRAM LISTING


```

COMMON/BLOCK25/MA, JM, NH, KER, KEM2
COMMON/BLOCK26/STC(40), CUC(40)
COMMON/BLOCK27/KKCC, MERM, NMM
COMMON/BLOCK28/CSNH, ERST, SCAL1, SCAL2
COMMON/BLOCK29/UU, VV, XL, XR, MER1, MER2, SAS(40), SLM(40), LAC
COMMON/BLOCK30/EX(40), BS(20)
COMMON D(6,6), DD(6,6), A(15,15), AK(15,15), S(15,15), TR(15,15), XXX(77
), YYY(77), NI(100), NJ(100), NK(100), KMAX(100), KB(100), FF(5), FG(385),
SNP(15), T(10), H(11), ZZ(10), NR(15), EFW(10), BMSL1(20), AG(15),
SP(3,15), EE(100,10), EE1(100,10), SIGR(100,10), SIGV(100,10), SICS(100,
S10), SM(13500), NN, NEL, NN1, NN2, NLAY, NIN, NSM, NB1, NUU, CAL, EMU, NALAW, AN
SUM, ND(77,5)
READ(5,5300) TITLE
WRITE(6,5301) TITLE
CALL DATA
CALL GEOMET
CAL=1.
C
READ(5,49) DB, TW, TF, BF, BI, DS, BS1, ZL
WRITE(6,50) DB, TW, TF, BF, BI, DS, BS1, ZL
READ(5,49) U, SD4, DC, DL, HARST, RPE, SLMAX, DEMAX
WRITE(6,50) U, SD4, DC, DL, HARST, RPE, SLMAX, DEMAX
READ(5,49) STRSY, STRPY, STRWY, STRFY, STSTF, STSBF, STBTF, STBBF
WRITE(6,50) STRSY, STRPY, STRWY, STRFY, STSTF, STSBF, STBTF, STBBF
END=ES
READ(5,31) DW1, DW2, DW3, DW4, DW5, DW6, DW7
WRITE(6,85) DW1, DW2, DW3, DW4, DW5, DW6, DW7
READ(5,31) W, WW3, WW4, WW5, WW6, WW7, WWB
WRITE(6,85) W, WW3, WW4, WW5, WW6, WW7, WWB
READ(5,1) N, NSHOR, LOAD, NW, NFU, NFD, NPL
WRITE(6,1) N, NSHOR, LOAD, NW, NFU, NFD, NPL
READ(5,49) WPL, TPL, PCUT
WRITE(6,49) WPL, TPL, PCUT
READ(5,1000) C2, C3, Q2, Q3, SLIN
WRITE(6,1000) C2, C3, Q2, Q3, SLIN
READ(5,237) NCE, NC, ER12, ER10, ACURA, TRYLD
WRITE(6,237) NCE, NC, ER12, ER10, ACURA, TRYLD
READ(5,238) (FAC(1), I=1,3)
READ(5,238) (FAC2(1), I=1,3)
READ(5,238) (EAC(1), I=1,3)
DO 7776 I=1,3
FAC(I+3)=2.-FAC(I)
FAC2(I+3)=2.-FAC2(I)
EAC(I+3)=2.-EAC(I)
7776 WRITE(6,7755) I, FAC(I), FAC2(I), EAC(I)
READ(5,79) ERIN, CFST, FRACT, EACL, EACS, FALA, NCHA
WRITE(6,79) ERIN, CFST, FRACT, EACL, EACS, FALA, NCHA
READ(5,7) ERST, FANEG
WRITE(6,7) ERST, FANEG
NH=(N-1)/2
DO 3002 I=1, NH
BS(I)=BS1
BSB(I)=BS1
DN(I)=DS
C
3002 CONTINUE
K=0
MA=0
JMK=0
KKCC=0
KER=0
KSCH=0
KN=0
KN=0
KN=0
FACTOR=1.
KNUL=0
SCAL1=1.
SCAL2=10.
KEM2=0
KNEC=0
AB=2.*TF=BF+TW*(DB-2.*TF)
STSY=STRSY/ES
STBY=STRPY/EB
STFY=STRFY/EB
MAI 750
MAI 760
MAI 770
MAI 780
MAI 790
MAI 800
MAI 810
MAI 820
MAI 830
MAI 840
MAI 850
MAI 860
MAI 870
MAI 880
MAI 890
MAI 900
MAI 910
MAI 920
MAI 930
MAI 940
MAI 950
MAI 960
MAI 970
MAI 980
MAI 990
MAI 1000
MAI 1010
MAI 1020
MAI 1030
MAI 1040
MAI 1050
MAI 1060
MAI 1070
MAI 1080
MAI 1090
MAI 1100
MAI 1110
MAI 1120
MAI 1130
MAI 1140
MAI 1150
MAI 1160
MAI 1170
MAI 1180
MAI 1190
MAI 1200
MAI 1210
MAI 1220
MAI 1230
MAI 1240
MAI 1250
MAI 1260
MAI 1270
MAI 1280
MAI 1290
MAI 1300
MAI 1310
MAI 1320
MAI 1330
MAI 1340
MAI 1350
MAI 1360
MAI 1370
MAI 1380
MAI 1390
MAI 1400
MAI 1410
MAI 1420
MAI 1430
MAI 1440
MAI 1450
MAI 1460
MAI 1470
MAI 1480

```

```

EBP=RPE*EB
N1=NFU+NW+NFD+NPL
DO 131 KL=1,N1
DDB(KL)=TF/FLOAT(NFU)
IF(KL.GT.NFU) DDB(KL)=(DB-2.*TF)/FLOAT(NW)
IF(KL.GT.(NFU+NW)) DDB(KL)=TF/FLOAT(NFD)
IF(KL.GT.(NFU+NW+NFD)) DDB(KL)=TPL/FLOAT(NPL)
BH(KL)=BF
IF(KL.GT.NFU) BH(KL)=TW
IF(KL.GT.(NFU+NW)) BH(KL)=BF
IF(KL.GT.(NFU+NW+NFD)) BH(KL)=WPL
131 CONTINUE
DFA(1)=DDB(1)
DO 132 I=2,N1
132 DFA(I)=DFA(I-1)+DDB(I)
WRITE(6,140)((DDB(L),DFA(L),BH(L)),L=1,N1)
BV=(G2*Q2-Q3-G3*Q3*Q2)/(G2*Q3-G3*Q2)
CV=(BV*G2*Q2-BV*BV*G2)/Q2
AV=CV/BV
DO 1100 I=1,30
SL(I)=FLOAT(I)/200.
Q(I)=(CV/(SL(I)-AV))+BV
1100 WRITE(6,6005) SL(I),Q(I)
NH1=NH+1
READ(5,32)(SS(I),I=1,NH)
WRITE(6,23)(SS(I),I=1,NH)
63 IF(JMK.LT.3) GO TO 54
READ(5,61) N,NLA
WRITE(6,35) N,NLA
NH=(N-1)/2
NH1=NH+1
READ(5,32)(SS(I),I=1,NH)
WRITE(6,64)(SS(I),I=1,NH)
READ(5,71)(LABAL(I),I=1,NLA)
WRITE(6,75)(LABAL(I),I=1,NLA)
W=WST
54 JN=0
XX(1)=SD4+.5*SS(1)
DO 3 I=2,NH
3 XX(I)=XX(I-1)+.5*(SS(I-1)+SS(I))
X(1)=SD4.
DO 36 I=2,NH1
36 X(I)=X(I-1)+SS(I-1)
QIN=(CV/(SLIN-AV))+BV
DO 1002 I=1,NH1
1002 ZK(I)=QIN/SLIN
WRITE(6,140)(ZK(I),I=1,NH1)
DO 58 I=1,NH
INELA(I)=0
58 DN(I)=DS
AREAP=TPL*WPL
YCN=(AD*(0.5*DB+TPL)+AREAP*0.5*TPL)/(AB+AREAP)
BP1=BI+AB*((0.5*DB-(YCN-TPL))**2)+(WPL*(TPL**3))/12.
I+AREAP*((YCN-0.5*TPL)**2)
DO 360 I=1,NH
360 BIT(I)=BI
DBT(I)=DB
CB(I)=0.5*DB
CDB(I)=0.5*DB
IF(XX(I).LE.PCUT) GO TO 360
BIT(I)=BP1
CDB(I)=YCN
CB(I)=DB+TPL-YCN
DBT(I)=DB+TPL
CCONTINUE
TDL2=.5*DL*ZL
DO 22 I=1,NH
22 BMDL(I)=TDL2*XX(I)-DL*XX(I)*XX(I)*.5
WRITE(6,99)((XX(I),BMDL(I)),I=1,NH)
BMDLN=TDL2*(0.5*ZL)-DL*((ZL*0.5)**2)*0.5
WRITE(6,7001) BMDLN
IF(NSHOR.GT.0) GO TO 43
DO 44 I=1,NH
44 CURD(I)=0.

```

MAI1490
MAI1500
MAI1510
MAI1520
MAI1530
MAI1540
MAI1550
MAI1560
MAI1570
MAI1580
MAI1590
MAI1600
MAI1610
MAI1620
MAI1630
MAI1640
MAI1650
MAI1660
MAI1670
MAI1680
MAI1690
MAI1700
MAI1710
MAI1720
MAI1730
MAI1740
MAI1750
MAI1760
MAI1770
MAI1780
MAI1790
MAI1800
MAI1810
MAI1820
MAI1830
MAI1840
MAI1850
MAI1850
MAI1870
MAI1880
MAI1890
MAI1900
MAI1910
MAI1920
MAI1930
MAI1940
MAI1950
MAI1960
MAI1970
MAI1980
MAI1990
MAI2000
MAI2010
MAI2020
MAI2030
MAI2040
MAI2050
MAI2060
MAI2070
MAI2080
MAI2090
MAI2100
MAI2110
MAI2120
MAI2130
MAI2140
MAI2150
MAI2160
MAI2170
MAI2180
MAI2190
MAI2200
MAI2210
MAI2220


```

GO TO 43
43 DO 46 I=1,NH
46 CURD(I)=BMDL(I)/(EB*BIT(I))
DO 48 I=1,NH
48 BMDL(I)=0.
45 IF(JMK.EQ.3.AND.JM.EQ.0) GO TO 300
GO TO 301
300 IF(NSHOR-1) 301,302,302
302 W=0.
BMLL=0.
BMSNP=BMDLM
DO 304 I=1,NH
CUR(I)=CURD(I)
CURB(I)=CURD(I)
STBT(I)=-CURB(I)*CB(I)
304 STBB(I)=CURB(I)*CBD(I)
WRITE(6,303)
WRITE(6,311)
WRITE(6,312) ((XX(I),STBT(I),STBB(I)),I=1,NH)
GO TO 305
301 CONTINUE
NMT=1
WST=W
DELW=DW1
18 CONTINUE
MERM=0
MER1=100
MER2=100
CURP=0.
LAG=0
JM=JM+1
JMK=JMK+1
IF(TRYLD.EQ.1.) GO TO 8000
IF(K.NE.0) DELW=DW2
IF(W.GE.WW3) DELW=DW3
IF(W.GE.WW4) DELW=DW4
IF(W.GE.WW5) DELW=DW5
IF(W.GE.WW6) DELW=DW6
IF(W.GE.WW7) DELW=DW7
GO TO 77
8000 DELW=1500.
IF(K.NE.0) DELW=1500.
IF(JMK.LE.6) GO TO 900
IF(STBB(NH).GT.0.008) DELW=500.
IF(STBB(NH).GT.0.02) DELW=250.
IF(LOAD.EQ.3) DELW=(2./ZL)*DELW
GO TO 77
900 IF(LOAD.EQ.3) DELW=(2./ZL)*DELW
77 W=W+DELW*FACTOR
IF(JM.EQ.1.AND.NSHOR.EQ.0) W=0.
IF(JM-4) 6100,6100,6101
6100 WNKJND=W
GO TO 6102
6101 DO 6103 I=1,3
6103 WNK(I)=WNK(I+1)
204 WNK(4)=W
6102 WRITE(6,34) W
REACL=W*0.5
IF(LOAD.EQ.2) GO TO 102
IF(LOAD.EQ.3) GO TO 1991
DO 4 I=1,NH
BM(I)=REACL*XX(I)+BMDL(I)
4 CONTINUE
BMLL=REACL*(ZL*0.5)
GO TO 103
102 DO 108 I=1,NH
IF(XX(I).GT.U.AND.XX(I).LE.(ZL/2.)) BM(I)=BMDL(I)+REACL*U
108 IF(XX(I).LE.U) BM(I)=BMDL(I)+REACL*XX(I)
BMLL=REACL*U
GO TO 103
1991 REACL=W*ZL*.5
DO 1992 I=1,NH
BM(I)=BMDL(I)+REACL*XX(I)-.5*W*XX(I)*XX(I)
1992 CONTINUE

```

- MA12230
- MA12240
- MA12250
- MA12260
- MA12270
- MA12280
- MA12290
- MA12300
- MA12310
- MA12320
- MA12330
- MA12340
- MA12350
- MA12360
- MA12370
- MA12380
- MA12390
- MA12400
- MA12410
- MA12420
- MA12430
- MA12440
- MA12450
- MA12460
- MA12470
- MA12480
- MA12490
- MA12500
- MA12510
- MA12520
- MA12530
- MA12540
- MA12550
- MA12560
- MA12570
- MA12580
- MA12590
- MA12600
- MA12610
- MA12620
- MA12630
- MA12640
- MA12650
- MA12660
- MA12670
- MA12680
- MA12690
- MA12700
- MA12710
- MA12720
- MA12730
- MA12740
- MA12750
- MA12760
- MA12770
- MA12780
- MA12790
- MA12800
- MA12810
- MA12820
- MA12830
- MA12840
- MA12850
- MA12860
- MA12870
- MA12880
- MA12890
- MA12900
- MA12910
- MA12920
- MA12930
- MA12940
- MA12950
- MA12960

```

103 BMLL=REACL*(.5*ZL)-.5*W*((.5*ZL)**2)
DO 5 I=1,NH
IF(NSHOR.EQ.0) TOTBM(I)=BM(I)
IF(NSHOR.EQ.1) TOTBM(I)=BM(I) + (TDL2*XX(I)-DL*XX(I)*XX(I)*0.5)
5 CONTINUE
BMTSP=BMDLM+BMLL
IF(JMK.CT.6) GO TO 8
IF(JMK.CT.3) GO TO 2001
AS1=AS11
AS2=AS21
DO 5101 I=1,NH
CALL TERMS(I,EB,ES)
B(I)=BB(I)
AC(2,I)=-((1./ZK(I)+1./ZK(I+1))+ALP(I)*SS(I))
AC(3,I)=1./ZK(I+1)
5101 AC(1,I)=1./ZK(I)
AC(1,1)=0.0
AC(3,NH)=0.0
AC(2,NH)=-((1./ZK(NH))+ALP(NH)*SS(NH))
CALL BNDSOL (AC,B,3,1,NH)
WRITE(6,1)JMK,JM
Q(I)=B(I)
DO 5105 I=2,NH
5105 Q(I)=B(I)-B(I-1)
Q(NH+1)=0.
DO 5665 I=1,NH
5665 SL(I)=Q(I)/ZK(I)
SL(NH+1)=0.
TRSL(JMK)=SL(I)
IF(JMK.LT.3) GO TO 18
IF(JMK.EQ.3) GO TO 63
8 CALL EXTRA(1,GSL,SUML)
WRITE(6,92) SUML
GSL(1,4)=SUML
DO 902 I=1,NH
CALL EXTRA(I,CC,SUML)
CC(1,4)=SUML
CALL EXTRA(I,CS,SUML)
CS(1,4)=SUML
CALL EXTRA(I,CST,SUML)
CST(1,4)=SUML
902 CONTINUE
GSNH=CS(NH,4)
IF(GSNH.GE.CFST) GO TO 9250
GO TO 851
9250 DO 9253 I=1,6
9253 FAC(I)=FAC2(I)
851 SAS(NH)=GSL(1,4)
WRITE(6,2958) SAS(NH)
C GREEN CARD-THE BEGINNING OF ELASTIC COMPUTATION*****
IF(K.NE.0) GO TO 70
2001 IF(JMK.EQ.4) SAS(NH)=TRSL(1)
IF(JMK.EQ.5) SAS(NH)=TRSL(2)
IF(JMK.EQ.6) SAS(NH)=GSL(1,2)+((GSL(1,2)-GSL(1,1))/(WM(2)-WM(1)))
1*(WM(3)-WM(2))
1624 SL(I)=SAS(NH)
I=1
NLAB=1
565 Q(I)=(CV/(SL(I)-AV))+BV
IF(SL(I).LT.0.0) Q(I)=-((CV/(ABS(SL(I))-AV))+BV)
IF(I.EQ.LABAL(NLAB)) GO TO 15
GO TO 16
15 NLAB=NLAB+1
Q(I)=0.
16 AS1=AS11*BS(I)/BS1
AS2=AS21*BS(I)/BS1
CALL TERMS(I,EB,ES)
IF(I-1) 800,300,801
801 B(I)=Q(I)+B(I-1)
GO TO 802
800 B(I)=Q(I)
802 HB(I)=B(I)*ALP(I)*SS(I)+BB(I)
SL(I+1)=SL(I)+HB(I)
IF(B(I).LT.(-299900.)) GO TO 289
MAI2970
MAI2980
MAI2990
MAI3000
MAI3010
MAI3020
MAI3030
MAI3040
MAI3050
MAI3060
MAI3070
MAI3080
MAI3090
MAI3100
MAI3110
MAI3120
MAI3130
MAI3140
MAI3150
MAI3160
MAI3170
MAI3180
MAI3190
MAI3200
MAI3210
MAI3220
MAI3230
MAI3240
MAI3250
MAI3260
MAI3270
MAI3280
MAI3290
MAI3300
MAI3310
MAI3320
MAI3330
MAI3340
MAI3350
MAI3360
MAI3370
MAI3380
MAI3390
MAI3400
MAI3410
MAI3420
MAI3430
MAI3440
MAI3450
MAI3460
MAI3470
MAI3480
MAI3490
MAI3500
MAI3510
MAI3520
MAI3530
MAI3540
MAI3550
MAI3560
MAI3570
MAI3580
MAI3590
MAI3600
MAI3610
MAI3620
MAI3630
MAI3640
MAI3650
MAI3660
MAI3670
MAI3680
MAI3690
MAI3700

```

```

IF(Q(I).LT.(-200000.)) GO TO 289
CO TO 290
289 SAS(MMD)=SAS(MMD)*FALA
    KSCH=KSCH+1
    WRITE(6,291)
    IF(KSCH.GE.80) GO TO 26
    GO TO 1624
290 I=I+1
    IF(I.LT.NH1) GO TO 565
    SLM(MMD)=SL(NH1)
    IF(JM.LE.3.AND.ABS(SLM(MMD)).LE.ERIN) GO TO 57
    IF(ABS(SLM(MMD))-ER12) 57,57,2323
2323 WRITE(6,1239) MMD,SAS(MMD),SLM(MMD)
    MMD=MMD+1
    IF(MMD.GT.NCE) GO TO 26
    IF(SLM(MMD-1).LE.(-.03)) SAS(MMD)=SAS(MMD-1)*EAC(1)
    IF(SLM(MMD-1).GT.(-.03).AND.SLM(MMD-1).LE.(-.001))
    ISAS(MMD)=SAS(MMD-1)*EAC(2)
    IF(SLM(MMD-1).GT.(-.001).AND.SLM(MMD-1).LE.0.) SAS(MMD)=
    ISAS(MMD-1)*EAC(3)
    IF(SLM(MMD-1).GE.(0.03)) SAS(MMD)=SAS(MMD-1)*EAC(4)
    IF(SLM(MMD-1).LT.(0.03).AND.SLM(MMD-1).GE.(.001))
    ISAS(MMD)=SAS(MMD-1)*EAC(5)
    IF(SLM(MMD-1).LT..001.AND.SLM(MMD-1).GE.0.) SAS(MMD)=
    ISAS(MMD-1)*EAC(6)
    IF(SLM(MMD-1).LE.(-.1)) SAS(MMD)=SAS(MMD-1)*EACL
    IF(SLM(MMD-1).GE.1.) SAS(MMD)=SAS(MMD-1)*EACS
    IF(MMD.LE.2) GO TO 1624
    CALL REGULA(MMD,MERMD)
    IF(ABS(SAS(MMD-1)-SAS(MMD-2)).LE.0.0000003) SAS(MMD)=(XL+XR)*0.5
    GO TO 1624
57 WRITE(6,1239) MMD,SAS(MMD),SLM(MMD)
    WRITE(6,1248)
    SREC=SAS(MMD)
    MNB=MMD-1
    MMD=1
    KSCH=0
    LAG=0
    IF(SL(NH1-2).LE.0.) GO TO 470
    GO TO 471
470 KNUL=KNUL+1
    W=W-(DELW/FLOAT(KNUL+1))
    IF(KNUL.EQ.5) GO TO 26
    IF(JM.GT.4) GO TO 204
    WM(JM)=W
    GO TO 6102
471 KNUL=0
C GREEN CARD-THE END OF ELASTIC COMPUTATION*****
DO 14 I=1,NH
CUR(I)=(DN(I)-B(I)*Z(I))/SEI(I)
CURS(I)=CUR(I)
CURB(I)=CUR(I)+CURD(I)
STST(I)=-B(I)/(ES*AS(I))-CS(I)*CURS(I)
STSB(I)=CURS(I)*DS+STST(I)
STBT(I)=B(I)/(EB*AB)-CURB(I)*CB(I)
STBB(I)=B(I)/(EB*AB)+CURB(I)*CBD(I)
DN(I)=(-STST(I)+STTEN)/CUR(I)
IF(CUR(I).LT.0.0) DN(I)=(-STSB(I)+STTEN)/ABS(CUR(I))
IF(DN(I).GT.DS) DN(I)=DS
IF(DN(I).LT.0.0) DN(I)=0.0
14 CONTINUE
WRITE(6,330) (STBB(I),I=1,NH)
C CHECK FOR THE YIELDING OF THE PANELS
DO 52 I=1,NH
IF(ABS(STST(I)).LE.STSY.AND.STBB(I).LE.STBY) GO TO 52
IF(K.EQ.0) GO TO 53
DO 84 LL=1,K
IF(INELA(LL).EQ.I) GO TO 52
84 CONTINUE
53 K=K+1
INELA(K)=I
52 CONTINUE
IF(K.EQ.0) GO TO 55
SAS(MMD)=SREC

```

- MAI3710
- MAI3720
- MAI3730
- MAI3740
- MAI3750
- MAI3760
- MAI3770
- MAI3780
- MAI3790
- MAI3800
- MAI3810
- MAI3820
- MAI3830
- MAI3840
- MAI3850
- MAI3860
- MAI3870
- MAI3880
- MAI3890
- MAI3900
- MAI3910
- MAI3920
- MAI3930
- MAI3940
- MAI3950
- MAI3960
- MAI3970
- MAI3980
- MAI3990
- MAI4000
- MAI4010
- MAI4020
- MAI4030
- MAI4040
- MAI4050
- MAI4060
- MAI4070
- MAI4080
- MAI4090
- MAI4100
- MAI4110
- MAI4120
- MAI4130
- MAI4140
- MAI4150
- MAI4160
- MAI4170
- MAI4180
- MAI4190
- MAI4200
- MAI4210
- MAI4220
- MAI4230
- MAI4240
- MAI4250
- MAI4260
- MAI4270
- MAI4280
- MAI4290
- MAI4300
- MAI4310
- MAI4320
- MAI4330
- MAI4340
- MAI4350
- MAI4360
- MAI4370
- MAI4380
- MAI4390
- MAI4400
- MAI4410
- MAI4420
- MAI4430
- MAI4440

70	L=1	MAI4450
C	THE BEGINNING OF INELASTIC COMPUTATION-----	MAI4460
	KOUT(L)=K	MAI4470
	WRITE(6,72) (FAC(I),I=1,6)	MAI4480
	NE=NI-K	MAI4496
	NE1=NE+1	MAI4500
	KREPT=0	MAI4510
73	SL(1)=SAS(MMM)	MAI4520
	WRITE(6,315)MMM,SAS(MMM)	MAI4530
	NLAB=1	MAI4540
C	COMPUTATION OF THE ELASTIC PANELS	MAI4550
	I=1	MAI4560
765	Q(I)=(CV/(SL(I)-AV))+BV	MAI4570
	IF(SL(I).LT.0.0) Q(I)=-((CV/(ABS(SL(I))-AV))+BV)	MAI4580
	IF(I.EQ.LABAL(NLAB)) GO TO 56	MAI4590
	GO TO 67	MAI4600
56	NLAB=NLAB+1	MAI4610
	Q(I)=0.	MAI4620
67	AS1=AS11*BS(I)/BS1	MAI4630
	AS2=AS21*BS(I)/BS1	MAI4640
	CALL TERMS(I,EB,ES)	MAI4650
	IF(I-1) 700,700,701	MAI4660
701	B(I)=Q(I)+B(I-1)	MAI4670
	GO TO 702	MAI4680
700	B(I)=Q(I)	MAI4690
702	HB(I)=B(I)*ALP(I)*SS(I)+BB(I)	MAI4700
	SL(I+1)=SL(I)+HB(I)	MAI4710
	I=I+1	MAI4720
	IF(I.LT.NE1) GO TO 765	MAI4730
	DO 60 I=1,NE	MAI4740
	CUR(I)=(DM(I)-B(I)*Z(I))/SEI(I)	MAI4750
	CURS(I)=CUR(I)	MAI4760
	CURB(I)=CUR(I)+CURD(I)	MAI4770
	STST(I)=-D(I)/(ES*AS(I))-CS(I)*CURS(I)	MAI4780
	STSB(I)=CURS(I)*DS+STST(I)	MAI4790
	STBT(I)=B(I)/(EB*AB)-CURB(I)*CB(I)	MAI4800
	STBB(I)=B(I)/(EB*AB)+CURB(I)*CB(I)	MAI4810
	DN(I)=(-STST(I)+STTEN)/CUR(I)	MAI4820
	IF(CUR(I).LT.0.0) DN(I)=(-STSB(I)+STTEN)/ABS(CUR(I))	MAI4830
	IF(DN(I).GT.DS) DN(I)=DS	MAI4840
	IF(DN(I).LT.0.0) DN(I)=0.0	MAI4850
60	CONTINUE	MAI4860
	II=NE1	MAI4870
	Q(NE1)=(CV/(SL(NE1)-AV))+BV	MAI4880
	IF(NE1.EQ.LABAL(NLAB)) GO TO 113	MAI4890
	GO TO 200	MAI4900
113	NLAB=NLAB+1	MAI4910
	Q(NE1)=0.	MAI4920
200	B(II)=B(NE)+Q(NE1)	MAI4930
	WRITE(6,78) B(NE),Q(NE1),SL(NE1)	MAI4940
C	COMPUTATION OF THE INELASTIC PANNELS	MAI4950
1235	STSTT(II)=GST(II,4)	MAI4960
	STDBT(II)=CS(II,4)	MAI4970
	CURT(II)=GC(II,4)	MAI4980
	CURD1(II)=CURD(II)	MAI4990
	BMREP=BM(II)	MAI5000
	IF(MERM.EQ.MER1.OR.MERM.EQ.MER2) GO TO 11	MAI5010
	GO TO 68	MAI5020
11	IF(ABS(SAS(MMM-1)-SAS(MMM-2)).GT.0.0000001) GO TO 68	MAI5030
	SCAL2=SCAL1	MAI5040
	SCAL1=SCAL1*0.5	MAI5050
68	AS1=AS11*BS(II)/BS1	MAI5060
	AS2=AS21*BS(II)/BS1	MAI5070
	CALL STRAIN(B,BM,CURD1,II)	MAI5080
	BM(II)=BMREP	MAI5090
	IF(KKCC.GT.4.AND.NMM.EQ.1) GO TO 201	MAI5100
	IF(KKCC.GT.4.AND.NMM.NE.1) GO TO 202	MAI5110
	GO TO 6106	MAI5120
201	IF(KN.EQ.6) GO TO 26	MAI5130
	W=(WM(3)+WM(4))*0.5	MAI5140
	IF(KREPT.EQ.1) GO TO 6	MAI5150
	IF(KN.EQ.1) GO TO 6	MAI5160
	FACTOR=0.75	MAI5170
6	KI=KI+1	MAI5180

```

WRITE(6,6112)
GO TO 204
202 IF(KN.EQ.NCHA) GO TO 26
SAS(NMMD)=SAS(MMM-1)+(SAS(NMMD)-SAS(MMM-1))/5.
KN=KN+1
IF(KN.EQ.1) GO TO 4444
DO 6111 I=1,6
IF(I.LE.3) FAC(I)=(FAC(I)-1.)*FRACT+1.
IF(I.GE.4) FAC(I)=2.-FAC(I-3)
FAC2(I)=FAC(I)
6111 CONTINUE
4444 WRITE(6,6110)
GO TO 73
6106 CUR(I)=CUR1(I)
CURS(I)=CURS1(I)
CURB(I)=CURB1(I)
DN(I)=(-STST(I)+STTEN)/CUR(I)
IF(CUR(I).LT.0.) DN(I)={-STSB(I)+STTEN}/ABS(CUR(I))
IF(DN(I).GT.DS) DN(I)=DS
IF(DN(I).LT.0.) DN(I)=0.
STSB1(I)=STSB(I)+CUR1(I)*DC
ANTEG(I)=(STBT(I)-STSB1(I))*SS(I)
SL(I+1)=SL(I)+ANTEG(I)
Q(I+1)=(CV/(SL(I+1)-AV))+BV
IF(SL(I+1).LT.0.0) Q(I+1)=-((CV/(ABS(SL(I+1))-AV))+BV)
IF((I+1).EQ.LABAL(NLAB)) GO TO 104
GO TO 12
104 NLAB=NLAB+1
Q(I+1)=0.
12 IF(I-NH) 1234,1236,1236
1234 II=II+1
B(II)=B(II-1)+Q(II)
IF(B(II).GT.0.) GO TO 1233
KNEG=KNEG+1
SAS(NMMD)=SAS(NMMD)*FANEG
IF(KNEG.EQ.10) GO TO 26
GO TO 73
1236 ER11=0.
IF(ABS(CURB(NH)-CURP).LE.(ACURA*CURB(NH))) ER11=1.
CURP=CURB(NH)
SLN(NMMD)=SL(NH+1)
IF(ABS(SLN(NMMD)).LE.ER10.AND.ER11.EQ.1) GO TO 59
WRITE(6,1239)NM, SAS(NMMD),SL(NH+1)
WRITE(6,4333)
NMN=NMN+1
KNEG=0
IF(NMN.GT.NC) GO TO 26
IF(SLN(NMN-1).LE.(-.025)) SAS(NMMD)=SAS(NMN-1)*FAC(1)
IF(SLN(NMN-1).GT.(-.025).AND.SLN(NMN-1).LE.(-.002))
1SAS(NMMD)=SAS(NMN-1)*FAC(2)
IF(SLN(NMN-1).GT.(-.002).AND.SLN(NMN-1).LE.0.) SAS(NMMD)=
1SAS(NMN-1)*FAC(3)
IF(SLN(NMN-1).GE.(0.025)) SAS(NMMD)=SAS(NMN-1)*FAC(4)
IF(SLN(NMN-1).LT.(0.025).AND.SLN(NMN-1).GE.(.002))
1SAS(NMMD)=SAS(NMN-1)*FAC(5)
IF(SLN(NMN-1).LT..002.AND.SLN(NMN-1).GE.0.) SAS(NMMD)=
1SAS(NMN-1)*FAC(6)
SASRE=SAS(NMMD)
IF(NMN.LE.2) GO TO 73
CALL REGULA(NMN,MERD)
IF(ABS(SAS(NMN-1)-SAS(NMN-2)).LE.0.0000003) SAS(NMMD)=SASRE
GO TO 73
59 WRITE(6,1239)NM, SAS(NMMD),SL(NH+1)
WRITE(6,1248)
SREC=SAS(NMMD)
NRD=NRD-1
NMN=1
LAC=0
CURP=0.
MER2=100
MERD=0
NER1=100
SCAL1=1.
SCAL2=10.

```

```

MA15190
MA15200
MA15210
MA15220
MA15230
MA15240
MA15250
MA15260
MA15270
MA15280
MA15290
MA15300
MA15310
MA15320
MA15330
MA15340
MA15350
MA15360
MA15370
MA15380
MA15390
MA15400
MA15410
MA15420
MA15430
MA15440
MA15450
MA15460
MA15470
MA15480
MA15490
MA15500
MA15510
MA15520
MA15530
MA15540
MA15550
MA15560
MA15570
MA15580
MA15590
MA15600
MA15610
MA15620
MA15630
MA15640
MA15650
MA15660
MA15670
MA15680
MA15690
MA15700
MA15710
MA15720
MA15730
MA15740
MA15750
MA15760
MA15770
MA15780
MA15790
MA15800
MA15810
MA15820
MA15830
MA15840
MA15850
MA15860
MA15870
MA15880
MA15890
MA15900
MA15910
MA15920

```

C	THE END OF INELASTIC COMPUTATION	RED	MAI5930
	DO 433 I=1,NH		MAI5940
	CURT(I)=CURB(I)		MAI5950
	STBBT(I)=STBB(I)		MAI5960
	STSTT(I)=STST(I)		MAI5970
433	CONTINUE		MAI5980
	KO=K		MAI5990
	DO 62 I=1,NH		MAI6000
	IF(ABS(STST(I)).LE.STSY.AND.STBB(I).LE.STBY) GO TO 62		MAI6010
	DO 66 LL=1,K		MAI6020
	IF(INELA(LL).EQ.I) GO TO 62		MAI6030
66	CONTINUE		MAI6040
	K=K+1		MAI6050
	INELA(K)=I		MAI6060
62	CONTINUE		MAI6070
	L=L+1		MAI6080
	KOUT(L)=K		MAI6090
	KNEW=KOUT(L)-KO		MAI6100
	WRITE(6,2352)KNEW		MAI6110
	WRITE(6,1247)		MAI6120
	NE=NH-K		MAI6130
	NE1=NE+1		MAI6140
	MM=1		MAI6150
	IF(KNEW.EQ.0) GO TO 55		MAI6160
	SAS(MM)=SREC		MAI6170
	KREPT=1		MAI6180
	DO 74 I=1,NH		MAI6190
	GST(I,4)=STST(I)		MAI6200
	GC(I,4)=CURB(I)		MAI6210
74	GS(I,4)=STBB(I)		MAI6220
	GO TO 73		MAI6230
55	CONTINUE		MAI6240
	DO 76 I=1,NH		MAI6250
	CURT(I)=CURB(I)		MAI6260
	STBBT(I)=STBB(I)		MAI6270
	STSTT(I)=STST(I)		MAI6280
76	CONTINUE		MAI6290
	DO 1110 I=1,MM		MAI6300
	DSAS=SAS(I)-SREC		MAI6310
	RATS=SREC/SAS(I)		MAI6320
	WRITE(6,1117) I,DSAS,RATS,SAS(I),SLM(I)		MAI6330
1110	CONTINUE		MAI6340
	MM=1		MAI6350
	Q(NH)=(CV/(SL(NH1)-AV))+BV		MAI6360
	NE1=NH+1-K		MAI6370
	DO 432 I=1,NH		MAI6380
	BMBE(I)=CURB(I) * EB * BIT(I)		MAI6390
	BMSL(I)=CURS(I) * ES * SI(I)		MAI6400
	BMSL1(I)=BMSL(I)-ABS(B(I))*(CS(I)-DS/2.)		MAI6410
	BMFDC(I)=BMBE(I)+BMSL1(I)+B(I)*Z(I)		MAI6420
432	CONTINUE		MAI6430
	IF(K.EQ.0) GO TO 142		MAI6440
	DO 141 I=1,K		MAI6450
	IN1=INELA(I)		MAI6460
	BMBE(IN1)=BMB(IN1)		MAI6470
	BMSL(IN1)=BMS(IN1)		MAI6480
	BMSL1(IN1)=BMSL(IN1)-ABS(B(IN1))*(CS(IN1)-DS/2.)		MAI6490
	BMFDC(IN1)=BMM(IN1)		MAI6500
141	CONTINUE		MAI6510
142	CONTINUE		MAI6520
	DO 9951 I=1,NH		MAI6530
	IF(DN(I)-DS) 9950,9951,9950		MAI6540
9950	WRITE(6,9952) I,DN(I)		MAI6550
9951	CONTINUE		MAI6560
C			MAI6570
305	XX1(I)=.66666667*SD4		MAI6580
	AREA(I)=CUR(I)*.5*SD4		MAI6590
	TAREA(I)=AREA(I)		MAI6600
	DO 37 I=2,NH1		MAI6610
	XX1(I)=XX(I-1)		MAI6620
	AREA(I)=CUR(I-1)*SS(I-1)		MAI6630
37	TAREA(I)=TAREA(I-1)+AREA(I)		MAI6640
	REACT=TAREA(NH1)		MAI6650
	DO 38 J=1,NE1		MAI6660

```

DDIO=REACTX(J)
SUM=0.
DO 39 I=1,NH1
IF(XX1(I).GT.X(J)) GO TO 40
SUM=SUM+AREA(I)*(X(J)-XX1(I))
39 CONTINUE
40 DEF(J)=DDIO-SUM
38 CONTINUE
C
IF(W.EQ.0.0) GO TO 2
IF(W.GT.WW1.AND.W.LT.WW2) GO TO 2
CALL FINITE(DEF)
NEW=0
DO 210 I=1,NH
IF(EFW(I).GT.BS1) EFW(I)=BS1
BSB(I)=(CUR(I)/CURF(I))*BSB(I)
IF(DSB(I).GT.BS1) BSB(I)=BS1
BSS=BS(I)
IF(ABS(EFW(I)-BS(I)).GT.(.05*BSS)) NEW=NEW+1
BS(I)=EFW(I)
210 CONTINUE
WRITE(6,212) (BSB(I),I=1,NH)
WRITE(6,212) (BS(I),I=1,NH)
IF(NEW.GT.0) GO TO 1624
WRITE(6,9) ((SM(I),SM(I+500),SM(I+1000),SM(I+1500),SM(I+2000)),I=1
S,NN)
C
IF(NLAY.EQ.10) GO TO 1003
WRITE(6,10) ((SIGR(III,JJJ),JJJ=1,NLAY),III=1,NEL)
GO TO 1004
1003 WRITE(6,20) ((SIGR(III,JJJ),JJJ=1,NLAY),III=1,NEL)
1004 CONTINUE
2 CONTINUE
WRITE(6,3001) W,BMLL
WRITE(6,700B) BMTSP
WRITE(6,41) (DEF(I),I=1,NH1)
IF(JM.EQ.0.AND.NSHOR.EQ.1) GO TO 301
WRITE(6,412)
WRITE(6,411) ((X(I),Q(I),SL(I)),I=1,NH1)
WRITE(6,144)
WRITE(6,33) ((XX(I),STST(I),STSB(I),STBT(I),STBB(I),CUR(I),CURB(I),
1B(I)),I=1,NH)
WRITE(6,1502)
WRITE(6,1501) ((XX(I),BMSL(I),BNBE(I),BMFD(I),TOTBM(I),BMSL1(I)),I=
S1,NH)
IF(K.EQ.0) GO TO 145
WRITE(6,143) K,(INELA(L),L=1,K)
145 DO 93 I=1,NH
IF(STDB(I).GE.STBDF.OR.ABS(STBT(I)).GE.STBTF) GO TO 94
IF(ABS(STST(I)).GE.STSTF.OR.STSB(I).GE.STSBF) GO TO 95
93 CONTINUE
DO 90 I=1,NH1
IF(ABS(SL(I)).GE.SLMAX) GO TO 91
IF(DEF(I).GT.DEMAX) GO TO 5000
90 CONTINUE
GO TO 100
91 WRITE(6,96)
GO TO 26
94 WRITE(6,97) I,STBB(I),STBT(I)
GO TO 26
95 WRITE(6,98) I,STST(I),STSB(I)
GO TO 26
5000 WRITE(6,3000)
GO TO 26
100 IF(JM.GE.4) GO TO 6000
DO 901 I=1,NH
GS(I,JM)=STBBT(I)
CC(I,JM)=CURT(I)
CSL(I,JM)=SL(I)
901 CST(I,JM)=STSTT(I)
GO TO 6104
6000 DO 6001 I=1,NH
DO 6001 MJ=1,2
CS(I,MJ)=CS(I,MJ+1)

```

```

MAI6670
MAI6680
MAI6690
MAI6700
MAI6710
MAI6720
MAI6730
MAI6740
MAI6750
MAI6760
MAI6770
MAI6780
MAI6790
MAI6800
MAI6810
MAI6820
MAI6830
MAI6840
MAI6850
MAI6860
MAI6870
MAI6880
MAI6890
MAI6900
MAI6910
MAI6920
MAI6930
MAI6940
MAI6950
MAI6960
MAI6970
MAI6980
MAI6990
MAI7000
MAI7010
MAI7020
MAI7030
MAI7040
MAI7050
MAI7060
MAI7070
MAI7080
MAI7090
MAI7100
MAI7110
MAI7120
MAI7130
MAI7140
MAI7150
MAI7160
MAI7170
MAI7180
MAI7190
MAI7200
MAI7210
MAI7220
MAI7230
MAI7240
MAI7250
MAI7260
MAI7270
MAI7280
MAI7290
MAI7300
MAI7310
MAI7320
MAI7330
MAI7340
MAI7350
MAI7360
MAI7370
MAI7380
MAI7390
MAI7400

```

```

        CC(I,MJ)=CC(I,MJ+1)
        GST(I,MJ)=GST(I,MJ+1)
6001  CSL(I,MJ)=CSL(I,MJ+1)
        DO 6003 I=1,NH
        CS(I,3)=STBT(I)
        CC(I,3)=CURT(I)
        GSL(I,3)=SL(I)
6003  GST(I,3)=STSTT(I)
6104  IF (W.LE.WH8) GO TO 18
3000  FORMAT(* DEFLECTION EXCEEDS THE ALLOWABLE LIMIT*)
98    FORMAT(IH0,26HCONC CRUSHES IN PANEL NO. ,I4,I5H STRAINS ARE ,2E1
25.4)
97    FORMAT(IH0,32HEXCESSIVE YIELDING IN PANEL NO. ,I4,I5H STRAINS AR
1E ,2E15.4)
96    FORMAT(*FAILURE OF CONNECTOR(S)*)
143  FORMAT(IH0,*NO. AND INELASTIC PANELS *,I6,18I4/)
1501  FORMAT(1X, F8.2,5E16.8)
1502  FORMAT(IH0,6X,*XX*,12X,*BMSL*,12X,*BMBE*,12X,*BMFD*,12X,*TOTBM*)
33    FORMAT(IH0,F8.2,7E16.8)
144  FORMAT(IH0,5X,*XN*,13X,*STST*,12X,*STSB*,12X,*STBT*,12X,*STBB*,12X
1,*CUR*,13X,*CURB*,12X,*F*,/)
411  FORMAT(IH0,F8.2, F12.0,F12.7)
412  FORMAT(IH0,/,6X,*X*,8X,*Q*,10X,*SL*,/)
41    FORMAT(IH0,*DEF*,13F9.5)
7008  FORMAT(* TOTAL B.M. AT MID-SPAN*,F14.2)
3001  FORMAT(1X,///,* LIVE LOAD FORCE*,F11.3,8X,*LIVE LOAD MOMENT AT MID
1-SPAN*,F13.0)
212  FORMAT(10F10.2)
9952  FORMAT( * PANEL NO *,I3,5X,*DN*,F10.3)
1117  FORMAT( * NO*,I3,5X,*SLIP DIFF*,F9.7,5X,*RATIO*,F10.8,5X,*SAS*,
1F11.8,5X,*MID-SPAN SLIP*,F10.7)
2352  FORMAT(1X,* NO OF NEW YIELDED PANELS IS *,I4)
1248  FORMAT(*SSSSSSSSSS THIS IS LAST CYCLESSSSSSSSSS*)
4333  FORMAT(*-----*,/)
1239  FORMAT(* CYCLE*,I3,5X,*END SLIP ASSUMED*,F12.8,6X,*MID-SPAN SLIP*
1,F12.8)
6110  FORMAT(* THE VALUE OF SLIP IS REASSUMED-----
1-----*,/)
6112  FORMAT(* THE LOADING INCREMENT IS CHANGED TO A SMALL VALUE-----
1-----*,/)
1247  FORMAT(*SSSSSSSSSSSSSSSSSSSSSSSSSSSSSSSSSSSSSSSSSSSSSSSSSS*,/)
78    FORMAT(3F30.2)
3151  FORMAT(1X, * CYCLE NO *,I5,9X,*SLIP ASSUMED*,F20.8)
72    FORMAT(/,* FAC*,8F10.6,/)
330   FORMAT( * STBB*,8E15.5)
291   FORMAT(* ORIGINAL SLIP ASSUMED IS TOO SMALL*)
2858  FORMAT(//,* SLIP ASSUMED*,F15.6)
92    FORMAT(F8.0)
34    FORMAT(IH0,///,4H W =,F11.3)
312   FORMAT(IH0,F8.2,2E16.8)
311   FORMAT(IH0,/,6X,*X*,8X,*STBT*,10X,*STBB*,/)
303   FORMAT(////,* AT THIS LOADING THE D.L. EFFECT IS COMPUTED*)
7001  FORMAT( * MID-SPAN B.M. DUE TO D.L. *,F12.2)
99    FORMAT( * XX*,F8.2,8X,*B.M.DUE TO D.L.*,F12.2)
61    FORMAT(2I5)
71    FORMAT(40I3)
75    FORMAT(* PSEUDO CONNECTOR*,40I3)
64    FORMAT(* NEW CONNECTOR SPACING*,16F7.2)
35    FORMAT(* NO OF TOTAL CONN.AFTER INTRODUCING PSEUDO ONES*,I3,5X,
1=NO OF PSEUDO CONN.*,I3)
23    FORMAT(* CONNECTOR SPACING*,16F6.2)
32    FORMAT(16F5.1)
6005  FORMAT(* SLIP AND FORCE*,F7.4,F13.2)
140   FORMAT(2X,3E20.6)
7     FORMAT(2F10.6)
79    FORMAT(6F10.7,1!0)
7755  FORMAT(* NO*,I2,5X,*FAC*,F9.5,5X,*FAC2*,F9.5,5X,*EAC *,F9.5)
238   FORMAT(3F8.5)
237   FORMAT(2I10,4F10.6)
1000  FORMAT(5F15.4)
1     FORMAT(16I5)
85    FORMAT(7F15.2)
31    FORMAT(8F10.2)
MAI7410
MAI7420
MAI7430
MAI7440
MAI7450
MAI7460
MAI7470
MAI7480
MAI7490
MAI7500
MAI7510
MAI7520
MAI7530
MAI7540
MAI7550
MAI7560
MAI7570
MAI7580
MAI7590
MAI7600
MAI7610
MAI7620
MAI7630
MAI7640
MAI7650
MAI7660
MAI7670
MAI7680
MAI7690
MAI7700
MAI7710
MAI7720
MAI7730
MAI7740
MAI7750
MAI7760
MAI7770
MAI7780
MAI7790
MAI7800
MAI7810
MAI7820
MAI7830
MAI7840
MAI7850
MAI7870
MAI7880
MAI7890
MAI7900
MAI7910
MAI7920
MAI7930
MAI7940
MAI7950
MAI7960
MAI7970
MAI7980
MAI7990
MAI8000
MAI8010
MAI8020
MAI8030
MAI8040
MAI8050
MAI8060
MAI8070
MAI8080
MAI8090
MAI8100
MAI8110
MAI8120
MAI8130
MAI8140

```


50 FORMAT(8F15.5)
49 FORMAT(8F10.5)
5300 FORMAT(20A4)
5301 FORMAT(1X,20A4,///)
9 FORMAT(5E15.8)
10 FORMAT(8E15.8)
20 FORMAT(10F12.2)
26 STOP
END

MA18150
MA18160
MA18170
MA18180
MA18190
MA18200
MA18210
MA18220
MA18230



C
C

```

SUBROUTINE DATA
*****
*****
COMMON/BLOCK1A/NLAYS1,NLAYS2
COMMON/BLOCK3A/ AS11,AS21,WWW1,WWW2,NU
COMMON/BLOCK3/STSY,STRSY,STRPY,STRNY,STRFY,EB,STFY,ES,ERP
COMMON/BLOCK5A/ NSP,JNSP(80),KTYPE(80),SK(80),SSTIF
COMMON/BLOCK 15/STRESST
COMMON/BLOCK 22/ AS1,AS2,DAS1,DAS2,STRYIE,STRYIE,STTEN
COMMON D(6,6),DD(6,6),A(15,15),AK(15,15),S(15,15),TR(15,15),XXX(77
*) ,YYY(77),NI(100),NJ(100),NK(100),KMAX(100),KB(100),FF(3),FG(385),
SNP(15),T(10),H(11),ZZ(10),NR(15),EPW(10),BMSL1(20), AC(15),
SP(3,15),EE(100,10),EE1(100,10),SIGR(100,10),SIGV(100,10),SIGS(100,
S10),SM(13J00),NN,NEL,NN1,NN2,NLAY,NIN,NSM,NB1,NUU,CAL,EMU,NALAW,AN
SUM,ND(77,5)
READ (5,*) NN,NEL,NN1,NN2,NLAY,NIN,NSM,NALAW
WRITE(6,1) NN,NEL,NN1,NN2,NLAY,NIN,NSM,NALAW
READ (5,*) (T(J),J=1,NLAY)
WRITE(6,2) (T(J),J=1,NLAY)
NLAY1=NLAY+1
READ (5,*)(H(J),J=1,NLAY1)
WRITE(6,2)(H(J),J=1,NLAY1)
READ (5,*)(ZZ(J),J=1,NLAY)
WRITE(6,2)(ZZ(J),J=1,NLAY)
READ (5,*) ES,EB,EMU,ANUM
WRITE(6,3) ES,EB,EMU,ANUM
READ (5,*) STRESST
WRITE(6,3) STRESST
STTEN=STRESST/ES
READ (5,*) AS11,AS21,DAS1,DAS2,STRYIE
WRITE(6,2) AS11,AS21,DAS1,DAS2,STRYIE
STRYIE=STRYIE/EB
READ (5,*) NLAYS1,NLAYS2
WRITE(6,1) NLAYS1,NLAYS2
READ (5,*) WWW1,WWW2
WRITE(6,3) WWW1,WWW2
DO 13 I=1,NN
READ (5,*) XXX(I),YYY(I)
13 CONTINUE
DO 19 N=1,NEL
READ (5,*) NI(N),NJ(N),NK(N)
19 CONTINUE
READ (5,1) ((ND(I,J),J=1,5),I=1,NN)
NU=1
DO 106 J=1,NN
DO 106 K=1,5
IF(ND(J,K).EQ.0) GO TO 106
ND(J,K)=NU
NU=NU+1
106 CONTINUE
WRITE(6,1) ((ND(I,J),J=1,5),I=1,NN)
READ (5,*) NSP,SSTIF
IF(NSP.EQ.0) GO TO 14
DO 15 I=1,NSP
READ (5,*) JNSP(I),KTYPE(I),SK(I)
15 CONTINUE
14 CONTINUE
1 FORMAT (16I5)
2 FORMAT (11F12.5)
3 FORMAT (3E15.0,F10.5)
RETURN
END

```

```

DAT 10
DAT 20
DAT 30
DAT 40
DAT 50
DAT 60
DAT 70
DAT 80
DAT 90
DAT 100
DAT 110
DAT 120
DAT 130
DAT 140
DAT 150
DAT 160
DAT 170
DAT 180
DAT 190
DAT 200
DAT 210
DAT 220
DAT 230
DAT 240
DAT 250
DAT 260
DAT 270
DAT 280
DAT 290
DAT 300
DAT 310
DAT 320
DAT 330
DAT 340
DAT 350
DAT 360
DAT 370
DAT 380
DAT 390
DAT 400
DAT 410
DAT 420
DAT 430
DAT 440
DAT 450
DAT 460
DAT 470
DAT 480
DAT 490
DAT 500
DAT 510
DAT 520
DAT 530
DAT 540
DAT 550
DAT 560
DAT 570
DAT 580
DAT 590
DAT 600
DAT 610

```

C
C

```

SUBROUTINE GEOMET
*****
*****
COMMON/BLOCK1A/NLAYS1,NLAYS2
COMMON D(6,6),DD(6,6),A(15,15),AK(15,15),S(15,15),TR(15,15),XXX(77
),YYY(77),NI(100),NJ(100),NK(100),KMAX(100),KB(100),FF(5),FC(385),
SNP(15),TY(10),H(11),ZZ(10),NR(10),EFW(10),BBSL1(20),AC(15),
SP(3,15),EE(100,10),EE1(100,10),SIGR(100,10),SIGV(100,10),SIGC(100,
)10),SM(13500),NN,NEL,NN1,NN2,NLAY,NIN,NSH,NB1,NUU,CAL,ENU,NALAW,AN
SUM,ND(77,5)
MAX=0
ND=0
DO 1 J=1,NEL
IN=NI(J)
JN=NJ(J)
KN=NK(J)
NP(1)=ND(IN,1)
NP(2)=ND(JN,1)
NP(3)=ND(KN,1)
NP(4)=ND(IN,2)
NP(5)=ND(JN,2)
NP(6)=ND(KN,2)
NP(7)=ND(IN,3)
NP(8)=ND(IN,4)
NP(9)=ND(IN,5)
NP(10)=ND(JN,3)
NP(11)=ND(JN,4)
NP(12)=ND(JN,5)
NP(13)=ND(KN,3)
NP(14)=ND(KN,4)
NP(15)=ND(KN,5)
MAX=0
MIN=3000
DO 127 I=1,15
IF(NP(I).EQ.0) GO TO 127
IF(NP(I)-MAX) 128,128,129
129 MAX=NP(I)
128 IF(NP(I)-MIN) 130,127,127
130 MIN=NP(I)
127 CONTINUE
NB1=MAX-NIN
IF(NB1.GT.NB) NB=NB1
KB(J)=NB
IF(MAX.GT.MAXD) MAXX=MAX
KMAX(J)=MAXX
YJ=ABS(XXX(JN)-XXX(IN))
YK=ABS(XXX(KN)-XXX(IN))
XK=ABS(YYY(KN)-YYY(IN))
YCG=YJ/2.
XCG=XK/4.
AL11=XK*YJ/2.
AL21=XK**2.*YJ/6.
AL31=XK**3.*YJ/12.
AL13=XK*YJ*(YJ**2.+YJ*YK+YK**2.)/12.
AL12=XK*YJ*(YJ+YK)/6.
AL22=(XK**2.)*YJ*(YJ+2.*YK)/24.
DO 115 I=1,15
DO 115 JJ=1,15
A(I,JJ)=0.0
TR(I,JJ)=0.0
115 CONTINUE
A(1,1)=1.
A(2,1)=1.
A(2,3)=YJ
A(3,1)=1.
A(3,2)=XK
A(3,3)=YK
A(4,4)=1.
A(5,4)=1.
A(5,6)=YJ
A(6,4)=1.
A(6,5)=XK
A(6,6)=YK
A(7,7)=1.

```

```

GEO 10
GEO 20
GEO 30
GEO 40
GEO 50
GEO 60
GEO 70
GEO 80
GEO 90
GEO 100
GEO 110
GEO 120
GEO 130
GEO 140
GEO 150
GEO 160
GEO 170
GEO 180
GEO 190
GEO 200
GEO 210
GEO 220
GEO 230
GEO 240
GEO 250
GEO 260
GEO 270
GEO 280
GEO 290
GEO 300
GEO 310
GEO 320
GEO 330
GEO 340
GEO 350
GEO 360
GEO 370
GEO 380
GEO 390
GEO 400
GEO 410
GEO 420
GEO 430
GEO 440
GEO 450
GEO 460
GEO 470
GEO 480
GEO 490
GEO 500
GEO 510
GEO 520
GEO 530
GEO 540
GEO 550
GEO 560
GEO 570
GEO 580
GEO 590
GEO 600
GEO 610
GEO 620
GEO 630
GEO 640
GEO 650
GEO 660
GEO 670
GEO 680
GEO 690
GEO 700
GEO 710
GEO 720
GEO 730

```

```

A(8,9)=1.
A(9,8)=-1.
A(10,7)=1.
A(10,9)=YJ
A(10,12)=YJ**2.
A(10,15)=YJ**3.
A(11,9)=1.
A(11,12)=2.*YJ
A(11,15)=3.*YJ**2.
A(12,8)=-1.
A(12,11)=-YJ
A(13,7)=1.
A(13,8)=XK
A(13,9)=YK
A(13,10)=XK**2.
A(13,11)=XK*YK
A(13,12)=YK**2.
A(13,13)=XK**3.
A(13,14)=(XK**2.)*YK
A(13,15)=YK**3.
A(14,9)=1.
A(14,11)=XK
A(14,12)=2.*YK
A(14,14)=XK**2.
A(14,15)=3.*YK**2.
A(15,8)=-1.
A(15,10)=-2.*XK
A(15,11)=-YK
A(15,13)=-3.*XK**2.
A(15,14)=-2.*XK*YK
CALL INVMAT(A,15,15,1.E-8,11,NB)
WRITE(1)((A(M,MM),MM=1,15),M=1,15),YJ,YK,XK,YCG,XCG,AL11,AL21,AL3
S1,AL13,AL12,AL22
C1=(XXX(JN)-XXX(IN))*(YYY(KN)-YYY(IN))
F1=ABS(XXX(JN)-XXX(IN))
AG1=-ABS(C1)
ANZ=C1/AG1
ALY=(XXX(JN)-XXX(IN))/F1
AFEX=-ANZ*ALY
TR(1,4)=ANX
TR(2,5)=ANX
TR(3,6)=ANX
TR(4,1)=ALY
TR(5,2)=ALY
TR(6,3)=ALY
TR(7,7)=ANZ
TR(8,9)=ANX
TR(9,8)=ALY
TR(10,10)=ANZ
TR(11,12)=ANX
TR(12,11)=ALY
TR(13,13)=ANZ
TR(14,15)=ANX
TR(15,14)=ALY
WRITE(1)((TR(M,MM),MM=1,15),M=1,15),(NP(K),K=1,15)
DO 120 JJ=1,NLAY
DO 160 MM=1,6
DO 160 NM=1,6
D(EM,MM)=0.0
CONTINUE
D(1,1)=T(JJ)
D(3,2)=D(1,1)
D(1,4)=-.5*(H(JJ+1)**2.-H(JJ)**2.)
D(2,5)=D(1,4)
D(4,1)=D(1,4)
D(5,2)=D(2,5)
D(4,4)=(H(JJ+1)**3.-H(JJ)**3.)/3.
D(5,5)=D(4,4)
IF(JJ.EQ.NLAYS1.OR.JJ.EQ.NLAYS2) GO TO 140
D(1,2)=T(JJ)*EMU
D(2,1)=D(1,2)
D(3,3)=((1.-EMU)/2.)*T(JJ)
D(1,5)=EMU*D(1,4)
D(2,4)=D(1,5)

```

160

GEO 740
GEO 750
GEO 760
GEO 770
GEO 780
GEO 790
GEO 800
GEO 810
GEO 820
GEO 830
GEO 840
GEO 850
GEO 860
GEO 870
GEO 880
GEO 890
GEO 900
GEO 910
GEO 920
GEO 930
GEO 940
GEO 950
GEO 960
GEO 970
GEO 980
GEO 990
GEO1000
GEO1010
GEO1020
GEO1030
GEO1040
GEO1050
GEO1060
GEO1070
GEO1080
GEO1090
GEO1100
GEO1110
GEO1120
GEO1130
GEO1140
GEO1150
GEO1160
GEO1170
GEO1180
GEO1190
GEO1200
GEO1210
GEO1220
GEO1230
GEO1240
GEO1250
GEO1260
GEO1270
GEO1280
GEO1290
GEO1300
GEO1310
GEO1320
GEO1330
GEO1340
GEO1350
GEO1360
GEO1370
GEO1380
GEO1390
GEO1400
GEO1410
GEO1420
GEO1430
GEO1440
GEO1450
GEO1460
GEO1470

```

D(3,6)=-((1.-EMU)/4.)*(H(JJ+1)**2.-E(JJ)**2.)
D(5,1)=D(1,5)
D(4,2)=D(2,6)
D(6,3)=D(3,6)
D(4,3)=EMU*D(4,4)
D(5,4)=D(4,5)
D(6,6)=(1.-EMU)/2.*D(4,4)
140 WRITE(1) ((D(L,LL),LL=1,6),L=1,6)
120 CONTINUE
1 CONTINUE
NB=KB(NEL)
NB1=NB
NUU=KMAX(NEL)
RETURN
END

```

- GEO1480
- GEO1490
- GEO1500
- GEO1510
- GEO1520
- GEO1530
- GEO1540
- GEO1550
- GEO1560
- GEO1570
- GEO1580
- GEO1590
- GEO1600
- GEO1610
- GEO1620

	SUBROUTINE ASM	ASM 10

C	*****	
	COMMON/BLOCK1A/NLAYS1,NLAYS2	ASM 20
	COMMON/BLOCK3A/ NSP,JNSP(80),KTYPE(80),SK(80),SSTIF	ASM 30
	COMMON D(6,6),DD(6,6),A(15,15),AK(15,15),S(15,15),TR(15,15),XXX(77	ASM 40
),YYY(77),NI(100),NJ(100),NK(100),KMAX(100),KB(100),FF(5),FG(385),	ASM 50
	SNP(15),T(10),H(11),ZZ(10),NR(15),EFW(10),BMSL(20),	ASM 60
	SP(3,15),EE(100,10),EE1(100,10),SIGR(100,10),SIGV(100,10),SIGC(100,	ASM 70
	810),SM(13500),NN,NEL,NN1,NN2,NLAY,NIN,NSM,NB1,NUU,CAL,EMU,NALAW,AN	ASM 80
	SUM,ND(77,5)	ASM 90
	DO 1 K=1,NSM	ASM 100
	SM(K)=0.0	ASM 110
1	CONTINUE	ASM 120
	DO 10 N=1,NEL	ASM 130
	READ(1) ((A(L,ND),MM=1,15),L=1,15),YJ,YK,XK,YCC,XCC,AL11,AL21,AL3	ASM 140
	S1,AL13,AL12,AL22	ASM 150
	READ(1) ((TR(LL,LD),LM=1,15),LL=1,15),(NP(LK),LK=1,15)	ASM 160
	CONSM=0.	ASM 170
	DO 20 II=1,6	ASM 180
	DO 20 JJ=1,6	ASM 190
	DD(II,JJ)=0.	ASM 200
20	CONTINUE	ASM 210
	DO 30 JJ=1,NLAY	ASM 220
	IF(EE(M,JJ).NE.EE1(M,JJ)) CONSM=CONSM+1.	ASM 230
	READ(1) ((D(L,LL),LL=1,6),L=1,6)	ASM 240
	EER=EE(M,JJ)/(1.-EMU**2.)	ASM 250
	IF(JJ.EQ.NLAYS1.OR.JJ.EQ.NLAYS2) EER=EE(M,JJ)	ASM 260
	DO 40 III=1,6	ASM 270
	DO 40 JJJ=1,6	ASM 280
	DD(III,JJJ)=DD(III,JJJ)+EER*D(III,JJJ)	ASM 290
40	CONTINUE	ASM 300
30	CONTINUE	ASM 310
	IF(CAL.EQ.1.) GO TO 90	ASM 320
	READ(2) ((AK(JII,IJJ),IJJ=1,15),JII=1,15).	ASM 330
	IF(CONSM.EQ.0.) GO TO 100	ASM 340
90	CALL STIFEL(AL11,AL12,AL13,AL21,AL31,AL22)	ASM 350
100	WRITE(4) ((AK(IIJ,JJI),JJI=1,15),IIJ=1,15)	ASM 360
	DO 50 J=1,15	ASM 370
	IF(NP(J).EQ.0) GO TO 50	ASM 380
	DO 60 I=J,15	ASM 390
	IF(NP(I).EQ.0) GO TO 60	ASM 400
	IF(NP(J)-NP(I)) 70,80,80	ASM 410
80	K=(NP(I)-1)*NB1+NP(J)	ASM 420
	SM(K)=SM(K)+AK(J,I)	ASM 430
	GO TO 60	ASM 440
70	K=(NP(J)-1)*NB1+NP(I)	ASM 450
	SM(K)=SM(K)+AK(J,I)	ASM 460
60	CONTINUE	ASM 470
50	CONTINUE	ASM 480
10	CONTINUE	ASM 490
	IF(NSP.EQ.0) GO TO 130	ASM 500
	NB=NB1+1	ASM 510
	DO 120 NKJ=1,NSP	ASM 520
	KT=KTYPE(NKJ)	ASM 530
	JN=JNSP(NKJ)	ASM 540
	IS=ND(JN,KT)	ASM 550
	ISS=(IS-1)*NB+1	ASM 560
	SM(ISS)=SM(ISS)+SM(NKJ)	ASM 570
120	CONTINUE	ASM 580
130	CONTINUE	ASM 590
	REWIND 2	ASM 600
	REWIND 4	ASM 610
	DO 110 IIK=1,NEL	ASM 620
	READ(4) ((AK(IIJ,JJI),JJI=1,15),IIJ=1,15)	ASM 630
	WRITE(2) ((AK(JII,IJJ),IJJ=1,15),JII=1,15)	ASM 640
110	CONTINUE	ASM 650
	RETURN	ASM 660
	END	ASM 670
		ASM 680

	SUBROUTINE STIFEL (AL11,AL12,AL13,AL21,AL31,AL22)	STI	10

	COMMON B(6,6),DD(6,6),A(15,15),AK(15,15),S(15,15),TR(15,15),XXX(77	STI	20
	B),YYY(77),NI(100),NJ(100),NK(100),KNAX(100),KB(100),FF(5),FG(385),	STI	30
	SNP(15),T(10),H(11),ZZ(10),NR(15),EFW(10),BMSL1(20),AC(15),	STI	40
	SP(3,15),EE(100,10),EE1(100,10),SIGR(100,10),SIGV(100,10),SIGS(100,	STI	50
	S10),SM(13500),NN,NEL,NN1,NN2,NLAY,NIN,NSM,NB1,NUU,CAL,EMU,NALAW,AN	STI	60
	SUM,ND(77,5)	STI	70
	DO 20 J=1,15	STI	80
	DO 20 IJ=1,15	STI	90
	AK(J,IJ)=0.0	STI	100
	S(J,IJ)=0.0	STI	110
20	CONTINUE	STI	120
	S(2,2)=DD(1,1)*AL11	STI	130
	S(2,6)=DD(1,2)*AL11	STI	140
	S(2,10)=2.*DD(1,4)*AL11	STI	150
	S(2,12)=2.*DD(1,5)*AL11	STI	160
	S(2,13)=6.*DD(1,4)*AL21	STI	170
	S(2,14)=2.*DD(1,4)*AL12	STI	180
	S(2,15)=6.*DD(1,5)*AL12	STI	190
	S(3,3)=DD(3,3)*AL11	STI	200
	S(3,5)=S(3,3)	STI	210
	S(3,11)=2.*DD(3,6)*AL11	STI	220
	S(3,14)=4.*DD(3,6)*AL21	STI	230
	S(5,3)=S(3,3)	STI	240
	S(5,5)=S(3,3)	STI	250
	S(5,11)=S(3,11)	STI	260
	S(5,14)=S(3,14)	STI	270
	S(6,2)=DD(2,1)*AL11	STI	280
	S(6,6)=DD(2,2)*AL11	STI	290
	S(6,10)=2.*DD(2,4)*AL11	STI	300
	S(6,12)=2.*DD(2,5)*AL11	STI	310
	S(6,13)=6.*DD(2,4)*AL21	STI	320
	S(6,14)=2.*DD(2,4)*AL12	STI	330
	S(6,15)=6.*DD(2,5)*AL12	STI	340
	S(10,2)=S(2,10)	STI	350
	S(12,2)=S(2,12)	STI	360
	S(13,2)=S(2,13)	STI	370
	S(14,2)=S(2,14)	STI	380
	S(15,2)=S(2,15)	STI	390
	S(11,3)=S(3,11)	STI	400
	S(14,3)=S(3,14)	STI	410
	S(11,5)=S(5,11)	STI	420
	S(14,5)=S(5,14)	STI	430
	S(10,6)=S(6,10)	STI	440
	S(12,6)=S(6,12)	STI	450
	S(13,6)=S(6,13)	STI	460
	S(14,6)=S(6,14)	STI	470
	S(15,6)=S(6,15)	STI	480
	S(10,10)=4.*DD(4,4)*AL11	STI	490
	S(10,12)=4.*DD(4,5)*AL11	STI	500
	S(10,13)=12.*DD(4,4)*AL21	STI	510
	S(10,14)=4.*DD(4,4)*AL12	STI	520
	S(10,15)=12.*DD(4,5)*AL12	STI	530
	S(11,11)=4.*DD(6,6)*AL11	STI	540
	S(11,14)=8.*DD(6,6)*AL21	STI	550
	S(12,12)=4.*DD(5,5)*AL11	STI	560
	S(12,13)=12.*DD(5,4)*AL21	STI	570
	S(12,14)=4.*DD(5,4)*AL12	STI	580
	S(12,15)=12.*DD(5,5)*AL12	STI	590
	S(13,13)=36.*DD(4,4)*AL31	STI	600
	S(13,14)=12.*DD(4,4)*AL22	STI	610
	S(13,15)=36.*DD(4,5)*AL22	STI	620
	S(14,14)=4.*DD(4,4)*AL13+16.*DD(6,6)*AL31	STI	630
	S(14,15)=12.*DD(4,5)*AL13	STI	640
	S(15,15)=36.*DD(5,5)*AL13	STI	650
	S(12,10)=S(10,12)	STI	660
	S(13,10)=S(10,13)	STI	670
	S(14,10)=S(10,14)	STI	680
	S(15,10)=S(10,15)	STI	690
	S(14,11)=S(11,14)	STI	700
	S(13,12)=S(12,13)	STI	710
	S(14,12)=S(12,14)	STI	720
		STI	730

S(15,12)=S(12,15)
S(14,13)=S(13,14)
S(15,13)=S(13,15)
S(15,14)=S(14,15)
CALL MULTP (A,S,AK,15,15,15,1,15,15,15)
CALL MULTP (AK,A,S,15,15,15,0,15,15,15)
CALL MULTP (TR,S,A,15,15,15,1,15,15,15)
CALL MULTP (A,TR,AK,15,15,15,0,15,15,15)
RETURN
END

STI 740
STI 750
STI 760
STI 770
STI 780
STI 790
STI 800
STI 810
STI 820
STI 830

	SUBROUTINE FINITE(DEF)	FIN 10

C	*****	FIN 20
C	DIMENSION DEF(20),DEF(31)	FIN 30
	DIMENSION PP(15)	FIN 40
	COMMON/BLOCK1A/NLAYS1,NLAYS2	FIN 50
	COMMON/BLOCK2A/B(40)	FIN 60
	COMMON/BLOCK4/BMS(40),BMB(40),BIT(40),TW,TF,BF,DS,AB,DC	FIN 70
	COMMON/BLOCK3/STSY,STRSY,STRPY,STRWY,STRFY,EB,STFY,ES,EBP	FIN 80
	COMMON/BLOCK3A/NSP,JNSP(80),KTYPE(80),SK(80),SSTIF	FIN 90
	COMMON/BLOCK7A/CURF(20),BSB(20)	FIN 100
	COMMON/BLOCK 15/STRESST	FIN 110
	COMMON/BLOCK 22/AS1,AS2,DAS1,DAS2,STYIE,STRYIE,STTEN	FIN 120
	COMMON/BLOCK25/MA,JM,NH,KER,KEM2	FIN 130
	COMMON D(6,6),DD(6,6),A(15,15),AK(15,15),S(15,15),TR(15,15),XXX(77	FIN 140
),YYY(77),NI(100),NJ(100),NK(100),KMAX(100),KB(100),FF(5),FG(385),	FIN 150
	SNP(15),T(10),H(11),ZZ(10),NR(15),EFW(10),BMSL1(20),	FIN 160
	AG(15),	FIN 170
	SP(3,15),EE(100,10),EE1(100,10),SICR(100,10),SICV(100,10),SICG(100,	FIN 180
	S10),SM(13500),NN,NEL,NN1,NN2,NLAY,NIN,NSM,NB1,NUU,CAL,EMU,NALAW,AN	FIN 190
	SUM,ND(77,5)	FIN 200
	NCYCL=1	FIN 210
490	CONTINUE	FIN 220
	REWIND 1	FIN 230
	REWIND 2	FIN 240
	REWIND 3	FIN 250
	REWIND 4	FIN 260
	IF(CAL.GT.1.) GO TO 1	FIN 270
	DO 2 I=1,NEL	FIN 280
	DO 2 J=1,NLAY	FIN 290
	EE(I,J)=ES	FIN 300
	EE1(I,J)=ES	FIN 310
	IF(J.EQ.NLAYS1.OR.J.EQ.NLAYS2) EE(I,J)=EB	FIN 320
	IF(J.EQ.NLAYS1.OR.J.EQ.NLAYS2) EE1(I,J)=EB	FIN 330
2	CONTINUE	FIN 340
1	CONTINUE	FIN 350
	DO 700 I=1,NUU	FIN 360
	FG(I)=0.0	FIN 370
700	CONTINUE	FIN 380
	NNL=NH+1	FIN 390
	CONF=0.0	FIN 400
	DO 10 I=1,NEL	FIN 410
	DO 10 J=1,NLAY	FIN 420
	IF(EE(I,J).NE.EE1(I,J)) CONF=CONF+1.	FIN 430
	IF(CONF.GT.0.) GO TO 14	FIN 440
10	CONTINUE.	FIN 450
14	IF(CONF.EQ.0.0.AND.CAL.GT.1.) GO TO 40	FIN 460
	CALL ASM	FIN 470
	WRITE(3) (SM(K),K=1,NSM)	FIN 480
	GO TO 50	FIN 490
40	READ(3) (SM(K),K=1,NSM)	FIN 500
50	JNU=NIN	FIN 510
	NH1=NH+1	FIN 520
	DEF1(I)=DEF(NH1)	FIN 530
	DO 3 JR=2,NH1	FIN 540
	DEF1(JR)=DEF(NH1)-DEF(JR-1)	FIN 550
3	CONTINUE.	FIN 560
	I=1	FIN 570
	DO 60 J=1,NNL	FIN 580
	FF(1)=0.	FIN 590
	FF(2)=0.	FIN 600
	FF(3)=0.	FIN 610
	FF(4)=0.	FIN 620
	FF(5)=0.	FIN 630
	IF(I.GT.2) GO TO 70	FIN 640
	IF(I.EQ.1) FF(1)=B(1)*2./(5.*ANUTD)	FIN 650
	IF(I.EQ.2) FF(1)=B(1)*3./(5.*ANUTD)	FIN 660
	GO TO 80	FIN 670
70	FF(1)=(B(I-1)-B(I-2))/ANUM	FIN 680
80	FF(3)=DEF1(I)*SSTIF	FIN 690
	I=I+1	FIN 700
	DO 90 L=1,5	FIN 710
	IF(ND(JNU,L).EQ.0) GO TO 90	FIN 720
	IK=ND(JNU,L)	FIN 730
	FG(IK)=FG(IK)+FF(L)	

```

90 CONTINUE
JNU=JNU+NR1
60 CONTINUE
DET=1.E-8
NB=NB1+1
CALL BAND (SM,FG,NUU,NB,1,DET)
IF (DET) 156,157,158
156 WRITE(6,159) DET
GO TO 1000
157 WRITE(6,160) DET
GO TO 1000
158 CONTINUE
DO 300 K=1,NSM
SM(K)=0.0
300 CONTINUE
II=0
DO 310 I=1,NN
DO 310 J=1,5
IF (ND (I,J).EQ.0) GO TO 320
II=II+1
IF (J.EQ.1) SM(I)=FG(II)
IF (J.EQ.2) SM(I+500)=FG(II)
IF (J.EQ.3) SM(I+1000)=FG(II)
IF (J.EQ.4) SM(I+1500)=FG(II)
IF (J.EQ.5) SM(I+2000)=FG(II)
GO TO 310
320 IF (J.EQ.1) SM(I)=0.0
IF (J.EQ.2) SM(I+500)=0.0
IF (J.EQ.3) SM(I+1000)=0.0
IF (J.EQ.4) SM(I+1500)=0.0
IF (J.EQ.5) SM(I+2000)=0.0
310 CONTINUE
REWIND 1
DO 330 N=1,NEL
READ(1) ((A(L,MD),MD=1,15),L=1,15),YJ,YK,XK,YCG,XCG,AL11,AL21,AL3
S1,AL13,AL12,AL22
READ(1) ((TR(LL,LM),LM=1,15),LL=1,15),(NP(LK),LK=1,15)
I=NI(N)
J=NJ(N)
K=NK(N)
AC(1)=SM(I)
AC(2)=SM(J)
AC(3)=SM(K)
AC(4)=SM(I+500)
AC(5)=SM(J+500)
AC(6)=SM(K+500)
AC(7)=SM(I+1000)
AC(8)=SM(I+1500)
AC(9)=SM(I+2000)
AC(10)=SM(J+1000)
AC(11)=SM(J+1500)
AC(12)=SM(J+2000)
AC(13)=SM(K+1000)
AC(14)=SM(K+1500)
AC(15)=SM(K+2000)
DO 351 NR=1,15
PP(NR)=0.0
DO 351 LR=1,15
PP(NR)=PP(NR)+TR(NR,LR)*AC(LR)
351 CONTINUE
DO 352 NR=1,13
S(NR,1)=0.0
DO 352 LR=1,15
S(NR,1)=S(NR,1)+A(NR,LR)*PP(LR)
352 CONTINUE
DO 350 JJ=1,NLAY
READ(1) ((D(L,LL),LL=1,6),L=1,6)
EMUL=ENU
EL=EE(N,JJ)/(1.-EMU**2.)
IF (JJ.EQ.NLAYS1.OR.JJ.EQ.NLAYS2) EMUL=0.0
IF (JJ.EQ.NLAYS1.OR.JJ.EQ.NLAYS2) EL=EE(N,JJ)
DO 354 NR=1,3
DO 354 LR=1,15
P(NR,LR)=0.0

```

```

FIN 740
FIN 750
FIN 760
FIN 770
FIN 780
FIN 790
FIN 800
FIN 810
FIN 820
FIN 830
FIN 840
FIN 850
FIN 860
FIN 870
FIN 880
FIN 890
FIN 900
FIN 910
FIN 920
FIN 930
FIN 940
FIN 950
FIN 960
FIN 970
FIN 980
FIN 990
FIN1000
FIN1010
FIN1020
FIN1030
FIN1040
FIN1050
FIN1060
FIN1070
FIN1080
FIN1090
FIN1100
FIN1110
FIN1120
FIN1130
FIN1140
FIN1150
FIN1160
FIN1170
FIN1180
FIN1190
FIN1200
FIN1210
FIN1220
FIN1230
FIN1240
FIN1250
FIN1260
FIN1270
FIN1280
FIN1290
FIN1300
FIN1310
FIN1320
FIN1330
FIN1340
FIN1350
FIN1360
FIN1370
FIN1380
FIN1390
FIN1400
FIN1410
FIN1420
FIN1430
FIN1440
FIN1450
FIN1460
FIN1470

```

```

354 CONTINUE
P(1,2)=EMUL*EL
P(1,6)=EL
P(1,10)=-2.*ZZ(JJ)*EMUL*EL
P(1,12)=-2.*ZZ(JJ)*EL
P(1,13)=-6.*ZZ(JJ)*YCC*EMUL*EL
P(1,14)=-2.*ZZ(JJ)*YCC*EMUL*EL
P(1,18)=-6.*ZZ(JJ)*YCC*EL
P(2,2)=EL
P(2,6)=EMUL*EL
P(2,10)=-2.*ZZ(JJ)*EL
P(2,12)=-2.*ZZ(JJ)*EMUL*EL
P(2,13)=-6.*ZZ(JJ)*YCC*EL
P(2,14)=-2.*ZZ(JJ)*YCC*EL
P(2,15)=-6.*ZZ(JJ)*YCC*EMUL*EL
IF(JJ.EQ.NLAYS1.OR.JJ.EQ.NLAYS2) GO TO 355
P(3,3)=((1.-EMUL)/2.)*EL
P(3,5)=P(3,3)
P(3,11)=-ZZ(JJ)*(1.-EMUL)*EL
P(3,14)=P(3,11)*XCC*2.
355 CONTINUE
DO 353 MR=1,3
AG(MR)=0.
DO 353 LR=1,15
AG(MR)=AG(MR)+P(MR,LR)*S(LR,1)
353 CONTINUE
SIGR(N,JJ)=AG(1)
SIGV(N,JJ)=AG(2)
SIGS(N,JJ)=AG(3)
350 CONTINUE
330 CONTINUE
NH1=NH+1
I=1
II=NN2-1
DO 9 II,J=1,NH1
DO 8 JJ=1,II,2
DO 7 JJ=1,NLAY
SIGA=(SIGR(JJ1,JJ)+SIGR((JJ1+1),JJ))/2.
SIGR(JJ1,JJ)=SIGA
SIGR((JJ1+1),JJ)=SIGA
7 CONTINUE
8 CONTINUE
I=I+NN2
II=II+NN2
9 CONTINUE
DO 410 N=1,NEL
DO 410 JJ=1,NLAY
EE1(N,JJ)=EE(N,JJ)
ESIGR=SIGR(N,JJ)
IF(JJ.EQ.NLAYS1.OR.JJ.EQ.NLAYS2) GO TO 402
IF(ESIGR) 430,430,440
440 IF(ESIGR) .GE. STRESST ) EE(N,JJ)=0.0
GO TO 410
430 CONTINUE
SIG=ESIGR
IF(SIG.EQ.0.) GO TO 5
IF(EE(N,JJ).LT.ES.AND.ABS(SIG).LT.STRSY) EE(N,JJ)=EE(N,JJ)*ABS(STR
SSY/SIG)
5 CONTINUE
IF(ABS(SIG).GT.STRSY) EE(N,JJ)=ABS(STRSY/SIG)*EE(N,JJ)
GO TO 410
402 IF(ABS(ESIGR).GT.STRYIE) EE(N,JJ)=ABS(STRYIE/ESIGR)*EE(N,JJ)
410 CONTINUE
NEW1=0
DO 480 JJ=1,NLAY
DO 480 N=1,NEL
IF(ABS(EE(N,JJ))-EE1(N,JJ)).GT.(.02*EE1(N,JJ)) NEW1=NEW1+1
480 CONTINUE
CAL=CAL+1.
WRITE(6,61) NCYCL
61 FORMAT(15)
IF(NCYCL.GT.2) GO TO 62
IF(NEW1.GT.NALAW) NCYCL=NCYCL+1
IF(NEW1.GT.NALAW) GO TO 490
FIN1480
FIN1490
FIN1500
FIN1510
FIN1520
FIN1530
FIN1540
FIN1550
FIN1560
FIN1570
FIN1580
FIN1590
FIN1600
FIN1610
FIN1620
FIN1630
FIN1640
FIN1650
FIN1660
FIN1670
FIN1680
FIN1690
FIN1700
FIN1710
FIN1720
FIN1730
FIN1740
FIN1750
FIN1760
FIN1770
FIN1780
FIN1790
FIN1800
FIN1810
FIN1820
FIN1830
FIN1840
FIN1850
FIN1860
FIN1870
FIN1880
FIN1890
FIN1900
FIN1910
FIN1920
FIN1930
FIN1940
FIN1950
FIN1960
FIN1970
FIN1980
FIN1990
FIN2000
FIN2010
FIN2020
FIN2030
FIN2040
FIN2050
FIN2060
FIN2070
FIN2080
FIN2090
FIN2100
FIN2110
FIN2120
FIN2130
FIN2140
FIN2150
FIN2160
FIN2170
FIN2180
FIN2190
FIN2200
FIN2210

```

```

62 CONTINUE
DO 81 N=1,NEL
DO 81 JJ=1,NLAY
IF(EE(N,JJ).EQ.0.0) GO TO 81
IF(JJ.EQ.NLAYS1.OR.JJ.EQ.NLAYS2) GO TO 82
IF(EE(N,JJ).LT.ES) EE(N,JJ)=EE1(N,JJ)*EE(N,JJ)/(2.*EE1(N,JJ)-EE(N,
*JJ))
IF(EE(N,JJ).LE.(.40*ES)) EE(N,JJ)=0.0
GO TO 81
82 IF(EE(N,JJ).LT.EB) EE(N,JJ)=EE1(N,JJ)*EE(N,JJ)/(2.*EE1(N,JJ)-EE(N,
*JJ))
81 CONTINUE
I=NN2+1
DO 500 J=1,NH
AREA=0.0
VOL=0.0
BMFF=0.0
TJJ=T(I)/2.
II=I+NN2-1
DO 510 JJ=1,NLAY
IF(JJ.EQ.NLAYS1) EQST1=(SIGR(I,JJ)-EMU*SIGV(I,JJ))/EE1(I,JJ)
IF(JJ.EQ.NLAYS2) EQST2=(SIGR(I,JJ)-EMU*SIGV(I,JJ))/EE1(I,JJ)
AREA=AREA+SIGR(I,JJ)*T(JJ)
DO 520 K=I,II
III=NI(K)
JJJ=NJ(K)
KKK=NK(K)
VOL=VOL+SIGR(K,JJ)*T(JJ)*ABS(YYY(III)-YYY(KKK))/2.0
BMFF=BMFF+SIGR(K,JJ)*ABS(YYY(III)-YYY(KKK))/2.*T(JJ)*(DS/2.-TJJ)
520 CONTINUE
IF(JJ.EQ.NLAY) GO TO 510
TJJ=TJJ+(T(JJ)+T(JJ+1))/2.
510 CONTINUE
EFW(J)=ABS(B(J)/AREA)
CURF(J)=ABS(BMFF)*2.
I=I+NN2
500 CONTINUE
159 FORMAT( 5X,*DET -VE *,E15.8)
160 FORMAT( 5X,*DET ZERO*,E15.8)
1000 RETURN
END
FIN2220
FIN2230
FIN2240
FIN2250
FIN2260
FIN2270
FIN2280
FIN2290
FIN2300
FIN2310
FIN2320
FIN2330
FIN2340
FIN2350
FIN2360
FIN2370
FIN2380
FIN2390
FIN2400
FIN2410
FIN2420
FIN2430
FIN2440
FIN2450
FIN2460
FIN2470
FIN2480
FIN2490
FIN2500
FIN2510
FIN2520
FIN2530
FIN2540
FIN2550
FIN2560
FIN2570
FIN2580
FIN2590
FIN2600
FIN2610
FIN2620

```

```

C      SUBROUTINE MULTP (A,B,C,I,J,K,IT,NA,NB,NC)
C      *****
DIMENSION A(NA,1),B(NB,1),C(NC,1)
DO 1 N=1,I
DO 1 N=1,J
C(M,N)=0.0
DO 1 L=1,K
IF(IT.EQ.0) C(M,N)=C(M,N)+A(M,L)*B(L,N)
IF(IT.NE.0) C(M,N)=C(M,N)+A(L,ND)*B(L,N)
1 CONTINUE
RETURN
END

```

```

MUL 10
MUL 20
MUL 30
MUL 40
MUL 50
MUL 60
MUL 70
MUL 80
MUL 90
MUL 100
MUL 110
MUL 120

```

C	SUBROUTINE TERMS(I,EB,ES)	TER 10
C	*****	
	COMMON/BLOCK4/BMS(40),BMB(40),BIT(40),TW,TF,BF,DS,AB,DC	TER 20
	COMMON/BLOCK7A/CURF(20),BSB(20)	TER 30
	COMMON/BLOCK10/AS(40),SI(40),SEI(40),EAB(40),EIB(40),Z(40),CS(40)	TER 40
	COMMON/BLOCK11/BET(40),ALP(40),BB(40),SS(40)	TER 50
	COMMON/BLOCK12/DN(40)	TER 60
	COMMON/BLOCK13/DBT(40),CBD(40),CB(40)	TER 70
	COMMON/BLOCK14/BN(40)	TER 80
	COMMON/BLOCK 22/ AS1,AS2,DAS1,DAS2,STYIE,STRYIE,STTEN	TER 90
	COMMON/BLOCK30/YX(40),DS(20)	TER 100
	AS(I)=DN(I)*BS(I)+(AS1+AS2)*EB/ES	TER 110
	STAT=BS(I)*DN(I)*DN(I)/2.+(AS1*DAS1+AS2*DAS2)*EB/ES	TER 120
	CS(I)=STAT/AS(I)	TER 130
	Z(I)=(DS-CS(I))+CB(I)+DC	TER 140
	SI(I)=BS(I)*DN(I)**3./12.+(AS1*(DAS1-CS(I))**2.+AS2*(DAS2-CS(I))*	TER 150
	9*2.)*EB/ES +BS(I)*DN(I)*(CS(I)-(DN(I)/2.))**2.	TER 160
	SI(I)=SI(I)*BSB(I)/BS(I)	TER 170
	SEI(I)=EB*BIT(I)+ES*SI(I)	TER 180
	EAB(I)=EB*AB*ES*AS(I)/(EB*AB+ES*AS(I))	TER 190
	EIB(I)=SEI(I)+EAB(I)*Z(I)**2.	TER 200
	BET(I)=Z(I)/SEI(I)	TER 210
	ALP(I)=EIB(I)/(EAB(I)*SEI(I))	TER 220
	BB(I)=-BET(I)*BN(I)*SS(I)	TER 230
	RETURN	TER 240
	END	TER 250

	SUBROUTINE FANS(STST,CURS1,I)	FAM 10
	=====	
C	*****	FAM 20
	DIMENSION STST(40),CURS1(40)	FAM 30
	COMMON/BLOCK2/FS(40),CS1	FAM 40
	COMMON/BLOCK4/BMS(40),BNB(40),BIT(40),TV,TF,BF,DS,AB,DC	FAM 50
	COMMON/BLOCK3/STSY,STRSY,STRPY,STRWY,STRFY,EB,STFY,ES,EBP	FAM 60
	COMMON/BLOCK7A/CURF(20),BSB(20)	FAM 70
	COMMON/BLOCK10/AS(40),SI(40),SEI(40),EAB(40),EIB(40),Z(40),CS(40)	FAM 80
	COMMON/BLOCK18/STSB(40)	FAM 90
	COMMON/BLOCK 22/ AS1,AS2,DAS1,DAS2,STYIE,STRYIE,STTEN	FAM 100
	COMMON/BLOCK30/XX(40),BS(20)	FAM 110
	STSB(I)=STST(I)+DS*CURS1(I)	FAM 120
	DNAS=(ABS(STST(I))+STTEN)/CURS1(I)	FAM 130
	IF(DNAS.GT.DS) DNAS=DS	FAM 140
	AREAS=BS(I)*DNAS+(AS1+AS2)*EB/ES	FAM 150
	STAT=BS(I)*(DNAS**2.)/2.+(AS1*DAS1+AS2*DAS2)*EB/ES	FAM 160
	DCC=STAT/AREAS	FAM 170
	CS(I)=DCC	FAM 180
	CS1=DS-DCC+DC	FAM 190
	IF(STST(I).LE.0.0.AND.STSB(I).LE.0.0) GO TO 10	FAM 200
	IF(STST(I).LE.0.0.AND.STSB(I).GT.0.0) GO TO 20	FAM 210
10	IF(ABS(STST(I)).GT.STSY) GO TO 11	FAM 220
	F1=STSB(I)*ES*BS(I)*DS	FAM 230
	F2=(STST(I)-STSB(I))*ES*DS*BS(I)*0.5	FAM 240
	FS(I)=F1+F2	FAM 250
	BMS(I)=F1*(DCC-DS/2.)+F2*(DCC-DS/3.)	FAM 260
	GO TO 100	FAM 270
11	DCON=(ABS(STST(I))-STSY)/CURS1(I)	FAM 280
	IF(DCON.GT.DS) DCON=DS	FAM 290
	F1=(-STRSY)*DS*BS(I)	FAM 300
	F2=(STSY-ABS(STSB(I)))*ES*(DS-DCON)*BS(I)*0.5	FAM 310
	FS(I)=F1+F2	FAM 320
	BMS(I)=F1*(DCC-DS/2.)+F2*(DS-(DS-DCON)/3.-DCC)	FAM 330
	GO TO 100	FAM 340
20	IF(ABS(STST(I)).GT.STSY) GO TO 25	FAM 350
	DNAS=(ABS(STST(I))+STTEN)/CURS1(I)	FAM 360
	IF(DNAS.GT.DS) DNAS=DS	FAM 370
	STDNAS=STST(I)+DNAS*CURS1(I)	FAM 380
	F1=STST(I)*ES*DNAS*BS(I)	FAM 390
	F2=(ABS(STST(I))+STDNAS)*ES*DNAS*BS(I)*0.5	FAM 400
	FS(I)=F1+F2	FAM 410
	BMS(I)=F1*(DS/2.-DNAS/2.)+F2*(DS/2.-2.*DNAS/3.)	FAM 420
	BMS(I)=ABS(BMS(I))+ABS(FS(I))*(DCC-DS/2.)	FAM 430
	GO TO 100	FAM 440
25	DCON=(ABS(STST(I))-STSY)/CURS1(I)	FAM 450
	IF(DCON.GT.DS) DCON=DS	FAM 460
	DNAS=(STSY+STTEN)/CURS1(I)	FAM 470
	DD=DS-DCON	FAM 480
	IF(DNAS.GT.DD) DNAS=DD	FAM 490
	STDNAS=DNAS*CURS1(I)-STSY	FAM 500
	F1=(-STRSY)*(DCON+DNAS)*BS(I)	FAM 510
	F2=(STSY+STDNAS)*ES*BS(I)*DNAS*0.5	FAM 520
	FS(I)=F1+F2	FAM 530
	BMS(I)=F1*(DS/2.-(DCON+DNAS)/2.)+F2*(DS/2.-DCON-2.*DNAS/3.)	FAM 540
	BMS(I)=ABS(BMS(I))+ABS(FS(I))*(DCC-DS/2.)	FAM 550
100	STREIN1=STST(I)+CURS1(I)*DAS1	FAM 560
	STREIN2=STST(I)+CURS1(I)*DAS2	FAM 570
	FSTEEL1=STREIN1*EB*AS1	FAM 580
	FSTEEL2=STREIN2*EB*AS2	FAM 590
	IF(ABS(STREIN1).GT.STYIE) FSTEEL1=STRYIE*AS1*STREIN1/ABS(STREIN1)	FAM 600
	IF(ABS(STREIN2).GT.STYIE) FSTEEL2=STRYIE*AS2*STREIN2/ABS(STREIN2)	FAM 610
	FSTEEL=(FSTEEL1+FSTEEL2)	FAM 620
	BMSTEEL=FSTEEL1*(DAS1-DCC)+FSTEEL2*(DAS2-DCC)	FAM 630
	IF(CURS1(I).LT.0.) BMS(I)=ABS(BMS(I))*(-1.)	FAM 640
	IF(CURS1(I).GE.0.) BMS(I)=ABS(BMS(I))	FAM 650
	FS(I)=FS(I)+FSTEEL	FAM 660
	BMS(I)=(BMS(I)+BMSTEEL)*BSB(I)/BS(I)	FAM 670
	RETURN	FAM 680
	END	FAM 690

```
C SUBROUTINE EXTRA( I, GYY, SUML )
C *****
C DIMENSION GYY( 40, 4 )
C COMMON / BLOCK1 / WM( 4 )
C SUML = 0.0
C DO 7273 J = 1, 3
C   PROL = GYY( I, J )
C   DO 7283 L = 1, 3
C     IF( J - L ) 7293, 7283, 7293
C     PROL = PROL * ( ( WM( 4 ) - WM( L ) ) / ( WM( J ) - WM( L ) ) )
7293 CONTINUE
7283 SUML = SUML + PROL
7273 RETURN
C END
```

```
EXT 10
EXT 20
EXT 30
EXT 40
EXT 50
EXT 60
EXT 70
EXT 80
EXT 90
EXT 100
EXT 110
EXT 120
EXT 130
EXT 140
```


C	SUBROUTINE REGULA(MMM, MERMD	REG 10
C	*****	
	COMMON/BLOCK29/ UU, VV, XL, XR, MER1, MER2, SAS(40), SLM(40), LAG	REG 20
	IF(LAG.LT.1) GO TO 2007	REG 30
	IF(SLM(MMM-1)*VV) 2009,2009,2010	REG 40
2010	XL=SAS(MMM-1)	REG 50
	VV=SLM(MMM-1)	REG 60
	MER1=MMM-1	REG 70
	GO TO 2005	REG 80
2009	XR=SAS(MMM-1)	REG 90
	UU=SLM(MMM-1)	REG 100
	MER2=MMM-1	REG 110
	GO TO 2005	REG 120
2007	IF(SLM(MMM-1)*SLM(MMM-2)) 2002,2002,25	REG 130
2002	LAG=LAG+1	REG 140
	IF(SLM(MMM-1)) 2003,2003,2004	REG 150
2003	VV=SLM(MMM-1)	REG 160
	UU=SLM(MMM-2)	REG 170
	XL=SAS(MMM-1)	REG 180
	XR=SAS(MMM-2)	REG 190
	MER1=MMM-1	REG 200
	MER2=MMM-2	REG 210
	GO TO 2005	REG 220
2004	UU=SLM(MMM-1)	REG 230
	VV=SLM(MMM-2)	REG 240
	XR=SAS(MMM-1)	REG 250
	XL=SAS(MMM-2)	REG 260
	MER2=MMM-1	REG 270
	MER1=MMM-1	REG 280
2005	SAS(MERD)=(XL*UU-XR*VV)/(UU-VV)	REG 290
	IF(MERH.EQ.MER1.OR.MERM.EQ.MER2) SAS(MMD)=(XL+XR)*0.5	REG 300
25	RETURN	REG 310
	END	REG 320
		REG 330

<p>C C 6 7 9 5 2 3 4</p>	<pre> SUBROUTINE STANS(FB,CURS1,I) ***** DIMENSION FB(40),CURS1(40),FB1(10) COMMON/BLOCK2/FS(40),CS1 COMMON/BLOCK3/BMK(40) COMMON/BLOCK4/BMS(40),BMB(40),BIT(40),TW,TF,BF,DS,AB,DC COMMON/BLOCK5/STSY,STRSY,STRPY,STRWY,STRFY,EB,STFY,ES,EBP COMMON/BLOCK13/DBT(40),CBD(40),CB(40) COMMON/BLOCK17/STST(40),STBB(40) COMMON/BLOCK18/STSB(40) COMMON/BLOCK23/CURT(40),STBT(40),STSTT(40) COMMON/BLOCK25/MA,JM,NH,KER,KEM2 COMMON/BLOCK28/CSNH,ERST,SCAL1,SCAL2 COMMON/BLOCK30/KK(40),DS(20) KEM2=0 KC=0 NNA=0 NNB=0 STST(I)=STSTT(I) CALL FAMS(STST,CURS1,I) FB1(I)=FS(I) DSTST=-5.0E-6 CONTINUE DO 2 L=1,6 IF(MA.EQ.1) DSTST=DSTST*(-1.0) STST(I)=STST(I)+DSTST CALL FAMS(STST,CURS1,I) FD1=FS(I) DFDE=(FD1-FB1(L))/DSTST IF(DFDE.NE.0.) GO TO 5 STST(I)=STSTT(I) IF(NNA.EQ.1) GO TO 7 DSTST=-1.0E-04 NNA=1 GO TO 6 IF(NNB.EQ.1) GO TO 9 DSTST=-5.0E-03 NNB=1 GO TO 6 KEM2=1 GO TO 4 DSTST1=(FB(I)-ABS(FB1(L)))/DFDE STST(I)=STST(I)-DSTST1-DSTST CALL FAMS(STST,CURS1,I) ERCOE=0.0001 IF(CSNH.GE.0.015) ERCOE=0.00001 IF(CSNH.GE.0.045) ERCOE=0.000002 ERR3=ABS(FB(I))*ERCOE IF(KER.GE.1) ERR3=ERR3+0.0001 IF(MA.EQ.1) DSTST=DSTST*(-1.0) IF(ABS(FB(I)-ABS(FS(I))).LE.ERR3) GO TO 5 FB1(L+1)=FS(I) CONTINUE Z1=CS1+CB(I) BMK(I)=BMB(I)+BMS(I)+FB(I)*Z1 RETURN END </pre>	<p>STA 10 STA 20 STA 30 STA 40 STA 50 STA 60 STA 70 STA 80 STA 90 STA 100 STA 110 STA 120 STA 130 STA 140 STA 150 STA 160 STA 170 STA 180 STA 190 STA 200 STA 210 STA 220 STA 230 STA 240 STA 250 STA 260 STA 270 STA 280 STA 290 STA 300 STA 310 STA 320 STA 330 STA 340 STA 350 STA 360 STA 370 STA 380 STA 390 STA 400 STA 410 STA 420 STA 430 STA 440 STA 450 STA 460 STA 470 STA 480 STA 490 STA 500 STA 510 STA 520 STA 530 STA 540 STA 550 STA 560 STA 570</p>
--	--	---

	SUBROUTINE FAMB(STBB,CURB1, I)	FAM 10

	DIMENSION STBB(40), CURB1(40), FBB(20), BMBB(20), TFBB(20),	FAM 20
	TBMBB(20), STBD(20), STRBD(20)	FAM 30
	COMMON/BLOCK4/BMS(40), BMB(40), BYT(40), TW, TF, BF, DS, AB, DC	FAM 40
	COMMON/BLOCK3/STSY, STBSY, STRPY, STRWY, STRFY, EB, STFY, ES, EBP	FAM 50
	COMMON/BLOCK6/FB(40)	FAM 60
	COMMON/BLOCK13/DBT(40), CBD(40), CB(40)	FAM 70
	COMMON/BLOCK19/STBT(40)	FAM 80
	COMMON/BLOCK21/BH(20), DDB(20), DFA(20), HARST, NFU, NFD, NW, NPL, PCUT	FAM 90
	COMMON/BLOCK30/XX(40), BS(20)	FAM 100
	STBT(I) = STBB(I) - CURB1(I) * DBT(I)	FAM 110
	STBD(I) = STBT(I)	FAM 120
	STRBD(I) = STBD(I) * EB	FAM 130
	IF(STBD(I) .GE. STFY .AND. STBD(I) .LE. HARST) STRBD(I) = STRFY	FAM 140
	IF(STBD(I) .GT. HARST) STRBD(I) = STRFY + (STBD(I) - HARST) * EBP	FAM 150
	IF(XX(I) .LE. PCUT) N1 = NFU + NFD + NW	FAM 160
	IF(XX(I) .GT. PCUT) N1 = NFU + NW + NFD + NPL	FAM 170
	DO 4 KL=1, N1	FAM 180
	STRY = STRFY	FAM 190
	IF((KL+1) .GT. NFU) STRY = STRWY	FAM 200
	IF((KL+1) .GT. (NFU + NW)) STRY = STRFY	FAM 210
	IF((KL+1) .GT. (NFU + NW + NFD)) STRY = STRPY	FAM 220
	STBY = STRY / EB	FAM 230
	SIBD(KL+1) = STBD(KL) + CURB1(I) * DDB(KL)	FAM 240
	STRBD(KL+1) = STBD(KL+1) * EB	FAM 250
	IF(ABS(STBD(KL+1)) .GE. STBY .AND. ABS(STBD(KL+1)) .LE. HARST)	FAM 260
	1STRBD(KL+1) = STRY * STBD(KL+1) / ABS(STBD(KL+1))	FAM 270
	IF(ABS(STBD(KL+1)) .GT. HARST) STRBD(KL+1) = (STRY + (ABS(STBD(KL+1)) -	FAM 280
	1HARST) * EBP) * STBD(KL+1) / ABS(STBD(KL+1))	FAM 290
	FBB(KL) = (STRBD(KL+1) + STRBD(KL)) * .5 * EB(KL) * BH(KL)	FAM 300
	BMBB(KL) = (DFA(KL) - DDB(KL) * .5) * FBB(KL)	FAM 310
	IF(KL .GT. 1) GO TO 8	FAM 320
	TFBB(KL) = FBB(KL)	FAM 330
	TBMBB(KL) = BMBB(KL)	FAM 340
	GO TO 4	FAM 350
8	TFBB(KL) = TFBB(KL-1) + FBB(KL)	FAM 360
	TBMBB(KL) = TBMBB(KL-1) + BMBB(KL)	FAM 370
4	CONTINUE	FAM 380
	FB(I) = TFBB(N1)	FAM 390
	YYY = DBT(I) - (TBMBB(N1) / FB(I))	FAM 400
	BMB(I) = ABS(CBD(I) - YYY) * FB(I)	FAM 410
	RETURN	FAM 420
	END	FAM 430
		FAM 440

```

SUBROUTINE STRAIN(FST,BMST,CURD1,I)
*****
C *****
C DIMENSION FST(40),DMST(40),CURD1(40) STR 10
COMMON/BLOCK3/BMM(40) STR 20
COMMON/BLOCK4/BMS(40),BMB(40),BIT(40),TW,TF,BF,DS,AB,DC STR 30
COMMON/BLOCK5/STSY,STRSY,STRPY,STRWY,STRFY,EB,STFY,ES,EBP STR 40
COMMON/BLOCK6/FB(40) STR 50
COMMON/BLOCK7/CUR1(40) STR 60
COMMON/BLOCK8/CURB1(40) STR 70
COMMON/BLOCK9/CURS1(40) STR 80
COMMON/BLOCK13/DBT(40),CBD(40),CB(40) STR 90
COMMON/BLOCK17/STST(40),STBB(40) STR 100
COMMON/BLOCK18/STSB(40) STR 110
COMMON/BLOCK19/STBT(40) STR 120
COMMON/BLOCK20/CUR(40) STR 130
COMMON/BLOCK23/CURT(40),STBBT(40),STSTT(40) STR 140
COMMON/BLOCK25/MA,JM,NH,KER,KEM2 STR 150
COMMON/BLOCK26/STC(40),CUC(40) STR 160
COMMON/BLOCK27/KKCC,NERM,MMM STR 170
COMMON/BLOCK28/GSNH,ERST,SCAL1,SCAL2 STR 180
COMMON/BLOCK30/XX(40),BS(20) STR 190
KER=0 STR 200
KKCC=0 STR 210
KK2=0 STR 220
CUR1(I)=CURT(I) STR 230
STBB(I)=STBBT(I) STR 240
BMST(I)=BMST(I)+CURD1(I)*EB*BIT(I) STR 250
CURB1(I)=CUR1(I) STR 260
WRITE(6,604) I,CUR1(I),STBB(I) STR 270
604 FORMAT(* INELASTIC PANEL NO*,I2,5X,*CURVATURE BAR*,E13.6,5X,*ST STR 280
IRAIN BAR*,E14.6) STR 290
CALL FAMB(STBB,CURB1,I) STR 300
CURS1(I)=CURB1(I)-CURD1(I) STR 310
CALL STAMS(FB,CURS1,I) STR 320
FB2=FB(I) STR 330
BMB2=BMM(I) STR 340
FB4=FB(I) STR 350
BMB4=BMM(I) STR 360
CUC(I)=0.1E-07 STR 370
STC(I)=0.1E-07 STR 380
8012 NLK=0 STR 390
NLN=0 STR 400
NLL=0 STR 410
GO TO 2 STR 420
7051 CUC(I)=0.1E-05 STR 430
STC(I)=0.1E-05 STR 440
NLK=1 STR 450
GO TO 2 STR 460
7052 CUC(I)=0.1E-06 STR 470
STC(I)=0.1E-08 STR 480
NLL=1 STR 490
GO TO 2 STR 500
7053 CUC(I)=0.1E-08 STR 510
STC(I)=0.1E-06 STR 520
NLN=1 STR 530
2 IF(KK2.EQ.2) GO TO 58 STR 540
GO TO 59 STR 550
58 CUC(I)=0.5E-08 STR 560
STC(I)=0.5E-08 STR 570
59 CURB1(I)=CUR1(I)+CUC(I) STR 580
CALL FAMB(STBB,CURB1,I) STR 590
CURS1(I)=CURB1(I)-CURD1(I) STR 600
IF(FB(I).LE.0.) GO TO 8019 STR 610
MA=1 STR 620
CALL STAMS(FB,CURS1,I) STR 630
MA=0 STR 640
IF(KEM2.EQ.1) GO TO 8019 STR 650
FBC=FB(I) STR 660
BMBC=BMM(I) STR 670
CURB1(I)=CUR1(I) STR 680
IF(KKCC.EQ.0) GO TO 505 STR 690
WRITE(6,606) CUC(I),FBC,BMBC STR 700
606 FORMAT(* DEL CUR*,E16.8,4X,*F DEL CUR*,F13.6,4X,*M DELT CUR*,F16. STR 710
STR 720
STR 730

```



```
4 CONTINUE
  IF(KK2.EQ.4) MERM=MM
  ERE1=ABS(FST(1))*ERFAC*SCAL2
  ERE2=ABS(BMST(1))*ERFAC*SCAL2
  IF(ABS(FST(1)-FB2).GT.ERE1.OR.ABS(BMST(1)-BMB2).GT.ERE2)
1GO TO 8019
  STBBT(1)=STBB(1)
  STSTT(1)=STST(1)
  CURT(1)=CUR1(1)
  CUR1(1)=CURS1(1)
  WRITE(6,6) KK2,1
6  FORMAT(2X,*(((((((( KK2= *,12.* )))))))))*,*PANNEL NO*,
113,/)
5  RETURN
  END
```

STR1480
STR1490
STR1500
STR1510
STR1520
STR1530
STR1540
STR1550
STR1560
STR1570
STR1580
STR1590
STR1600
STR1610
STR1620

REFERENCES

1. Newmark, N.M., Siess, C.P. and Viest, I.M., "Tests and Analysis of Composite Beams with Incomplete Interaction", Proceedings of the Society for Experimental Stress Analysis, vol. IX, no. 1, 1951, pp. 75-92.
2. Timoshenko, S.P. and Goodier, J.N., "Theory of Elasticity", McGraw-Hill Book Company, New York, 1951.
3. Hognestad, E., Hansen, N.W. and McHenry, D., "Concrete Stress Distribution in Ultimate Strength Design", Journal of the American Concrete Institute, vol. 52, Dec. 1955.
4. Beedle, L.S., "Plastic Design of Steel Frames", John Wiley & Sons Inc., New York, 1958.
5. Allan, D.N. and Savern, R.T., "Composite Action Between Beams and Slabs under Transverse Load", The Structural Engineer, vol. 39; no. 5, May 1961, pp. 149-154.
6. Mackey, S. and Wong, F.K.C., "Effective Width of Composite Tee-Beam Flange", The Structural Engineer, vol. 39, no. 9, Sept. 1961, pp. 277-285.
7. Robinson, H., "Preliminary Investigation of a Composite Beam with Ribbed Slab Formed by Cellular Steel Decking", Engineering Dept. Report No. 35, McMaster University, Oct. 1961.
8. Savern, R.T., "The Deformation of a Rectangular Slab Stiffened by Beams under Transverse Load", Magazine of Concrete Research, vol. 14, no. 41, July 1962, pp. 73-78.
9. Savern, R.T., "The Effective Width of T-Beams", Magazine of Concrete Research, vol. 16, no. 47, June 1964, pp. 99-102.
10. Barnard, P.R. and Johnson, R.P., "Plastic Behaviour of Continuous Composite Beams", Proceedings, Institution of Civil Engineers, vol. 32, Oct. 1965, pp. 180-197.
11. Mattock, A.H., "Rotational Capacity of Hinging Regions in Reinforced Concrete Beams", Proceedings of the International Symposium "Flexural Mechanics of Reinforced Concrete", 1965.
12. British Standard Code of Practice, CP 117, Part I, "Simply Supported Beams in Buildings", 1965.

13. Slutter, R.G. and Driscoll, G.C., Jr., "Flexural Strength of Steel-Concrete Composite Beams", Journal of the Structural Division, American Society of Civil Engineers, vol. 91, no. ST2, April 1965, pp. 71-99.
14. British Standard Code of Practice, CP 117, Part II, "Beams For Bridges", 1967.
15. Robinson, H., "Tests on Composite Beams with Cellular Deck", Journal of the Structural Division, American Society of Civil Engineers, vol. 93, no. ST4, Aug. 1967, pp. 139-164.
16. Teraszkiewicz, J.S., "Static and Fatigue Behaviour of Simply Supported and Continuous Composite Beams of Steel and Concrete", Ph.D. Thesis, University of London, 1967.
17. Van Dalen, K., "Composite Action at the Support of Continuous Beams", Ph.D. Thesis, University of Cambridge, 1967.
18. Adekola, A.O., "Effective Widths of Composite Beams of Steel and Concrete", The Structural Engineer, vol. 46, no. 9, Sept. 1968, pp. 285-289.
19. Canadian Sheet Steel Building Institute, "Composite Beam Manual", 1968.
20. Hagood, T.A., Jr., Guthrie, L. and Hoadley, P.G., "An Investigation of the Effective Concrete Slab Width for Composite Construction", Engineering Journal, American Institute of Steel Construction, Jan. 1968.
21. Nilson, A.H., "Nonlinear Analysis of Reinforced Concrete by the Finite Element Method", Journal of the American Concrete Institute, vol. 65, no. 9, Sept. 1968, pp. 757-766.
22. Yam, L.C.P. and Chapman, J.C., "Inelastic Behaviour of Simply Supported Composite Beams of Steel and Concrete", Proceedings, Institution of Civil Engineers, vol. 41, Dec. 1968, pp. 651-683.
23. Barnard, P.R., "New Developments in Composite Floor Systems", Proceedings, Symposium on Composite Construction, June 1969.
24. Johnson, R.P., Green Wood, R.D. and Van Dalen, K., "Stud Shear Connectors in Hogging Moment Regions of Composite Beams", The Structural Engineer, vol. 47, Sept. 1969, pp. 345-350.
25. Kupfer, H., Hilsdorf, H.K. and Rusch, H., "Behaviour of Concrete Under Biaxial Stresses", Journal of the American Concrete Institute, Vol. 66, Aug. 1969, pp. 656-665.

26. Robinson, H., "Composite Beams with Cellular Steel Decking", Journal of the Structural Division, American Society of Civil Engineers, vol. 93, No. ST3, March 1969, pp. 355-360.
27. Thiruvengadam, T.R., "A Method for Inelastic Analysis of Single Span Composite Beams", Ph.D. Thesis, University of Illinois, Urbana, Illinois, 1969.
28. Cervenka, V., "Inelastic Finite Element Analysis of Reinforced Concrete Plates Under In-plane Loads", Ph.D. Thesis, University of Colorado, 1970.
29. Daniels, J.H., Kroll, G.D. and Fisher, J.W., "Behaviour of Composite Beam-to-Column Joints", Journal of the Structural Division, American Society of Civil Engineers, vol. 96, no. ST3, March 1970, pp. 671-685.
30. Fisher, J.W., "Design of Composite Beams with Formed Metal Deck", Engineering Journal, American Institute of Civil Engineering, vol. 7, no. 2, July 1970, pp. 88-96.
31. Johnson, R.P., "Research on Steel-Concrete Composite Beams", Journal of the Structural Division, American Society of Civil Engineers, vol. 96, No. ST3, March 1970, pp. 445-459.
32. Rawtani, S., "Vibration Analysis of Rotating Low Aspect Ratio Blades", Ph.D. Thesis, McMaster University, 1970.
33. Tachibana, Y., "Experiment on Non-Prestressed Continuous Composite Beams", International Association for Bridge and Structural Engineering, Publication 30-1, 1970, pp. 203-215.
34. ACI Committee 442, "Response of Buildings to Lateral Forces", Journal of the American Concrete Institute, vol. 68, Feb. 1971, pp. 81-104.
35. Gracia, I. and Daniels, J.H., "Negative Moment Behaviour of Composite Beams", Fritz Engineering Laboratory Report No. 359.4, Lehigh University, 1971.
36. Jofriet, J.C. and McNeice, G.M., "Finite Element Analysis of Reinforced Concrete Slabs", Journal of the Structural Division, American Society of Civil Engineers, vol. 97, March 1971, pp. 785-806.
37. Scanlon, A., "Time Dependent Deflections of Reinforced Concrete Slabs", Ph.D. Thesis, University of Alberta, 1971.
38. Zienkiewicz, O., "The Finite Element Method in Engineering Science", McGraw-Hill Book Company, New York, 1971.

39. Naka, T., Wakabayashi, M. and Murata, J., "Steel Reinforced Concrete Construction", Preliminary Report, International Association for Bridge and Structural Engineering, Ninth Congress, Amsterdam, May 1972, pp. 165-172.
40. Daniels, J.H., "Recent Research on Composite Beams for Bridges and Buildings", Civil Engineering Transaction, I.E. Australia, vol. CE14, no. 2, Oct. 1972, pp. 228-233.
41. Duplessis, D.P. and Daniels, J.H., "Experiments on Composite Beams under Positive End Moment", Fritz Engineering Laboratory Report No. 374.2, Lehigh University, 1972.
42. Fisher, J.W., Daniels, J.H. and Slutter, R.G., "Continuous Composite Beams for Bridges", International Association for Bridge and Structural Engineering, Amsterdam, 1972.
43. Johnson, R.P. and Hope Gill, M., "Semi-Rigid Joints in Composite Frames", Preliminary Report, International Association for Bridge and Structural Engineering, Ninth Congress, Amsterdam, 1972.
44. Scordelis, A.C., "Finite Element Analysis of Reinforced Concrete Structures", Proceedings of the Specialty Conference on Finite Element Method in Civil Engineering, Montreal, June 1972, pp. 71-113.
45. Valliappan, S. and Doolan, T., "Nonlinear Stress Analysis of Reinforced Concrete", Journal of the Structural Division, American Society of Civil Engineers, vol. 98, no. ST4, April 1972, pp. 885-898.
46. Wanchoo, M.K., "Post-Elastic Finite Element Analysis of Reinforced Plates", Ph.D. Thesis, University of New Mexico, 1972.
47. Yam, L.C.P. and Chapman, J.C., "The Inelastic Behaviour of Continuous Composite Beams of Steel and Concrete", Proceeding, The Institution of Civil Engineers, vol. 53, Dec. 1972, pp. 487-501.
48. Duplessis, D.P. and Daniels, J.H., "Strength of Composite Beam-to-Column Connections", Fritz Engineering Laboratory Report No. 374.3, Lehigh University, 1973.
49. Hand, F.R., Pecknold, D.A. and Schnobrich, W.C., "Nonlinear Layered Analysis of RC Plates and Shells", Journal of the Structural Division, American Society of Civil Engineers, vol. 99, no. ST7, July 1973, pp. 1491-1505.
50. Khatua, T.P. and Cheung, Y.K., "Bending and Vibration of Multi-Layer Sandwich Beams and Plates", International Journal for Numerical Methods in Engineering, vol. 6, 1973, pp. 11-24.

51. Lin, C.S., "Nonlinear Analysis of Reinforced Concrete Slabs and Shells", Ph.D. Thesis, University of California, Berkeley, 1973.
52. Loo, Y.K., "Moment Connection for Vierendeel Trusses of Square Hollow Structural Sections", M.Eng. Project, McMaster University, 1973.
53. Ma, K.P., "Inelastic Analysis of Composite Beams with Partial Connection", M.Eng. Project, McMaster University, 1973.
54. Robinson, H. and Wallace, I.W., "Composite Beams with 1 1/2 inch Metal Deck and Partial and Full Connection", Transaction of the Canadian Society for Civil Engineering, vol. 16, no. A-8, Sept. 1973, pp. I-VIII.
55. Adekola, A.O., "The Dependence of Shear Lag on Partial Interaction in Composite Beams", International Journal of Solid Structures, vol. 10, 1974, pp. 389-400.
56. Adekola, A.O., "On the Influence Curves for Effective Widths in Non-Prismatic Composite Beams", Proceeding, Institution of Civil Engineers, vol. 57, March 1974, pp. 51-66.
57. Brady, F.J., "An Experimental Investigation of Unequal Width HSS Moment Connections for Vierendeel Trusses", M.Eng. Project, McMaster University, 1974.
58. Fahmy, E.H., "Inelastic Analyse of Composite Open-Web Steel Joists", M.Eng. Thesis, McMaster University, 1974.
59. "Hand Book of Steel Construction", Canadian Institute of Steel Construction, 1974.
60. Mawenya, A.S. and Davies, J.D., "Finite Element Analysis of Multi-Layer Plates", International Journal for Numerical Methods in Engineering, vol. 8, 1974, pp. 215-225.
61. Moffatt, K.R. and Lin, P.T., "On the Influence Curves for Effective Widths in Non-Prismatic Composite Beams", Discussion, Proceeding, Institution of Civil Engineers, vol. 57, Sept. 1974, pp. 553-557.
62. CSA Standard S16.1, 1974.
63. Szilard, R., "Theory and Analysis of Plates, Classical and Numerical Methods", Prentice-Hall Inc., New Jersey, 1974.
64. Ansourian, P., "An Application of the Method of Finite Elements to the Analysis of Composite Floor Systems", Proceeding, Institution of Civil Engineers, vol. 59, Dec. 1975, pp. 699-726.

65. Architectural Institute of Japan Standard for Structural Calculation of Steel-Reinforced Concrete Structures, 3rd Edition, Nov. 1975, English Translation by Prof. M. Wakabayashi in private correspondence.
66. Johnson, R.P., "Composite Structures of Steel and Concrete", Volume 1, John Wiley & Sons, New York, 1975.
67. Lin, C.S. and Scordelis, A.C., "Nonlinear Analysis of RC Shells of General Form", Journal of the Structural Division, American Society of Civil Engineers, vol. 101, No. ST3, March 1975, pp. 523-538.
68. Wanchoo, M.K. and May, G.W., "Cracking Analysis of Reinforced Concrete Plates", Journal of the Structural Division, American Society of Civil Engineers, Vol. 101, No. ST1, Jan. 1975, pp. 201-215.
69. Ansourian, P. and Roderick, J.W., "Composite Connections to External Columns", Journal of the Structural Division, American Society of Civil Engineers, vol. 102, No. ST8, -Aug. 1976, pp. 1609-1625.
70. Hamada, S. and Longworth, J., "Ultimate Strength of Continuous Composite Beams", Journal of the Structural Division, American Society of Civil Engineers, vol. 102, No. ST7, July 1976, pp. 1463-1478.
71. Heins, C.P. and Fan, H.M., "Effective Composite Beam Width at Ultimate Load", Journal of the Structural Division, American Society of Civil Engineers, vol. 102, No. ST11, Nov. 1976, pp. 2163-2179.
72. Lyengar, H.S., "State-of-the-Art Report on Composite or Mixed Steel-Concrete Construction for Buildings", Published by the American Society of Civil Engineers, 1977.
73. Cheung, M.S. and Chan, M.Y.T., "Finite Strip Evaluation of Effective Flange Widthh for Bridge Girders", Canadian Journal of Civil Engineering, vol. 5, June 1978, pp. 174-185.
74. Moffatt, K.R. and Dowling, P.J., "British Shear lag Rules for Composite Girders", Journal of the Structural Division, American Society of Civil Engineers, vol. 104, No. ST7, July 1978, pp. 1123-1130.